# STRUCTURE AND METAMORPHISM IN THE DALRADIAN OF NW CONNEMARA, IRELAND

'Thesis submitted in accordance with the requirements of the University of Liverpool for the degree of Doctor in Philosophy by

Ian Peter Dawes

July 1988

**List of Tables**

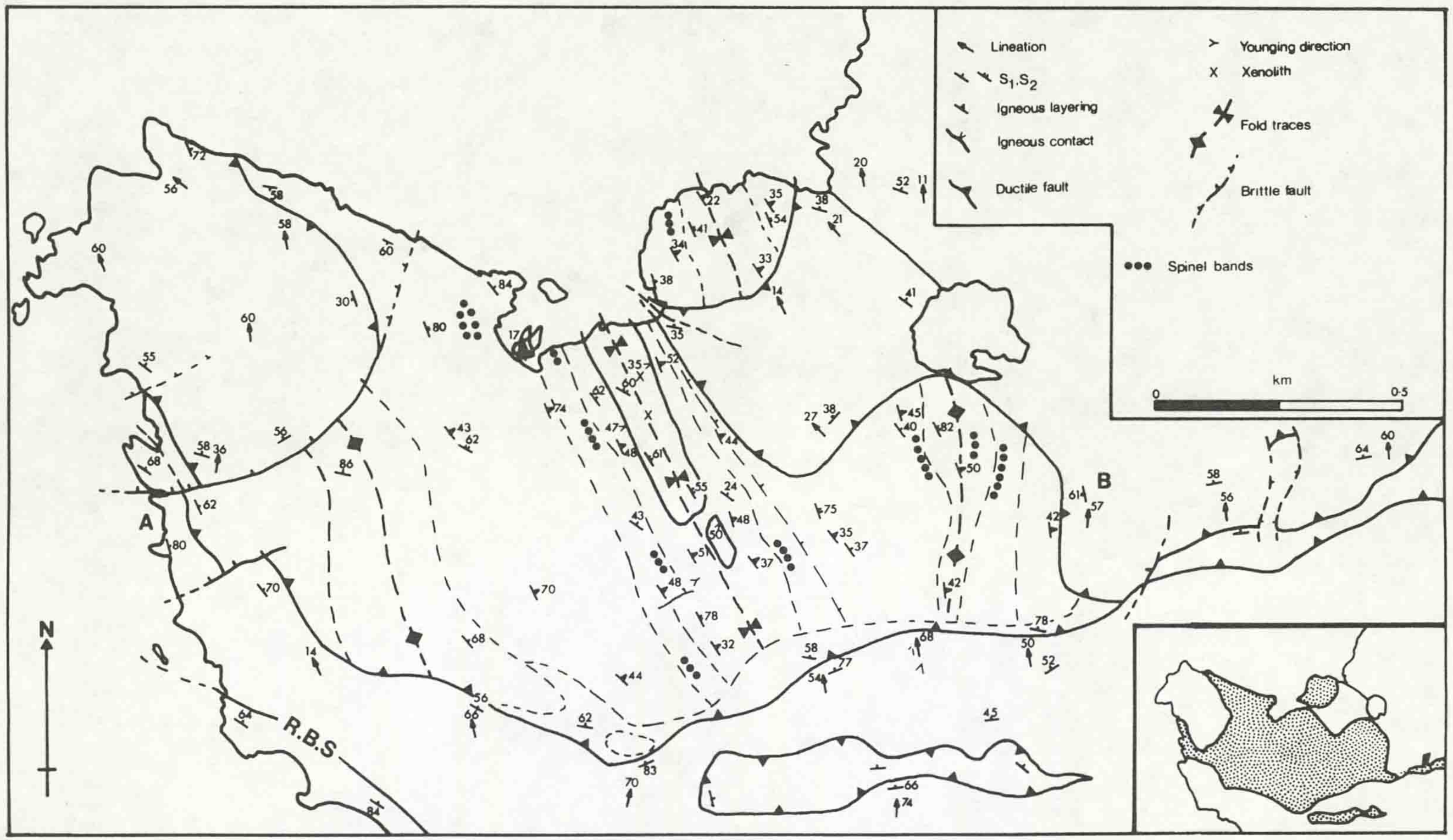


**Figure 3.36a: Simplified structural map of the main outcrop of the Dawros peridotite and its aureole. Inset map shows the extent of the peridotitic lithologies (stippled)**

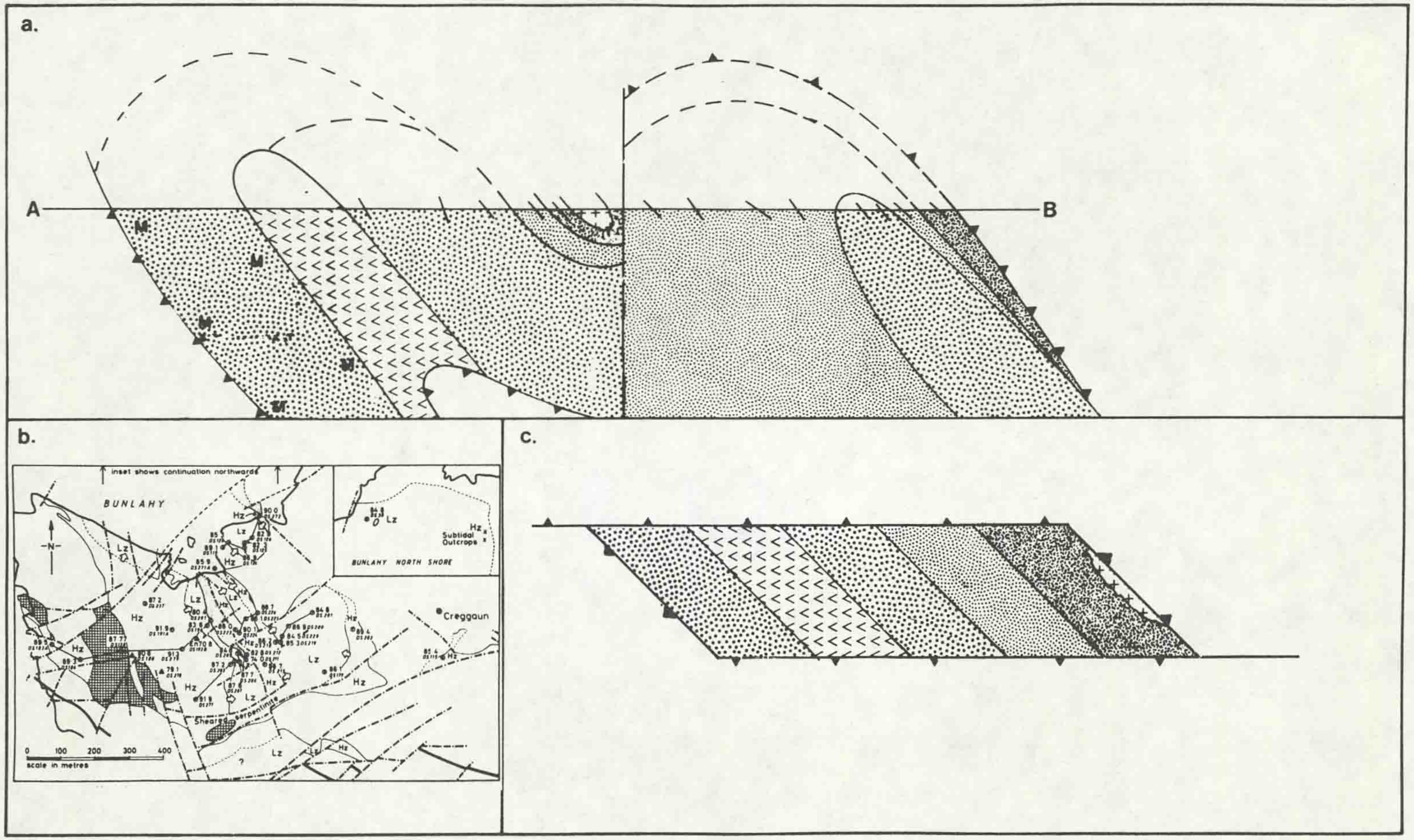


**Figure 3.36b: Cross section and schematic interpretation of the Dawros peridotite area. Inset map shows Bennett & Gibb's (1983) interpretation of the younging evidence.**

peridotite the form of the body is contentious, with disagreements on fundamental problems like the way - up and facing direction, the relation of gabbroic lithologies to the peridotite and the timing of emplacement and deformation of these bodies. This section covers the structure and tectonic fabrics developed in the peridotite and the nature of its contacts with the Kylemore Fm metasediments. The structure and contact relations of the gabbroic bodies are discussed in {3.4.2} with the relations between the peridotite and gabbros and their implications for the regional development covered in {3.5}.

3.4.1.1 Previous work: Rothstein (1954, 1957, 1961) considered the peridotite to be an essentially undeformed igneous sequence, having a lensoid shape with a rim of massive peridotite and a core of layered lithologies (Figure 3.34).

Leake (1964, 1970b) reinterpreted the structure of the peridotite body using the tectonic fabrics developed in the peridotite (primarily foliations) to define the internal structure of the peridotite. Leake's interpretation considers the gabbroic lithologies to be a continuation of the peridotite fractionation sequence, the gabbro representing the youngest part of the peridotite body.

Leake (Figure 3.34) envisages the peridotite to be downward facing and deformed by two phases of folding, a downward facing $F_2$ synform, the axial trace of which runs though the gabbro, and a later pair of upright NW/SE $F_3$ folds which deform the $F_2$ fold. The $F_2$ structure in the peridotite is traced by Leake (1970b) into the Currywongaun and Doughruagh bodies, with the entire DCD complex lying in an $F_2$ synformal core.

Kanaris-Sotiriou & Angus (1976) show the Dawros peridotite body as being tectonically separated from the developing Dawros - Currywongaun - Doughruagh igneous complex during $F_2$, with the peridotite schematically shown as being deformed into a syncline during this separation event.

Bennett & Gibb (1983) consider the peridotite to be upward facing, although locally inverted, and younging to the ENE. They consider the body to have a folded, originally tabular, form and to be lying in the limb of an $F_2$ fold. The gabbroic material is described as intrusive in nature, having been

emplaced syn - $D_2$, possibly by the autointrusive mechanism suggested by Angus, Middleton & Kanaris-Sotiriou (1980). The $F_2$ structures are deformed around $F_3$ and $F_4$ folds, possibly related to the $F_3$ Tully Mountain synform to the NW, which Bennett & Gibb suggest can be traced into the Kylemore Fm metasediments (Figure 3.34).

3.4.1.2 Fabrics: As described in {2.2.1.2}, two foliation fabrics are developed in the peridotite lithologies. The earliest of these fabrics, $S_1$, is developed at a low angle to the layering (Figure 3.35), but shows a variable vergence to the layering. This vergence can be used in the same way as cleavage-bedding relations to determine the structure of the body. The $S_1$ foliation is most obviously developed in olivine - rich lithologies as a spaced (10 - 40mm) planar fabric, the planes being defined by 2 - 10mm zones of serpentinised peridotite.

A variably orientated second foliation is developed, generally occurring as an upright fabric which is again most evident in the olivine rich units. This fabric is patchily developed, being absent in some areas and completely obscuring the early fabric in others. Veins of fibrous serpentinite are often developed parallel to the $S_2$ foliation. The mineralogical effects of the serpentinisation produced within the two foliations are described in {4.2.3.6}.

3.4.1.3 Folding: Use of the $S_1$ foliation-layering intersection as a structural indicator defines the structure of the peridotite shown in Figure 3.36. The body is deformed around NNW-SSE trending tight to isoclinal folds which are overturned to the south such that the lithological sequence is locally inverted, but consistently upward facing. The control of outcrop pattern by the folding is most clear in the centre and east of the peridotite where the lherzolite, the upper portion of the sequence, is developed in the cores of synclinal folds (Figure 3.36). The younging directions deduced by Bennett & Gibb (1983) fit closely with the structure proposed by this work (Figure 3.36). However, the tracing by Bennett & Gibb (1983) of the internal structures of the peridotite into apparently contiguous

structures in the metasediments of the Kylemore Fm is considered by this worker to be incorrect owing to the more complex behaviour of migmatitic lithologies during deformation {3.2.2.4}. The structures and fabrics developed within the Kylemore Fm are discussed in {3.2.2}.

3.4.1.4 Contact relations of the Dawros peridotite

3.4.1.4.1 Introduction: Previous workers generally pass over the nature of the contacts between the metasediments and the peridotite, providing no detailed descriptions of the contact zones. They do, however, agree that the body has been tectonically displaced from its original location to its present environs. The occurrence of hornfelsic and locally migmatitic material at the contacts is cited by Rothstein (1957) and Leake (1970b) as evidence of the body's original intrusive nature.

3.4.1.4.2 Field observations: The contacts between the peridotite and Kylemore Fm metasediments are generally unexposed, but often marked by a narrow gully. In most areas the contact can often be located within 2-5m. Where exposed the contact zones are marked by the development of characteristic fabrics within the peridotite and metasedimentary lithologies. The degree of development of these fabrics is variable, with the best development of fabrics seen in the most complete section [GR 705 590].

3.4.1.4.2.1 Fabric changes in the metasediments at the contacts with the peridotite: The typical fabrics and folding developed within the Kylemore Fm around the igneous bodies have already been described {3.2.2.4}. Adjacent to the contacts with the peridotite these fabrics and folds become modified with mylonitisation and recrystallisation of the metasediments increasing towards the contact. The foliation developed within the metasediments becomes regular in nature, as irregular migmatitic features {3.2.2.4} are overprinted by a more regular foliation. The foliation associated with the contacts also shows a strong grain shape lineation (Figure 3.37) which is

**Figure 3.37: Typical lineation developed within Kylemore Formation adjacent to the peridotite [GR 696 596]. Lens cap is 49mm diameter.**


**Figure 3.38: Talc carbonate schist from the Creggaun shear zone [GR 705 590] (X 56) XPL.**

locally the dominant fabric. In thin section the lithologies around the contacts show strong mylonitisation features (see Figure 3.24) often with evidence of recovery; polygonal and subgrain textures being developed. The fabrics and mineralogies seen in the metasedimentary lithologies at the contact with the peridotite are similar to those described in {3.2.2.4} as being associated with ductile shear zones.

3.4.1.4.2.2 Fabrics developed within the peridotite adjacent to its contacts: The degree of pervasive serpentinisation of the peridotite {4.2} increases towards its margins. At the contact the peridotite is entirely serpentinitic, locally being replaced by talc - carbonate assemblages. The width of the zone affected by the pervasive effects is variable from 2 - 3m up to 20m. The fabrics within this serpentinised zone are best seen in the area around [GR 699 589] where a N to S transect from the peridotite into the Kylemore Fm metasediments reveals the following effects:

i, the degree of serpentinisation of the peridotite increases from 20 - 25% approximately 20m from the contact, to complete serpentinisation 2 - 5m from the contact;

ii, the increase in serpentinisation is paralleled by a loss of layering within the peridotite;

iii, a strong E - W striking and shallowly N dipping foliation becomes the dominant fabric within the peridotite at the marginal zones;

iv, within 1 - 2 metres of the contact the serpentinised peridotite becomes increasingly well foliated, and local developments of talc - carbonate schist are common e.g. [GR 705 590, 699 589].

In thin section the serpentinised lithologies show an increasingly strained nature towards the contact. Polygonal textures (Maltman 1978) are developed in the serpentinised peridotite 4-5m away from the contacts. These polygonal textures are lost closer to the contact and replaced by carbonate - rich talcose schists (Figure 3.38). Similar fabrics are described by Cruse (1963) as occurring at the margins of serpentinite pods adjacent to the RBS on Inishbofin. The serpentinisation and textural changes at the margins of the peridotite developed after

the igneous crystallisation of the body {4.2.3.6}.

3.4.1.5 Summary of the structure and contact relations of the Dawros peridotite: The Dawros peridotite body consists of a sequence of ultrabasic igneous rocks with a well developed stratigraphic (fractionation) sequence {2.2.1}. A series of massive peridotitic lithologies in the western part of the body may represent a marginal / basal facies which passes northeastwards into a layered sequence of more evolved layered lithologies. Primary phase layering showing current and graded bedding features reveals the structure of the peridotite to be a series of upward facing tight to isoclinal NNW - SSE folds, which locally invert the lithological sequence in fold limbs (Figure 3.36). The body as a whole plunges to the north beneath a cover of Kylemore Fm metasediments. Folding in the peridotite is not contiguous with structures in the surrounding metasediments {3.2.2.4}, although the orientations of the the structures in the peridotite are similar to $F_3$ folds within the metasediments (Figure 3.35).

The peridotite is separated from the Kylemore Fm metasediments by a zone of tectonised metasedimentary and serpentinitic lithologies. There is less evidence of migmatisation of metasedimentary lithologies in this contact zone than for contact rocks adjacent to the gabbroic bodies. Towards the east, the peridotite thins into a serpentinitic zone which structurally underlies the Creggaun gabbro and its migmatitic aureole. This feature is the structural roof of the peridotite body, the floor being best exposed at [GR 695 593] and on the southern margin of the body.

The present form of the body is of a tightly folded, tectonically bounded, 'lens' which dips away to the N / NE and thins to the east. A schematic reconstruction of the original form of the exposed portions of the body is shown in Figure 3.36.

The implications of the form and contact relations of the peridotite are discussed in {3.5}.

3.4.2 The structure of the gabbroic bodies

**Figure 3.39: Previous interpretations of the form of the gabbroic bodies;**
**a, Leake (1970b),**

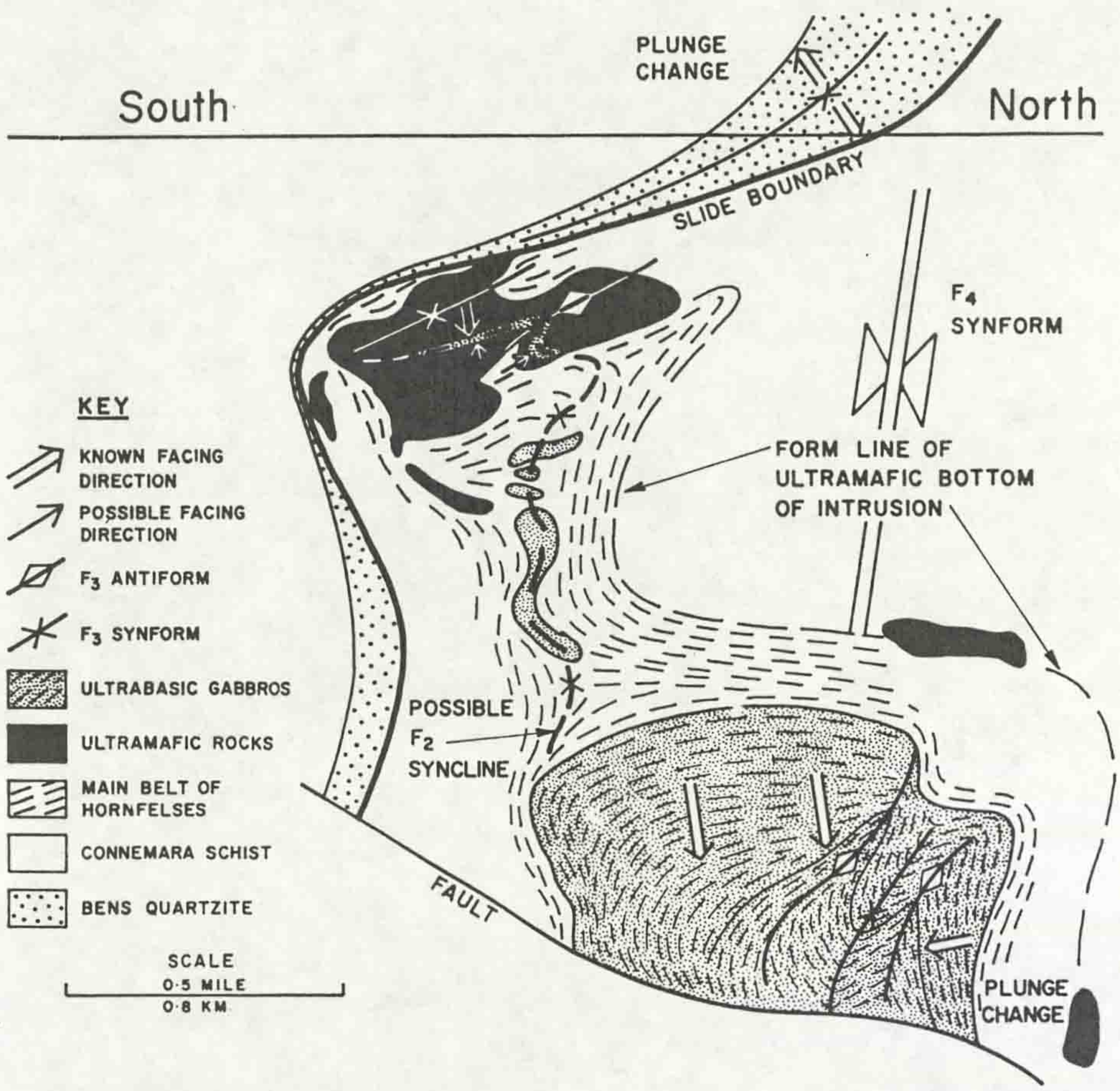


**b, Kanaris – Sotiriou & Angus (1976).**

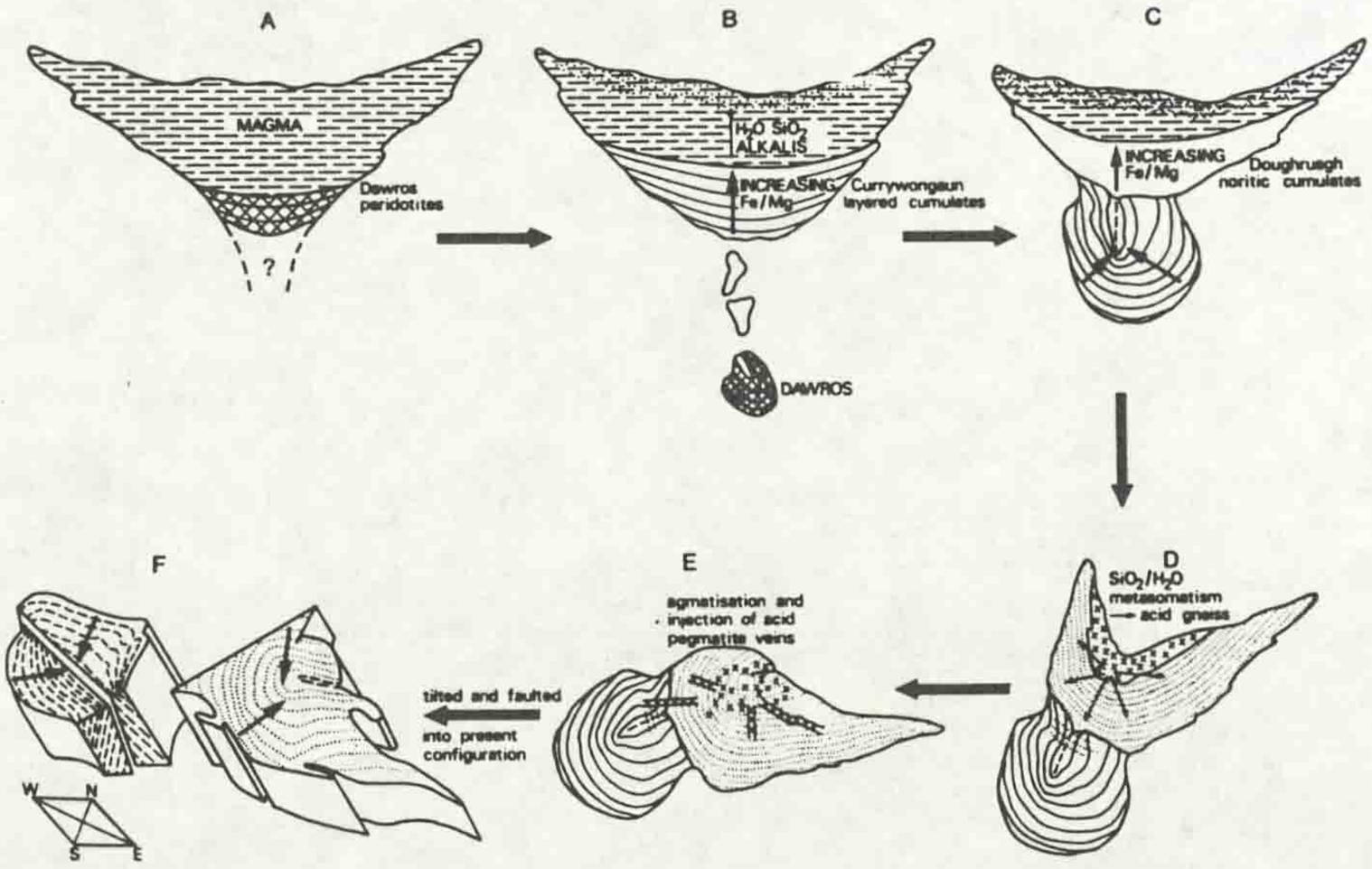

3.4.2.1 Previous work: Initial studies of the Currywongaun - Doughruagh gabbros by Ingold (1937) showed that the two intrusive bodies represented one original intrusion, now separated by a fault. The pre - faulted form of the intrusion is considered by Ingold to be a thick inclined sheet or laccolith. Leake (1964, 1970b) also considers the two bodies to represent one original intrusion but describes the structure of Currywongaun as being a downward facing tight to isoclinal syncline or synform (Figure 3.39).

Kanaris - Sotiriou & Angus (1976) investigated the form of the internal layering in the igneous lithologies. They conclude that the overall structure of Currywongaun is a tight, NW plunging, anticline or antiformal syncline, although no conclusive way up could be defined. Doughruagh is described as possessing a similar form. However, the lack of primary layering features prevent the clear definition of the fold structure. They suggest that these structures are $F_3$ in age. The form of the Currywongaun - Doughruagh bodies appears to be a tight antiformal syncline which plunges west with a northerly dipping axial plane. This structure is considered by Leake (1970b) to continue through the smaller gabbroic bodies to the west of Currywongaun and into the Dawros peridotite.

3.4.2.2 Contact relations of the gabbros

3.4.2.2.1 Previous work: All the previous authors note the existence of sillimanite bearing, hornfelsic contact lithologies and consider the original nature of the contacts to be intrusive. Ingold (1937) noted the contacts to be sharp, with local *lit-par-lit* relations between gabbro and gneissose metasediments. 'Sheet - like' xenoliths of metasedimentary lithologies are common at the margins of the gabbros, along with rare peridotite fragments (Angus *et al.* 1980). Leake (1970b) states that the area to the west of Currywongaun, containing the Dawros river and Creggaun gabbros, consists of *'fragments of ultrabasic and gabbroic rocks together with clots and patches of kneaded, partially melted hornfels, all torn off the original major intrusion and its envelope'*. This idea that the Dawros River and Creggaun gabbros represent fragments separated from the

## Acknowledgements

I am indebited to Dr A.P. Boyle for his advice and guidance during the course of this research, for forming the other half of the hockey defence and for buying the ice creams!

I am extremely grateful to Micky and Josie Aspell for their hospitality and for preserving my sanity when it rained. Letterfrack football team are to be thanked for providing bruised shins and twisted ankles.

Of the cast of thousands who provided 'technical support' during the production of this thesis, the following deserve special thanks:

Julie Sharman for all her help with the XRF analyses,

Mike Brotherton for the NAA analyses,

Tim Hopkins And Dave Plant at the Department of Geology, The University of Manchester and Ian Young at UCL, London for their help during the probe work,

Dr A.C. Barnicoat for kindly providing the thermal modelling programs,

Dr M.A. Khan of Leicester University for the loan of the gamma spectrometer.

I would like to thank the A3.05 'boys', Nick Lindsay, Colin Grant, Phil Rose and Keith Westhead for friendship, discussion, distraction and generally lowering the work rate.

The residents of Devonshire House, especially Peter Ditchfield for the loan of his guitars, Jon Rowse for organizing the sport (and sometimes picking me), Tony Reynolds for the noises and Cat, Huw, Greg, Mark and the others for intellectual discussion and general debauchery.

I am very grateful to my mother and sister for their encouragement, financial support and letting me get on with it.

I would like to thank Susan Russell for her friendship.

Norris, the Ford Fiasco, rates a mention for its (almost) unflagging support.

I acknowledge the receipt of a University of Liverpool University Research Studentship in Science.

**Figure 3.40: Mobilised semipelitic xenoliths (pale weathering) within the Creggaun Gabbro [GR 702 595]. Compass is 100mm long.**

**Figure 3.41: Sharp contact between gabbro and pale weathering Kylemore Formation psammites at [GR 702 595], Creggaun Gabbro. Compass is 100mm long.**

**Figure 3.42: Strongly lineated gabbro and pale weathering Kylemore Formation psammite at [GR 731 606], the northern contact of the Currywongaun gabbro. Lens cap is 49mm diameter.**

Currywongaun and Doughruagh intrusions during syn-crystallisation deformation is also put forward by Kanaris-Sotiriou & Angus (1976) as part of their model for the evolution of the DCD {2.2.1}. Kanaris-Sotiriou & Angus note that the contacts of the larger intrusives are sheared to greater or lesser amounts and are thus tectonic *sensu stricto*.

3.4.2.2.2 Field relations at the gabbro contacts: At the margins of the Creggaun gabbro a zone of sheet-like xenoliths is developed (Figure 3.40). These xenoliths consist of migmatised and mobilised psammites, semipelites and pelites. Associated with the xenolithic areas are quartzofeldspathic veins up to 200mm across which contain large (≃ 100mm) prismatic tourmaline crystals. Similar tourmaline rich veins are associated with xenolithic zones within the other gabbros. The contact of Creggaun gabbro with the Kylemore Fm is sharp, though irregular in nature, and can be seen in the steep crag at [GR 703 595] (Figure 3.41). The grain size of the gabbroic material is coarse (5 - 10 mm) at the contact which no chilled zone developed. No evidence of shearing or displacement is apparent along this contact, although a mineral lineation fabric is variably developed in both the gabbro and metasediments.

On the northern margin of Currywongaun the gabbro/metasediment contact is exposed in a stream section [GR 731 606]. In this exposure lineated psammitic and gabbroic lithologies are interlayered in a highly deformed zone (Figure 3.42) approximatly 10 - 15m wide. The fabrics developed in this zone die away rapidly into the gabbro to the south and into the foliated metasediments to the north. This contact shows features typical of the tectonised contacts described by Kanaris - Sotiriou & Angus (1976). In some areas adjacent to the main igneous bodies, such as at [GR 761 596] on the east of Doughruagh, the contact zones show little or no tectonic effects, preserving original igneous features.

Tectonic contacts appear to be best developed on the northern and southern margins of the larger intrusions , with the smaller intrusions and zones on the eastern and western edges of Currywongaun and Doughruagh showing the preservation of original igneous contacts.

<u>Kylemore Formation</u>

$D_1$: Evident as inclusion fabrics within pre / syn $D_2$ garnet and plagioclase porphyroblasts and in rare relict zones within the later foliation.

$D_2$: Penetrative bedding parallel / sub parallel foliation with E - W strike and general N dip. Limited evidence for folding, with eye structures and double vergence suggesting sheath fold forms. Strongly developed linear fabrics (rodded grain aggregates and vein bodies) typically with E - W azimuths and shallow plunges (along strike), although adjacent to the igneous bodies of the DCD a steeper N - S (down - dip) lineation is common. Within the contact zones of the DCD $D_2$ structures and fabrics include complex fold patterns within syn - deformational migmatites and a linked system of mylonitic zones which form a ductile thrust system.

$D_3$: Variably plunging folds with E - W axial planes and local crenulation cleavage (best developed in pelitic units). E - W trending ductile shear zones in contact zones show evidence of reactivation.

$D_4$: Kink bands. Tilting of the entire area to the north associated with the development of the Connemara Antiform.

<u>Lithologies to the south of the Renvyle - Bofin slide</u>

$D_1$: Inclusion fabrics in garnet and feldspar porphyroblasts.

$D_2$: Penetrative bedding parallel / sub parallel foliation with E - W strike and N dip. Strong lineation fabrics (grain aggregates, clasts) with E - W azimuths and generally shallow dip (lineations run along strike). Sheath folding

$D_3$: Upright to S overturned downward facing folds with variable shallow plunges, the dominant large scale structures in the study area. Axial planar crenulation cleavages.

$D_4$: Kink bands. Tilting of the entire area to the north associated with the development of the Connemara Antiform.

<u>Renvyle - Bofin Slide</u>: The timing of the RBS is not clear, with syn - $D_2$ mylonitic fabrics associated with the slide zone suggesting an early movement history although the present form of the slide suggests a syn / post $D_3$ timing. It is likely that the RBS initially developed during $D_2$ and was reactivated in later deformation.

**Figure 3.43: Summary of the deformation sequence determined in the study area.**

The significance of the variation in contact styles is discussed in {3.5}.

## 3.5 Discussion and interpretation of the structure of the study area

The structural evolution of the study area is complex, although it can be subdivided into a series of stages (Figure 3.43). The earliest fabric, $S_1$, is only preserved in porphyroblasts and in rare matrix zones.

The $S_2$ fabrics, and the evidence of its mechanism of formation preserved in porphyroblasts, suggest that the $D_2$ deformation was achieved by non - coaxial bulk inhomogeneous shortening (Bell & Rubenach 1983). Under such conditions an overall flattening is accompanied by an element of simple shear. The strain ellipsoid calculated by Kelly & Max (1979), using data from strained clasts within the Trawmore Psammite Mb of the Lakes Marble Fm, shows an X:Y:Z ratio of 23:13:1. This value indicates an overall flattening strain with an element of extension. Ferguson (1984) considers this strain estimate to represent the effects of $D_2$, with $D_3$ simply folding these earlier fabrics. Treloar & McInnes (1981) also consider $D_2$ to have produced flattening, with an associated layer parallel extension, which was buckle folded in $D_3$. The $L_2$ mineral stretch lineation is associated with the development of curvilinear $F_2$ folds {3.2.1.3 and 3.2.2.3} which suggest that simple shear was at least locally important in $D_2$.

The dominant effect of the $D_3$ deformation is the production of folds, typically hybrid type 3/1c folds (Yardley 1976). These folds with thinned limbs and thickened hinges can be produced by flattening an initial buckle fold normal to the axial surface (Ramsay 1967). $F_3$ folds show non - cylindrical hinges, a feature described by Ramsay as being produced by strain variation along the length of a fold.

Evidence of $D_4$ deformation is limited, kink bands being the only obvious $D_4$ structures. The primary effect of $D_4$ is the regional tilting associated with formation of the Connemara antiform {3.2.1.3 and 3.2.2.3}.

This four stage deformation history is comparable to previously proposed deformation histories (Figure 3.44).

The deformation histories to the south of the RBS and in the Kylemore Fm to the north are comparable although where the Kylemore Fm is adjacent to the igneous bodies of the DCD it has a somewhat modified history. The timing of intrusion of the DCD is generally accepted as syn $D_2$ (Kanaris - Sotiriou & Angus 1976).

The folding and fabrics developed within the Dawros peridotite show orientations similar to $D_3$ features in the metasediments, as do the large scale folds reported as being present in the Currywongaun and Doughruagh gabbros. The contacts of the larger gabbroic bodies show preservation of original igneous contacts only at the east and west sides of the bodies, ie, in the fold noses. The northern and southern contact zones show considerable evidence of high strains {3.4.2.2.2}. The variation in contact zones is here interpreted as being due to the effects of flexural slip in the limbs of the Currywongaun - Doughruagh folds being concentrated at the contact as the marked competence contrast between gabbroic and psammitic and semipelitic lithologies would tend to localise such strain. The effects of deformation synchronous with the intrusion of the gabbros is clear in the migmatitic zones adjacent to the Creggaun gabbro {3.2.2.4} where migmatitic lithologies show complex, syn migmatisation, folding. These fold fabrics are locally reorientated into high strain zones showing strong mylonitic fabrics which are associated with sillimanite growth {4.1.3.8}. The high strain zones are typically flat lying although they locally pass into steep N-S striking zones. The overall form of these zones is here considered to present a system of linked ductile displacments with the flat zones representing floor thrusts which pass into steep walls or lateral ramp thrusts {Enclosure 2}. These thrust forms are stacked in a ductile duplex, with the gabbroic material and its contacts being emplaced over metasediments which in turn are emplaced over the peridotite. The movement sense on these structures is unclear although the dominant N-S linear fabrics seen in the in the aureole lithologies suggest the movement to have a N - S direction, although the polarity of movement is not apparent. The mylonitic fabrics are cut by veins of granitic material similar in appearance to the irregular segregation veins evident

in the convolutely folded migmatitic areas. Although the syn migmatisation folding is overprinted by the high strain zones there need be no significant time interval between the two. It is likely that the two processes occurred over the same time span (syn - $D_2$) as both groups of lithologies have comparable sillimanite bearing mineralogies {4.1}. However, certain of the shear zones, especially those associated with serpentinitic lithologies, show retrogression and further mylonitisation of the high grade mineral assemblages suggesting that movement on these zones also occurred at lower temperatures than the initial movements, possibly being reactivated syn - $D_3$.

The peridotite and its metasedimentary envelope show a more complex structural history than that seen in and around the gabbros. All the contacts between peridotite and metasediment are tectonic in nature and show limited migmatisation, with no late granitic veins cutting the fabrics. No zones of xenoliths or hybridised igneous lithologies are present at the margins of the peridotite which are strongly serpentinised and locally converted into talc schist. The layering in the peridotite is at a high angle to the contacts. The peridotite is considered to have been emplaced in a solid state, syn - $D_2$, but still retaining sufficient heat to produce sillimanite in the contact mylonites although not extensive migmatisation. Subsequent deformation (during $D_3$) led to the formation of serpentinitic and retrograde mylonitic assemblages in the contact lithologies as the contact zones were reactivated. The most evident ductile shear zone, seen at [GR 705 590], which places the Creggaun gabbro and its aureole over the peridotite, is associated with low grade mineral assemblages and represents one such reactivated zone. It is noteworthy that the most obvious reactivation can be seen in contacts striking E - W, in a manner similar to the fabrics seen in the larger gabbroic bodies, possibly indicating the reactivation of these contacts to be syn - $D_3$. It is likely that the E - W striking peridotite contact zones were also reactivated by flexural slip effects during the $F_3$ folding.

The Renvyle - Bofin Slide juxtaposes two groups of lithologies which show similar structural histories. The RBS itself, however, remains rather an obscure feature. Its timing can be

constrained as post - intrusion of the DCD because the aureole effects appear to be truncated by the slide, but prior to the regional metamorphic peak (post - $D_2$) as the peak regional assemblages on either side of the RBS are comparable {Chapters 4 and 5}. The RBS can be seen to cross cut the stratigraphy, truncating the northern limb of the Tully Mountain Synform, an $F_3$ fold, which suggests that the present form of the slide developed post $D_3$. The fabrics associated with the slide zone itself {3.3.2} show that both ductile and brittle deformation have occurred. The early ductile fabrics are partly defined by biotite, a mineral developed in $D_2$ fabrics and generally replaced by chlorite in $D_3$ fabrics {3.2.1.1 and 3.2.2.1}. This suggests that the slide was active during $D_2$, under P - T conditions suitable for the production of biotite, and was subsequently reactivated to produce the fabrics associated with the more brittle deformation and chlorite growth seen in the actual slide itself {3.3.2}. It is here suggested that the slide represents a late $D_2$ feature (with the DCD having cooled such that its thermal effects were not transmitted across the slide), which was subsequently reactivated in $D_3$ to give its present, N dipping, form. The movement senses of both events are unclear in the field, although P-T path work {5.5} suggests the Kylemore Fm to have remained at a constant crustal level and the lithologies south of the RBS to have been loaded during $MP_2$, giving the RBS, in its present form, a dip - slip thrust sense. The lineation present along the RBS has an overall E - W orientation with variable gentle plunges, suggesting that any motion along the slide related to this fabric was of a 'strike - slip' nature. Thus, the RBS shows a complex movement history, with at least two possible displacement vectors.

Addendum to {3.2.2.4}

As discussed in {3.2.2.4} the main fabrics and folding in the Kylemore Formation metasediments which form the aureole to the DCD are here considered to be of $D_2$ age. This age is the same as that considered by Kanaris - Sotiriou & Angus (1976) for the syn - deformational intrusion of the DCD. A variety of criteria have been used to determine the timing of fabric development in the aureole rocks.

Firstly, the foliation fabric developed in the aureole zones passes laterally into the $S_2$ fabrics of the regional metamorphic lithologies and no evidence of one fabric overprinting the other can be seen. In the outermost parts of the aureole contact metamorphic garnets contain inclusion trails of an $S_1$ fabric. However, contact metamorphic garnets developed near to the igneous bodies contain xenoblastic inclusions. The fabrics preserved in aureole garnets are straight, unlike the regional garnets which show a range in form {3.2.3}. This suggests that the garnet growth associated with the contact metamorphic effects of the DCD was relatively early in $D_2$ and as such the syn - intrusive fabrics within the aureole are early $D_2$ in age. These observations suggest the foliation in the aureole zones to be an $S_2$ foliation.

Secondly, chlorite commonly occurs as a late mineral replacing garnet and biotite. In places it is developed in a crenulation fabric similar to the $S_3$ crenulation fabrics seen in the adjacent regional metamorphic lithologies. Although no clear $F_3$ folding can be recognised within the aureole zones, the folds and fabrics within the igneous bodies, i.e. the folding and foliation in the peridotite as discussed in {3.4} and the form of the gabbroic bodies of Currywongaun and Doughruagh as suggested by Kanaris - Sotiriou & Angus (1976), show orientations and styles typical of the $F_3$ structures elsewhere in the study area.

Finally, although the stretching lineation in the aureole trends N - S, rather than E - W as in the regional rocks, it is associated with sheath folds characteristic of $D_2$ and with orientated fibrolite growth. The lineation is thus regarded as being formed during $D_2$, synchronous with the emplacement of the DCD. The orientation of this lineation fabric may be related to an early $D_2$ movement in a N - S sense or to the strain

related to the emplacement of the DCD. It is possible that the increased ductility of the heated aureole rocks may have led to an enhancement of the early $D_2$ event whatever its cause.
The balance of evidence favours the fabrics (foliation and lineation) found in the aureole of the DCD being $D_2$ in age.

## Preface

References to sections of the thesis are marked as { }.

Grid references are denoted by [GR ... ...] and refer to Irish Ordnance Survey sheet 10 (Connemara), all falling within sub - zone L of the Irish National grid.

Abbreviations used in the text

DCD : Dawros - Currywongaun - Doughruagh igneous complex

RBS : Renvyle - Bofin Slide

CA : Connemara Antiform

Abbreviations for mineral names are after Kretz (1983).

Act: actinolite
Alm: almandine
And: andalusite
Ann: annite
An: anorthite
Bt: biotite
Cpx: clinopyroxene
Cal: calcite
Chl: chlorite
Cld: chloritoid
Ctl: chrysotile
Crd: cordierite
Ep: epidote
Grt: garnet
Grs: grossular
Kfs: K - feldspar
Ky: kyanite
Lz: lizardite
Ms: muscovite
Ol: olivine
Or: orthoclase
Opx: orthopyroxene
Pg: paragonite
Phl: phlogopite
Pl: plagioclase
Prp: pyrope
Qtz: quartz
Sil: sillimanite
Sps: spessartine
Spl: spinel
St: staurolite
Tlc: talc
Tur: tourmaline
Tr: tremolite
Ts: tschermakite

# Chapter 4: Whole rock chemistry, petrography and mineral chemistry

## 4.1 Metasedimentary and metaigneous lithologies

### 4.1.1 Introduction

Forty nine rocks were analysed by XRF {Appendix B} for their major ($SiO_2$, $TiO_2$, $Al_2O_3$, $Fe_2O_3$, MnO, MgO, CaO, $Na_2O$, $K_2O$) and trace (Ba, Ce, Co, Cr, La, Nd, Ni, Pb, Rb, Sc, Sr, Th, V, Y, Zn, Zr) element concentrations (the results are tabulated in {Appendix C}). The analysed rocks comprise 26 regional metamorphic pelites, 10 contact metamorphic pelites, with 7 amphibolites and 6 ultrabasic 'pods'.

Thirty five samples were made in to polished thin sections and their mineral compositions were analysed by electron microprobe techniques {Appendix B} with the results of analyses tabulated in {Appendix C}. The samples selected for this analytical method were typically garnetiferous pelites and semi - pelites, which show a range in mineral assemblages. Two main groups of metamorphic assemblages can be defined in the study area, one which is related to the aureole effects of the DCD, the 'contact assemblages', and a second group which can be related to the main regional metamorphism, the 'regional assemblages'.

The work undertaken in this study largely covers the pelitic and semipelitic lithologies, as the assemblages developed in these units enable the application of exchange thermobarometry and P - T path modelling methods {Chapter 5}.

### 4.1.2 Whole rock Chemistry

4.1.2.1 Amphibolitic lithologies: The amphibolitic material studied was sampled from either side of the RBS (2 Kylemore Fm, 5 from the Doongill Amphibolite Mb of the Streamstown Fm). The compositions of these analyses on a ternary ACF plot (Figure 4.1) fall in to the field of Connemara striped amphibolite compositions of Evans & Leake (1960). The results of a statistical comparison (using F and t tests of significance) are shown in Table 4.1. This comparison shows the data from the study area to show significant correlations with Evans & Leakes' data as far as the elements $Al_2O_3$, CaO, $Na_2O$ (1% significance) and $TiO_2$ (5% significance). The compositional data from the amphibolitic material suggests that they are

Figure 4.1: ACF plot of analysed regionally metamorphosed amphibolitic lithologies and their relation to the Connemara striped amphibolite field defined by Evans & Leake (1960). Triangles indicate Kylemore Fm amphibolites.

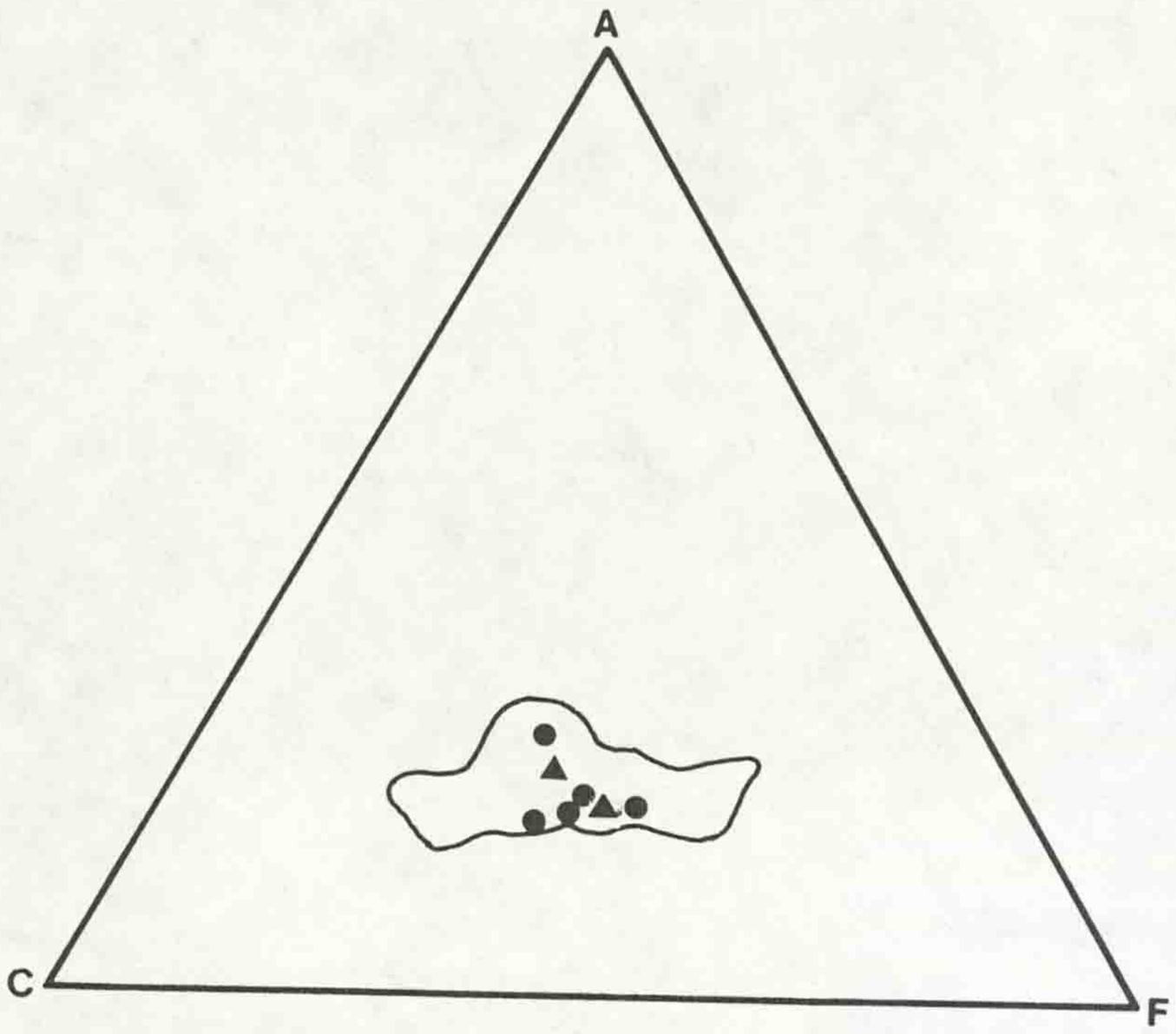


Table 4.1: Statistical comparison (using F and t tests of significance) of analysed amphibolitic material with the Connemara striped amphibolite analyses of Evans & Leake (1960, Table 1). The mean and standard deviation of the data are also shown.

| | | | Analysed | | Evans & Leake | |
|---|---|---|---|---|---|---|
| Element | F | t | Mean | S.D | Mean | S.D |
| $SiO_2$ | ** | - | 49.18 | 1.58 | 48.88 | 8.82 |
| $TiO_2$ | - | * | 1.22 | 0.55 | 1.73 | 0.60 |
| $Al_2O_3$ | - | ** | 13.39 | 1.37 | 14.95 | 1.22 |
| FeOT | * | - | 12.56 | 1.57 | 11.52 | 2.70 |
| MnO | ** | - | 0.21 | 0.05 | 0.23 | 0.12 |
| MgO | - | * | 7.59 | 1.42 | 6.52 | 2.30 |
| CaO | ** | * | 8.96 | 1.03 | 3.60 | 1.05 |
| $Na_2O$ | - | * | 0.68 | 0.61 | 0.79 | 0.71 |

- = <95% correlation
* = >95% correlation
** = >99% correlation

| | Study Area | | | | | | | | Connemara | | | | Scottish | | | |
|---|---|---|---|---|---|---|---|---|---|---|---|---|---|---|---|---|
| | All | | Regional pelites Kylemore Fm | | Other Fms | | Contact pelites (Kylemore Fm) | | Regional pelites | | Contact pelites | | Dalradian | | | |
| | mean | s.d. | mean | s.d. | mean | s.d. | mean | s.d. | mean | s.d. | mean | s.d. | mean | s.d. | mean | s.d. |
| n | 26 | | 16 | | 10 | | 10 | | 27 | | 16 | | 230 | | | |
| SiO2 | 54.37 | 5.81 | 57.30 | 6.81 | 51.31 | 3.17 | 62.46 | 6.76 | 56.55 | 3.16 | 52.23 | 3.18 | 59.88 | 10.87 | 61.54 | 4.68 |
| TiO2 | 1.80 | 0.52 | 1.78 | 0.49 | 1.77 | 0.54 | 1.43 | 0.36 | 1.32 | 0.15 | 1.15 | 0.19 | 1.03 | 0.46 | 0.82 | 0.61 |
| Al2O3 | 19.90 | 2.97 | 18.02 | 3.09 | 22.06 | 1.66 | 16.39 | 3.31 | 20.08 | 1.85 | 22.79 | 2.61 | 19.15 | 6.02 | 16.95 | 4.21 |
| FeOT* | 8.96 | 1.83 | 8.88 | 1.93 | 8.82 | 1.66 | 8.01 | 2.14 | 8.85 | 1.02 | 9.40 | 1.04 | 7.39 | 4.61 | 6.02 | 4.02 |
| MnO | 0.12 | 0.06 | 0.11 | 0.06 | 0.12 | 0.03 | 0.15 | 0.05 | 0.15 | 0.05 | 0.19 | 0.05 | 0.12 | 0.09 | == | == |
| MgO | 2.58 | 0.46 | 2.42 | 0.48 | 2.72 | 0.44 | 2.49 | 0.66 | 2.62 | 0.29 | 2.76 | 0.35 | 2.34 | 1.07 | 2.52 | 1.91 |
| CaO | 1.70 | 0.69 | 1.67 | 0.69 | 1.73 | 0.59 | 1.40 | 0.49 | 1.41 | 0.65 | 1.72 | 1.38 | 1.03 | 0.75 | 1.76 | 2.03 |
| Na2O | 1.86 | 0.56 | 1.73 | 0.47 | 1.90 | 0.51 | 1.30 | 0.45 | 2.04 | 0.67 | 1.98 | 0.88 | 2.10 | 1.05 | 1.84 | 1.18 |
| K2O | 3.56 | 0.79 | 3.29 | 0.77 | 3.95 | 0.53 | 2.69 | 0.71 | 3.23 | 0.63 | 3.54 | 0.99 | 3.50 | 1.52 | 3.45 | 1.32 |
| MFM | 0.34 | 0.05 | 0.32 | 0.03 | 0.35 | 0.06 | 0.35 | 0.05 | 0.34 | 0.02 | 0.34 | 0.02 | == | == | == | == |

Table 4.2: Means and standard deviations of pelite data.

Data sources

Connemara

Regional pelites: Yardley (1977c) Table 1, Senior & Leake (1978) Table 7 (average garnetiferous northern pelite) and Ferguson & Al - Ameen (1982) Table 2.

Contact pelites: Yardley (1977c) Table 2, Senior & Leake (1978) Table 7 (average southern pelite).

Scottish

Data from Atherton & Brotherton (1982) Table 1.

Average pelite from Shaw (1956).

| | Regional metamorphic pelites | | | | Contact metamorphic pelites | | | | | |
|---|---|---|---|---|---|---|---|---|---|---|
| | Connemara Dalradian | | Scottish Dalradian | | Regional pelites | | Connemara Dalradian | | Scottish Dalradian | |
| Variable | F | t | F | t | F | t | F | t | F | t |
| $SiO_2$ | * | - | - | - | - | ** | * | ** | - | - |
| $TiO_2$ | ** | - | - | * | - | - | * | * | - | - |
| $Al_2O_3$ | * | - | - | - | - | * | ** | ** | - | - |
| FeOT | ** | - | - | - | - | - | ** | - | - | - |
| MnO | - | * | - | - | - | - | - | ** | - | - |
| MgO | * | - | - | - | - | - | * | - | - | - |
| CaO | - | - | - | - | - | - | - | ** | - | - |
| $Na_2O$ | - | - | - | - | - | ** | ** | * | - | - |
| $K_2O$ | - | - | - | - | - | ** | ** | * | - | - |
| MFM | ** | - | - | - | - | - | ** | - | - | - |

Table 4.3: Results of statistical comparison between regional and contact metamorphosed pelites from the study area, Connemara pelites (data from Yardley 1977c, Senior & Leake 1978 and Ferguson & Al - Ameen 1986 for Sill - bearing assemblages, compared with contact pelites, and staurolite - bearing assemblages, compared with regional pelites).
FeOT is total iron as FeO
MFM is $\frac{MgO}{(FeOT + MgO)}$

\- = <95% correlation
* = >95% correlation
** = >99% correlation

F = Fisher's ratio of variances
t = Students t - test on means

similar in many respects to other amphibolitic material in the Connemara massif, and hence can be considered as 'Connemara amphibolites'.
The ultrabasic pod material is interpreted as being related to the DCD and so is discussed in {4.2.2}.

4.1.2.2 Pelitic lithologies: The pelitic rocks analysed can divided into two groups on the basis of their mineral assemblages, one group consisting of Kylemore Formation associated with the contact aureole of the DCD and containing:
Grt + Bio + Pl + Kfs + Qtz ± Sil assemblages.

The other group consists of regional metamorphic pelites which are typified by the assemblage:
Grt + Bt + Ms + Pl + St + Qtz ± Tur ± Chl.

The regional metamorphic pelites can be further divided into two groups, a group of Kylemore Formation pelites, and a group of pelites collected from lithologies which lie to the south of the Renvyle - Bofin slide (predominantly Streamstown Formation pelites).

The mean compositional values of the analysed rocks (Table 4.2) are similar to the 'average pelite' values calculated by Shaw (1956). The contact pelite data shows lower mean concentrations of $TiO_2$, $Al_2O_3$, FeOT, MgO, CaO, $Na_2O$ and $K_2O$ than the group of all pelites, the contact pelites being rather more siliceous. However if the contact pelite data is compared with regionally metamorphosed Kylemore Formation, the differences in mean element concentrations are rather less marked. Senior & Leake (1978) note that pelites in the south Connemara migmatite zone are depleted in $SiO_2$ relative to non - migmatitic northern pelites, the opposite of the relations observed here. Senior & Leake note that the causes of variation in major elements are equivocal and difficult to interpret, with primary sedimentary variation being a contributary factor. They do show the southern pelites to be relatively enriched in CaO and $Na_2O$ (as seen in the contact pelites from the study area), and suggest that this is due to metasomatic effects either mobilising elements from the surrounding more siliceous metasediments, or partial melt processes leading to the relative concentration of CaO and

**Figure 4.2: Thompson AFM projection (from muscovite) showing the field of regional metamorphic pelite compositions.**

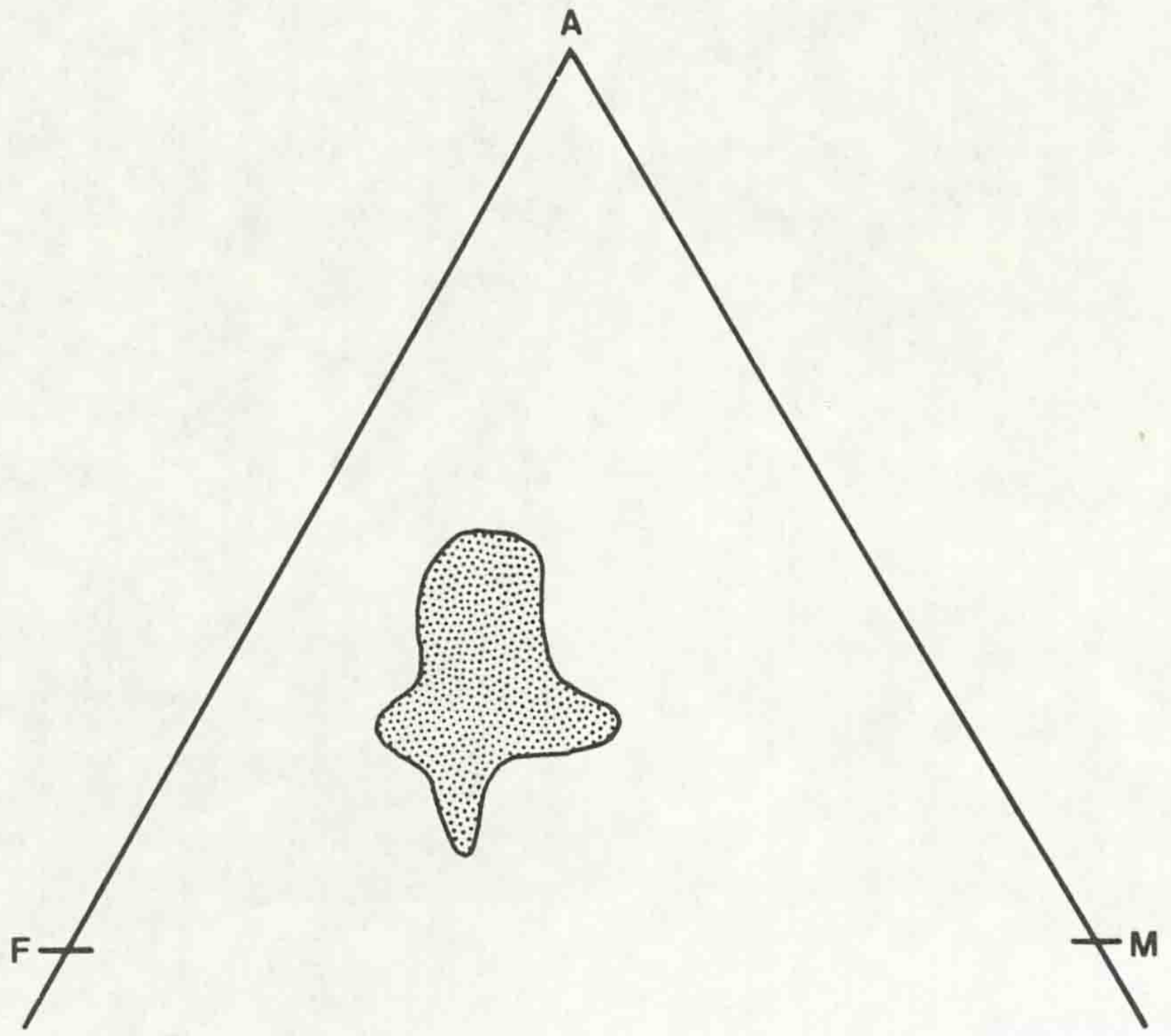


**Figure 4.3: Thompson AFM projection (from K - feldspar) showing the field of contact metamorphic pelite compositions.**

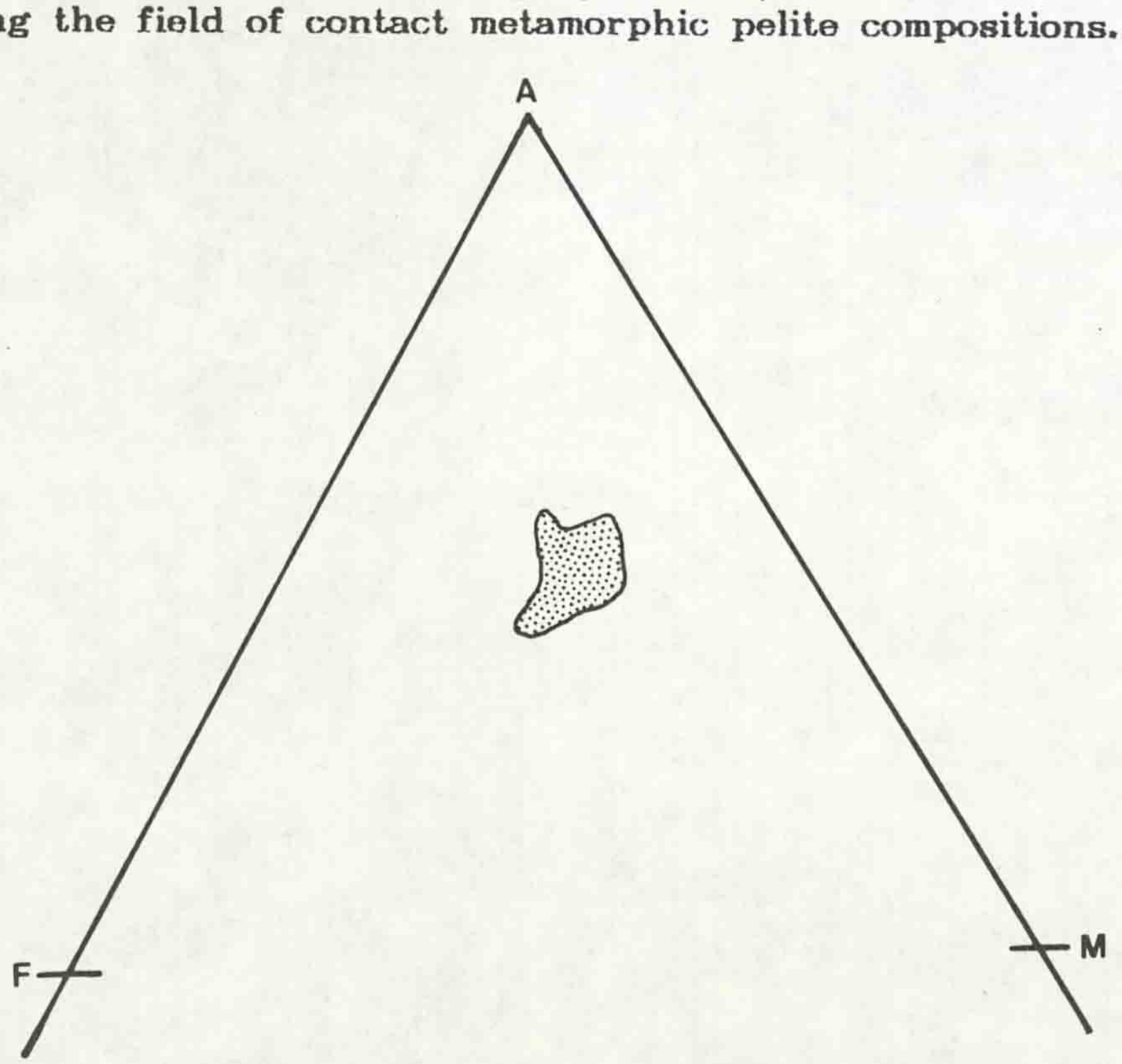

$Na_2O$.

The contact and metamorphic pelite data were compared statistically (F and t tests of significance) with each another, with the mean Scottish Dalradian pelite composition data of Atherton & Brotherton (1982) and with data from high (Sil / Kfs - bearing) and medium (St / Ms - bearing) grade pelites from Connemara (data from Yardley 1977c, Senior & Leake 1978 and Ferguson & Al - Ameen 1986). The results of these comparisons are shown in Table 4.3.

The contact pelites have higher $SiO_2$ and $TiO_2$ than both Scottish and the Connemara high grade pelites, higher MFM values than the Connemara pelites, and higher CaO than the Scottish pelites. The regional pelites are lower in $SiO_2$, $Al_2O_3$, MgO, $Na_2O$ and MnO than the Connemara lower grade pelites, and show a similar relation to the Scottish pelites although $Al_2O_3$ is lower in the regional pelites.

The fields defined by analysed pelitic lithologies on a Thompson (1957) AFM projection are shown in Figures 4.2 (regional pelites, projected from Ms) and 4.3 (contact pelites, projected from Kfs). The AFM fields defined by mineral compositions and the reaction topologies leading to the development of the mineral assemblages seen are discussed in {4.1.4}, along with the influence of whole rock composition on these assemblages.

4.1.3 Mineral Textures and Chemistry:

The descriptions and discussion of minerals in this section are confined largely to pelitic lithologies, covering both the regional and contact metamorphic grades. The mineral analyses for garnet, biotite, muscovite, chlorite, plagioclase, K - feldspar and staurolite are tabulated in {Appendix C}.

4.1.3.1 Garnet: Garnet is common within pelitic and semipelitic rocks throughout the study area, being developed in both regional and contact metamorphic rocks. The garnet population can be subdivided into two groups, those garnets developed in regional metamorphic assemblages (regional garnets), which show a range of forms from euhedral to anhedral and contain a variety of inclusion fabrics indicating syndeformational

development {3.2.3}, and garnets developed in contact metamorphic assemblages (contact garnets). Garnet is typically developed as a dark red/brown sub to anhedral porphyroblast phase, generally 2 - 5mm in size, but can reach up to 15mm in contact aureole lithologies. Euhedral garnets are rarely developed, although euhedral rhombdodecahedral and trapezohedral garnets can be found in highly micaceous pelites within the Streamstown [GR 661 606] and Kylemore [GR 695 631] Formations. Within the aureole of the DCD, garnets reach larger grain sizes than within the regionally metamorphosed rocks, xenolithic and contact lithologies being typically highly garnetiferous. Rare vein developments of garnets, within a Ms + Qtz + Tur vein, are seen in the Currywongaun gabbroic body [GR 721 597], although this lithology is probably related to mobilized xenolithic material within the gabbro.

The typical fabrics within syn - deformational regional metamorphic garnets have been described previously {3.2.3} and will not be considered in this section. The textures seen in contact metamorphic garnets are different from those seen in syn - deformational garnets.

Within the aureoles of the DCD garnets are variably poikiloblastic containing rounded and xenoblastic inclusions (Figure 4.4), although rare, apparently spherical inclusion trails are also evident (Figure 4.5). Similar trails were noted by Harvey & Ferguson (1973) in garnets from the regionally metamorphosed Kylemore Fm at Renvyle Point. They consider that such spherical trails, defined by elongate ilmenite plates, as being produced by garnet growth displacing the surrounding matrix, reorientating and then overgrowing ilmenite plates to produce a spherical shell of included material. Within the aureole garnets the inclusions are typically of fibrolitic sillimanite and quartz, although the overall appearance of the trail is identical to those described by Harvey & Ferguson. Garnets containing spherical trails are present within mylonitic lithologies, the garnet being wrapped by anastomosing foliae of sillimanite and quartz (Figure 4.6). This relation suggests that the initial garnet growth was static, displacing a passive matrix to produce the trails seen, and that subsequent to the inclusion of the trails the lithology was mylonitised at high temperatures

**Figure 4.4: Contact aureole garnet containing rounded, xenoblastic inclusions (X 29) PPL.**


**Figure 4.5: Contact aureole garnet with 'spherical' inclusion trail (X 29) PPL.**

# Chapter 1: Introduction and regional setting

**Figure 4.6: Garnets wrapped by fibrolitic sillimanite in mylonitic hornfels lithology (X 29) PPL.**

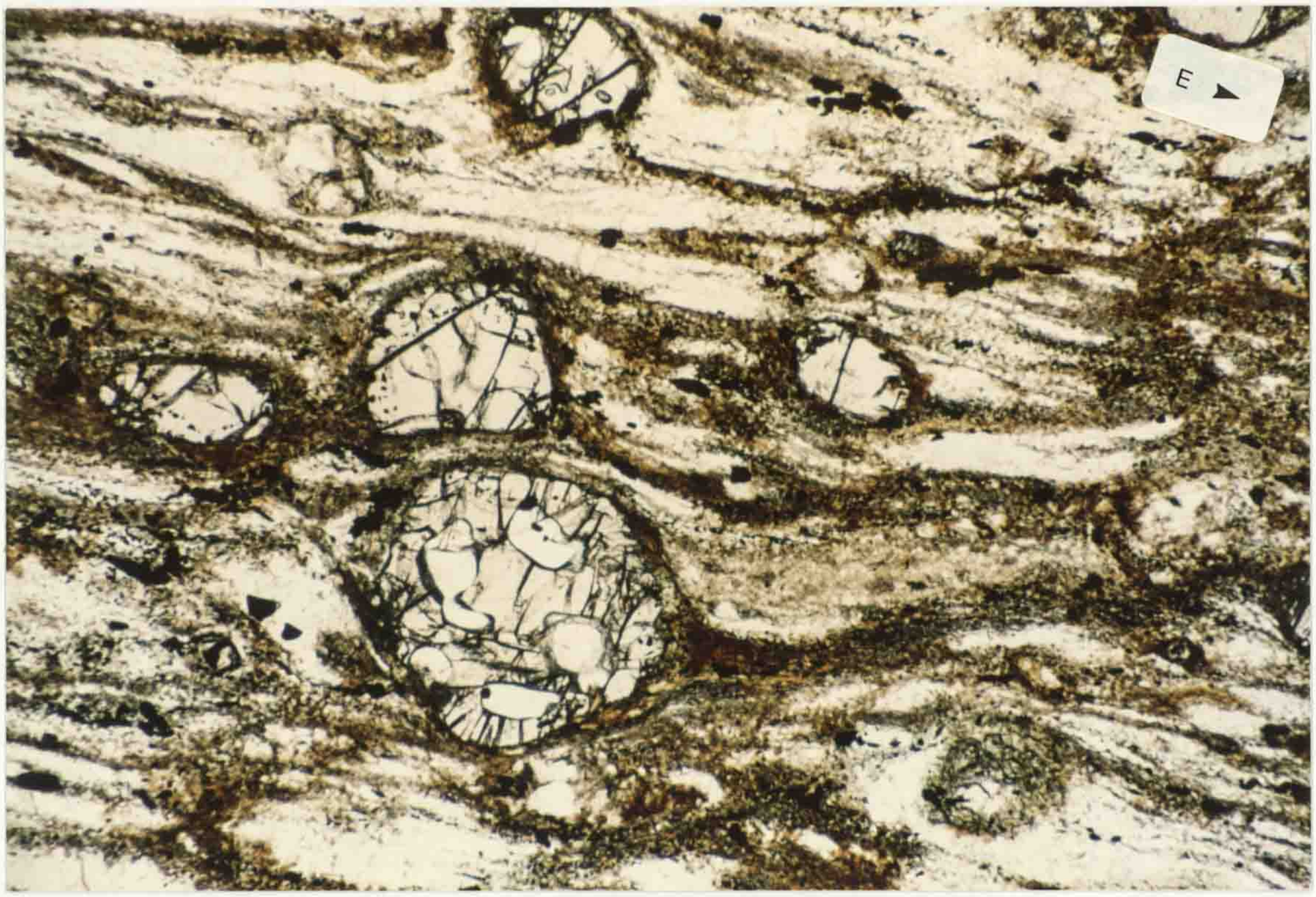


**Figure 4.7: Skeletal garnet within hornfelsic contact lithology with shape apparently controlled by grain boundaries (X 29) PPL.**

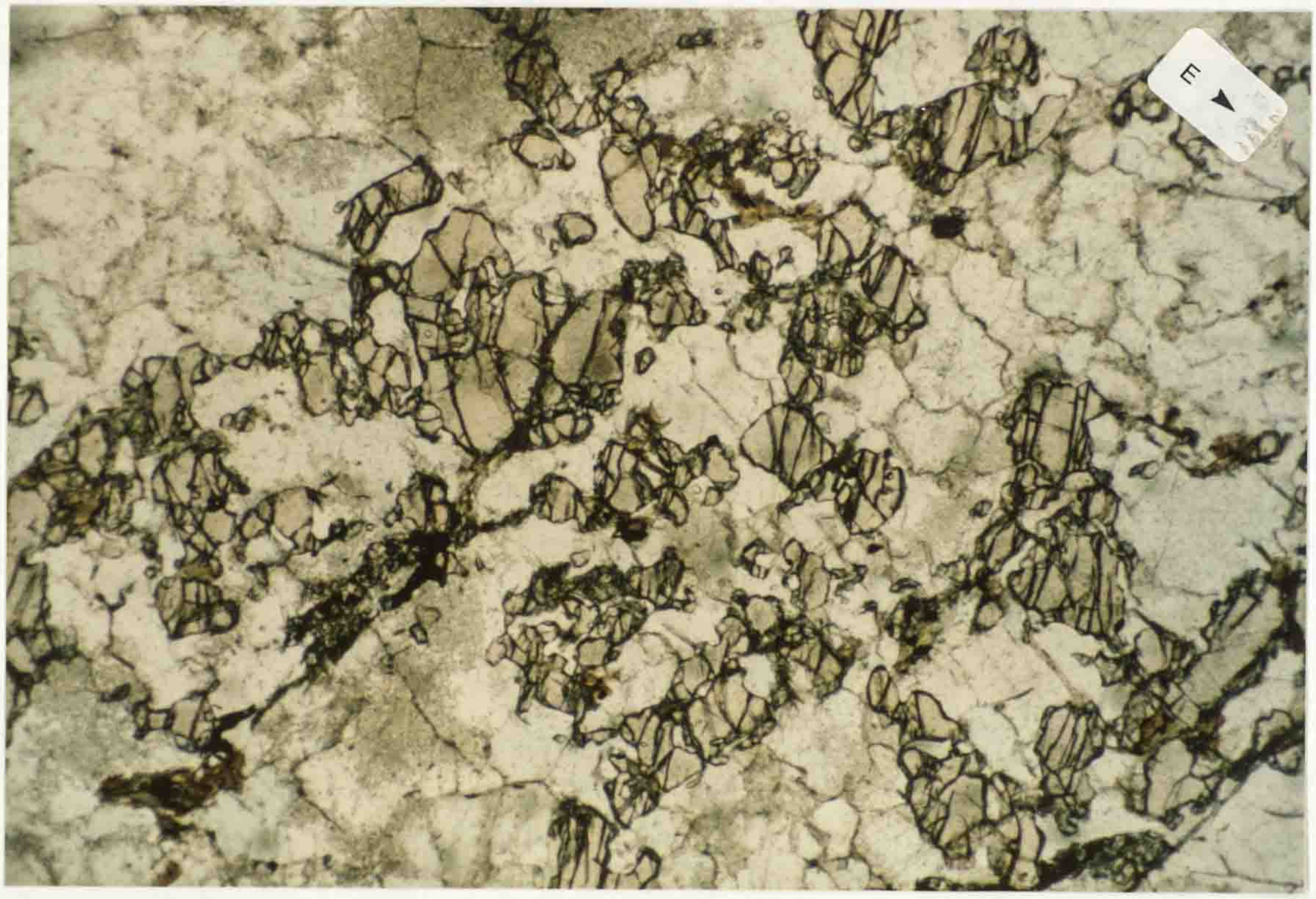

**Figure 4.8: Variation of $Fe_{(total)}$, Ca, Mn, Mg in garnet rims with $Fe_{(total)}$, Ca, Mn, Mg in whole rock for regional metamorphic lithologies.**

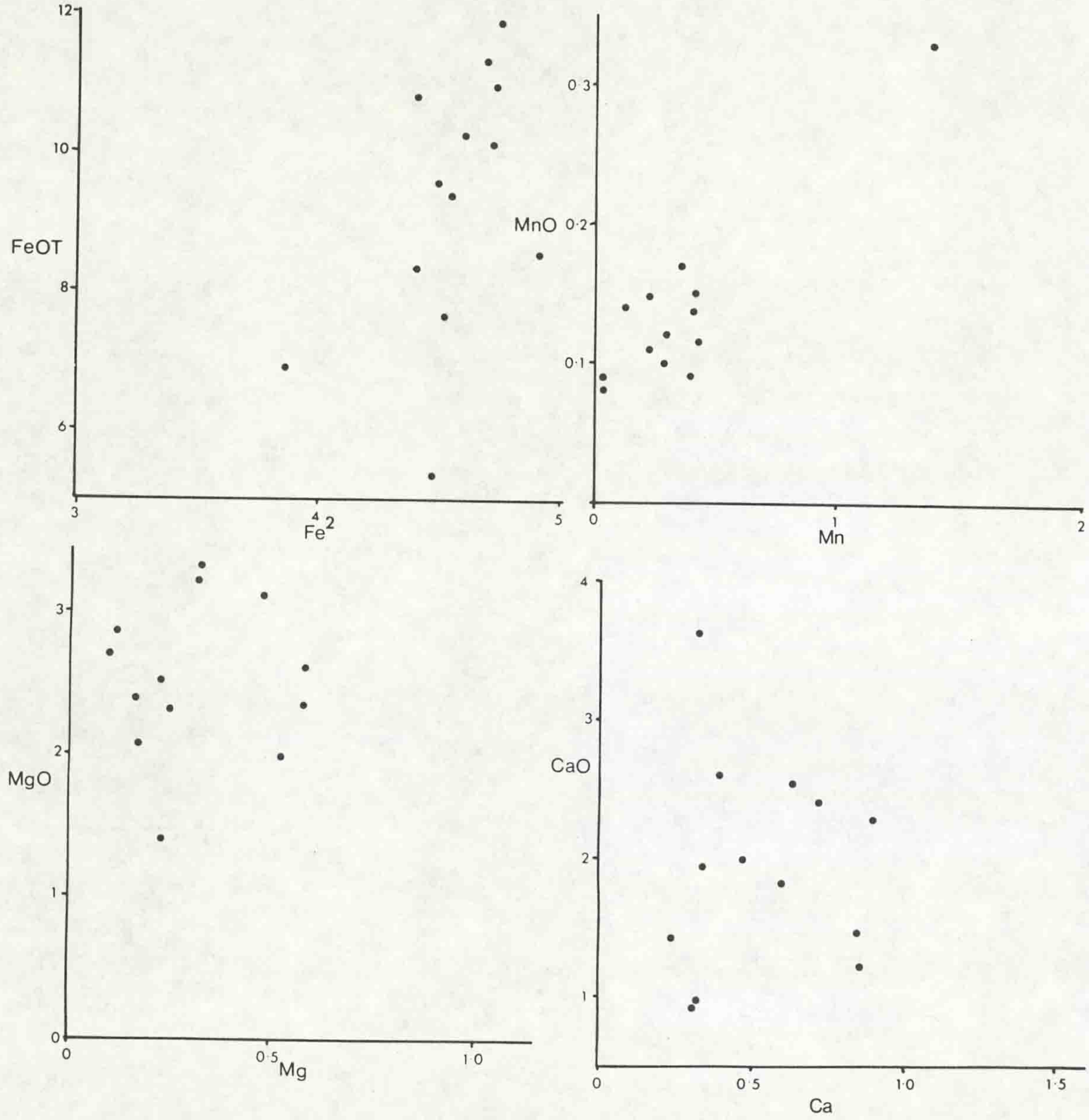

Figure 4.9: Compositional zoning profiles in regional metamorphic garnets. Profiles given in percentage end member content ( ■ Alm, ● Sps, □ Prp, ○ Grs). Scale bars = 1mm.
a, 68806
b, 69229
c, 69230
d, 69236
e, 69238
f, 69277
g, 69317
h, 69623
i, 71912
j, 71923
k, 71934
l, 71941
m, 71916 (1/2 profile)

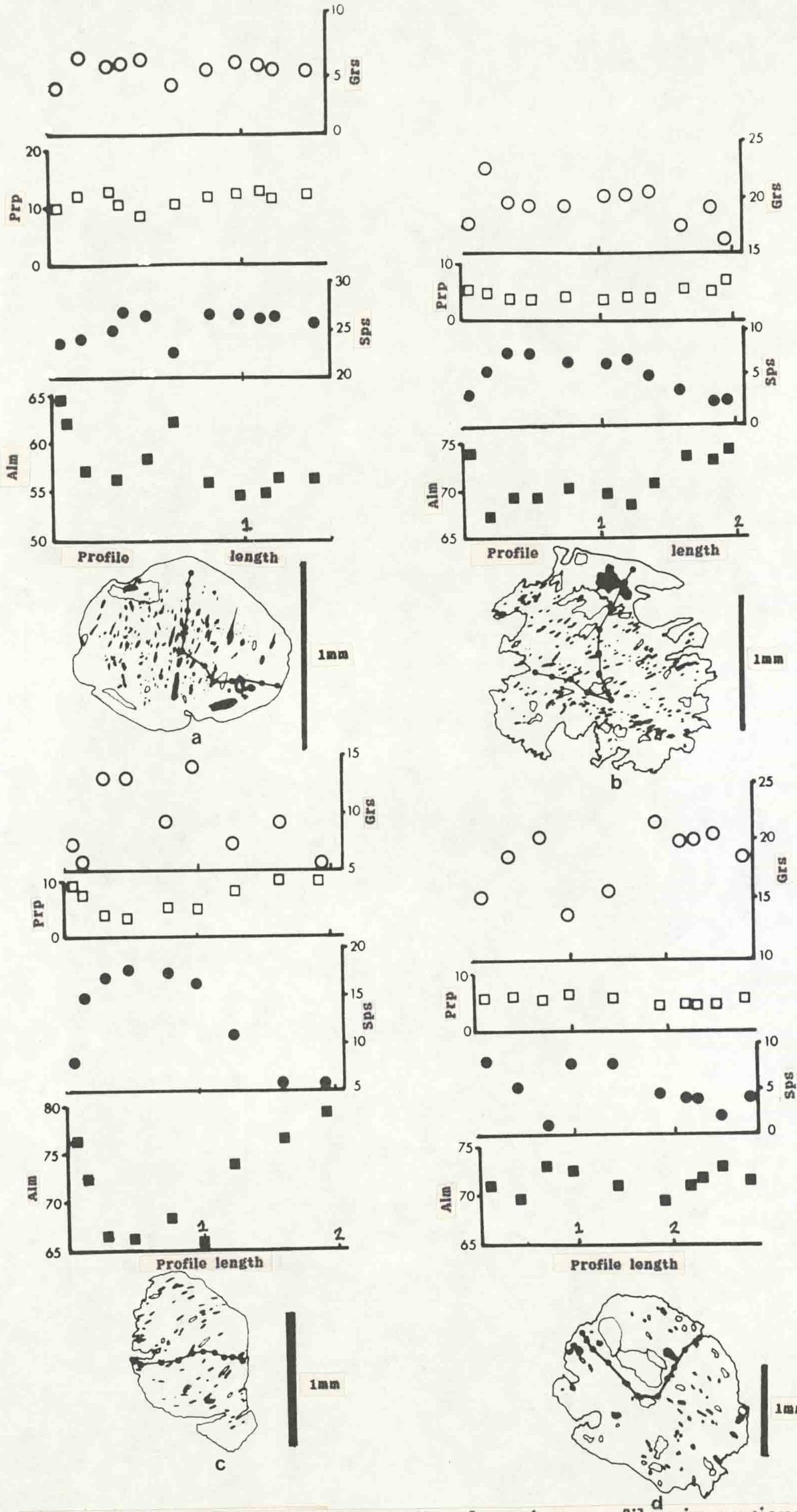


(Figure 4.9 continued) Compositional zoning profiles in regional metamorphic garnets. End member (Alm, Sps, Prp, Grs) in percent. Profile length scales in mm.

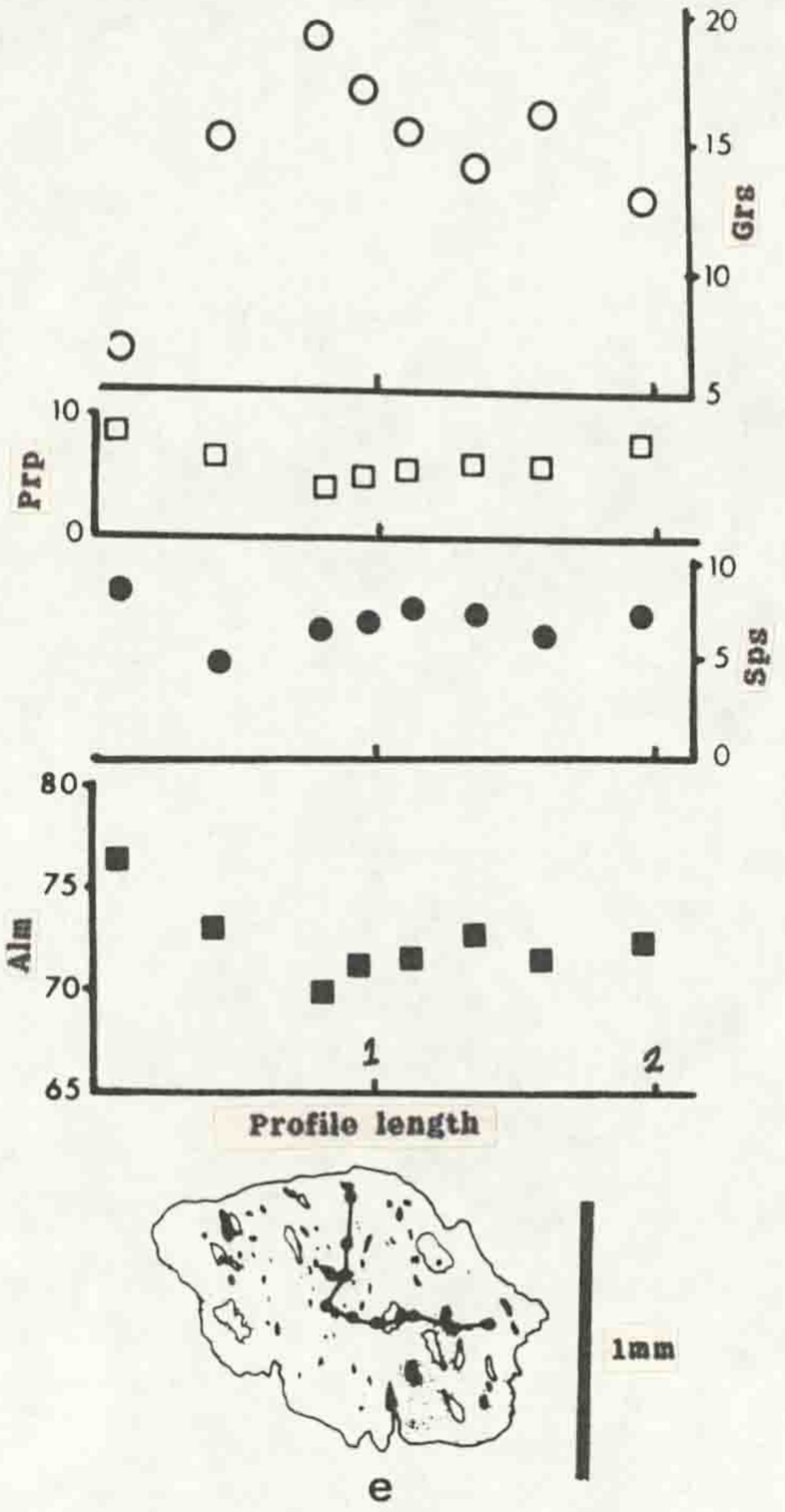


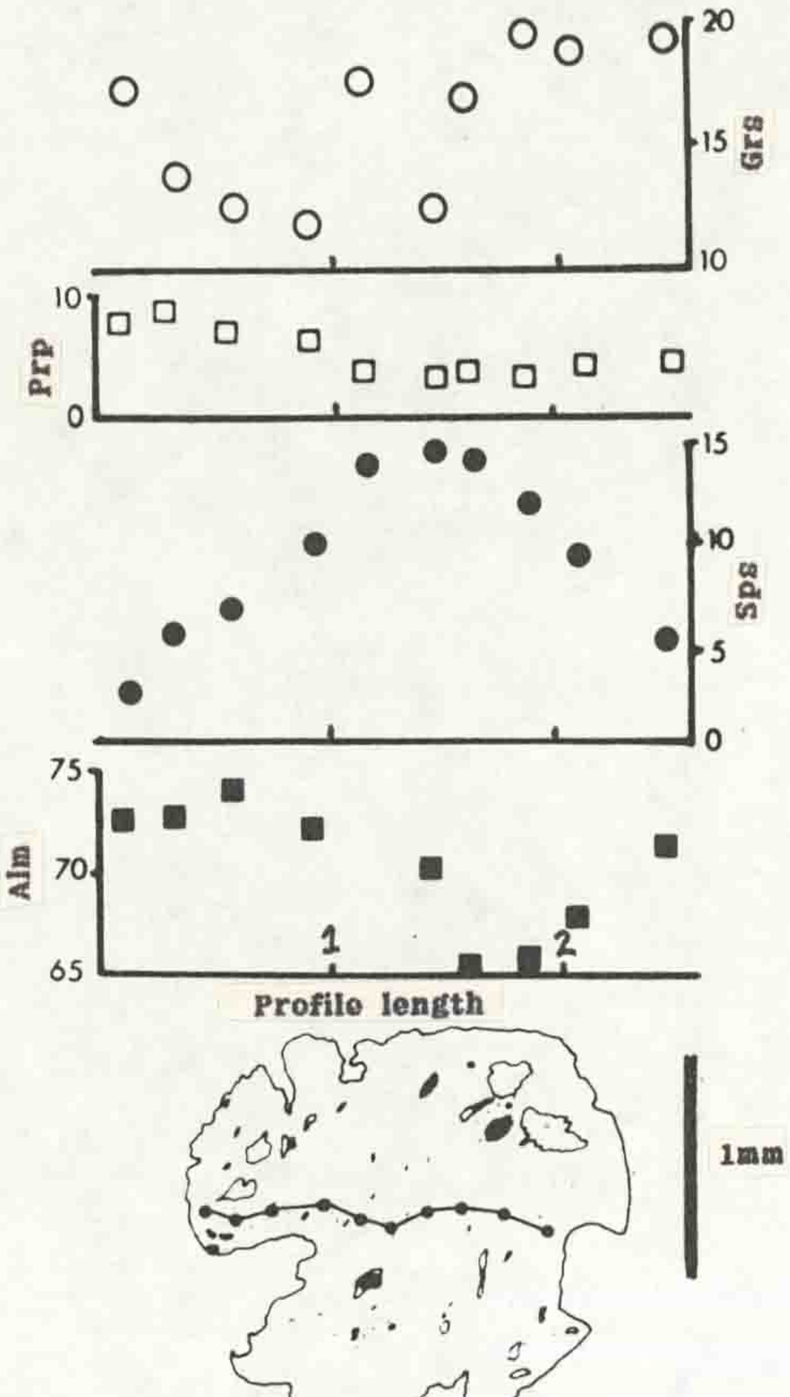


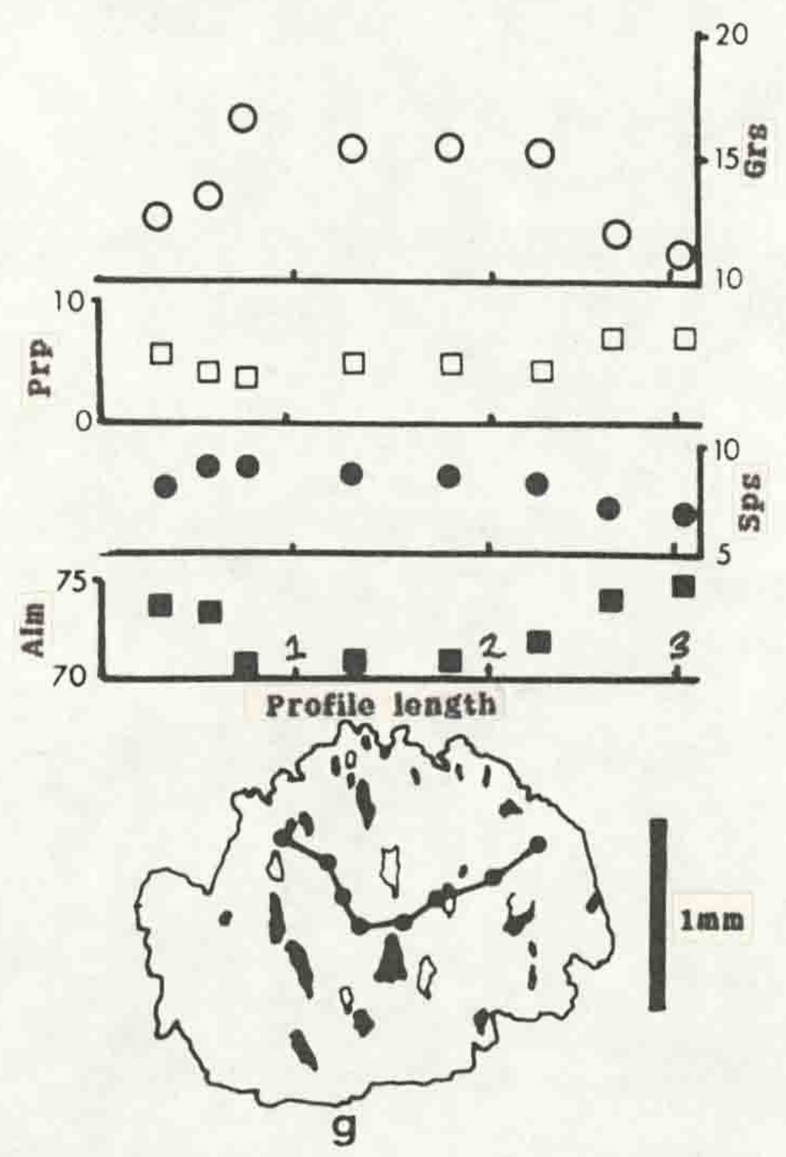


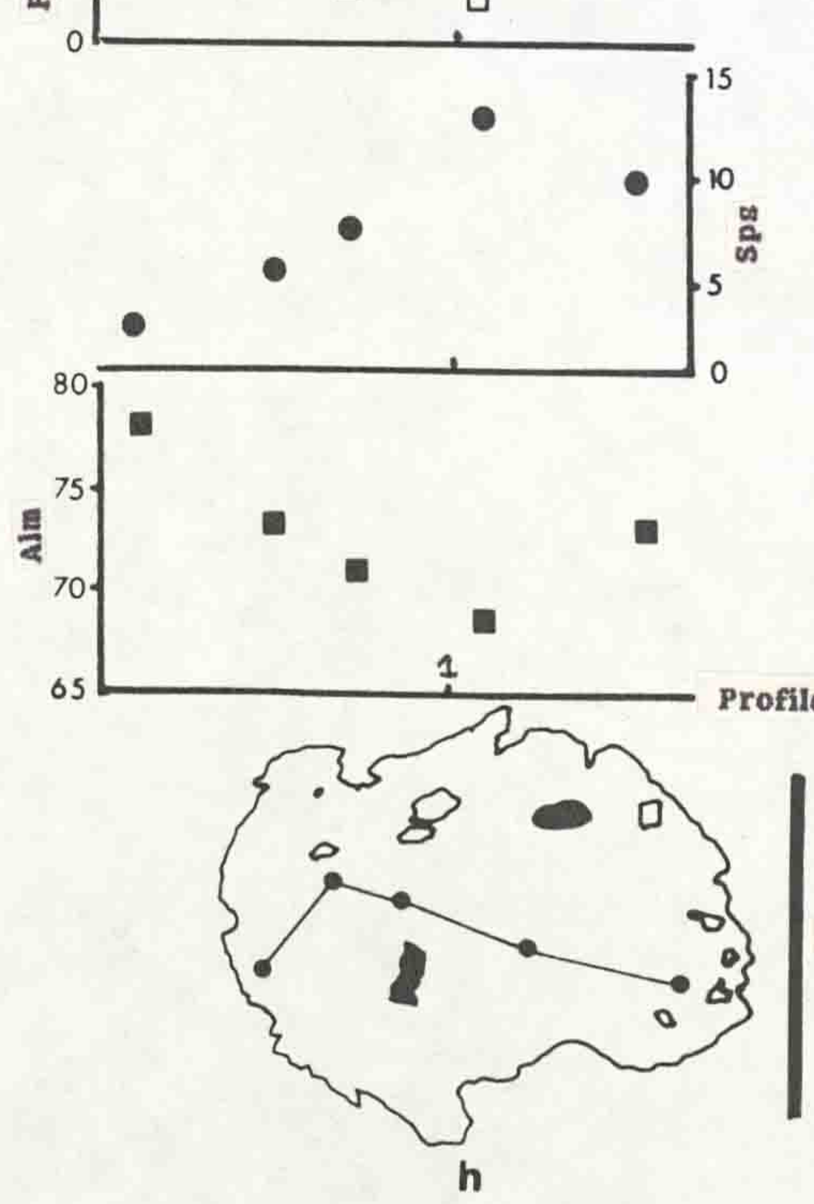


(Figure 4.9 continued) Compositional zoning profiles in regional metamorphic garnets. End member (Alm, Sps, Prp, Grs) in percent. Profile length scales in mm.

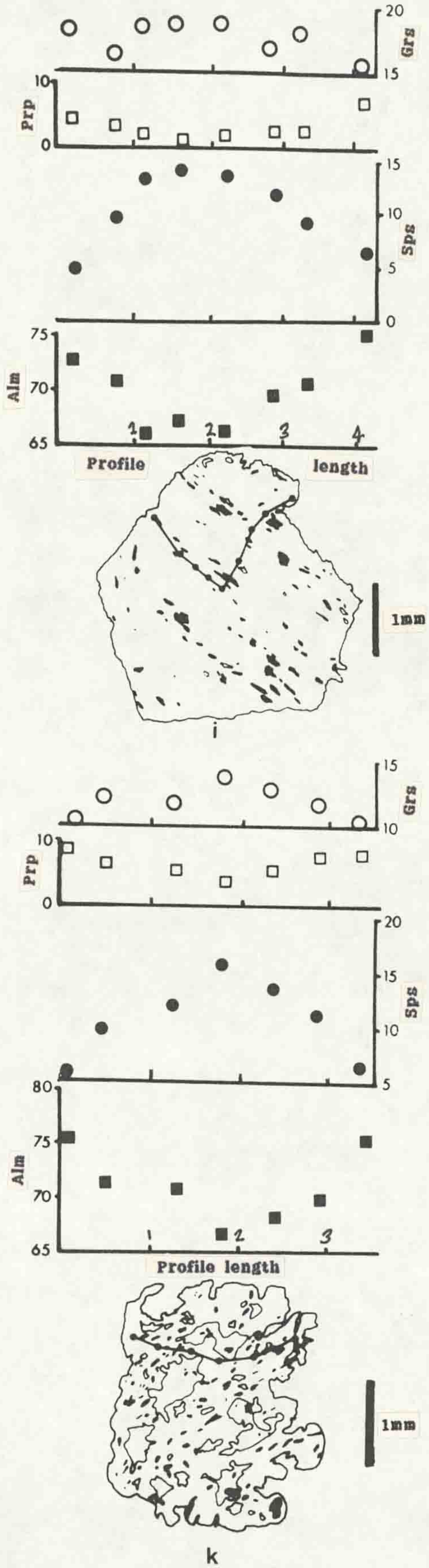


(Figure 4.9 continued) Compositional zoning profiles in regional metamorphic garnets. End member (Alm, Sps, Prp, Grs) in percent. Profile length scales in mm.

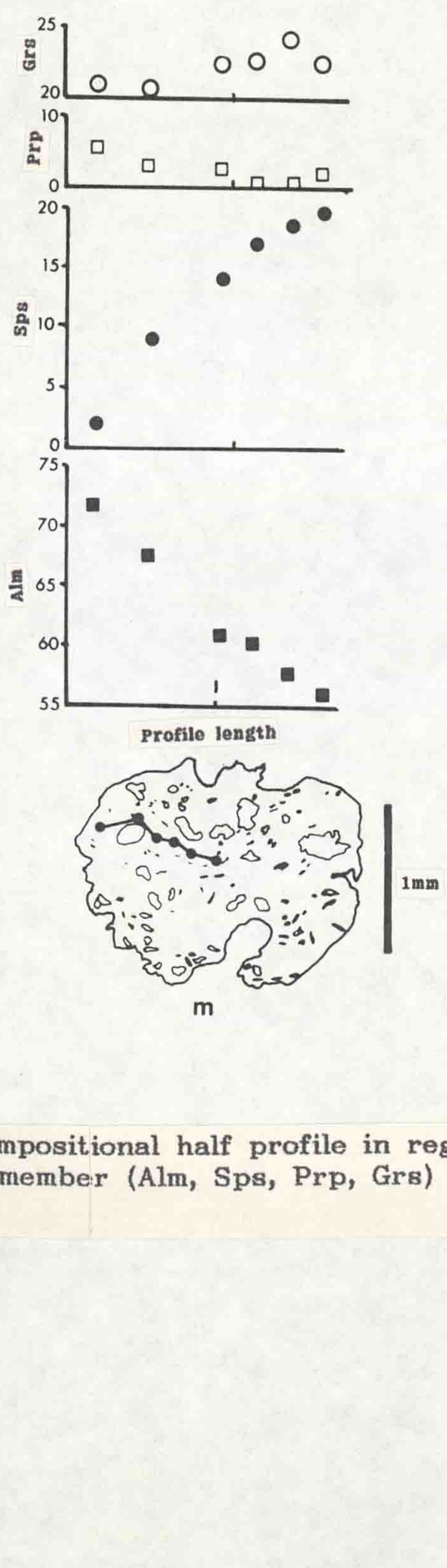


(Figure 4.9 continued) Compositional half profile in regional metamorphic garnet. End member (Alm, Sps, Prp, Grs) in percent. Profile length scale in mm.

with syndeformational ($D_2$) development of sillimanite {4.1.3.8}.

Within non - mylonitic aureole lithologies, garnets often display skeletal forms suggesting that garnet growth was controlled by pre - existing grain boundaries (Figure 4.7).

In considering the chemistry of garnets in the study area the regional and contact aureole garnets will be discussed separately.

Regional garnets are typically almandine rich although there is a wide range in element concentrations (as end members), from 51% to 82% for Alm, <1% to 22% for Grs, 1% to 13% for Prp and <1% to 27% for Sps. The mean formula for all the analysed regional garnets (based on 24 oxygens) is:

$Fe_{4.19}\ Ca_{0.85}\ Mg_{0.37}\ Mn_{0.59}\ Al_4\ Si_6\ O_{24}$

The variation in composition cannot be wholly ascribed to the variation in lithological composition (Figure 4.8), as plots of the element concentrations in garnet rims against whole rock element concentrations show only slight linear relations for $Fe^{2+}$ and Mg.

Element concentration profiles across regional metamorphic garnets (Figure 4.9) reveal the existence of compositional zoning.

The zoning in almandine (Alm, filled squares on Figure 4.9) is characterised by low values in garnet cores, increasing outwards to maximum values at the garnet rims. The magnitude of the variation is typically 15%, with the Alm - poor garnets showing core to rim variation from 55% to 70%$_{Alm}$ and Alm - rich garnets ranging from 65% to 80%$_{Alm}$. Certain of the garnets show variations from this simple pattern:

68806 (a, Fig 4.9) shows a high value of Alm in the core which then decreases outwards to a minimum value and then shows an increase towards the rim.

69299 (b, Fig 4.9) the variation of Alm content in this garnet falls slightly from the core to a minimum value of 66 - 67% and then increases towards the rim.

69236 (d, Fig 4.9) This garnet shows an increase in Alm from 70% in the core to a maximum of 74% at approximately 1/2 the radius, and then decreases towards the rim.

It should be noted that, although the overall trend in Alm

zoning is typically symmetrical within a particular garnet, the absolute values of the variation often show no clear symmetry. The zoning also shows no clear relation to the inclusion fabrics developed within the garnets, suggesting that the inclusion fabric did not interfere with the development of the compositional zoning.

Spessartine (Sps, dots on Figure 4.9) zoning in regional garnets shows a similar magnitude to Alm, Sps showing a variation of up to 15%, although the maximum Sps contents are considerably lower than Alm (Sps shows maximum values of <20%). The general trend in Sps zoning is from high values in the garnet cores to low values in the rims. This variation is typically smooth in nature and the profiles are often 'bell' shaped (e.g. 69230, 69277, 71912, 71934, 71941, c, f, i, k, l in Fig 4.9). Three of the zoning paths (69230, 69236, 69238) show compositional profiles in which the concentration of Sps decreases from the core to a minimum at approximately 1/3 of the garnet radius from the rim, giving a central bell shaped profile, Sps values then increase towards the rim itself. The profiles are again largely assymmetric and the variation in Sps appears unrelated to inclusion fabrics, although in 69230 the increase in Sps at the garnet rim is associated with an inclusion - poor zone near the garnet rim.

Pyrope (Prp, open squares on Figure 4.9) contents of the garnets show a much more restricted range of variation than Alm and Sps, although the general trend is from lower values in the cores to higher values in the rims (similar in style to Alm). The magnitude of this variation is typically less than 5%.

The magnitude of variation in grossular (Grs, open circles on Figure 4.9) contents of garnets is comparable to Alm and Sps with variation of up to 15%, although the zoning profiles are typically complex in nature. The style of Grs zoning can be subdivided into four groups:

(i), zoning profiles in which the variation in Grs is sympathetic to Sps (highest in core, lowest at rim, garnets 68806, 69229, 69317, 69623, 71934, a, b, g, h, k in Fig 4.9). The detailed trends for each of these garnets show a degree of variation from this simple trend.

(ii), zoning profiles in which Grs variation is sympathetic to

**Figure 4.10: Alm V. Sps plot for regional garnets.**

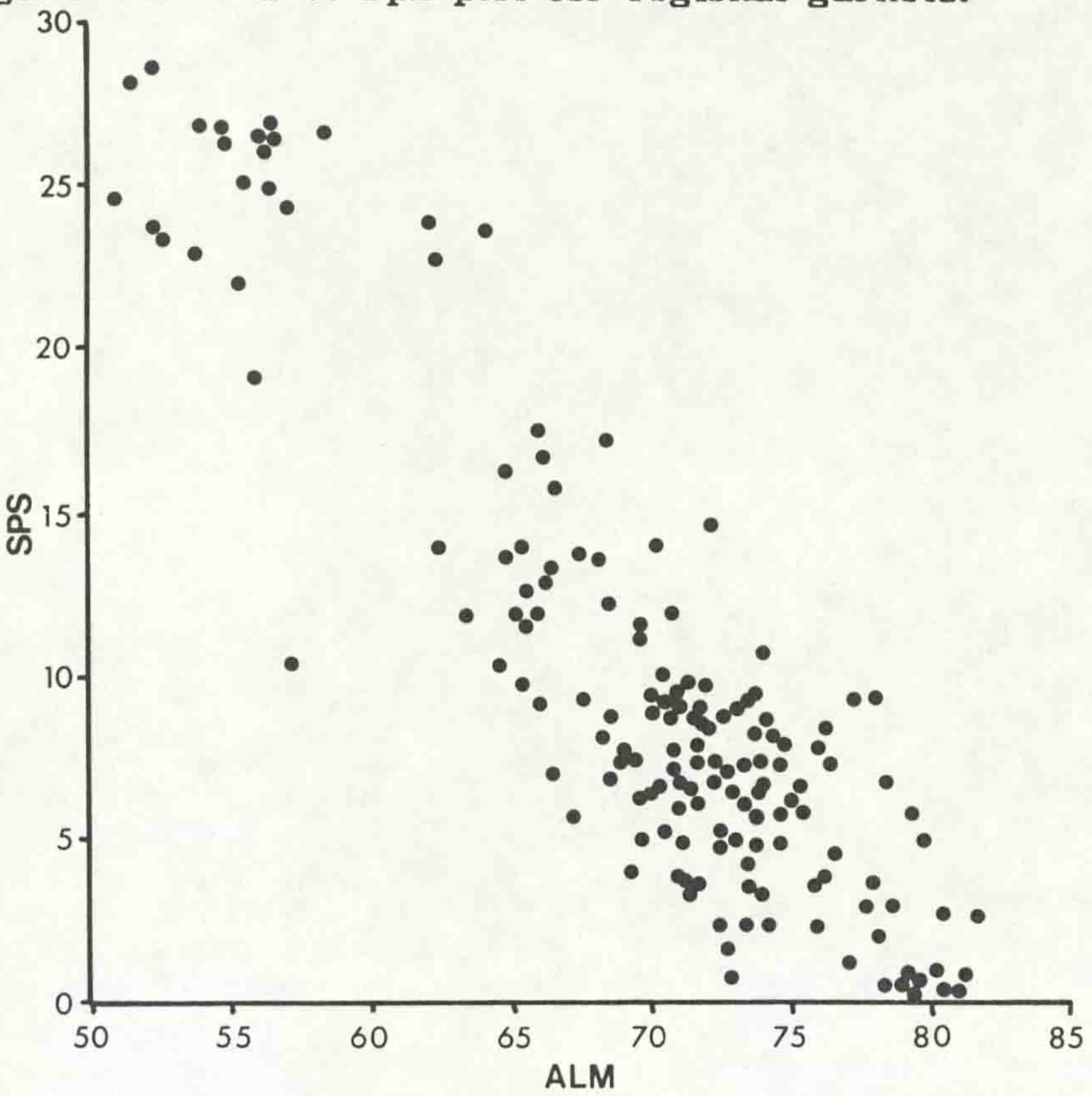


**Figure 4.11: Prp V. Grs plot for regional garnets.**

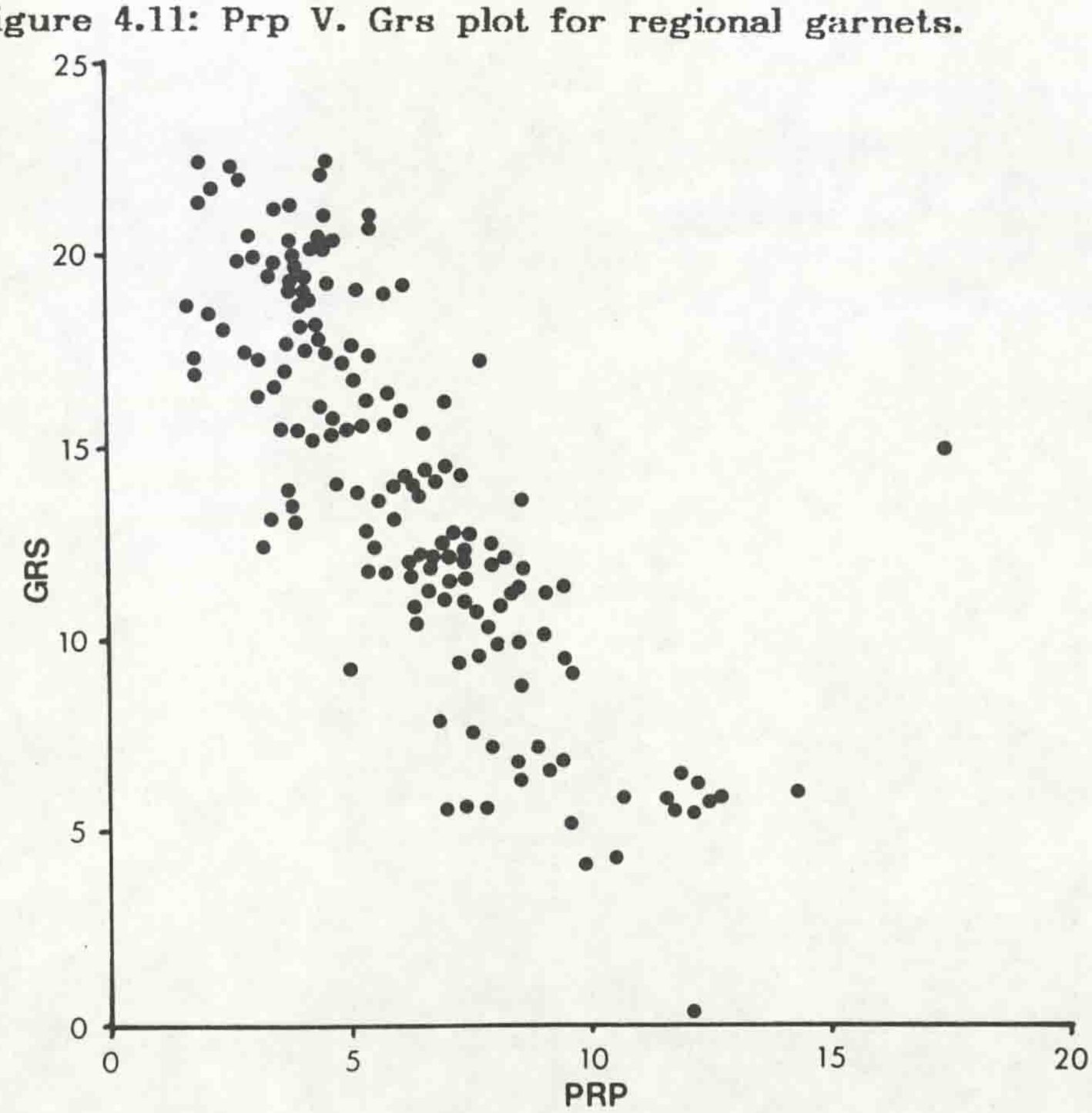

## 1.1 Geographic setting

Connemara is the westernmost region of County Galway and lies on the Atlantic coast of the Irish Republic (Figure 1.1). The study area lies to the north - west of the Twelve Bens group of mountains and is bounded to the north and west by the Atlantic coast, to the south by the N59 Clifden to Westport road and to the east by the mountains of Altnagaighera and Garraun. The bulk of the study area has a relatively low ( <50m), but rugged, relief, with three main peaks: Tully Mountain (358m) which forms an NW trending ridge on the Renvyle peninsula; Currywongaun (275m) and Doughraugh (536m) which lie on the north side of the Kylemore valley.

Exposure is highly variable, much of the low-lying land being blanketed by peat bog and thus poorly exposed, and the north - eastern corner of the area having a thick cover of glacial drift which reduces the exposure to a narrow, largely continuous, coastal strip. The higher ground is generally better exposed with 70% to total exposure on Tully Mountain, Currywongaun and Doughraugh, although the flat area between and to the north of Currywongaun and Doughraugh is peat covered and lacking in exposure.

Access is generally good, with much of the area being within 1km of a road or track, although after heavy rain the areas of peat bog are often passable only with extreme care. Connections with Galway and Westport are good with the N59 passing through the main settlement, Letterfrack.

## 1.2 Geological setting

The rocks of the Connemara massif (Figure 1.2) consist of a multiply deformed sequence of pelitic, psammitic, calc-silicate, amphibolitic, and quartzitic metasedimentary and metaigneous rocks, correlated on a lithostratigraphic basis (Kilburn, Shackleton & Pitcher 1965) with the Appin and Argyll Groups of the Dalradian of Scotland. The stratigraphy is established over much of Connemara (e.g. Tanner & Shackleton 1979, Treloar 1982, Leake 1986). A range of intrusive rocks, from syn - deformational basic and ultrabasic (Leake 1970b), to extensive late/post - tectonic granitic bodies (Townend 1966), are present within the metasedimentary sequence.

Alm (lowest in core, highest at rim, garnet 69277, f in Fig 4.9). In this garnet the Alm profile is not a simple curve but the variation in Grs tends to follow the same overall trend.
(iii), 'Flat' profiles in which Grs variation is restricted (71923, 71941, j, l in Fig 4.9).
(iv), More complex, often assymetric profiles where the Grs values show no clear relation to the other end member profiles (garnets 69230, 69236, 69238, 71912, 71916, c, d, e, i, m in Fig 4.9).

The overall nature of compositional zoning in the regional garnets analysed is for low Alm and Prp along with high Sps contents in the garnet core, with high Alm and Prp along with low Sps at the garnet rim. The Sps zoning is often characterised by a bell shaped curve. Grs zoning is rather more complex in nature and cannot be simply characterised for the whole group of garnets. It should be noted that a degree of variation from these simple trends exists within the analysed garnets. The overall style of compositional zoning developed in the regional metamorphic garnets studied here is commonly seen in garnets from low and medium grade metamorphic terrains (Tracy 1982) and referred to as *'normal'* zoning.

The antipathy between Sps and Alm noted in the zoning profiles can also be seen in a plot of Alm V. Sps (Figure 4.10) which reveals the expected negative relation. A similar negative relation is also seen, albeit to a lesser extent, between Grs and Prp (Figure 4.11).

Contact garnets are also almandine rich and show a wide range of compositional variation of the components (as end members) with ranges of 80% to 46% for Alm, 3% to 16% for Grs, 6% to 26% for Prp and 1% to 33% for Sps, and have a mean formula (based on 24 oxygens) of:

$Fe_{4.05}\ Ca_{0.38}\ Mg_{1.10}\ Mn_{0.51}\ Al_4\ Si_6\ O_{24}$

Like the regional metamorphic garnets the variation in composition in the contact garnets shows only limited relation to whole rock composition (Figure 4.12).

Zoning profiles through garnets developed within aureole lithologies (Figure 4.13) show less compositional variation than those seen in regional garnets, with core to rim variation in Alm, Sps, Prp and Grs typically being <5%. Despite this lack of

**Figure 4.12: Variation of FeO, MnO, MgO, CaO in garnet rims with FeOT, MnO, MgO, CaO in whole rock for contact metamorphic lithologies.**

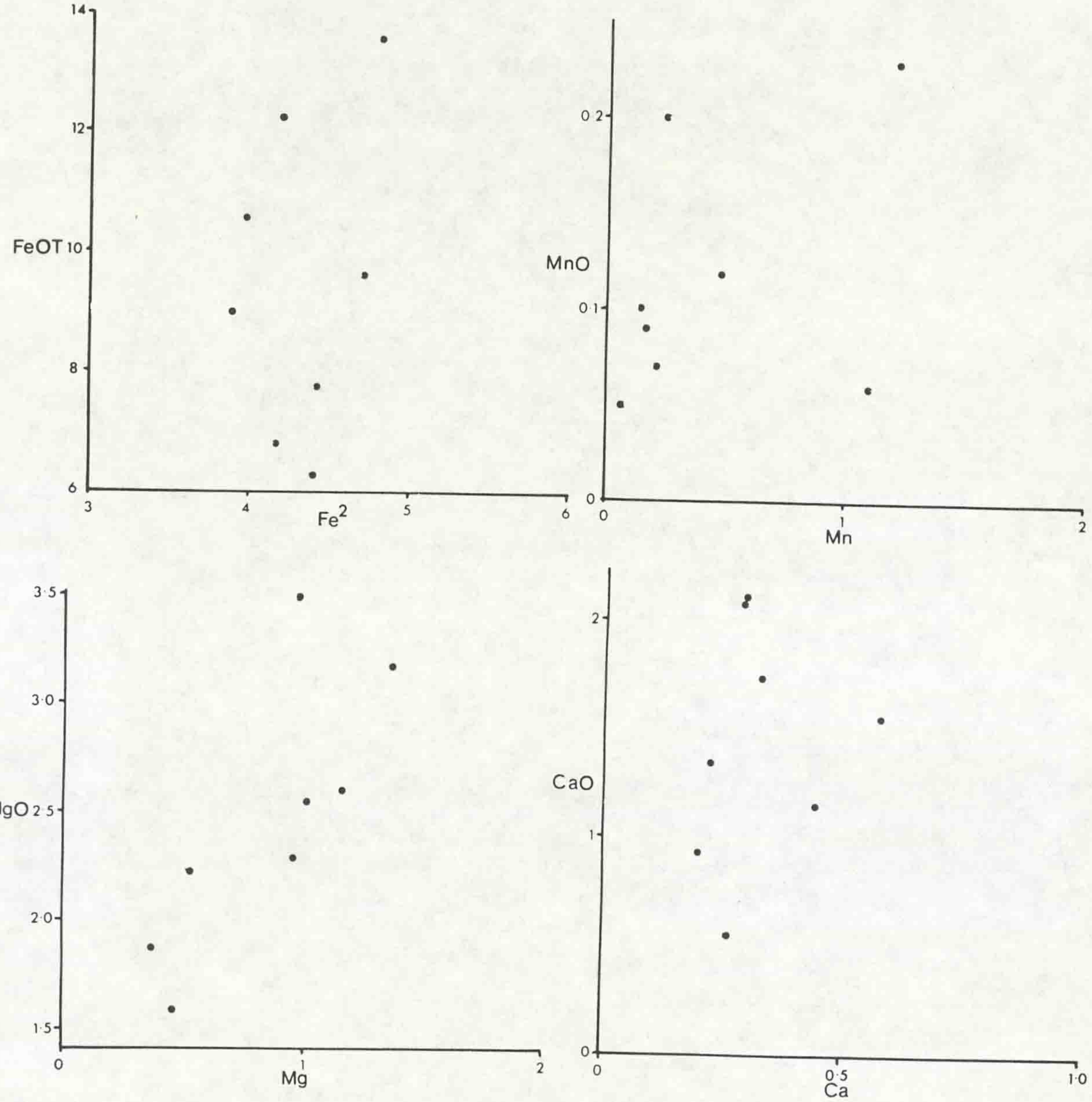

Figure 4.13: Compositional zoning profiles in contact metamorphic garnets. Profiles given in percentage end member content ( ■ Alm, ● Sps, □ Prp, ○ Grs). Scale bars = 1mm.
a, 66795
b, 68780
c, 68793 (1/2 profile)
d, 68799
e, 68804
f, 69215
g, 69219
h, 69635

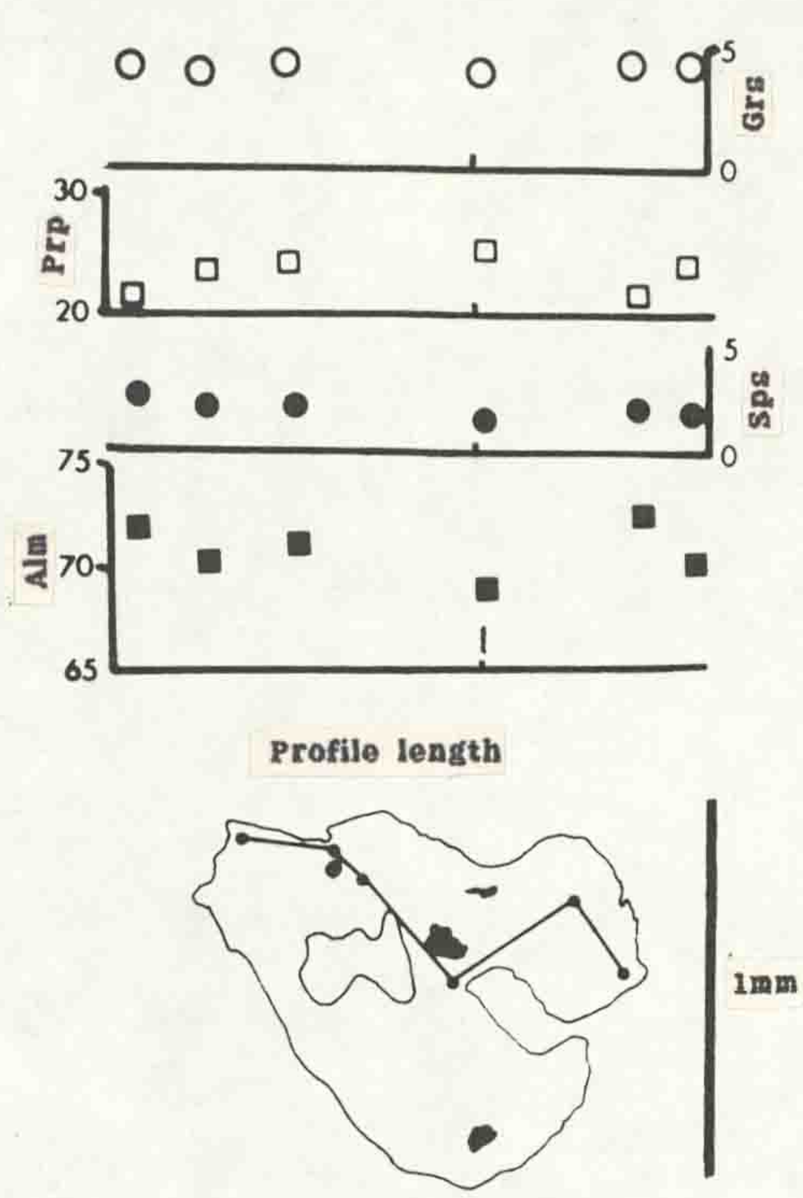


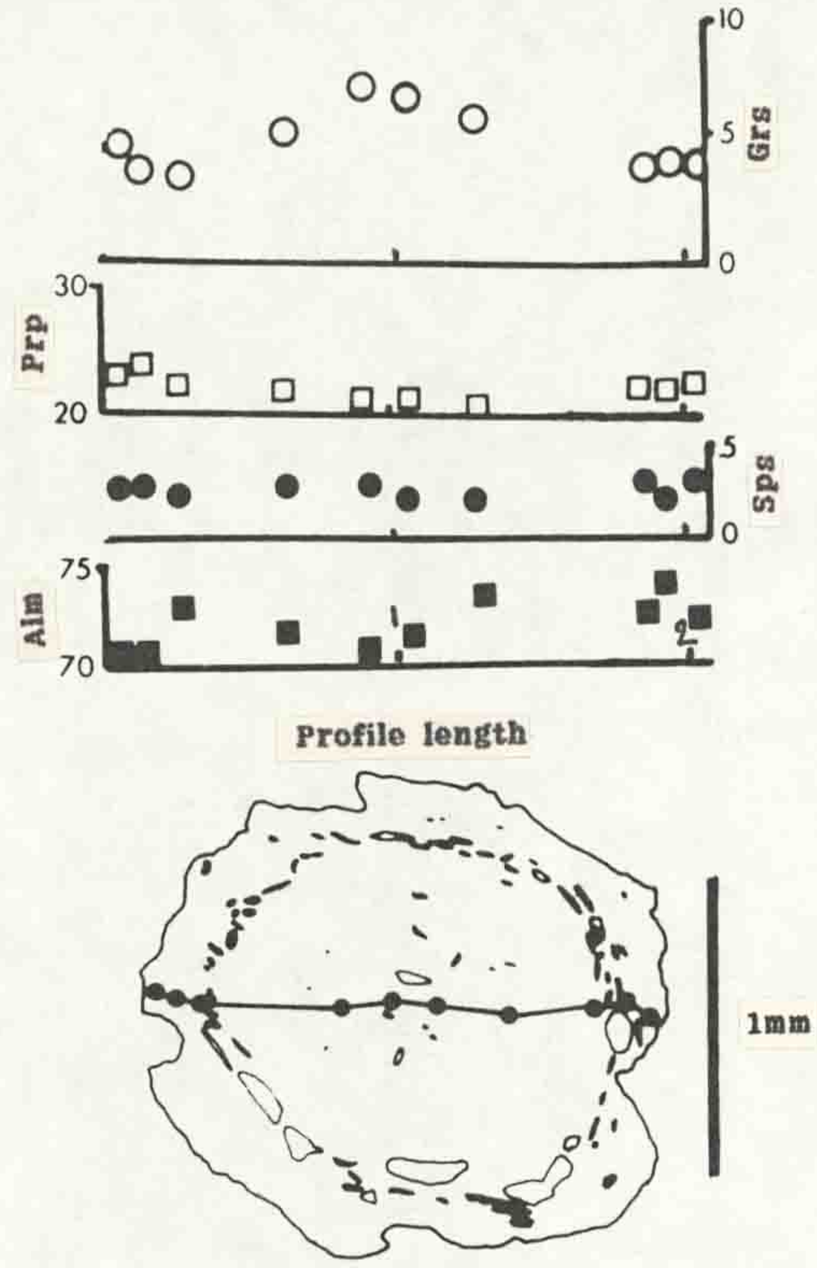


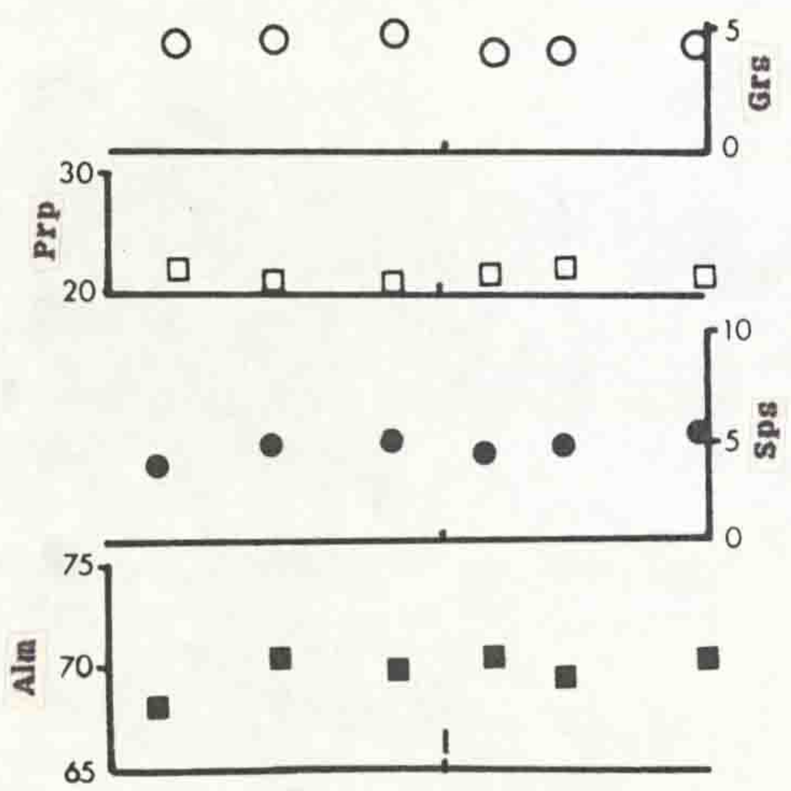


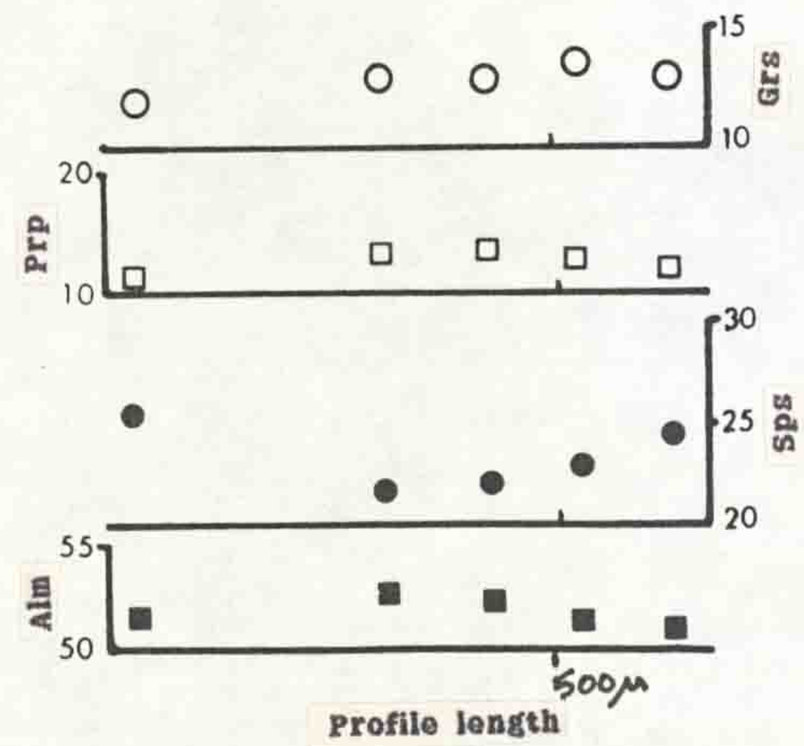


(Figure 4.13 continued) Compositional zoning profiles in contact metamorphic garnets. End member (Alm, Sps, Prp, Grs) in percent. Profile length scales for garnets a, b, and c, in mm, scale for garnet d is in *u*.

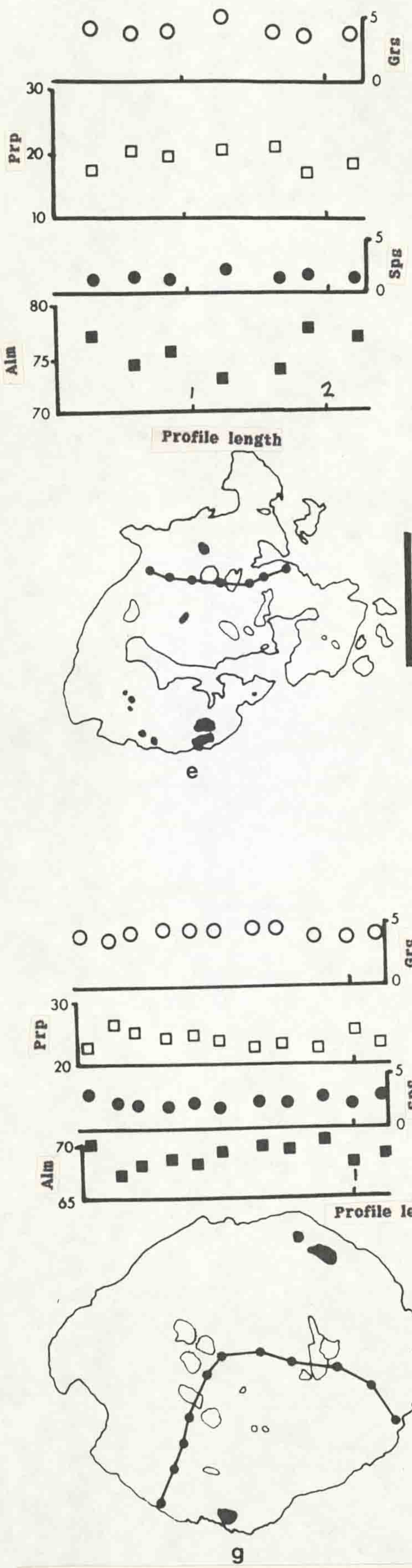


(Figure 4.13 continued) Compositional zoning profiles in contact metamorphic garnets. End member (Alm, Sps, Prp, Grs) in percent. Profile length scales in mm.

compositional variation in garnets the antipathy between Alm and Sps (Figure 4.14) and Prp and Grs (Figure 4.15) remain apparent.

Almandine profiles (Alm, filled squares on Figure 4.13) through contact garnets generally show limited variation in composition, although the slight variations present fall into three groups:

(i), Garnets where Alm values are low in the cores and high at the rims (66795, 68804, 69635, a, e, h in Fig 4.13).

(ii), Garnets in which Alm concentrations fall from core to rim (68793, 68799, 69215, 69219, c, d, f, g in Fig 4.13). Two of these garnets (69215, 69219) show evidence of Alm increase at the rim, the minimum concentrations being developed inside the rim.

(iii), One garnet (68780, b in Fig 4.13) in which the Alm values increase from a minimum in the core to maximum values inside an inclusion rich zone (this zone represents the spherical inclusion trail discussed earlier), the values of Alm then fall between this inclusion zone and the rim.

Spessartine (Sps, dots on Figure 4.13) variation is again restricted in its variation, typically defining 'flat' profiles with <3% variation (66795, 68780, 69215, 69219, 69635). In those garnets where variation is more evident, the variation in Sps either decreases (68793, 68804) or increases (68799) from core to rim.

Pyrope (Prp, open squares on Figure 4.13) variation in contact garnets generally has the appearance of flat ( <2% variation) profiles, although certain of the garnets do display some degree of zoning. High values of Prp in garnet cores and low values at the rims are evident in garnets 66795, 68799, 68804, with the opposite being the case in garnets 68780, 68793, 69215, 69219, 69635. Certain of the garnets which show low Prp in their cores (68780, 69215, 69219) display slight fall in Prp at the rim, with the maximum Prp concentrations being developed inside the rim.

The variation in Grossular (Grs, open circles on Figure 4.13) is rather more simple in nature than that developed in regional garnets, the profiles showing slight and relatively regular variations. The Grs profiles of garnets 68780, 68804, 69219 and 69635 show increased Grs in their cores with the concentration falling towards the rim. In garnets 68780, 68804 and 69219 the minimum concentration of Grs occurs inside the rim, and slight

**Figure 4.14: Alm V. Sps plot for contact garnets.**

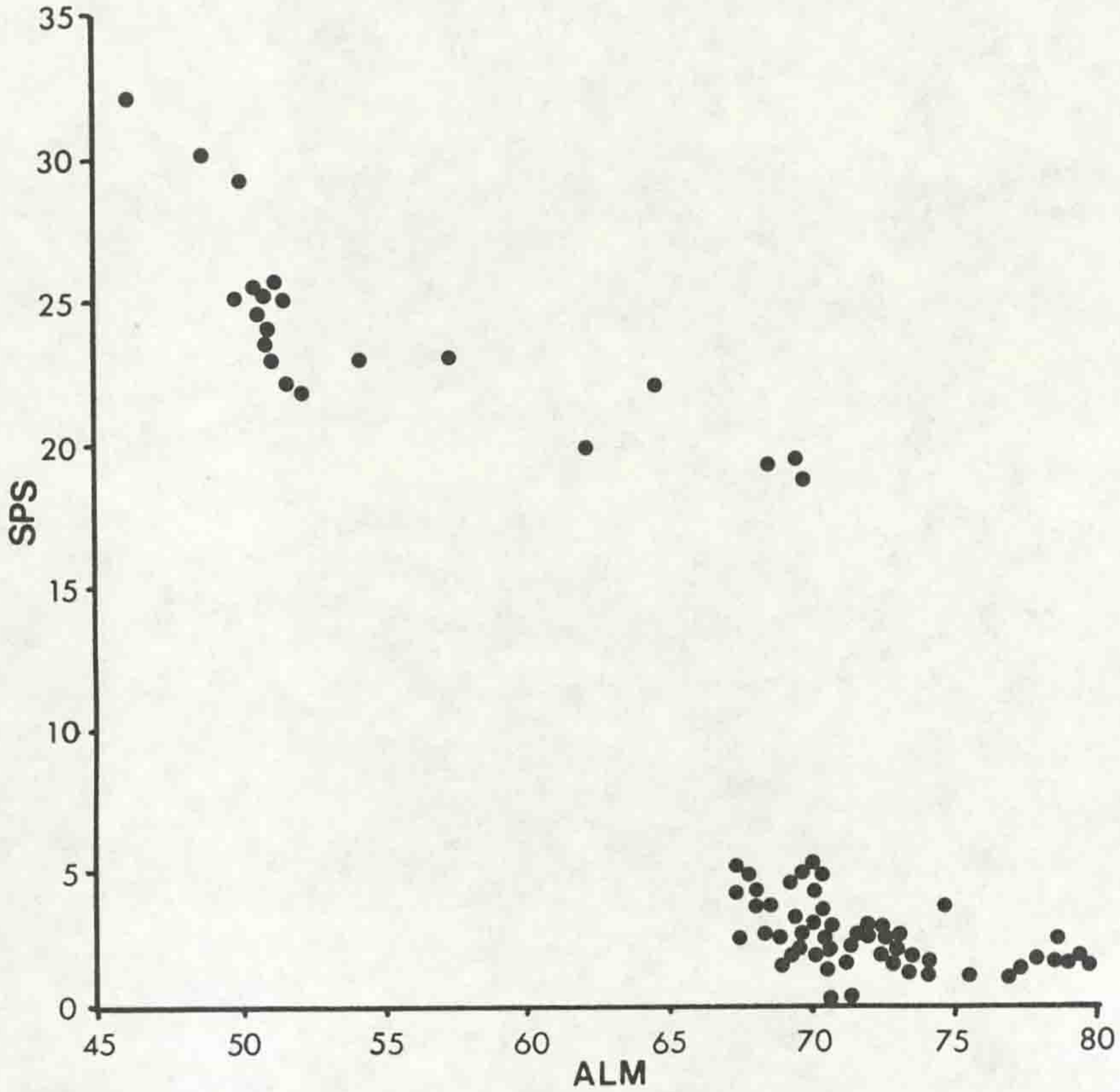


**Figure 4.15: Prp V. Grs plot for contact garnets.**

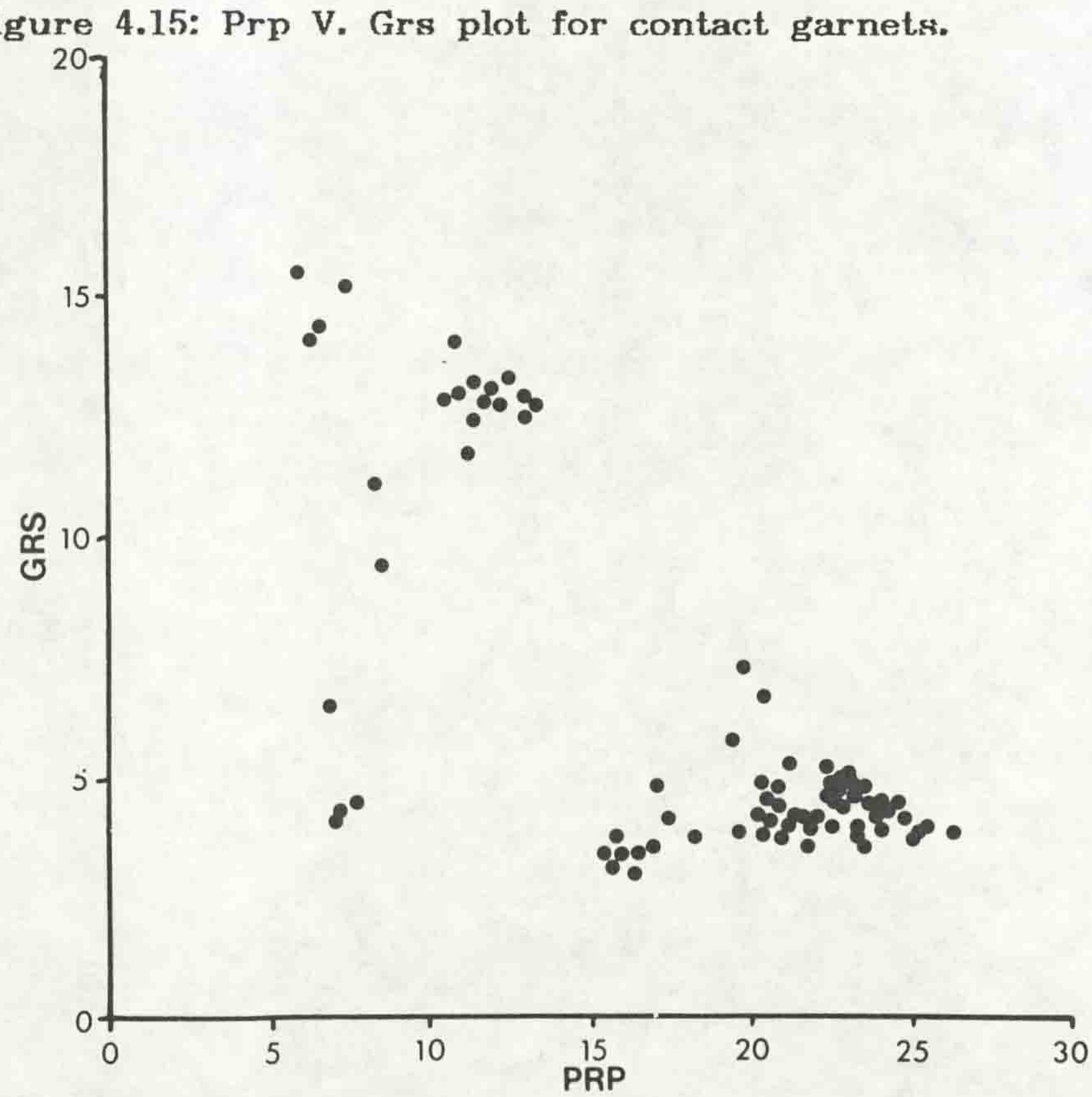

increase in Grs is seen near to the rim. Garnets 66795, 68793, 68799 and 69215 show a slight tendency towards lower Grs in their cores and higher values at the rims, although the range of variation is very low.

The zoning patterns developed in contact garnets can be divided into two groups, a group which show, albeit to an attenuated degree, *normal* zoning (66795, 68804), and a second group (68793, 68799, 69215, 69219) which show slight zoning in Alm and Sps end members, where Alm concentrations are high in the garnet core and low in the rims, with Sps showing an antipathetic relation to Alm. Such zoning is the reverse of that developed in normally zoned garnets and is (logically) referred to as *'reverse'* zoning (Tracy, 1982).

A variety of models have been proposed to explain the development of *normal* zoning by preferential partitioning of elements (Mn and Ca being prefered to Fe and Mg) into garnet during growth (e.g. Hollister 1966, Atherton 1968). Such models typically concentrate on the partition of Mn into a growing garnet. As the concentration of Mn within typical pelitic lithologies is relatively low any preferential partition of Mn into garnet will lead to a depletion of Mn from the surrounding rock. As the garnet continues to grow it continues to extract Mn from the matrix, which is now relatively depleted in this element. In order to continue growth, the garnet draws on other suitable elements such as Fe. Such a process results in a garnet with a core enriched in Mn (Sps), the Mn content falling towards a minimum at the garnet rim. The Fe content (Alm) of such a garnet will be minimum in the core rising to a maximum at the rim. A similar process is considered to occur in the substitution of Ca (Grs) and Mg (Prp), with Ca being preferentially fractionated relative to Mg, although the controls on availability of these elements are rather more complex than for Mn because Ca and Mg are involved in other phases (e.g. plagioclase, biotite, epidote) in the assemblage. These models rely on the garnet behaving in a refractory manner after its growth; ie, the diffusion rates within garnet are such that once incorporated into a garnet elements no longer take any part in the reaction system. This isolation of elements within garnets during growth has implications for the use of garnets as

'recorders' of the evolution of an assemblage, because the composition of the rim of the garnet will, at any time in the development of the assemblage, be controlled by the composition of the external assemblage and its P - T conditions. This relation is used as the basis for the P - T path modelling method of Spear & Selverstone (1983) {5.5}.

The profiles resulting from the development of garnets by a partition process during growth are typically 'bell - shaped' and the garnet core is enriched in Sps and Grs, and the rim being depleted in these end members and enriched in Alm and Prp (Figure 4.16).

The zoning profiles seen in regional garnets typically show relatively smooth variation in end member concentrations (excepting Grs) suggesting that the development of garnet was not controlled by univariant (crossing tie-line) reactions, but occurred during continuous exchange reactions (Tracy 1982). When plotted on ternary diagrams in the method suggested by Tracy (1982) the core to rim variations in end member concentrations (Figure 4.17) show zoning trends consistent with garnet growth being due to a single reaction. The majority of the paths show an overall increase in Alm (with relatively constant Prp) with falling Sps (and Grs) for core to rim. These paths show the similarity in trends of element concentration within garnets from different lithologies. AFM topologies {4.1.4} suggest that the peak assemblage Grt + St + Bt was produced by the consumption of chlorite in a reaction leading to the formation of a tie - line defining the field Grt + St + Bt (the staurolite + biotite isograd of Carmichael, 1970). Certain of the paths show an increase in Sps at the garnet rim. This style of zoning was modelled by Kretz (1973) and Trzienski (1977) as being due to garnet growth involving the consumption of Mn bearing chlorite. In such models the diffusion rate of Mn in chlorite is considered to be greater than the rate of reaction with the result that the core of the chlorite becomes relatively enriched in Mn during the removal of chlorite from the reaction system. When the remnant chlorite is finally consumed it releases Mn into the reaction system, resulting in an increase in Mn (Sps end member) in garnet.

The ternary plot (Figure 4.17b) of Alm, Grs and Prp shows an

**Figure 4.16: Typical zoning profile seen in regional metamorphosed garnet (Hollister 1966).**

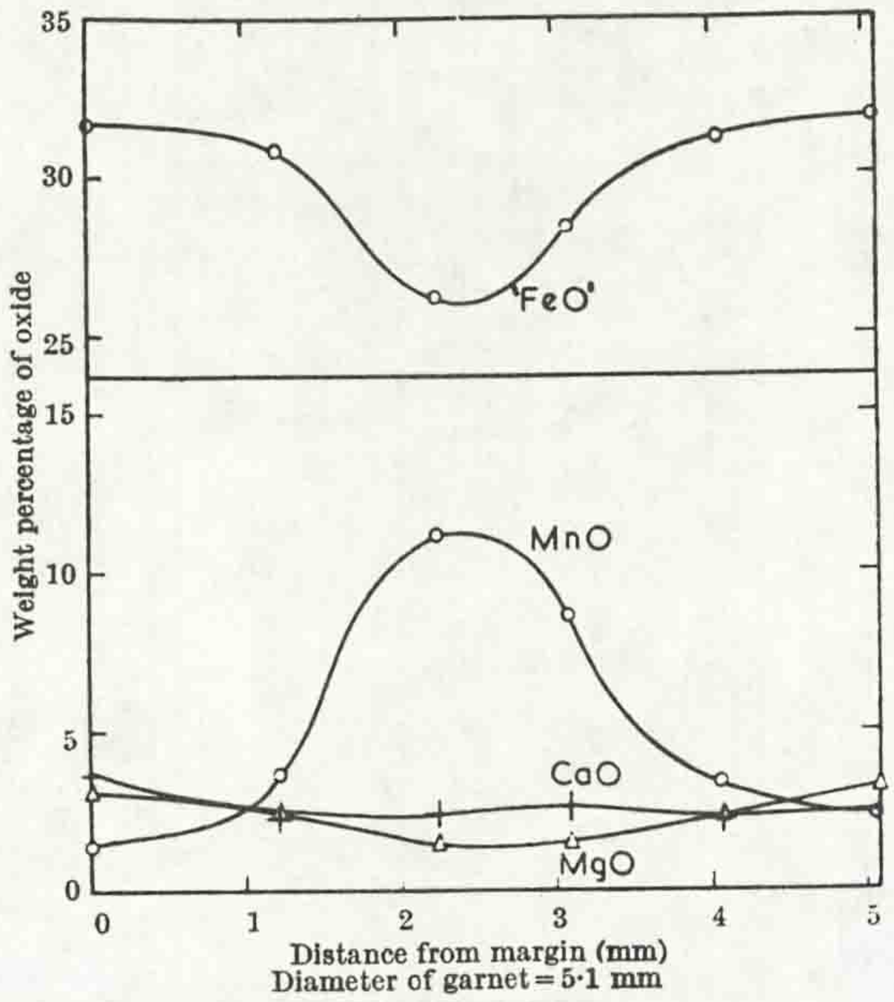

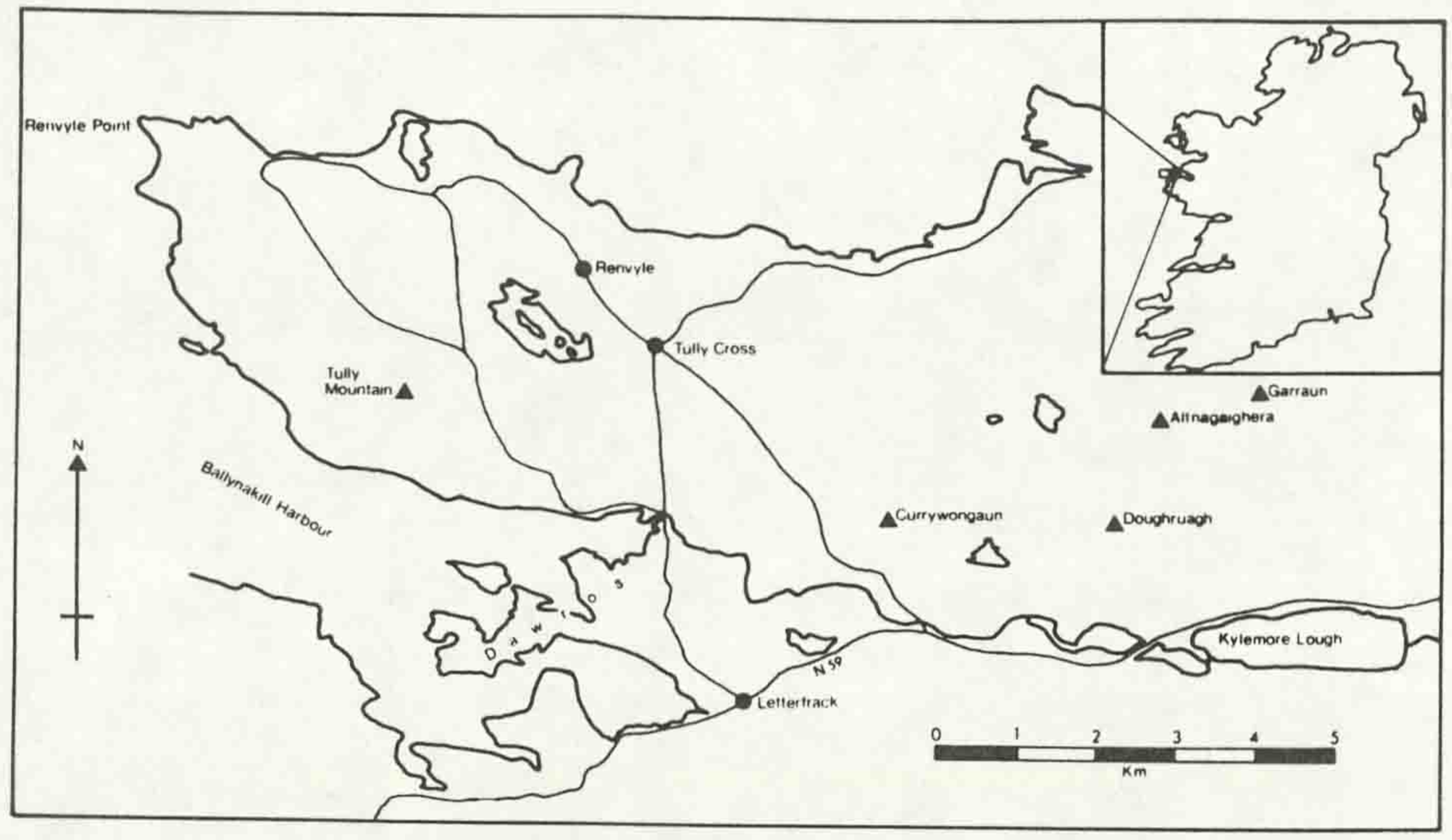


Figure 1.1. Location and key features of the study area.

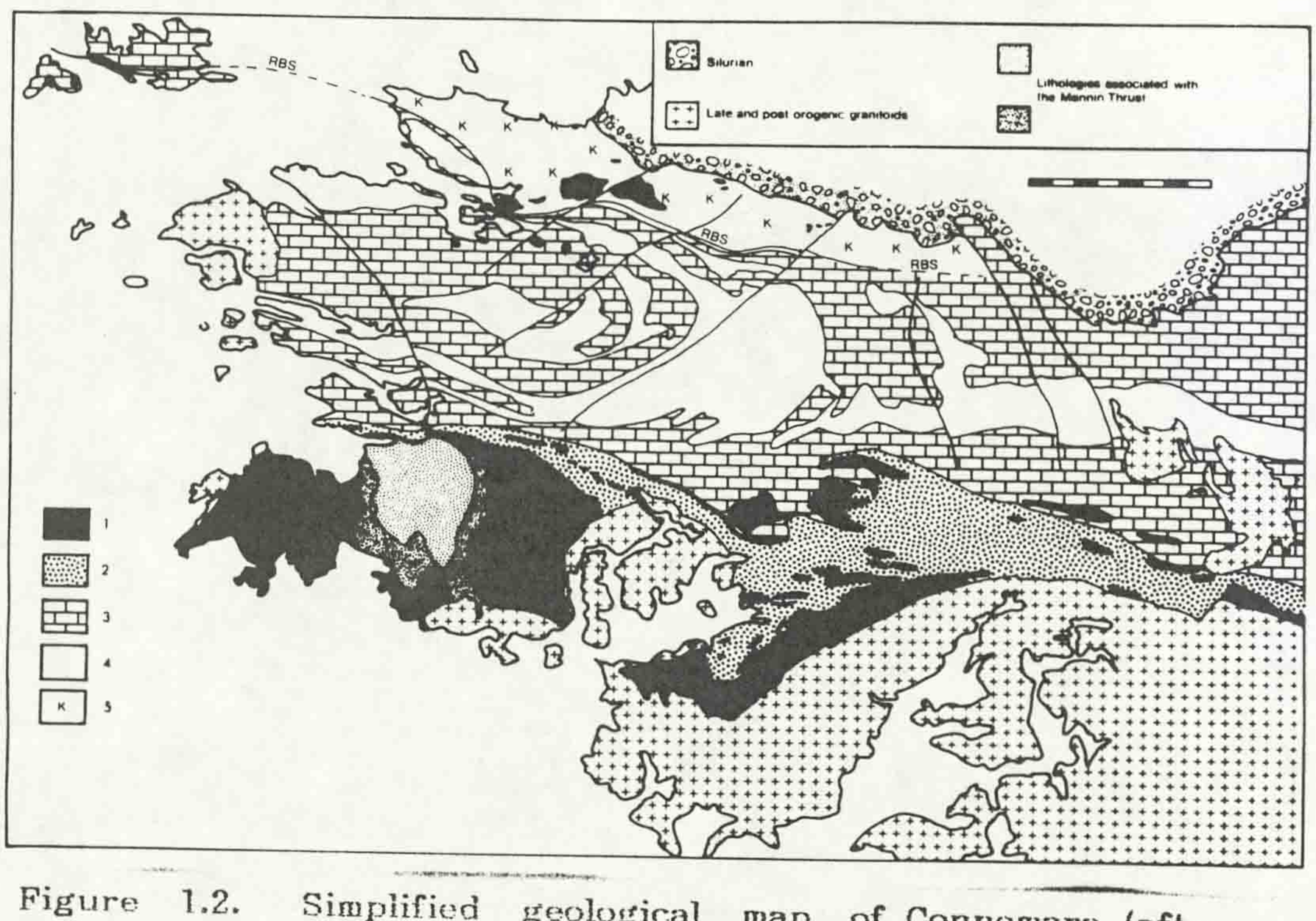


Figure 1.2. Simplified geological map of Connemara (after Leake, Tanner & Senior 1983. 1: Basic and ultrabasic igneous bodies, 2: Migmatitic and synorogenic intrusive lithologies, 3: Middle to Upper Argyll Group Dalradian lithologies (Lakes Marble, Streamstown, Ballynakill and Cornamona Formations), 4: Lower Argyll and Appin Group Dalradian lithologies (Bennabeola Quartzite, Cleggan Boulder Bed, Barnanoraun, Connemara Marble and Clifden Formations), 5: Kylemore Formation. RBS: Renvyle - Bofin Slide.

**Figure 4.17: Ternary plots of end member concentration in regional garnets (after Tracy 1982):**
**a, Alm, Sps, Prp ternary diagram,**

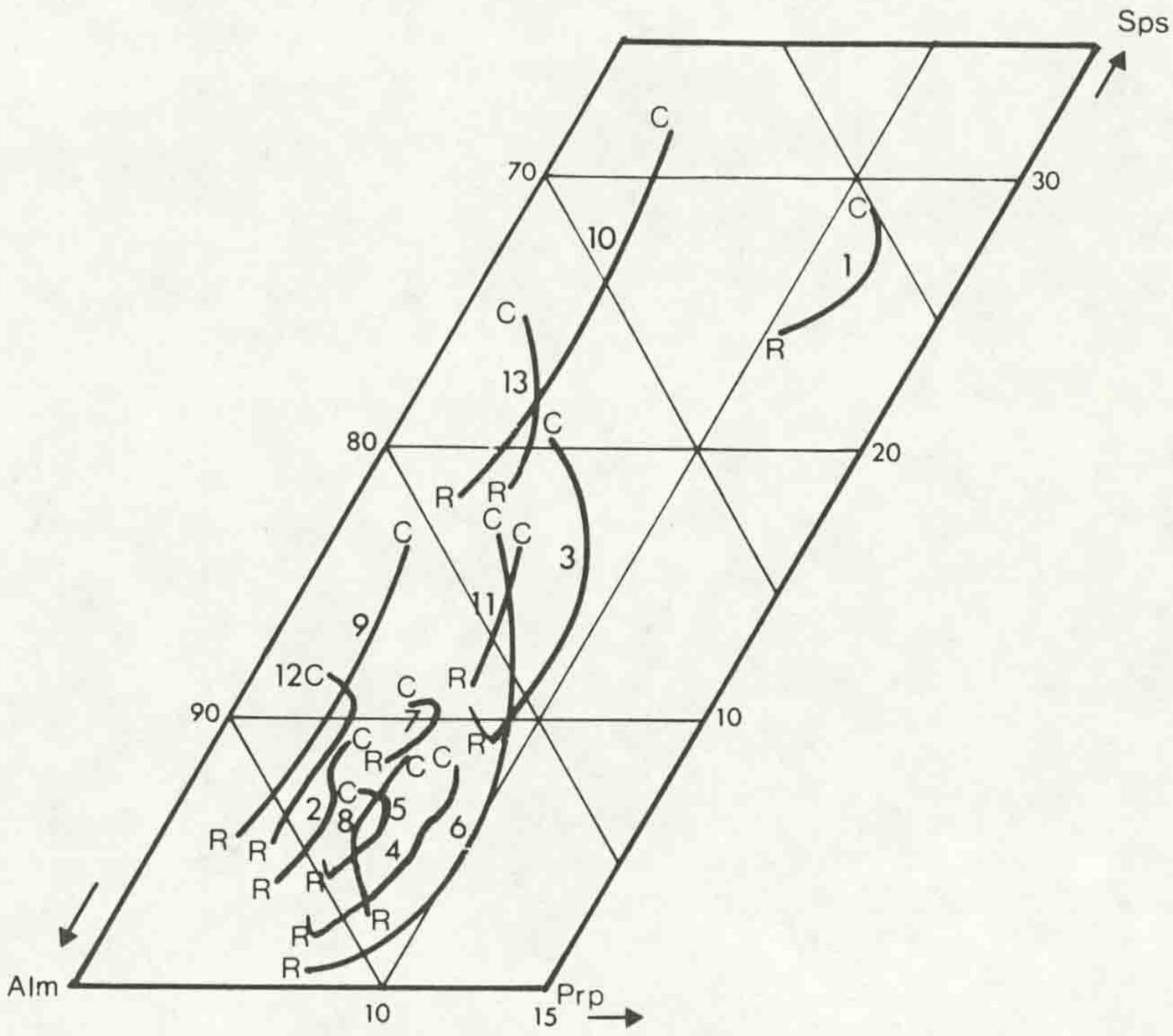


1, 68806.
2, 69229.
3, 69230.
4, 69236.
5, 69238.
6, 69277.
7, 69317.
8, 69623.
9, 71912.
10, 71916.
11, 71923.
12, 71934.

**b, Alm, Grs, Prp ternary diagram.**

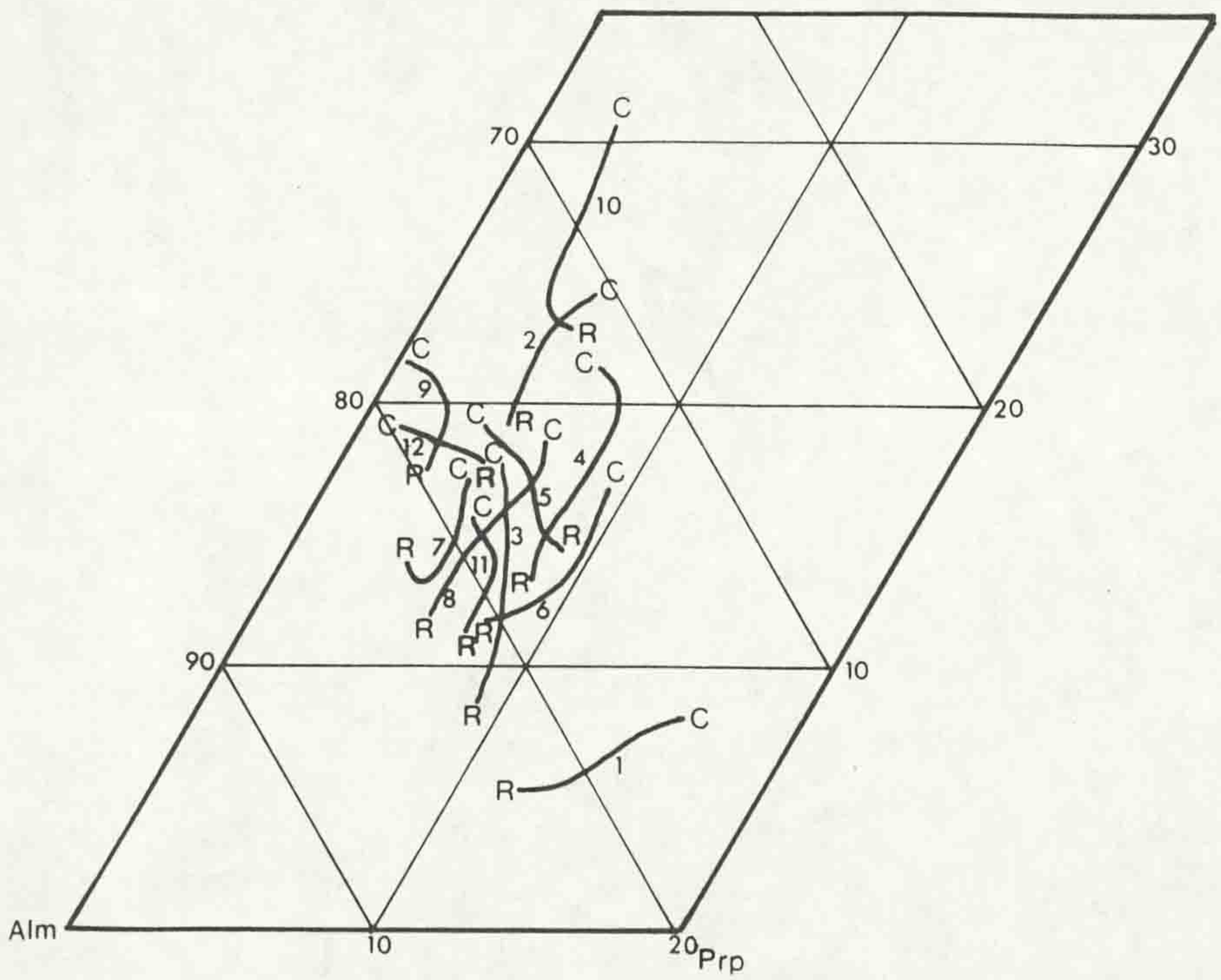


1, 68806.
2, 69229.
3, 69230.
4, 69236.
5, 69238.
6, 69277.
7, 69317.
8, 69623.
9, 71912.
10, 71916.
11, 71923.
12, 71934.

increase of Alm, with constant or falling Prp, and decreasing Grs from core to rim. Some of these paths are slightly more complex than the Sps paths, but the overall compositional trend for regional metamorphic garnets remains relatively consistent.

The preservation of zoning within garnets requires that the intracrystalline diffusion rate is sufficiently slow to allow compositional gradients to persist. The rate of cation diffusion in garnet is largely temperature controlled (Lasaga 1983) and it is suggested (Yardley 1977a) that at temperatures below 640° C ± 30° C diffusional re - equilibration of compositional zoning in garnet is not significant. The regional pelitic assemblages containing compositionally zoned garnets in the study area yield mean temperatures (calculated by exchange thermobarometry {5.4}) of 510 ± 65° C suggesting that the zoning represents an original growth feature and not the effects of intracrystalline diffusion.

At temperatures above 640° C ± 30° C, at or near the the Sil + Kfs - in isograd (Tracy, 1982), the effects of cation diffusion in garnet become increasingly significant with the effect that chemical gradients within garnets tend to be reduced. The mean temperatures calculated by cation exchange thermometry {5.4} for contact aureole rocks are 769 ± 95° C for sillimanite - bearing, and 695 ± 64° for non - sillimanite - bearing assemblages. These results suggest the temperatures developed in the aureole were sufficiently high to allow intracrystalline diffusion processes to be significant. At such temperatures it is possible that any pre - existing compositional zoning could be lost, the garnet tending to become compositionally homogeneous. Incomplete homogenisation of pre - existing compositional zonation results in 'flattened' zoning profiles (Anderson & Olimpio, 1977), where profiles retain the form of any initial compositional variation but the magnitude of variation is greatly reduced from the 'original' profile. The restricted compositional ranges evident within the normally zoned contact garnets (66795, 68804) are likely to be the result of diffusional homogenisation of compositional zoning.

The reverse zoned profiles seen in garnets 68793, 68799, 69215 and 69219 are also the result of diffusional zoning, with

**Figure 4.18: Ternary plots of end member concentration in contact garnets (after Tracy 1982):**
**a, Alm, Sps, Prp ternary diagram.**

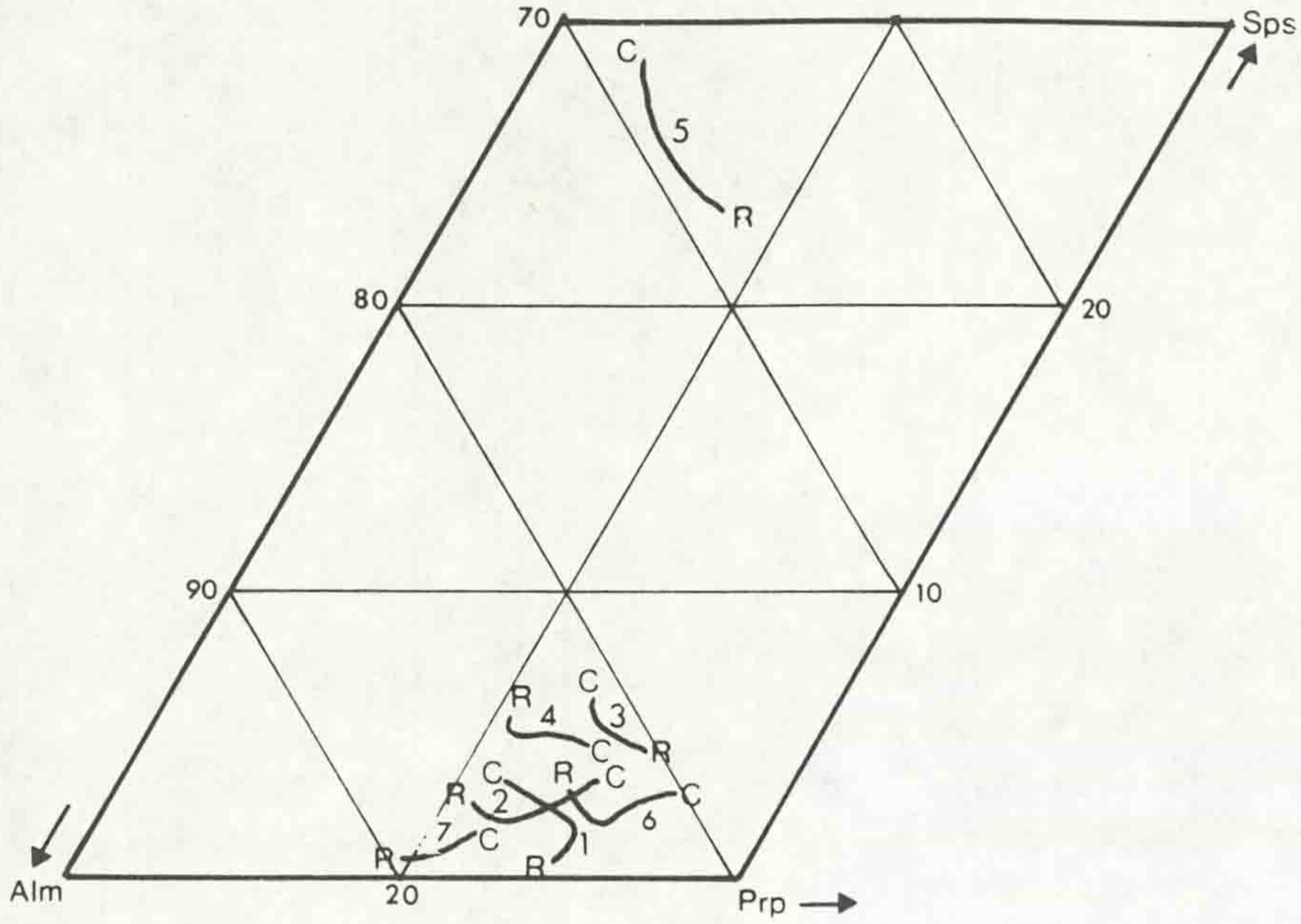


1, 66795.
2, 68780.
3, 68793.
4, 68799.
5, 68804.
6, 69215.
7, 69219.

**b, Alm, Grs, Prp ternary diagram.**

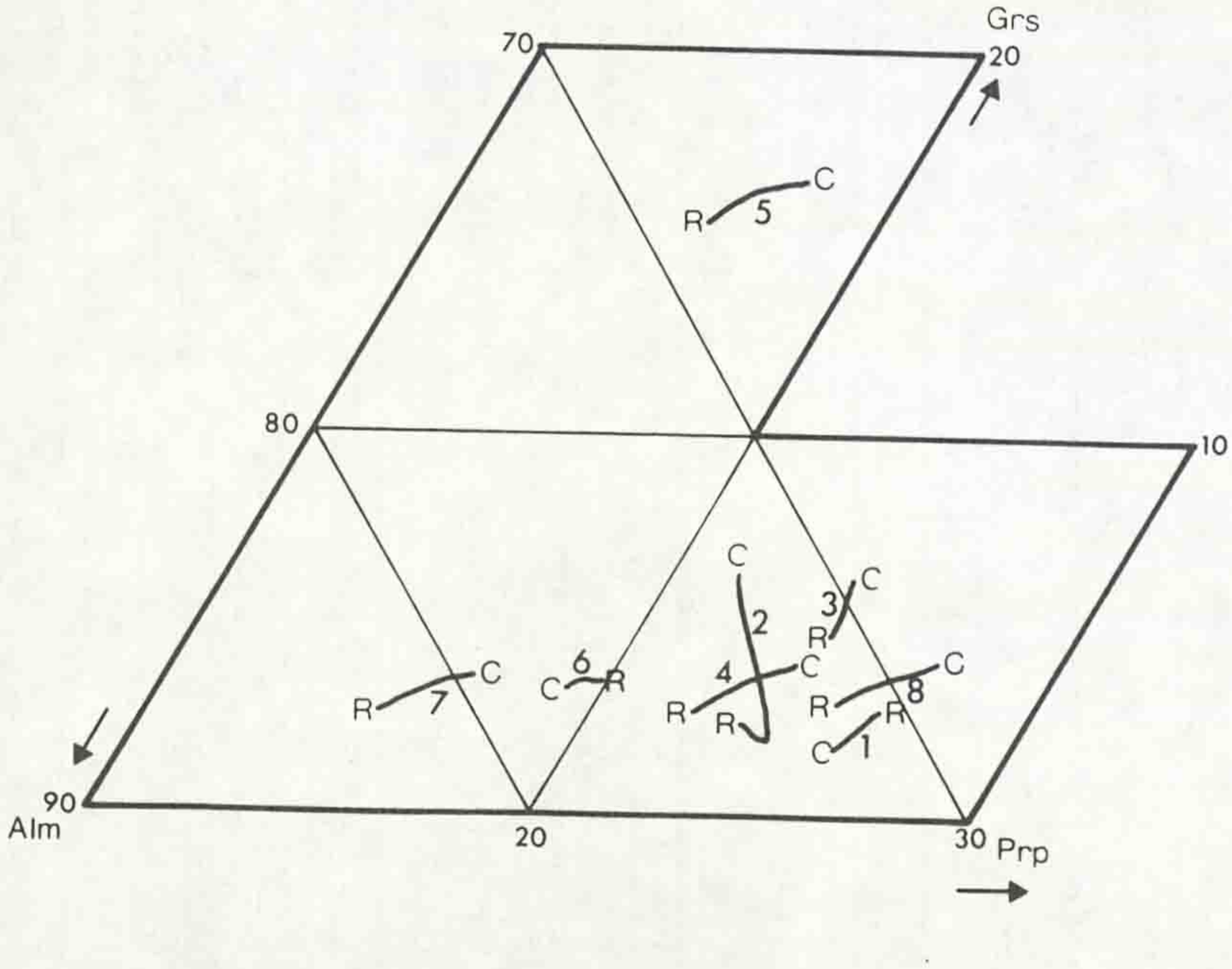


1, 66795.
2, 68780.
3, 68793.
4, 68799.
5, 68804.
6, 69215.
7, 69219.

**Figure 4.19: Biotite developed in $S_2$ foliation (X 29) PPL.**

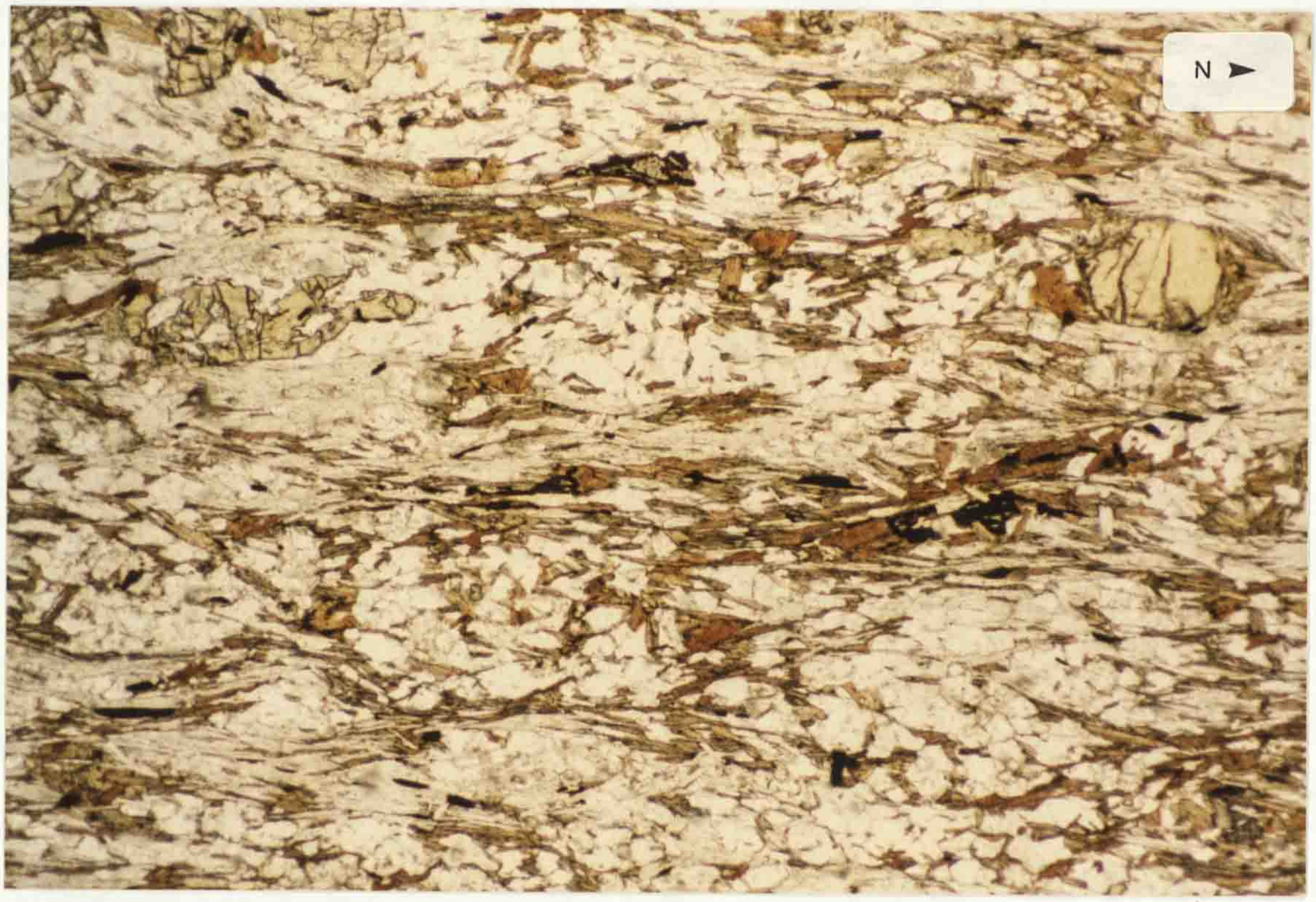


**Figure 4.20: Irregular decussate biotite developed within aureole lithologies (X 29) PPL.**

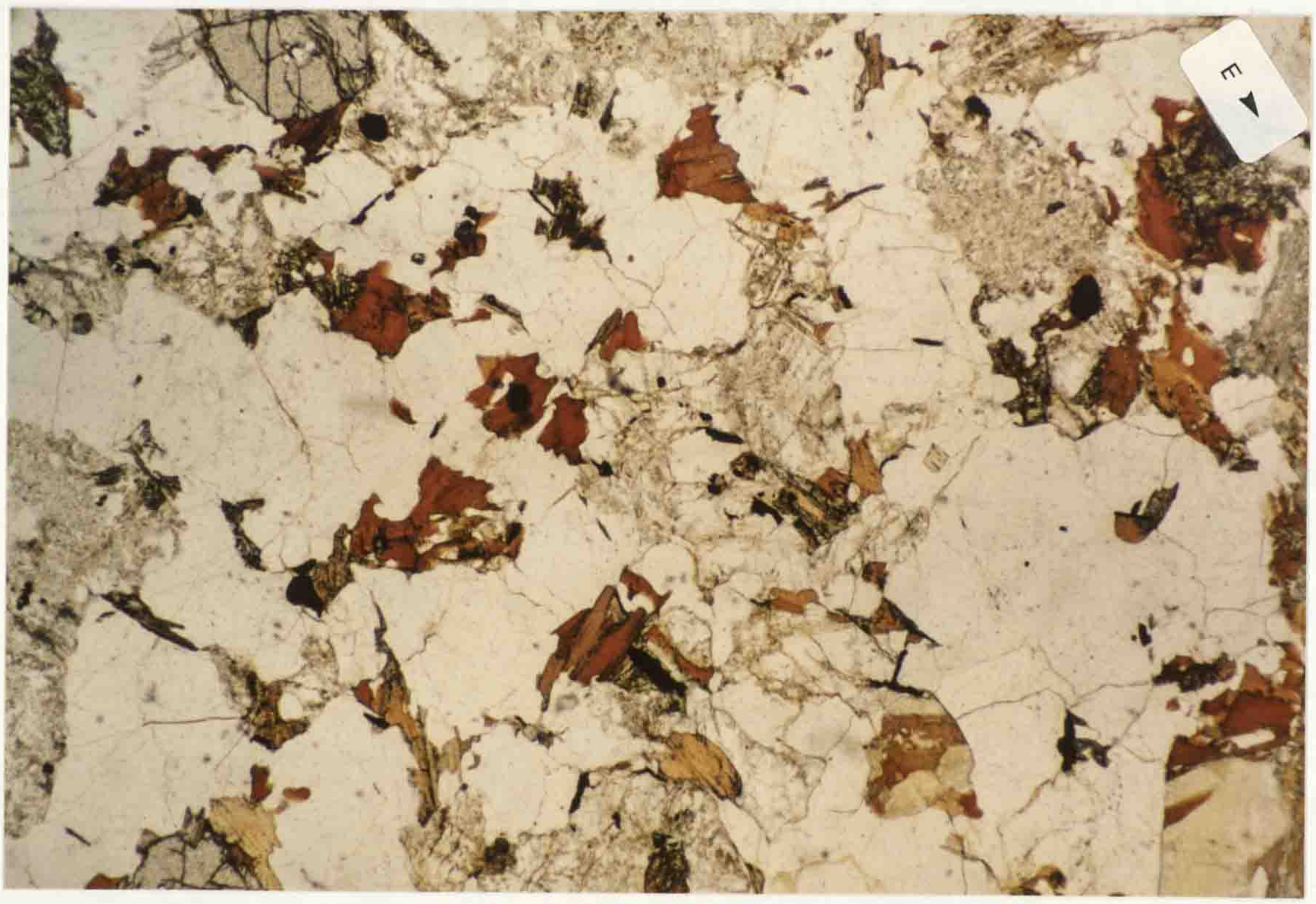

**Figure 4.21: Porphyroblastic biotite within regional metamorphic lithologies (X 29) PPL. Note the pleiochroic haloes developed around included zircon grains.**

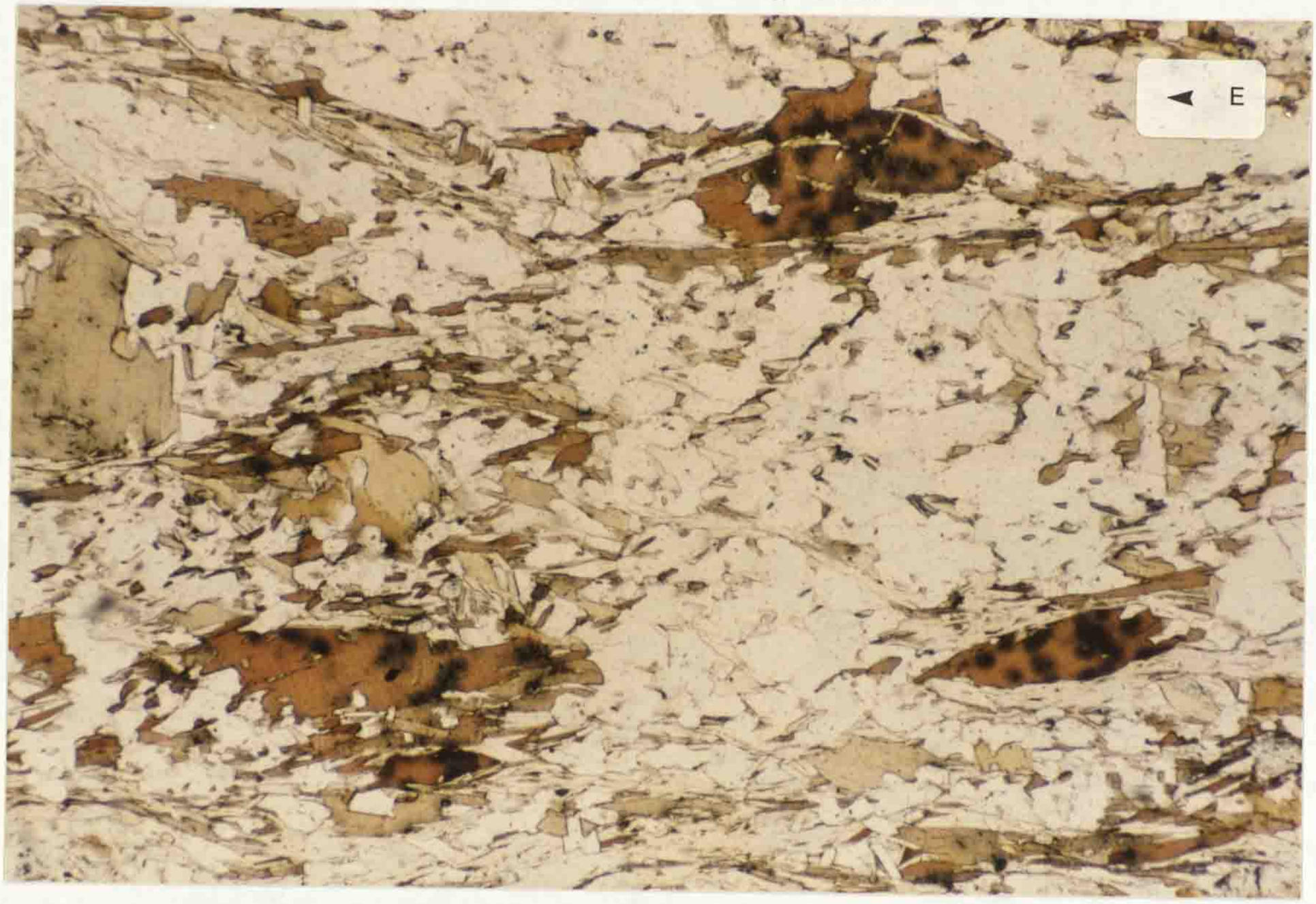


**Figure 4.22: Regional Metamorphic MFM biotite V. MFM whole rock**

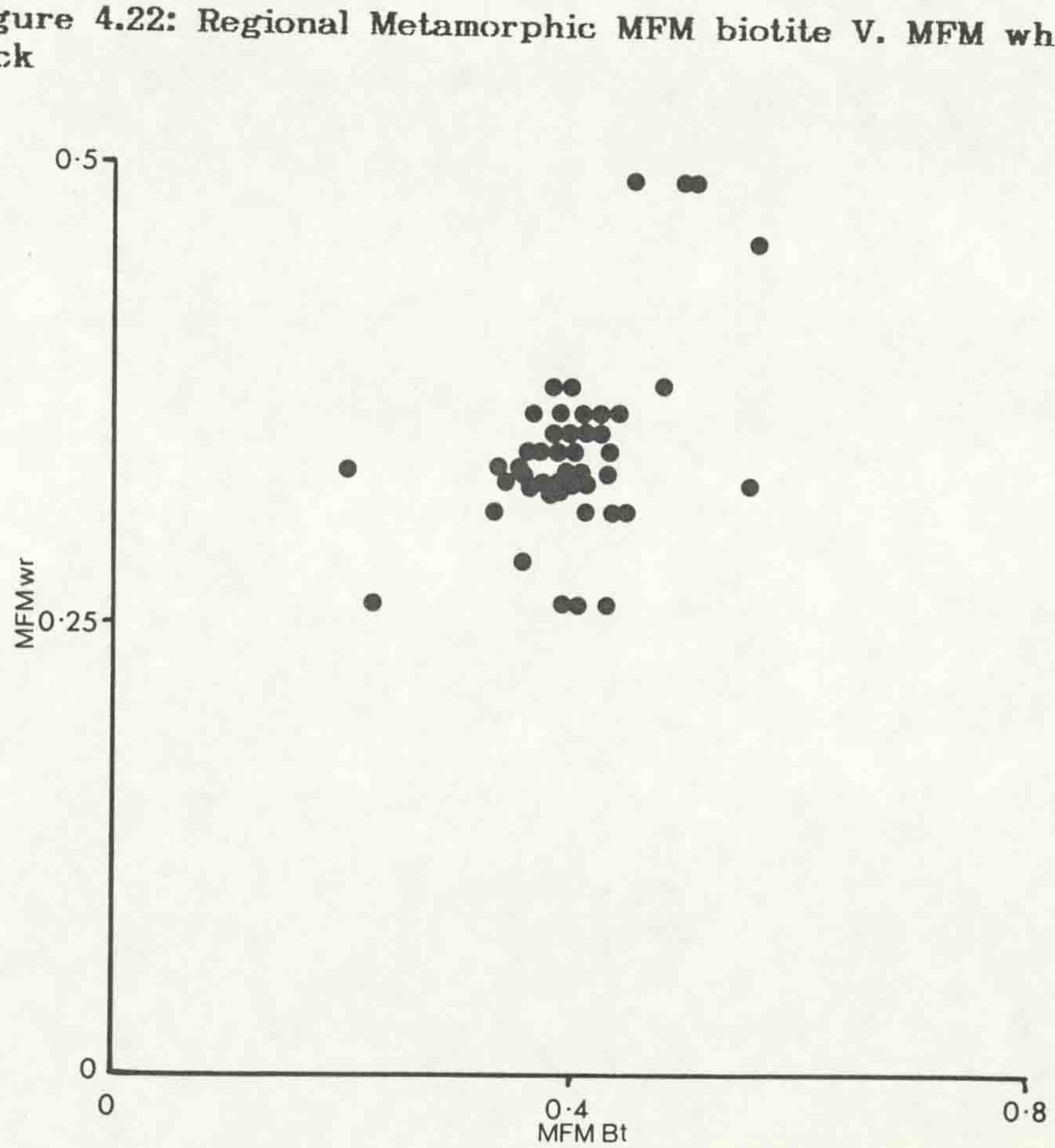

diffusion occurring during the retrograde stage of metamorphism. Two main mechanisms for the production of reverse zoning are suggested, cation exchange between garnet and coexisting ferromagnesian minerals (mainly biotite) during retrogression (Tracy, Robinson & Thompson 1976), and the retrograde resorption of garnet rims with Mn selectively diffusing into the garnet rim and enriching it (De Bethune 1975).* The garnets with reverse zoning show no clear evidence of retrogression, but are associated with ferromagnesian minerals (biotite), suggesting that retrograde cation exchange effects have produced the zoning. The reaction invoked by Tracy *et al.* (1976):

$Grt + Kfs + H_2O = Bt + Al_2SiO_5 + Qtz$

results in the effective depletion of the garnet rim of Fe.

Ternary plots of the contact garnet data (Figure 4.18) yield core to rim paths different in form to those seen in regional garnets. The relative shortness of the paths reflects the relative homogeneity of aureole garnets. An overall increase in Alm with falling Sps is apparent, although Prp shows more variation than in regional garnets. The paths for garnets 68780, 68799, 69219 show the increase in Sps seen in their profiles. The form of these 'tails' of Sps enrichment is identical to those described by Tracy (1982) as being due to retrograde cation exchange between garnet and biotite, further indicating that this mechanism is likely to be the cause of the zoning.

* De Bethune, Laduron & Bocquet (1975)

4.1.3.2 Biotite: Biotite is common throughout the study area, being developed in pelitic and semipelitic lithologies with both regional and contact metamorphic assemblages. A wide range of crystal habits are developed, ranging from subhedral foliation parallel forms within regional lithologies (Figure 4.19) to decussate anhedral crystals within granoblastic aureole lithologies (Figure 4.20).

Biotite within regionally metamorphosed schistose lithologies is typically fine grained ( >0.5mm) with porphyroblastic grains up to 2mm sometimes being present (Figure 4.21). Inclusion fabrics within biotites are rare, although randomly orientated zircon grains are seen (Figure 4.21). Biotite is developed within the dominant regional fabric ($S_2$) and shows evidence of deformation (strained grains) in $S_3$ crenulation fabrics

**Figure 4.23: Fe2 + Mg V. AlVI + Ti in all analysed biotites showing the relation to ideal biotite compositions (dots represent regional biotites, triangles represent contact biotites).**

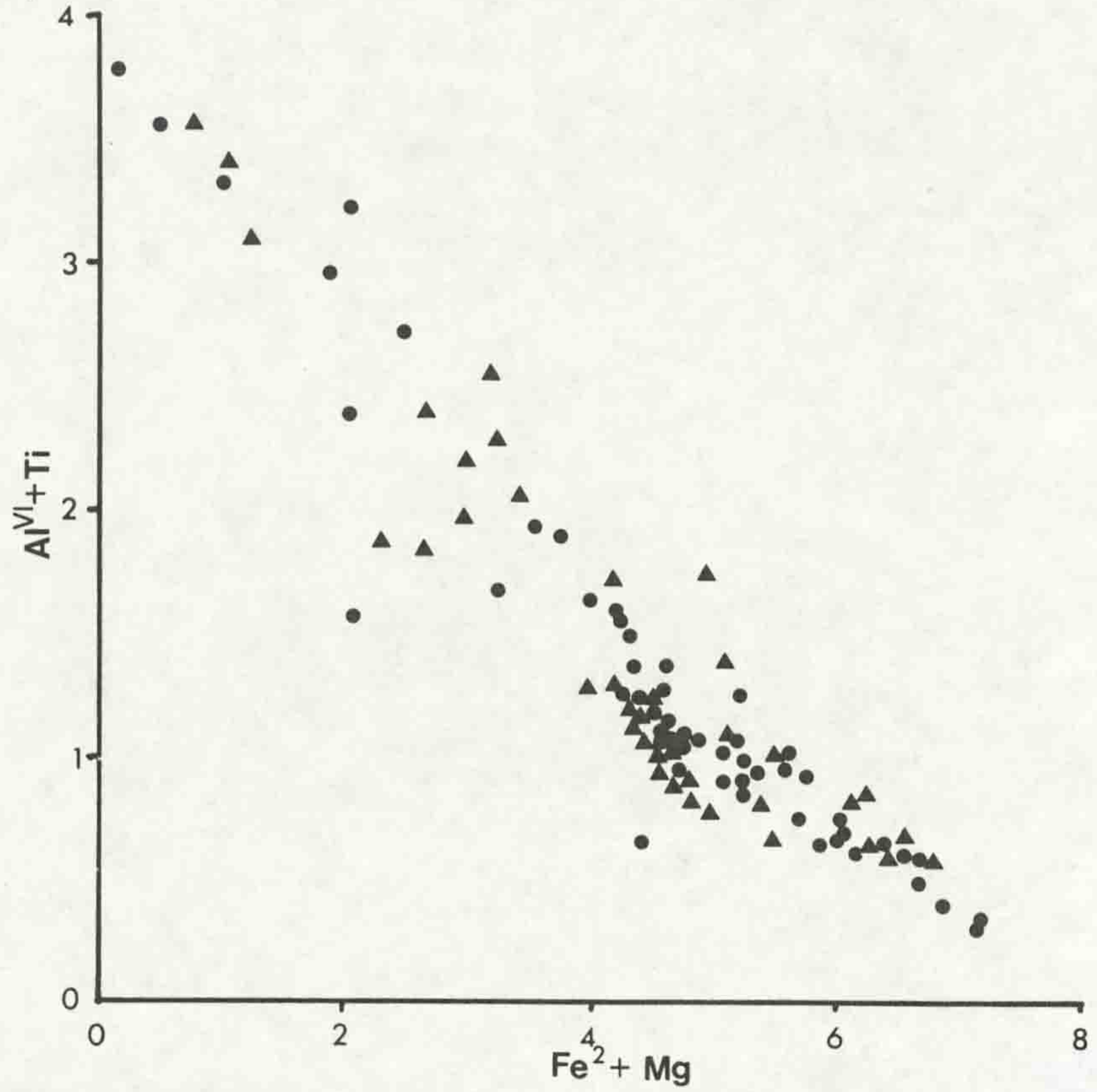


**Figure 4.24: Mesh of fine rutile needles developed in contact biotite (X 110) PPL.**

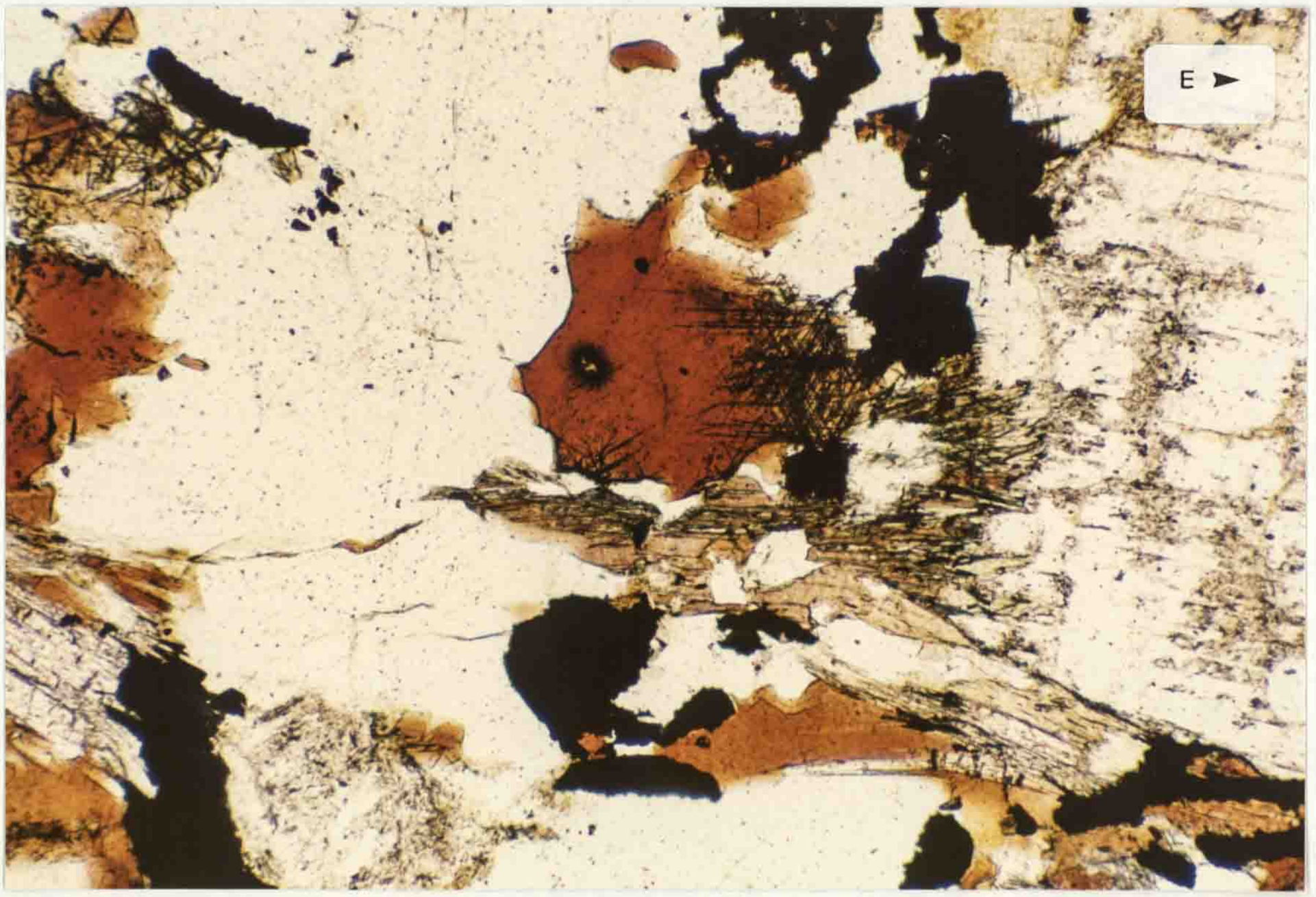

**Figure 4.25: Contact biotite MFM V. MFM whole rock.**

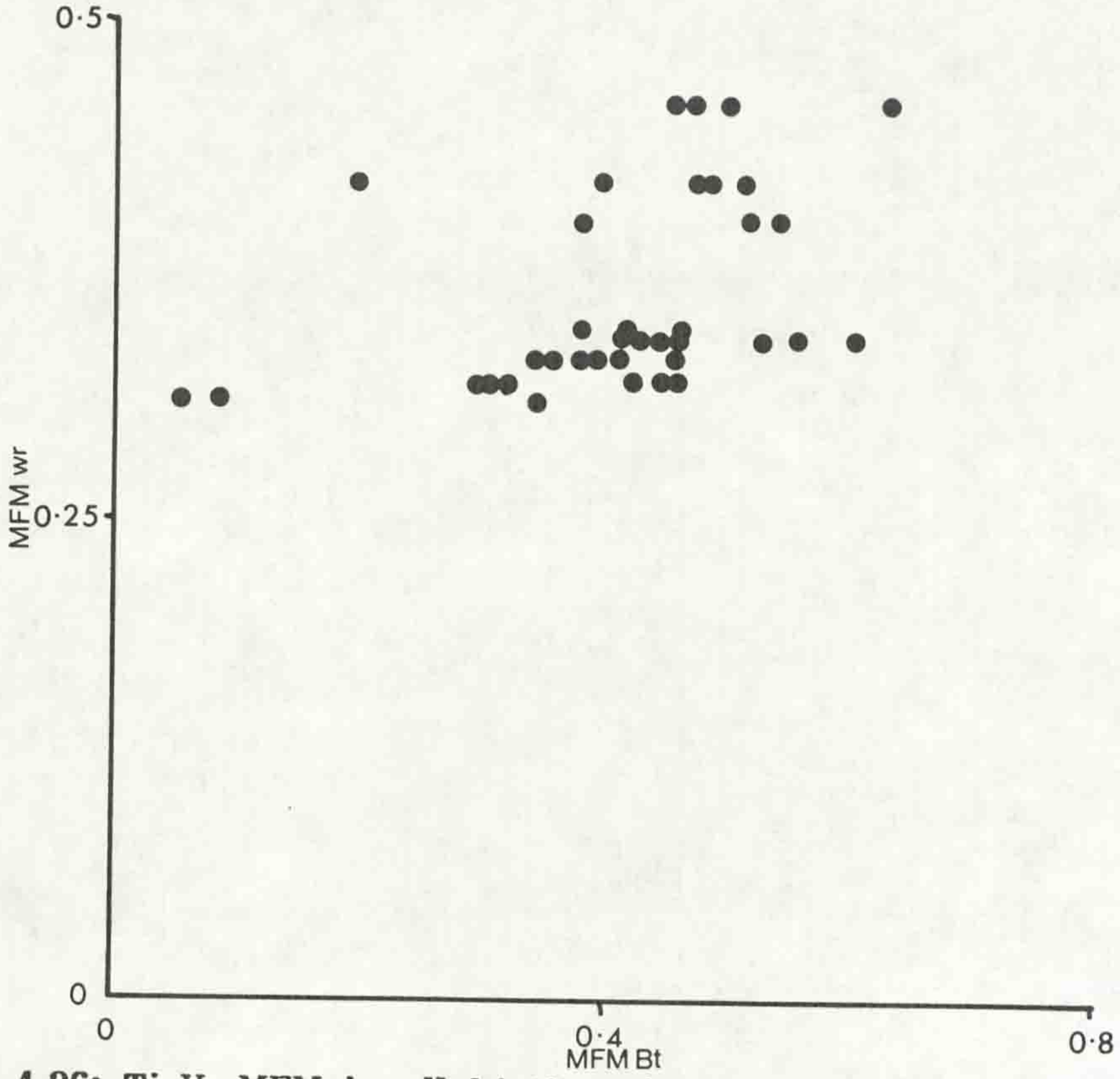


**Figure 4.26: Ti V. MFM in all biotites (dots represent regional metamorphic biotites, triangles represent contact biotites).**

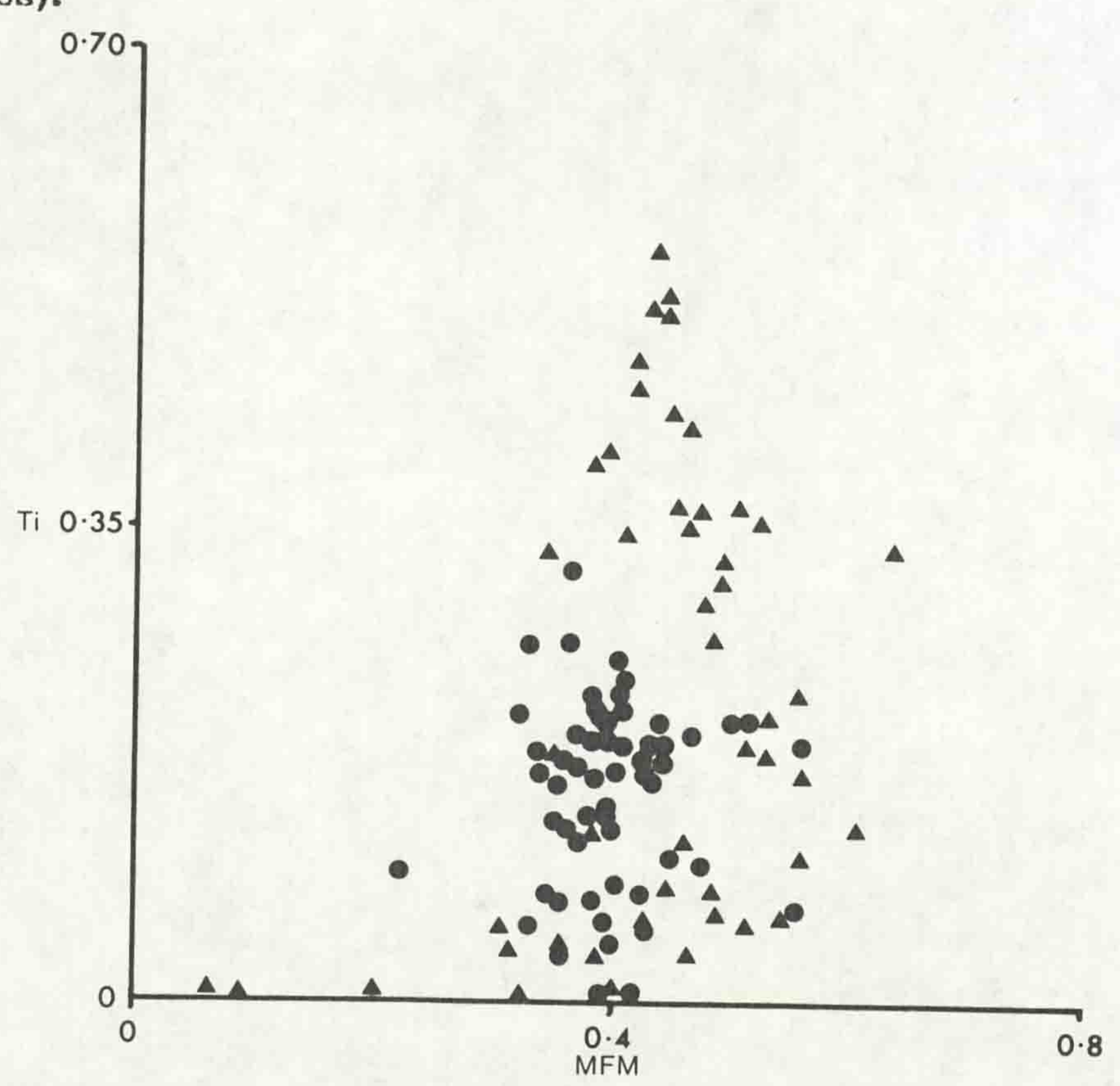

{3.2}. It also occurs within the mylonitic fabrics associated with ductile displacement on the RBS {3.3}. Where $S_2$ biotite fabrics are strongly deformed by $S_3$ the biotites are often replaced by chloritic micas {4.1.3.4.}. Where unaffected by such replacement regional biotites are strongly yellow to red - brown pleochroic, a colouration suggestive of either high $Fe^{2+}$ or Ti compositions (Guidotti 1984). Where chloritic retrogression of assemblages is evident biotites are often green to brown pleochroic, suggesting higher ferric iron than those biotites within less retrogressed lithologies.

The mean formula of the regional metamorphic biotites is:

$$K_{1.074}\ Mg_{1.859}\ Fe_{2.836}\ Ti_{0.165}\ Al^{VI}_{2.648}\ Al^{IV}_{1.116}\ Si_{5.361}\ O_{20}\ (OH)_2$$

No evidence for compositional zoning in individual biotites was found.

The MFM ratios for regional biotites range from 0.225 to 0.561, with a mean of 0.397. No direct correlation is apparent in a plot of MFM ratios in biotite and MFM whole rock, the data being somewhat clusters (Figure 4.22).

The substitution of $Al^{VI}$ + Ti for Fe + Mg in octahedral sites is well documented (e.g. Guidotti 1984) and shows a strong linear negative relationship in the analysed biotites (Figure 4.23). The $TiO_2$ contents of the regional metamorphic biotites show a relatively wide range, from below detection limits to 2.892 wt%. The presence of a coexisting Ti rich phase, ilmenite, suggests that biotites are Ti - saturated. The occurrence of ilmenite also suggests (Guidotti 1984) that the lithology is relatively low in ferric iron, an observation which supports the compositions suggested by the biotite colours.

In contrast to the limited variation in form seen in regional metamorphic biotites, those developed in contact aureole lithologies display a wide range of textures. Within granoblastic lithologies, biotites reach grain sizes up to 2mm, with 0.5 - 1 mm grains being most common. These grains show no prefered orientation, although where a pre - existing compositional banding is developed variably orientated biotites replace the original phyllosilcates. In granoblastic lithologies the development of fibrolite and prismatic sillimanite is often associated with biotite grains {4.1.3.8}. Where mylonitic fabrics are present in aureole lithologies {3.2.2.4, 3.4} biotite

and sillimanite are developed in anastomosing zones which wrap porphyroclastic/blastic garnets and feldspars. The biotite and sillimanite zones are interpreted as representing high strain zones (after Vernon 1987) within the mylonitic lithology {4.1.3.8}.

Inclusion fabrics within aureole biotites are rare, although fine meshes of rutile needles are seen (Figure 4.24) in basal sections. These rutile inclusions are apparently crystallographically controlled, suggesting that the rutile is either intergrown with, or exsolved from, the biotite. The colour of contact aureole biotites is generally strongly pleochroic yellow to red - brown, although in lithologies where högbomite is present the pleochroism tends to greener brown colours, suggesting a relatively oxidising environment was prevalent during the development of the mineral assemblage.

The mean formula of contact biotites is:

$$K_{1.147}\ Mg_{1.923}\ Fe_{2.451}\ Ti_{0.234}\ Al^{VI}_{2.470}\ Al^{IV}_{1.132}\ Si_{5.538}\ O_{20}\ (OH)_2$$

No evidence for compositional zoning in biotite grains was seen.

The range in MFM ratios for contact biotites is from 0.201 to 0.767, with a mean of 0.443, and as with regional biotites no clear correlation between MFM in biotite and in whole rocks MFM is apparent (Figure 4.25). The mean Ti concentrations in contact biotites is somewhat higher than in regional biotites, with a range from below detection limits to 6.419 wt%. The presence of rutile within biotites suggests that the biotites are Ti - saturated. The association of higher Ti content in biotite with coexisting rutile with higher metamorphic grade is well established (e.g. Kwak 1968, Dymek 1983). A plot of MFM against Ti for regional and contact biotites (Figure 4.26) shows the wider range of Ti contents in contact biotites. It is possible that the spread of Ti content in contact biotites may be due to down temperature re - equilibration of Ti - rich contact biotites to give a Ti mineral and Ti - poor biotite. The Ti contents of contact biotites which are associated with rutile meshes are lower than biotites in the same rock which show few or no rutile inclusions, suggesting that the development of rutile has resulted in the loss of Ti from the biotite, possibly through exsolution.

The massif shows a complex structural history. The main regional structure is the E-W trending, open, Connemara antiform ($F_4$ Tanner & Shackleton 1979) around which are deformed features produced in two earlier deformational events. E-W trending $F_3$ folds (the '*Glencoaghan*' phase of Tanner & Shackleton) deform an earlier set ($F_2$) of southerly closing and facing nappe-scale folds (the '*Derryclare anticline*' phase, Tanner & Shackleton; Leake, Tanner, Singh & Halliday 1983). The $F_3$ folding possibly represents a northerly directed 'backfolding' event post-dating the emplacement of the $D_2$ structures (Ferguson & Al-Ameen 1986). Mesoscopic evidence for $D_1$ is limited, the main evidence for the existence of this event being microscopic, and based on the existence of pre - $D_2$ fabrics preserved within $MS_2$ garnets (e.g. Badley 1976, Treloar 1982). The existence of tectonic slides which disrupt and thin the stratigraphic sequence has been proposed (Tanner & Shackleton 1979). One such slide, the Renvyle - Bofin slide (RBS) (Cruse 1963), runs through the study area. This slide separates a sequence of psammites, semi-pelites, and pelites (the Kylemore Formation, Morris & Tanner 1977) containing basic and ultrabasic igneous bodies (the Dawros - Currywongaun - Doughruagh igneous complex, DCD), against a well stratified sequence of metasediments (the Ballynakill, Lakes Marble, Streamstown, and Bennabeola Quartzite Formations of Tanner & Shackleton 1979).

Leake, Tanner, Singh & Halliday(1983) noted the existence of a major ductile thrust zone (the Mannin Thrust) in southern Connemara and postulated that this feature ran under the whole of Connemara, with the massif being emplaced southwards ( >50km), over a now deformed and metamorphosed sequence of possibly Ordovician acid volcanics (the Delaney Dome Formation). Leake *et al.* (1984) concluded that this southerly directed emplacement was associated with major uplift and occurred at 454Ma either during the late stages of, or immediately after, $D_3$. The existence of such a major displacement zone, which is considered to underlie the entire massif, has led to the interpretation of Connemara as a major allochthon.

The metamorphic evolution of Connemara (Yardley, Barber & Gray 1987) shows a simple two phase development:

4.1.3.3 Muscovite: Muscovite is developed in a wide range of lithologies throughout the study area. With biotite it defines the $S_2$ foliation in regional metamorphic pelites and semipelites (Figure 4.27) {3.2}. Muscovite is often absent from sillimanite bearing aureole lithologies, K - feldspar being developed instead {4.1.3.6}. In the migmatitic aureole lithologies, muscovite is commonly present as a porphyroblastic phase, most apparent in quartz - tourmaline - muscovite veins and segregations. The porphyroblastic muscovites are typically sub to euhedral, and can reach grain sizes of up to 20 - 30mm, although 3 - 5mm porphyroblasts are more usual. Porphyroblastic muscovites occurring within foliated lithologies are less regular in form than those developed in vein associations (Figure 4.28).

The mean composition of regional muscovites is:

$$K_{1.621}\ Na_{0.212}\ Fe_{0.288}\ Mg_{0.106}\ Al^{IV}_{1.758}\ Si_{6.242}\ Al^{VI}_{3.640}\ O_{20}\ (OH)_2$$

Contact muscovites have a mean composition of:

$$K_{1.798}\ Na_{0.083}\ Fe_{0.268}\ Mg_{0.052}\ Al^{IV}_{1.795}\ Si_{6.205}\ Al^{VI}_{3.160}\ O_{20}\ (OH)_2$$

Analyses of muscovite are tabulated in {Appendix C}. The compositions of both the regional and contact muscovites suggest that both phengitic (Mg) and paragonitic (Na) substitutions are present. Values of Si : $Al^{IV}$ in excess of 3 indicate that muscovites contain phengite (Deer, Howie & Zussman 1966). The analysed muscovites yield mean values of 3.550 for regional muscovites and 3.456 for contact muscovites. A plot of $Al^{VI}$ v. ($Fe^{2+}$ + Mg) (Figure 4.29) shows that the degree of phengitic substitution is relatively low, the bulk of analyses plotting near to muscovite composition. Paragonitic substitution in muscovite occurs when Na replaces K, and a plot of K v. Na for muscovites containing Na (Figure 4.30), although showing a degree of scatter (probably due to either probe error or lattice vacancies), has the expected inverse ratio between the two cations.

Figure 4.31 shows a plot of Al content against (Fe + Mg + Si), the primary octahedral cations, and indicates that the data plot close to an ideal Tschermak substitution although they are displaced away from the ideal. This scatter away from the ideal Tschermak line may be due to dioctahedral - trioctohedral substitution, to the presence of minor amounts of $Fe^{3+}$, or to the effects of probe error. As noted in {4.1.3.2} evidence

**Figure 4.27: Muscovite in $S_2$ foliation (X 110) PPL.**

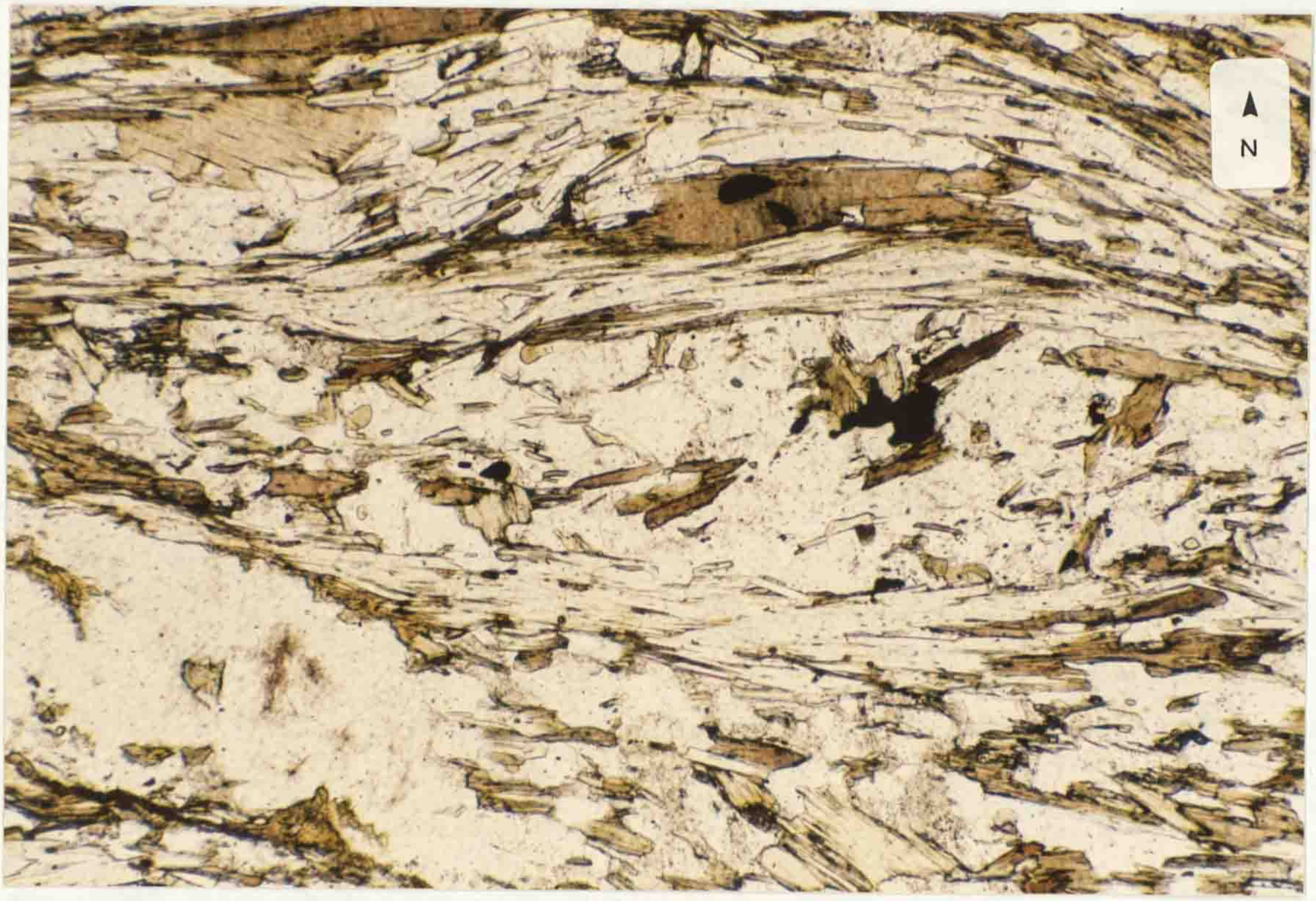


**Figure 4.28: Porphyroblastic muscovite in migmatitic contact aureole lithology (X 29) PPL.**

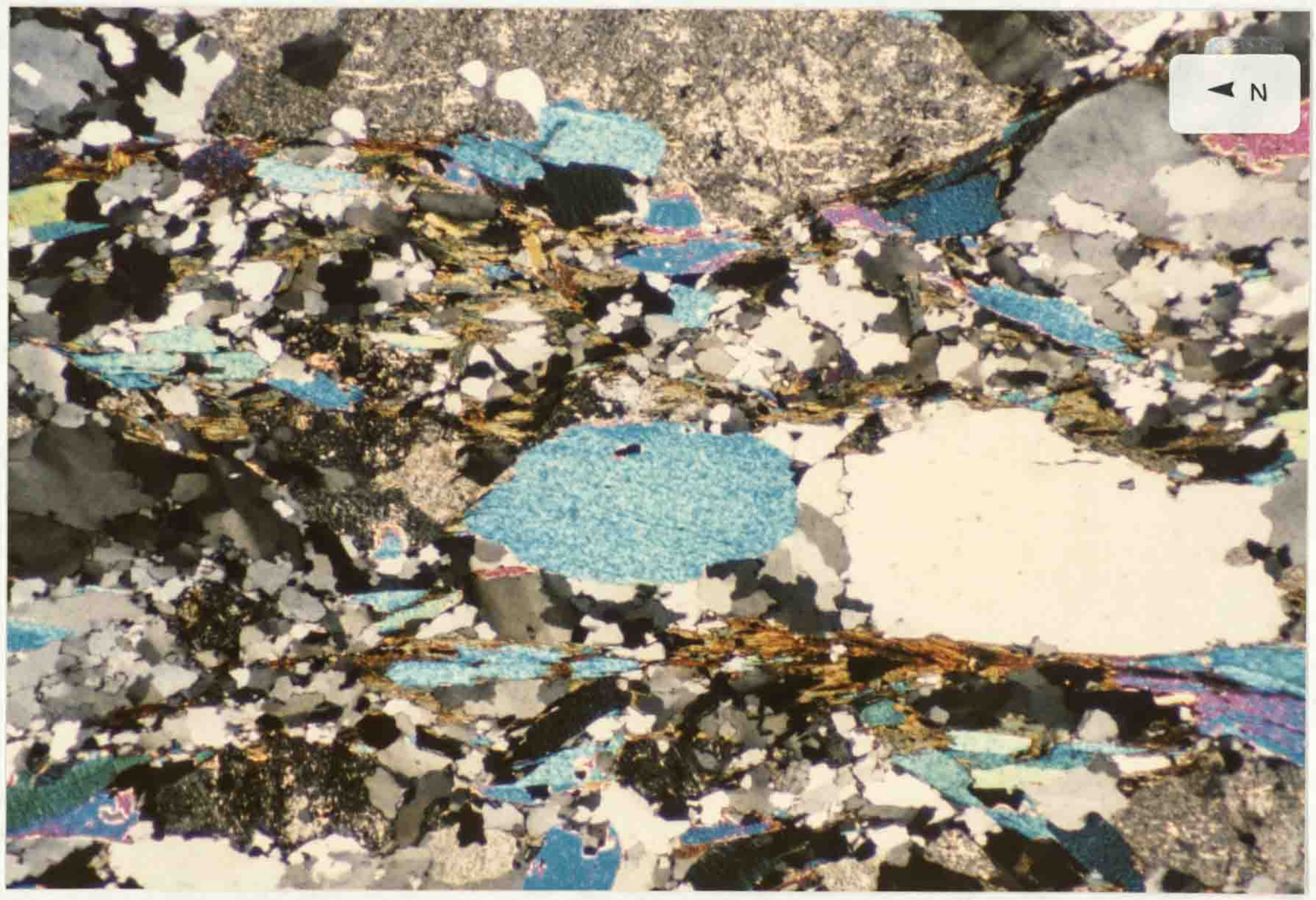

**Figure 4.29: $Al^{VI}$ V. ($Fe^{2+}$ + Mg) plot showing the degree of phengitic substitution in muscovite (P = phengite, M = muscovite, dots regional muscovites, triangles contact muscovites).**

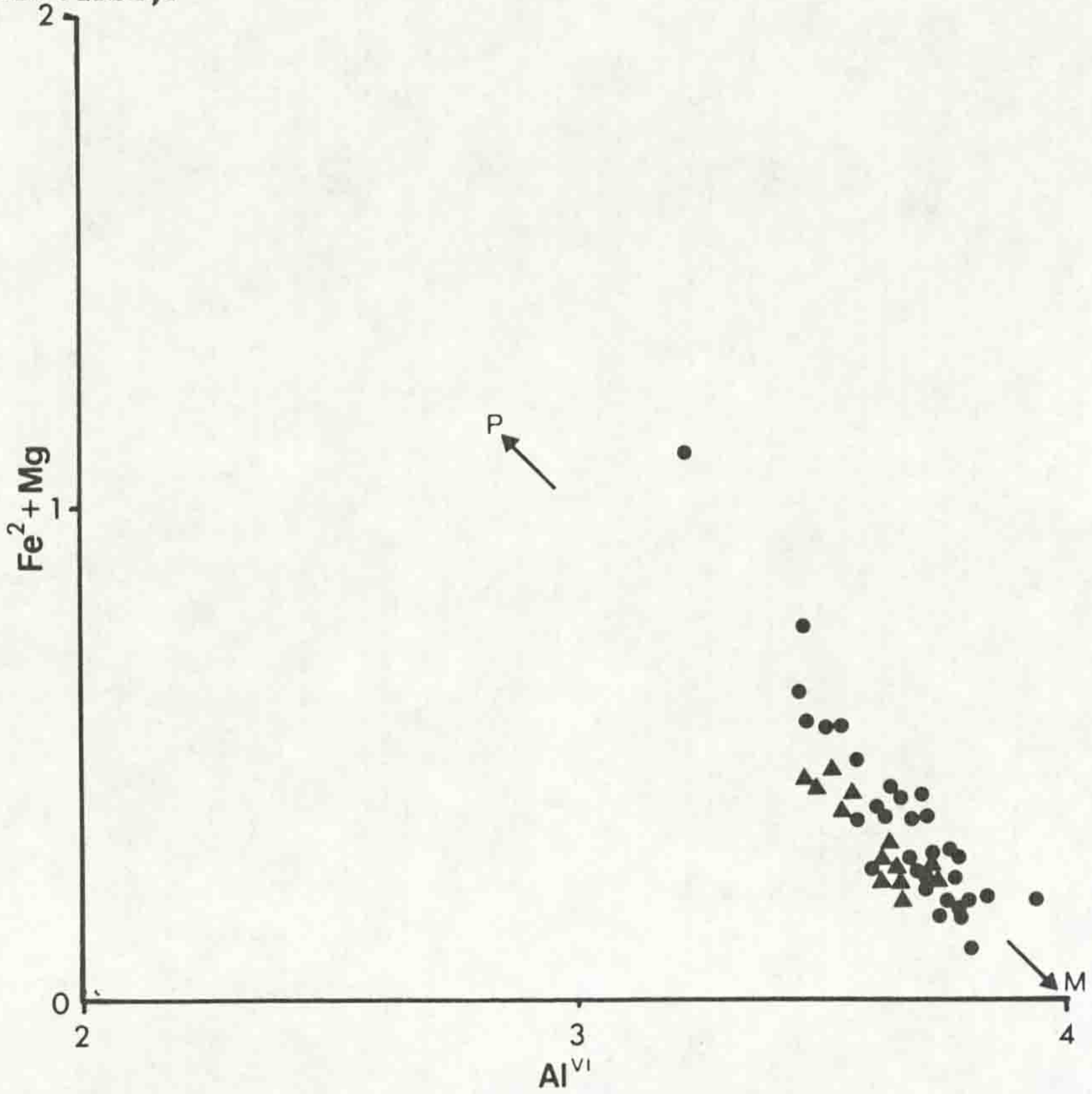


**Figure 4.30: K V. Na in muscovites (dots = regional muscovites, triangles = contact muscovites).**

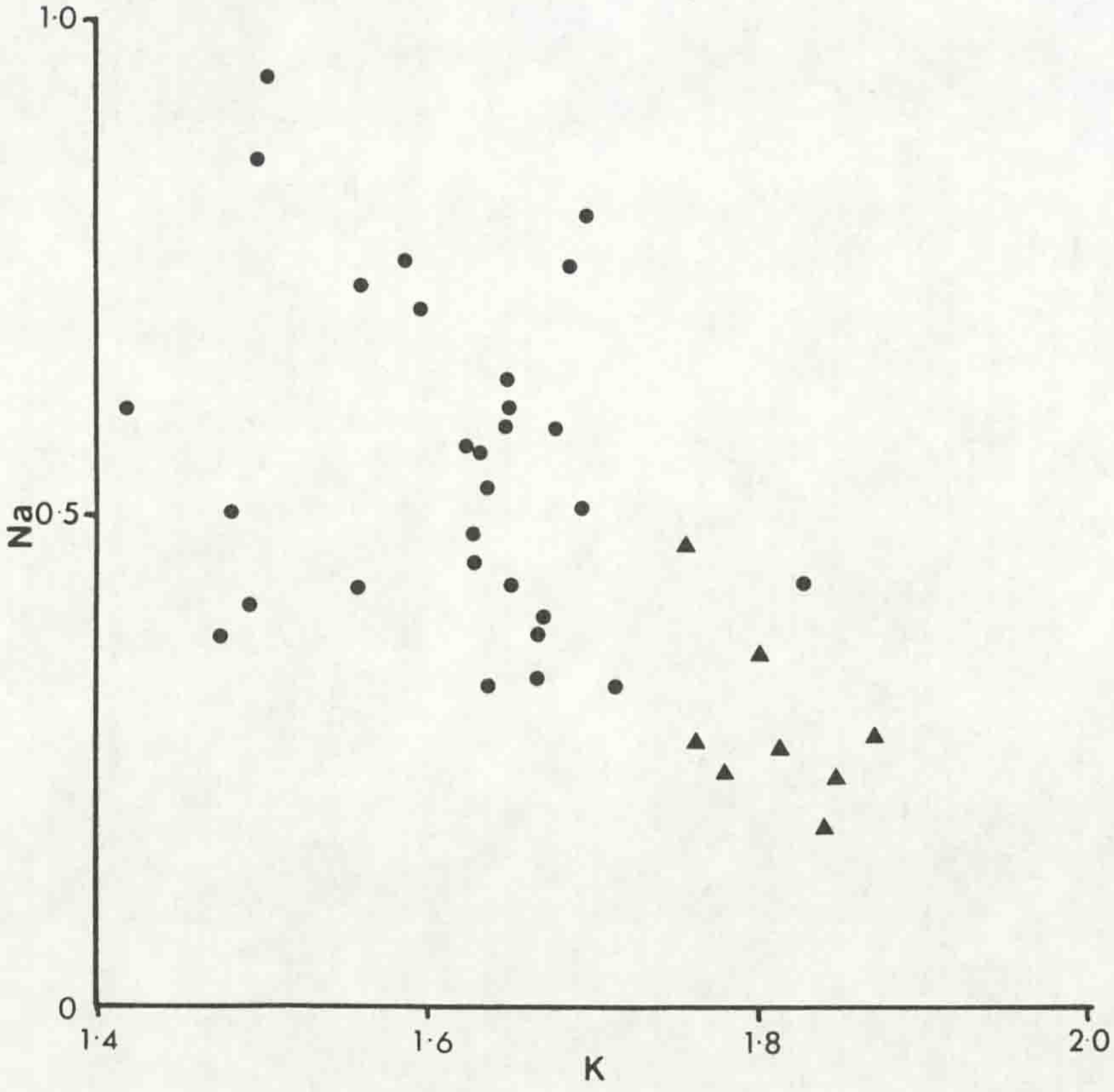

**Figure 4.31: ($Al^{VI}$ + $Al^{IV}$) V. ($Fe^{2+}$ + Mg + Si) in analysed muscovite showing the spread of data away from the ideal Tschermak line (dots indicate regional metamorphic muscovite, triangles muscovite developed in contact lithologies).**

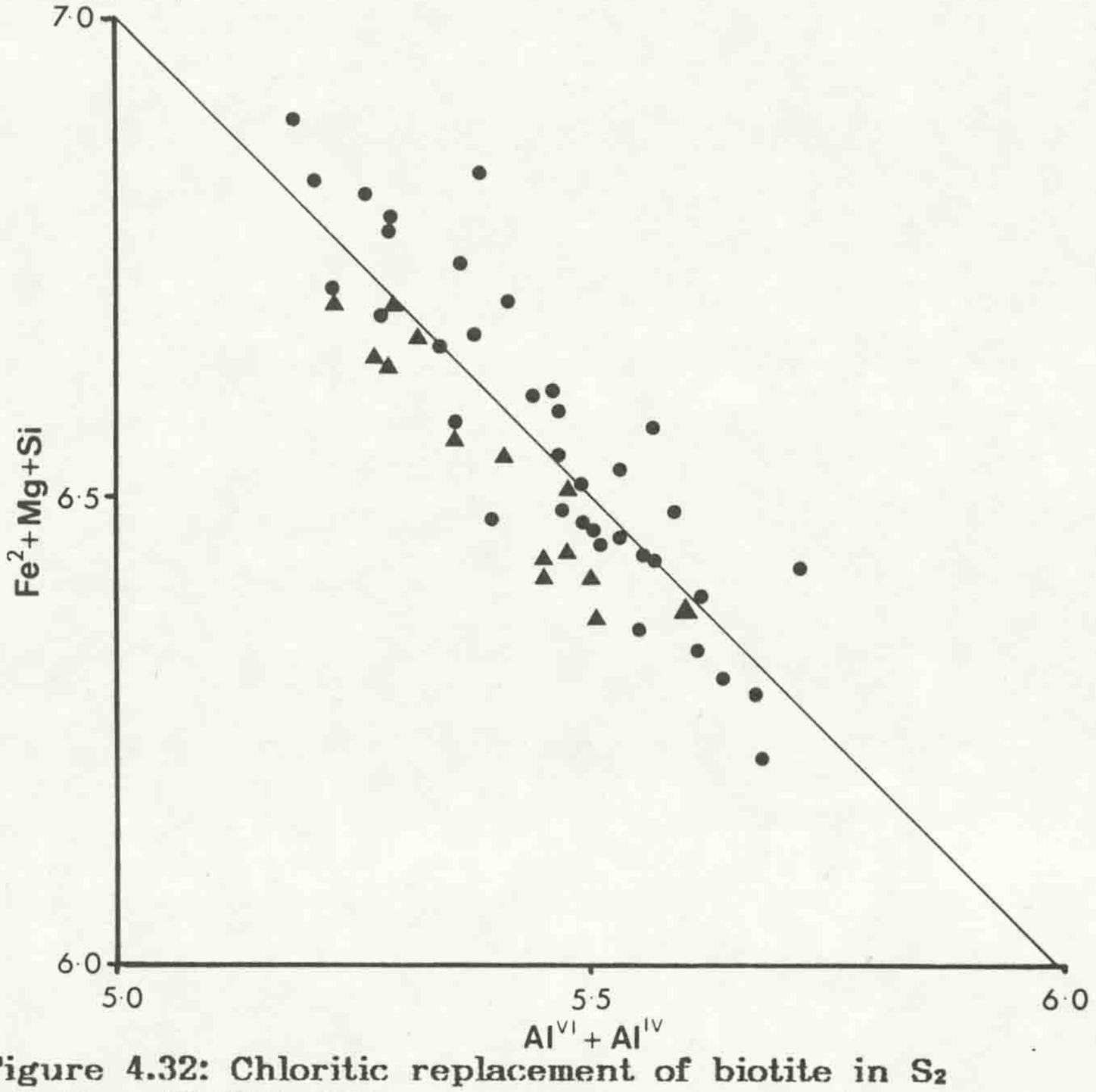


**Figure 4.32: Chloritic replacement of biotite in $S_2$ foliation (X 110) PPL.**

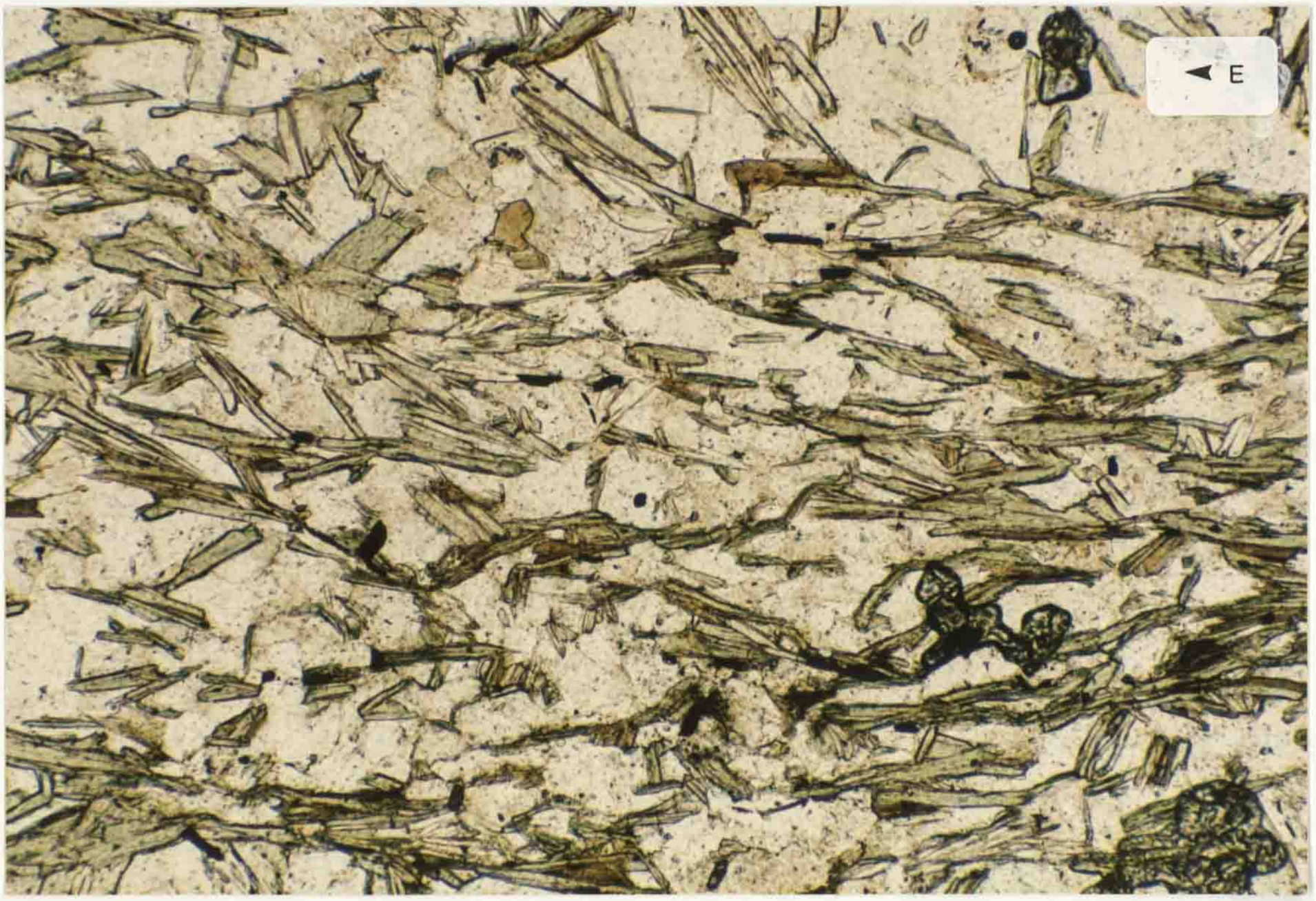

for ferric iron within the contact lithologies can be seen, and it is evident from Figure 4.31 that the contact muscovite data (triangles) plot to one side of the ideal line, suggesting that one mechanism (ferric iron substitution ?) is dominant in these lithologies.

In the contact aureole lithologies, muscovite is generally absent from K - feldspar bearing assemblages, suggesting that muscovite breakdown has occurred. The mean temperature and pressure obtained for sillimanite bearing (Ms absent) assemblages is 769° C at 6.7 kilobars, which lies on the K - feldspar + sillimanite + $H_2O$ side of the muscovite + quartz breakdown curve of Chatterjee & Johannes (1974). The actual placement of this breakdown curve relies on the relation of $PH_2O$ to $P_{total}$. Treloar (1985), in considering the aureole rocks of the south Connemara ultrabasic bodies, suggests the value of $PH_2O$ to be less than $P_{total}$.

$PH_2O$ : $P_{total}$ ratios less than one would tend to shift the breakdown curve to higher temperatures for a given pressure, and, if the south Connemara aureole conditions relate to those seen in the study area, suggest that conditions suitable for muscovite breakdown may not have been present throughout the aureole lithologies. Such conditions may explain the occasional coexistence of muscovite and K - feldspar within sillimanite bearing assemblages {4.1.3.6}.

4.1.3.4 Chlorite: The development of chlorite in the study area is largely retrograde, although rare, textural relations suggest that primary chlorite may occur locally. Chlorite is typically developed as an alteration product of biotite or garnet. Within regional metamorphic lithologies the replacement of biotite by chlorite is often restricted to biotites which are crenulated in $S_3$ fabrics {3.2} (Figure 4.32). Chlorite is developed at the margins and along the cleavages of such biotites. The chlorite which replaces biotites in foliated lithologies shows a variety of habits, ranging from orientated intergrowths with biotite to decussate aggregates. Chloritic replacement of garnets results in 'clots' of chlorite which mimic the original form of the garnet (Figure 4.33).

Within the reactivated (syn - $D_3$) shear zones developed

**Figure 4.33: Chloritic clots replacing garnet (X 56) PPL.**

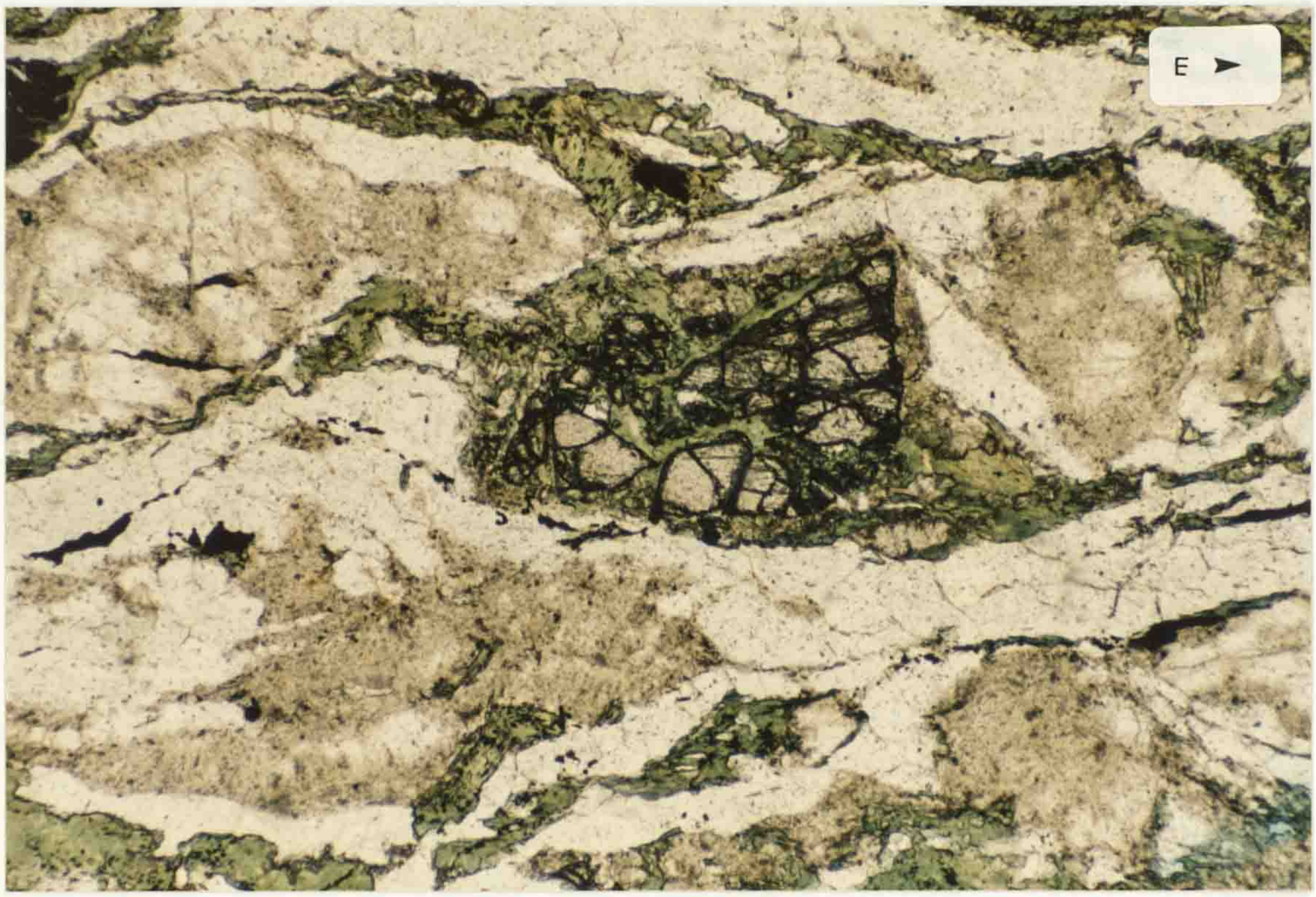


**Figure 4.34: Chlorite developed in reactivated mylonitic lithology (X 56) PPL.**

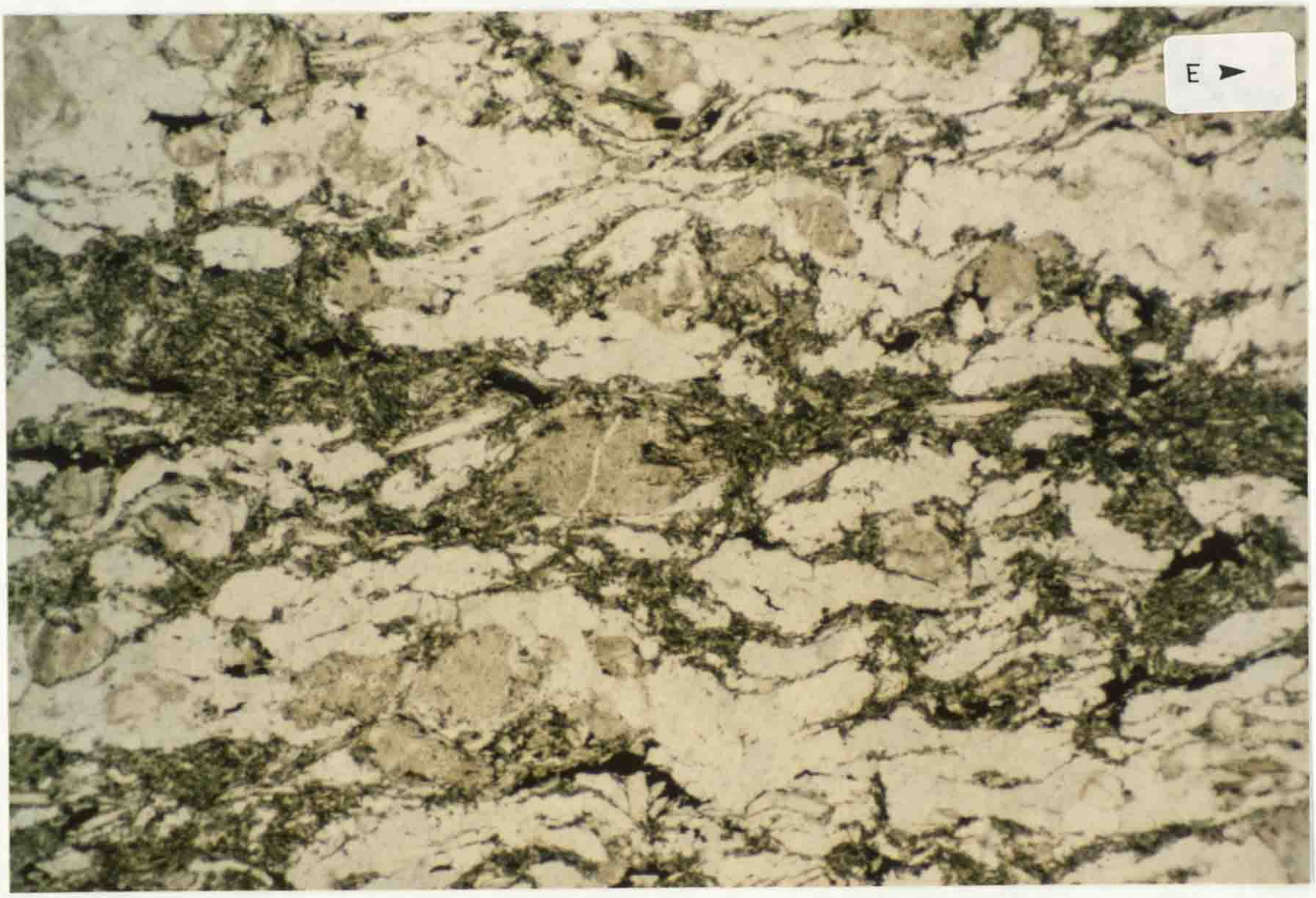

**Figure 4.35: Si V. $Fe_{total}$ plot (after Hey 1954) for classification of chlorite compositions showing analysed chlorites. (Pth = psuedo - thuringite, C = corundophilite, Dph = daphnite, R = ripidolite, Cl = clinochlore, B = brunsvigite, P = pycnochlorite, Pe = penninite, D = diabantite, Tc = talc - chlorite).**

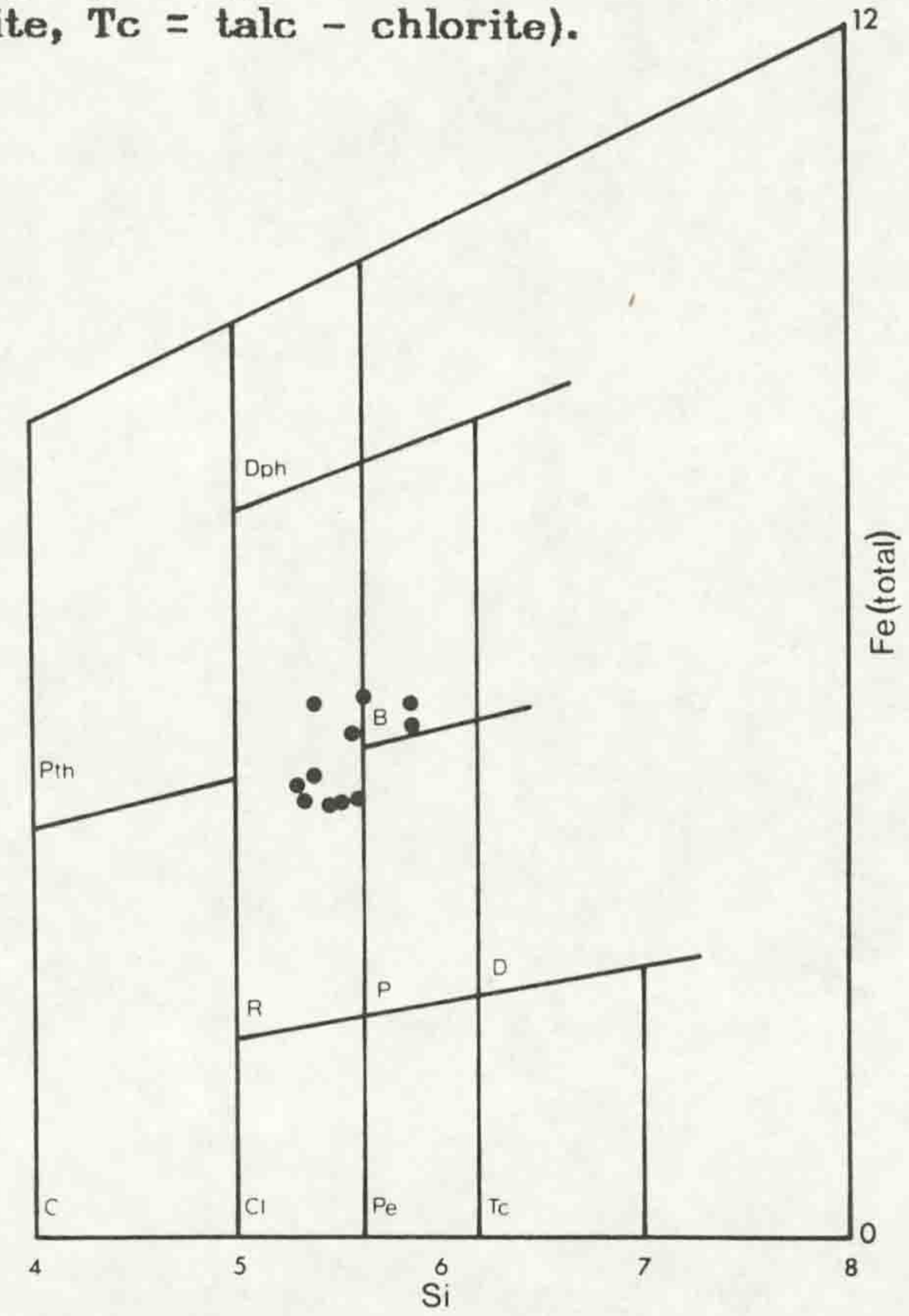


**Figure 4.36: Plagioclase feldspars developed in foliae in schistose regional metamorphic lithology (X 56) XPL.**

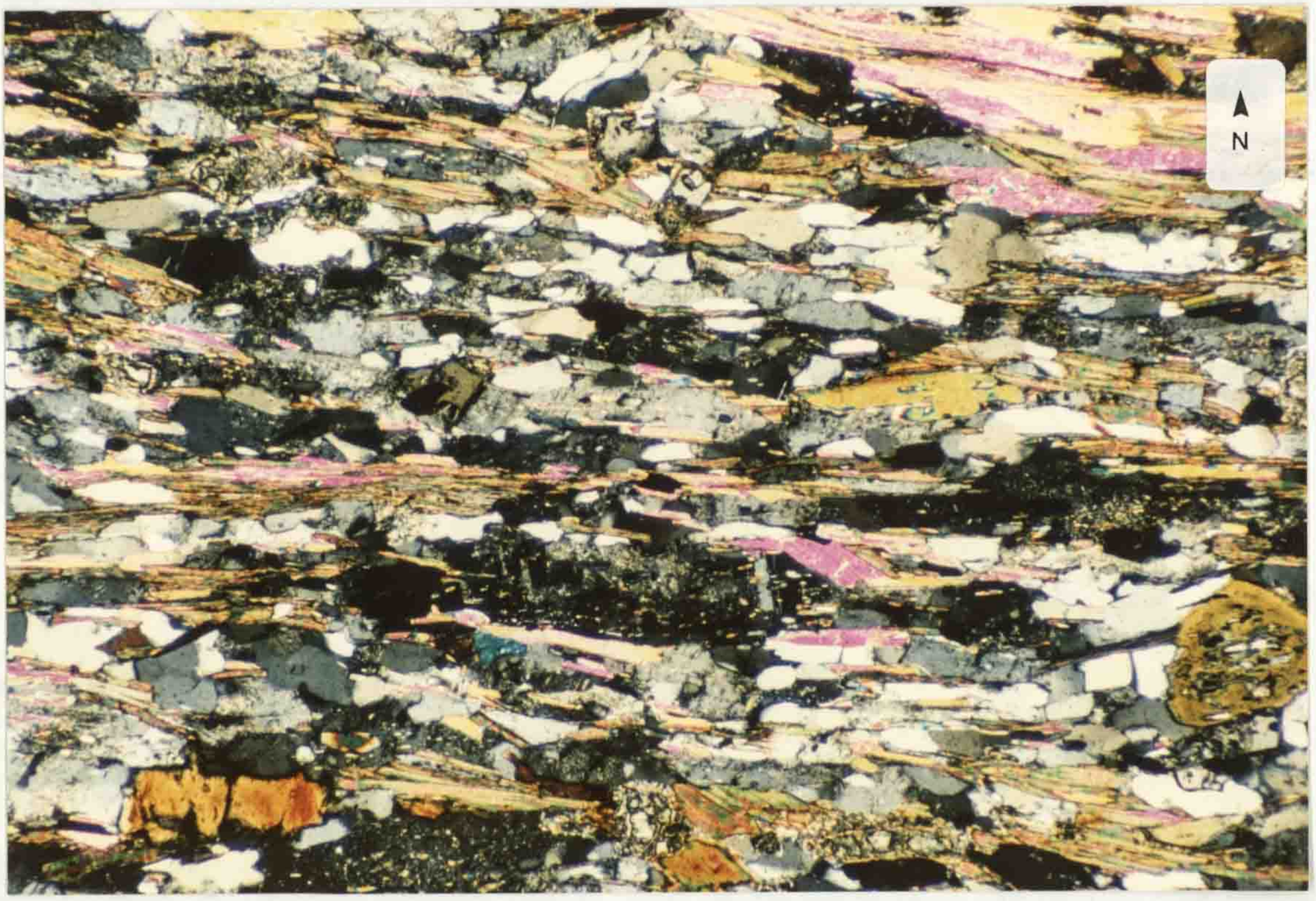

in aureole lithologies {3.2.2.4, 3.4.1.4} chlorite is found in anastomosing zones within the mylonitic fabrics (Figure 4.34).

The mean composition of chlorites within the study area is:

$Fe_{5.144}\ Mg_{3.651}\ Al^{VI}_{2.771}\ Al^{IV}_{2.419}\ Si_{5.565}\ O_{20}\ (OH)_2$

Minor amounts of Ti (0.095), Mn (0.026), Ca (0.012), Na (0.033) and K (0.022) are present in the mean formula, being present in some of the analysed chlorites. The octahedral site occupancy ($Al^{VI}$ + Fe + Mg + Mn + Ca + Na + K) shows a range from 9.897 to 11.912, the mean composition being 11.659. Values of octahedral site occupancy of <12 indicate that the chlorite may be partially di - octahedral (Deer *et al.* 1966). The occurrence of Mn, Ca, Na and K in some of the analyses, along with values of $Al^{VI} > Al^{IV}$, may indicate the presence of smectite and illite interlayers in the chlorite (Aguirre & Atherton 1987), suggesting that these chlorites were produced in sub - greenschist conditions.

Assuming that the analysed chlorites are unoxidised (all iron as FeO) their compositions plot in the Ripidolite and Brunsvigite fields of Hey (1954) (Figure 4.35).

The values of MFM range between 0.333 and 0.466, with a mean of 0.415. These values are comparable with the MFM ratios calculated for regional metamorphic biotites {4.1.3.2}.

4.1.3.5 Plagioclase Feldspar: Plagioclase feldspar is common throughout the study area occurring in a wide range of lithologies. In amphibolitic rocks, plagioclase defines part of a compositional striping {2.1.2.1.4, 3.2}, and where such compositional segregations are developed in foliated pelites plagioclase is typically found in quartz - plagioclase foliae (Figure 4.36).

The development of compositional segregation by differentiation of phyllosilicate from quartzofeldspathic minerals is evident in pelitic lithologies throughout the study area. Within regionally metamorphosed lithologies of this type plagioclase is typically fine grained ( >0.25mm) and anhedral in form, although rare porphyroblastic plagioclases are developed (Figure 4.37) which often display inclusion fabrics {3.2.3} which suggesting pre/syn - $D_2$ development of plagioclase.

Within the aureole lithologies plagioclase commonly forms a

Figure 4.37: Porphyroblastic feldspar in regional lithology (X 56) XPL.

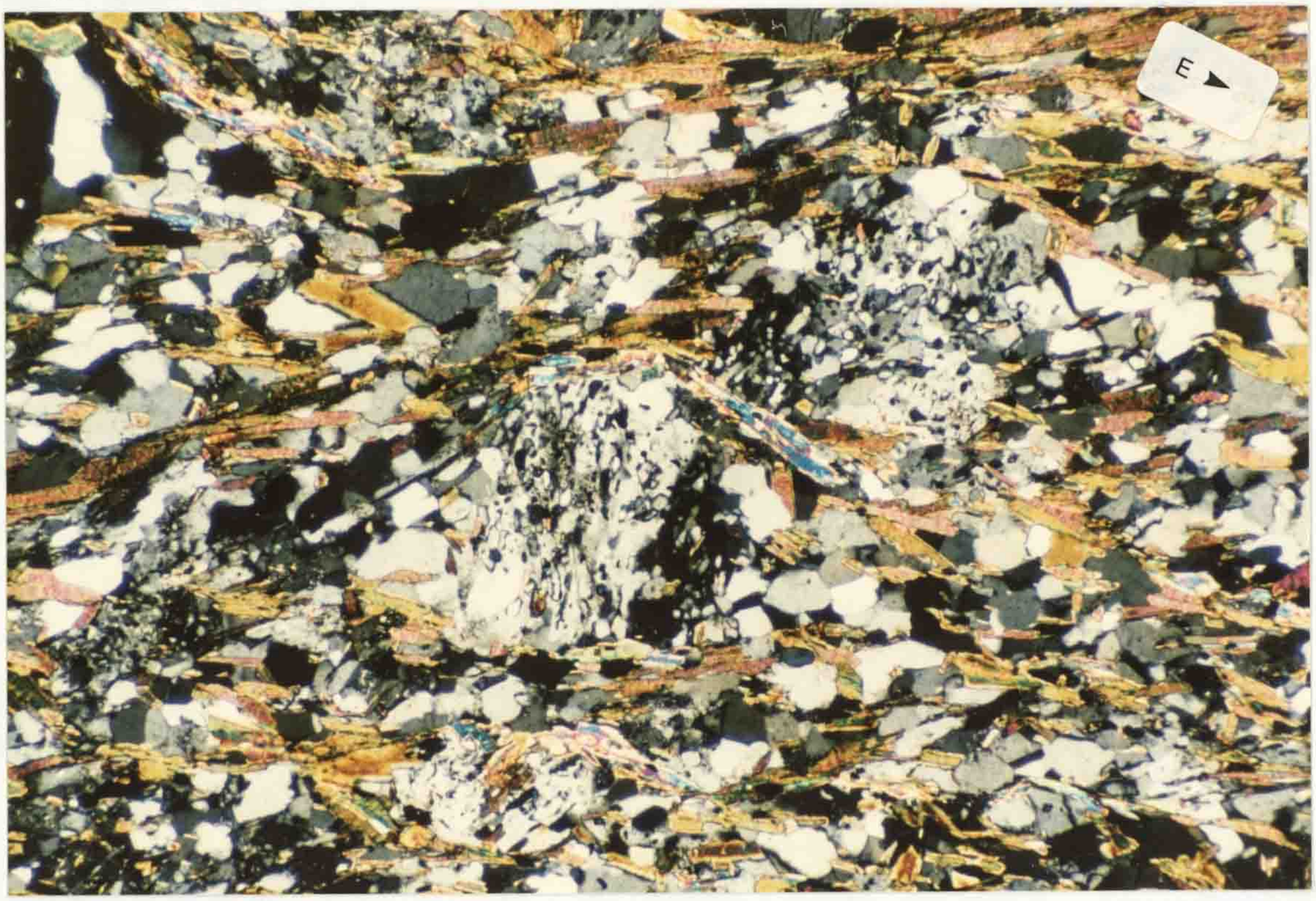


Figure 4.38: Plagioclase feldspars developed in granoblastic aureole lithologies (X 29) XPL.

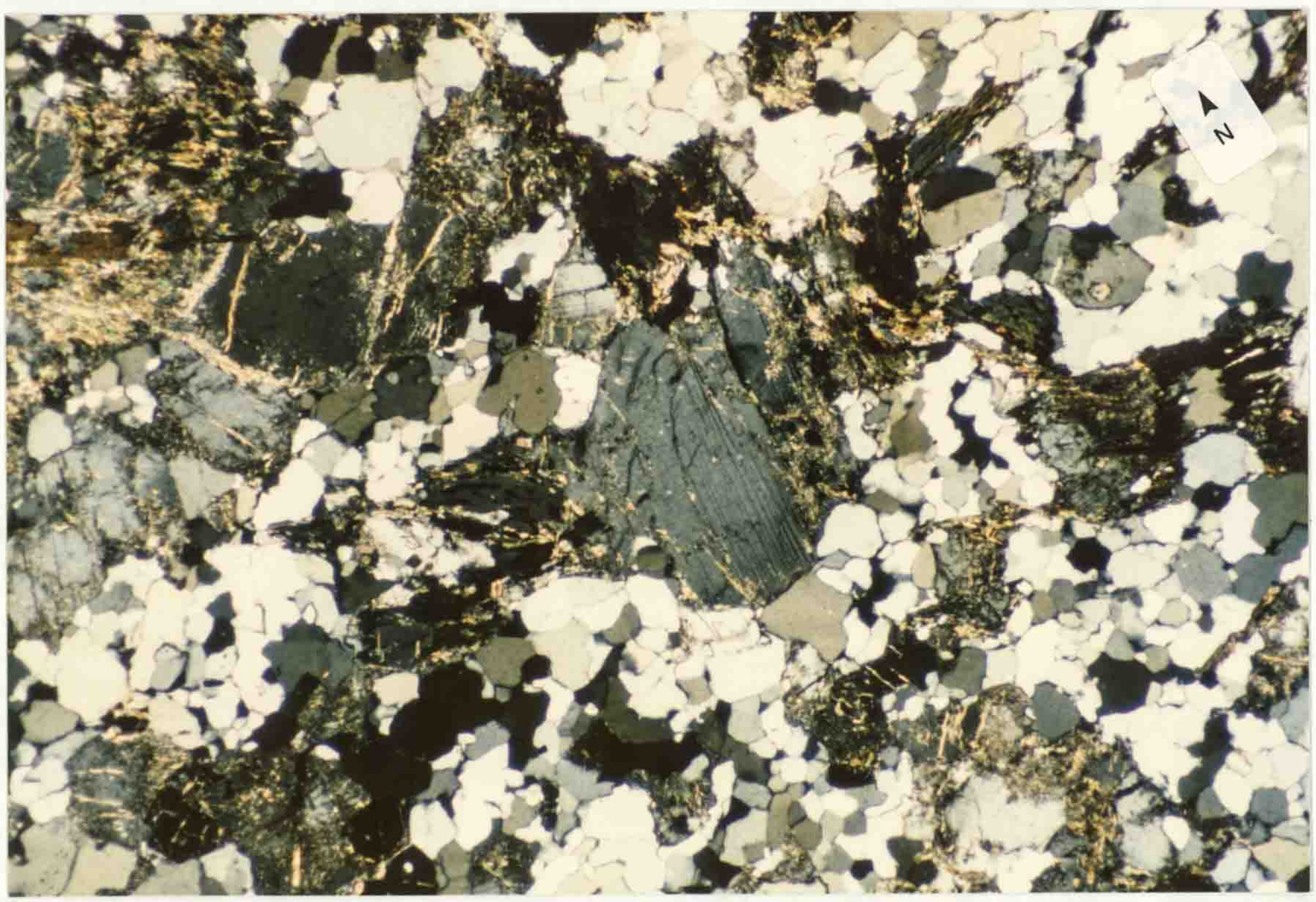

**Figure 4.39: Porphyroclasts of plagioclase feldspar in mylonitic aureole lithologies (X 29) XPL.**

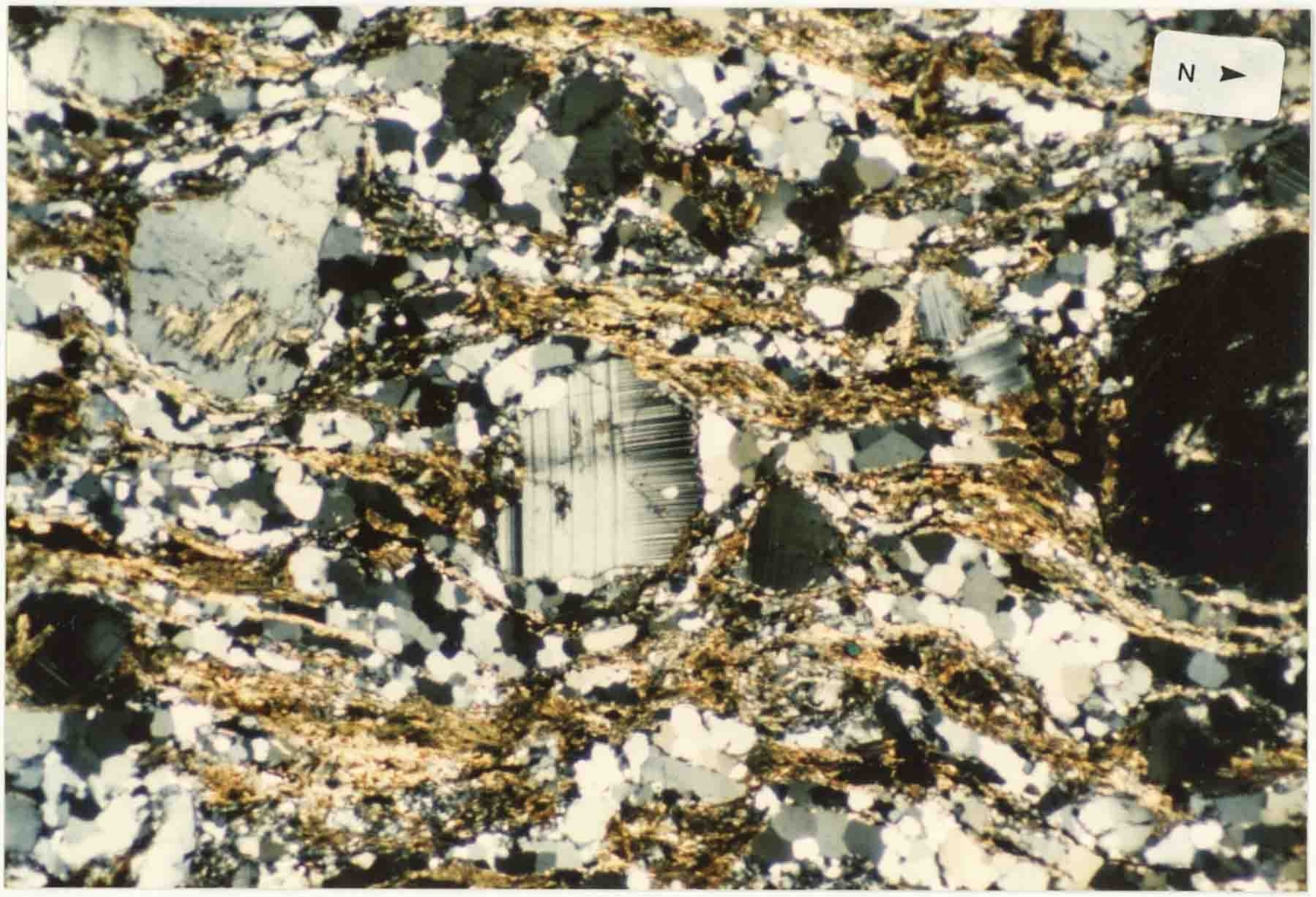


**Figure 4.40: Myrmekitic intergrowth of plagioclase feldspar and quartz in contact aureole lithology (X 56) XPL.**

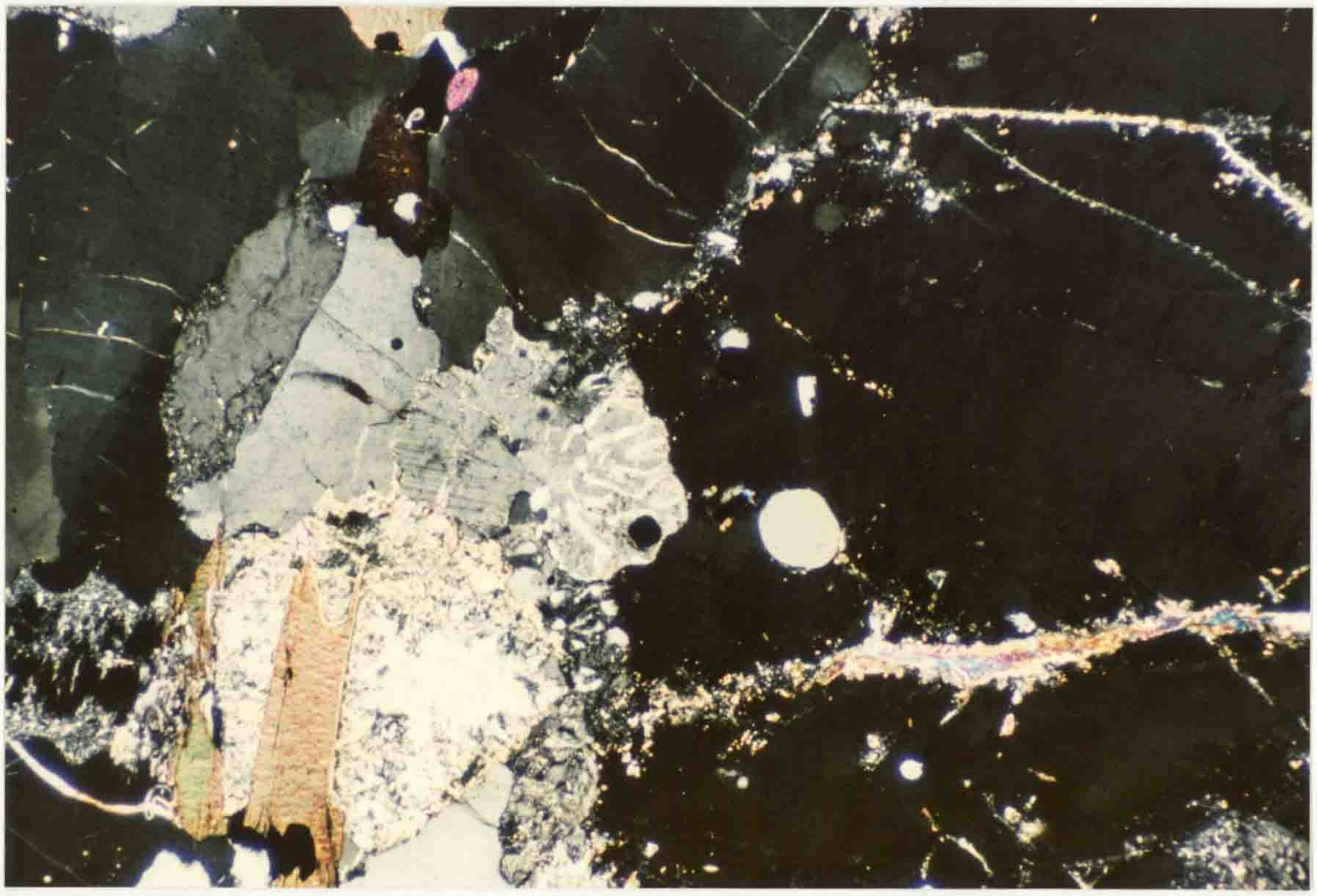

Figure 1.3. Metamorphic zones within the Connemara Dalradian (after Yardley, Barber & Gray 1987) showing the closed sillimanite - in isograd developed around the Dawros - Currywongaun - Doughruagh igneous complex (from Leake *et al.* 1983). 1: Garnet zone, 2: Staurolite zone, 3: Sillimanite - Muscovite zone, 4: Sillimanite - K-Feldspar zone, 5: Migmatite zone and synorogenic intrusive bodies.

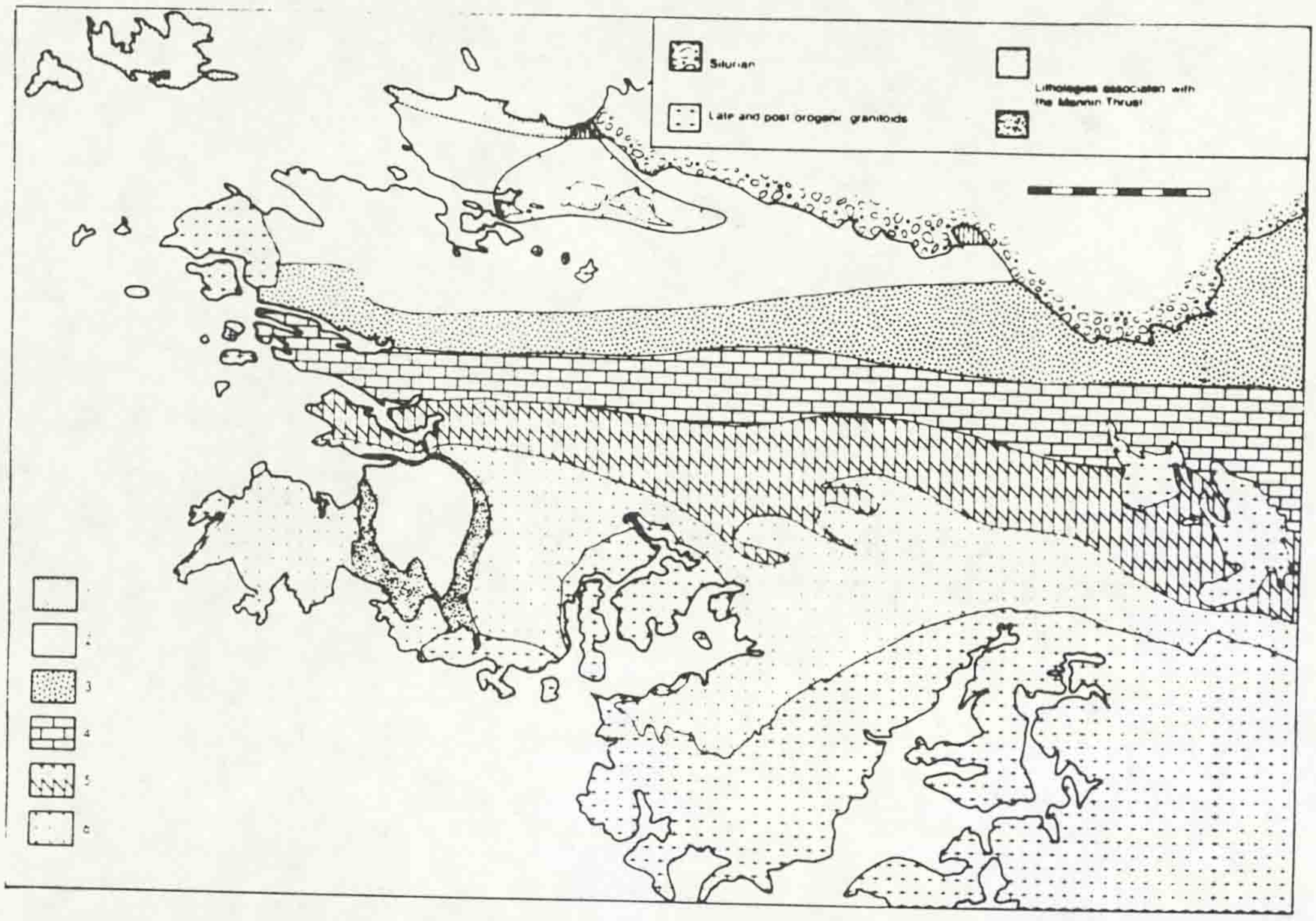


Figure 1.4. Location of the Connemara Dalradian lithologies (C) relative to the main Dalradian outcrop (stippled) (after Leake, Tanner, Singh & Halliday 1983). IS: Iapetus Suture, SUF: Southern Uplands Fault, HBF: Highland Boundary Fault, GGF: Great Glen Fault.

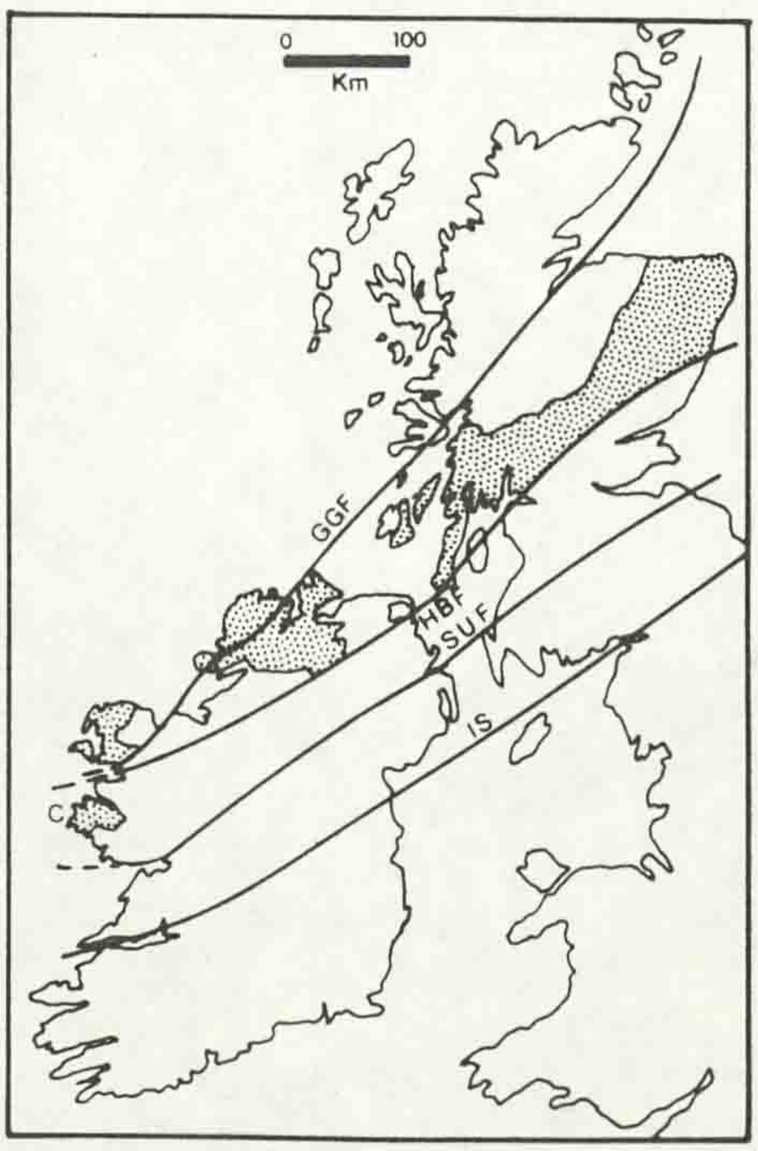

porphyroblastic phase within granoblastic (Figure 4.38) and mylonitic lithologies (Figure 4.39). In the mylonitic lithologies plagioclase is typically developed as rounded porphyroclasts which show evidence of internal strain; undulose extinction and deformed twinning being apparent. In mylonites containing phyllosilicate and fibrolite foliae, plagioclase porphyroclasts are less evidently strained than those in lithologies poor in such foliae. This suggests that strain is partitioned into the fibrolitic and micaeous foliae because they are more ductile, being able to undergo non - coaxial deformation through grain - boundary sliding (Vernon 1987). The rounded form of plagioclase porphyroclasts within mylonitic lithologies is commonly reported (e.g. Shaocheng & Mainprice 1988).

Myrmekitic intergrowths of plagioclase and quartz (Figure 4.40) are developed within granoblastic migmatitic lithologies. These intergrowths are most evident where plagioclase and K - feldspar grains abut. Smith (1974) notes that, although no specific mechanism for myrmekite development has been defined, the process involves synchronous crystallization of quartz and sodic plagioclase within an heterogeneous stress field. The lithologies which show myrmekite development are typically syn - deformational migmatitic lithologies {3.2.2.4} which show the development of tectonic fabrics. The assemblages within such lithologies (Pl + Kfs + Bt + Sil + Qtz ± Crd) are identical to those reported by Barber & Yardley (1985) from apparently anatectic migmatites in southern Connemara, although they report no evidence of myrmekite development.

The compositions of plagioclase grains developed within both regional and contact lithologies are tabulated in {Appendix C}. Plagioclase feldspars developed within regional metamorphic lithologies are sodic, with a mean composition of $An_{19.7}$ (oligoclase), contrasting with contact aureole plagioclases which have mean compositions of $An_{39.3}$ (andesine). It should be noted that whilst the mean composition of regional plagioclase falls outside the range of compositions known as the peristerite gap ($An_2$ - $An_{16}$, Ribbe 1983) individual feldspar compositions fall into this range indicating that metamorphic conditions were sufficient to enable the formation of low temperature plagioclase structures (Deer *et al.* 1966). No

**Figure 4.41: Coexisting K - feldspar and muscovite in contact aureole lithology (X 29) XPL.**

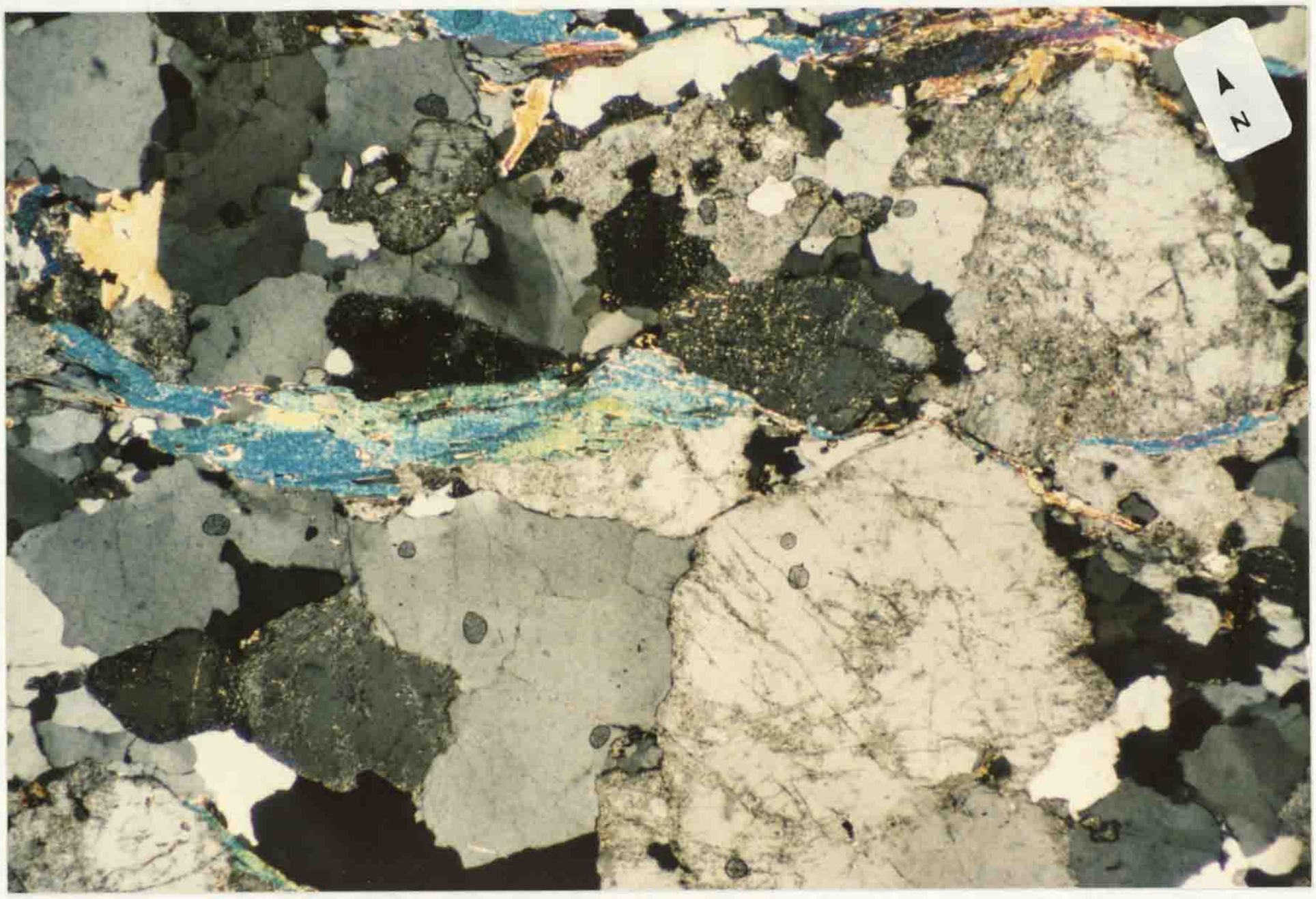


**Figure 4.42: Porphyroblastic K - feldspar in contact aureole lithology (X 29) XPL.**

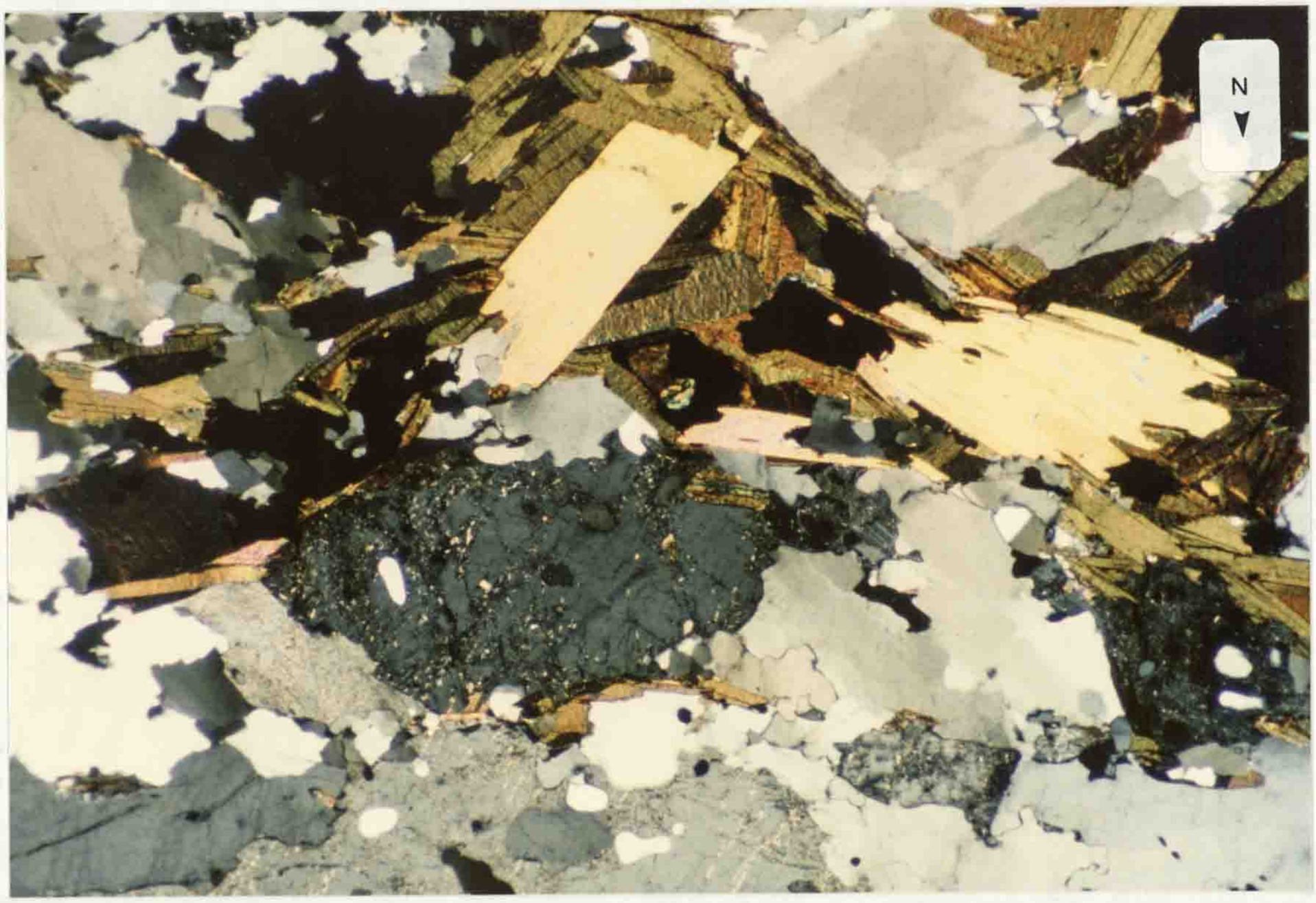

optical evidence for peristerite exsolution was seen. Rare pure albitic plagioclases are developed in lithologies which show local retrogression and it is probable that such albites represent a retrograde feldspar development. Plagioclase within regional metamorphic lithologies are commonly untwinned, and only rarely exhibit compositional zoning. When developed such zoning is typically from calcic cores to more sodic rims. The contact metamorphic plagioclases are more commonly zoned, and typically become more sodic rimwards, although rare reverse zoning is also developed.

4.1.3.6 <u>K - Feldspar</u>: K - feldspar is common within contact aureole assemblages but only one occurrence of K - feldspar was found in the regional lithologies [GR 679 630] and it coexists with muscovite. This lithology is developed near to the Rushenduff pegmatite body (Cruse 1963), a late - $D_3$, highly - evolved, intrusive pegmatitic lithology, and may represent an effect of this body. It is noteworthy that the thermobarometric results from this rock {5.4} are at variance with those of adjacent lithologies, possibly indicating a degree of resetting of exchange reactions. Cruse (1963) suggests the Rushenduff pegmatitic lithologies are derived from the injection of a fluid enriched in K, Na, Si, $CO_2$ and $H_2O$, although he does not record any instances of K - feldspar development associated with this fluid phase away from the main pegmatite body. It is possible that the occurence of K - feldspar recorded here is due to the effects of this fluid.

The main occurrences of K - feldspar are within sillimanite - bearing aureole lithologies where muscovite is largely absent, although coexisting muscovite and K - feldspar are occasionally found (Figure 4.41). K - feldspar in aureole lithologies is typically porphyroblastic (up to 15mm) forming subhedral grains (Figure 4.42), often clearly evident at outcrop. These grains show the same styles of occurrence as plagioclase grains {4.1.3.5}, being developed as porphyroblasts within granoblastic lithologies and as porphyroclasts in mylonitic zones. The compositions of K - feldspar grains analysed are tabulated in {Appendix C}.

**Figure 4.43: Porphyroblastic staurolite developed within $S_2$ foliation, note the tabular ilmenite inclusions aligned parallel to ilmenites in the external foliation (X 29) PPL.**

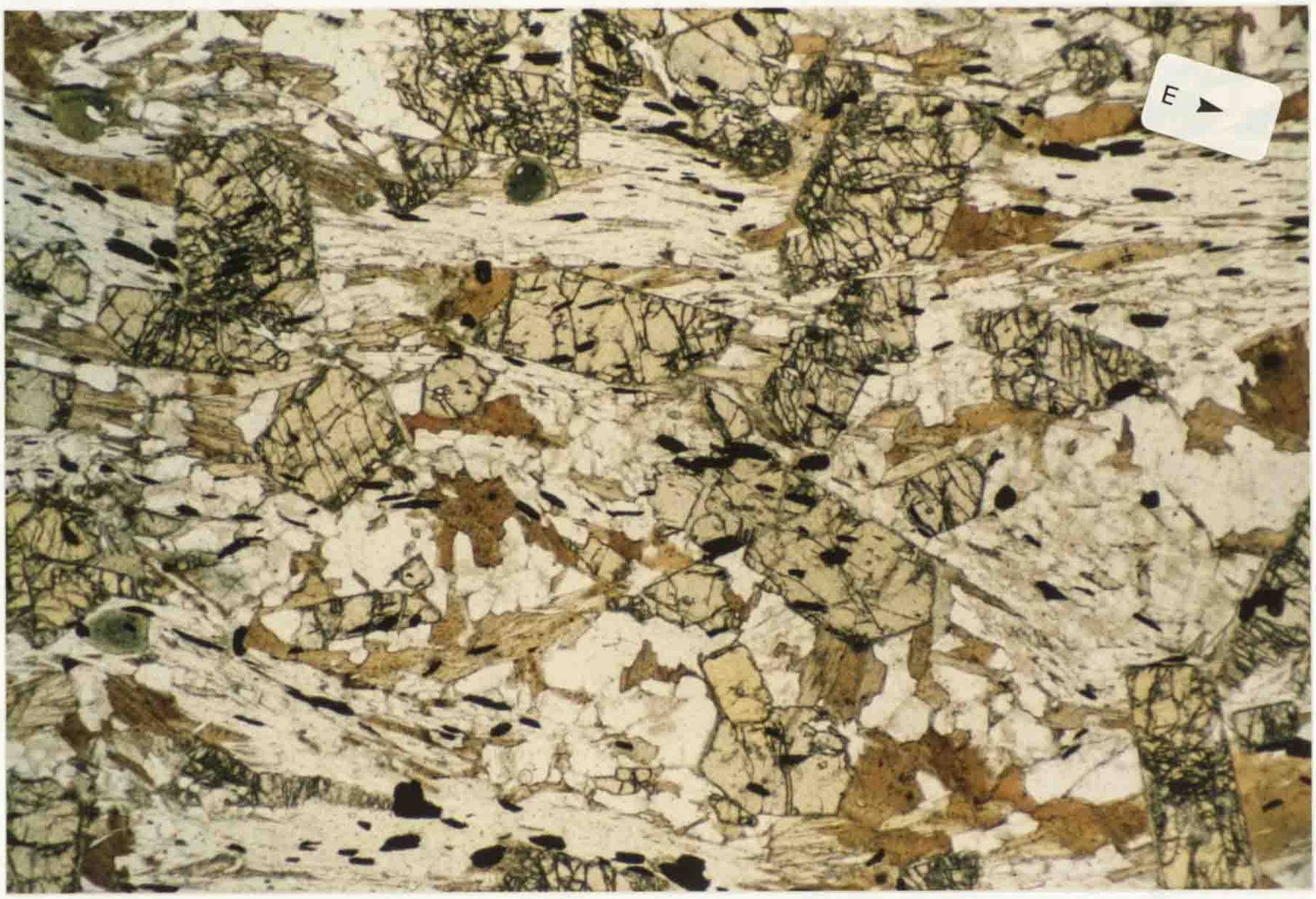


**Figure 4.44: Curved, syn deformational inclusion trail developed within staurolite (X 110) PPL.**

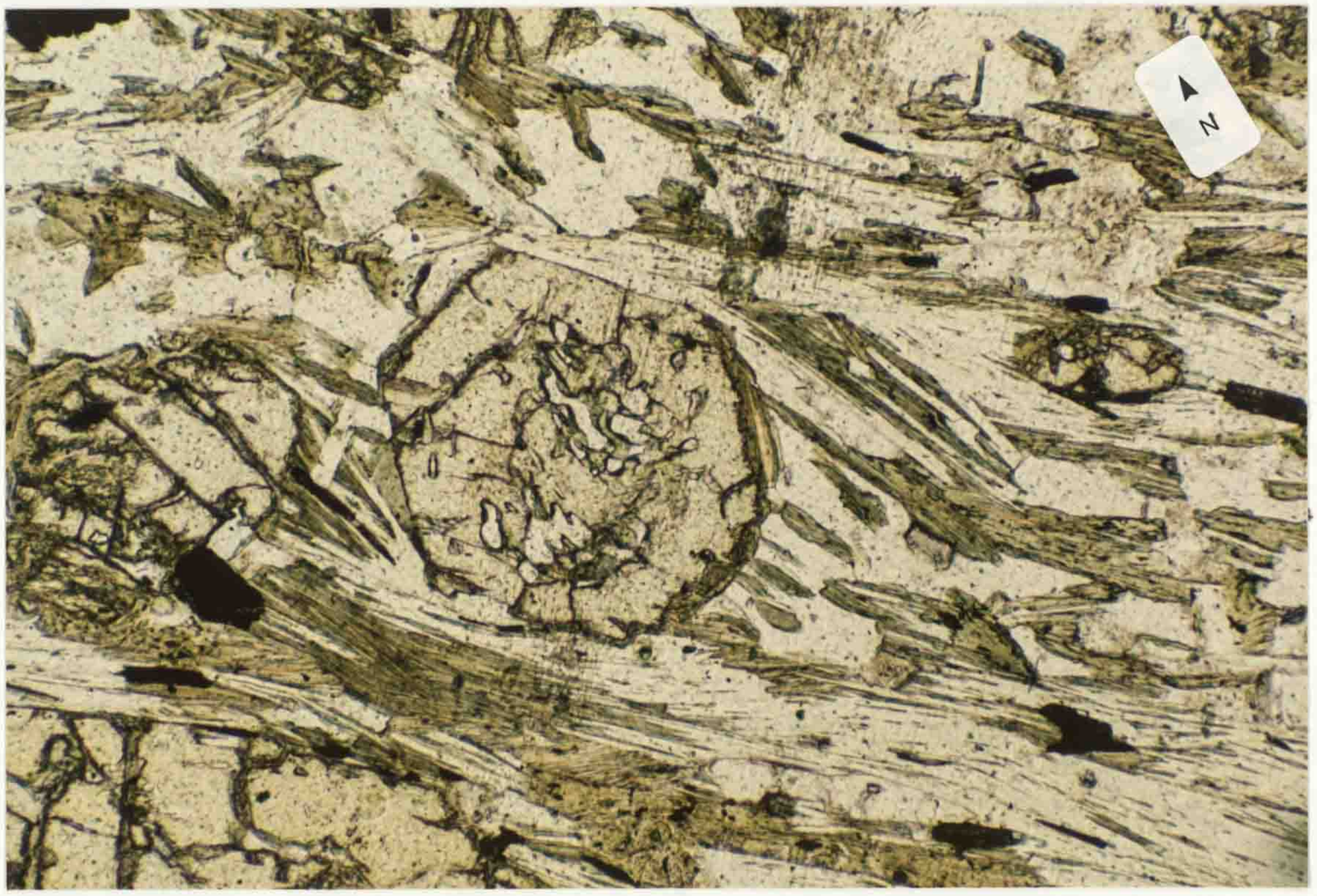

**Figure 4.45: Rounded and embayed staurolite grains included in porphyroblastic andalusite (X 29) XPL.**

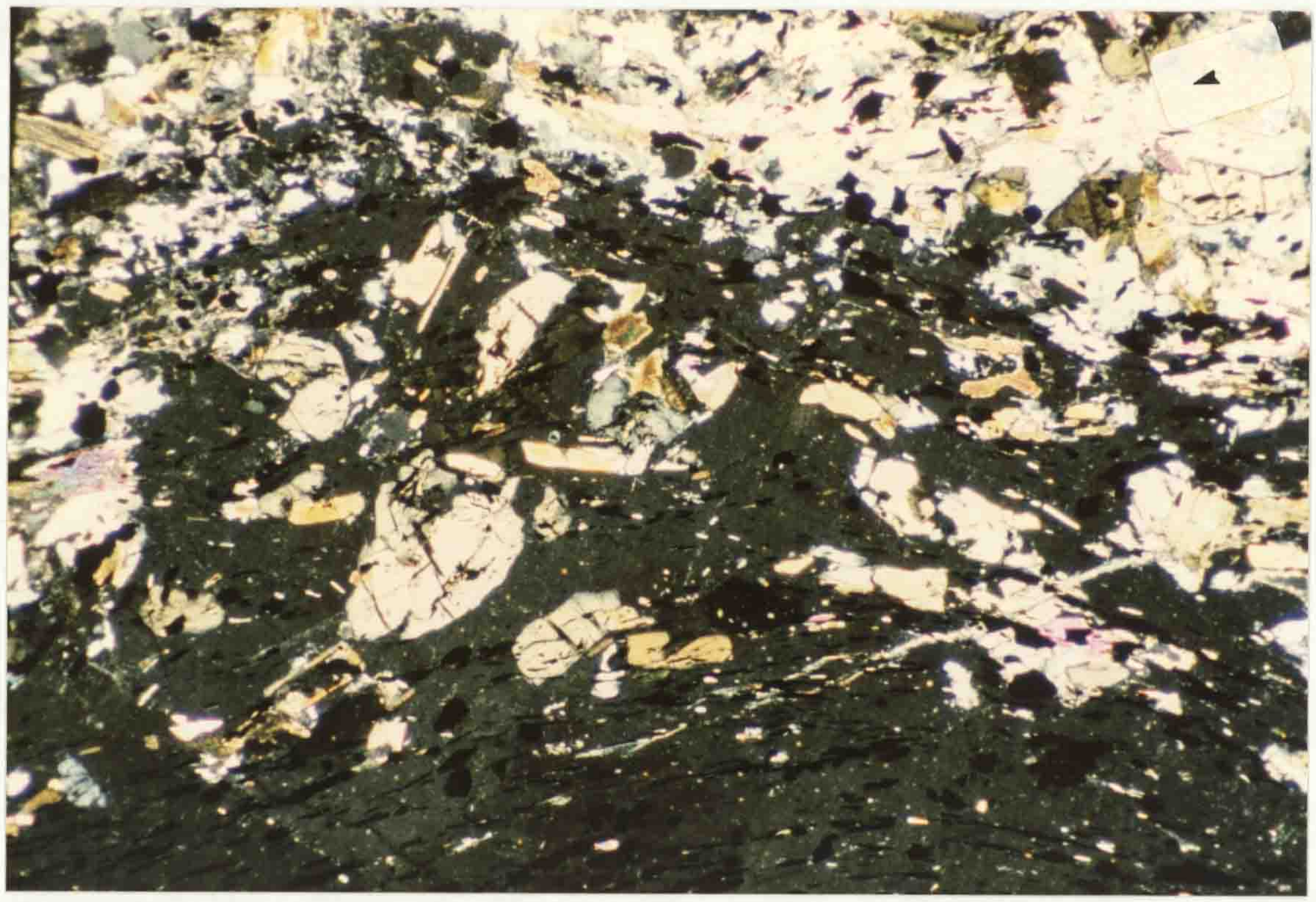

**Figure 4.46: Sillimanite developed on biotite in contact aureole lithology (X 56) PPL.**

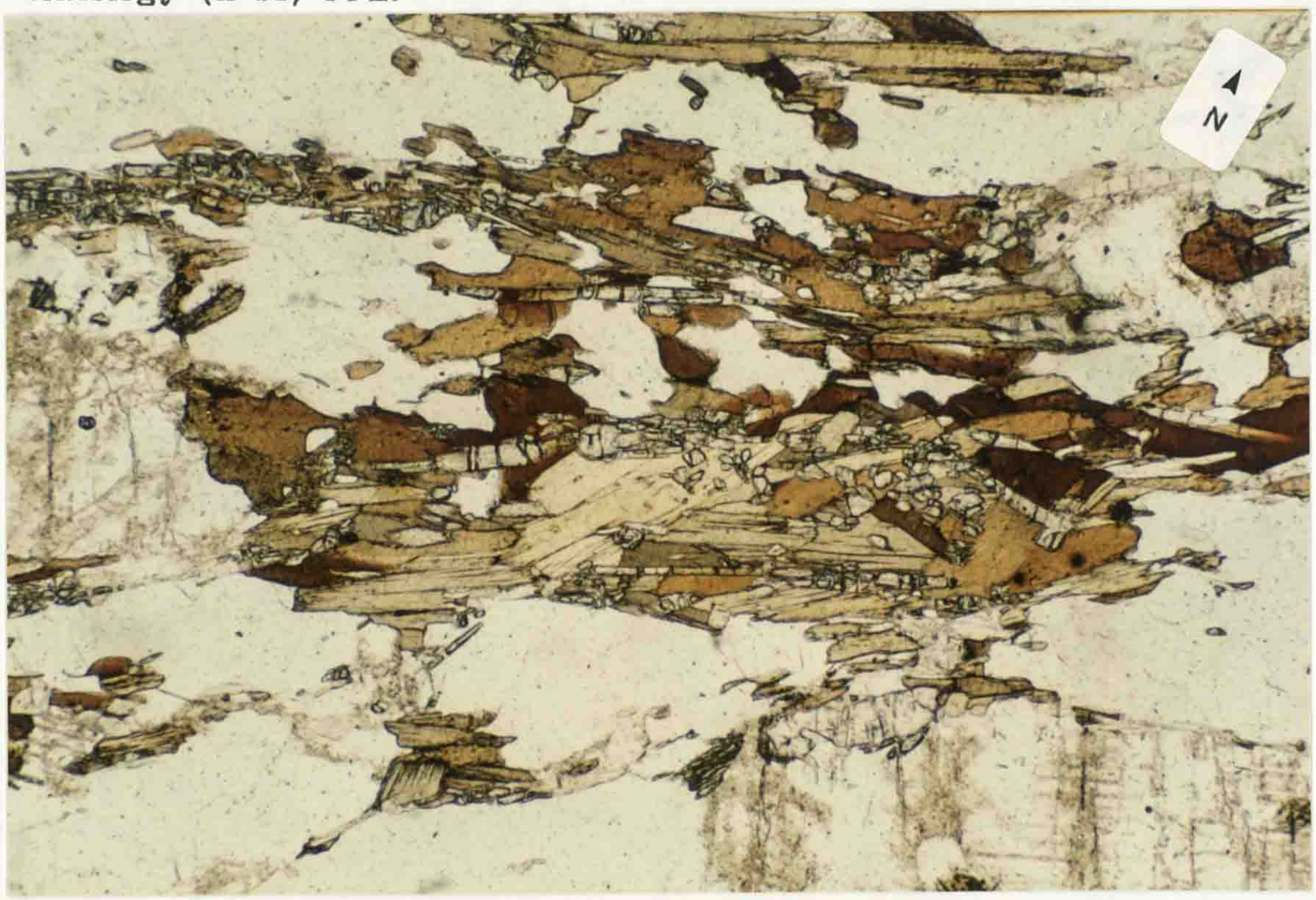

4.1.3.7 Staurolite: Staurolite is developed within regionally metamorphosed pelitic lithologies throughout the study area, forming the peak assemblage with garnet and biotite.

Staurolite commonly forms porphyroblastic, euhedral to subhedral grains which overgrow and include the $S_2$ foliation (Figure 4.43). Where $S_3$ crenulation fabrics are developed the staurolite grains appear to be displaced by the $F_3$ microfolds. This evidence suggests that the timing of staurolite development was post - $D_2$ and pre - $D_3$, although rare syn - deformational inclusion trails in staurolites (Figure 4.44) and wrapping fabrics suggest some staurolites may have developed syn/late - $D_2$.

In andalusite bearing lithologies {4.1.3.9} staurolite grains occur both as inclusions within the andalusite porphyroblasts and within the matrix of the rock. The included grains show rounded and embayed forms (Figure 4.45), whereas those staurolites in the matrix are typically subhedral to euhedral. This suggests that the development of andalusite was associated with the dissolution of staurolite, possibly through the reaction:

$St + Ms + Qtz = And + Bt + H_2O$ (Yardley 1976).

The mean staurolite composition (calculated on an anhydrous basis to 46 oxygens with all iron in the ferrous state) is:

$Fe_{(3.001)}\ Mg_{(0.402)}\ Ti_{(0.113)}\ Al_{(17.517)}\ Si_{(8.002)}\ O_{46}\ (O,OH)_2$

No evidence of compositional zonation in staurolite grains was detected.

The MFM ratios for staurolite range from 0.075 to 0.204, with a mean value of 0.156. The occurrence of Ti in the staurolite suggests that the growth of this phase involved the breakdown of a Ti - bearing phase (possibly chlorite) {4.1.4}.

4.1.3.8 Sillimanite: Sillimanite is restricted to the north of the Renvyle-Bofin slide in Kylemore Formation lithologies adjacent to the Dawros - Currywongaun - Doughruagh igneous complex (DCD). Its development is due to the contact metamorphic effects of the DCD (Ingold 1937, Leake 1970b). A minor development of fibrolitic sillimanite occurs on the north coast of the Renvyle peninsula, probably associated with the thermal aureole of the Crump Island basic body, a satellite of the DCD (Leake 1970b).

Sillimanite occurs as either fibrolitic bundles or prismatic grains. Within granoblastic hornfels lithologies the prisms and fibres show no preferred linear orientation, typically growing within the cleavage of biotite (Figure 4.46) or as radiating needles within quartz or plagioclase grains.

Within the mylonitised hornfelsic lithologies anastomosing zones of foliated fibrolitic sillimanite with biotite are common (Figure 4.47). Scattered prismatic grains are variably aligned in the fabric (Figure 4.48).

The association of biotite and sillimanite has been noted by various workers (e.g. Chinner 1961, Carmichael 1969), who suggest two possible mechanisms to explain this relation:

i, The biotite lattice provides favourable sites for sillimanite nucleation and growth (Chinner 1961).

ii, Biotite and sillimanite grow simultaneously, with the sillimanite developing indirectly from the breakdown of other $Al_2SiO_5$ polymorphs, in a reaction which is catalysed by the presence of muscovite (Carmichael 1969).

Sillimanite intergrowths with biotite commonly run parallel to biotite cleavage planes suggesting that preferred nucleation has occurred along such surfaces. This observation, coupled with the lack of relict kyanite and andalusite within sillimanite bearing lithologies and the occurrence of sillimanite in muscovite - free lithologies, favours sillimanite growth by the mechanism of Chinner (1961).

Sillimanite in mylonitic rocks displays features similar to those described by Vernon (1987) in which sillimanite is concentrated in anastomosing zones by either growth within pre-existing mica-rich folia or syndeformational growth of sillimanite in zones of strong non-coaxial strain. Features such as sillimanite inclusions in pre/syndeformational porphyroblasts (porphyroclasts?) and within ribbon aggregates of quartz show that sillimanite growth was syndeformational, not post deformational. In non-mylonitic lithologies the growth of sillimanite is concentrated within the mica folia which define the $S_2$ fabric and the timing of growth cannot be clearly constrained.

The timing of sillimanite growth in the study area (syn-$D_2$) is earlier than sillimanite growth in the rest of

**Figure 4.47: Anastoming fibrolitic sillimanite zones in contact aureole lithology (X 56) PPL.**

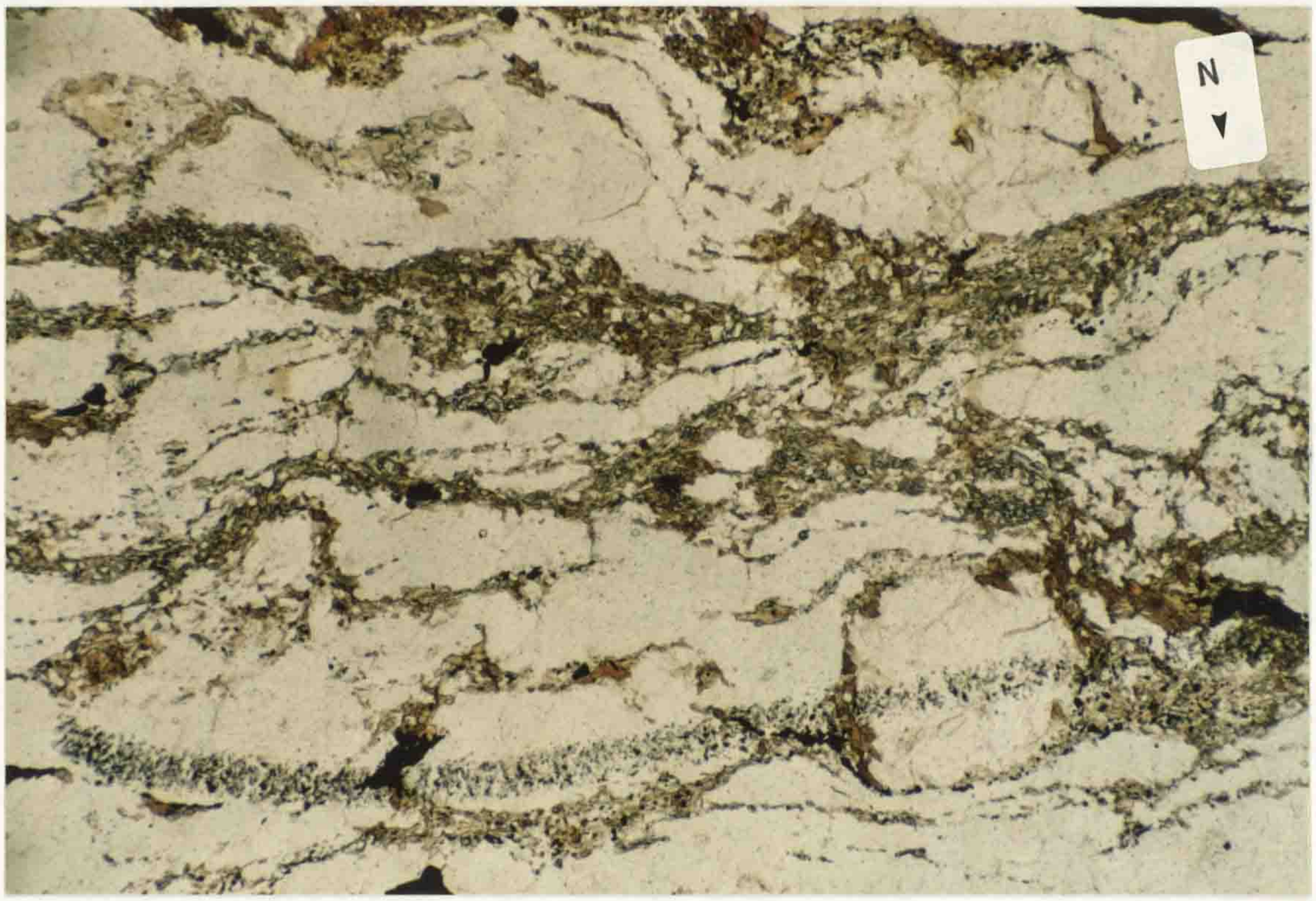


**Figure 4.48: Prismatic sillimanite, with local fibrolite developments in contact aureole lithology (X 56) PPL.**

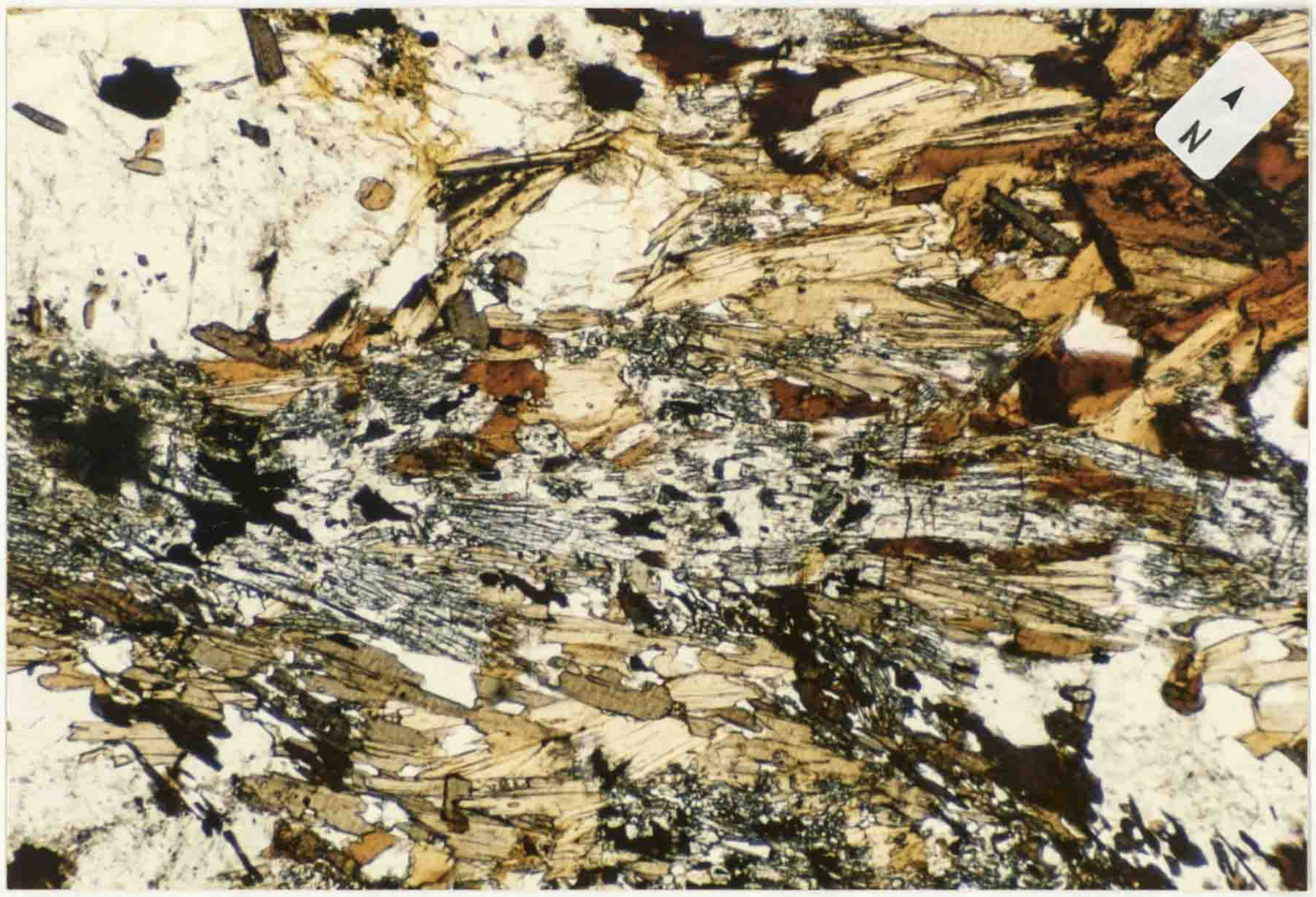

Connemara which is typically post-$D_2$/ syn-$D_3$ (Yardley *et al.* 1987). This syn - $D_2$ age within the mylonitic contact aureole zones of the DCD fits well with the model suggested by Kanaris-Sotiriou & Angus (1976) for syn - $D_2$ intrusion of the bodies (3.4).

Prismatic sillimanite is only developed within 200 - 300m of the DCD. This distribution is interpreted as being due to the initial widespread nucleation of fibrolite on suitable sites followed by the coarsening of grains to give prismatic sillimanite immediately adjacent to the igneous bodies. This suggests that within a zone close to the igneous bodies the sillimanite forming reactions occurred either more rapidly or for a longer period of time than in lithologies further away. Prismatic sillimanite is restricted to low strain (i.e. non-mylonitic) zones, with fibrolite being present in high strain zones within 200 - 300m of the intrusives . This implies that the growth of prismatic crystals in the mylonitic lithologies was restricted by either grain boundary sliding inhibiting the growth of large crystals, or by large grains being reduced in size by post - growth deformation (Vernon 1987).

4.1.3.9 Andalusite: Andalusite is restricted to the Kylemore Fm within 200 - 300 m of the Rushenduff pegmatite body on the northern side of the Renvyle peninsula. It forms subhedral to rounded porphyroblasts in Grt + St + Bt + Ms + Pl + Qtz + Tur ± fibrolite schists. Porphyroblasts are typically 5 - 10 mm. in size, although sizes up to 20 - 30 mm. are evident in clean coastal outcrops [GR 692 638]. In thin section the porphyroblasts are often ragged in outline, commonly containing inclusions of magnetite, ilmenite, biotite, partially resorbed staurolite and tourmaline. No occurrences of andalusite overgrowing fibrolite are evident. The magnetite and ilmenite inclusions show plate - like forms and define straight inclusion trails (Figure 4.49) which are continuous with the external ($S_2$) foliation, but lack the typical strong ($D_3$) crenulation seen in the external foliation. The development of andalusite appears to have been largely pre - crenulation ($S_3$) although rare crenulated inclusion trails can be seen in porphyroblasts. $F_3$ crenulation folds often appear to

**Figure 4.49: Porphyroblastic andalusite in schistose Kylemore Fm lithology (X 29) XPL.**

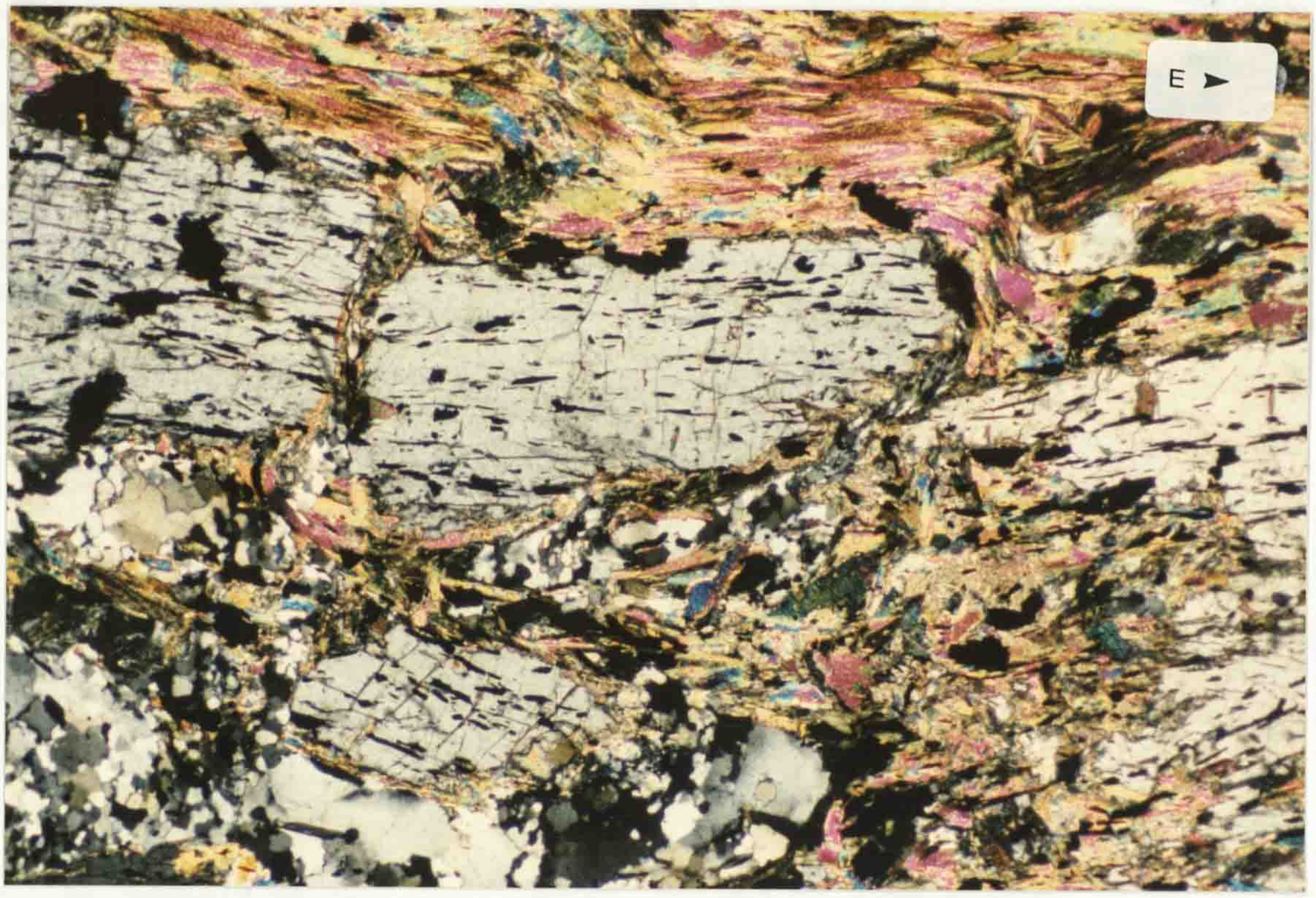


**Figure 4.50: Corroded and embayed kyanite within Kylemore Fm lithology (X 56) PPL.**

1. an early Barrovian type metamorphism syn to post $D_2$ reaching staurolite/kyanite grades;
2. a later higher temperature, lower pressure type metamorphism with sillimanite/andalusite grades developed.

The metamorphic zoning pattern now seen (Figure 1.3) increases in grade from garnet/biotite grades (Yardley *et al.* 1987) in the north to extensive migmatisation in the south and is the result of the later metamorphic event. It is noteworthy that the $F_3$ folds appear to have little or no influence on the orientation of the isograds produced during the second metamorphic event.

The Dalradian terrane of Connemara occupies an anomalous geographic position (Figure 1.4) as, unlike other areas of Dalradian outcrop, it lies to the south of the Highland Boundary Fault. Explanations of this location, based on plate tectonic reconstructions (Dewey & Shackleton 1984, Soper & Hutton 1984, Barker & Gayer 1985, Dewey & Hutton 1986, Hutton 1987), generally consider that Connemara was displaced away from the main Dalradian outcrop and in to its present position by sinistral displacement on a braided system of strike - slip faults associated with the closure of the Iapetus ocean. In these models Connemara is thus regarded as a suspect terrane, emplaced during the closure of Iapetus.

## 1.3 The aims of this research

This project aims to determine:

1. the stratigraphic and deformational sequences of the Dalradian lithologies of the NW Letterfrack area;
2. the metamorphic sequence;
3. the relation of the metamorphism to deformation, with particular bearing on the timing and effects of the Renvyle - Bofin slide;
4. the timing and manner of emplacement of the Dawros - Currywongaun - Doughraugh igneous bodies.

This information, along with pressure and temperature data determined using published calibrations of mineral geothermometers and barometers, and P - T paths calculated from the zoning profiles of garnets using the method of Spear & Selverstone (1983), is used to ascertain the tectonothermal

have nucleated on the andalusite porphyroblasts. Cruse (1963) and Cruse & Leake (1968) regarded the andalusites around Rushenduff as having grown either prior to, or after, $D_4$.

Andalusite growth in the rest of Connemara is late in terms of the tectonic sequence, occurring syn/post $D_3$ (Yardley *et al.* 1987). Most andalusite occurrences in Connemara appear to be of regional metamorphic origin, although local developments can be related to the contact aureole effects of post - tectonic granites (e.g. Ferguson & Harvey 1978). The development of regional andalusite is considered by Yardley *et al.* (1987) to be due to the progressive northward migration of isotherms through the Connemara massif, driven by the 'heat engine' of the migmatite zone intrusive gneisses in S Connemara. This migration of isotherms is synchronous with uplift and erosion in the massif resulting in the development of peak temperatures at progressively lower pressures from south to north. Yardley *et al.*'s model explains the development of andalusite within the northern staurolite zone lithologies and the more complex $Al_2SiO_5$ relations seen in the higher grade lithologies of southern Connemara. Ferguson & Al-Ameen (1986) suggest that the uplift during heating is related to the development of the Connemara antiform (a $D_4$ structure).

The growth of andalusite in the study area appears to be earlier than in the rest of Connemara, being of post $D_2$ - early $D_3$ age, and as such it is difficult to relate such an occurrence to either of the models suggested. Given the spatial distribution of andalusite, it is possible that its development in the study area could be related either to the emplacement of the Crump Island body (Cruse 1963) or associated with pre - $D_3$ uplift of the Kylemore Fm, possibly due to movement on the Renvyle - Bofin slide {3.3}.

4.1.3.10 <u>Kyanite</u>: Kyanite is typically absent over much of Connemara and was found in only one locality in the study area [GR 702 602]. It is developed as scattered 2 - 3mm corroded porphyroblasts (Figure 4.50), within muscovite and quartz rich pods, in Grt + Bt + Ms + Pl + Qtz + Tur schists. No unequivocal timing relationships between the kyanite and the rock fabrics could be ascertained, although the quartz - muscovite pods are

wrapped by the dominant composite ($S_{2/3}$) foliation, suggesting the kyanite probably developed early in the foliation evolution (pre/syn - $D_2$).

Throughout the rest of Connemara kyanite occurs sparsely, developing after $D_2$ (Yardley *et al.* 1987) synchronous with the growth of staurolite. Two explanations for the lack of kyanite within the Connemara massif have been put forward:

i, Ferguson & Al-Ameen (1986) consider that the restricted spatial distribution of kyanite is due to the effects of lithological composition, with P-T conditions (as calculated from absolute thermobarometry) suitable for kyanite growth having occurred over much of the massif. They suggest that kyanite growth occurred only in those lithologies where infiltrations of $CO_2$ rich fluids led to suitable compositional conditions.

ii, Yardley *et al.* (1987) consider that the lack of kyanite occurs simply because suitable P-T conditions were only narrowly reached over much of the massif. They suggest that systematic errors within the commonly used cation exchange thermobarometers (especially the Grt - Pl Ca exchange barometer), due to the use of non - equilibrium assemblages, lead to overestimations in the peak P - T reached in the massif. This leads Yardley *et al.* to suggest that 'peak' pressure values, calculated using Grt - Pl Ca exchange systems, may overestimate pressure by as much as 2-3 Kb, and suggest that the true maximum pressures recorded are 5-6 Kb (against the 7-8 Kb stated by Ferguson & AL-Ameen 1986).

Apart from the pelite already discussed, the pelites in the study area are kyanite free and show a mean MFM ratio of 0.339 in the regionally metamorphosed lithologies and 0.348 in the contact lithologies, a value less than the 0.353 suggested by Naggar & Atherton (1970) as being the minimum MFM for the development of kyanite in Dalradian pelitic lithologies (NB, the value of MFM is recalculated for Naggar & Atherton's (1970) data set as MgO / ($MgO + FeO^{total}$) with all iron in the ferrous state). This is consistent with the restricted development of kyanite in the study area being controlled by lithological composition rather than P - T conditions, the bulk of pressure - temperature estimates (using apparent equilibrium assemblages) lying in the kyanite field {5.4}.

**Figure 4.51: Tabular cordierite crystals replaced by pale yellow pinnite within granoblastic contact aureole lithology (X 29) PPL.**

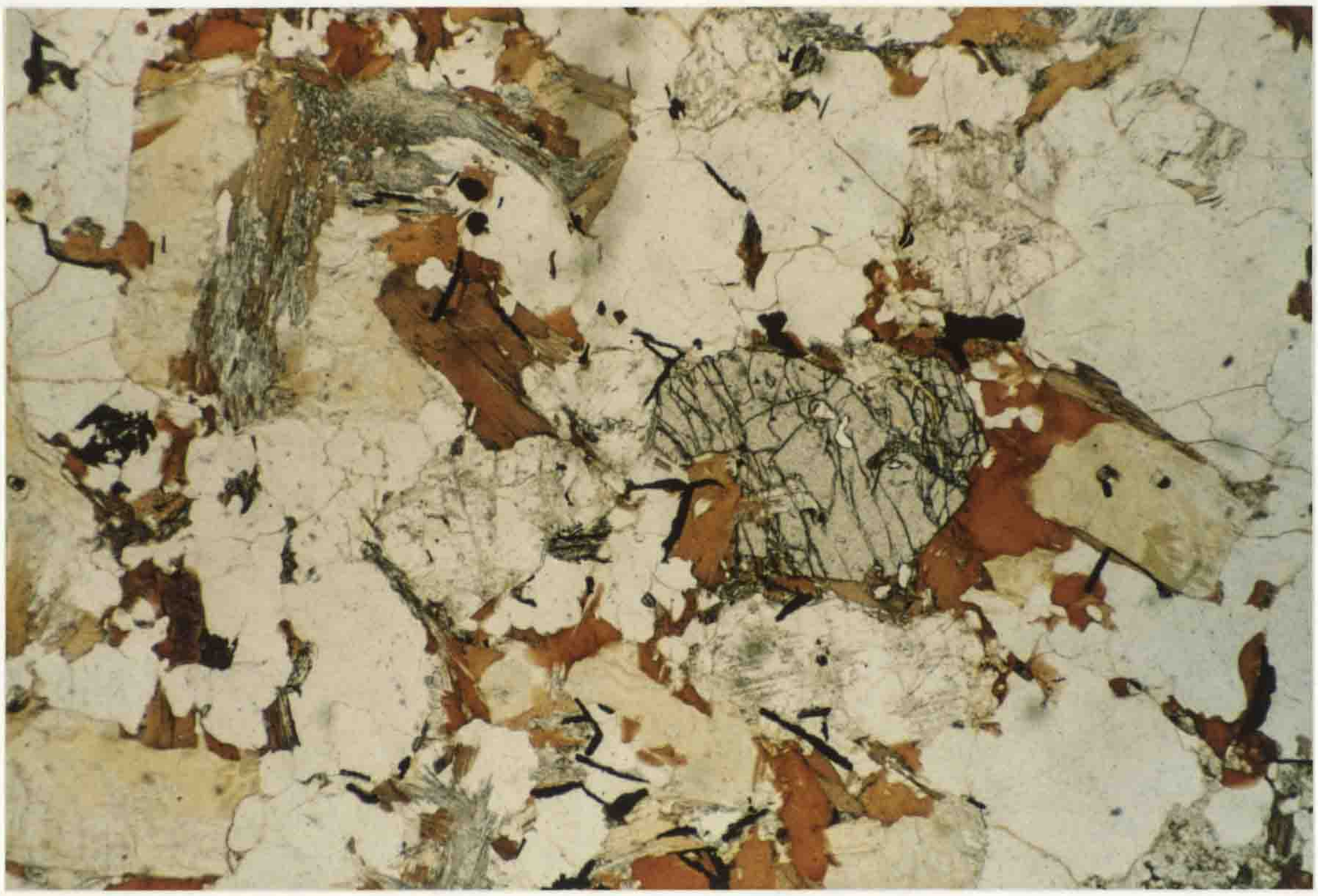

**Figure 4.52: Colour zoned tourmaline developed in schistose Streamstown Fm regional metamorphic lithology (X 110) PPL.**

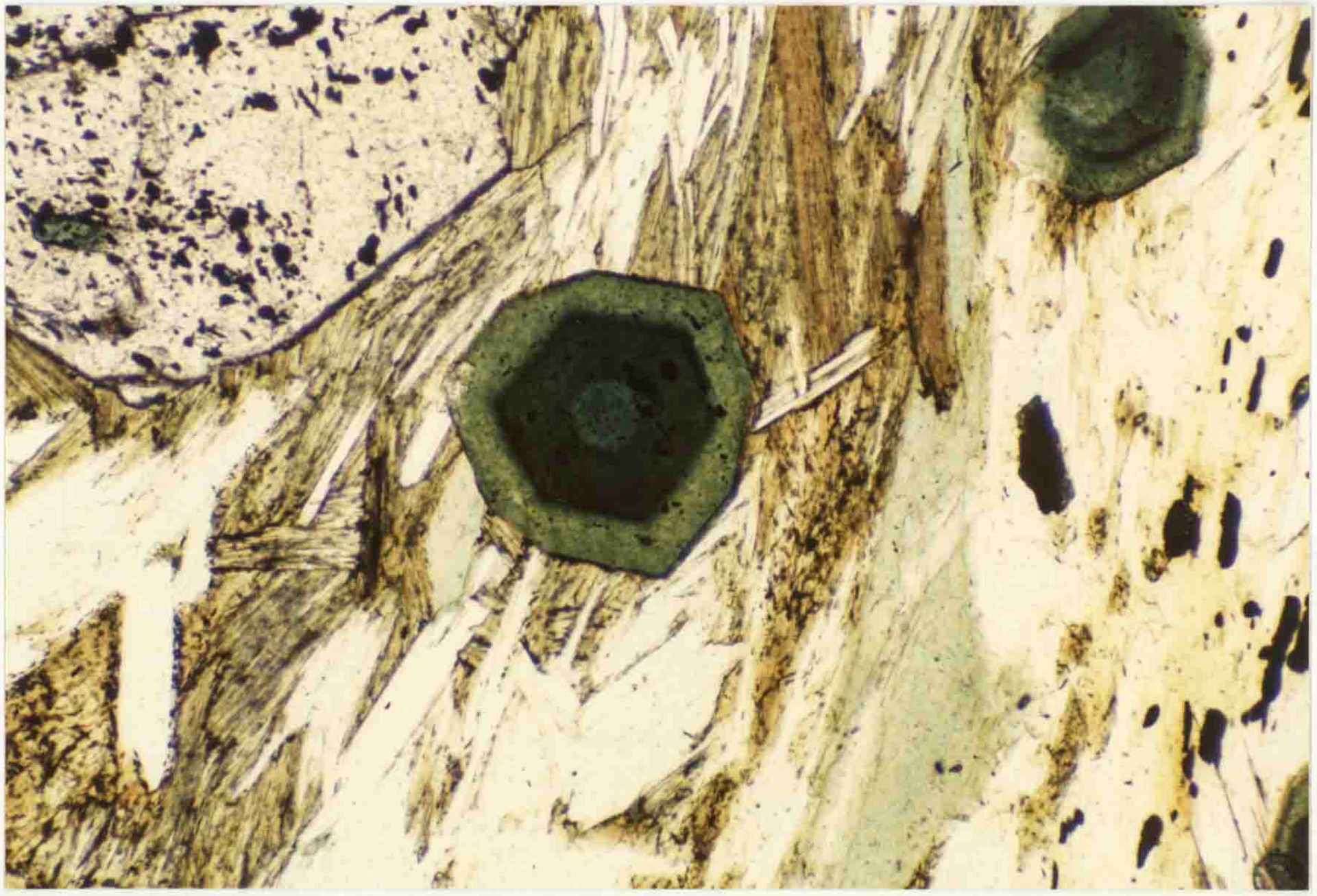

4.1.3.11 Cordierite: The development of cordierite in the contact aureole of the DCD has been noted by several authors (e.g. Ingold 1939, Leake 1965). This study identified no completely fresh cordierite within such lithologies, only variably altered rounded to subhedral porphyroblasts up to 3mm diameter within granoblastic hornfels lithologies. The altered cordierite porphyroblasts are often mantled by biotite which is associated with sillimanite, suggesting that cordierite broke down to produce Bt and Sil and the pinitic alteration product. Two styles of alteration of cordierite are present: a micaceous pinitic, and a yellow - brown isotropic alteration product which partially or completely replaces cordierite porphyroblasts (Figure 4.51). The yellow - brown isotropic alteration product has been described from cordierites in Malawian gneisses by Haslam (1983), who notes a significant increase in $K_2O$ in the alteration products in comparison with the unaltered cordierite. Similar yellow - brown isotropic alteration of cordierite has been noted by Ferguson & Harvey (1978) in western Connemara, although pinitic alteration of cordierite is more commonly reported in the 'migmatite belt' of south Connemara (e.g. Barber & Yardley 1985).

4.1.3.12 Tourmaline: Black tourmaline (Schorl) is a common accessory mineral within pelitic and semipeltic lithologies in the study area. Occurrences vary from <1mm needles lying randomly in the foliation of 'regional' schists to 100 - 150mm prismatic crystals developed in Qtz ± Pl ± Ms migmatite veins within the contact rocks of the DCD.

The tourmalines in regional metamorphic assemblages are wrapped by the main ($S_2/S_3$) foliation and show euhedral to subhedral forms. The grains are strongly pleochroic and often display a characteristic colour zoning in thin section (Figure 4.52) with blue-grey cores passing through green zones to pale yellow-green rims. The boundaries between these zones are sharp and typically parallel to the crystal faces. The cause of colour zoning in tourmalines is commonly attributed one of two mechanisms:

i, variations in $Fe^{2+}/Fe^{3+}$ concentrations (McCurry 1971);

ii, variations in Fe/(Fe + Mg) ratios (Tracy 1982).

**Figure 4.53: Uniform colour tourmaline developed in Kylemore Fm contact aureole lithology (X 56) PPL.**

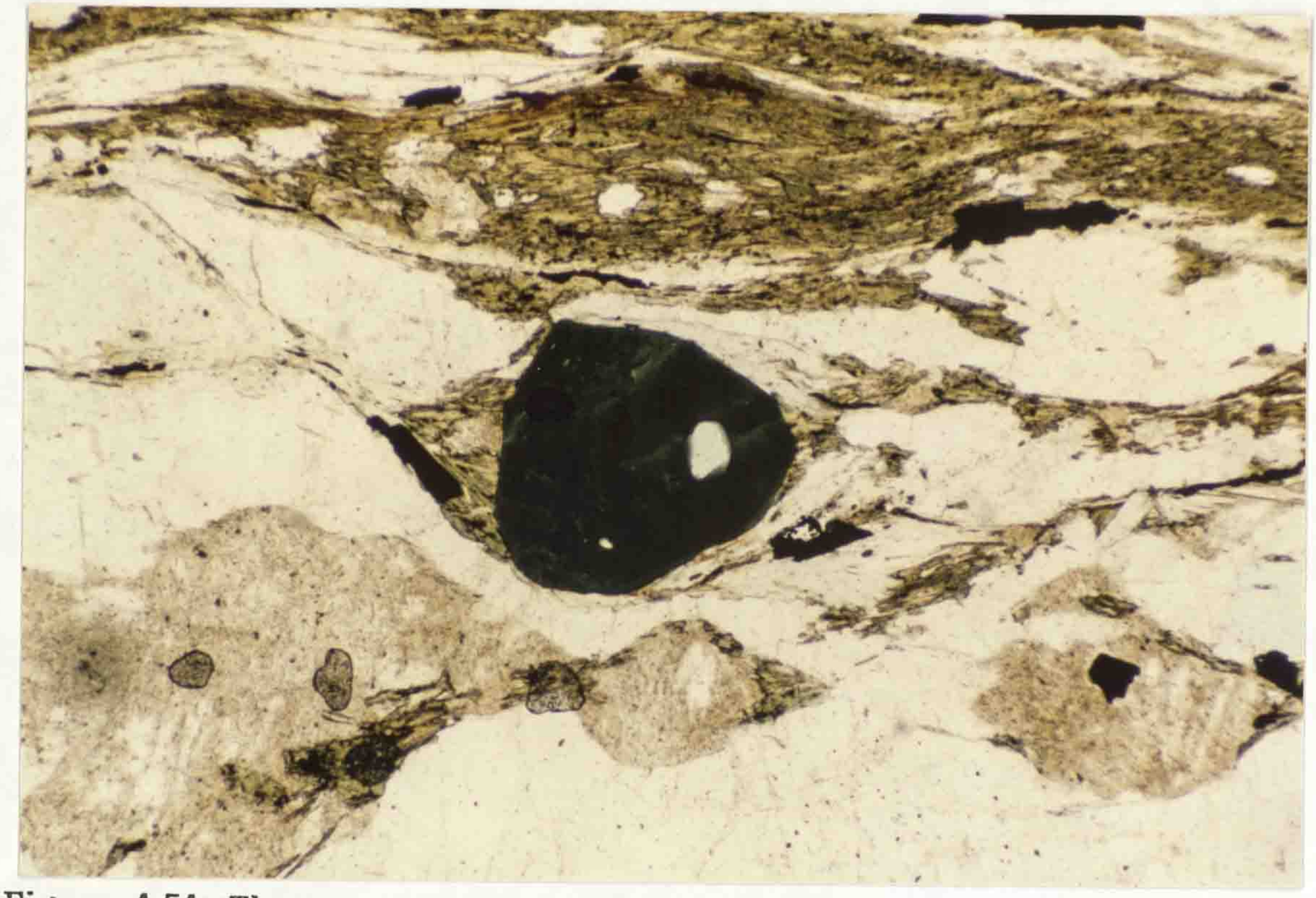

**Figure 4.54: Thompson AFM projection (from Ms) showing the fields of mineral compositions in regional metamorphic pelites. G: garnet field, B: biotite field, S: staurolite field, C: chlorite field. Dashed line defines field of whole rock compositions.**

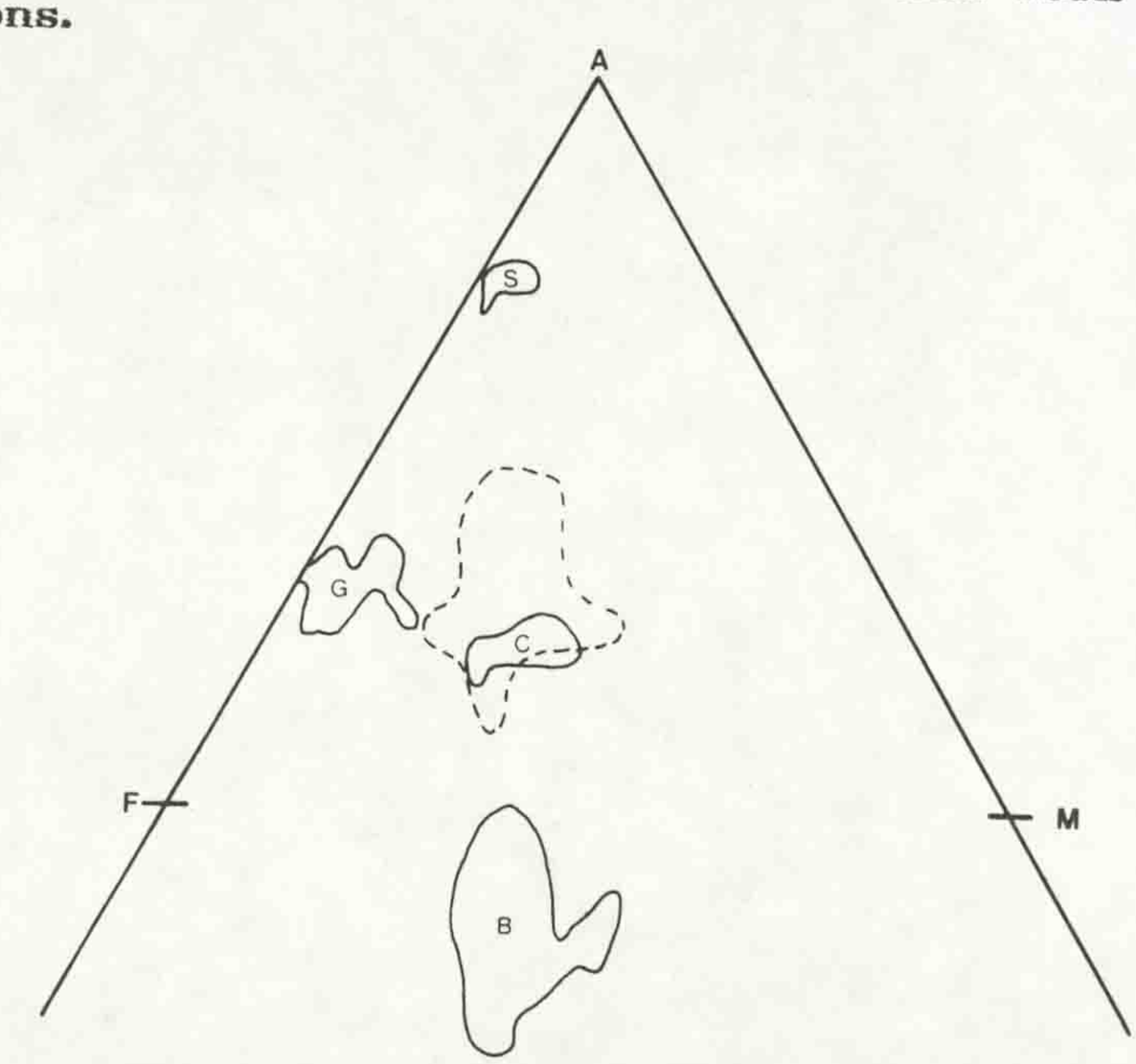

No study of the chemistry of the zoning was undertaken so the cause of the zoning developed in these tourmalines could not be determined.

The tourmaline associated with the intrusive bodies is typically strongly pleochroic olive green and displays sub to anhedral crystal forms with no internal colour zoning (Figure 4.53). Tourmaline - bearing veins are restricted to Kylemore Fm lithologies adjacent to the igneous bodies and are more abundent closer to the bodies. Tourmaline is developed as a matrix mineral within pelitic and semipelitic regional metamorphic rocks.

It is likely that the vein tourmaline is derived from components in the metasediments rather than igneous bodies, as its sole association in the ultrabasic rocks is within metasedimentary xenoliths and mobilised migmatitic lithologies. The development of tourmaline may therefore reflect the original composition of the metasedimentary lithologies, possibly being due to the mobilisation of original detrital grains (a feature apparent in many Dalradian metasedimentary lithologies (Deer *et al.* 1966) during the metamorphism. Alternatively, given the association of tourmaline with the more pelitic lithologies of the study area, it is possible that the tourmaline may be the product of boron bearing metasomatic fluids, the boron being held in the original sedimentary minerals (primarily phyllosilicates) and released during the metamorphism (Frondel & Collette 1957).

### 4.1.4 AFM topologies and the sequence of reactions in pelitic lithologies

The mineral assemblages developed in regional and contact metamorphic pelites are noted in {4.1.1}. The development of these assemblages are considered in the system KFMASH (after Thompson 1957).

The regional metamorphic pelites are typified by two assemblages:

Qtz + Pl + Grt + Bt + Chl ±Tur

Qtz + Pl + Grt + Bt + St + Chl ±Tur.

These assemblages are developed in pelitic rocks on either side of the Renvyle - Bofin slide, suggesting that the slide may

**Figure 4.55: AFM topology for peak mineral assemblages in regional metamorphic pelites.**

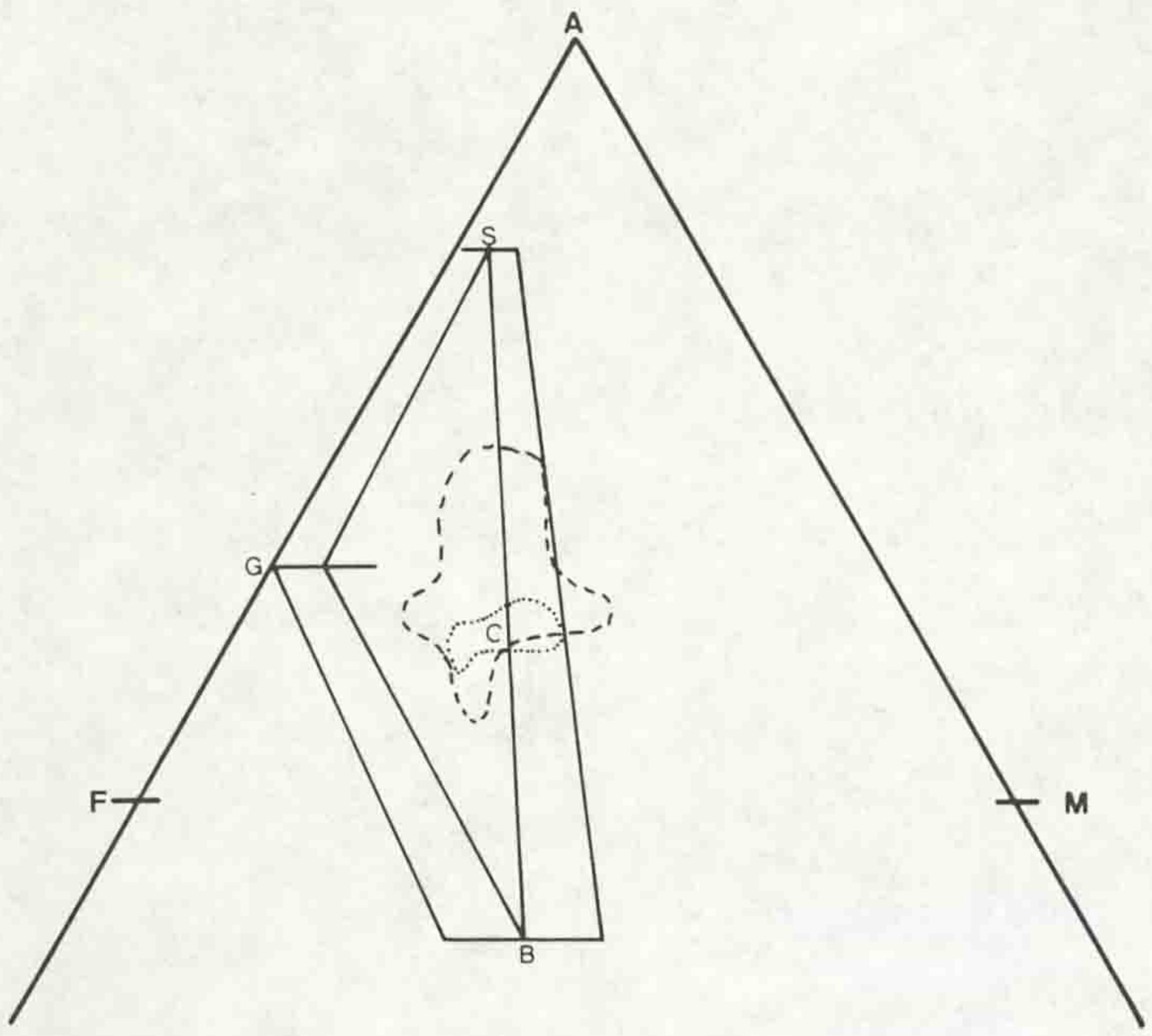

Figure 4.56: Isobaric psuedobinary T - X section (at A = 0), after Atherton (1977), showing the expected sequence of reactions within regionally metamorphosed pelites. Stability fields: 1 = Grt + Bt, 2 = Grt + Bt + Chl, 3 = Bt + Chl, 4 = Grt + Bt + St, 5 = St + Bt, 6 = St + Bt + Chl, 7 = Ky + St + Bt, 8 = Ky + Bt, 9 = Ky + Bt + Chl. The line WR indicates the range of whole rock compositions. The schematic AFM projections (from Ms, with Qtz + Pl + $H_2O$) show the topological change caused by the up - temperature breakage of the Grt - Chl tie - line and the field of Grt + Bt + St becoming stable. Note that the range of whole rock compositions fall only into the Grt + Bt and Grt + Bt + St fields at high temperatures.

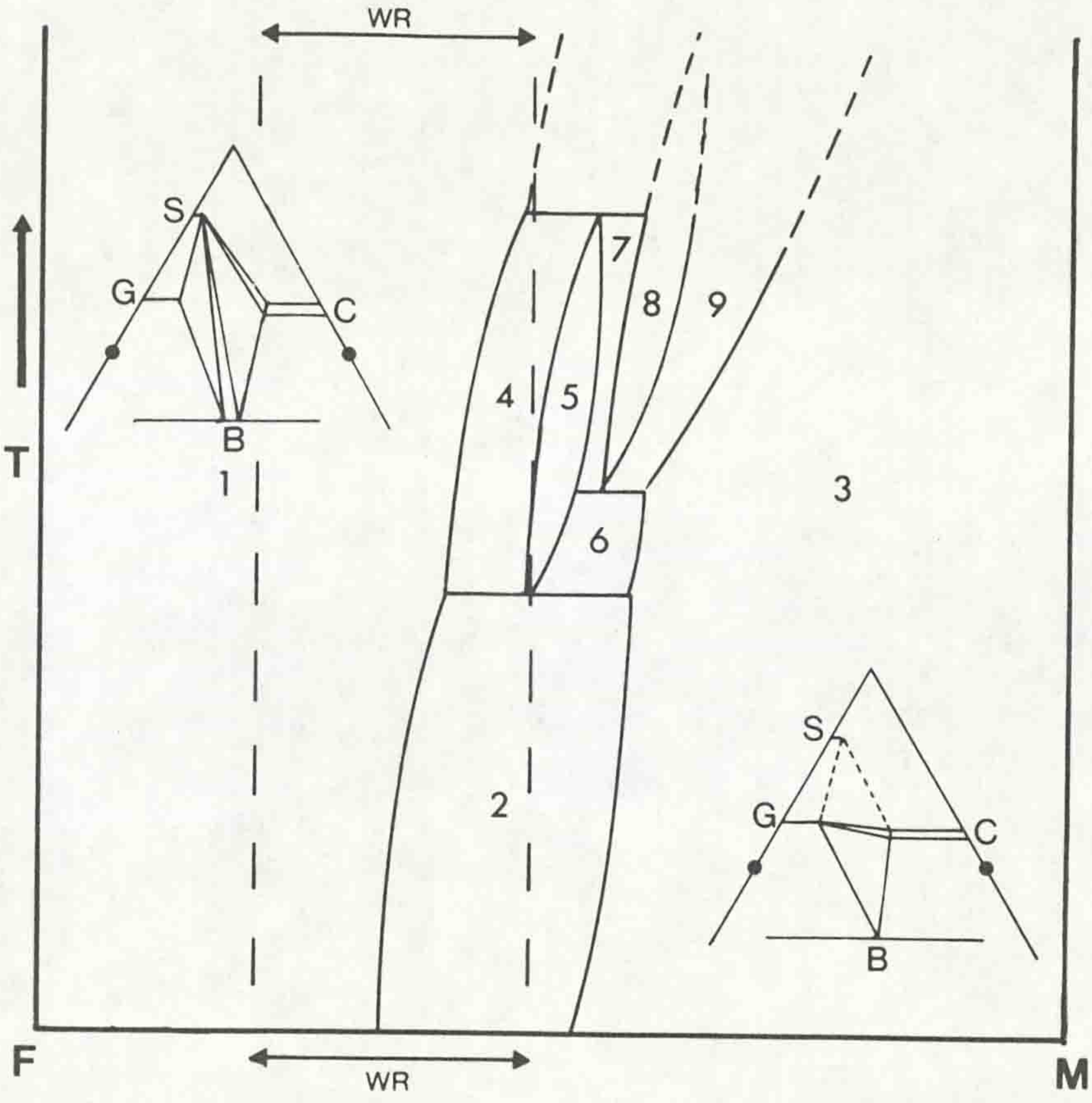

predate the development of the regional metamorphic assemblages {Chapter 3}. The timing of mineral growth, as determined by textures and fabrics, suggests that the stable coexistence of Grt + Bt (+ St) represents the peak metamorphic assemblage, developing syn to late $D_2$ ($MS_2$ in the terminology of Sturt & Harris, 1961) with chlorite growth occurring later ($MS_3$). The assemblage lacking staurolite as a stable phase is of limited use in determining the sequence of AFM reactions as the Grt + Bt tie - line is stable throughout many other changes in topology.

The fields defined by the compositions of garnet, biotite, staurolite and chlorite on a Thompson AFM projection (from muscovite, with Qtz, Pl and Ilm) are shown in Figure 4.54. The configuration of tie - lines during the development of the peak mineral assemblage is shown in Figure 4.55. It is notable that this topology indicates the instablity of chlorite, breakdown of which provides material towards the development of the Grt + Bt + St assemblage. Certain of the chemical features (Mn zoning in garnet {4.1.3.1}, Ti in staurolite {4.1.3.7}) of the peak minerals suggest that chlorite breakdown occurred during the development of the peak assemblage. Such a reaction sequence requires that the garnet - chlorite tie - line breaks early in the development of the assemblage (e.g. Labotka 1980) with the resulting reaction;

$$Grt + Chl + Ms = St + Bt + Qtz + H_2O \quad \text{--- (1)}$$

consuming the chlorite. This reaction defines the staurolite - biotite isograd of Carmichael (1970). A psuedobinary T - X section (after Atherton 1977) shows the location of the Grt + Bt and Grt + Bt + St fields and the range of whole rock compositions (Figure 4.56). As is evident from this diagram an increase in metamorphic grade for a lithology within the compositional field will lead to either the continuous stability of Grt + Bt or a change from a continuous reaction between garnet, chlorite and biotite to a discontinuous reaction as the garnet - chlorite tie breaks. The continuous reaction between garnet, chlorite and biotite will, with increasing grade, move to progressively more magnesium - rich compositions. Atherton (1977) notes that, at the onset of the discontinuous reaction resulting in the loss of chlorite, the MFM ratios of biotites should have values of less

than 0.56. The MFM ratios for analysed biotites from regional metamorphic assemblages range from 0.22 to 0.56, with a mean of 0.39, implying that the biotite compositions developed in the Grt + St + Bt stability field.

As the development of staurolite appears to be later than the initial nucelation of garnet and biotite it is possible that the early stages of the development of garnet and biotite were controlled by the continuous reaction:

Chl + Ms + Qtz = Grt + Bt + $H_2O$ --- (2)

With the breaking of the garnet - chlorite tie - line through reaction (1) the production of staurolite leads to the consumption of chlorite. The final breakdown of chlorite may have resulted in the release of Mn and to the Mn enrichment seen in the rims of certain regional garnets {4.1.3.1} and may have released the Ti evident in staurolite.

The late chlorite typically replaces biotite within regional metamorphic assemblages suggesting that during retrogression the garnet - chlorite tie - line reformed with the effective bulk compositions falling into the Grt + St + Chl stability field. It is significant that the compositions of chlorites fall partially into the Grt + St + Bt field, showing further the lack of relation of Chl to the development of the peak assemblage.

Cruse & Leake (1963) report the development of late chloritoid in Qtz + Ms + Grt + Chl pelites of Renvyle and Inishbofin, relating this to a *'hidden igneous mass'*. No chloritoid was detected in this study and this lack, along with the paucity of information on chloritoid in Cruse & Leake, renders the interpretation of possible chloritoid - forming reactions difficult. Assuming that the assemblage Qtz + Ms + Grt + Chl + Cld given by Cruse & Leake represents a stable assemblage it suggests that the form of the AFM reactions were as shown in Figure 4.57, with the Grt - Chl tie established and effective bulk rock compositions falling into the Grt + Chl + Cld field.

The development of andalusite within certain of the regional metamorphic pelites has been discussed {4.1.3.9}, the relations of andalusite with staurolite suggesting that the reaction:

St + Ms + Qtz = And + Bt + $H_2O$ (Yardley 1976) --- (3)

leads to andalusite formation (Figure 4.57).

From reactions (1), (2) and (3) it is clear that a fluid phase

evolution of the area, and to constrain models of its evolution.

## 1.4 Techniques used

1.4.1 Field studies: The stratigraphic and structural sequences of the area were determined by field mapping (approx 40km²) at 1:10,000 using enlarged air photographs in conjunction with the available base maps (O.S sheets 83, 84, 93, 94, which date from 1898 and show no contour information). The Dawros peridotite and its contact zones, an area of approximately 1.5km², were mapped using both photos and enlarged base maps at 1:2,500.

The area was surveyed using a Gamma ray spectrometer {Appendix A} to ascertain the distribution of the primary radiogenic heat producing elements (U, Th, K%) to provide data on the potential magnitude of radiogenic heating.

1.4.2 Laboratory studies: Petrological work performed includes mineral assemblage and fabric/textural description using light microscopy, X-ray fluorescence measurement of whole-rock chemistry, measurement of radioelement abundances through neutron activation of selected samples (used in calibrating the field data on radiogenic element distribution), and electron microprobe analysis of mineral compositions {Appendix B}. The probe data were used in the calculation of temperature and pressures, and, as profile paths through garnets, in the Spear (1986) calculation of P-T trajectories.

These pressure and temperature data, along with the heat production information, were used to constrain computer programs which modelled the temporal evolution of 1-D temperature profiles, and these models enabled an assessment of the contributions of heat flux variations during the evolution of the Connemara massif.

## 1.5 Previous work

Rather than provide an extensive review of previous work on the thesis area, this section is intended to provide an overview, and a brief discussion of the bias of previous work. More specific detail is discussed later in the relevant sections.

The study area was first covered by the Irish Geological

was present during the development of the regional metamorphic assemblages. The nature of this fluid is unclear, although the absense of a carbonate phase within the pelites suggests that the fluid was $H_2O$ rich. The ubiquitous presense of colour zoned tourmaline within regional metamorphic pelites {4.1.3.12} indicates that fluid transport of ions was significant in the development of at least part of the mineral assemblage. The consistent nature of the colour zoning (blue / grey core through green zone to pale yellow - green rim) in tourmalines throughout regionally metamorphosed pelitic rocks may suggest that the fluid was relatively mobile during tourmaline growth. The nature of the fluid phase in regional metamorphic pelites and its significence in the evolution of the mineral assemblage are discussed in {5.6}.

The reaction sequence of the contact metamorphic pelites of the Kylemore Formation is somewhat different from that developed in regional pelites, with the typical assemblage being:

Qtz + Pl + Grt + Bt + Sil + Kfs ± Crd ± Ms

The most common assemblage is Crd and Ms free, Ms breakdown through the reaction:

$Ms + Qtz = Kfs + Sil + H_2O$ --- (4)

leading to the development of Sil and Kfs {4.1.3.3}. The AFM topology for these assemblages is shown in Figure 4.58, along with the compositional fields of analysed Grt and Bt. Coexisting Ms, Kfs and Qtz are seen in some of the contact pelites, a relation which suggests the Ms breakdown reaction {4.1.3.3} did not reach completion locally.

The assemblages which contain Crd are Ms - free, typically containing Kfs and Sil, a relation noted by Yardley, Leake & Farrow (1980) in the south Connemara migmatite belts. Barber & Yardley (1985) suggest two possible reactions which lead to the development of cordierite:

$Sil + Bt + Qtz = Kfs + Crd + H_2O$ --- (5)

$Grt + Sil + Qtz + H_2O = Crd$ --- (6)

As the textural relations of Grt and Crd (now present only as altered relics) suggest that the two minerals coexisted in a stable assemblage it is likely that reaction (6) was not responsible for Crd development. The relation of Sil and Bt to Crd {4.1.3.11} suggest that the Crd became unstable and was

**Figure 4.57: AFM projection showing reaction topologies for andalusite and chloritoid bearing assemblages.**

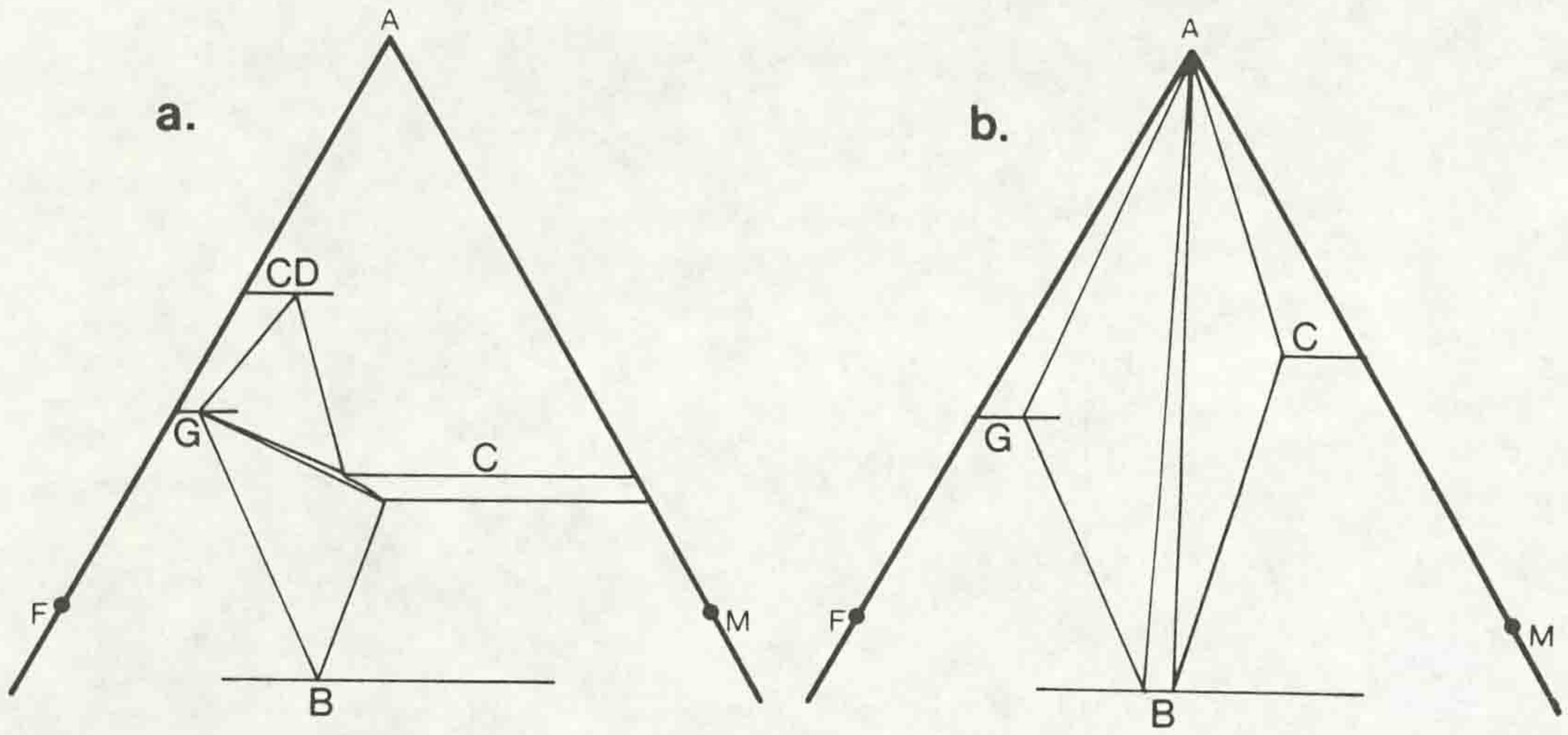


**Figure 4.58: Thompson AFM projection (from Kfs) showing the field of mineral compositions in contact metamorphic pelites. G: garnet field, B: biotite field. Dashed line indicates field of whole rock compositions.**

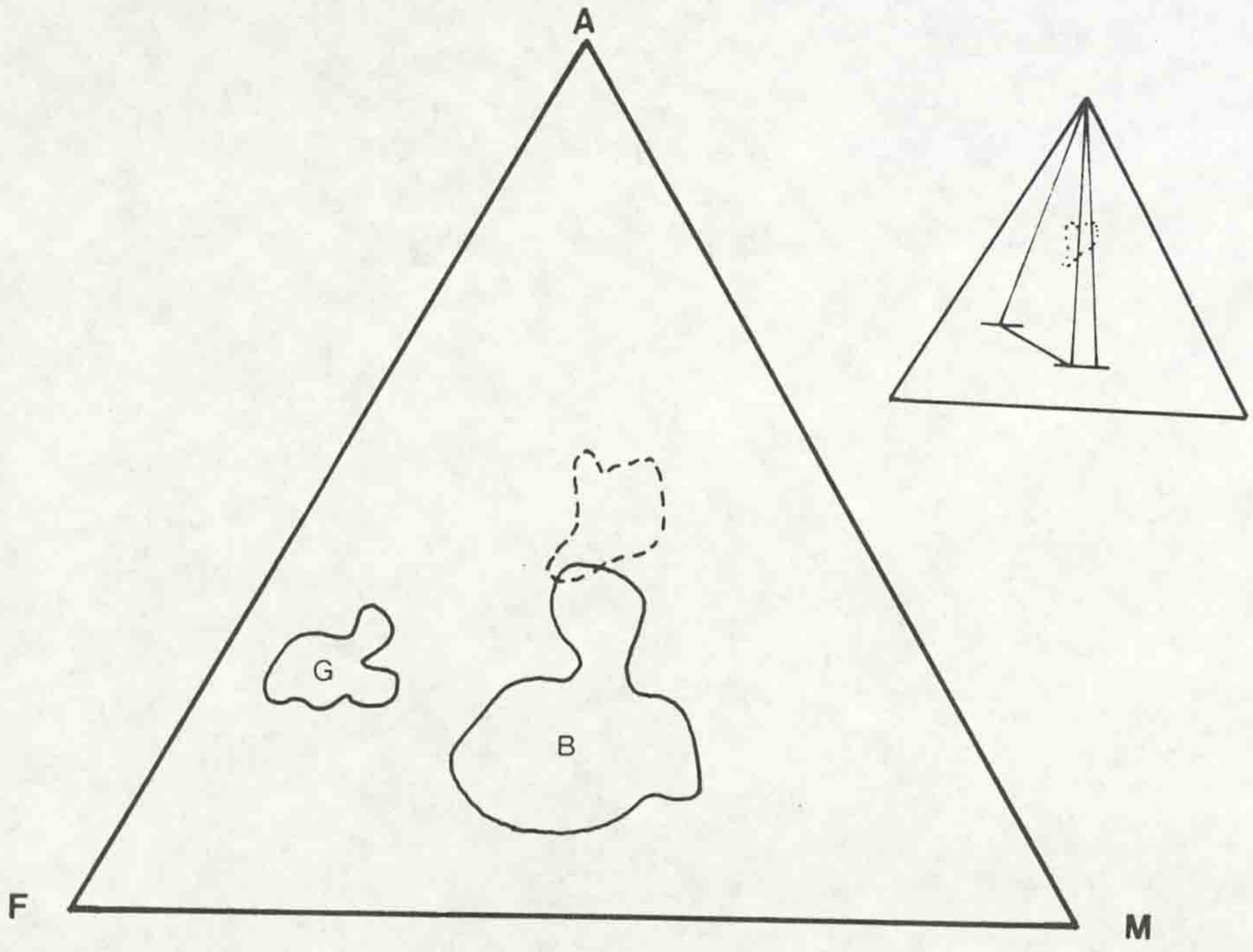

**Figure 4.59: AFM projections (after Thompson, 1976a Fig 3) for Grt + Bt + Sil + Crd + Kfs + Qtz + $H_2$) assemblages.**
**a, Grt + Crd tie - line established (Grt + Crd + Bt stable), high temperature, early assemblage.**
**b, Bt + Sil tie - line established (Grt + Bt + Sil stable), lower temperature, later assemblage.**

replaced by Sil and Bt. The sequence of reactions likely to produce the phase relations seen are shown in Figure 4.59. The initial stable assemblage Grt + Crd + Bt (with Kfs and Qtz) became unstable, with the assemblage Grt + Bt + Sil becoming stable. The discontinuous reaction leading to Crd instability requires the breaking of the Grt - Crd tieline and occurs in a down temperature sense (Thompson 1976a). The initial stability of Grt + Crd + Bt represents a high temperature assemblage, with the subsequent Grt + Bt + Sil overprint representing a lower temperature stability system. The sequence of stable assemblages may represent the initial intrusion of the gabbroic bodies, leading to temperature conditions in which the Crd - bearing assemblages were stable, with the subsequent cooling phase producing lower temperatures at which the Sil - bearing assemblage was stable.

## 4.2 Igneous lithologies

### 4.2.1 Introduction

The igneous rocks covered in this section belong to the basic and ultrabasic material which makes up the DCD. The lithologies in this complex range from feldspar - free ultrabasic to gabbroic and quartz - diorite assemblages. Six samples of ultrabasic material from 'pods' {2.2.3} were analysed by XRF {Appendix B}, in an attempt to assess their relation to the main part of the DCD.

#### 4.2.1.1 Igneous assemblages

The assemblages developed in the basic and ultrabasic lithologies fall into two groups, original igneous assemblages and secondary metamorphic overprint/alteration assemblages, which range from amphibolitic to serpentinitic.

The peridotite assemblages are typically feldspar free {2.2} and fall into three main groups:

Ol + Opx ± Spl ± Phl

Ol + Opx + Cpx ± Spl ± Phl

Ol + Opx ± Spl ± Phl

Within gabbroic lithologies the original assemblages are feldspar bearing and are typically (after Kanaris - Sotiriou &

Angus 1976):

Opx + Cpx + Pl (commonly An>90) ± opaques ±
Bt

The proportions of the minerals are highly variable, giving lithologies which range from pyroxenites to anorthosites.

4.2.1.2 Metamorphic overprint assemblages

These assemblages overprint the original igneous mineralogies and are often variably developed.

In the peridotitic lithologies, especially within the small isolated pods {2.2.3}, assemblages containing amphibole are patchily developed and typically consist of:

Tr + Tlc

with relict pyroxene and spinels.

More commonly the alteration assemblages in ultrabasic lithologies are serpentinitic {4.2.3.6}

Ctl + Lz + Cal

with relict olivine and pyroxene.

At the tectonised margins of the Dawros peridotite foliated schists with the assemblage:

Tlc + Cal ± opaques

are developed.

In the gabbroic lithologies alteration of the original assemblage to give:

Tr/Act + Ep + White mica ± Chl

is common. The amphibole minerals often form rims on relict pyroxenes.

4.2.2 Whole rock chemistry

The chemical compositions of five igneous lithologies were analysed by XRF {Appendix C}. The samples analysed consisted of material from the serpentinic 'pods' developed within the Kylemore Fm {2.2.3} at [GR 729 628] (samples 68790, 68792), [GR 713 605] (sample 71890) and [GR 705 630] (samples 71943, 71944). These lithologies were sampled because their mineral assemblages (serpentinitic or talc / tremolite with rare relict pyroxene and olivine nb, Pl absent assemblages) and field relations {2.2.3} suggested that their original affinities were somewhat different from the amphibolitic lithologies discussed in {4.1.2}.

Figure 4.60: Ternary AFM (A = ($Na_2$ + $K_2O$), F = (total iron as $Fe_2O_3$ + MnO), M = MgO all as molar %) plot of analyses from ultrabasic pods (Dots) within the study area and data from other ultrabasic lithologies within Connemara (data from Leake (1958b) Cashel ultrabasic material (Open circles), Kanaris - Sotiriou & Angus (1976) Ultrabasic material from Currywongaun (Open squares), Boyle, McCarthy & Stewart (1987) Creggaun gabbro material (Open triangles)). The arrow indicates Kanaris - Sotiriou & Angus's (1976) petrogenetic evolution trend.

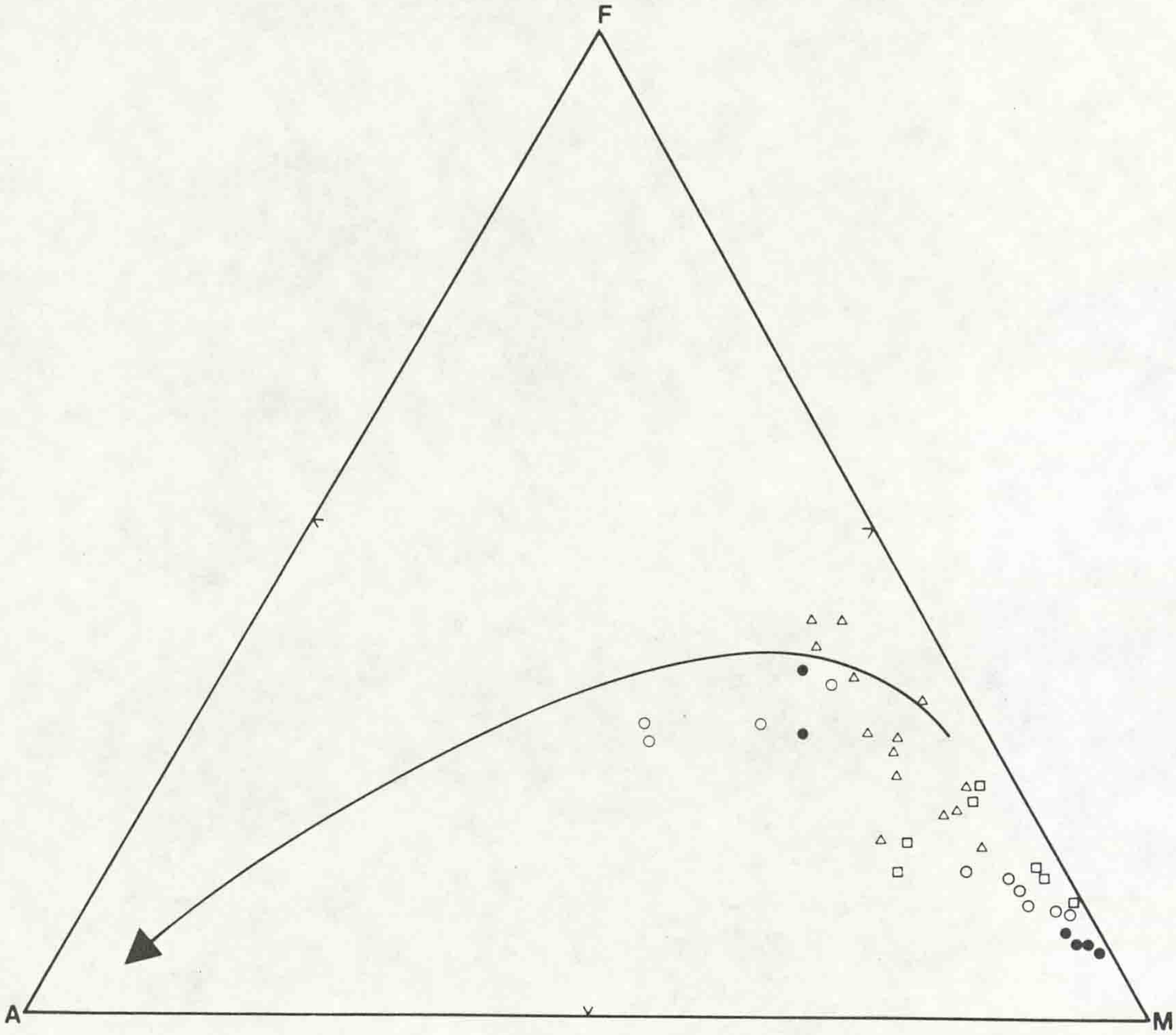

**Figure 4.61: Massive Harzburgitic lithology (X 29) XPL.**

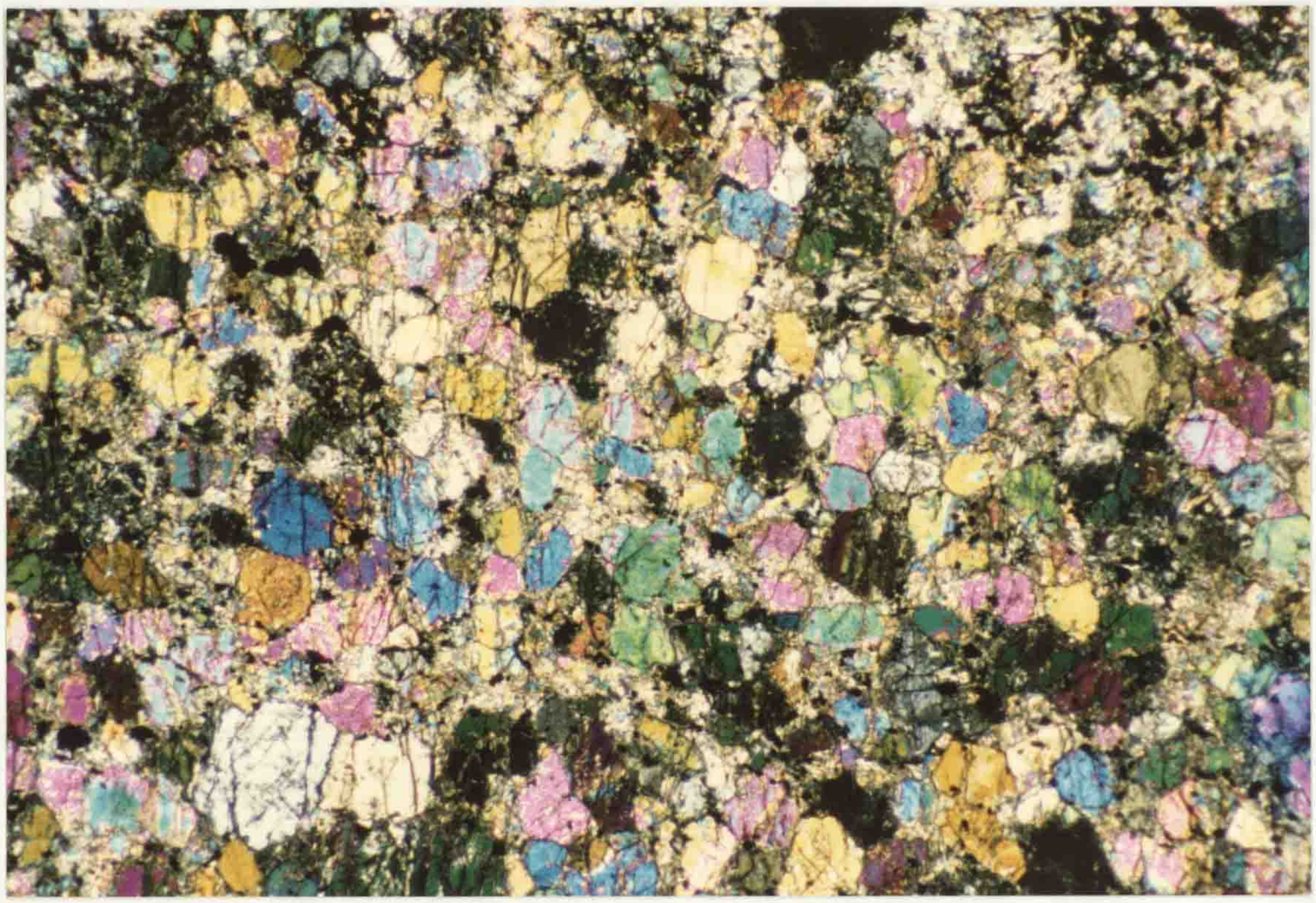

**Figure 4.62: Orthopyroxenite (X 29) XPL.**

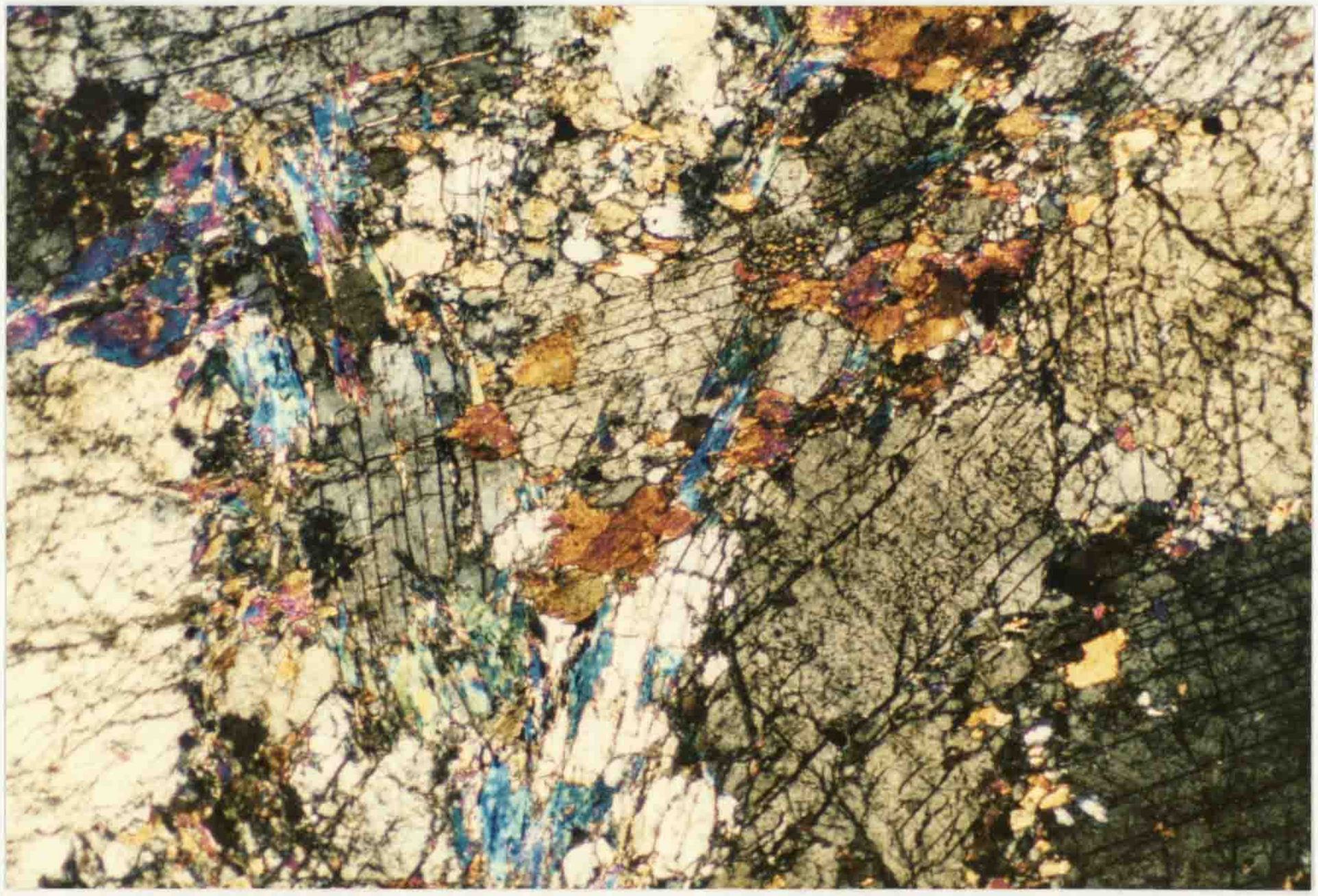

A ternary plot of A ($Na_2O + K_2O$), F ($FeO^* + MnO$), M (MgO) as molar percentages (Figure 4.60) shows the analysed lithologies to plot on or near to the F - M join, at the basic end of Kanaris - Sotiriou & Angus (1976) petrogenetic evolution curve for the Connemara ultrabasic suite. The data plot close to Leakes' (1958b) data for the basic and ultrabasic parts of the Cashel intrusion.

It is evident that the ultrabasic pod material shows affinities with the ultrabasic lithologies, both in the DCD and in the rest of Connemara, suggesting that they represent part of the same magmatic system.

4.2.3 Petrography

4.2.3.1 Massive Harzburgites: These lithologies are characterised by an anhedral equigranular olivines and pyroxenes (Figure 4.61). Both enstatitic orthopyroxene and diopsidic clinopyroxene are present, commonly showing 0.5 to 1mm grain sizes, although enstatitic orthopyroxene is rarely developed as laths upto 5mm. Enstatitic pyroxenes often contain exsolved blebs of clinopyroxene in (100) planes and the larger grain size laths contain inclusions of olivine and clinopyroxene. Interstitial phlogopitic mica is present in small quantities (2 - 3% of the rock); some grains are included in the orthopyroxenes. Rare rounded spinels occur as inclusions within the pyroxenes. A variably developed serpentinitic alteration and associated growth of opaque phases (generally magnetite) locally obscures the original igneous textures and mineralogies.

4.2.3.2 Massive Orthopyroxenite: The euhedral laths seen in outcrop are enstatitic orthopyroxene and form up to 80% of the total rock. These orthopyroxenes show irregular, locally consertal, boundaries and vary in form from lath - like to equigranular in texture (Figure 4.62). No evidence of compositional zoning is seen in the orthopyroxenes, although strained extinctions are evident and small blebs of exsolved clinopyroxene are developed along the (100) cleavages. A fine ( <1mm) interstitial growth of diopsidic clinopyroxene is present, with minor development of opaque oxide minerals (mostly

**Figure 4.63: Strongly altered gabbroic lithology (X 29) PPL.**

**Figure 4.64: Tremolite - Talc lithology developed at the peridotite - gabbro contact [GR 696 590] (X 29) XPL.**

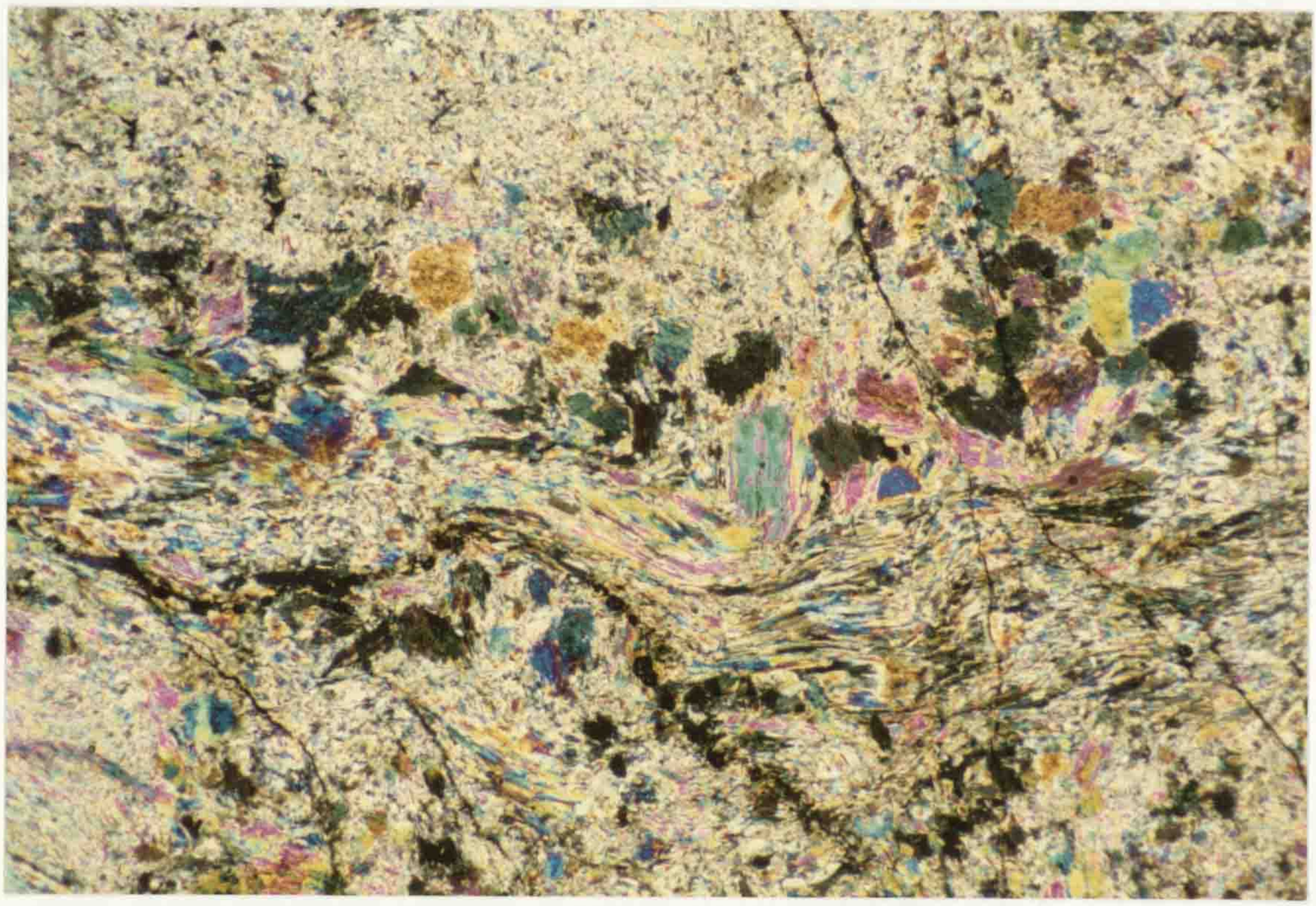

magnetite) and rare spinels.

4.2.3.3 Transition zone of layered lithologies

This lithology consists of anhedral, equigranular forsteritic olivine, enstatitic orthopyroxene and diopsidic clinopyroxene of 0.5 - 1mm grain size. Olivine forms 5-10% of the total rock with varying proportions of ortho and clinopyroxene making up the remaining percentage. The proportions of the two pyroxenes show a change in the dominant pyroxene from orthopyroxene at the base of the zone to clinopyroxene at its top. Minor amounts ( <5%) of anhedral chrome spinel, 0.1 - 0.2mm grain size, are present either as rare inclusions in pyroxenes or more commonly as interstitial phases.

4.2.3.4 Lherzolite

The lithology consists of layers of granular clinopyroxene with scattered inclusions of rounded olivine and rare orthopyroxene as interstitial material, and granular, olivine rich material with scattered pyroxenes. Spinels are evident as scattered grains; no spinel horizons were seen.

4.2.3.5 Gabbroic lithologies

The gabroic lithologies are typically strongly altered to amphibole - epidote rich assemblages, although relict olivine and pyroxenes are evident (Figure 4.63). The original igneous textures are often preserved in the alteration products and show evidence of tabular feldspar grains (reaching upto 15mm) with interstitial finer grained pyroxene. Where strong foliation fabrics have developed the original igneous fabrics are obscured. The included blocks of more basic material seen at [GR 697 591] consist of fresh olivine - orthopyroxene - clinopyroxene assemblages, similar to those developed in the adjacent peridotite, and are in sharp contrast to the tremolite - actinolite - epidote assemblages typical of the gabbro.

The glassy serpentinitic lithology developed at the contact between the peridotite and gabbro consists of a locally foliated mesh of fine grained ( upto 1mm) tremolitic amphiboles and talc with minor chlorite (Figure 4.64). The gabbro in contact with this material shows a high degree of alteration, with the

# Structure and metamorphism in the Dalradian of NW Connemara, Ireland

Ian Peter Dawes

ABSTRACT: The Dalradian of Connemara has a metamorphic and structural history dissimilar to that of the Scottish Dalradian. An early phase of nappe scale folding, accompanied by the emplacement of basic and ultrabasic igneous bodies and a 'Barrovian' metamorphism, is followed by further folding and high temperature / medium to low pressure metamorphism leading to the development of extensive migmatisation in south Connemara.

The area studied in this work lies in the NW of the Dalradian massif and has not suffered the migmatitic overprint seen in equivalent rocks to the east and south. The lithologies studied belong to the Bennabeola Quartzite, Streamstown, Lakes Marble and Kylemore Formations (Tanner & Shackleton 1979). An important tectonic break, the Renvyle - Bofin slide (RBS), runs through the study area separating the Kylemore Fm from the other lithologies. The RBS shows evidence of several phases of movement. The lithologies on either side of the RBS show similar structural histories, with an early deformation ($D_2$) associated with the southerly directed nappe emplacement and significant E - W extension, followed by a phase of folding ($D_3$) due to N - S shortening, which is then folded by the regional scale Connemara antiform.

The regional metamorphic peak is reached syn/post $D_2$, the assemblage Grt - Bt - St being typical throughout the study area. Geothermobarometric studies in the regional metamorphic assemblages yield mean P - T conditions of 574 °C at 7.33 kb in the Kylemore Fm and 490°C at 6.67 kb in the Streamstown Fm.

Modelling compositionally zoned garnets using the method of Spear & Selverstone (1983) on material from the study area show that the development of the syn - deformational peak assemblage to be associated with uplift of the Kylemore Fm and burial in those rocks to the south of the RBS. This evidence, coupled with the orientation of fabrics associated with the RBS, suggests that the RBS initially developed as a $D_2$ thrust, emplacing the Kylemore Fm over the rocks to the south. The application of one - dimensional crustal thermal modelling methods to the RBS system shows that the peak metamorphic conditions recorded in the study area can be produced by simple crustal thickening through the emplacement of an overthrust unit.

A number of syn - $D_2$ basic and ultrabasic bodies, the Dawros - Currywongaun - Doughraugh igneous complex, are developed within the Kylemore Formation. The contact aureole lithologies of these bodies yield mean P - T conditions of 807 °C at 8.03 kb, equivalent to conditions recorded for similar lithologies in south Connemara.

Subsequent deformational events led to the formation of the $F_3$ folds and the probable reactivation, in a dominantly strike - slip sense, of the RBS. The metamorphic grade fell during $D_3$, with chlorite growth being the only significant syn - $D_3$ metamorphic effect. The formation of the Connemara antiform led to tilting of the study area to the north and possible reactivation of the RBS as a brittle normal fault.

The area studied records important evidence as to the nature of the early metamorphism in Connemara, along with the nature of the early deformation and the emplacement of the basic and ultrabasic igneous bodies.

Survey as part of the survey for sheets 93 & 94 and their accompanying memoir (Kinahan, Nolan, Leonard & Cruise 1878). No stratigraphy or measured section for the area were produced although the existence of limestone, schistose (locally hornblendic) and quartzitic units was recorded. Importantly, this work reports the existence of a large scale dislocation, the *'Kylemore valley fault'*, which separates the limestone, schist and quartzite sequence in the south of the area from a northerly series of schists and gneisses within which ophitic, steatic (talc-schist) and amphibolitic bodies are developed.

Following the publication of the survey memoir (1878) the detailed local stratigraphy remained undetermined for 85 years, although descriptions of metasediments (as 'contact rocks') are given in work discussing the igneous bodies (eg, Ingold 1937, Rothstein 1954, 1958), until Cruse (1963) studied the Renvyle peninsula as part of a Ph.D thesis which also covered the islands of Inishshark and Inishbofin. In this work Cruse erected a stratigraphy and noted the existence a major tectonic break in the stratigraphic sequence (the Kylemore valley fault of the survey), and named it the *'Renvyle - Bofin slide'* (RBS). Cruse also determined that the stratigraphy in the lithologies to the south of this slide was inverted. In Cruse & Leake (1968) the lithologies of the area are correlated (after Kilburn *et al.* 1965) with the Dalradian of Donegal and Scotland. This correlation with the Dalradian, and also with the rest of Connemara, was further clarified by Tanner and Shackleton (1979). It should be noted that stratigraphic correlations are best for the lithologies to the south of the Renvyle - Bofin slide, the sequence north of this feature, the Kylemore Formation (Morris & Tanner 1977), lacks a firm position within the regional stratigraphy.

The detailed structure of the area is generally not considered in the early work, the survey being content to note that the Rinvyle (Renvyle) peninsula consists of a *'great synclinal curve'* which trends NW/SE. Cruse (1963) noted that this fold was a synformal anticline (the Tully Mountain synform) and proposed that it was a $D_3$ structure. Tanner & Shackleton (1979) also considered the Tully Mountain synform to be a $D_3$ structure {3.2}.

**Figure 4.65: Classification of serpentinitic textures after Maltman (1978, Figures 1 and 2).**

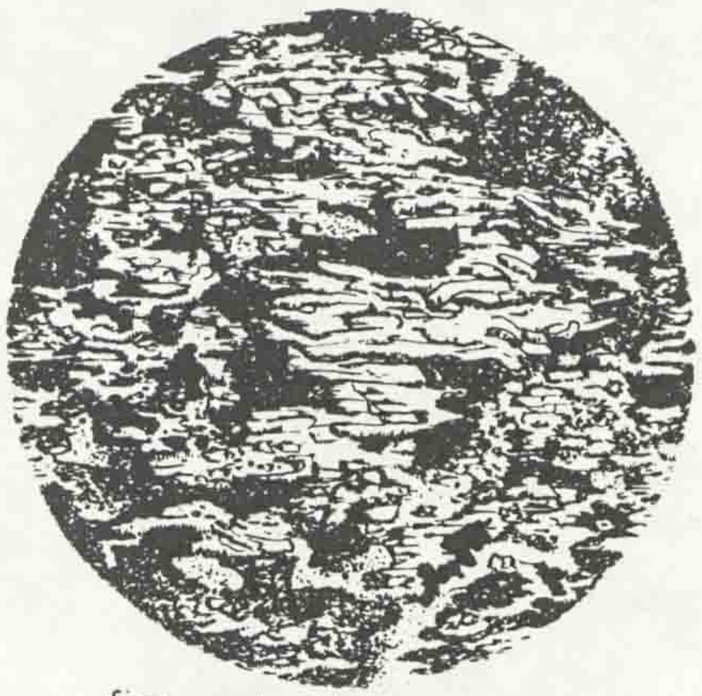

fine-grain bladed serpentine replacing ribbon texture

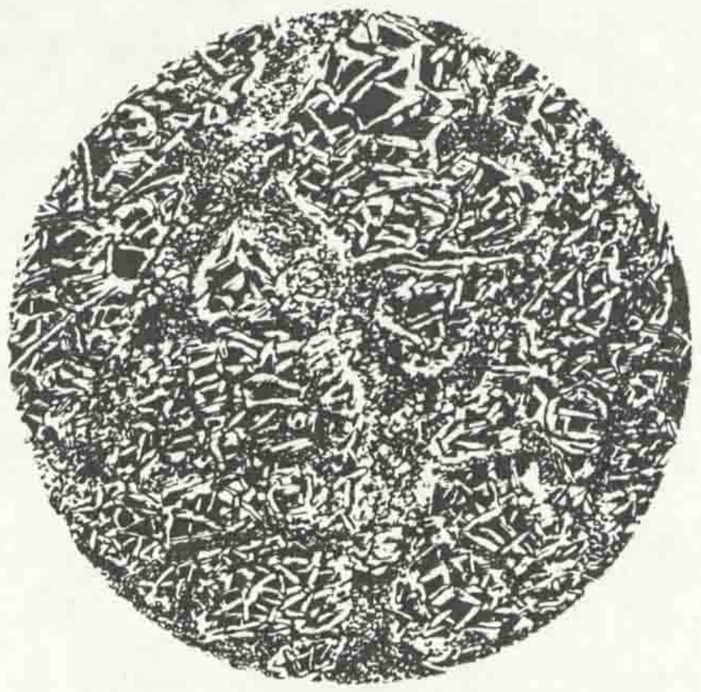

fine-grain bladed serpentine replacing mesh texture

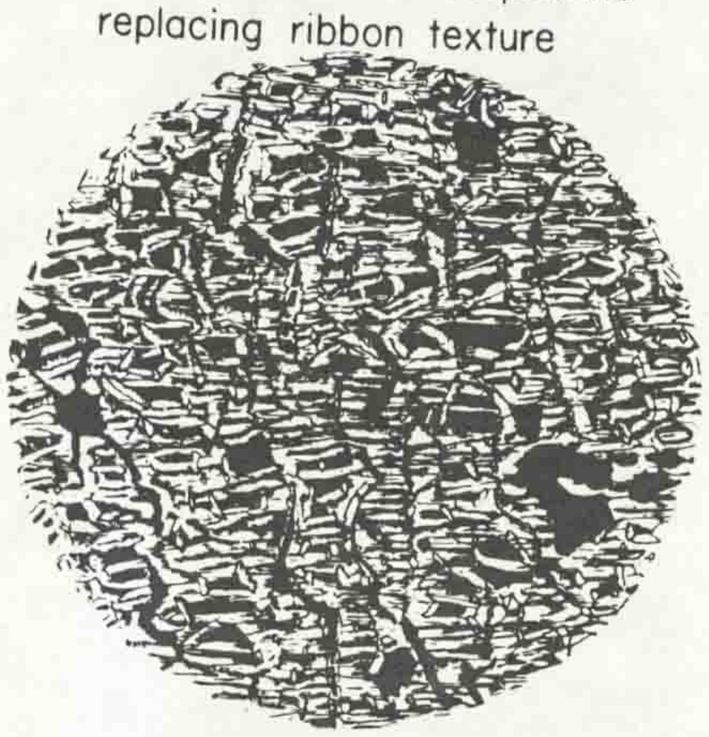

'mesh' serpentine, with incipient ribbon texture

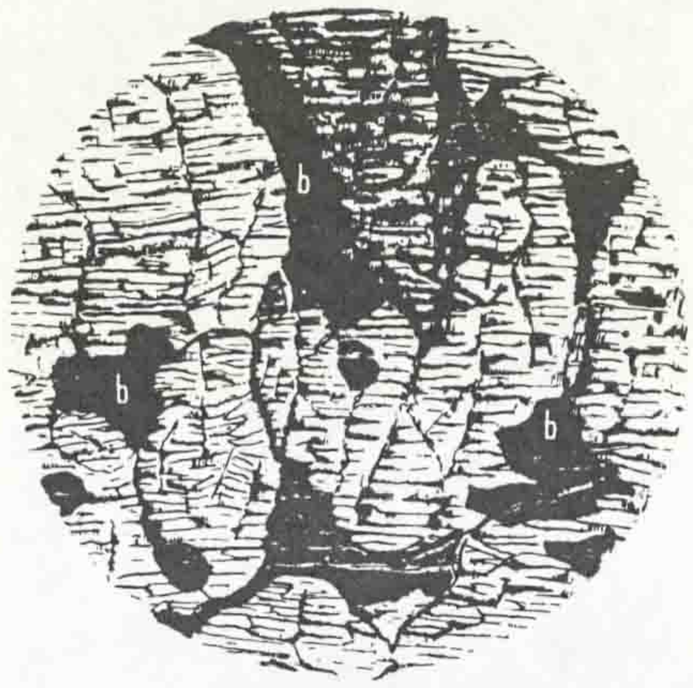


'ribbon' texture serpentine (b=bastite)

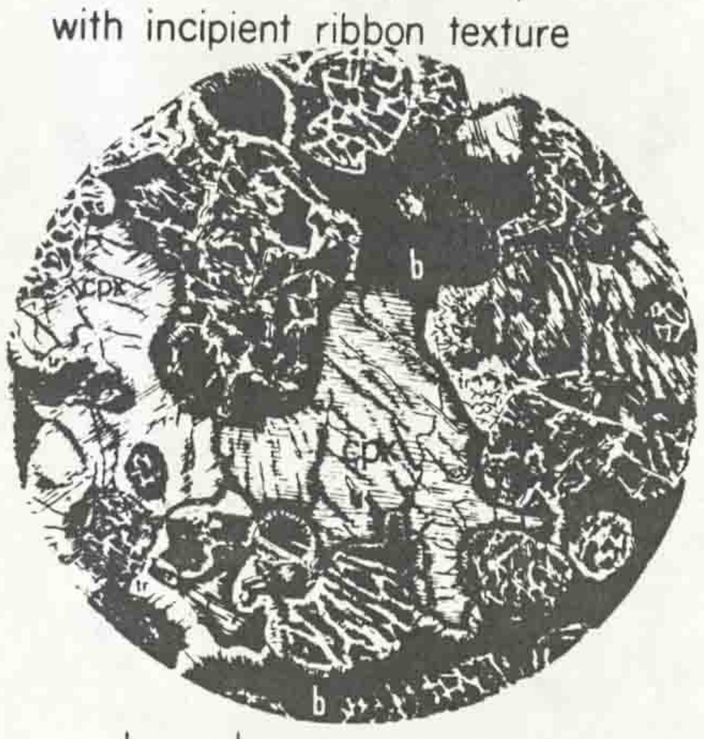


'mesh' texture serpentine, after olivine in lherzolite. (b=bastite; cpx=clinopyroxene; tr=tremolite)

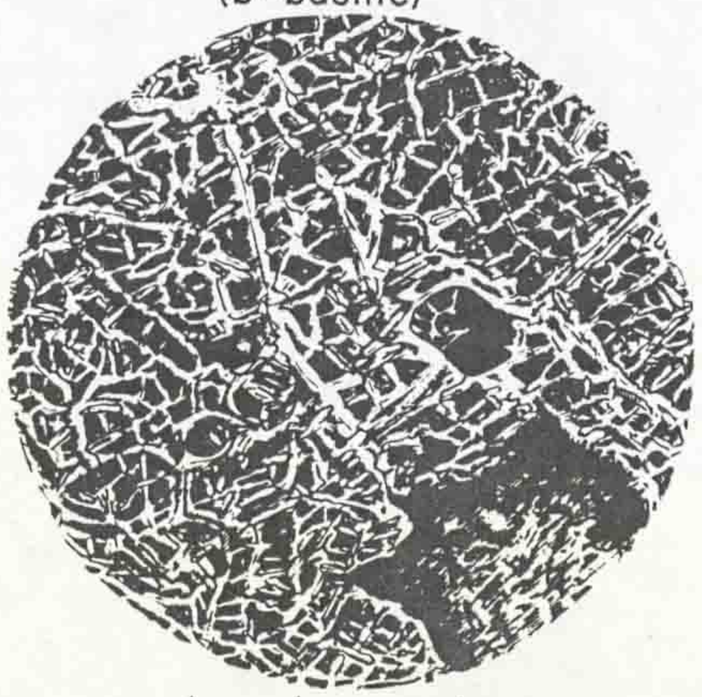

'mesh' serpentine (b=bastite)

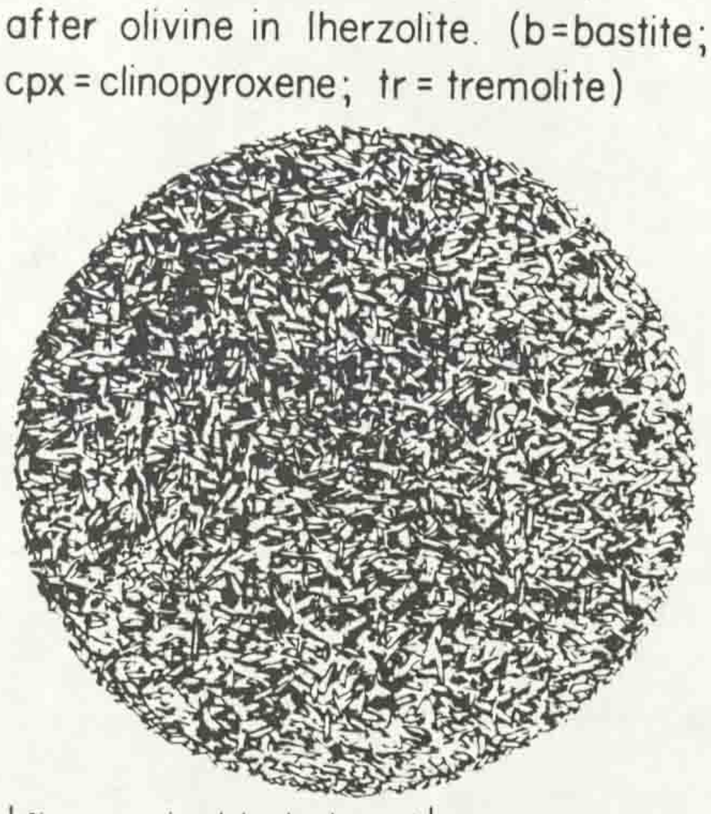

'fine-grain bladed mat' texture

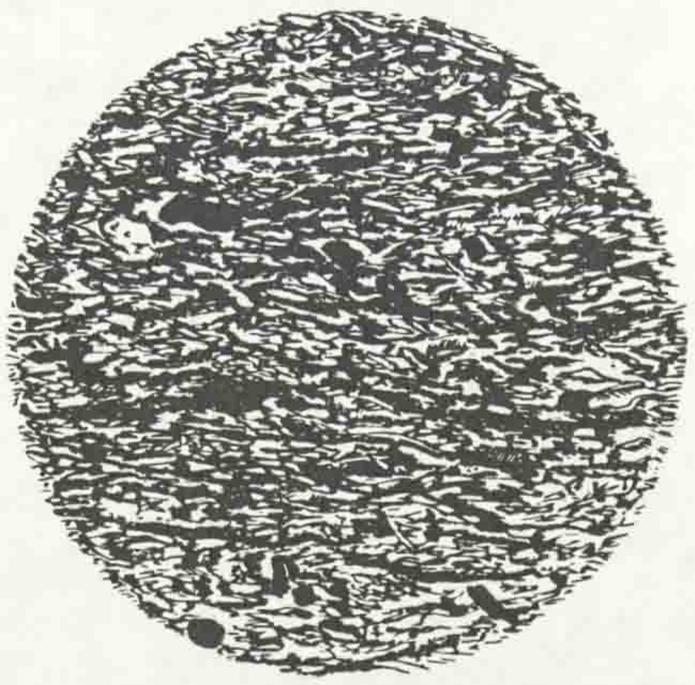

fine-grain bladed serpentine, highly deformed

original igneous minerals (now seen as rare unaltered grains of feldspar and pyroxene) being replaced by tremolite/actinolite meshes and sericitic patches.

4.2.3.6 Serpentinisation effects: The serpentine minerals, chrysotile, lizardite and antigorite, are all hydrated magnesium silicates ($Mg_3Si_2O_5(OH)_n$), and result from reactions between olivine/pyroxene - bearing assemblages and hydrous phases. The parent minerals show variable susceptabilities to the serpentinisation reactions such that, the reactivity of olivine > orthopyroxene > clinopyroxene.

The textural scheme of Maltman (1978) (Figure 4.65) is used in describing the effects of serpentinisation on the rocks of the peridotite.

The serpentinisation is variably developed on the scale of a single thin section, such that a 30 X 50mm section can contain both fresh igneous and complete serpentinite replacement textures. The map scale distribution of the serpentinisation is more regular with the most pervasive serpentinisation occurring at the margins of the body. As the small scale textures are irregularly developed the textural descriptions cover the changes in mineralogy resulting from progressivly higher degrees of serpentinitic alteration.

In the peridotite lithologies the serpentinisation can be subdivided into two main 'styles':

(i) A foliation serpentinisation is seen throughout the central portions of the body although it is obscured near the margins by more pervasive effects. Two phases of foliation serpentinisation are developed, an early layering parallel/subparallel group and a later, finer, set at high angles to the layering (Figure 4.66). The early phase fabric shows a zonation of serpentinite textures across a 5-10mm zone. At the margins of the zone a mixed mesh/ribbon texture is developed, grading over <1mm into relatively fresh igneous material. This zone passes into a central zone of opaque magnetite plates lying parallel to the vein walls; fibres of chrysotile lying at high angles to the vein walls, occur between the magnetite plates. This fabric is evident in foliation parallel veins throughout the body. The upright fabric consists of regular, but discontinous, thin zones

**Figure 4.66: Typical serpentinised foliation textures in peridotite, showing early wide foliation parallel serpentinitic veins cross cut by higher angle, thin serpentinitic veins (X 29) XPL.**

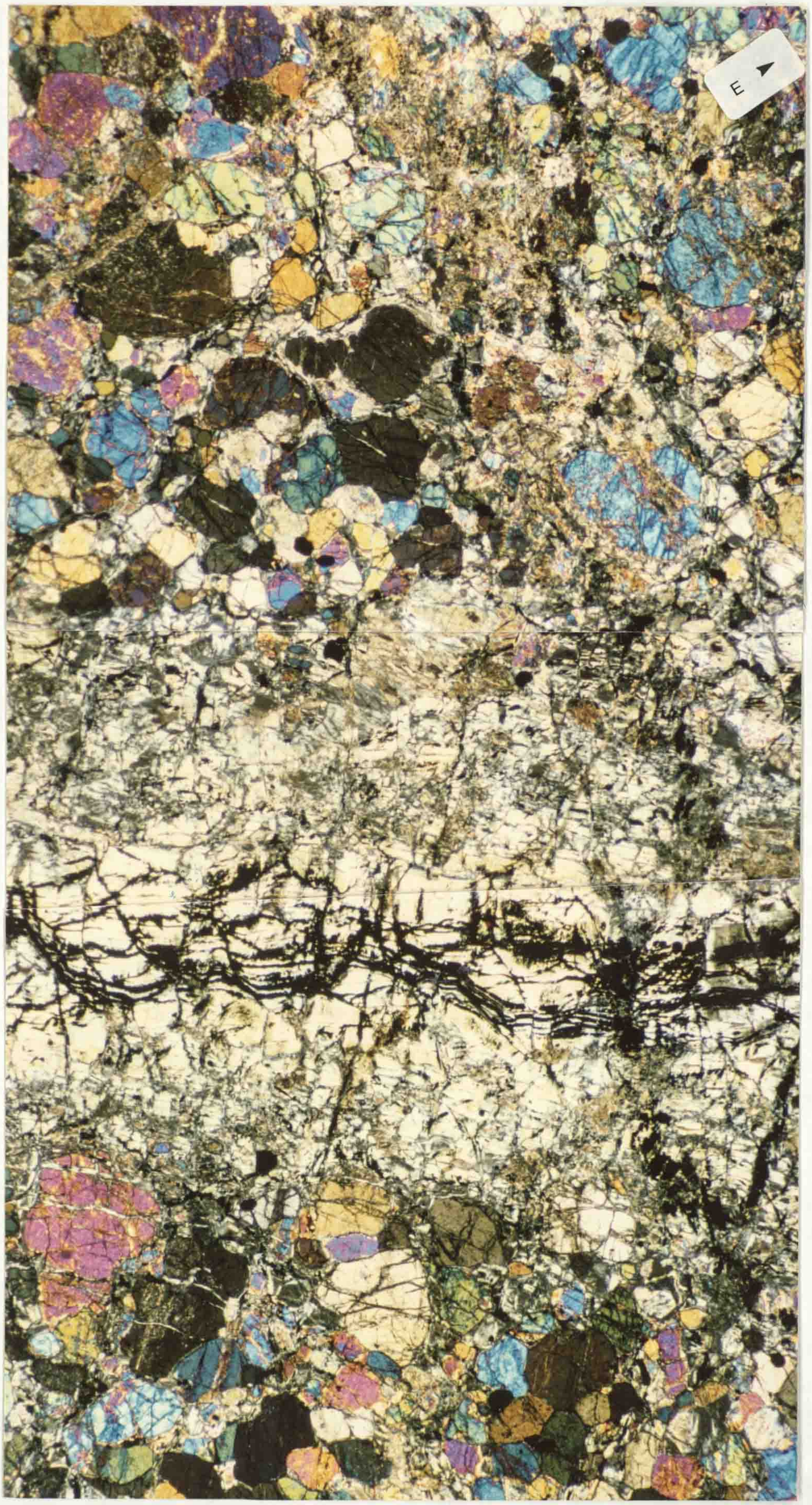

**Figure 4.67: Pervasively serpentinised ultrabasic lithology showing polygonal arrangement of opaque minerals (mesh texture) containing ribbon textured serpentinite (X 29) XPL.**

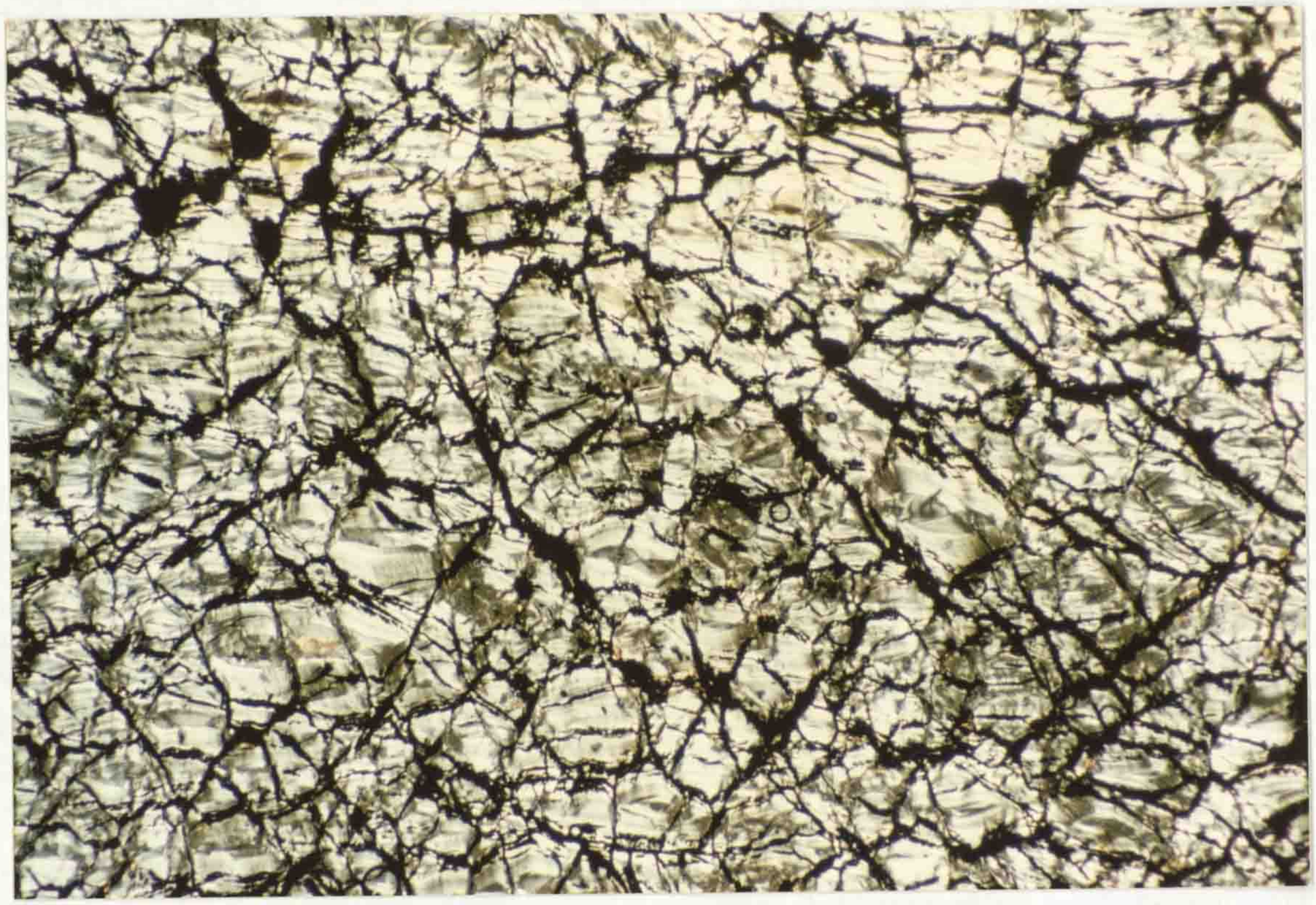

Figure 4.68: Talc - carbonate schist. (X 29) PPL.

( <1mm) of often incomplete chrysotile and lizardite alteration which crosscut the thicker lower angle veins.

(ii) A matrix serpentinisation, in which olivine crystals range in alteration from partial serpentinisation to give a 'mesh' texture of fresh olivine and fibrous chrysotile to complete replacement giving a polygonal texture, defined by opaques, within which fibrous chrysotile shows the development of incipent ribbon forms (Figure 4.67). The pyroxenes show change from fresh igneous material, with a slight cloudiness evident in crystals adjacent to affected olivines, to extreme alteration giving bastitic meshes which often pseudomorph the cleavages of the pyroxenes. In some areas immediately adjacent to the metasediments, such as around [GR 705 590] the peridotite is completely replaced by a fine grained ( <0.25mm), foliated, talc - carbonate schist (Figure 4.68). The tectonic implications of the appearance of talc - carbonate assemblages at the contacts of the peridotite have been discussed in {3.5}.

# Chapter 5: Pressure / Temperature determinations and P - T paths

# Chapter 5: Pressure / Temperature determinations and P - T paths

## 5.1 Geothermometry and geobarometry: An introduction

A number of different methods and systems for assessing the pressure and temperature conditions of a metamorphic terrain are available to the metamorphic petrologist. The use of methods such as facies series analysis, isograd sequence mapping, mineral phase relations and absolute/relative thermobarometry have enabled the determination of P - T conditions in many metamorphic systems. The application of methods like facies series analysis (after Miyashiro 1973), isogradic mapping (after Tilley 1924b), and mineral phase relations (after Winkler 1965), which rely on discontinuous reactions to provide the assemblage changes which allow metamorphic grade to be determined, proved of limited use in this study. Much of the study area shows assemblages typical of amphibolite facies metamorphism {4.1}; the prevalent reactions developed continuous (Thompson 1976a) rather than discontinuous {4.1.4}. The development of isograds is restricted to the aureole of the Dawros - Currywongaun - Doughruagh igneous complex, where a sillimanite - in isograd is developed (Leake, Tanner & Senior 1981).

In order to assess variations in P - T across the study area absolute geothermobarometry was employed. This method uses the measured compositions in coexisting mineral phases within an equilibrium assemblage, as determined using electron microprobe techniques {Appendix B}, within a calibration of the Van't Hoff isotherm equation (after Wood & Fraser 1977):

$$G^{\circ} = -RT\ln \frac{a^{c}_{C} \cdot a^{d}_{D}}{a^{a}_{A} \cdot a^{b}_{B}} \quad * \qquad \text{--- (5.1)}$$

$$* \text{ as } \Delta G^{\circ}_{1,T} = \Delta H^{\circ}_{1,T} - T\Delta S^{\circ}_{T} + (P-1)\Delta V^{\circ}_{solids} \text{ --- (5.2)}$$

(these two equations can be combined to produce calibrations for either temperature or pressure).

a represents the activity of components A, B, C and D in phases a, b, c and d in a reaction:

$$\underset{\text{phase}}{\underset{a}{wA} + \underset{b}{xB}} = \underset{c}{yC} + \underset{d}{zD} \qquad \text{--- (5.3)}$$

w, x, y and z are the number of moles of components A, B, C and D respectively.

**Table 5.1: Formulae used to calculate mole fractions, X (after Hodges & Spear 1982 and Hodges & Crowley 1985, mineral symbols after Kretz 1983). All iron as $Fe^{2+}$.**

Garnet

$$X_{Alm} = \frac{Fe}{Fe+Mn+Mg+Ca}$$

$$X_{Sps} = \frac{Mn}{Fe+Mn+Mg+Ca}$$

$$X_{Pyr} = \frac{Mg}{Fe+Mn+Mg+Ca}$$

$$X_{Grs} = \frac{Ca}{Fe+Mn+Mg+Ca}$$

Muscovite

$$X^{Fe}_{Ms} = \frac{Fe}{Al^{VI}+Ti+Fe+Mn+Mg}$$

$$X^{Al^{VI}}_{Ms} = \frac{Al^{VI}}{Al^{VI}+Ti+Fe+Mn+Mg}$$

$$X^{K}_{Ms} = \frac{K}{Ca+Na+K+Ba}$$

$$X^{Na}_{Ms} = \frac{Na}{Ca+Na+K+Ba}$$

Biotite

$$X_{Ann} = \frac{Fe}{Al^{VI}+Ti+Fe+Mn+Mg}$$

$$X_{Phl} = \frac{Mg}{Al^{VI}+Ti+Fe+Mn+Mg}$$

$$XAl^{VI} = \frac{Al^{VI}}{Al^{VI}+Ti+Fe+Mn+Mg}$$

$$X_{K} = \frac{K}{Ca+Na+K+Ba}$$

Plagioclase

$$X_{An} = \frac{Ca}{Ca+Na+K}$$

$$X_{Ab} = \frac{Na}{Ca+Na+K}$$

Staurolite

$$X^{Fe}_{St} = \frac{Fe}{(Fe+Mg+Mn+Zn)}$$

$$X^{Mg}_{St} = \frac{Mg}{(Fe+Mg+Mn+Zn)}$$

$$X^{Mn}_{St} = \frac{Mn}{(Fe+Mg+Mn+Zn)}$$

Work on the ultrabasic igneous bodies of the area forms the bulk of the literature covering the study area. The survey initially recognized the Currywongaun - Doughraugh intrusions, along with the serpentinitic rocks of the Dawros peninsula and the existence of similar serpentinitic bodies on the North coast of the Renvyle peninsula. Ingold (1937) studied the Currywongaun - Doughraugh intrusions, the gabbroic bodies found along the Dawros River, and the Dawros peridotite. This work was mentioned in Wager (1939) who considered the relation between these bodies and the similar ultrabasic bodies in South Connemara, concluding that the two intrusive suites bore little or no relation to one another. The Dawros peridotite was studied by Rothstein (1954, 1956, 1958, 1961, 1964) who defined its internal layering and structure. Leake (1964b & 1970b) reassessed this body, attempting to relate it to the Currywongaun - Doughraugh bodies and the Southern suite of intrusives. The relation between the peridotite and gabbroic bodies was considered by Kanaris-Sotiriou & Angus (1976) who produced a model to explain the present spatial distribution and contact relations of the bodies. Bennett & Gibb (1983) re-examined the structure of the peridotite and its surrounding metasedimentary envelope, along with the nearest gabbroic body, the Creggaun gabbro. Details of the work covering the igneous bodies are discussed in {2.2, 3.4 and 4.2}.

The metamorphic grade of the area is not considered in detail by any of the early work, although Ingold (1937) and Rothstein (1954, 1956) discuss the contact metamorphism around the igneous bodies, noting the formation of sillimanite grade hornfelsic aureoles (locally with hypersthene–corundum–bearing rocks). Both authors consider that the aureole metamorphism overprints an earlier regional staurolite - garnet grade metamorphism. Cruse (1963) describes two metamorphic events, an early ($D_2$) staurolite grade event (possibly locally reaching sillimanite grade), showing a possible increase in grade to the south, followed by a retrogressive event (syn $D_3$) which produced a greenschist facies overprint in the north of the area, and an epidote - amphibolite overprint to the south. Local occurrences of post-tectonic andalusite and chloritoid are recorded by Cruse. Leake, Tanner & Senior (1981) show the development a sillimanite

**Table 5.2: Activity and activity coefficient calculation methods used in thermobarometric calibrations (mineral symbols after Kretz 1983). The calculations are in joules unless stated otherwise.**

$a$ is activity
$Y$ is activity coefft (gamma)
$R$ is gas constant (8.3144 joules/Kelvin, 1.9862 calories/Kelvin)

## Garnet

### Hodges & Spear (1982)

$$a_{Alm} = (Y_{Alm} \cdot X_{Alm})^3$$
$$a_{Prp} = (Y_{Prp} \cdot X_{Prp})^3$$
$$a_{Grs} = (Y_{Grs} \cdot X_{Grs})^3$$

Where:

$$Y_{Alm} = \exp \frac{(-13807 - 6.3T) \cdot (X_{Prp} \cdot X_{Grs})}{RT}$$

$$Y_{Prp} = \exp \frac{(-13807 - 6.3T) \cdot (X_{Grs} \cdot (1 - X_{Prp})}{RT}$$

$$Y_{Grs} = \exp \frac{(-13807 - 6.3T) \cdot (X_{Prp} \cdot (1 - X_{Grs})}{RT}$$

### Hodges & Crowley (1985)

$$a_{Alm} = X_{Alm} \cdot \exp \frac{(1.5T - 3300) \cdot (X_{Prp} \cdot X_{Grs})}{RT}^3$$

$$a_{Prp} = X_{Prp} \cdot \exp \frac{(3300 - 1.5T) \cdot (X_{Grs}^2 + (X_{Alm} \cdot X_{Grs}) + (X_{Grs} \cdot X_{spe}))}{RT}^3$$

$$a_{Grs} = X_{Grs} \cdot \exp \frac{(3300 - 1.5T) \cdot (X_{Prp}^2 + (X_{Alm} \cdot X_{Prp}) + (X_{Prp} \cdot X_{spe}))}{RT}^3$$

### Ganguly & Saxena (1984)

These calculations use values of $Y$ in calories.

$$a_{Alm} = (Y_{Alm} \cdot X_{Alm})^3$$
$$a_{Prp} = (Y_{Prp} \cdot X_{Prp})^3$$
$$a_{Grs} = (Y_{Grs} \cdot X_{Grs})^3$$
$$Y_{Alm} = \exp \{X_{Prp}^2 \cdot (0.13 + (2.995 \cdot X_{Alm})) + X_{Grs}^2 \cdot (2.253 - (6.836 \cdot X_{Alm})) + (X_{Prp} \cdot X_{Grs} \cdot (3.958 - (8.82 \cdot X_{Alm}))) - (1.984 \cdot (X_{Pyp} - X_{Grs}))\}$$

$$Y_{Prp} = \exp \{(X_{Grs}^2 \cdot (-0.104 + (3.968 \cdot X_{Prp}))) + (X_{Alm}^2 \cdot (1.628 - (2.995 \cdot X_{Prp}))) + (X_{Grs} \cdot X_{Alm} \cdot (4.673 - (6.414 \cdot X_{Prp}))) - (3.418 \cdot (X_{Grs} \cdot X_{Alm})) + (X_{Sps} \cdot X_{Alm} (3.482 \cdot X_{Prp}))\}$$

$$Y_{Grs} = \exp \{(X_{Prp}^2 \,.\, (1.88 - (3.968 \,.\, X_{Grs}))) + (X_{Alm}^2 \,.\, (-1.165 + (6.836 \,.\, X_{Grs})))$$
$$+ ((X_{Prp} \,.\, X_{Alm}) \,.\, (4.003 - (5.467 \,.\, X_{Grs})))$$
$$+ (1.497 \,.\, (X_{Prp} \,.\, X_{Alm})) + ((X_{Sps} \,.\, X_{Alm}) \,.\, (-1.165 + (6.836 \,.\, X_{Grs})))\}$$

## Biotite

$a_{Phl} = X^{Bt}{}_K \,.\, X_{Phl}^3$ (after Holdaway 1978)

$a_{Ann} = X_{Ann}^3$

after Hodges &Crowley (1985)

$a_{Phl} = X_{Phl}^3$

## Feldspars

Newton & Hasleton (1981)

$$a_{An} = \frac{X_{An} \,.\, (1 + X_{An})^2}{4} \,.\, \exp \frac{(1 - X_{An})^2}{T} \,.\, (1032 + (4726 \,.\, X_{An}))$$

Hodges & Crowley (1985)

$$a_{An} = X_{An} \,.\, \exp \frac{610.34}{(T - 0.3837)}$$

## Muscovite

Hodges & Crowley (1985)

$$a_{Ms} = (X^{K}_{Ms} \,.\, X^{AlVI}{}_{Ms}{}^2) \,.\, \exp \frac{(X^{Na}_{Ms} \,.\, X^{AlVI}{}_{Ms}{}^2) \,.\, (W_{Ms} + (2X^{K}_{Ms} \,.\, X^{AlVI}{}_{Ms}{}^2)) \,.\, (W_{Pg} - W_{Ms})}{RT}$$

$$a_{Ts} = \frac{2X^{AlVI}{}_{Ms} - 1}{2X^{Fe}_{Ms}}$$

Where the interaction (Margules) parameters are

$W_{Ms} = 4650.1 + 0.109P + 0.3954T$

$W_{Pg} = 2923.1 + 0.159P + 0.1698T$

The activity term in brackets is known as the equilibrium constant, K

$$K = \frac{a^c{}_C \;.\; a^d{}_D}{a^a{}_A \;.\; a^b{}_B} \qquad \text{--- (5.4)}$$

In systems where the mixing of components within phases is ideal the equilibrium constant can be replaced by a distribution coefficient, $K_D$, which can be empirically determined such that:

$$K_D = \frac{X^c{}_C \;.\; X^d{}_D}{X^a{}_A \;.\; X^b{}_B} \qquad \text{--- (5.5)}$$

X represents the mole fractions of components A, B, C and D in phases a, b, c and d. Table 5.1 shows the formulations used in calculation of mole fractions for the minerals used in the geothermometric and geobarometric calculations in this work.

In systems where ideal mixing is not developed the calculation of $K_D$ values is more complex (e.g. Ganguly & Saxena 1984). Non - ideal mixing models are discussed where relevant to the geothermometer and geobarometer calibrations (the formulae for calculation of activities in non - ideal systems are in Table 5.2). One geothermometer (Grt - Bt exchange) and two geobarometers (Grt - Bt - Pl - Ms and Grt - Pl - Sil - Qtz) have been used to calculate P - T conditions. Details of the calibrations are given in {5.2, 5.3.1 and 5.3.2}.

## 5.2 Geothermometry: The garnet - biotite exchange thermometer

The reaction system used in determining temperatures in this work is an ionic exchange reaction between garnet and biotite. This system is commonly applied to pelitic lithologies and is based on the temperature dependent exchange of Fe and Mg between coexisting garnet and biotite in the reaction:

$Fe_3Al_2Si_3O_{12} + KMg_3AlSi_3O_{10}(OH)_2 = Mg_3Al_2Si_3O_{12} + KFe_3AlSi_3O_{10}(OH)_2$ --- (A)

almandine + phlogopite = pyrope + annite

This exchange reaction (Ferry & Spear 1978) is considered to involve $Fe^{2+}$ and $Mg^{2+}$ cations only, with the effects of $Fe^{3+}$ being disregarded.

Thompson (1976b) applied the garnet - biotite cation exchange reaction in temperature determination following previous discussion on the use of garnet - biotite exchange as a thermometer (e.g. Perchuk 1967, Saxena 1969). Thompson's (1976b) calibration was calculated using the available thermodynamic data to give (T in Kelvin, P in bars):

$$T = \frac{2740 + 0.0234P}{\ln K_{DT1} + 1.56} \qquad \text{--- (5.6)}$$

The distribution coefficient, $K_{DT1}$, was determined as

$$K_{DT1} = \frac{X_{Alm} \cdot X_{Phl}}{X_{Prp} \cdot X_{Ann}} \qquad \text{--- (5.7)}$$

This calibration is more reliable at lower temperatures as it was calculated using thermodynamic data from low temperatures which were then extrapolated to higher temperatures. The reported errors for this calculation are ±50°C at 500°C but rise to ±100°C at 1000°C.

Ferry & Spear (1978) calibrated the garnet biotite exchange experimentally using mixtures of synthetic $Fe^{2+}$/Mg garnet and biotite:

$$T = \frac{4151 + 0.019P}{RT\ln K_{DT2} + 1.554} \qquad \text{--- (5.8)}$$

$$\text{where } K_{DT2} = \frac{(X_{Prp}/X_{Alm})}{(X_{Phl}/X_{Ann})} \qquad \text{--- (5.9)}$$

Ferry & Spear suggest the errors on this calculation to be ±50°C and, because of the effects of other cations (Ca, Mn) on the Fe - Mg exchange reaction, they indicate that the calibration is not valid when:

$$\frac{(Ca+Mn)}{(Ca+Mn+Fe+Mg)} \leq 0.2 \text{ in garnet} \qquad \text{--- (5.10)}$$

$$\frac{(Al^{VI}+Ti)}{(Al^{VI}+Ti+Fe+Mg)} \leq 0.15 \text{ in biotite.} \qquad \text{--- (5.11)}$$

Studies of the influence of Ti, $Al^{VI}$, $Fe^{3+}$, Ca and Mn cations on the partition of $Fe^{2+}$ and Mg between

garnet and biotite (e.g. Dallmeyer 1974, Ganguly & Saxena 1984, Indares & Martingole 1985) show that Ti, $Al^{VI}$ and $Fe^{3+}$ substitution in biotite and Ca, $Fe^{3+}$, and Mn substitution in garnet distort the lattices of those minerals. Such lattice distortions mean that certain cations are more readily partitioned into the lattice. The occurrence of substitutions in the reaction system alters the nature of the mixing in the phases leading to non - ideal mixing (e.g. Geiger, Newton & Kleppa 1987), which in turn affects the $K_D$. The Ferry & Spear (1978) calibration calculates $K_{DT2}$ values based on the assumption that only $Fe^{2+}$ and Mg are involved in the exchange reaction and that the resultant minerals show ideal mixing characteristics. They suggest a limit on the use of the calibration to systems with low Ca + Mn in garnet and $Al^{VI}$ + Ti in biotite. Thompson's (1976b) calibration, although calculating $K_{DT1}$ using only $Fe^{2+}$ and Mg, is based on a natural pelitic assemblage where minor cation substitutions will be present in the minerals. The reliability of the Thompson calibration is dependent on the similarities in composition between the assemblage under analysis and the original assemblage used in the calibration.

In order to more rigorously apply the garnet - biotite reaction several authors have attempted to recalibrate the reaction, by comparison with another geothermometer (e.g. Goldman & Albee 1977), by re - evaluating the thermodynamics of the exchange reaction (e.g. Anovitz & Essene 1987), or attempting to refine the $K_D$ calculation method in such a way that cation substitution and non - ideal behaviour is accounted for (e.g. Hodges & Spear 1982, Ganguly & Saxena 1984).

Pigage & Greenwood (1982) produced a calibration of the Ferry & Spear system for staurolite bearing assemblages which also incorporates corrections for non - ideal mixing of Mn and Ca in garnet (after the mixing models of Ganguly 1979):

$$T = \frac{1586 \,.\, X_{Grs} + 1308 \,.\, X_{Sps} + 2089 + 0.00956 \,.\, P}{0.78198 - \ln K_{DT3}} \quad \text{---} \quad (5.12)$$

where:

$$K_{DT3} = \frac{X_{Alm} \cdot X_{Phl}}{(Mg/(Mg + Fe))_{Bt}} \qquad \text{--- (5.13)}$$

Hodges & Spear (1982) reassessed the Ferry & Spear (1978) calibration and, assuming ideal mixing in biotites (except those with *'high Ti contents'*), attempted to allow for non - ideal mixing in garnets. By breaking the quaternary garnet mixing system down into a series of binary solution systems (Alm - Prp, Grs - Prp, Prp - Sps, Grs - Alm, Grs - Sps and Alm - Sps) and accounting for the interaction energies (W the Margules parameter) of the binary systems, the following calibration was produced.

$$T = \frac{2089 + 9.56P + (1661 \cdot X_{Grs})}{\ln K_{DT2} + 0.782 + (0.755 \cdot X_{Grs})} \qquad \text{--- (5.14)}$$

This calibration assumes ideal behaviour for all the binary systems except Grs - Prp and corrects for this nonideality. This calibration uses the Ferry & Spear (1978) distribution coefficient, $K_{DT2}$.

Ganguly & Saxena (1984) attempt in their calibration to account for the interaction between cations in garnets, using thermodynamic data (Cressey, Schmidt & Wood 1980) which allowed more control on the interaction energies than previous systems.

The calibration,

$$T = \frac{1175 + 9.45P + {}^{1}/_{1.987} \cdot \{W_{FeMg}(X_{Alm} - X_{Prp}) + 3000(X_{Grs} + X_{Sps})}{\ln K_{DT2} + 0.782} \qquad \text{--- (5.15}$$

uses the simple $K_{DT2}$ calculation of Ferry & Spear (1978).
The formulae used in calculating X and W parameters are shown in Tables 5.1 and 5.2.

These five calibrations were used to calculate the temperature values from electron microprobe data on mineral assemblages. The results of the temperature calculations are shown in table 5.3, with tables 5.4 and 5.5 showing the variations in $K_D$ and activity values respectively.

## 5.3 Geobarometry

Two geobarometric systems were used in this study, Grt - Pl -

Ms - Bt {5.3.1} and Grt - Pl - $Al_2SiO_5$ - Qtz {5.3.2}.

5.3.1 Garnet - Plagioclase - Muscovite - Biotite Barometry

This system of geobarometry is based on the reactions:

Pyrope + Grossular + Muscovite = 3 Anorthite + Phlogopite ---(B)

Almandine + Grossular + Muscovite = 3 Anorthite + Annite ---(C)

(after Ghent & Stout 1981).

Reaction (B) is pressure sensitive and reaction (C) is temperature sensitive, the simultaneous solution of the two reactions providing both pressure and temperature estimations for a given assemblage (Ghent & Stout 1981). In this work reaction (B) is used to determine pressure, the relevant temperature being calculated from the garnet - biotite systems described in {5.2}.

The initial formulation of this system by Ghent & Stout (1981), based on a comparison of the pressure and temperature results obtained from Grt - Bt thermometry (after Ferry & Spear 1978) and Grt - Pl - $Al_2SiO_5$ - Qtz barometry (after Ghent 1976) with calibrations of reactions B and C, yields the following (T in Kelvin):

$$P = \frac{37189 + 69.768T - RT\ln K_{DP1}}{7.725} \quad \text{--- (5.16 after B)}$$

$$P = \frac{-17257 + 92.303T - RT\ln K_{DP2}}{7.543} \quad \text{--- (5.17 after C)}$$

The values of $K_{DP1}$ and $K_{DP2}$ are the solid activity products of the reactions and are based on the assumption of ideal cation solution models to give:

$$K_{DP1} = \frac{X_{An}^3 \cdot X_{Phl}^3}{(X_K^{Ms} \cdot X^{AlVI}{}_{Ms})\, X_{Alm}^3 \cdot X_{Grs}^3} \quad \text{--- (5.18)}$$

$$K_{DP2} = \frac{X_{An}^3 \cdot X_{Ann}^3}{(X_K^{Ms} \cdot X^{AlVI}{}_{Ms})\, X_{Alm}^3 \cdot X_{Grs}^3} \quad \text{--- (5.19)}$$

The assumptions of ideality lead to errors in the calibrations, giving high pressure estimates at low temperatures and low pressures at high temperatures (Ashworth & Evirgen 1985 ).

Ganguly & Saxena (1984) attempted to overcome such problems by

using non - ideal mixing models in their calibration (NB, this calibration is in calories):

$$P = \frac{1778.2 + 129.62T + RT\ln K_{DP3}}{7.254} + 1 \qquad \text{--- (5.20)}$$

$$K_{DP3} = \frac{a_{Phl} \cdot a_{An}^3}{a_{Prp} \cdot a_{Grs} \cdot a_{Ms}} \qquad \text{--- (5.21)}$$

The activity models used in this calibration (Table 5.2 ) assume ideal mixing in biotite and muscovite, with non - ideal mixing in plagioclase (modelled after Newton & Hasleton 1981) and garnet. The garnet mixing model is based on a quaternary mixing between Alm, Prp, Sps and Grs, although at low $X_{Sps}$ values in garnet a ternary mixing model can be applied (Table 5.2). Ashworth & Evirgen (1985) apply the ternary system on garnets with up to $X_{Mn} = 0.06$. The mean value of $X_{Sps}$ in this study is 0.0916 with a range from 0.006 to 0.25.

Hodges & Spear (1982) use the same H and S values as Ganguly & Saxena (1984) but calculate the $K_{DP}$ value differently.

$$P = \frac{1778.2 + 129.62T + RT\ln K_{DP4}}{7.254} + 1 \qquad \text{--- (5.22)}$$

$$K_{DP4} = \frac{a_{Phl} \cdot a_{An}^3}{a_{Prp} \cdot a_{Grs} \cdot a_{Ms}} \qquad \text{--- (5.23)}$$

The *a* (activity) values used in this $K_{DP}$ calculation are based on garnet mixing models which assume that end member interaction parameters (Margules parameters) are negligible for all mixing except for Grs - Prp.

Hodges & Crowley (1985) recalibrate the Ganguly & Saxena system by fitting regression lines to a plot of [(P - 1)$\Delta$V + RTlnK] versus T to give:

$$P = \frac{-69965 + 162.99T - RT\ln K_{DP3}}{7.543} \qquad \text{--- (5.24)}$$

$$K_{DP5} = \frac{a_{Ann} \cdot a_{An}^3}{a_{Alm} \cdot a_{Grs} \cdot a_{Ms}} \qquad \text{--- (5.25)}$$

All the above calibrations use simple models for mixing in

plagioclase (after Newton & Hasleton 1981), which may lead to errors in the under - estimation of $a_{An}$. A more recent model for plagioclase mixing (Newton 1983) accounts for variation in a and Y due to temperature.

$$a_{An} = Y_{An} \cdot \frac{X_{An}\ (1 + X_{An})^5}{4} \qquad \text{--- (5.26)}$$

$$\ln Y_{An} = X_{Ab}^2\ \{W_{An} + 2X_{An} \cdot (W - W_{An})\} \qquad \text{--- (5.27)}$$

5.3.2 Garnet - Plagioclase - $Al_2SiO_5$ - Quartz barometry

This system of geobarometry is based on the reaction (Ghent 1976):

3 Anorthite = Grossular + 2 $Al_2SiO_5$ + Quartz --- (D)

which has been calibrated for reactions involving the three main $Al_2SiO_5$ polymorphs (andalusite, kyanite and sillimanite). Essene (1982) noted the large temperature dependence of calibrations of this reaction, terming it a 'thermobarometric' rather than barometric system. In those lithologies used in theromobarometry $Al_2SiO_5$ occurs as sillimanite, developed as both prismatic and fibrolitic crystal forms. The calibrations presented below are for sillimanite bearing assemblages.

The reaction was initially calibrated by Ghent (1976):

$$P = \frac{-11675 - 32.815 - RT\log K_{DP6}}{1.301} + 1 \qquad \text{---- (5.28)}$$

$$\text{Where } K_{DP6} = \frac{X_{Grs}^3}{X_{An}^3} \qquad \text{---- (5.29)}$$

The solid activity product ($K_{DP6}$) used in this calibration is based on the assumption of ideal solid solution in both garnet and plagioclase, although Ghent (1976) does note that the mixing system is unlikely to be ideal.

Ghent, Robbins & Stout (1979) modify the Ghent calibration to account for the activity coefficients of garnet and plagioclase, such that:

$$K_{DP7} = \frac{X_{Grs}^3}{X_{An}^3} \cdot \frac{Y_{Grs}^3}{Y_{An}^3} \qquad \text{--- (5.30)}$$

Ghent *et al.* suggest that the calibrations give the best results when:

$$\ln KY = \frac{Y_{Grs}^3}{Y_{An}^3} = -0.4$$

Recent data by Salje (1986) suggest that fibrolitic sillimanite has a different entropy to that of prismatic sillimanite, due largely to lattice disordering. Saljes' work suggests that applications of a sillimanite calibrated geobarometer in fibrolite - bearing lithologies may produce erroneous results, and that this problem should be considered in interpretation of sillimanite geobarometer results where both fibrolitic and prismatic sillimanite are developed.

## 5.4 The results of geothermometry and geobarometry

The various calibrations of the Grt - Bt thermometer and the Grt - Pl - Bt - Ms and Grt - Pl - Sil - Qtz barometers yield temperatures of:

412 to 963 °C (mean of 629°C)

and pressures between:

4.53 and 13.14 kilobars (mean of 7.42 kilobars).

The results are summarized on Figure 5.1. The mean values encompass lithologies associated with the regional metamorphic peak and those lithologies developed in the migmatitic aureole of the DCD. To clarify the situation the lithologies can be subdivided into three groups:

i, Sillimanite bearing contact aureole assemblages of the Kylemore Fm (Figure 5.2), which yield a mean pressure of:

8.03 ± 1.8 kb

and a mean temperature of:

807 ± 96 °C

(variations ± sigma).

ii, Non - sillimanitic Kylemore Fm lithologies, two groups including regional, Grt + Bt ± St bearing lithologies which yield:

mean pressure of 7.33 ± 1.5 kb,

mean temperature of 574 ± 66 °C

isograd around the igneous bodies within a garnet - staurolite regional grade. However, no evidence for the timing of these events is given. The work covering the metamorphic grade of the area is discussed in {Chapters 4 and 5}.

## 1.6 Outline of this Thesis

This thesis consists of seven chapters, where chapters two and three are concerned with the stratigraphy and structure of the study area. Chapters four and five cover the petrography, rock chemistry, mineral chemistry, geothermometric and barometric calculations, and the P-T path calculations. Chapter six covers the thermal modelling of the area. Chapter seven is a regional synthesis and discussion of the conclusions of this work.

Figure 5.1: Mean results of Grt - BT thermometry, Grt - Pl - Ms - Bt and Grt - Pl - $Al_2SiO_5$ - Qtz barometry for all the lithologies studied. Diamonds = Streamstown Fm, Dots = Kylemore Fm (regional metamorphic assemblages), Triangles = Kylemore Fm (contact metamorphic assemblages.

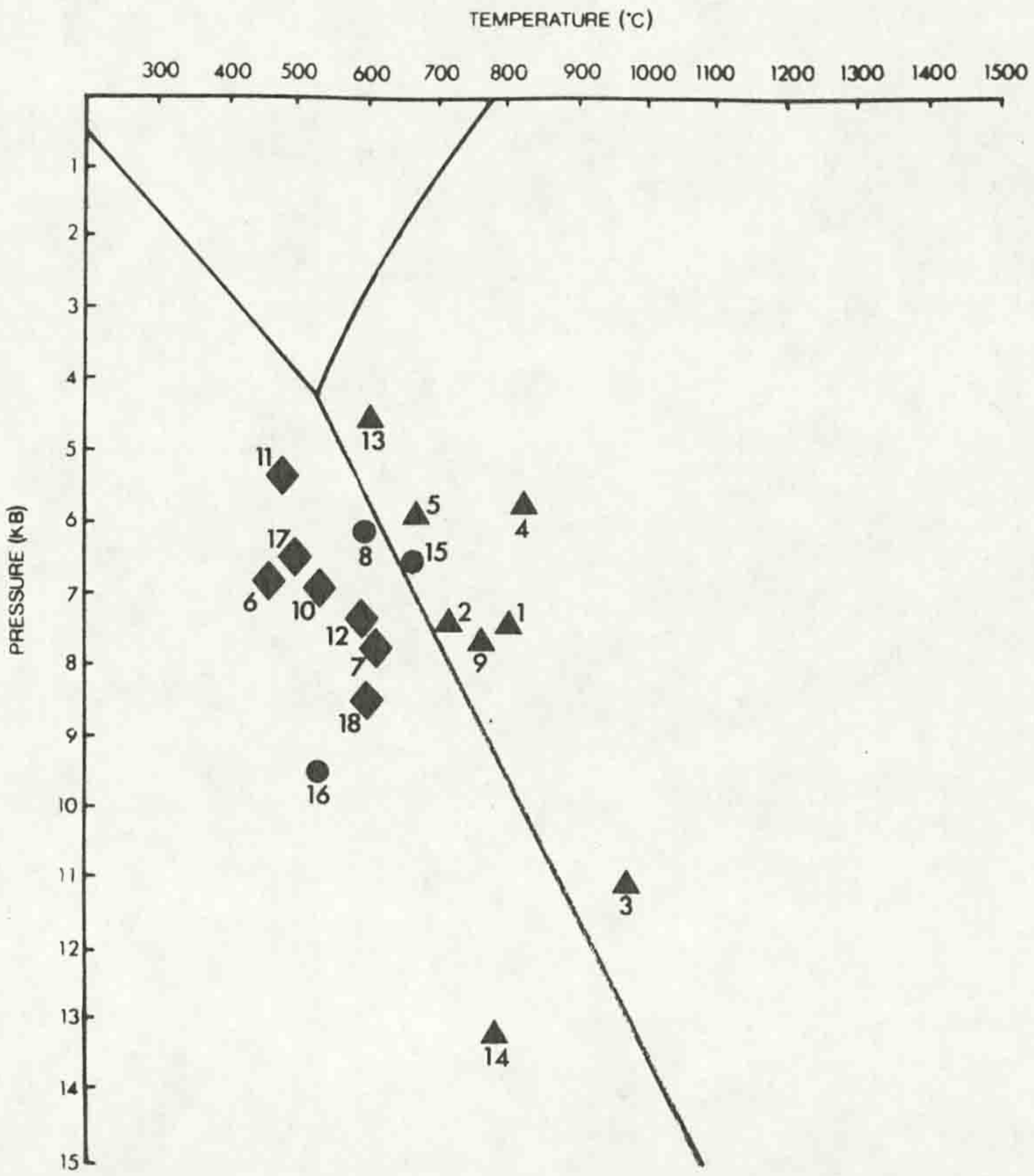


1: 66795
2: 68799
3: 68804
4: 68806
5: 69215
6: 69229
7: 69230
8: 69238
9: 69619
10: 69623
11: 69625
12: 69627
13: 69635
14: 71898
15: 71901
16: 71912
17: 71916
18: 71918

Figure 5.2: Results of Grt - BT thermometry and Grt - Pl - Ms - Bt barometry for Streamstown Fm lithologies. The error boxes are calculated for 2 sigma variations in mineral composition. $Al_2SiO_5$ curves after Salje (1986).

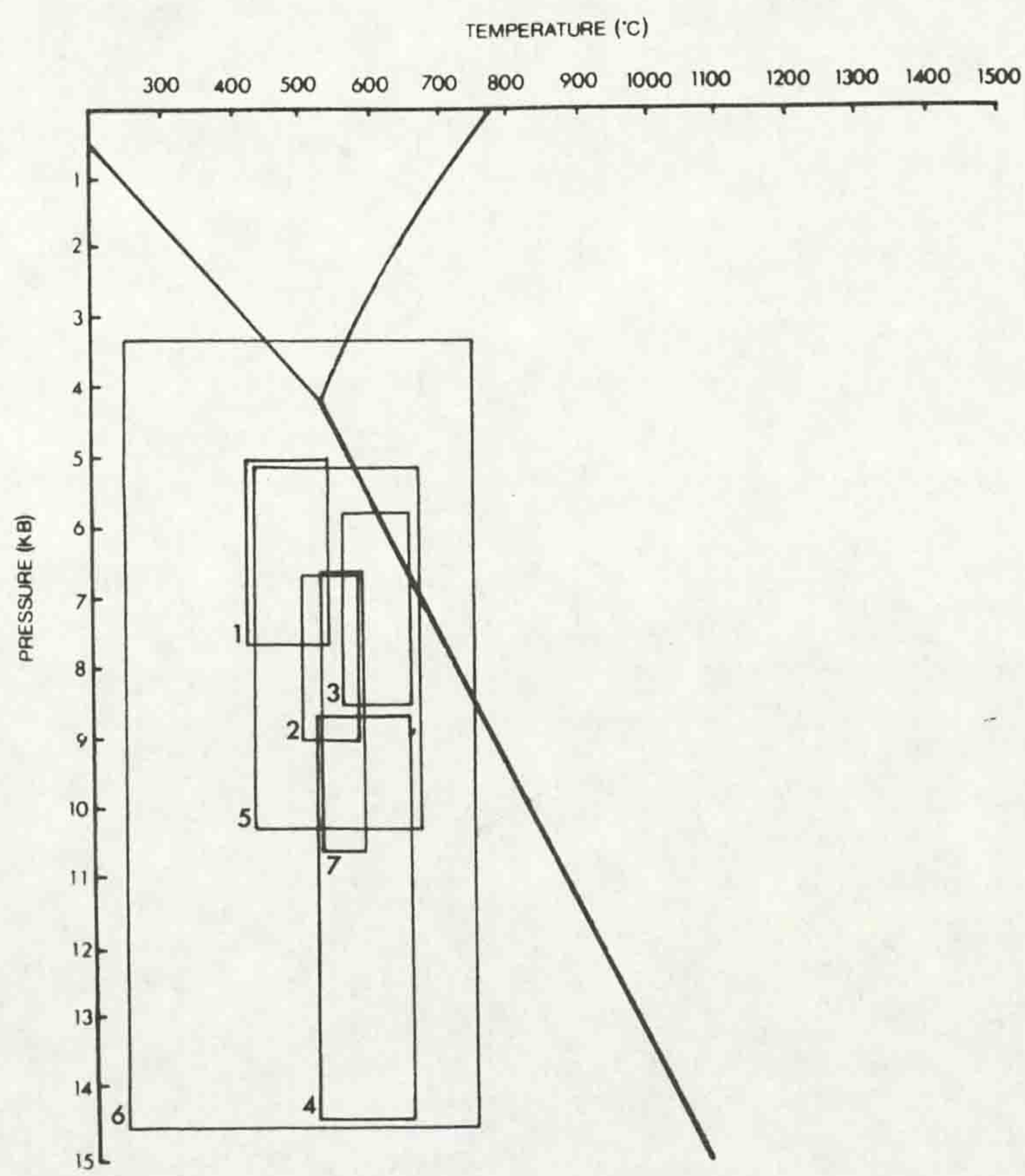


1: 69229
2: 69230
3: 69623
4: 69625
5: 69627
6: 71916
7: 71918

Figure 5.3: Results of Grt - BT thermometry and Grt - Pl - Ms - Bt barometry for Kylemore Fm lithologies. The error boxes are calculated for 2 sigma variations in mineral composition. $Al_2SiO_5$ curves after Salje (1986).

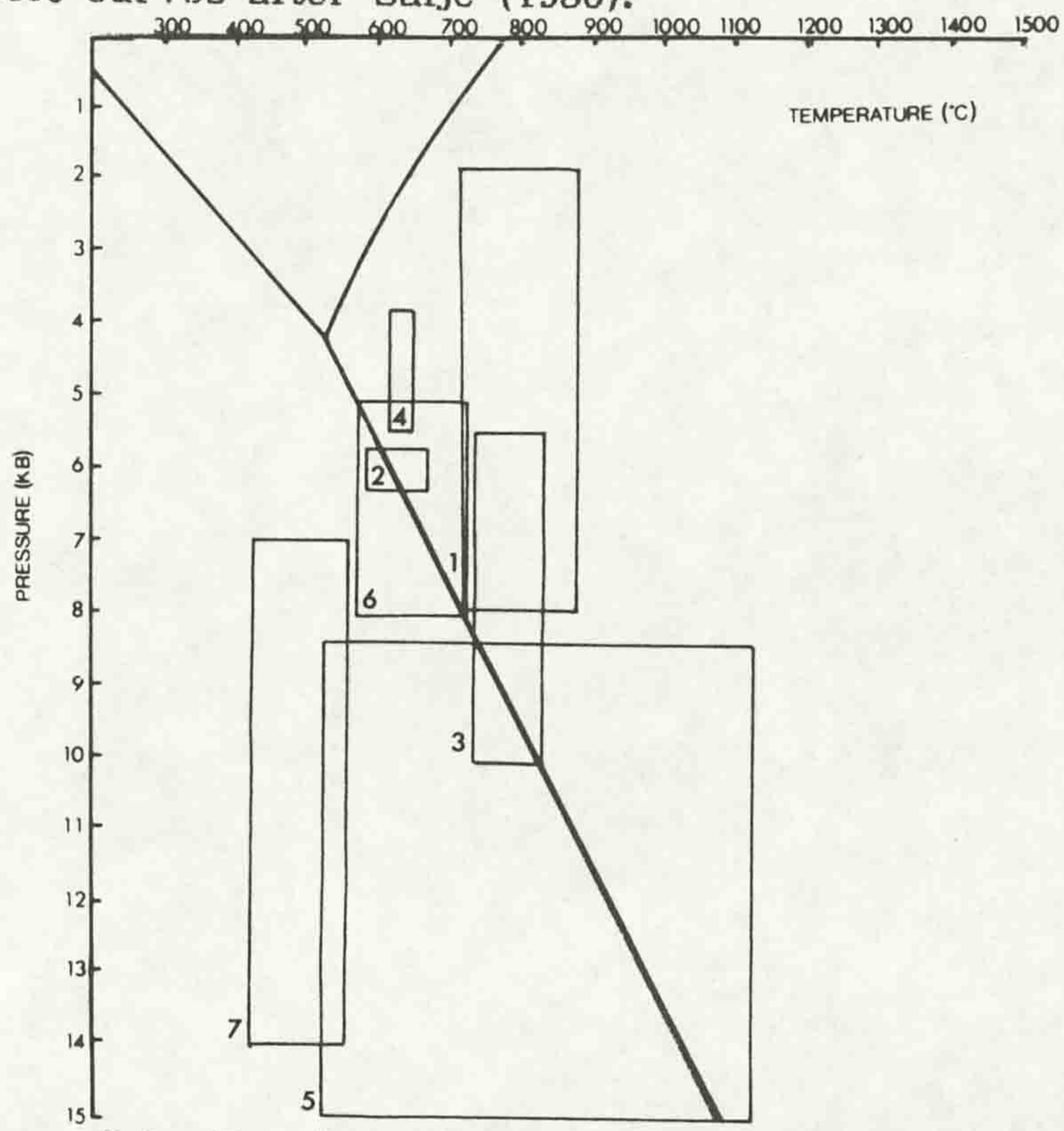


1: 68806
2: 69238
3: 69619
4: 69635
5: 71898
6: 71901
7: 71912

Figure 5.4: Results of Grt - BT thermometry and Grt - Pl - $Al_2SiO_5$ - Qtz barometry for sillimanite and fibrolite bearing assemblages in the Kylemore Fm. The error boxes are calculated for 2 sigma variations in mineral composition. $Al_2SiO_5$ curves after Salje (1986).

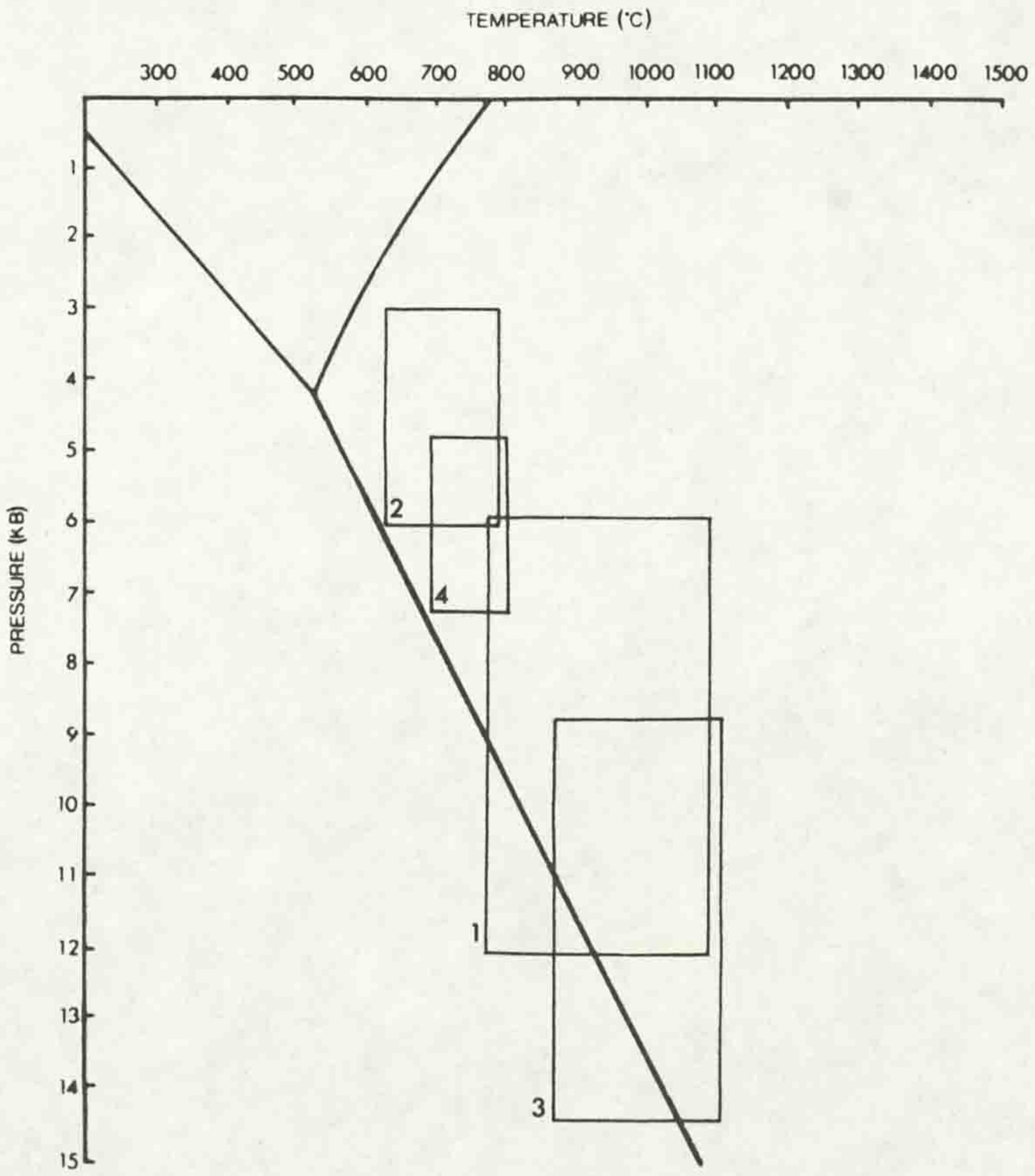


1: 66795
2: 68799
3: 68804
4: 69215

| | Garnet | | Biotite | | Muscovite | | | | Plagioclase | |
|---|---|---|---|---|---|---|---|---|---|---|
| Sample | $X_{Sps}$ | $X_{Phl}$ | $X_{Ti}$ | $X_{AlVI}$ | $X_{AlVI}$ | $X_{Fe}$ | $X_{K}$ | $X_{Na}$ | $X_{Ab}$ | $X_{or}$ |
| 66795 | 0.023(3) | 0.556(3) | 0.005(3) | 0.074(3) | * | * | * | * | 0.456(4) | 0.008(4) |
| 68799 | 0.246(2) | 0.401(6) | 0.049(6) | 0.116(6) | * | * | * | * | 0.591(1) | 0.005(1) |
| 68804 | 0.015(3) | 0.501(2) | 0.033(2) | 0.045(2) | * | * | * | * | 0.617(3) | 0.015(3) |
| 68806 | 0.262(2) | 0.461(3) | 0.012(3) | 0.278(3) | 0.792(2) | 0.395(2) | 0.925(2) | * | 0.732(5) | 0.009(5) |
| 69215 | 0.022(2) | 0.576(5) | 0.042(5) | 0.030(5) | * | * | * | * | 0.614(4) | 0.031(4) |
| 69229 | 0.027(2) | 0.563(3) | 0.027(3) | 0.021(3) | 0.789(4) | 0.036(4) | 0.051(4) | 0.175(4) | 0.651(4) | 0.199(4) |
| 69230 | 0.172(1) | 0.496(4) | 0.027(4) | 0.075(4) | 0.873(4) | 0.045(4) | 0.067(4) | 0.197(4) | 0.895(2) | = = |
| 69238 | 0.091(1) | 0.464(4) | 0.029(4) | 0.067(4) | 0.867(3) | 0.082(3) | 0.046(3) | 0.246(3) | 0.654(3) | 0.039(3) |
| 69619 | 0.104(5) | 0.300(2) | 0.017(2) | 0.353(2) | 0.889(3) | 0.047(3) | 0.040(3) | 0.103(3) | 0.705(7) | 0.032(7) |
| 69623 | 0.056(3) | 0.492(3) | 0.016(3) | 0.131(3) | 0.904(2) | 0.044(2) | 0.037(2) | 0.314(2) | 0.166(1) | 0.003(1) |
| 69625 | 0.092(2) | 0.451(3) | 0.022(3) | 0.033(3) | 0.922(4) | 0.032(4) | 0.028(4) | 0.127(4) | 0.698(1) | 0.004(1) |
| 69627 | 0.021(4) | 0.474(4) | 0.021(4) | 0.080(4) | 0.863(1) | 0.065(1) | 0.057(1) | 0.166(1) | 0.814(4) | 0.011(4) |
| 69635 | 0.105(2) | 0.324(4) | 0.004(4) | 0.243(4) | 0.579(2) | 0.136(2) | 0.161(2) | 0.102(2) | 0.646(2) | 0.033(2) |
| 71898 | 0.225(3) | 0.310(2) | 0.025(2) | 0.291(2) | 0.899(3) | 0.072(3) | = = | = = | 0.849(3) | 0.108(3) |
| 71901 | 0.255(3) | 0.472(3) | 0.049(3) | 0.019(3) | 0.861(3) | 0.112(3) | = = | = = | 0.718(2) | 0.006(2) |
| 71916 | 0.124(2) | 0.347(2) | 0.020(2) | 0.212(2) | 0.923(2) | 0.147(2) | 0.200(2) | = = | 0.777(2) | 0.015(2) |
| 71918 | 0.020(2) | 0.411(2) | 0.017(2) | 0.154(2) | 0.942(2) | 0.053(2) | = = | = = | 0.766(2) | 0.010(2) |

**Table 5.3: Mean values of molar fractions used in calculating pressure and temperature. (= = indicates element concentrations below detection limits, * indicates mineral not present in assemblage, number in brackets number of analyses used to calculate mean).**

| Sample | $X_{Alm}$ | $X_{Prp}$ | $X_{Ann}$ | $\ln K_{DT1}$ | $\ln K_{DT2}$ | $T_1$ | $T_2$ | $T_3$ | $T_4$ | $T_5$ | $T_{mean}$ |
|---|---|---|---|---|---|---|---|---|---|---|---|
| 66795 | 0.701(2) | 0.225(2) | 0.376(3) | 1.158 | -1.144 | 800.4 | 841.2 | 858.4 | 664.5 | 898.5 | 812.6 |
| 68799 | 0.509(2) | 0.122(2) | 0.434(6) | 1.375 | -2.061 | 720.5 | 728.7 | 780.6 | 749.1 | 669.0 | 729.6 |
| 68804 | 0.747(3) | 0.198(3) | 0.505(2) | 0.930 | -1.000 | 930.5 | 1008.1 | 1024.4 | 847.3 | 1004.6 | 963.0 |
| 68806 | 0.595(4) | 0.117(2) | 0.537(3) | 1.218 | -1.747 | 762.1 | 799.2 | 817.0 | 814.7 | 728.2 | 784.2 |
| 69215 | 0.755(2) | 0.184(2) | 0.411(4) | 1.366 | -1.257 | 711.0 | 725.9 | 742.8 | 616.8 | 823.6 | 724.0 |
| 69229 | 0.755(2) | 0.058(2) | 0.443(3) | 2.364 | -2.332 | 460.2 | 408.8 | 464.8 | 468.6 | 508.0 | 462.1 |
| 69230 | 0.741(2) | 0.083(2) | 0.424(3) | 1.980 | -1.995 | 549.5 | 506.4 | 530.7 | 543.4 | 595.4 | 545.1 |
| 69238 | 0.748(1) | 0.077(1) | 0.500(3) | 1.776 | -1.881 | 590.6 | 566.0 | 603.5 | 613.3 | 628.2 | 600.3 |
| 69619 | 0.734(4) | 0.108(4) | 0.500(1) | 1.310 | -1.492 | 743.2 | 759.9 | 781.6 | 768.4 | 773.8 | 765.4 |
| 69623 | 0.759(3) | 0.073(3) | 0.459(3) | 2.227 | -2.139 | 493.4 | 443.2 | 486.6 | 486.8 | 550.6 | 492.1 |
| 69625 | 0.687(2) | 0.038(2) | 0.510(2) | 2.448 | -2.704 | 441.8 | 389.5 | 457.0 | 475.4 | 458.7 | 444.5 |
| 69627 | 0.799(4) | 0.080(4) | 0.544(3) | 1.851 | -1.806 | 581.7 | 547.5 | 586.8 | 584.1 | 633.2 | 586.7 |
| 69635 | 0.766(2) | 0.075(2) | 0.509(1) | 1.681 | -1.789 | 605.3 | 592.8 | 613.6 | 642.6 | 642.1 | 619.3 |
| 71898 | 0.689(3) | 0.076(3) | 0.625(2) | 1.491 | -1.837 | 725.8 | 701.3 | 718.6 | 766.7 | 693.0 | 721.1 |
| 71901 | 0.615(3) | 0.079(3) | 0.485(3) | 1.635 | -2.100 | 632.4 | 617.0 | 652.9 | 679.5 | 620.2 | 640.4 |
| 71912 | 0.717(2) | 0.038(2) | 0.541(2) | 2.306 | -2.545 | 492.6 | 432.6 | 493.2 | 520.1 | 491.4 | 483.0 |
| 71916 | 0.645(2) | 0.043(2) | 0.371(2) | 2.658 | -2.868 | 412.5 | 352.3 | 420.8 | 430.9 | 442.9 | 411.9 |
| 71918 | 0.772(2) | 0.055(2) | 0.462(2) | 2.042 | -2.119 | 542.3 | 495.1 | 522.5 | 563.0 | 566.5 | 543.9 |

**Table 5.4: Results of garnet - biotite thermometry. (The calibrations used are Thompson (1976), $T_1$; Ferry & Spear (1978), $T_2$; Hodges & Spear (1982), $T_3$; Ganguly & Saxena (1984), $T_4$; Pigage & Greenwood (1982), $T_5$. T in °C.**

Table 5.5: Variations in $K_D$ values for garnet - biotite thermometry. $K_{DT1}$ and $K_{DT2}$ are the distribution coefficients of Thompson (1976b) and Ferry & Spear (1978) respectively.

| sample | $\ln K_{DT1}$ | | | $\ln K_{DT2}$ | | |
|---|---|---|---|---|---|---|
| | min | mean | max | min | mean | max |
| 66795 | 0.754 | 1.158 | 1.285 | -1.208 | -1.144 | -0.903 |
| 68799 | 1.209 | 1.375 | 1.534 | -2.136 | -2.061 | -1.977 |
| 68804 | 0.765 | 0.930 | 1.094 | -1.086 | -1.000 | -0.914 |
| 68806 | 1.070 | 1.281 | 1.375 | -1.795 | -1.747 | -1.710 |
| 69215 | 1.247 | 1.366 | 1.484 | -1.314 | -1.257 | -1.198 |
| 69229 | 2.067 | 2.364 | 2.529 | -2.469 | -2.332 | -2.138 |
| 69230 | 1.842 | 1.980 | 2.155 | -2.093 | -1.995 | -1.905 |
| 69238 | 1.724 | 1.776 | 1.828 | -1.913 | -1.881 | -1.849 |
| 69619 | 1.205 | 1.310 | 1.424 | -1.561 | -1.492 | -1.434 |
| 69623 | 1.632 | 2.227 | 2.581 | -2.232 | -2.139 | -1.825 |
| 69625 | 2.340 | 2.448 | 2.563 | -2.793 | -2.704 | -2.622 |
| 69627 | 1.591 | 1.851 | 2.121 | -1.983 | -1.806 | -1.636 |
| 69635 | 1.645 | 1.681 | 1.717 | -1.812 | -1.767 | -1.789 |
| 71898 | 0.828 | 1.491 | 2.132 | -1.347 | -1.837 | -2.233 |
| 71901 | 1.449 | 1.635 | 1.830 | -2.191 | -2.100 | -2.021 |
| 71912 | 2.071 | 2.306 | 2.554 | -2.731 | -2.545 | -2.375 |
| 71916 | 1.505 | 2.658 | 3.817 | -3.523 | -2.868 | -2.098 |
| 71918 | 1.966 | 2.042 | 2.119 | -2.143 | -2.119 | -2.095 |

| | Garnet | | | | | | | | | Biotite | | |
|---|---|---|---|---|---|---|---|---|---|---|---|---|
| | Ganguly & Saxena | | | Hodges & Spear | | | Hodges & Crowley | | | Holdaway | Hodges & Crowley | |
| Sample | $a_{Alm}$ | $a_{Prp}$ | $a_{Grs}$ | $a_{Alm}$ | $a_{Prp}$ | $a_{Grs}$ | $a_{Alm}$ | $a_{Prp}$ | $a_{Grs}$ | $a_{Phl}$ | $a_{Phl}$ | $a_{Ann}$ |
| 66795 | 0.462 | 0.092 | 0.000 | 0.344 | 0.013 | 0.000 | 0.355 | 0.012 | 0.000 | 0.026 | 0.055 | 0.053 |
| 68799 | 0.130 | 0.047 | 0.003 | 0.123 | 0.003 | 0.003 | 0.130 | 0.002 | 0.002 | 0.067 | 0.069 | 0.082 |
| 68804 | 0.505 | 0.083 | 0.000 | 0.402 | 0.009 | 0.000 | 0.413 | 0.008 | 0.000 | 0.026 | 0.039 | 0.129 |
| 68806 | 0.221 | 0.043 | 0.000 | 0.208 | 0.002 | 0.000 | 0.210 | 0.002 | 0.000 | 0.045 | 0.045 | 0.155 |
| 69215 | 0.506 | 0.079 | 0.000 | 0.417 | 0.007 | 0.000 | 0.427 | 0.006 | 0.000 | 0.061 | 0.061 | 0.070 |
| 69229 | 0.329 | 0.029 | 0.005 | 0.413 | 0.000 | 0.005 | 0.426 | 0.000 | 0.004 | 0.047 | 0.047 | 0.087 |
| 69230 | 0.395 | 0.033 | 0.000 | 0.398 | 0.000 | 0.000 | 0.404 | 0.001 | 0.000 | 0.042 | 0.042 | 0.076 |
| 69238 | 0.381 | 0.036 | 0.001 | 0.408 | 0.001 | 0.001 | 0.416 | 0.000 | 0.001 | 0.025 | 0.028 | 0.125 |
| 69619 | 0.373 | 0.056 | 0.000 | 0.363 | 0.002 | 0.000 | 0.367 | 0.002 | 0.000 | 0.017 | 0.020 | 0.125 |
| 69623 | 0.373 | 0.038 | 0.001 | 0.421 | 0.001 | 0.002 | 0.433 | 0.000 | 0.002 | 0.066 | 0.070 | 0.097 |
| 69625 | 0.237 | 0.010 | 0.012 | 0.313 | 0.000 | 0.009 | 0.322 | 0.000 | 0.008 | 0.035 | 0.035 | 0.133 |
| 69627 | 0.450 | 0.043 | 0.001 | 0.496 | 0.001 | 0.001 | 0.507 | 0.001 | 0.001 | 0.039 | 0.042 | 0.161 |
| 69635 | 0.443 | 0.027 | 0.000 | 0.445 | 0.000 | 0.000 | 0.449 | 0.000 | 0.000 | 0.019 | 0.019 | 0.132 |
| 71898 | 0.334 | 0.022 | 0.000 | 0.331 | 0.000 | 0.000 | 0.334 | 0.000 | 0.000 | 0.015 | 0.015 | 0.143 |
| 71901 | 0.224 | 0.027 | 0.000 | 0.228 | 0.001 | 0.001 | 0.232 | 0.001 | 0.001 | 0.033 | 0.033 | 0.114 |
| 71912 | 0.282 | 0.010 | 0.006 | 0.359 | 0.000 | 0.006 | 0.366 | 0.000 | 0.005 | 0.023 | 0.023 | 0.158 |
| 71916 | 0.198 | 0.012 | 0.015 | 0.256 | 0.000 | 0.011 | 0.265 | 0.000 | 0.009 | 0.044 | 0.044 | 0.051 |
| 71918 | 0.352 | 0.027 | 0.004 | 0.446 | 0.000 | 0.005 | 0.457 | 0.000 | 0.004 | 0.017 | 0.017 | 0.099 |

**Table 5.6: Calculated activities of garnet and biotite.**

| Sample | $X_{Grs}$ | $X_{An}$ | $X_{KMs}$ | $\ln K_{DP1}$ | $\ln K_{DP2}$ | $\ln K_{DP3}$ | $\ln K_{DP4}$ | $\ln K_{DP5}$ | $P_1$ | $P_2$ | $P_3$ | $P_4$ | $P_5$ | $P_{mean}$ | |
|---|---|---|---|---|---|---|---|---|---|---|---|---|---|---|---|
| 68806 | 0.043(4) | 0.244(5) | 0.933(3) | 8.656 | 5.002 | 7.184 | 9.514 | 5.871 | 4512 | | 4818 | 9939 | 7116 | 6724 | 5793 |
| 69229 | 0.160(2) | 0.263(2) | 0.877(4) | 7.124 | 0.031 | 4.432 | 8.709 | 1.453 | 5816 | | 6681 | 9155 | 5552 | 5429 | 5869 |
| 69230 | 0.064(2) | 0.096(2) | 0.860(4) | 5.661 | -0.321 | 3.561 | 6.263 | 0.880 | 7217 | | 8012 | 11033 | 8500 | 7606 | 7834 |
| 69238 | 0.096(1) | 0.297(3) | 0.823(3) | 7.708 | 2.337 | 5.606 | 8.933 | 3.498 | 5455 | | 6107 | 9745 | 6416 | 6221 | 6050 |
| 69619 | 0.053(4) | 0.231(6) | 0.933(4) | 7.288 | 3.356 | 5.210 | 7.705 | 4.093 | 6046 | | 6573 | 12104 | 9136 | 8470 | 7556 |
| 69623 | 0.120(3) | 0.153(1) | 0.769(2) | 6.154 | -0.527 | 3.605 | 7.215 | 0.790 | 6655 | | 7519 | 10264 | 7099 | 6588 | 6965 |
| 69625 | 0.196(2) | 0.277(1) | 0.873(4) | 7.615 | 0.269 | 4.573 | 9.206 | 1.803 | 5413 | | 6273 | 8809 | 5002 | 4792 | 5370 |
| 69627 | 0.102(4) | 0.181(4) | 0.885(1) | 6.233 | 0.679 | 3.751 | 7.162 | 1.823 | 6812 | | 7592 | 11425 | 8063 | 7579 | 7511 |
| 69635 | 0.052(2) | 0.296(2) | 0.904(2) | 9.146 | 4.103 | 8.103 | 10.707 | 5.303 | 4089 | | 4593 | 7409 | 4747 | 4784 | 4533 |
| 71898 | 0.043(3) | 0.028(2) | 1.000(3) | 2.373 | -2.103 | -0.872 | 1.707 | -1.251 | 11252 | | 12176 | 18512 | 15576 | 13573 | 13143 |
| 71901 | 0.090(3) | 0.261(2) | 1.000(3) | 7.376 | 2.470 | 5.523 | 8.603 | 3.557 | 5811 | | 6398 | 10290 | 7067 | 6873 | 6537 |
| 71912 | 0.173(2) | 0.073(3) | 1.000(1) | 3.490 | -3.442 | -0.862 | 3.744 | -2.087 | 8817 | | 9868 | 14068 | 10060 | 8870 | 9404 |
| 71916 | 0.207(2) | 0.181(4) | 1.000(2) | 5.906 | -2.063 | 3.343 | 7.701 | -0.192 | 6645 | | 7655 | 9371 | 5949 | 5671 | 6480 |
| 71918 | 0.156(2) | 0.179(3) | 1.000(2) | 4.999 | -1.127 | 1.454 | 5.898 | 0.035 | 7796 | | 8725 | 12993 | 8831 | 8346 | 8425 |

**Table 5.7: Results of garnet - plagioclase - biotite - muscovite barometry. $\ln K_{DP1}$: Ghent & Stout (1981); $\ln K_{DP2}$: Ghent & Stout (1981); $\ln K_{DP3}$: Ganguly & Saxena (1984) $\ln K_{DP4}$: Hodges & Spear (1982); $\ln K_{DP5}$: Hodges & Crowley (1985). P in Bars.**

| Sample | $\ln K_{DP1}$ i | | $\ln K_{DP2}$ i | | $\ln K_{DP3}$ i | | $\ln K_{DP4}$ i | | $\ln K_{DP5}$ i | |
|---|---|---|---|---|---|---|---|---|---|---|
| | min | max | min | max | min | max | min | max | min | max |
| 68806 | 6.907 | 11.810 | 3.696 | 7.685 | 4.879 | 11.037 | 7.471 | 13.081 | 4.446 | 8.694 |
| 69229 | 5.503 | 7.929 | -0.697 | 0.339 | 2.176 | 5.375 | 6.511 | 9.711 | 0.493 | 1.887 |
| 69230 | 4.854 | 6.522 | -0.673 | 0.058 | 2.367 | 4.832 | 5.173 | 7.424 | 0.411 | 1.383 |
| 69238 | 7.493 | 7.912 | 2.319 | 2.427 | 5.299 | 5.894 | 8.643 | 9.204 | 3.401 | 3.586 |
| 69619 | 5.675 | 8.686 | 2.057 | 4.413 | 2.996 | 7.081 | 5.615 | 9.443 | 2.701 | 5.247 |
| 69623 | 4.250 | 7.751 | -0.646 | 7.968 | 0.433 | 6.505 | 4.484 | 9.400 | 0.238 | 1.580 |
| 69625 | 7.316 | 7.931 | 0.295 | 0.239 | 4.132 | 5.035 | 8.772 | 5.032 | 1.746 | 1.858 |
| 69627 | 4.671 | 7.617 | -0.102 | 1.253 | 1.442 | 5.817 | 4.969 | 9.115 | 0.841 | 2.607 |
| 69635 | 8.364 | 9.834 | 3.427 | 4.681 | 7.101 | 8.945 | 9.768 | 11.484 | 4.591 | 5.916 |
| 71898 | 0.006 | 4.784 | -2.476 | -1.614 | -4.268 | 2.628 | -1.518 | 5.062 | -2.128 | -0.289 |
| 71901 | 6.403 | 8.536 | 2.054 | 3.043 | 4.097 | 7.219 | 7.332 | 10.096 | 3.000 | 4.280 |
| 71912 | -0.441 | 5.562 | -6.907 | -2.103 | -5.809 | 2.056 | -1.123 | 6.587 | -5.521 | -0.555 |
| 71916 | 1.141 | 9.085 | -3.381 | -2.364 | -3.729 | 8.242 | 0.958 | 12.346 | -2.343 | 0.314 |
| 71918 | 3.071 | 6.553 | -2.830 | 0.195 | -1.518 | 3.962 | 3.295 | 7.918 | -1.742 | 1.432 |

**Table 5.8: The results of Grt - Pl - Ms - Bt geobarometry. Variations in $K_S$ results for -sigma and +sigma variation in input data. $\ln K_{DP\ 1\ to\ 5}$ refer to the distribution coefficients of Ghent & Stout (1981) (1 and 2) , Ganguly & Saxena (1984), Hodges & Spear (1982) and Hodges & Crowley (1985) respectively.**

Table 5.9: Calculated muscovite and plagioclase activities.

| | Holdaway | Hodges & Crowley | | Newton & Haselton | Hodges & Crowley |
|---|---|---|---|---|---|
| Sample | $a_{Ms}$ | $a_{Ms}$ | $a_{Ts}$ | $a_{An}$ | $a_{An}$ |
| 68806 | 0.551 | 0.658 | 3.499 | 0.308 | 0.296 |
| 69229 | 0.721 | 0.774 | 13.154 | 0.564 | 0.412 |
| 69230 | 0.649 | 0.718 | 8.455 | 0.126 | 0.137 |
| 69238 | 0.578 | 0.656 | 4.875 | 0.496 | 0.407 |
| 69619 | 0.709 | 0.778 | 9.514 | 0.293 | 0.283 |
| 69623 | 0.609 | 0.673 | 10.549 | 0.263 | 0.231 |
| 69625 | 0.684 | 0.746 | 12.943 | 0.622 | 0.442 |
| 69627 | 0.632 | 0.710 | 6.416 | 0.274 | 0.250 |
| 69635 | 0.532 | 0.636 | 5.522 | 0.479 | 0.399 |
| 71898 | 0.739 | 0.817 | 5.793 | 0.023 | 0.036 |
| 71901 | 0.655 | 0.754 | 3.535 | 0.402 | 0.347 |
| 71912 | 0.852 | 0.899 | 8.624 | 0.100 | 0.111 |
| 71916 | 0.563 | 0.682 | 3.374 | 0.399 | 0.300 |
| 71918 | 0.850 | 0.897 | 9.158 | 0.294 | 0.099 |

| Sample | $X_{Grs}$ | $X_{An}$ | $Al_2SiO_5$ | $\log K_{s6}$ | $\log K_{s7}$ | $P_1$ | $P_2$ | $P_{Mean}$ |
|---|---|---|---|---|---|---|---|---|
| 66795 | 0.041(2) | 0.506(3) | S/F | -3.274 | -3.874 | 7346 | 7839 | 7592.5 |
| 68799 | 0.129(2) | 0.404(1) | S | -1.487 | -1.887 | 7758 | 7313 | 7535.5 |
| 68804 | 0.041(3) | 0.268(4) | F/S | -2.446 | -2.846 | 11310 | 10734 | 11022.0 |
| 69215 | 0.041(2) | 0.354(4) | F/S | -2.808 | -3.208 | 6183 | 5741 | 5962.0 |

**Table 5.10: Results of Grt - Pl - $Al_2SiO_5$ - Qtz geobarometry. The calibrations are $P_1$ Ghent (1976) and $P_2$ Ghent, Robbins & Stout (1979). P in bars.**

# Chapter Two: The metasedimentary sequence and igneous bodies

Table 5.11: Variations in $K_{DP6}$ (Ghent, 1976) and $K_{DP7}$ (Ghent, Robbins & Stout, 1979) values.

| sample | $\log K_{DP6}$ | | | $\log K_{DP7}$ | | |
|---|---|---|---|---|---|---|
| | minimum | mean | maximum | minimum | mean | maximum |
| 66795 | -3.289 | -3.274 | -3.224 | -3.874 | -3.689 | -3.624 |
| 68799 | -1.497 | -1.487 | -1.467 | -1.897 | -1.887 | -1.867 |
| 68804 | -2.700 | -2.446 | -2.195 | -3.100 | -2.846 | -2.595 |
| 69215 | -2.933 | -2.808 | -2.720 | -3.333 | -3.208 | -3.120 |

and contact (locally migmatitic) lithologies (Figure 5.3) with
mean pressure of 7.75 ± 3.3 kbb
mean temperature of 722 ± 64 °C.
iii, Regional metamorphic assemblages south of the RBS (Figure 5.4), giving
mean pressure of 6.67 ± 0.9 kbb,
mean temperature of 490 ± 59 °C.

The error boxes shown in Figure 5.2, 5.3 and 5.4, are calculated on plus or minus sigma for the variation in mineral composition in an analysed assemblage (the means of the data are tabulated in Table 5.3). The variation in mineral compositions were used to calculate maximum and minimum $K_{DT}$ and $K_{DP}$ values (ie, the variation in $K_{DT}$ values given by using maximum values of $X_{Phl}$ / $X_{Ann}$ in biotite with minimum values of $X_{Prp}$ / $X_{Alm}$ in garnet and vice versa, and $K_{DP}$ variations using maximum $X_{Grs}$ with minimum $X_{An}$ and vice versa). The values of P and T for a given composition assemblage were calculated iteratively by repeated solution of the geothermometer and geobarometer calibrations using the mean P from one run as an input parameter to calculate T on the next run and the mean T value as an input to the P calculation, until both P (Tables 5.7 and 5.10) and T (Table 5.4) remained constant. The error boxes plotted on Figures 5.2, 5.3 and 5.4 show the results for maximum and minimum $K_{DT}$ and $K_{DP}$ (Tables 5.5, 5.78 5.11) values, and, as the mean temperatures and pressures for a number of calibrations were used, are plotted with no slope, unlike error boxes for specific calibrations (e.g. Spear & Rumble 1986). The results of the various activity calculations are tabulated in Tables 5.6 and 5.9

As is evident in Figs. 5.2, 5.3 and 5.4 the magnitude of errors due to compositional variation in certain assemblages is very high . Such assemblages may represent a variably disequilibrated system, and in those sections where obvious retrograde mineralogies replace the earlier assemblage it is possible to determine if retrogression is a significant error source. However, where retrograde minerals are not obviously developed, error may be due to a variety of other effects.

Where minerals are compositionally zoned the data used in the

thermobarometric calculations should be restricted to those areas of minerals likely to be in equilibrium with the rest of the assemblage (ie, the 'rim' composition). As the garnets studied are often conspicuously zoned {4.1.3.1} only compositional data from the rims of garnets were used in the calculations. Some problems may arise in assemblages where garnet has been resorbed, although the resorption reactions are likely to maintain a degree of equilibrium between the garnet and the external assemblage.

Biotite shows a range of compositions {4.1.3.2}, although evidence for chemical zoning within individual biotites is scant. It is likely that the relatively rapid rates of intracrystalline diffusion in biotite (Tracy 1982) have prevented the formation of compositional gradients during mineral growth, or have facilitated the loss of any gradients developed during growth. Any retrograde diffusive re - equilibration of biotite may also lead to resetting of overall $X_{Phl}$ / $X_{Ann}$ ratios in biotite and subsequent effects on thermometry using these ratios.

Feldspar shows a variety of zoning styles {4.1.3.5}. Only rim compositions were used in barometric calculations when zoning was evident. The persistence of chemical gradients within plagioclase feldspars in contact assemblages where biotite is homogenized and garnet profiles are strongly affected by post - growth diffusion suggests that the rates of such processes within feldspars are relatively slow. This may lead to problems in barometric systems where a significant degree of diffusive resetting of biotite and garnet has occurred with minimal effects on feldspars.

The effects of ionic substitution within thermometric systems have been discussed. The primary substitution within the minerals studied involves Ti which occurs in both biotite and muscovite in a range from below detection limits to $\tilde{=}$ 6% {4.1.3.2}.

In keeping with 'traditional' practice in thermobarometry all iron involved in exchange reactions is considered to be in the ferrous state ($Fe^{2+}$) although there is optical evidence for ferric ($Fe^{3+}$) iron in some biotites in this study {4.1.3.2}, and high oxidation ratios within hornfelsic lithologies are reported in Angus & Middleton (1985). The effects of ferric iron on Grt - Bt exchange are not considered in this work, although

the presence of $Fe^{3+}$ will change Mg/Fe ratios and the subsequent $K_{DT}$ values leading to incorrect temperature estimates. Ghent *et al.* (1979) note that the assumption of total iron as ferrous iron in mole fraction calculations leads to high values for $X_{Grs}$ in garnet and to the production of higher pressure values for systems at given temperatures and $X_{An}$.

The various calibrations of the thermobarometric systems used produce a wide range of results, this effect being due simply to the thermodynamic and mixing data used in the calibrations. In order to avoid the problems associated with specific calibrations mean values of the temperatures and pressures for each sample were calculated. Certain of the calibrations (e.g. the Pigage & Greenwood (1982) calibration of the Grt - Bt thermometer) are based on a fixed mineral assemblage containing the calibration minerals, and where such minerals are absent then the result obtained from applications of the calibration will be erroneous. Problems with the type of $Al_2SiO_5$ polymorph considered in calibrations have been noted, as both fibrolitic and prismatic sillimanite are present in all the $Al_2SiO_5$ - bearing assemblages.

Analytical errors are not accounted for in this study, although Hodges & McKenna (1987) suggest errors, derived from analytical uncertainties, of up to 10 - 20% on the results of Grt - Bt exchange and as high as 30% on Grt - Pl - $Al_2SiO_5$ - Qtz results.

Three of the mean P - T values fall well outside the main cluster of points (Figure 5.1), showing pressures of between 9.40 and 13.14 kb, but at temperatures equivalent to other similar lithologies. These high pressure values may indicate that these assemblages developed at significantly higher pressures than the bulk of the area (although they show assemblages and textures similar to lithologies which yield lower pressures), or that these assemblages have been altered subsequent to their initial development in such a way as to perturb the thermobarometric systems.

Sample 69236 contains K - feldspar which is probably due to metasomatism associated with the Rushenduff Pegmatite body (4.1.3.6) and plagioclase which shows a degree of sericitic alteration. Samples 71898 and 71912 show significant

chloritic alteration of biotite and garnet, along with sericitisation of feldspar. Although the altered areas were avoided during probe analysis, it is apparent that retrograde effects are developed throughout the samples, and that these effects may significantly perturb the barometric systems (probably through loss of Ca in feldspars) with limited effects on the thermometric exchange. In sample 68804 a limited amount of alteration is developed, typically concentrated in narrow (1 - 2mm) zones of grain size reduction, and the bulk of the lithology remains unaltered. However, the lithology yields high pressure estimates, which can be ascribed to the presence of högbomite as an accessory mineral in the assemblage. The development of högbomite in the aluminous migmatitic aureole lithologies of the DCD (Leake 1965, Angus & Middleton 1985) suggests high oxidation ratios within these lithologies (where oxidation ratio (O.R) = $Fe^{3+}/(Fe^{2+} + Fe^{3+})$) and possible substitution of ferric iron into suitable sites in the thermobarometric phases. As discussed earlier, failure to account for ferric iron substitution results in high pressure estimates for the assemblage studied.

P - T estimates calculated using the calibrations given in {5.2, 5.3.1 and 5.3.2} fall largely into the kyanite field of the $Al_2SiO_5$ diagram (Figures 5.1, 5.2, 5.3 and 5.4), except within those lithologies which are either sillimanite bearing or in the aureole of the DCD (Figure 5.2). The sillimanite bearing assemblages are developed within the migmatitic contact aureoles of the DCD and yield temperatures equivalent to the >700°C recorded in the Cashel aureole, South Connemara, by Treloar (1981). The 'regional' metamorphic lithologies (ie, those which show no apparent relation to aureole effects) show a range of temperatures and pressures similar to those reported in equivalent lithologies in the rest of Connemara (Yardley *et al.* 1987). Importantly, the pressures and temperatures within the regional metamorphic assemblages on either side of the RBS show similar conditions. The timing of the regional metamorphic peak in these lithologies, as determined from textural relations {4.1.3, 4.1.4}, is syn / post D2, which coupled with the P - T results suggests that the material on either side of the RBS reached similar crustal conditions during / immediately after

Figure 5.5: Schematic P-T diagram (after Spear, Selverstone, Hickmott, Crowley & Hodges, 1984) showing the P-T paths followed by a series of samples (1, 2, 3) involved in a single metamorphic event. $T_{Max}$ and $P_{Max}$ are the peak temperature and pressure experienced by sample 3. Between these two maxima 'peak' P - T conditions are obtained from thermobarometry (the stippled areas). The resultant array of 'peak' P-T conditions yields the *piezothermic array* ('PA') as discussed by Richardson & England (1979).

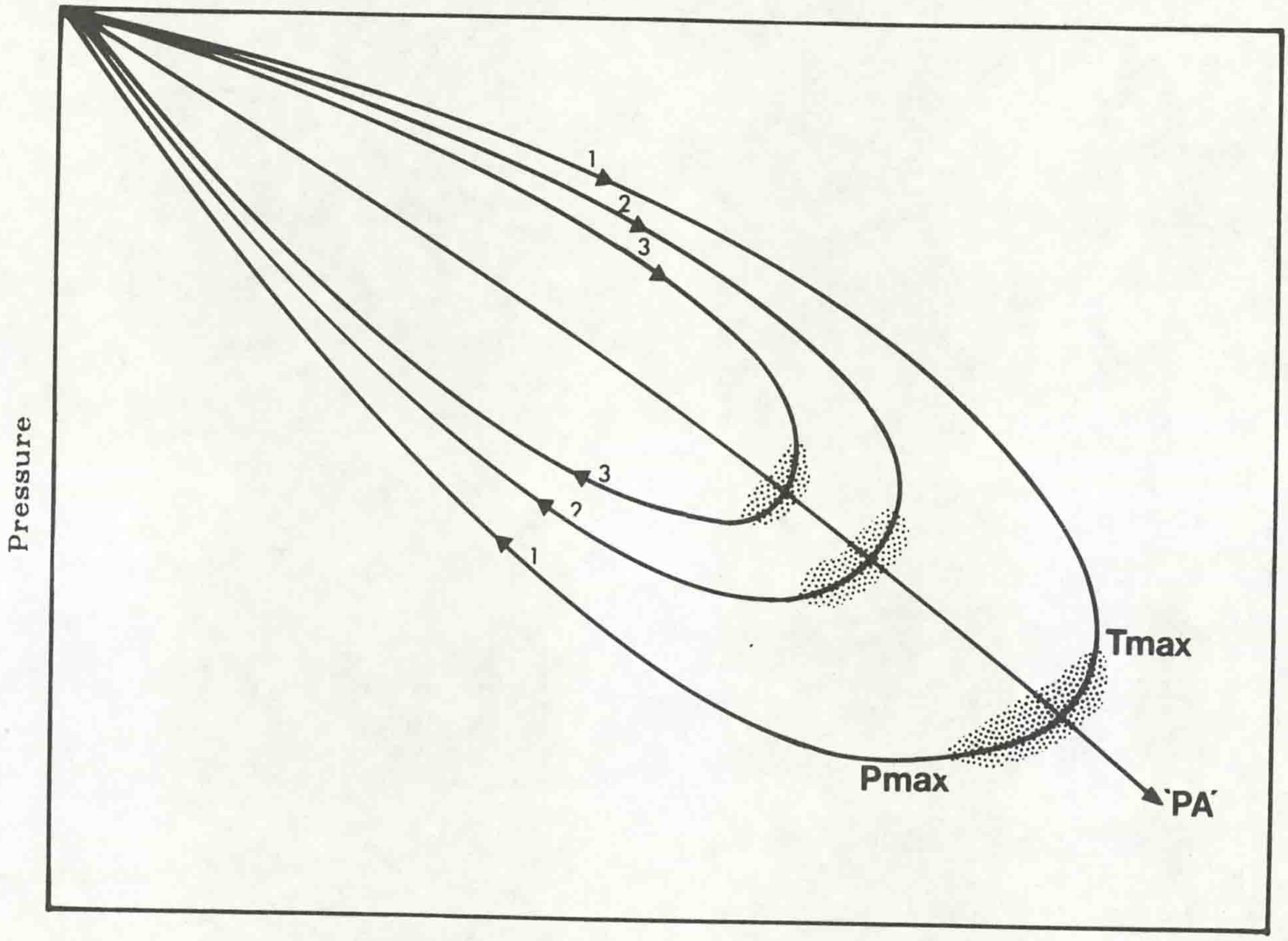

$D_2$.

## 5.5 P - T paths

### 5.5.1 Introduction and basic concepts

With the increasing use of tectono - thermal modelling to assess the theoretical evolution of metamorphic terrains (e.g England & Thompson 1984) the need for quantitative data on the pressure - temperature path followed by a metamorphic system has become increasingly apparent. 'Traditional' methods of P - T determination, such as the use of petrogenetic grids and geothermobarometry, are aimed at the determination of peak metamorphic conditions for mineral assemblages. Information on the P - T paths of a metamorphic event can be obtained by the use of several assemblages within a thermal system. However, the resultant array of pressures and temperatures, the '*piezothermic array*' of Richardson & England (1979), bears only limited relation to the actual P - T path followed by individual samples (Figure 5.5). To determine the actual P - T path followed by a metamorphic rock a method of monitoring the P - T variation over time is required.

Several authors (e.g. Loomis 1975, Kretz 1973) noted the control on zoning in porphyroblastic metamorphic minerals, most commonly garnet, by reactions between the phases of a mineral assemblage during the growth of the porphyroblast phase. Under such conditions any compositional zoning within porphyroblasts is controlled by the composition of the external assemblage and the prevalent P -T conditions. Spear & Selverstone (1983) produced a technique which uses the compositional zoning in garnet to assess any changes in temperature and pressure during the development of this zoning. By taking the compositions of the external equilibrium phases of an assemblage, and then using the compositional changes in the zoned mineral, the variation in pressure and temperature during the development of these minerals can be calculated. Details of the calculation method are given in Spear & Selverstone (1983) and Spear (1986).

The method relies on the relation between the compositional zoning of a mineral and the pressure and temperature conditions during the growth of that mineral, thus:

$T = f(X_1, X_2, X_3 \ldots\ldots X_n)$ --- (5.31)

$P = f(X_1, X_2, X_3 \ldots\ldots X_n)$ --- (5.32)

both T and P are functions of the composition (n represents the number of independent compositional terms).

As this approach looks at the relative changes of P and T with the development of a mineral assemblage it use the differential forms of the thermodynamic equations, rather than the intergral forms used in absolute thermobarometry {5.1}. The differentials of the compositional equations are:

$$dT = \left(\frac{dT}{dX_1}\right)_{X_{j\neq n}} dX_1 + \left(\frac{dT}{dX_2}\right)_{X_{j\neq n}} dX_2 + \ldots\ldots \left(\frac{dT}{dX_n}\right)_{X_{j\neq n}} dX_n \quad \text{--- (5.33)}$$

$$dP = \left(\frac{dP}{dX_1}\right)_{X_{j\neq n}} dX_1 + \left(\frac{dP}{dX_2}\right)_{X_{j\neq n}} dX_2 + \ldots\ldots \left(\frac{dP}{dX_n}\right)_{X_{j\neq n}} dX_n \quad \text{--- (5.34)}$$

The changes in pressure and temperature , $\Delta P$ and $\Delta T$, for a compositional change $\Delta X_i$ are given by:

$$\Delta T = \lesssim \left(\frac{dT}{dX}\right)_{X_{j\neq i}}^{X_i} \quad \text{--- (5.35)}$$

$$\Delta P = \lesssim \left(\frac{dP}{dX}\right)_{X_{j\neq i}}^{X_i} \quad \text{--- (5.36)}$$

The values of $(dT/dX_i)$ and $(dP/dX_i)$ are calculated using

*'the Gibbs method'* (Spear, Ferry & Rumble 1982) which involves the solution of a series of linear differential equations:

a, The Gibb - Duhem equation of each phase:

$$0 = \bar{S}\, dT - \bar{V}\, dP + \lesssim X_i\, d\,u_i \quad \text{--- (5.37)}$$

($u_i$ is the chemical potential of the phase under consideration and i is the number of components in that phase).

b, The sum of chemical potentials at chemical equilibrium:

$$0 = \lesssim v_i u_i \quad \text{---- (5.38)}$$

($v_i$ is the stoichiometric coefficient of the component i).

c, A set of equations which monitors the compositional changes as functions of pressure and temperature.

These equations use a variety of solution models to calculate

the activity of components within the different phases. For example, in a binary solution phase:

$$0 = -(d u_2 - d u_1) - (\bar{S}_2 - \bar{S}_1)dT + (\bar{V}_2 - \bar{V}_1)dP + \left(\frac{d^2 \bar{G}}{dX^2_2}\right)_{P,T} dX_2 \text{ ---- } (5.39)$$

The algebraic solutions of these three sets of equations give the isopleth slopes (dP/dT, dX/dT or dX/dP) used to determine T and P.

The required input set comprises the compositions of the coexisting phases at a reference pressure and temperature, the molar entropies and volumes of the phases at the reference P and T, the partial molar entropies and volumes of the components of any solid solution systems present, and expressions for the curvature of Gibbs free energy surfaces of the solid solution phases. Monitor parameters, such as the variation in $X_{Alm}$ and $X_{Grs}$ in garnet are used to calculate the changes in temperature and pressure during the growth of the garnet.

The resultant P - T path records the changes in pressure and temperature during the growth of a compositionally zoned mineral phase within an equilibrium assemblage. Calculations were performed using the FORTRAN program PTPATH (Spear 1986).

The use of this method of P - T path determination is not without its problems. These fall into two groups: those problems connected with the assumptions made in the model and those problems associated with the analytical assessment of the metamorphic mineral assemblage under study. The assumptions made in the model are:

(i) The compositional zoning in garnet (or the zoned phase being used for the calculation) is due solely to reactions occurring during the growth of that mineral.

(ii) The rim compositions of all the phases within the assemblage remain in equilibrium throughout the development of the assemblage.

(iii) The compositions of minerals produced in the development of the assemblage are not reset by retrograde effects.

(iv) The solid solutions developed within phases follow simple mixing models.

(v) The reaction history of the assemblage is known and can

be constrained relative to zones within the garnet.

Work on garnet compositional zoning by various authors (see Tracy 1982) has shown that not all compositional zoning is produced during the growth of porphyroblasts. Garnets without compositional zoning can be produced above temperatures of 640°C± 30° (Yardley 1977a) as rapid diffusion of cations within the solid garnet leads to homogenization of the garnet and the loss of any pre - existing zoning profile {4.1.3.1}. This diffusional homogenization often leads to the loss of zoning within garnets produced during lower temperature conditions (e.g. Dempster 1985, Anderson & Olimpo 1977). Tracy, Robinson & Thompson (1976) found evidence that initially homogeneous high grade garnets could have zoning imposed on them by retrograde cation exchange reactions after the cessation of garnet growth. It is apparent that zoning in garnets can have several possible causes and in applying the Spear & Selverstone (1983) method it is important to identify the nature of the zoning used to monitor P and T.

The controls on the attainment of equilibrium during a metamorphic reaction are complex (Spear, Ferry & Rumble, 1982) with the magnitude of reaction, diffusion and/or heat transfer rates controlling the degree of equilibrium developed in a reaction system. Whilst the development of disequilibrium textures can provide useful information towards the petrogenetic and P - T history of a system (Lasaga 1983), the use of the Spear & Selverstone method requires that equilibrium is maintained at least between the edges of all phases within a developing mineral assemblage. As the detection of the degree of disequilibrium within a system can be problematical, Selverstone & Spear (1985) suggest that an analysed assemblage can be tested for consistency by using the mineral compositions predicted by their method and comparing them with the actual values derived from inclusions within the garnet porphyroblast, or from zoned matrix grains (provided that these grains can be related to a particular growth phase in the porphyroblast).

The possibility of reactions occurring after porphyroblast growth and either resetting the matrix or the internal zoning of the garnet, or causing resorption of the garnet cause problems in the use of the Spear & Selverstone method. They do, however,

## 2.1 The metasedimentary sequence: lithologies and stratigraphy

2.1.1 Previous work: The Dalradian geology of the Letterfrack area was first investigated by the Irish Geological Survey as part of the mapping for the 1" regional series (sheets 83, 84, 93, 94) and the accompanying memoir (Kinahan *et al.* 1878). This work records no stratigraphy or measured section across the area, although the presence of schists, limestones and quartzites around Letterfrack, south Renvyle and Ballynakill with the NE of the area containing schists and gneisses with igneous bodies. The contact between these two lithological groups is considered to be a fault (the *'Kylemore valley fault'*) which runs E-W, passing in to the sea on the Dawros peninsula. The structure of the area is not considered in detail, with the only large scale structure noted being the synform developed on the Renvyle peninsula. This failure to define the structure led to the survey misinterpreting the lithological succession such that lithologies which are structurally repeated were considered as representing a stratigraphic sequence. A sequence of non - metamorphic Silurian sediments lying to the NE, and forming the ridge of Altnagaighera and Garraun, are noted as being unconformable on the metamorphic lithologies.

Kilroe (1907) studied the area adjacent to, and south of, Kylemore Abbey. He compared the stratigraphy in this area with sequences in South Mayo and Central Connemara, noting several important features:

(i) The metamorphic rocks are Dalradian in age. A conglomeratic horizon, the Cleggan boulder bed, developed in Connemara can be correlated with the Port Askaig Tillite of the Scottish Dalradian.

(ii) The Dalradian metamorphic sequence is unconformably overlain by Silurian sediments.

(iii) The sequence of lithologies in the Kylemore area, with limestones underlying quartzite, is the converse of the sequence in South Connemara. This inversion of the stratigraphy is due, in the opinion of Kilroe, to the effects of large scale overfolding.

(iv) The stratigraphic sequence is complicated by the repetition

indicate the qualitative effects of such reactions on a calculated profile. Where matrix re - equilibration occurs without any effect on the porphyroblast zoning the resetting of the exchange reactions used to estimate pressure and temperature will lead to incorrect starting conditions in the calculation of P and T. As the method does not calculate absolute pressures and temperatures, and merely iterates the change in P and T from known starting values, any errors in the starting data will result in the calculated path being quantitatively wrong, but qualitatively useful. Should reactions lead to the resorption of part of the porphyroblast any P - T path calculated will be incorrect in detail, but again the sense of the starting and finishing points of the path will be qualitatively useful. In such circumstances, where resorption of porphyroblasts is evident (or suspected) Spear & Selverstone (1983) suggest that only the total values of P and T between core and rim of the porphyroblast be calculated.

In order to produce an accurate P - T path for a porphyroblast growing under variable P - T conditions it is required to know what mineral phases are/were present in equilibrium with each growth phase of the porphyroblast and the compositions of these mineral phases. Where porphyroblasts possess a rich inclusion suite it is possible to determine the type and composition of the equilibrium phases at each stage of porphyroblast growth. Such information is, however, often sparse or absent, leading to problems in determining the assemblages present during porphyroblast growth. It is important that external assemblages be related to specific phases of porphyroblast zoning, as failure to accurately constrain the relative timings of zoning and assemblage growth will lead to errors.

Other errors are introduced into the method through uncertainties in the input parameters (the importance of the assemblage has already been stressed). Simple sources of error such as the use of porphyroblasts which are sectioned so that they do not display full zoning profiles, or asymmetric profiles are obtained can be relatively easily avoided. The nature of the solid solutions present in certain phases can also be assessed and suitable formulations be used in the calculation of path information. Work by Spear & Selverstone (1983) has shown that if the simple solution models used in the PTPATH program are

| | Biotite | | | Plagioclase | | Staurolite | | | Chlorite | | | | | | | | |
|---|---|---|---|---|---|---|---|---|---|---|---|---|---|---|---|---|---|
| Sample | $X_{Ann}$ | $X_{Phl}$ | $X_{MnBt}$ | $X_{An}$ | $X_{Ab}$ | $X_{Fe}$ | $X_{Mg}$ | $X_{Mn}$ | $X_{Fe}$ | $X_{Mg}$ | $X_{Mn}$ | Ms | Kfs | Qtz | $Al_2SiO_5$ | Tstart | Pstart |
| 69229 | 0.558 | 0.448 | = = | 0.263 | 0.713 | 0.843 | 0.166 | = = | * | * | * | + | * | + | * | 462 | 5869 |
| 69230 | 0.594 | 0.406 | = = | 0.096 | 0.904 | 0.797 | 0.199 | 0.003 | * | * | * | + | * | + | * | 545 | 7834 |
| 69238 | 0.581 | 0.535 | 0.065 | 0.297 | 0.649 | 0.867 | 0.133 | = = | 0.745 | 0.245 | 0.010 | + | + | + | * | 600 | 6050 |
| 69623 | 0.583 | 0.413 | 0.004 | 0.153 | 0.843 | 0.834 | 0.149 | 0.016 | * | * | * | + | * | + | * | 492 | 6965 |
| 69625 | 0.608 | 0.390 | 0.002 | 0.277 | 0.716 | 0.843 | 0.142 | 0.014 | * | * | * | + | * | + | * | 444 | 5370 |
| 69627 | 0.609 | 0.388 | 0.003 | 0.181 | 0.807 | 0.921 | 0.065 | 0.013 | * | * | * | + | * | + | * | 586 | 7511 |

**Table 5.12: PTPATH input data. (* indicates phase not present in assemblage, + indicates phase present in assemblage, = = indicates element below detection limit). T in °C, P in bars.**

replaced by more realistic models the resultant paths are largely unaffected. The effect of errors inherent in probe data has been assessed by Spear & Rumble (1986) in a study where errors of ±0.005 mole fraction for major elements and ±0.001 mole fraction for minor elements were propagated through the calculation of a series of paths for a single zoning profile. The resultant paths show considerable variation in absolute values but are qualitatively the same. Spear & Rumble's work indicates the qualitative nature of the method, and as such the resultant paths should not be interpreted as absolutes, but as qualitative indicators of the pressure and temperature variation during the zoned porphyroblast development. Where rich inclusion suites provide suitable assemblages it is possible to more accurately constrain the path calculated from zoning information with data from appropriate geothermobarometric systems.

## 5.6 P - T path results and interpretation

Six garnets from regional metamorphic rocks were modelled by the Spear & Selverstone method, and were selected on the nature of their compositional zoning profiles {4.1.3.1}. All the garnets show smooth continuous zoning, suggesting that their growth has not involved any discontinuous reactions, and that exchange reactions dominated the system. Of the six garnets modelled, one possesses an assemblage which is bivariant in the model system KNCFMnMASH: Sample 69627 (Roeillaun schist Member of the Streamstown Formation) which has the assemblage Grt - Bt - Pl - Ms - Chl - St - Qtz. Of the other assemblages modeled, four (69229, 69230, 69623, 69625) are from the Roeillaun Schist, and the remaining sample (69238) comes from the Kylemore Fm. Both samples from the Kylemore Fm are taken from the Renvyle Peninsula, and are typical of the regionally metamorphosed Kylemore Fm, containing garnets with well developed zoning profiles, unlike garnets in the aureole assemblages which typically show diffusionally perturbed zoning {4.1.3.1}.

The assemblages in samples 69229, 69230, 69238, 69623 and 69625 are trivariant in the model system KNCFMnMASH and they cannot be modelled simply from the variation in $X_{Alm}$,

$X_{Grs}$ and $X_{Sps}$, requiring a further variable to constrain the modelling. As no suitable included minerals such as plagioclase are present the compositional variation between these grains and the external plagioclase cannot be used to constrain the modelling. However, an assumption that the chemical potential of $H_2O$ remains constant is made, thus enabling the monitor parameter $duH_2O$ to be held at 0 and providing a fourth monitor on the assemblage. The validity of this assumption and the possible nature of the fluids involved in the metamorphism are discussed subsequently.

An AFM plot of the coexisting Grt + St + Bt assemblages (Figure 5.6) shows crossing tie - lines. Several possible mechanisms may have produced these crossing tie relations (after Burton 1986).

(i) A retrograde phase, chlorite is present in all of the samples. The development of this phase {4.1.4} may have led to compositional change in the peak phases.

(ii) The composition of muscovite within the assemblages is not pure, with both paragonitic and phengitic components being present {4.1.3.3}. The presence of such compositional variations make the projection for pure muscovite on to the AFM plane invalid.

(iii) The presence of additional components (Ca, Mn) may be stabilising the assemblage. A projection from Qtz - Ms - $H_2O$ into the $Al_2O_3$ - FeO - MgO - (MnO + CaO) tetrahedra (Figure 5.7) leads to the loss of all of the crossing tie - line relationships. This projection also shows that the variation in the three phase planes is due largely to MnO + CaO contents.

(iv) The value of $uH_2O$ is variable within and between samples. As the tetrahedral plot (Figure 5.7) shows, the

Figure 5.6: AFM plot (from muscovite) showing the mineral compositions in the coexisting Grt + Bt + St assemblages modelled. Note the crossing tie - line relations.

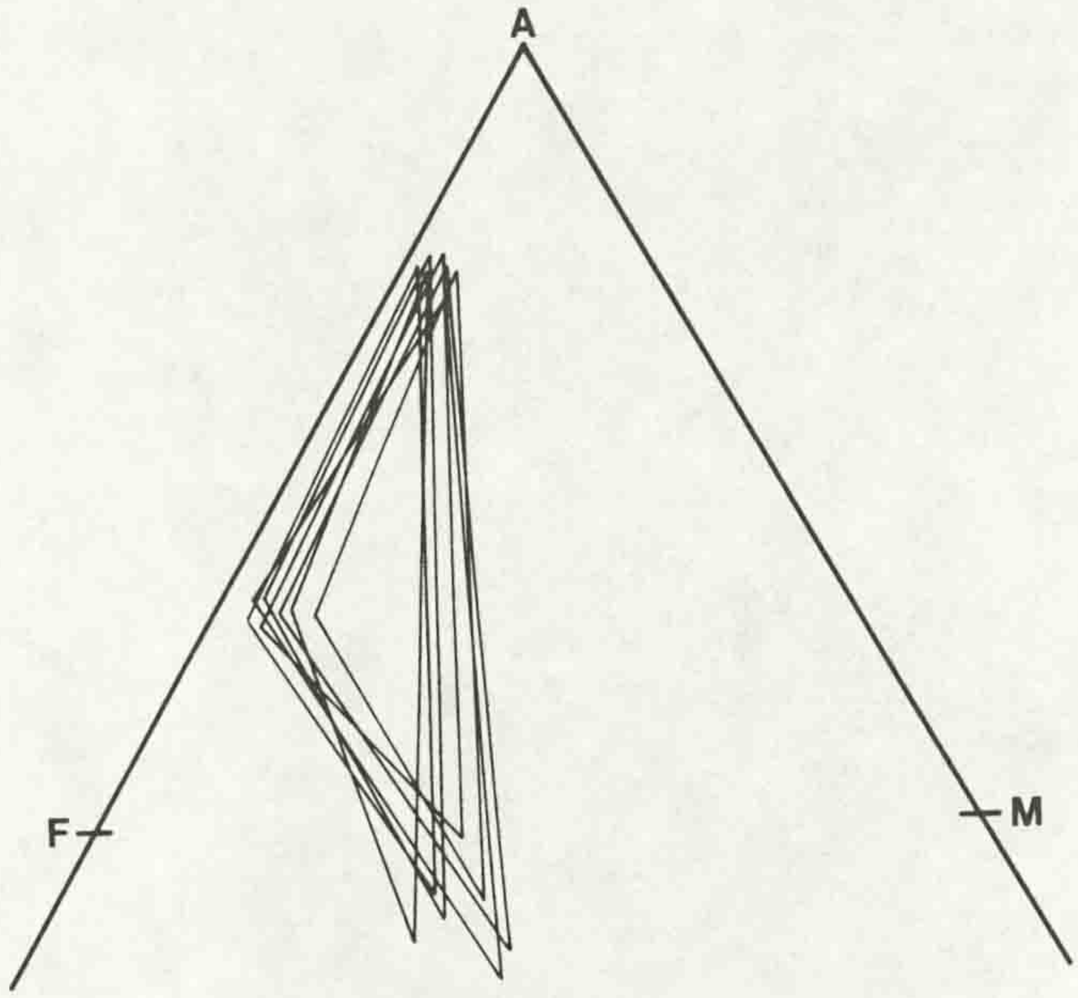


Figure 5.7: Projection from Ms, Qtz and $H_2O$ into the Al' - Fe' - Mg' - (Mn' + Ca') tetrahedron. The consideration of Mn and Ca in this system removes the crossing tie - line relations.

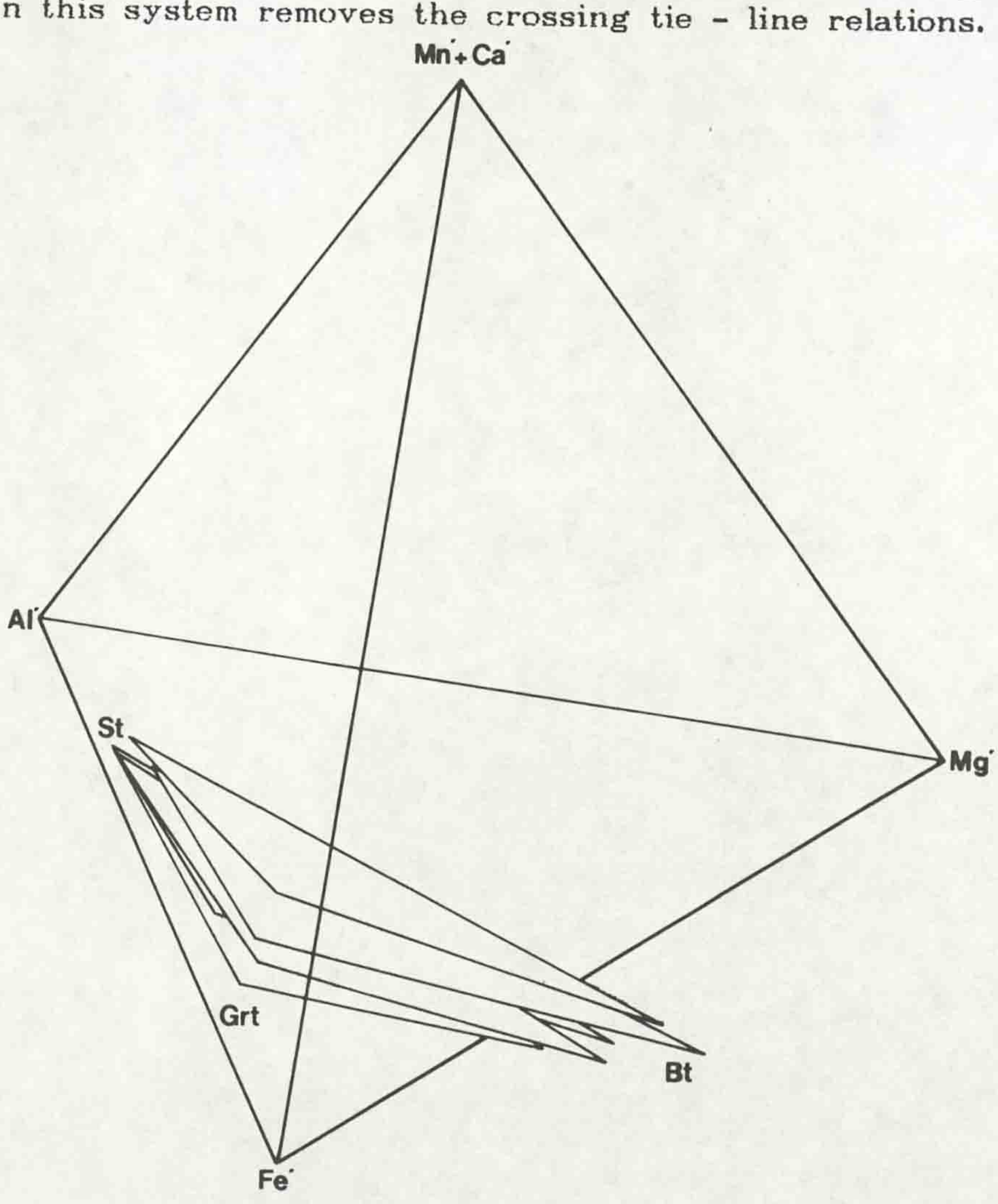

majority of crossing tie - line relations can be resolved by allowing for the MnO and CaO components in the system, suggesting the value of $uH_2O$ has relatively little influence on the equilibrium relations in these samples. The investigation of fluid movement within metamorphic systems has been an important field of study in recent years (e.g. Norris & Henley 1976, A.B. Thompson 1987), and a significant body of work has shown evidence for variation in $H_2O$ on outcrop scales (e.g. Ferry 1979, Rumble, Ferry, Hoering & Boucot 1982). However, evidence for considerable fluid release associated with prograde dehydration reactions has been cited (e.g. Walther & Orville, 1982), and the role of lithological units as zones of pervasive fluid flow (*metamorphic aquifers*), have become increasingly apparent in recent research (e.g. Ferry 1988, Rye, Schuiling, Rye & Jansen 1976).

The development of a chacteristically colour zoned tourmaline phase, probably having a syn - $D_2$ metasomatic origin {4.1.3.12}, within the schistose pelites, suggests that a pervasive, mobile fluid phase was present during the development of the peak mineral assemblage. The absence of phases such as graphite and (primary) carbonate within the mineral assemblages suggests that the fluid phase was $H_2O$ rich. Yardley, Shepherd & Barber (1983) conclude that the composition of the fluid phase in similar, although higher grade, graphite - free pelites was close to pure $H_2O$. A mobile fluid phase is unlikely to be buffered by any coexisting mineral assemblage as the fluid residence time within any particular volume of rock will be too short (Walther & Orville, 1982). In such circumstances, the fluid composition will be externally buffered and the value of $uH_2O$ shows no variation (i.e. $duH_2O = 0$, Spear, Ferry & Rumble 1982).

The assumption that $duH_2O = 0$ is made in modelling Grt - Bt - Pl - Ms - St - Qtz assemblages where suitable mineral (plagioclase) inclusion data is unavailable in this work, as such assemblages are quadravariant. Unpublished work by R.K. Westhead (*pers. comm.*) has shown that the modelling of assemblages using $duH_2O = 0$ as a monitor parameter produces P - T paths which are not significantly different from those derived by standard modelling methods. In such circumstances the sense of

the P - T path is maintained, although its absolute value is altered. As the P - T path technique is only qualitative in nature {5.5}, the effects of holding $uH_2O$ constant have limited influence on the interpretation of the resultant paths.

(v) The final equilibration of the assemblage do not occur at the same P -T conditions for all the samples, or for the individual minerals within samples. The samples plotted on Figure 5.7 were collected from lithologies (largely from the Roeillaun schist member of the Streamstown Fm) which are separated by 4 - 5km laterally and as such it is possible that the peak metamorphic conditions showed a degree of variation over such a distance. P - T results from the samples show ranges of:

444 - 600°C (mean of 536°C),

5.37 - 10.59kb (mean of 7.10kb),

suggesting that the assemblages equilibrated under different conditions. As such the assemblages modelled show internal equilibrium, but have equilibrated under conditions different from one another.

The results of the P - T path modelling are shown in Tables 5.13 and 5.14 and Figures 5.8 and 5.10. As noted earlier the magnitudes of the calculated P - T paths should not be viewed as the true magnitude of P - T variation during garnet growth, but rather as a qualitative measure of that variation.

The paths calculated for samples 69229, 69230, 69623, 69625 and 69627, from the Streamstown Fm, are shown in Figure 5.8 and schematically in Figure 5.9. The typical form of these paths is of a progressive increase in pressure, accompanied with slight temperature increase, from the garnet core to rim, suggesting garnet growth during burial. The actual form of some of the paths is rather more complex, with the paths from garnet 69229 and 69230 showing an initial pressure decrease (of up to 3kb) followed by an increase in pressure (of up to 5kb). A similar change in the polarity of the path is seen in garnet 60625 albeit to a much more restricted degree (a decrease of <100bars followed by an increase of nearly 3 kb). Garnets 69623 and 69627 produce paths which show consistent pressure increases from core to rim (69623: 2.7kb increase, 69627: 3.5kb increase). It may be significant that the garnets which show reversals of polarity in P - T paths contain

Table 5.13: Streamstown formation, garnet composition data used in P - T path modelling and the calculated P -T results.
* indicates starting presures and temperatures calculated using Grt - Bt thermometry and Grt - Bt - Pl - Ms barometry.
T in °C, P in bars

| Sample | $X_{Alm}$ | $X_{Sps}$ | $X_{Prp}$ | $X_{Grs}$ | T | P |
|---|---|---|---|---|---|---|
| 69229 | | | | | | |
| | 0.738 | 0.033 | 0.051 | 0.171 | 462* | 5869* |
| | 0.671 | 0.057 | 0.046 | 0.224 | 447 | 4448 |
| | 0.690 | 0.076 | 0.039 | 0.193 | 443 | 4099 |
| | 0.693 | 0.075 | 0.039 | 0.191 | 443 | 4129 |
| | 0.700 | 0.066 | 0.041 | 0.191 | 446 | 4357 |
| 69230 | | | | | | |
| | 0.760 | 0.078 | 0.090 | 0.071 | 545* | 7834* |
| | 0.721 | 0.146 | 0.075 | 0.056 | 534 | 6787 |
| | 0.659 | 0.175 | 0.034 | 0.130 | 552 | 8556 |
| | 0.684 | 0.172 | 0.050 | 0.092 | 562 | 9518 |
| 69623 | | | | | | |
| | 0.776 | 0.030 | 0.090 | 0.101 | 492* | 6962* |
| | 0.731 | 0.048 | 0.052 | 0.167 | 475 | 5339 |
| | 0.710 | 0.067 | 0.049 | 0.171 | 472 | 5074 |
| | 0.685 | 0.122 | 0.037 | 0.155 | 463 | 4245 |
| 69625 | | | | | | |
| | 0.770 | 0.012 | 0.073 | 0.142 | 444* | 5370* |
| | 0.682 | 0.081 | 0.040 | 0.194 | 423 | 3390 |
| | 0.660 | 0.092 | 0.044 | 0.202 | 424 | 3480 |
| 69627 | | | | | | |
| | 0.810 | 0.009 | 0.066 | 0.113 | 586* | 7511* |
| | 0.759 | 0.037 | 0.064 | 0.138 | 583 | 6692 |
| | 0.733 | 0.073 | 0.057 | 0.136 | 578 | 5874 |
| | 0.704 | 0.101 | 0.040 | 0.154 | 569 | 4090 |

Table 5.14: Kylemore Formation, garnet composition data used in P - T path modelling and the calculated P -T results.
* indicates starting pressure and temperature calculated using Grt - Bt thermometry and Grt - Bt - Pl - Ms barometry.
T in °C, P in bars

| Sample | $X_{Alm}$ | $X_{Sps}$ | $X_{Prp}$ | $X_{Grs}$ | T | P |
|---|---|---|---|---|---|---|
| 69238 | | | | | | |
| | 0.748 | 0.079 | 0.096 | 0.077 | 600* | 7834* |
| | 0.731 | 0.048 | 0.153 | 0.067 | 624 | 8211 |
| | 0.698 | 0.064 | 0.197 | 0.040 | 610 | 6820 |
| | 0.712 | 0.066 | 0.174 | 0.047 | 615 | 7318 |

Figure 5.8: Modelled P - T paths for the Streamstown Fm (Roeillaun schist Mb) samples. Filled diamonds indicate calculated rim P - T, open diamonds modelled core P - T.
1: 69229, 2: 69230, 3: 69623, 4: 69625, 5: 69627.

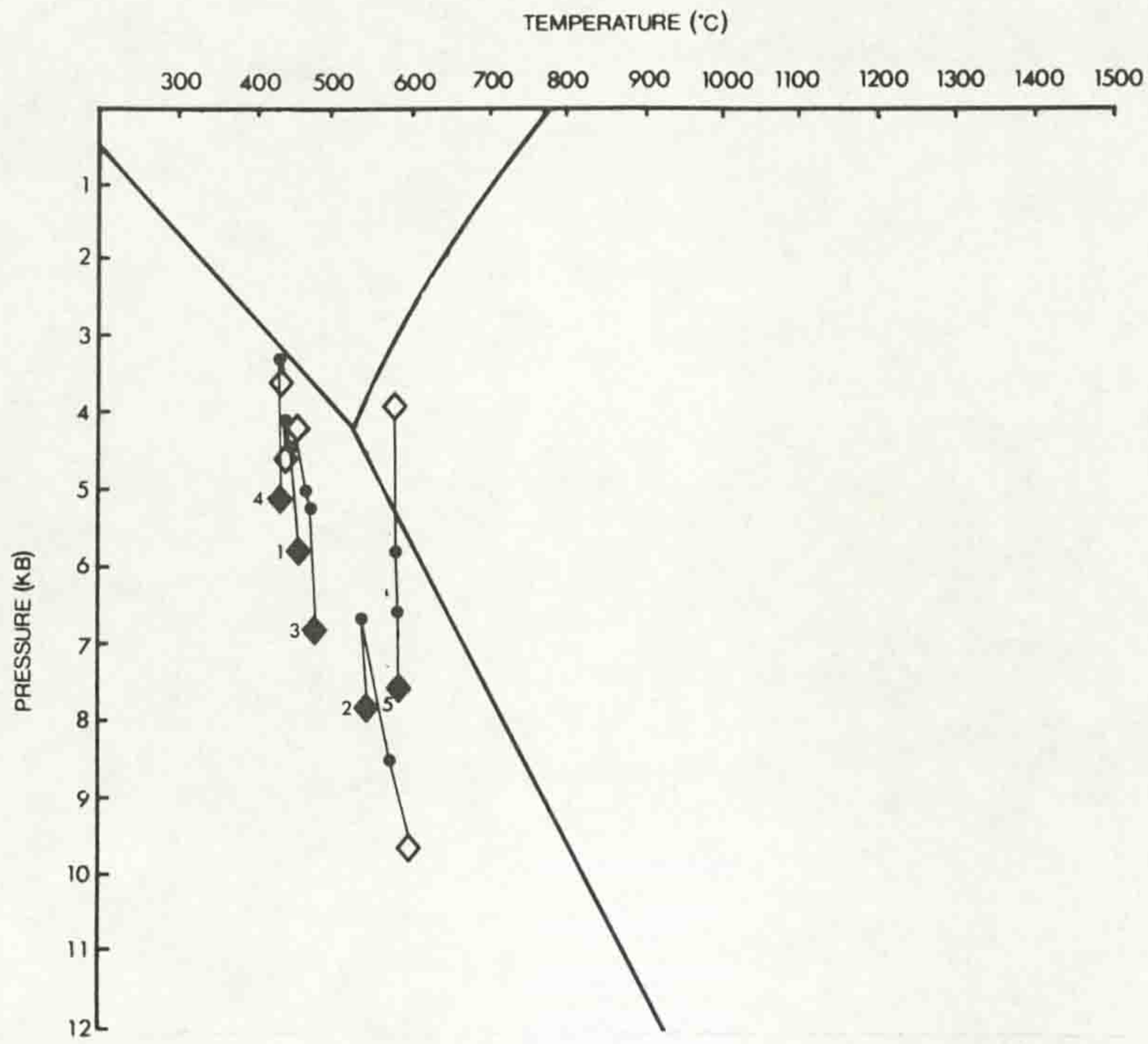


Figure 5.9: Schematic diagram of particle paths (after Jamieson & Beaumont *in press*) from the Streamstown Fm lithologies. Arrows indicate the direction of movement.

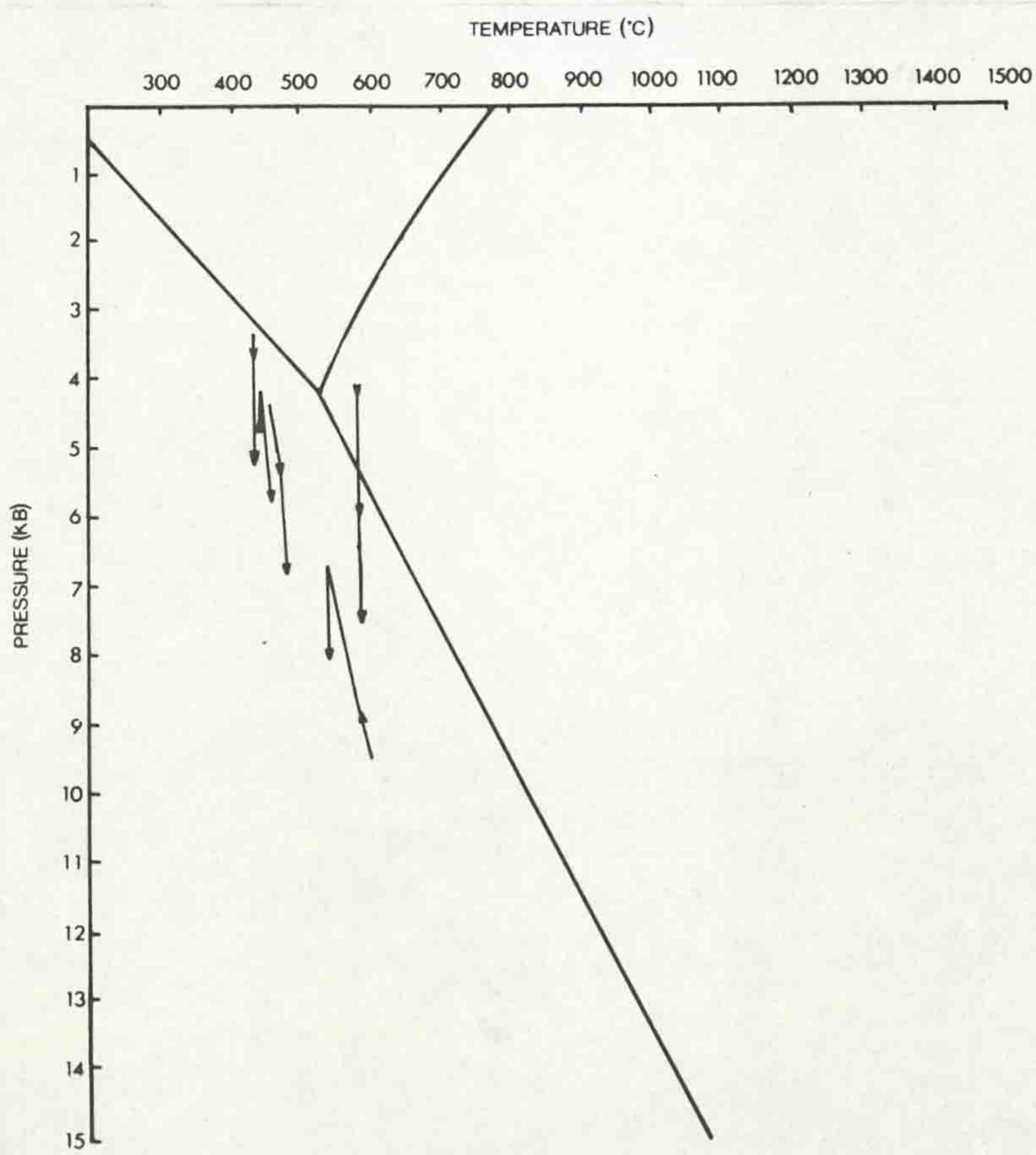

inclusion trails which suggest the garnet growth was relatively early in the $D_2$ deformation {3.2.3}, before the initiation of staurolite growth {4.1.4}. The timing of mineral growth seen in samples 69229 and 69230 suggests that the early phases of garnet development were in an assemblage lacking staurolite {4.1.4} but with chlorite present, and as such the modelling of the rim assemblage (including staurolite) through to the core is incorrect. It is possible that those parts of the P - T paths modelled from garnet compositions close to the garnet core (i.e. early in the garnet development, the external assemblage containing chlorite) are an artifact of modelling through an assemblage change and do not represent 'real' P - T paths. However, within the rims of such garnets (where the coexisting assemblage contained staurolite) modelling conditions will be consistent with the external assemblage.

In 69623, the growth of garnet and staurolite was synchronous, as determined from inclusion textures {3.2.3 and 4.1.3.7}. The modelling of the P - T paths using the same external assemblage from core to rim is valid in this case and the resulting paths represent the 'real' P - T variation during the development of the garnet. The assemblage in 69627 which contains primary chlorite and produces a P -T path showing the same polarity of movement as the paths for 69623, 69625 and the later growth stages of garnets 69229 and 69230.

The results of P - T path modelling on the garnets from the Streamstown Formation (which lies to the south of the RBS) show the syn - $D_2$ garnet growth to be accompanied with a pressure increase (and a possible early pressure decrease).

The garnet modelled from the Kylemore Formation (north of the RBS), 69238, produces the results in Table 5.24 and the path shown in Figures 5.10 and 5.11. This path has a complex form, with an initial pressure decrease (of 500bars) followed by an increase (of 1.4kb) and a final decrease (of 2kb). The overall effect is of a net decrease in pressure during the, syn - $D_2$, garnet growth.

The two sets of P - T path data indicate that the two 'units'

**Figure 2.1: Comparison of the stratigraphy erected in this work with that of Cruse (1963) and the regional stratigraphical correlation (after Tanner & Shackleton 1979).**

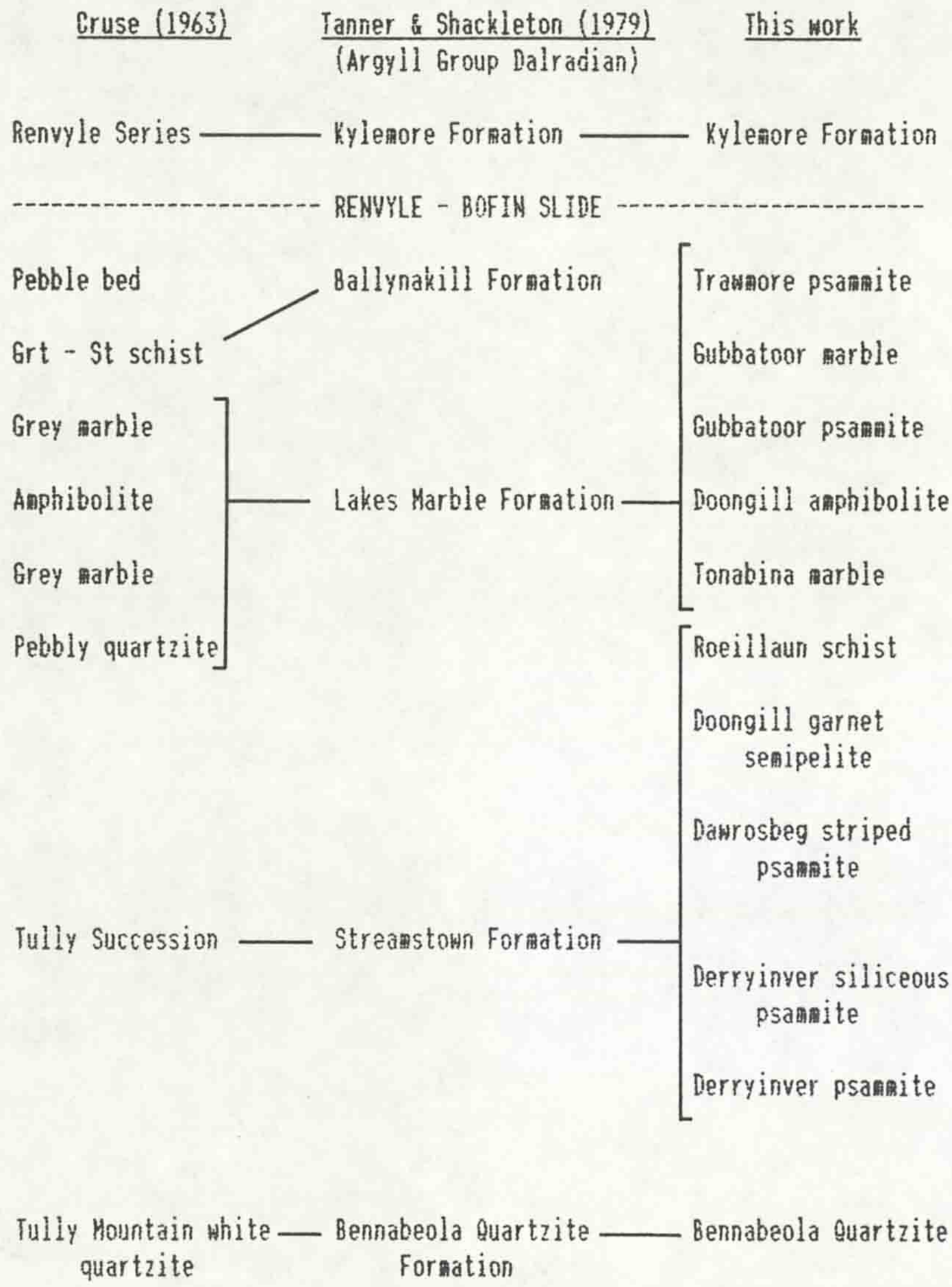


**Nb, The Renvyle - Bofin slide, although separating the Kylemore and Bennabeola Quartzite Formations for much of its length, cuts up through the stratigraphy to locally juxtapose the Kylemore Fm with parts of the Streamstown (Dawrosbeg striped psammite) and Lakes Marble (Doongill amphibolite) Formations.**

Figure 5.10: Modelled P - T path for sample 69238 from the Kylemore Fm. Dot indicates calculated rim P - T, open circle modelled core P - T.

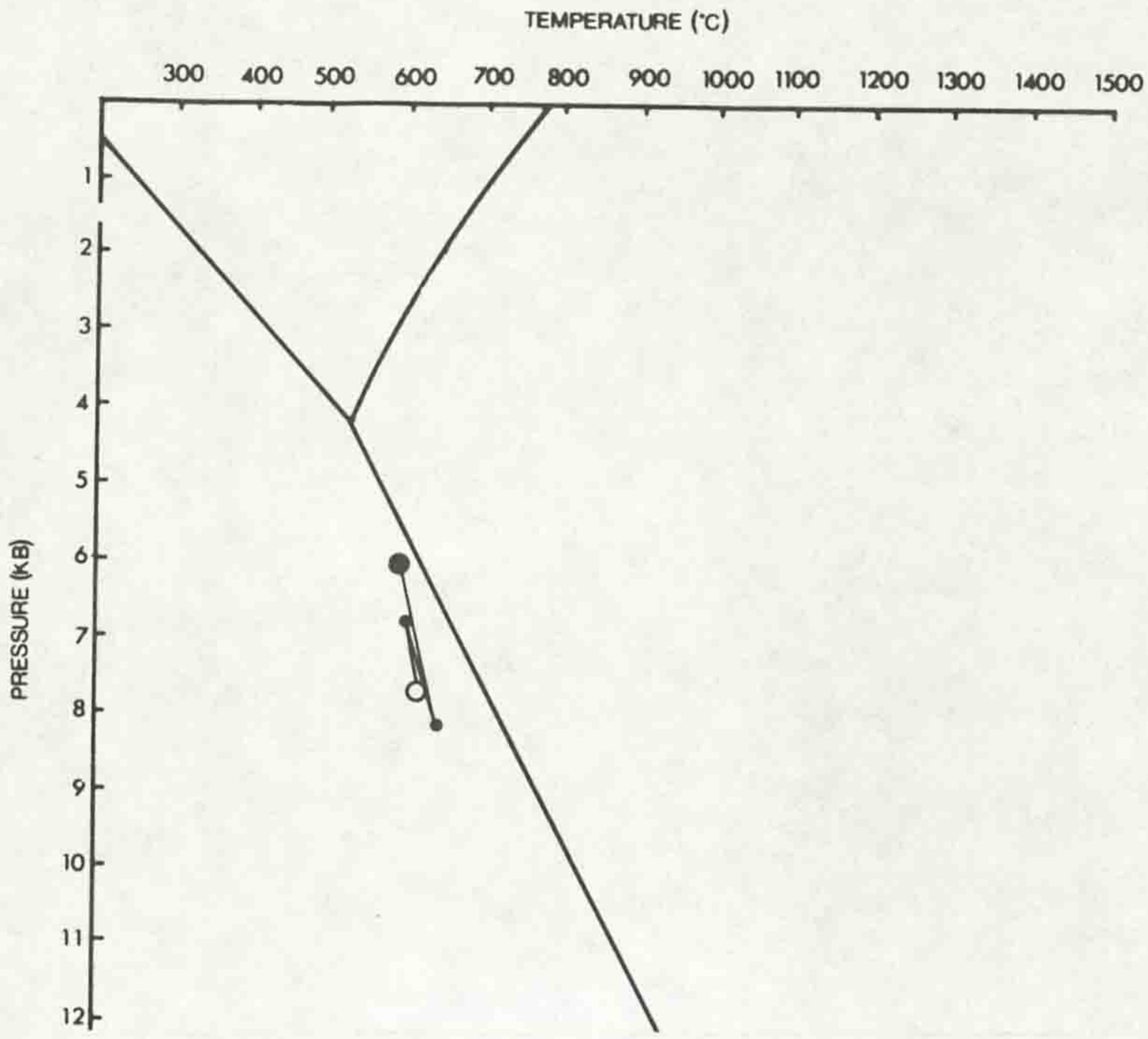


Figure 5.11: Schematic diagram of particle paths (after Jamieson & Beaumont *in press*) from the Kylemore Fm lithology. Arrow indicates the direction of movement.

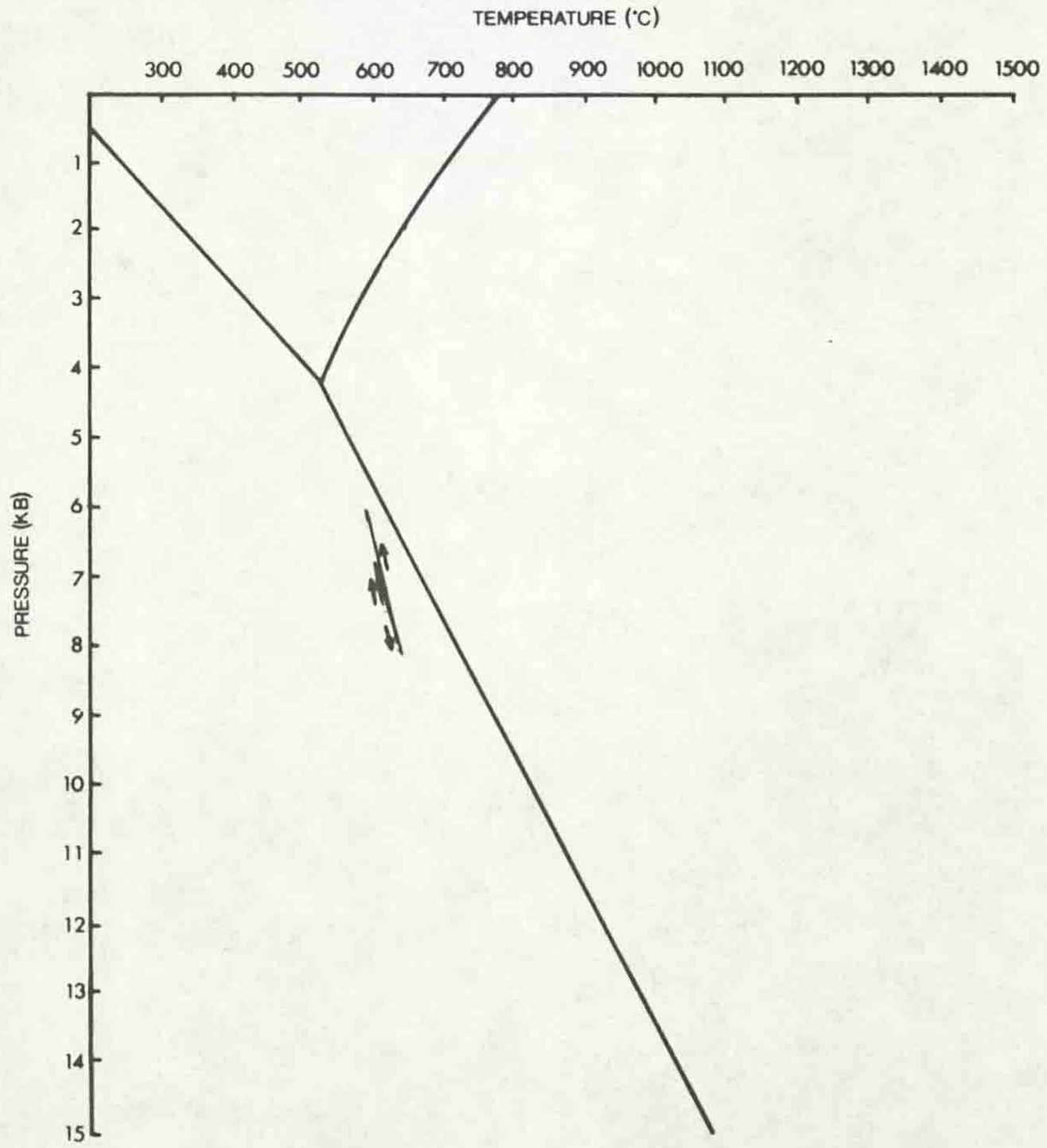

separated by the RBS show different polarities of movement during the syn - $D_2$ growth of garnets. The Kylemore Formation, to the north of the RBS, shows evidence of syn - deformational pressure decrease (uplift associated with exhumation as described by Jamieson & Beaumont, *in press*), whereas the lithologies to the south of the RBS record syn - deformational pressure increase (burial). This suggests that the $D_2$ deformation involved movement on the RBS such that the Kylemore Fm was uplifted and the lithologies to the south of the RBS were buried.

# Chapter 6: The modelling of thermal systems in the crust

## 6.1 Introduction

The application of techniques such as P - T path modelling {5.5} and absolute thermobarometry, has enabled the qualitative and quantitative determination of thermobarometric histories within orogenic systems. P - T paths derived from mineral assemblages can be compared with those produced by modelling the evolution of idealised crustal scale thermal systems. This chapter considers the application of simple one - dimensional thermal modelling (after England & Richardson 1977) to the study area, and compares the results of this approach with the P - T paths calculated using the method of Spear & Selverstone (1983).

## 6.2 The basic terminology used in describing crustal thermal systems

6.2.1 Geothermal gradient: The relation between temperature (T) and vertical depth (x) within the Earth's crust at any one time. The resultant thermal gradient may represent a steady state, equilibrium geothermal gradient, or a transient geothermal gradient which will change with time (Thompson & England 1984). The geothermal gradient may be either linear or non - linear.

6.2.2 Isobar: Surfaces of equal pressure. Because such surfaces are largely dependent on the load of overlying rocks the pressure gradient is generally considered to have its maximum development in the vertical direction.

6.2.3 Isotherm: Surfaces of equal temperature. The spacing of these surfaces is controlled by the geothermal gradient, which is in turn controlled by factors such as the heat flux and thermal properties of the rock pile. Where the geothermal gradient is linear the spacing of the isotherms is constant. However, where non - linear geothermal gradients are developed, the spacing of the isotherms varies and is dependent on the nature of the geothermal gradient.

P.H. Thompson (1976) suggests that the orientation of the maximum thermal gradient is not always that of the vertical geothermal gradient, with the result that isothermal surfaces are

Figure 6.1: Schematic diagram showing the relations of isotherms (bold lines) to isobars (faint lines), within a 'thermal dome' after P.H. Thompson 1976.

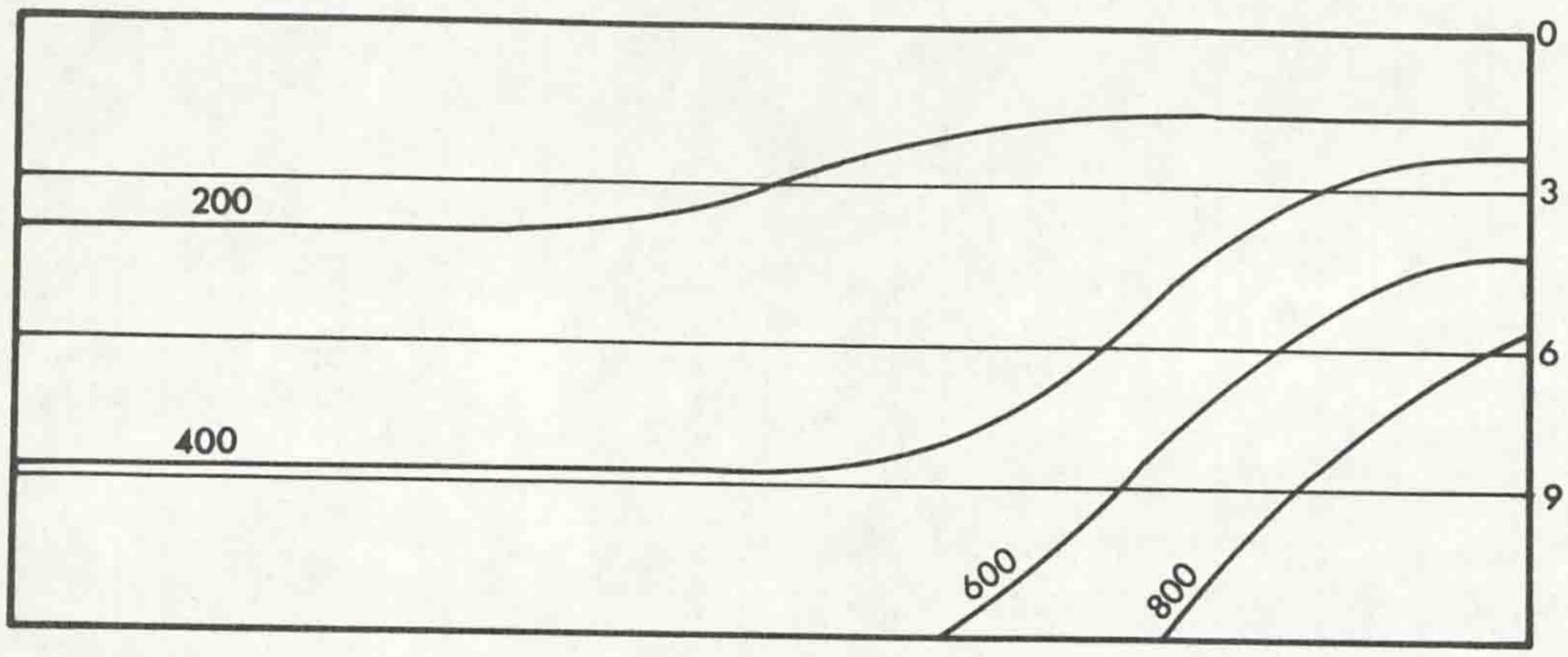

not parallel to isobaric surfaces (Figure 6.1). Such non - parallel geometries of isothermal and isobaric surfaces are rare within equilibrated crustal thermal systems, although common within crustal systems which have been disturbed (A.B. Thompson 1981, Fowler & Nisbet 1982).

6.2.4 Heat flux: The heat flux through a system is the flow of heat per unit area per unit time. Fourier's law defines the heat flux in one dimension as being directly proportional to the temperature gradient:

$q = -k \, dT/dx$

In equilibrated crustal thermal systems, the surface heat flux is controlled by subsurface heat addition to the crustal pile, such that:

$q = q_m + bA$

where $q_m$ is the fraction of heat flow derived from the lower crust and mantle, b is the fraction of heat added to the system by crustal heat generation (A). The heat flux (q, $q_m$) is measured in $uW/m^2$.

The heat flux through a sequence of lithologies is also controlled by the thermal conductivity of the lithologies involved (Oxburgh & Turcotte 1974).

## 6.3 Controls on the development of equilibrium geothermal gradients

### 6.3.1 Heat addition

6.3.1.1 Internal radiogenic heat production (A): The decay of radioactive elements such as U, Th and K within the crustal material provides a significant source of heat to crustal thermal systems. The concentration of the radioactive elements and their spatial distribution are major controls in the form of equilibrium geothermal gradients (England & Thompson 1984).

Heat production is measured in $uW/m^3$.

6.3.1.2 External heat sources ($q_m$): The heat flux from the lower crust and mantle contributes towards the surface heat flux {6.2.4} and variations in this heat flux affect the

shape of equilibrium geotherms (Roy, Blackwell & Birch 1968). However, the production of models which allow for $q_m$ variation show that the effects of varying $q_m$ take a considerable amount of time ( >100 Ma) to be transmitted through the entire system (Nisbet & Fowler 1982).

The value of $q_m$ does, however, appear to vary laterally (Roy *et al.*, 1968) and this variation is related to the tectonic setting of the equilibrated system.

6.3.2 Heat loss

6.3.2.1 Conductive heat transfer: The rate of heat transfer through a rock is controlled by its heat capacity (Cp) and conductivity ($k$) (Oxburgh & Turcotte 1974).

6.3.2.2 Convective heat transfer: The transport of heat away from a crustal system by either hydrothermal or magmatic fluids would have a considerable influence of the nature of the geothermal gradient. Such effects are more likely to be developed in crustal systems where the thermal gradient of perturbed by some mechanism, rather than in equilibrated crustal conditions.

6.3.2.3 The geometry of the crustal system: The internal geometry of the crust, such as layers of different heat producing values, $k$ and Cp, show considerable control on the form of the equilibrium geotherm.

## 6.4 The perturbation of equilibrium geothermal gradients

By modelling metamorphic facies seen at the surface using petrogenetic grids, Richardson (1970) showed that the 'normal' equilibrium geothermal gradients would not be able to produce many of the facies observed. Indeed, the normal equilibrium geotherm *'passes through a singularly uninteresting area of the petrogenetic grid'* (Richardson 1970), many metamorphic facies being the products of anomalous geothermal gradients. Such anomalous geotherms are typically transitory in nature (Thompson

& England 1984), being produced by the perturbation of a pre - existing thermal system. Non - equilibrium perturbed geotherms are, by their very nature, unstable. Thermal relaxation will occur over a period of time until an equilibrium geotherm is obtained. The mechanisms which can lead to the perturbation of a thermal system are discussed below.

6.4.1 Variation of $q_m$ and its consequences: As previously discussed {6.3.1.2}, variation in the values of $q_m$ will produce changes in the equilibrium conditions for a particular section of crust. These changes in thermal conditions will be transmitted at a relatively slow rate through the system. If the value of $q_m$ is increased significantly, large amounts of partial melting may occur at depth long before the near surface geothermal gradient is affected (Nisbet & Fowler 1982). The upward buoyant rise of the resultant magma would transfer heat upwards into higher crustal levels perturbing the geotherm. The volume of rock affected by the thermal effects of intrusions is controlled by several factors such as the volume of the intrusion, the magma temperature and $k$, the country rock temperature and $k$ and the presence or absence of fluids (e.g. Jaeger 1961).

As the intrusion of new material is adding to the crust, the thermal properties of the intrusive rock will determine how closely the post - intrusive thermal system will resemble the pre - intrusive one. Intrusions which are relatively enriched in heat producing elements will have a significant heating effect due to their radiogenic heat production. Where the heat production within the intrusion is significantly higher than that in the surrounding rocks the intrusion will act as a heat source, locally increasing the crustal temperature and raising the geothermal gradient. Intrusive bodies which are poor in heat producing elements tend to act as heat sinks, locally depressing the thermal gradient around themselves (Nisbet & Fowler 1982).

6.4.2 Heat transfer through the convection of a fluid phase: The effects of heat transfer by fluids has been largely neglected in the modelling of regional thermal systems, the majority of quantitative studies of this process having

considered the effects contact metamorphic systems. Studies which consider the effects of fluid movement within regionally metamorphosed areas (eg, Ferry 1976, 1980, Wickham & Taylor 1987) are relatively rare. Whilst it is evident that fluids play a major role in the evolution of such terrains the actual effects of fluid movement are not yet sufficiently well understood to allow anything other than qualitative assessments.
England & Thompson (1984) consider the transfer of heat by magmatic fluids to be unimportant in the overall thermal budget, the magmatic fluids just redistributing the heat within a regional thermal system. However, it is evident (e.g. Richardson 1970, England & Richardson 1977) that the upward transport of heat by the movement of fluids is of considerable importance.

6.4.3 Endothermic Reactions: The role played by heat consuming chemical reactions, such as dehydration reactions at high amphibolite facies, has been considered by England & Thompson (1984). Their calculations show that the heat required to produce a 5% (by volume) dehydration of the continental crust over a 30 Ma period is approximately 0.6 uW / $m^3$. This figure is considerably less than the internal heat production over a similar time period. If a large volume of rock were to be dehydrated in a very short time period the resultant heat loss would be on a suitable scale to produce a change in the regional heat budget. The rates of dehydration and the volume of rock needed to undergo such a reaction are such that heat loss on a large scale is unlikely to be significant in the thermal evolution of a system (England & Thompson 1984).

6.4.4 Tectonic processes: Sleep (1979) showed that if crustal deformation occurs at a rate which is greater than the rate at which isothermal surfaces are able to re - equilibrate then the isothermal surfaces will be deformed. The effects of such deformation of isothermal surfaces have been considered in both compressional and extensional tectonic regimes.

6.4.4.1 Compressional tectonic regimes: Compressional tectonic systems can achieve crustal thickening by two main processes, overthrusting or folding. Systems in which the

crustal thickening is achieved by overthrusting form the bulk of models of crustal thermal evolution (e.g. Oxburgh & Turcotte 1974, England & Richardson 1977). Limited studies have been undertaken in modeling the thermal effects of crustal thickening due to folding (e.g. Sleep 1979, Chamberlain & Karabinos 1987).

The modelling of the thermal evolution of the study area carried out in this work {6.5} considers a thermal system which is perturbed by the emplacement of an overthrust. The methods of calculation of overthrust models and their results are discussed later {6.5, 6.6}.

6.4.4.2 Extensional tectonic regimes: The evolution of extensional tectonic systems and their effects on the thermal structure is becoming an important field of investigation in relation to hydrocarbon development and maturation (e.g. McKenzie 1978). The modelling of extensional thermal systems is not considered in this work.

## 6.5 Modelling of tectonically perturbed crustal thermal systems

### 6.5.1 Introduction

The modelling technique discussed below is based on the time dependent solution of a one - dimensional conductivity equation given by Carslaw and Jaeger (1959). The thermal models were calculated using a FORTRAN computer program, REGIONAL, which was kindly supplied by Dr A.C. Barnicoat.

It is noteworthy that the model does not consider convective fluid movement as a mechanism of heat transfer, conduction (in a vertical direction) being the only heat transfer process occurring. The model also does not account for the thermal effects of dehydration reactions or the effects of melting within the crustal system and the subsequent heat transfer.

The model used in this work follows the system of England & Richardson (1977) in considering the effect of erosion on the thermal evolution of an overthrust system. The model uses fixed erosion rates to control the uplift of the crustal section. The resultant model is of a system in which ' *temperature increases*

of beds by folding. This effect is evident in the area to the east of Kylemore where the '*numerous limestones*' noted by the survey are due to the repetition of '*one or two beds*' by folding.

(v) The igneous rocks forming the Currywongaun - Doughruagh upland area are intrusive into the sedimentary rocks and are not the result of metamorphism and melting of these sediments.

After the work of Kilroe no specific stratigraphic study was undertaken, although Wager & Andrew (1930) agreed with Kilroe as to the age of the lithologies, noting that the unconformable boundary with the Silurian marks a considerable metamorphic break. Studies of the igneous rocks of the Letterfrack area by Ingold (1937) and Rothstein (1954, 1956) provide descriptions of the contact and adjacent lithologies.

The most detailed previous study of the area is that of Cruse (1963) as part of a Ph.D study which covers the islands of Inishshark and Inishbofin to the west of Renvyle Point, and the Renvyle peninsula, stopping at a N-S line which cuts through Tully Lough and Derryinver. The stratigraphy erected by Cruse (Figure 2.1) was determined taking account of the structure of the area, an important advance. Evidence from graded and cross bedding preserved within the metasediments show that the bulk of the stratigraphy is inverted, with the major structures ($F_3$) being downward and North facing. The stratigraphy is interrupted by a tectonic break (the westward extension of the Kylemore valley fault of the Survey) which runs E - W through the islands of Inishshark and Inishbofin onto the Renvyle peninsula, where its path swings NW - SE. This break, the '*Renvyle - Bofin slide*' (RBS) separates a well - stratified sequence to the south (the Bennabeola Quartzite, Streamstown, Ballynakill and Lakes Marble Formations of Tanner & Shackleton 1979) from a more homogeneous sequence associated with the Dawros - Currywongaun - Doughruagh igneous complex, the Kylemore Formation (Morris & Tanner 1977). Cruse determined that the facing in the Kylemore Formation is generally upwards, whereas the lithologies to the south of the RBS are downward and north facing.

Cruse & Leake (1968) follow the correlation of Kilburn *et al.* (1965) of the Connemara rocks with the Dalradian of Scotland and Donegal, again using the Cleggan boulder bed as a

*by conductive relaxation whilst concurrently pressure decreases by erosion of the pile'* (England & Richardson 1977). Erosional parameters, essentially the rate of uplift, are used to calculate the change in the temperature gradient due to the erosion.

The model follows a sequence of events where an instantaneous tectonic event (the formation of the overthrust) produces a disequilibrium geothermal gradient, which then relaxes during uplift. The results of such a model show a three stage thermal evolution in the lithologies beneath the thrust (England & Thompson 1984) (Figure 6.2).

(i) An initial isothermal pressure increase associated with the emplacement of the overthrust sheet. The model assumes that the thrust emplacement is instantaneous (after Oxburgh & Turcotte 1974) with no re - equilibration of the isothermal surfaces within either the overthrust or underthrust sheets during the thrusting process.

(ii) A period of increasing temperature associated with decreasing pressure. This phase is due to the re - equilibration of the perturbed isothermal surfaces during uplift.

(iii) A final phase of falling temperature and pressure as the largely thermally equilibrated material continues to be uplifted.

The overthrust sheet shows a more simple evolution with both pressure and temperature falling after the thrust emplacement.

The model enables the calculation of complete pressure - temperature - time (P - T - t) loops for individual points within the model system. However, the use of such 'single event' systems are of limited use in modelling polyphase terrains where tectonism continues to affect the equilibrating thermal system. The results of polyphase models (Thompson & Ridley 1987) which consider the effects of a sequence of tectonic, or combined tectonic and igneous events on the thermal evolution, are rather more complex. Figure 6.3 shows the qualitative effects of several different tectonic and intrusive histories on a system.

The results of garnet profile modelling {5.6} suggest that the lithologies to the south of the RBS were loaded and the Kylemore Fm was uplifted during $D_2$. The thermal modelling in this work is based on the interpretation of the RBS represents a thrust surface, with the Kylemore Fm being the overthrust sheet.

**Figure 6.2: Schematic thermal evolution of an overthrust system showing the evolution of the overthrust (Ot) and the underthrust (Ut), after Thompson & England (1984).**

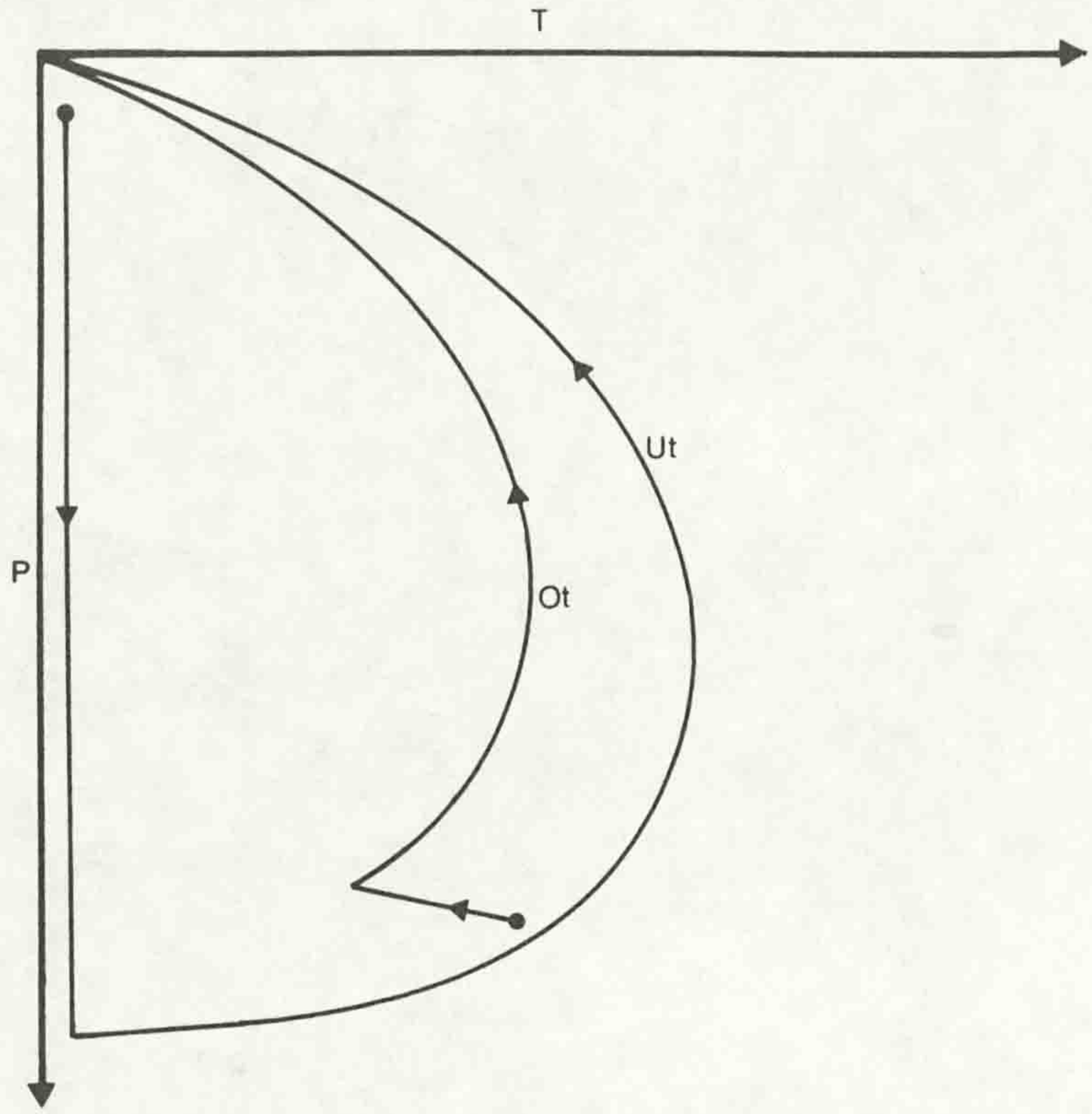


**Figure 6.3: Complex P - T paths resulting from modelling of polyphase thermal systems, after Thompson & Ridley (1987).**

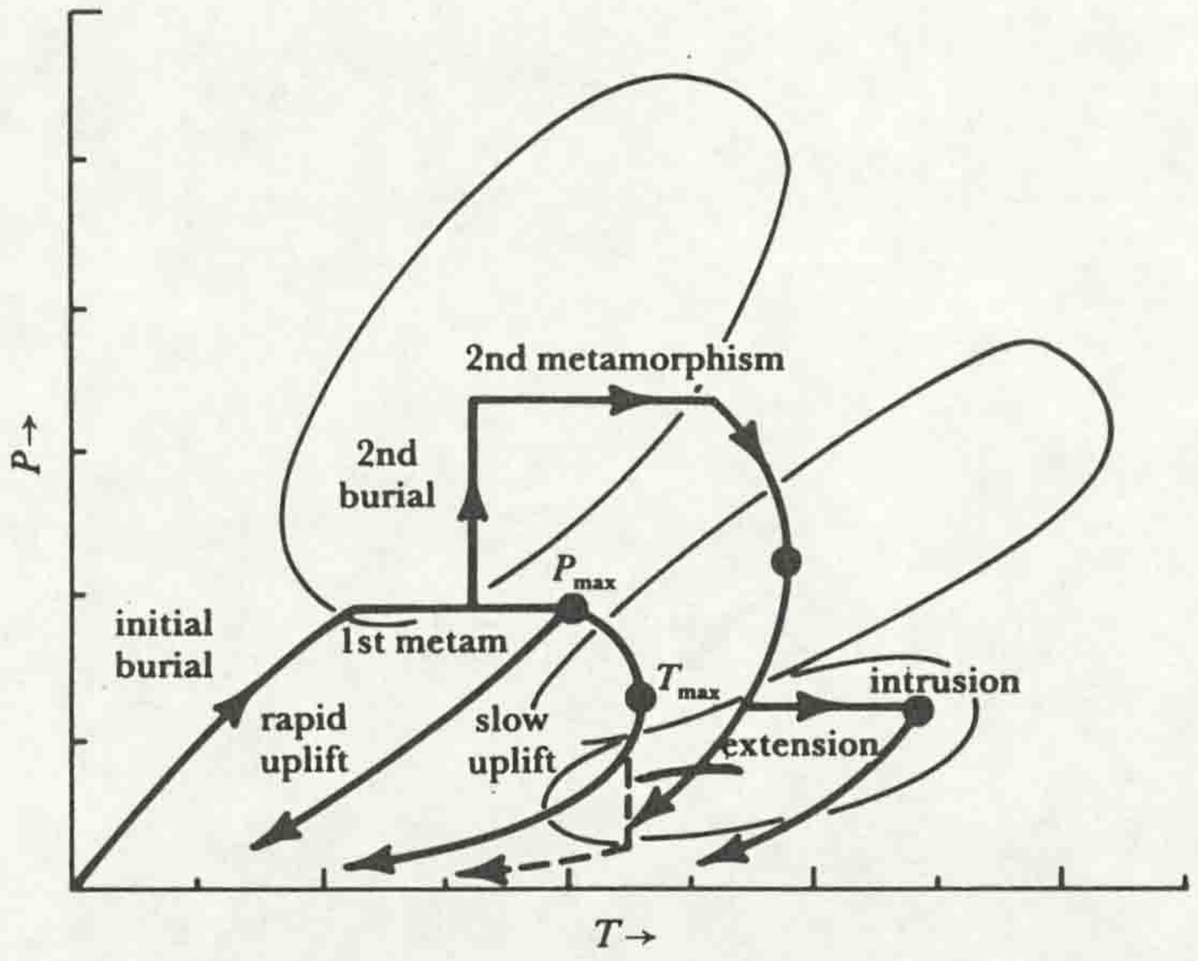

The results of such models are then compared with the P - T paths produced in garnet modelling {6.7}.

6.5.2 Input parameters required by the thermal model

6.5.2.1 Initial thermal gradient: It is assumed that the thrust emplacement occurs instantaneously, and the initial thermal gradients are preserved in both the overthrust and underthrust sheets immediately after the thrust emplacement. It is difficult to ascertain the original thermal gradients in the study area as no clear evidence is preserved for either the original plate tectonic setting or the degree of equilibrium developed in the thermal systems prior to any tectonism. In the modelling it is assumed that the initial thermal gradients within both the overthrust (Kylemore Formation) and the underthrust sheets were the same and represent equilibrium gradients. Anderton (1985) interprets the deposition of the Scottish Dalradian (with which the Connemara rocks are correlated) as occurring within a basin developing due to lithospheric extension as described by McKenzie (1978). It is not clear if the development of equilibrium thermal gradients within such settings is common, although McKenzie (1978) suggests that the upwelling of hot athenosphere during extension often precludes equilibrated systems.

The initial thermal gradient used in the modelling is a simple linear gradient of 25°C $km^{-1}$ in the overthrust and the upper part of the underthrust sheet. The gradient beneath 60km depth in the underthrust is of 15°C $km^{-1}$ (after Nisbet & Fowler 1982). The form of the starting gradients, immediately after the overthrusting, is shown in Figure 6.4. The assumption of linear thermal gradients in the starting temperature profiles is a gross over - simplification of the probable nature of the original thermal system, but it represents a base state which can be used in comparison with the P - T conditions calculated through thermobarometry {5.4}. It should be noted that the heating effects of the DCD on the initial thermal gradient are ignored in the modelling.

6.5.2.2 The magnitude of the mantle heat flux $q_m$: As

Figure 6.4: The starting gradients use in the thermal modelling.
a, System (1)
b, System (2)

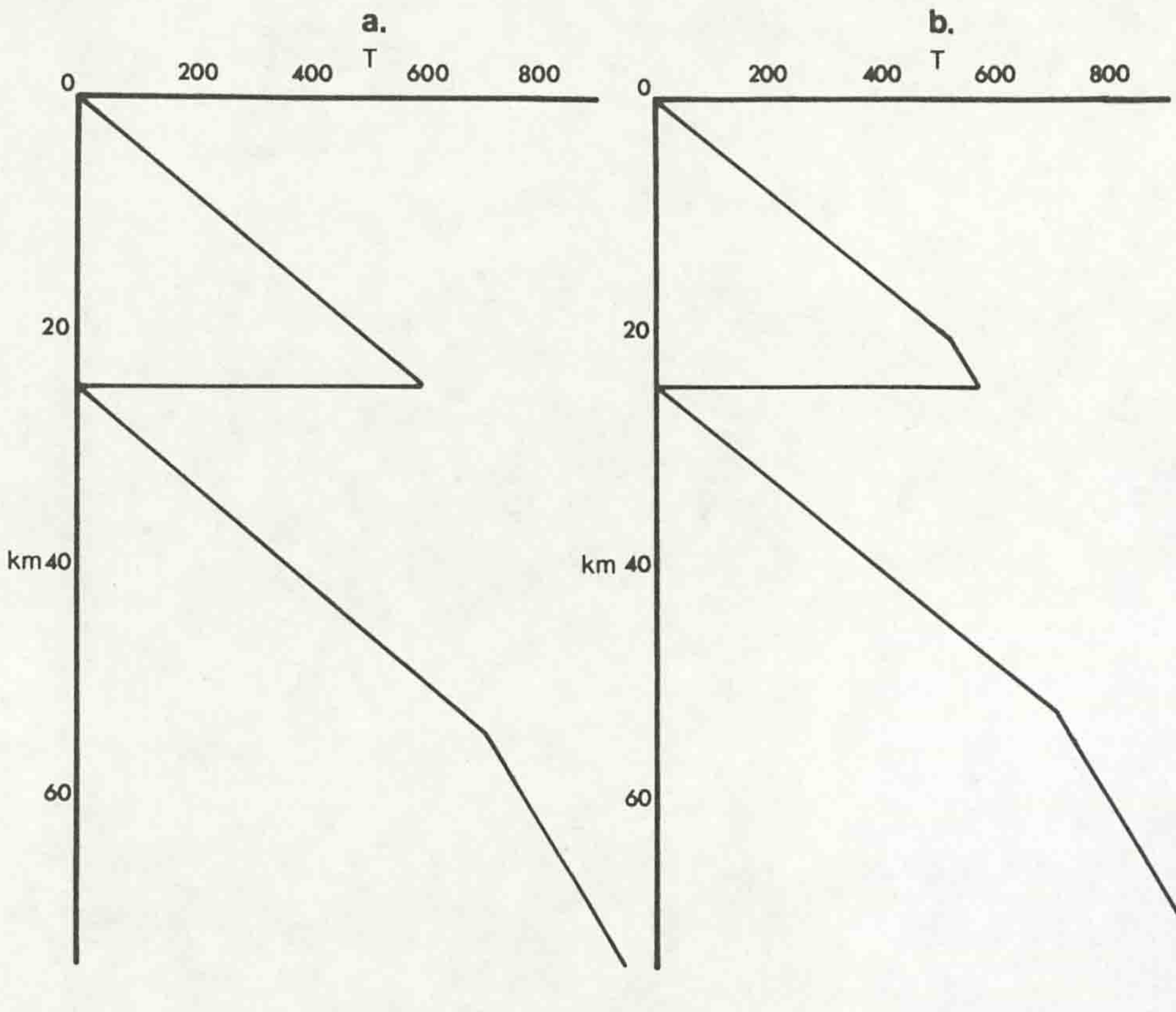

noted in {6.3.1.2} the magnitude of $q_m$ has a control on the thermal system, and is also controlled by tectonic setting. Yardley, Vine & Baldwin (1982) suggest that the tectonic setting of the Dalradian rocks of Connemara changed with time, from an initial subduction zone site, where heat fluxes would be relatively low, to being the roots of a volcanic arc system (Yardley & Senior 1982) within which heat fluxes would be above crustal averages.

As the computation of the model does not allow for any changes in $q_m$ over time, the value of 38 uW / $m^2$ (after England & Richardson 1980) was used in the modelling because it represents a heat flux intermediate to the reduced fluxes associated with subduction zones and the enhanced fluxes seen in volcanic arc settings.

6.5.2.3 <u>The magnitude of radiogenic heating (A)</u>: The amount of heat added to an equilibrating thermal system by radiogenic heating is a major controlling factor in the evolution of that system (England & Thompson 1984). In an attempt to reduce the error introduced into the modelling by using assumed or average values of A, the concentration of radiogenic elements within the study area was assessed by field measurement {Appendix A} and by laboratory determination of the primary radiogenic heat producing elements (U, Th, K) {Appendix B}.

The U and Th concentrations in the different lithologies of the study area are tabulated in {Appendix C}. The variation in the magnitude of radiogenic heating in the study area (in uW / $m^3$) is shown on {Enclosure 3}. The mean heat production (A) values for the different lithologies of the study area are shown in Table 6.1.

The magnitude of radiogenic heating of relatively constant within lithologies, the primary differences being between the lithological units. In the metasedimentary lithologies north of the RBS (the Kylemore Fm) the primary variation is between psammitic and more pelitic lithologies, with the psammites showing a mean A (in uW / $m^3$) of 1.415 and the pelites showing a mean of 1.903. No clear variation in heat production between regional and contact metamorphic lithologies is apparent. The ultrabasic and basic igneous bodies are characterized by low

Table 6.1: Mean heat production values, in $uWm^{-3}$, in the different lithologies of the study area.

| Lithology | n | mean | s.d. |
|---|---|---|---|
| Peridotite | 8 | 0.247 | 0.081 |
| Gabbro | 23 | 0.485 | 0.191 |
| Kylemore Fm | | | |
| Pelite | 44 | 1.903 | 0.416 |
| Semipelite | 46 | 1.594 | 0.404 |
| Psammite | 13 | 1.415 | 0.290 |
| Bennabeola Quartzite Fm | | | |
| Quartzite | 17 | 0.712 | 0.246 |
| Streamstown Fm | | | |
| Pelites | 4 | 1.915 | 0.222 |
| Psammites | 14 | 1.721 | 0.593 |
| Lakes Marble Fm | | | |
| Psammites | 5 | 1.600 | 0.070 |
| Marbles | 4 | 0.468 | 0.361 |
| Amphibolite | 7 | 0.439 | 0.168 |

concentrations of radiogenic elements, and hence, by low heat production values (mean values of 0.485 for gabbros, and 0.247 for ultrabasic lithologies).

In rocks to the south of the RBS the control of lithology, and particularly the mica content, on the heat production is clear. The Bennabeola Quartzite Fm shows a mean heat production of 0.712 uW / $m^3$, with the micaceous psammites and semipelites of the Streamstown Fm having a mean of 1.721 and the highly aluminous schists of the Roeillaun schist Mb having a mean heat production of 1.915 uW / $m^3$. The marbles and amphibolites of the Lakes Marble Fm show mean heat productions of 0.468 and 0.439 uW / $m^3$ respectively, with the psammitic lithologies having a mean of 1.6 uW / $m^3$.

The relation between weight percent K (K%) and Th concentration is discussed by Atherton & Brotherton (1979), who note that, whilst Th may be concentrated in layered silicates it may also be present in minerals such as zircon and K - feldspar. Zircon is a common accessory within pelitic schists in the study area, often being apparent as inclusions in biotite mica {4.1.3.2}, surrounded by pleochroic haloes. K - feldspar is common within the migmatitic aureoles of the DCD {4.1.3.6}. A plot of K% V. Th (Figure 6.5) shows a wide spread of values, suggesting that Th is present in mica, K - feldspar and zircon grains (Atherton & Brotherton 1979).

A plot of Th V. U (Figure 6.6) shows a spread away from ideal ratios, suggesting either original sedimentary differences, or element mobility during metamorphism. No clear relation between the grade of metamorphism and the Th / U ratio is apparent.

The heat production values used in modelling are shown in Figure 6.7.

6.5.2.4 <u>The geometry of the system being modelled</u>: The geometry of the thermal system has a degree of control over its resultant equilibration. The orientation of the thrust plane and the lithological layering are considered to be horizontal for the model, with heat conduction being in the vertical sense. This geometry may well be consistent with the initial form of the RBS {3.3}. The thickness of the Kylemore Fm and other lithologies above the RBS at the time of thrust emplacement is based on the

Figure 6.5: Plot of K% V. Th in the metasedimentary rocks of the study area (fields after Atherton & Brotherton, 1979: a, Th in K - feldspar, b, Th in mica, c, Th in zircon). Triangles indicate Kylemore Fm contact metamorphic lithologies, dots Kylemore Fm regional metamorphic lithologies, squares other lithologies.

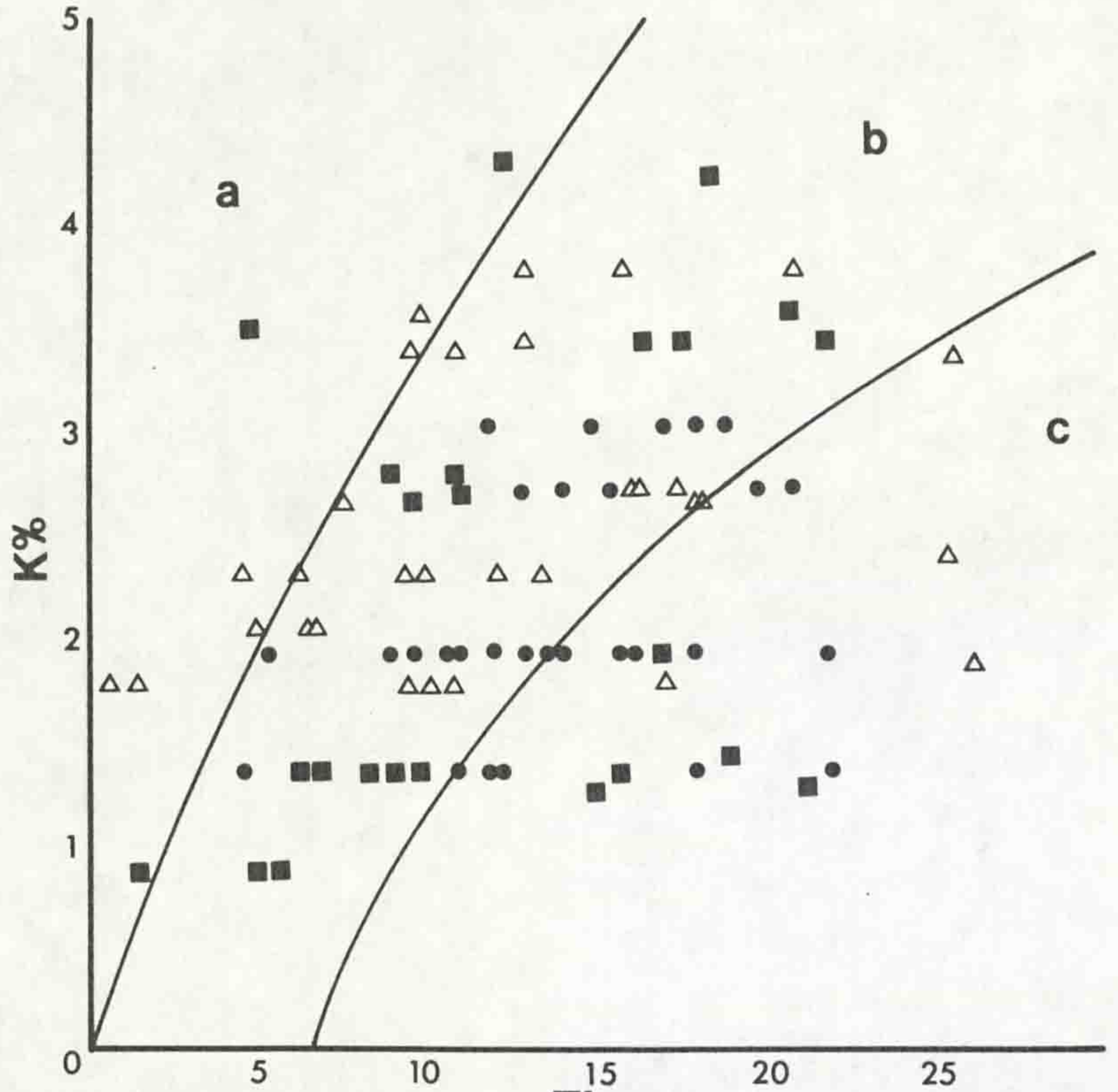


Figure 6.6: Plot of Th V. U in all lithologies in the study area.

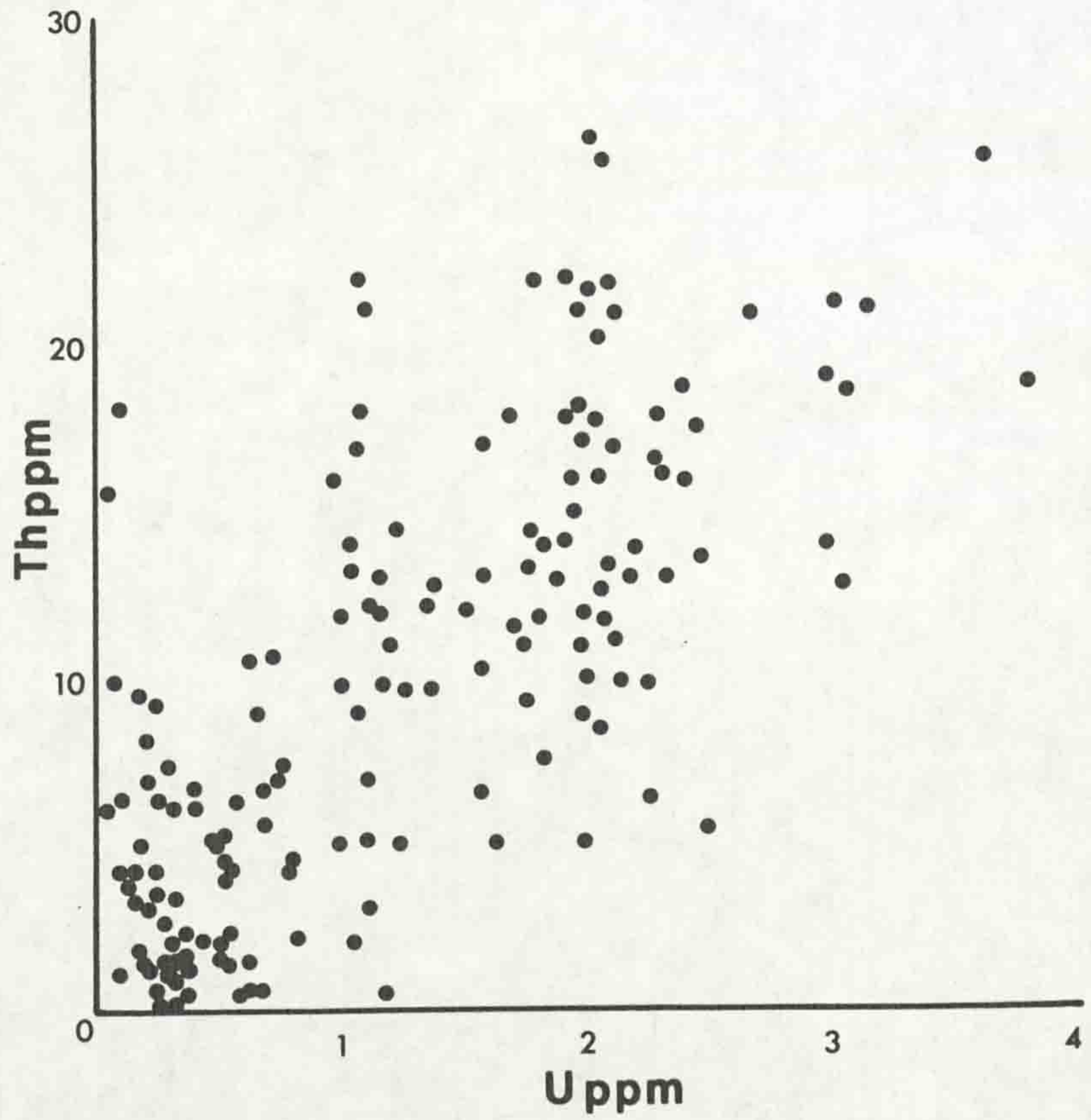

**Figure 6.7:** The lithological thicknesses and heat production values (in uW / $m^3$) used in the thermal modelling.
1, Kylemore Fm; 2, Gabbro; 3, Bennabeola Quartzite Fm; 4, Streamstown Fm; 5, Lakes Marble Fm and miscellaneous semipelites; 6, Undifferentiated lower crustal rocks (heat production values from Nisbet & Fowler 1982).
a, System (1).
b, System (2).

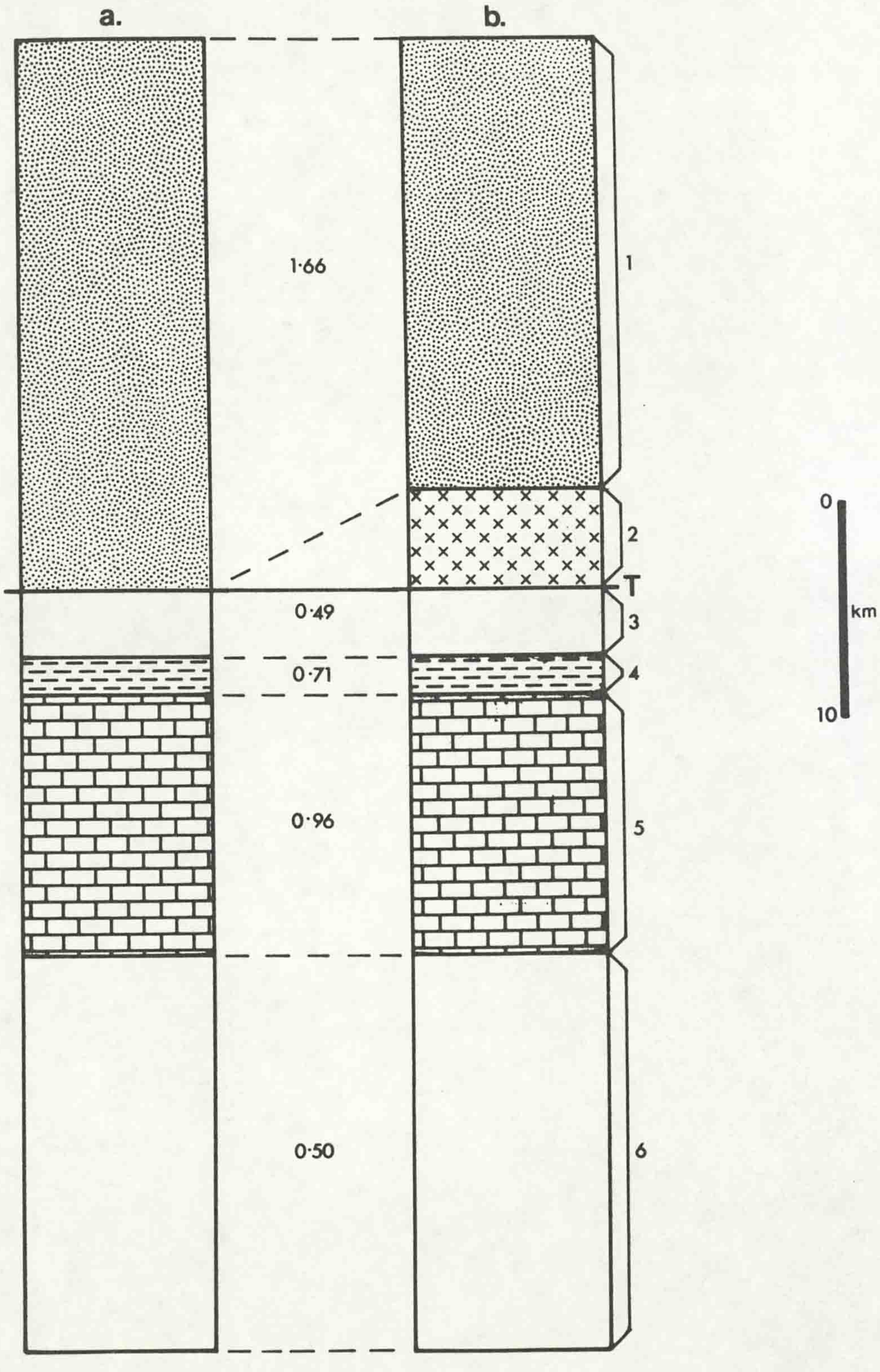

calculated pressures {5.4} in lithologies beneath the slide. The mean pressure of 7.88kb suggests that the thickness of material above the slide (assuming a mean density of ≃ 2.81 g $cm^{-3}$ for the pelites and psammites of the Kylemore Fm) of between 20 and 25km. The thickness of overthrust used in the modelling is 25km.

The scale of the internal layering in the two vertical sections modelled is based on the true thicknesses of the lithological succession. The internal heat production values {6.5.2.3} ascribed to each of the layers are based on the measured element concentrations. The thicknesses of lithological units and the heat production ascribed to them are shown in Figure 6.7.

The model system used could not allow for differing values of conductivity ($k$) and density within the lithological sequence. The value of $k$ used in the modelling is 2.2 W/ m / °K an intermediate value for $k$ in metamorphic lithologies similar to those in the study area (Clark 1966). A model density of 2.81 g $cm^{-3}$ is also an intermediate value for metamorphic rocks similar to those within the study area (Daly, Manger & Clark 1966).

6.5.2.5 <u>The rate of uplift of the overthrust system</u>: The time available for a rock unit to undergo a thermal event in the model is the period between the overthrusting and the arrival of that particular rock unit at the surface. In modelling the study area it is possible to constrain the time period between the syn - $D_2$ movement on the thrust plane (RBS) and the time at which the Kylemore Formation reached the surface. The timing of the syn - $D_2$ emplacement of the Connemara ultrabasic suite at c. 515 ± 15 Ma. (Leggo & Pidgeon 1970) provides an age for the emplacement of the Kylemore Fm as an overthrust. The Kylemore Formation is overlain by unmetamorphosed sediments of Silurian age (the Upper Llandovery Kilbride Fm, Ryan 1983). The absolute age of Llandovery sedimentation is considered by Harland, Cox, Llewellyn, Pickton, Smith & Walters (1982) to be 428 - 438 Ma.

These dates suggest that the time available between overthrusting and the unroofing of the thrust was between 80 and

marker horizon.

Regional stratigraphic correlations were considered by Tanner (1968) and Tanner & Shackleton (1979) who produced a stratigraphy for the entire Bennabeola area of NW Connemara. This stratigraphy (Figure 2.1) was again correlated lithostratigraphically with the Scottish Dalradian and the work also noted that the stratigraphic succession in a major part of the Bennabeola area was inverted. This work further emphasised the need to clarify the structure in determining the stratigraphy, as the existence of early ($F_2$) fold closures produces repetitions in stratigraphy, along with attenuation and local loss of stratigraphic horizons along slides. The effect of slides on the stratigraphic sequence is particularly evident in the study area where the RBS cuts across the stratigraphy. Tanner & Shackleton (1979) tentatively suggest a correlation between the Kylemore Formation and a similar sequence of lithologies associated with the south Connemara ultrabasic bodies, the Cashel Formation, and the Ballynakill Formation.

The stratigraphy erected in this work is described below (and Figure 2.1), the mineralogical and textural features of the rocks being covered in {Chapter 4}. In the lithological descriptions given it should be noted that:

(i) all thicknesses of units are post - tectonic thicknesses {Enclosure 2};

(ii) the bulk of the stratigraphy is inverted such that the structurally highest units are the stratigraphically lowest;

(iii) the stratigraphy is interrupted by the RBS and the relation between the Kylemore Formation, to the north of the slide, and the main stratigraphic sequence to the south is not clear.

### 2.1.2 Stratigraphic Sequence

#### 2.1.2.1 Lithologies to the south of the Renvyle - Bofin slide

The lithologies to the south of the Renvyle - Bofin slide show a well-developed stratigraphic sequence which is correlated with the sequence in the Twelve Bens area (Tanner & Shackleton, 1979). It should be noted that the stratigraphy established in this work

100 Ma., which gives a minimum uplift rate (calculated from the overthrust thickness of 25km noted in {6.5.2,4}) of 0.25km per Ma, or 0.25mm per year. This value is slightly lower than the range suggested for typical Alpine and Himalayan uplift rates by England & Richardson (1980). It has been suggested (Leake, Tanner, Singh & Halliday 1983, Bluck & Leake 1986) that the rate of uplift was very rapid at around 460 Ma as this period corresponds with the development of low pressure metamorphic assemblages (Crd / And). Although evidence of rapid uplift is present in the Scottish Dalradian (Dempster 1985), both the timing and rate of uplift in the Connemara massif remain enigmatic.

Pidgeon (1969) notes the occurrence of clasts of Dalradian quartzite and schist within Lower Ordovician conglomerates and implies that this represents an age of unroofing for the Dalradian of Connemara (470 - 455 m.a). However, no sedimentary contact between Ordovician and Dalradian lithologies is evident. As the evidence for the duration and rates of uplift is so limited, a value of 0.25mm per year is used in the modelling.

## 6.6 The results of thermal modelling

The thermal evolution of two vertical crustal sections was modelled. System (1) consisted of an homogeneous sequence of metasedimentary lithologies (25km thick), corresponding to the Kylemore Fm, emplaced over a sequence of varying heat production, corresponding to the lithologies to the south of / beneath the RBS. System (2) was essentially the same, although a 4km thickness of material with lower heat production values and a thermal gradient of 15°C / km equivalent to the gabbroic material was placed at the base of the Kylemore Fm (above the RBS). The starting conditions for these systems are shown in Figure 6.7.

The results of system (1) are shown in Figure 6.8. The thermal relaxation of the initial saw - tooth geotherm (Oxburgh & Turcotte 1974) occurs within the first 8 Ma of the thermal evolution to give a continuous temperature gradient. The variation of heat production in the lithologies beneath the thrust have an influence on the initial stages of the thermal

**Figure 6.8: The results of the thermal modelling of system (1). The values adjacent to the curves indicate time in Ma.**

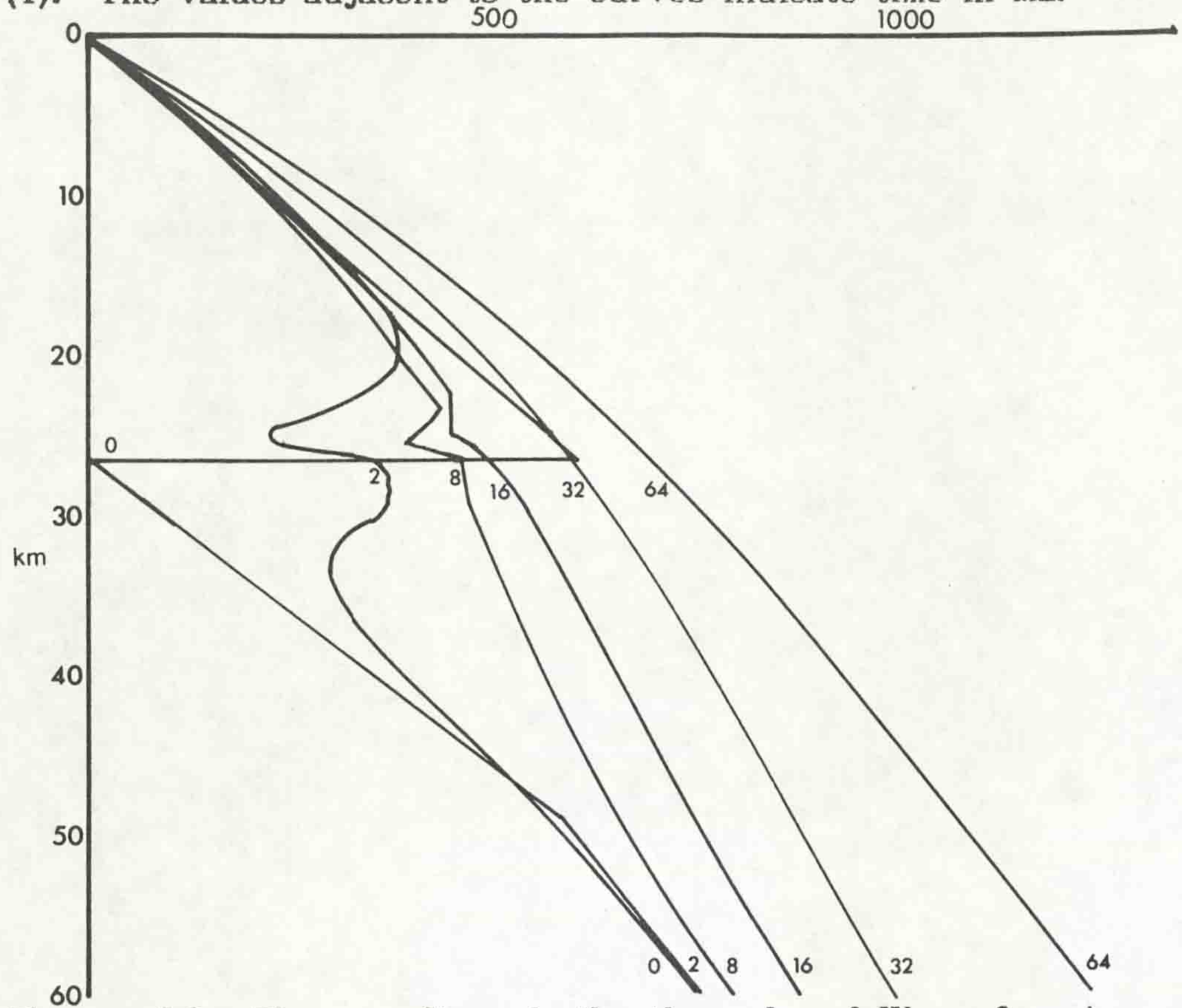


**Figure 6.9: The results of the thermal modelling of system (2). The values adjacent to the curves indicate time in Ma.**

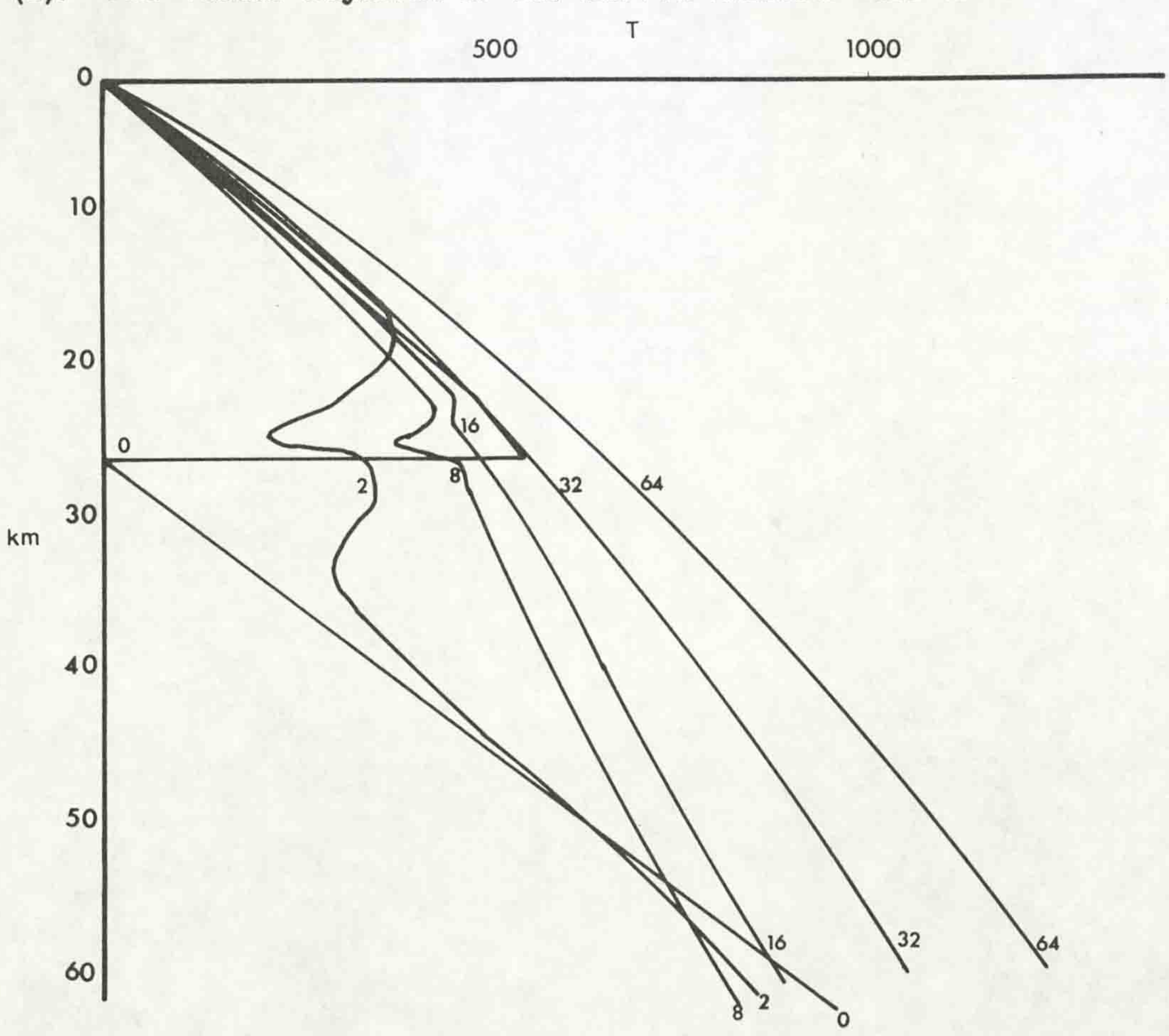

evolution, although after 32 Ma the effects of heat production variation are no longer significant. The thermal gradient after 32 Ma is higher than that developed in the initial system. The results of system (2) (Figure 6.9) are similar to those of system (1) although some minor differences do occur. The modelled pressure - temperature - time (P - T - t) paths for the overthrust and underthrust units are shown Figures 6.10 and 6.11. The overthrust unit in both systems shows a simple thermal evolution (Figure 6.10) with an initial period of falling temperature in lithologies near to the thrust surface followed by heating. The temperature fall is due to the relaxation of the temperature inversion of the saw - tooth gradient. The maximum temperatures reached during the heating phase are lower than the starting temperatures. The heating during uplift ceases after $\tilde{=}$ 20 Ma, after which the rocks cool during uplift. The sequence of initial temperature fall followed by a period of heating is seen only in lithologies less than 7km above the thrust plane (i.e. at depth of 18 - 25km). The lithologies which occur more than 7km above the thrust show paths with continuous cooling during uplift. In system (2) a 4 km thickness of gabbro occurs immediately above the thrust and the initial temperature at the thrust is slightly lower (560°C against 600°C in system (1)) and the P - T - t path follows a slightly lower temperature route during uplift.

The underthrust unit in both system (1) and system (2) shows a rather more complex P - T - t history (Figure 6.11), with an initial period of thrust induced isothermal loading followed by a period of heating during uplift, and then an uplift and cooling phase. The initial loading phase is isothermal because the model considers thrust sheet emplacement to be instantaneous, thus allowing no time for the isothermal surfaces to migrate. The problems involved in the consideration of instantaneous thrust emplacement are discussed later. In the period within 20 Ma of the thrust emplacement, the underthrust sheet undergoes rapid heating to a maximum temperature of over 500°C and then cools at a rate similar to that seen in the overthrust sheet. Both model systems show similar evolution curves (Figures 6.10 and 6.11) although system (2) follows a slightly lower temperature path, the temperature difference probably being

Figure 6.10: Pressure - temperature - time (P - T - t) paths for a point 1km above the base of the overthrust sheet. Dots indicate system (1), triangles system (2). Values the the right of the points indicate time in Ma.

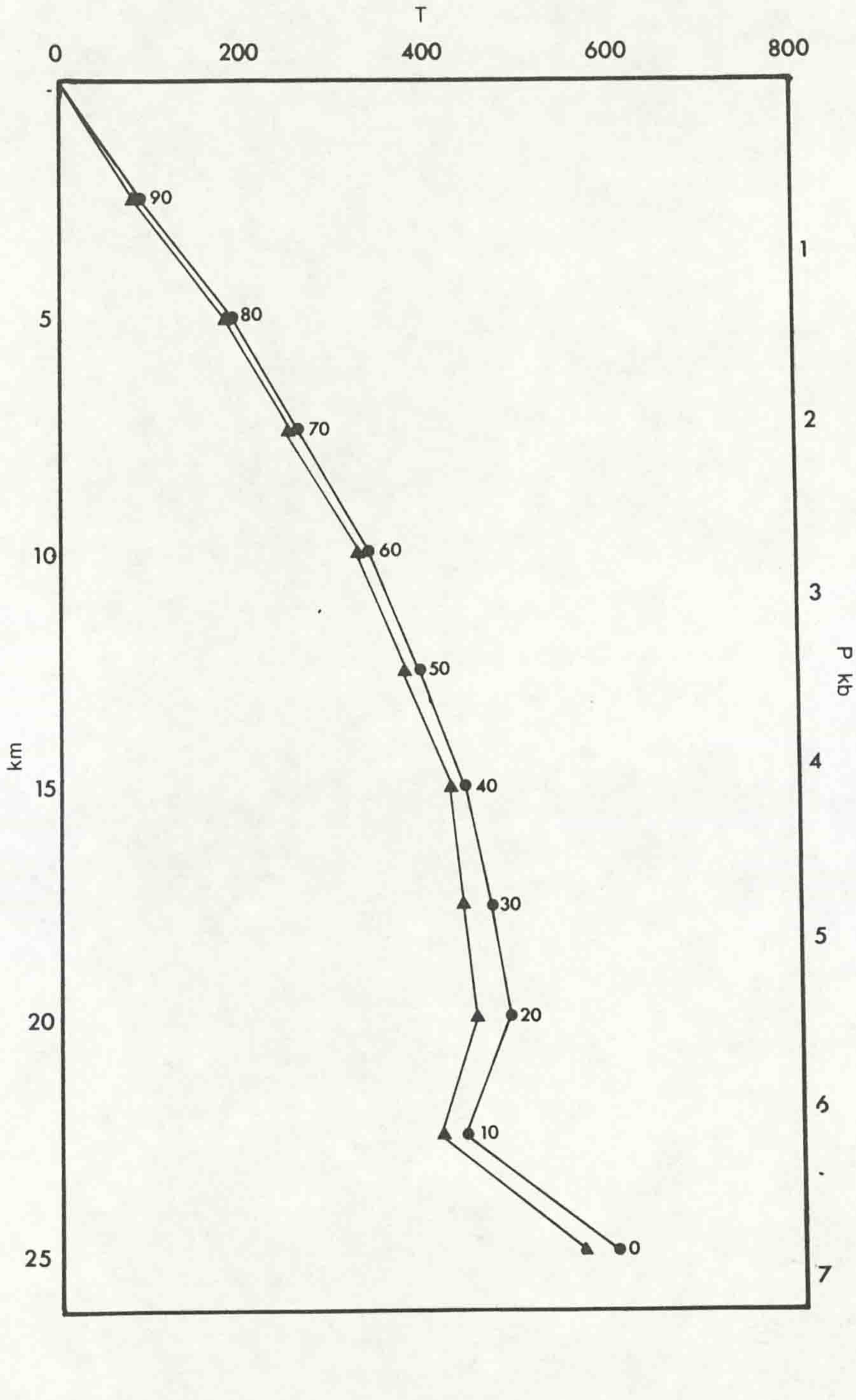

Figure 6.11: Pressure - temperature - time (P - T - t) paths for a point 1km below the base of the overthrust sheet. Dots indicate system (1), triangles system (2). Values the the right of the points indicate time in Ma.

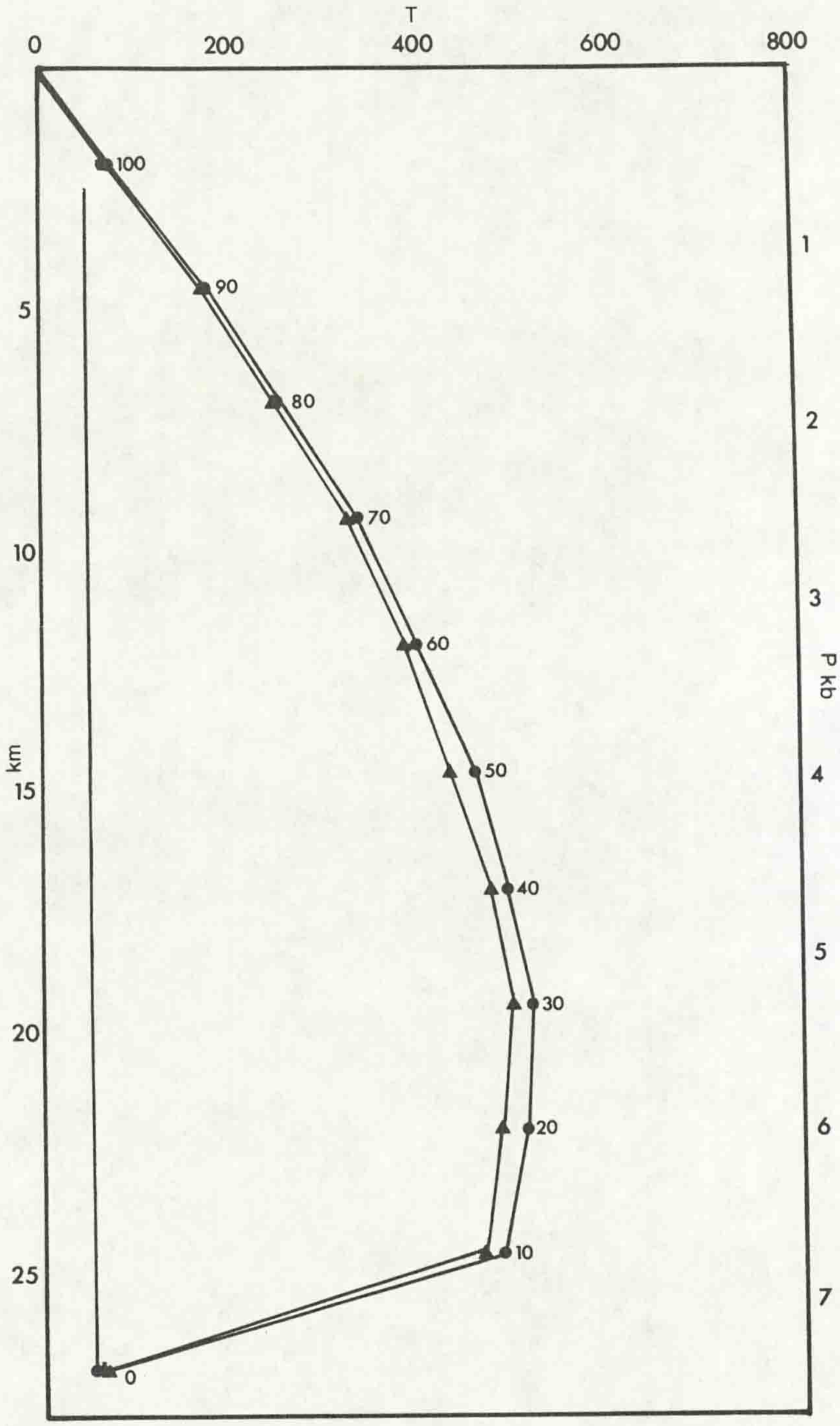

controlled by the lower initial temperatures at the thrust plane in system (2) and the lower radiogenic heating in the gabbroic unit.

## 6.7 Discussion

The pressure - temperature - time (P - T - t) paths produced by thermal modelling can be compared with the pressure - temperature (P - T) paths produced by garnet zoning modelling {5.6}. As noted in {6.5.1} the thermal modelling was based on the assumption that the Kylemore Fm represents the overthrust unit, and the lithologies to the south of the RBS (the Bennabeola, Streamstown and Lakes Marble Fms), the upper part of the underthrust sheet.

At first sight, only those P - T paths produced in modelling zoned garnets from the Streamstown Formation show any obvious relation to the P - T - t paths produced in the thermal modelling (Figure 6.12). It is important to note that the garnets record information on only the early stages of the thermal evolution, since the timing of garnet growth within regional metamorphosed rocks can be constrained as being syn - $D_2$ {3.2.3} (i.e. during the movement on the RBS). This factor being considered, the P - T paths derived from the garnets should be correlated with those stages of the thermal model which involve the thrust emplacement.

As the model system used in this work considers the thrust sheet to have been emplaced instantaneously, and natural thrust systems take a finite period to be emplaced (e.g. Thompson & Ridley 1987), the model will not produce a result which is directly comparable with the garnet P - T paths.

The complete form of the thermally modelled P - T - t path for the underthrust sheet (Figure 6.11) is not seen in the garnet paths, which record only a pressure increase (and a possible earlier slight pressure decrease {5.6}), here interpreted as being due to the thrust sheet emplacement. Whilst the P - T - t path derived from the thermal modelling shows the pressure increase phase to be isothermal, the garnet paths show a slight increase in temperature during this burial. Modelling of thermal systems where thrust emplacement is non - instantaneous (e.g.

Davy & Gillet 1986, Shi & Wang 1987) show that thermal relaxation leads to re - equilibration of the overthrust (saw - tooth) geotherm during the thrust movement. In such models the underthrust sheet undergoes a temperature increase synchronous with the loading event. The resultant P - T - t path shows an initial period of rapid loading associated with a temperature increase, an event sequence recorded in the garnet zoning of the underthrust sheet. However, the starting temperatures of the underthrust sheet material in the model (50°C 2km beneath the thrust) are considerably different from those produced in garnet modelling (≃ 500°C). The high temperatures may be ascribed to a variety of reasons:

(i) The present top of the underthrust sheet may not represent the highest portion of the sheet, later reactivation of the RBS {3.3} possibly cutting the stratigraphically higher material out of the sequence.

(ii) The top of the underthrust may not have been at the surface before the thrusting event, i.e. the RBS represents either a ramp cutting up section, or a mid crustal flat.

(iii) Emplacement rates on the RBS were such that the re - equilibration of isothermal surfaces resulted in equivalent temperatures either side of the thrust.

(iv) Garnet growth may be relatively late in the thrust movement history, such that thermal equilibration across the thrust may have raised the temperature to give conditions suitable for the growth of garnets.

There is no clear evidence as to the original form of the underthrust sheet or to rates of thrust emplacement on the RBS, and consideration that the growth of garnet would not occur at low temperatures suggests that the P - T paths produced from garnet zoning may only record the late, higher temperature, stages of the overthrusting. As such, the garnet derived P - T paths would represent only the later portion of the burial phase in the P - T - t paths calculated from thermal modelling and the apparently high temperatures recorded in the garnet paths are due to the initiation of garnet growth as syn - deformational thermal re - equilibration raised temperatures to suitable levels.

The P - T paths calculated from garnet zoning in the overthrust sheet (the Kylemore Fm) {5.6} show uplift associated

Figure 6.12: Comparison of P - T - t paths produced by thermal modelling with the P - T paths produced in garnet profile modelling.
a, The underthrust sheet P - T - t and the P - T paths produced by modelling Streamstown Fm garnets.

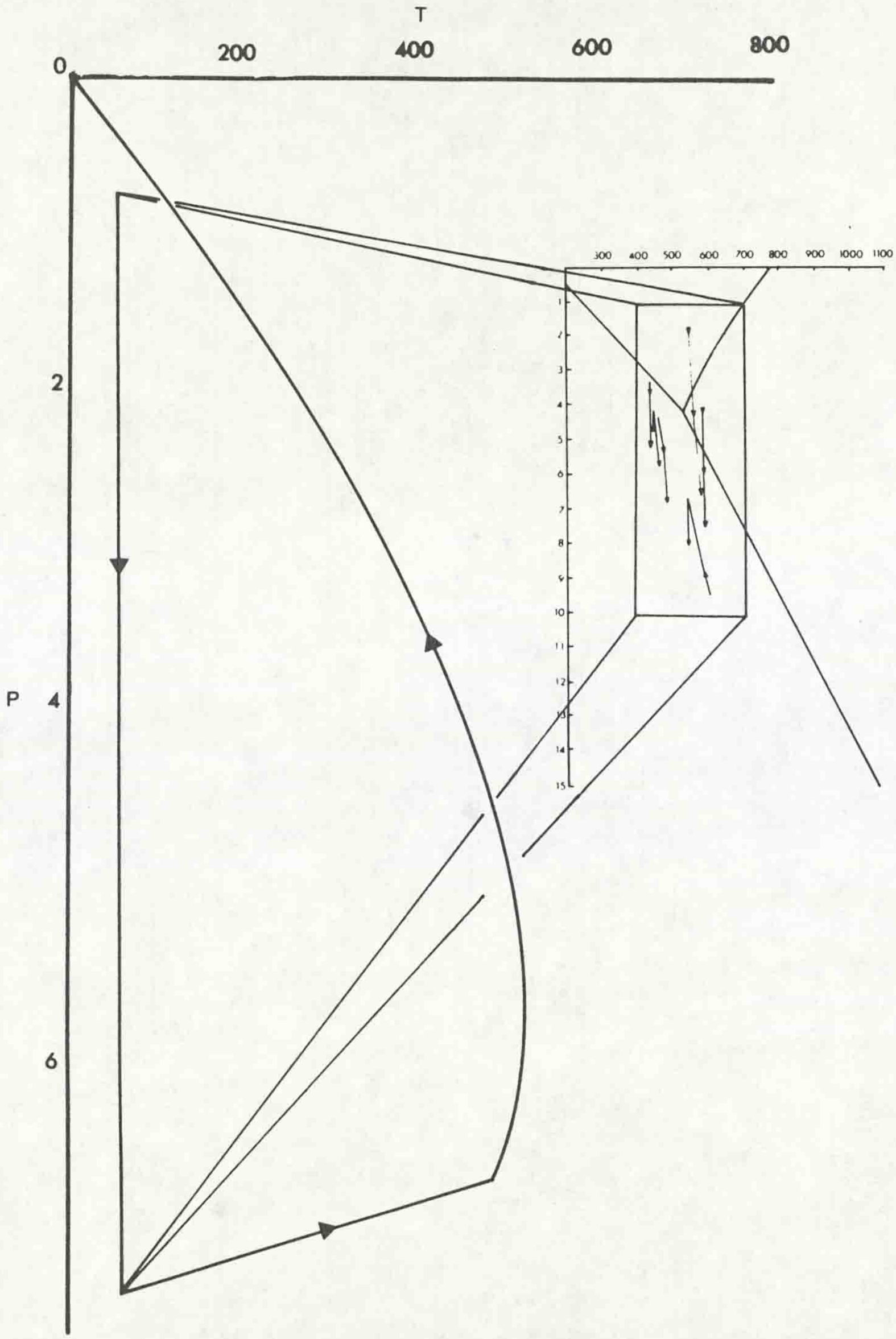

Figure 6.12 (cont)
b, The overthrust sheet P - T - t paths and Kylemore Fm garnet P - T paths.

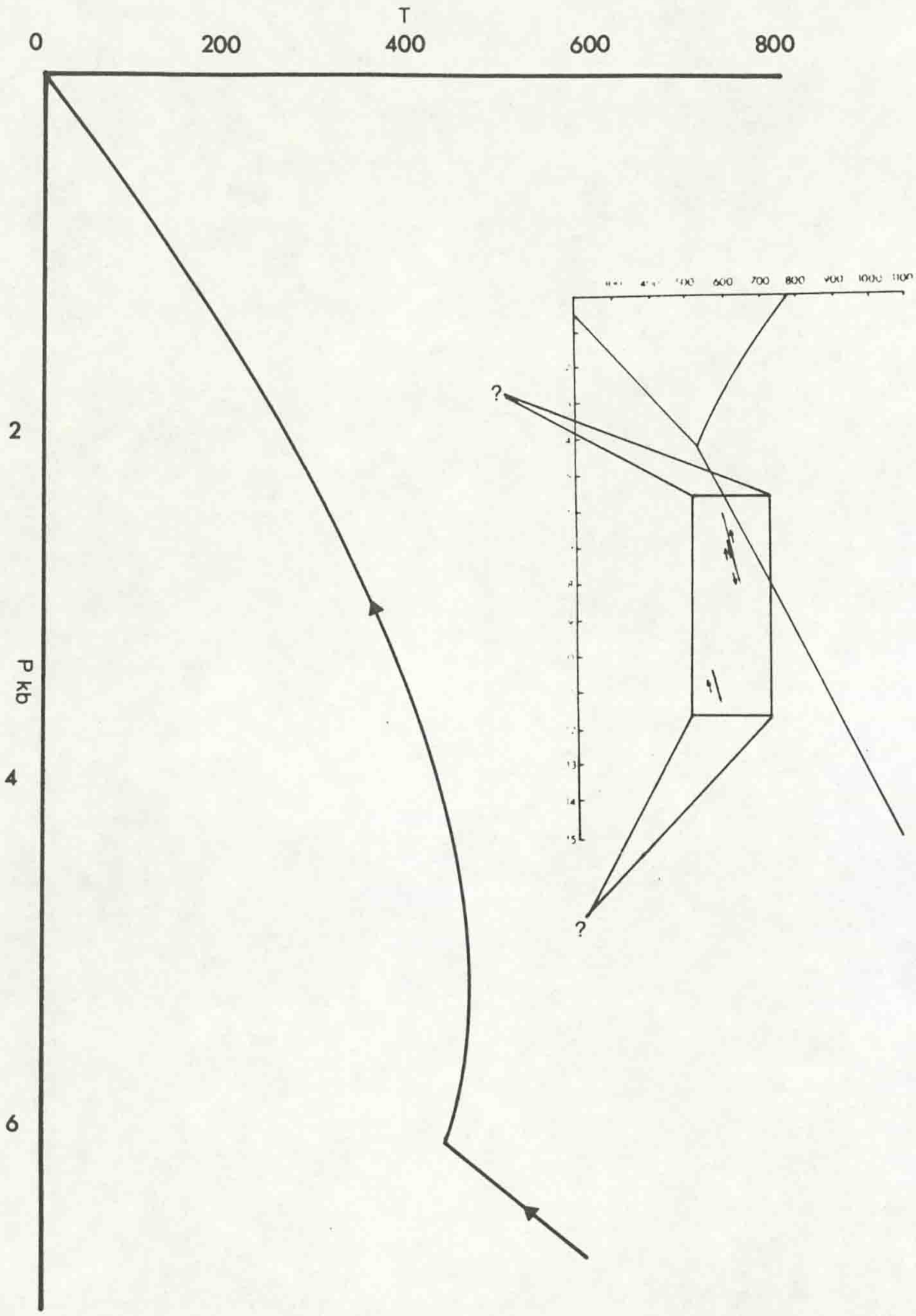

with a slight temperature decrease (Figure 6.12). The thermally modelled P - T - t paths for the overthrust show an initial temperature decrease associated with the immediate post - thrust equilibration of the saw - tooth geotherm. As the P - T paths derived from garnet modelling are syn - deformational it is unlikely that these paths represent the immediately post - thrusting system, but are more likely to be related to syn - deformational thermal re - equilibration of the thrust sheet. Davy & Gillet (1986) show that a time - dependent thrust emplacement results in cooling of the lower portions of the overthrust during the period of thrust motion along with the heating of the upper portion of the underthrust.

The results of different values of $q_m$ or uplift rates are not considered in this modelling, as metamorphic evidence for events after $D_2$ is poor {4.1.4}. However, qualitatively, the effects of increased basal heating or more rapid uplift would lead to higher temperatures at shallow depths (Nisbet & Fowler 1982). It is possible that the period of rapid uplift discussed by Bluck & Leake (1986) may have occurred within the study area, as post - $D_2$ andalusite is locally developed {4.1.3.9}. This andalusite may be due to rapid uplift leading to high temperatures at relatively shallow depths. Variation in $q_m$ values takes longer to transmit through the crustal system, but it is possible that such variation did occur in the study area though the thermobarometric data is too sparse or insufficiently sensitive to determine such variation.

The P - T paths produced by the modelling of garnet zoning profiles can be related to the initial stages of overthrust development in a 1 - dimensional thermal model system. However, the thermal model used in this work, whilst being qualitatively valid, produces unrealistic results as the assumption of instantaneous thrust emplacement is made. The rates of emplacement of natural thrust systems are such that partial thermal re - equilibration of the material adjacent to the thrust surface occurs (Davy & Gillet 1986) and the P - T paths calculated from garnet zoning suggest that this was the case during the development of the RBS. Taking this thermal equilibration during the thrust movement into account the garnet zoning paths suggest that during the $D_2$ deformation the RBS

differs from the Tanner & Shackleton stratigraphy in the omission of the Ballynakill Formation. Although the Ballynakill Formation overlies the Lakes Marble Formation in much of western and central Connemara Tanner & Shackleton note that it is only tentatively correlated with garnet - staurolite bearing pelites in northern Connemara. The garnet - staurolite pelites in the study area which have been previously correlated with the Ballynakill Fm (the Roeillaun schists) actually form part of the Streamstown Fm. Cruse (1963), on whose study Tanner & Shackleton base the stratigraphy in the Letterfrack area, failed to identify an antiformal $F_3$ fold in the Doongill area, and as a result misinterpreted the succession.

2.1.2.1.1 Bennabeola Quartzite Formation

This is the structurally highest and stratigraphically lowest lithology present in the study area. Its thickness is highly variable, ranging from several hundred metres in the cores of the $F_3$ synformal structures (Tully Mountain and Diamond Hill synform), to <15m adjacent to the RBS on the Dawrosmore peninsula.

In outcrop the quartzite is typically white, occasionally with a blue - grey tint, with crustose lichen patches (Figure 2.2), and shows a strongly developed spaced foliation. Locally the quartzite shows a pink colour, with scattered angular 1 - 5mm clasts of pink feldspar. The foliation fabric is defined by an L-S shape fabric in quartz grains and by thin ( <1mm) partings of muscovite and chlorite flakes. Where the feldspar clasts are present they are flattened in the foliation. Bedding is largely absent, seen only where thin (2 - 10mm) dark bands of heavy minerals (typically magnetite and pyrite) reveal layering on 100 - 150mm scale. Locally developed, foliation parallel, heavy mineral bands reach thicknesses of up to 100mm. Cross - bedding is evident where the heavy mineral bands reveal the original bedding. Grit units up to 200mm thick, consisting of strongly lineated 5 - 10mm quartz clasts are common in the lower parts of the quartzite.

The contact of the quartzite with the overlying Streamstown Formation is locally well exposed e.g. [GR 683 586] and is typically marked by a 5 - 10m thick transitional zone of

acted as a thrust plane, the Kylemore Fm being emplaced over the Bennabeola Quartzite, Streamstown and Lakes Marble Formations.

It has been suggested by Yardley, Barber & Gray (1987) that the early phase of metamorphism in Connemara (the *Barrovian* phase) was the result of thermal relaxation after the emplacement of a large scale overthrust sheet. The later high temperature metamorphism, which is most evident in the south of Connemara, is ascribed by Yardley *et al.* to the thermal effects of the voluminous syn - orogenic magma suite developed in south Connemara.

The evidence presented in this chapter, along with {3.3, 5.6}, is consistent with the hypothesis of Yardley *et al.* (1987), the RBS representing an early thrust (possibly part of a sequence of thrusts?) which emplaces the Kylemore Fm over the formations to the south, the resultant thermal evolution leading to the development of staurolite - garnet grade metamorphism. The study area, having 'escaped' the high temperature effects of the later metamorphism, preserves important evidence as to the mechanism which lead to the early metamorphism in the Connemara massif.

# Chapter 7: Synthesis and conclusions

## 7.1 Introduction

This chapter attempts to summarize the tectonothermal history of the study area {7.2} and to relate this development to the evolution of the rest of the Connemara massif {7.3}. Suggestions for possible further work, both on the study area and further applications of the methods used, are made {7.4}.

## 7.2 Summary of the depositional, metamorphic and structural evolution of the study area

### 7.2.1 Stratigraphic sequence

The stratigraphic sequence and lithologies of the study area are similar to those in much of north - western Connemara (Tanner & Shackleton 1979), although the Ballynakill Fm, common further south, is not present. Ferguson & Al - Ameen (1986) interpret the spatial variation in lithologies in NW Connemara as being due to deposition within a system of basins and swells similar in nature to that suggested by Anderton (1985) for the Scottish Dalradian. In their model Ferguson & Al - Ameen (1986) consider the thin strips of staurolite pelite within the Bennabeola area (the Roeillaun schist Mb of the Streamstown Fm in this study) to be either a transitional facies between basin and swell (Figure 7.1) or tectonically intercalated sheets. The staurolite pelites show sedimentary boundaries with other Streamstown Fm units, and are here interpreted as a facies variation in the Streamstown Fm. No evidence for a tectonic intercalation of these units was found. The calc - silicate units of the Lakes Marble Fm (the Gubbatoor and Tonabina Marble Members) have been interpreted as turbiditic in origin by Ferguson & Al - Ameen (1986).

The amphibolitic unit within the Lakes Marble Fm, the Doongill amphibolite, can be correlated with the Finnisglin member (Badley 1976) an amphibolite unit which is traceable throughout much of the rest of Connemara. This amphibolite unit is considered (e.g. Evans & Leake 1960, Badley 1976) to represent a volcanic event, the material probably representing an ash flow or similar large scale volcanic depositional event.

Whilst the lithologies to the south of the RBS can be directly related to rocks in the main part of the Connemara massif, the correlations of the Kylemore Formation are somewhat more

Figure 7.1a: Schematic facies relations in NW Connemara during the deposition of the Lakes Marble Fm, although prior to the deposition of the amphibolitic unit (the Finnisglin Mb ≡ Doongill Amphibolite Mb), after Ferguson & Al - Ameen (1986). Black indicates shale, cc indicates carbonate rich slate/silt, brick ornament indicates carbonate material.

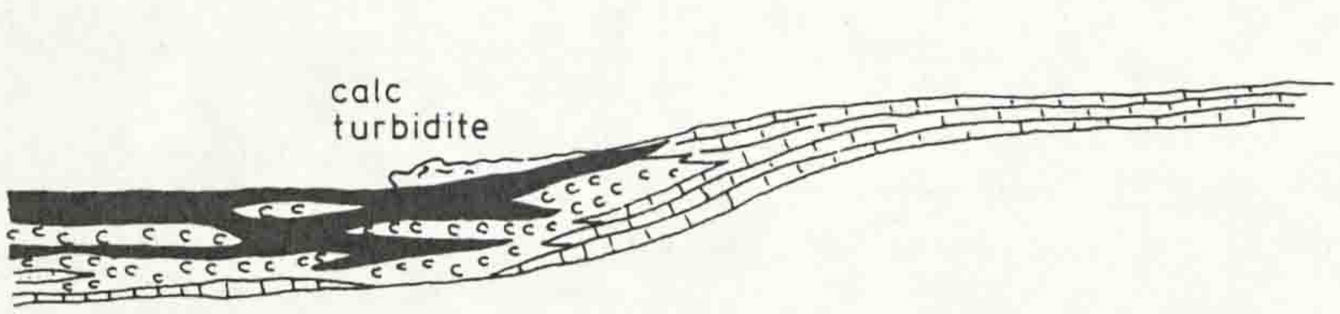


Figure 7.1b: Schematic cross - section of the depositional system for the Easdale subgroup (Mid - Argyll group) from Anderton (1985).

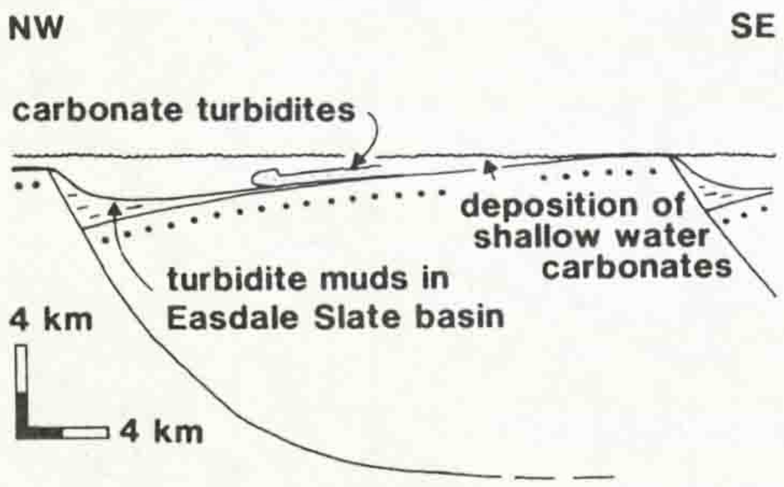

contentious. The lithologies of the Kylemore Fm, typically thinly interlayered pelites and psammites with local graded grit horizons, are correlated by Morris & Tanner (1977) with the Cashel Formation in south Connemara, although no interpretation of the original sedimentary nature of either of these units is made. It is possible that direct correlation of the Kylemore Formation with other lithologies in the Connemara Dalradian may not be viable and that the RBS represents a terrane boundary between the Kylemore Fm and the rest of the Dalradian. However, the similarities in deformation sequences in the lithologies either side of the RBS, and the lithological correlations of the Kylemore Fm with lithologies in south Connemara (Morris & Tanner 1977, Tanner & Shackleton 1979) argue against consideration of the Kylemore Formation as a suspect terrane *sensu stricto* (Jones, Howell, Coney & Monger 1983).

Overall, the lithologies and stratigraphic sequence within the majority of the study area are directly comparable with the rest of the Connemara massif. The depositional history of the area can be considered in terms of the development of a basin margin from an extensive open shelf system to local, fault controlled, compartmentalized basins, a sequence of events similar to that suggested by Anderton (1985) for the Scottish Dalradian.

### 7.2.2 Structural and metamorphic sequence

The structural and metamorphic development of the study area, although locally complicated, is on the whole relatively simple {3.5, 4.1.4}. The earliest deformational fabrics ($S_1$) seen are evident only locally as inclusion trails and in microscopic domains within later fabrics. Little evidence as to the origin of these fabrics is preserved, although it has been suggested (e.g. Yardley 1976, Tanner & Shackleton 1979) that they represent a mimetic fabric after bedding.

A second foliation fabric, $S_2$, is common throughout the study area, and is associated with a variably shallowly plunging, E - W trending lineation, $L_2$. These two fabrics are common in much of the Connemara massif, and have been related to large, nappe - scale fold closures (e.g. Treloar 1982). Evidence from extended clasts (Kelly & Max 1979), the development of fabrics in porphyroblasts {3.2.4} and locally developed sheath folds suggest

that the $D_2$ deformation involved a significant component of simple shear leading to extension in an overall E - W sense, although in the Kylemore Fm around the DCD a N - S directed extension is evident.

Within the regionally metamorphosed rocks the development of the peak metamorphic assemblage, Grt - Bt - St, begins during the $D_2$ deformation, although the assemblage is locally post - $D_2$. It is possible that the deformation enabled the metamorphic reactions to progress, either by promoting recrystallization and/or increasing the mobility of fluid phases (Thompson & Ridley 1987). Yardley, Barber & Gray (1987) suggest that the relatively fine grain sizes seen in the Connemara rocks (as compared with material from the Ox Mountains) is due to the rapid heating rates experienced by the Connemara Dalradian. However, as the peak metamorphism in the study area is largely syn - deformational it is perhaps more likely that the grain size of the minerals was controlled by the deformation, leading to overall finer grain sizes within the deformed lithologies of Connemara (Bell, Fleming & Rubenach 1986).

The syn - $D_2$ orientation of the RBS was flat - lying / sub - horizontal (Morris & Tanner 1977), and the modelling of garnet zoning profiles yields P - T paths which show the RBS to have been active as a thrust during $D_2$. The thrust motion emplaced the Kylemore Formation over the lithological sequence to the south perturbing the thermal layering within the Dalradian lithologies. The relaxation of this system led to the development of the metamorphic assemblages seen in the study area. The movement sense on the RBS is suggested by the $L_2$ fabric to be in an overall E - W sense, although around the DCD a N - S $L_2$ lineation is developed.

The $D_2$ structures and fabrics developed around the igneous bodies of the DCD are rather more complex than those in the regionally metamorphosed Kylemore Formation. A strong N - S lineation associated with a system of ductile shear zones {3.5}, along with locally developed convolutely folded migmatite patches, are present within the aureole rocks. The shear zones show evidence of syn - $D_2$ N - S movement, although the polarity of, and reasons for, this movement are unclear. The lower yield strengths and non - ideal behaviour of melt - rich

migmatites (McLellan 1988) may have led to the development of complex convolute folding patterns in the migmatitic aureoles of the DCD. These folding patterns, which have previously been interpreted as fold interference patterns (Bennett & Gibb 1983), can be ascribed to a single syn - migmatisation deformation.

The timing of mineral growth, and the presence of deformed migmatitic and sillimanite - bearing rocks, suggest that the emplacement of the igneous bodies was a syn - $D_2$ event. The gabbroic bodies show sharp igneous contacts (locally overprinted by later deformation) whereas the peridotite contacts are typically tectonic, showing the peridotite to have been tectonically emplaced during the $D_2$ deformation. It is likely that a mechanism similar to that described by Kanaris - Sotiriou & Angus (1976) led to the tectonic emplacement of the peridotite {3.5}. The gabbroic bodies were intruded into the Kylemore Fm, and also show evidence of being intrusive into the peridotite {2.2.1.2.2.3}. Although showing petrogenetic affinties with the peridotite {4.2}, the gabbroic bodies show a different mechanism of emplacement, and retain good contact aureole zones. At Creggaun the gabbroic material and its aureole are emplaced over the peridotite on a syn - $D_2$ ductile thrust {3.5}. Evidence for regional metamorphic assemblages overprinting the assemblages in the DCD and its contact lithologies is relatively sparse, although the development of amphibolitic assemblages within the ultramafic lithologies {4.2.1.2} suggest the igneous bodies to predate the regional metamorphic peak. The contact effects of the DCD are truncated by the RBS, suggesting at least some post DCD movement of the RBS.

The $D_3$ deformation shows evidence for strong N - S compression, with the development of large scale folds, with locally penetrative axial planar fabrics. Chlorite growth in the foliation fabrics and local early/pre - $D_3$ andalusite suggest that the grade of metamorphism was, on the whole, falling during $D_3$; the andalusite possibly being due to rapid (near isothermal?) uplift in the early stages of $D_3$. Shear zones within the aureole lithologies and fabrics associated with the RBS show evidence of reactivation, possibly in response to flexural slip on $F_3$ folds.

The $D_4$ deformation is not immediately apparent in the study area, but reference to other studies (e.g. Morris & Tanner 1977) indicates that the, largely $D_4$, formation of the Connemara antiform led to the tilting of the area to the north by up to 70°. It is possible that the RBS was again reactivated during this tilting, this time behaving as a normal fault and down throwing to the north.

The Dalradian rocks of the study area are unconformably overlain by Silurian age sediments (Ryan 1983), showing the system to have been exhumed by this time.

## 7.3 Regional synthesis and the development of the Connemara massif

The structural evolution of the study area is largely consistent with the rest of the Connemara massif, whereas the metamorphic history differs from that seen elsewhere in the massif. The rocks of the study area show no evidence of the later, high temperature event recorded in the rocks of south Connemara (Yardley, Barber & Gray 1987). This event is ascribed to the contact effects of the voluminous intrusive bodies in the south. It is likely, therefore, that these effects did not extend into the study area.

Initial geochronological studies within the rocks of the Connemara massif (e.g. Leggo, Compston & Leake 1966, Moorbath, Bell, Leake & McKerrow 1968, Pidgeon 1969) enabled an absolute deformation and intrusion chronology to be determined. However, recent studies (Kennan, Feely & Mohr 1987 and Jagger, Max, Aftalion & Leake 1988) have cast doubt on two of the *'golden spikes'* in the Connemara massif, the intrusion ages of the syn - $D_2$ ultrabasic bodies and the late / post tectonic Oughterard granite. Table 7.1 presents a summary of the timing of events in the Connemara massif in the light of the recent work. Work by Elias, MacIntyre, & Leake (1988) has attempted to determine the cooling history of the Connemara massif. The results of such geochronological studies provide a temporal framework within which the evolution of the study area and its relation to the development of the Connemara massif as a whole can be interpreted.

| Sequence of geological events | Isotopic age | Geological age | Notes |
|---|---|---|---|
| Deposition of Dalradian sediments | =( 700 M.a. A2W<br>)572 ± 20 M.a A2W | Late Precambrian<br>Early Cambrian | Scottish Dalradian deposition age 700 - 600 M.a. Anderton (1982) |
| $D_1$ deformation | ——— | ——— | Fabrics only locally preserved (porphyroblast inclusion trails etc) |
| $D_2$ deformation,<br>Barrovian regional metamorphism,<br>Intrusion of Connemara ultrabasics. | 490 ± 1 M.a. D3Z | Tremadoc/Arenig | Zircon age for the Cashel gabbro |
| Connemara migmatite suite<br>Peak of 'Buchan' metamorphism | 480 to 440 M.a. A1MAm2MW<br>480 ± 10 M.a. E (mean value) | Arenig/Ashgill | Associated with rapid uplift and cooling |
| $D_3$ deformation | 426 ± 10 M.a. C2AmW | Wenlock | Rapid uplift<br>Age of movement on the Mannin thrust, probable culmination of $D_3$ movements. |
| $D_4$ deformation, formation of the Connemara antiform | ——— | ——— | ——— |
| Intrusion of post - tectonic granitoids | c. 400 M.a. B<br>(407 ± 23 M.a B2W) | | Intrusion of the Oughterrard granite. |

Data sources
A: Moorbath, Bell, Leake & McKerrow (1968)
B: Kennan, Feely & Mohr (1987)
C: Kennan & Murphy (1987)
D: Jagger, Max, Aftalion & Leake (1988)
E: Elias, MacIntyre & Leake (1988)

Dating methods
1: K - Ar
2: Rb - Sr
3: $^{207}Pb$ - $^{206}Pb$
W: whole rock
Z: zircon
M: mica
Am: amphibole

**Table 7.1: The sequence and absolute timings of events in the Connemara massif.**

Recent plate tectonic syntheses which consider the Caledonides in the light of terrane models, (e.g. Dewey & Shackleton 1984, Soper & Hutton 1984, Barker & Gayer 1985, Hutton 1987) interpret Connemara as being a suspect / displaced terrane, having displaced away from the main Dalradian outcrop on the Laurentian margin by collision - related sinistral strike - slip movements. More detailed plate tectonic models consider the sequential evolution of the Connemara massif within a plate collision involving significant amounts of sinistral strike - slip (Figure 7.2). These plate tectonic models, used in conjunction with the geochronological data and the evidence presented in this work, enable an overall event sequence for the Connemara massif to be determined.

Initial deposition of the metasediments of the Connemara Dalradian probably occurred between 700 and 600 M.a., in an extending ensialic basin on the Laurentian continental margin (Anderton 1985). The subsidence of this basin was largely fault controlled and the later stages of extension were marked by the compartmentalization of the initially shallow shelf setting into a series of small basins. Anderton (1985) suggests that the thickness and facies variations seen within the Scottish Dalradian are largely fault controlled, and it is likely that a similar mechanism operated during the deposition of the Connemara Dalradian (e.g. Ferguson & Al - Ameen 1986). The extension of the basin was also associated with igneous activity, both extrusive and high level intrusive bodies being evident in the Scottish Dalradian and numerous amphibolite bodies being present in Connemara.

With the end of basin subsidence and the onset of collision, the evolution of the Connemara Dalradian begins a structural and metamorphic phase comparable with the Scottish Dalradian, although the later history of Connemara is somewhat different from the Scottish Dalradian. A phase of nappe scale folding, associated with the emplacement of the Connemara ultrabasic bodies, and the development of their contact aureoles (the DCD in the study area) occurred around 490 ± 1 M.a. (Jagger *et al.* 1988), a timing comparable to the Grampian deformation in Scotland which led to the development of the Tay Nappe. The nappe folds in Connemara ($F_2$ *Derryclare anticline* folds

**Figure 2.2: Field appearance of the Bennabeola Quartzite Formation showing the typical pale weathering colour and crustose lichen. Lens cap is 49mm diameter.**


**Figure 2.3: Schematic diagram showing the lateral variation in the Streamstown Formation in the central Tully Mountain area . DP: Derryinver Psammite Member, DS: Derryinver Siliceous Psammite Member, DB: Dawrosbeg Striped Psammite Member, DG: Doongill garnet semipelite member, RS: Roeillaun Schist Member. Striped ornament indicates Bennabeola Quartzite Fm, brick ornament indicates the Lakes Marble Fm.**

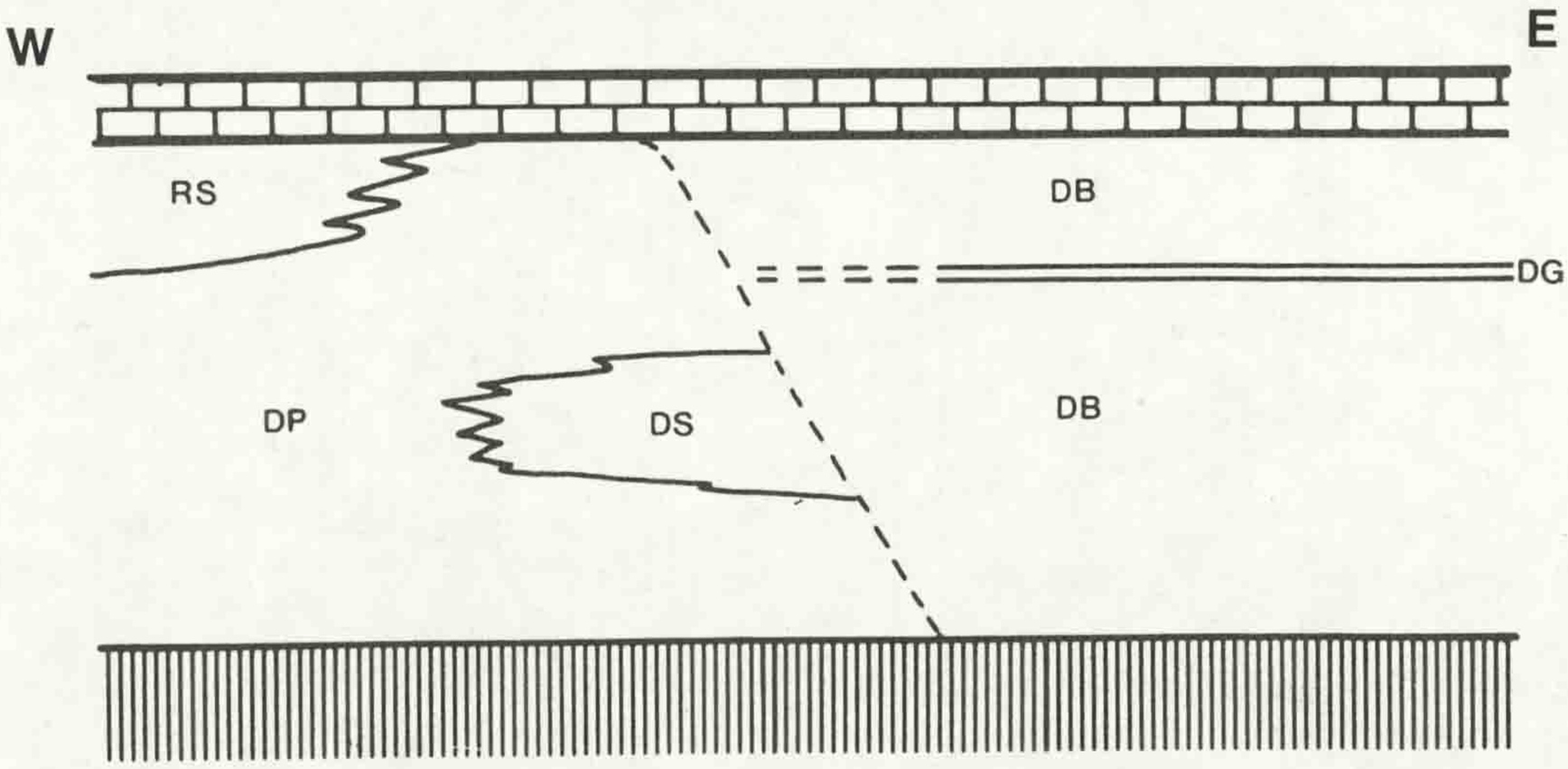

Figure 7.2: Stylized model for the evolution of the British Isles sector of Iapetus from Arenig to mid - Devonian times, Hutton (1987).

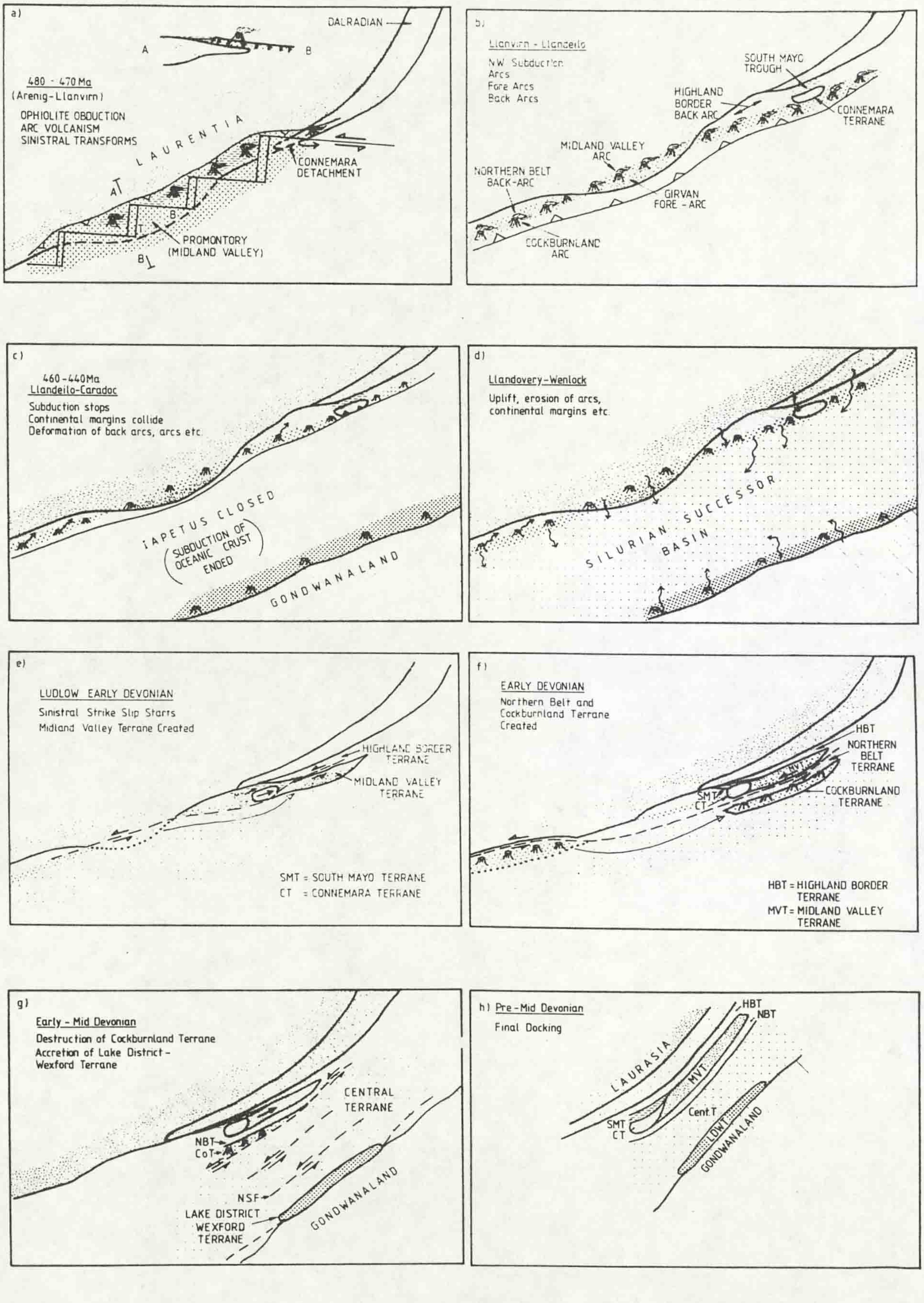

of Tanner & Shackleton 1979) are generally evident only from mapping stratigraphic repetition around later folds, although early large scale south facing and closing folds have been reported (e.g. Bremner & Leake 1980, Treloar 1982). The original orientation of these nappe folds was generally flat - lying to sub - horizontal. A southward emplacement direction has been postulated for the nappes (Treloar 1982), although the evidence cited in this work for the orientations of $L_2$ stretching lineations and $F_2$ sheath fold closures {3.2} suggests that a significant component of E - W simple shear, not consistent with south - directed emplacement, was involved in the $D_2$ deformation. Hutton & Dewey (1986) suggest that the Connemara massif remained attached to the main Dalradian outcrop during this period of nappe emplacement, the whole system being involved in a period of basin closure with oblique, NW directed, subduction and local ophiolite obduction. Ellis (1986) and Ellis & Watkinson (1987) show that oblique subduction regimes are typically associated with significant ductile extension and the formation of stretching lineations which run sub - parallel to large scale fold axes and to the length of the orogen. Although the evidence for the orientation of the nappe scale fold axes is limited, evidence for orogen parallel extension in the Connemara massif during the $D_2$ deformation is clear. The plate tectonic setting of the massif, close to a NW oblique subduction zone, suggests that a transpressive regime, compression associated with strike - slip movement, is likely to have controlled the deformation of the Connemara Dalradian.

The initial movements on the Renvyle - Bofin slide also occur during $D_2$, evidence in this work suggesting movement as a thrust during $D_2$, emplacing the Kylemore Fm over the rocks to the south, although the dominant E - W extension lineations in the study area suggest that the slide was principally a strike - slip feature. It is possible that the RBS is a mid - crustal structure analogous to the fault surfaces seen within upper - crustal transpressional structures (flower structures) (e.g. Lewis, Ladd & Bruns 1988) and had elements of both strike - slip and dip - slip in its movement.

Subsequent to the formation of the nappe scale folds the Connemara massif was displaced away from the main Dalradian

massif, either through the obduction of a sinistral tranform fault (Hutton 1987) or by the braiding of the strike - slip faults developed in the collision zone (Soper & Hutton 1984, Barker & Gayer 1985). The element of strike - slip movement involved in the development of the $D_2$ structures in the study area suggests that the detachment of the Connemara massif from the main Dalradian outcrop through movement on a braided tranpressional fault system may have occurred during $D_2$. It is possible that the thrust movement on the RBS is related to the plate convergence, in a manner similar to the convergence - related thrusting seen in recent oblique collision systems (Lewis *et al.* 1988), although modified by elements of lateral movement.

The peak of metamorphism due to the re - equilibration of the thrust - perturbed isotherms, the *Barrovian* metamorphism of Yardley, Barber & Gray (1987), was reached at around the same time as the detachment of the Connemara massif occurred. This metamorphism produced the peak regional assemblages (Grt - Bt - St) seen in the study area. However, the continuation of north - westerly directed subduction to the south of the Connemara massif led to the emplacement of large volumes of island arc related calc - alkaline magma in the south of Connemara (Yardley & Senior 1982). The heat added to the massif by the emplacement of such large volumes of magma, along with rapid uplift rates (Elias, MacIntyre & Leake 1988), led to the high temperature, low pressure metamorphism associated with the development of the Connemara migmatite belt (Yardley, Barber, Gray 1987). The timing of this metamorphism is not well constrained; a range of ages between 480 - 440 M.a. are cited by Moorbath, Bell, Leake & McKerrow (1968). Evidence for metamorphism related to the calc - alkaline igneous bodies is not seen in the study area.

The $D_3$ deformation and the large scale north - facing folds related to it have been related by Yardley, Barber & Gray (1987), Leake (1986) and Ferguson & Al - Ameen (1986) to the *en masse* uplift of the massif, possibly through ramp climb on the Mannin thrust (Yardley *et al.* 1987). The north facing $F_3$ folds may thus represent backfolds formed during the northerly directed collapse of the overthickened metamorphic pile. Such a collapse may have led to the reactivation of the RBS with a movement

vector different from its original sense. A collapse and thinning of the orogen would lead to rapid uplift rates, as noted by Elias, MacIntyre & Leake (1988) who describe a period of closure of K - Ar systems in minerals across much of the Connemara massif at around 480 M.a., although the overall timings produced are complicated by the movement of tectonic slides during $D_3$. Anderton (1988) suggests that many of the major fold structures developed in the Scottish Dalradian are related to the syn - sedimentary intrabasinal faults and the stratigraphic variation related to these folds. It is possible that some of the folding in Connemara is related to early fault locations, either through reactivation of the fault or through lithological thickness variation providing heterogeneities on which folds nucleated. It is possible that the numerous tectonic slides seen in Connemara represent reactivated faults, although information on the relations of these features is limited at present.

At the time the $D_3$ deformation was occurring Connemara was lying inboard of the subduction zone, adjacent to (Bluck & Leake 1986), or docked with, the subsiding South Mayo Trough (Hutton & Dewey 1986). Soper & Hutton (1984) have suggested that the $D_3$ deformation was due to an overall N - S compression within the continental margins related to the cessation of subduction. The structures seen in the study area produced in the $D_3$ deformation indicate a dominant N - S shortening, although lineations associated with the RBS suggest its reactivation in a strike - slip sense {3.5}. It is possible that strike - slip movement, associated with the N - S collision, was localized on the RBS during $D_3$.

Movement on the Mannin thrust, dated at 426 ± 10 M.a. (Kennan & Murphy 1987), ended the $D_3$ deformation and emplaced the Connemara allochthon over a sequence of acid volcanics of probable Ordovician age (Leake, Tanner, Singh & Halliday 1983). This movement is related by Kennan & Murphy (1987) to the docking of the Connemara massif with the South Mayo Trough and the initiation of folding within the Ordovician sedimentary sequence.

A sequence of Silurian sedimentary rocks of upper Llandoverian age unconformably overlie the Dalradian and Ordovician, providing

a younger age limit for the terrane accretion event. Bluck & Leake (1986) suggest that the Dalradian had completed its uplift path significantly before the deposition of the Silurian, and had undergone a *'prolonged weathering cycle'* prior to the deposition of the terrane linking sediments.

With the cessation of movement on the Mannin thrust the continued shortening of the continental margin was accommodated by the formation of the Connemara antiform, along with folding and the reactivation of strike - slip faults in the Ordovician and Silurian rocks (Hutton & Dewey 1986). It is possible that the RBS was again reactivated during the formation of the Connemara antiform, possibly acting as a normal fault, downthrowing to the north, as suggested by Leake (1986).

End - Silurian events, probably related to continued N - S continental collision (Soper & Hutton 1984), led to sinistral shear between the terranes, although the movement was concentrated on the bounding faults between the terranes (Hutton & Dewey 1986). This period was associated with the intrusion of voluminious granitic bodies into much of Connemara.

The evolution of the Connemara massif can be considered as part of a long - lived oblique continental collision, with deformation switching between dominantly compressive to dominantly strike - slip over time.

The area studied in this work differs from much of the Connemara massif in that it contains evidence of the early stages of the metamorphic, igneous and structural history which are generally overprinted by later events in other parts of the Connemara massif. As such, the study area provides an important 'window' into the early history of the Connemara massif, preserving the early Barrovian metamorphism along with pre - regional contact metamorphism and evidence for the mechanisms of emplacement of the DCD. The RBS, an important tectonic boundary, is preserved in the study area and, although poorly exposed, shows evidence of a long and varied movement history.

## 7.4 Suggestions for possible future work

Although the results of this work shed some light on the important events early in the evolution of Connemara massif there

is much scope for further investigations both within the study area and in the rest of the Connemara massif.

(i) An investigation of the fabrics and microstructures associated with the Renvyle - Bofin slide, especially on the island of Inishbofin where the slide is better exposed, in order to refine the movement history of this feature.

(ii) Further to the study of Kanaris - Sotiriou & Angus (1976) an investigation of the petrology, petrogenesis, internal structure and contact relations of the gabbroic bodies, particularly the Currywongaun and Doughruagh intrusions , would provide important evidence as to the relations of these bodies to the south Connemara ultrabasic bodies.

(iii) Microstructure and fabric analyses of the aureole zones of the Dawros peridotite and Creggaun gabbro to elucidate the local kinematic history and attempt to clarify the emplacement mechanisms.

(iv) Further P - T path modelling, based on garnet zoning, coupled with structural investigations, both within the study area and in the main Connemara massif, to determine the overall 'particle paths' followed by rock units during the metamorphic evolution of the massif. This work would be helpful in determining the effects of the many tectonic slides within the Connemara Dalradian.

(v) Detailed study of the migmatites of the DCD aureole zone to determine the melting reactions involved and the interactions between deformation and migmatite development.

(vi) Further application of garnet zoning P-T path modelling in areas with a well constrained tectonic framework which would provide a direct test on the validity of the modelling system.

# Appendix A

## Gamma - spectrometer survey techniques

In order to assess the degree of heat production due to radiogenic elements (U, Th and K) a reconnaissance field survey using a portable gamma - ray analyser was undertaken. The spectrometer used was a Exploranium type DISA 300 intergral gamma spectrometer, kindly loaned by Dr M.A Khan of Leicester University. The field sampling method used was similar to that of Cassidy (1981), although the variablity in outcrop over the northern parts of the study area prevented the use of a regularly spaced sampling grid. The raw field data was recalculated to give both stripped count rates and concentrations (ppm) using the method suggested by Cassidy. The magnitude of heat production due to radioelement decay was calculated using the formula in Drury & Lewis (1983). The stripped data, calculated ppm and heat production values are tabulated in {Appendix C}.

# Appendix B

X - ray fluorescence spectrometry

Sample preparation: Samples selected for chemical analysis were typically large ( >1kg in weight), although the removal of weathered external surfaces and altered joint / fracture planes resulted in final weights being somewhat lower. Inspite of efforts to remove any alteration and use only the freshest material in the analysis some altered material may still be present in the final analyses.

The 'clean' material was first crushed to grit size and 100g palced in a tungsten carbide tema for 4 - 5 minutes (a 5g sample of homogenised powder was removed after 30 seconds grinding for FeO determinations, although no analyses for FeO were made). The resultant powder was homogenised and a sample of 10 - 15g passed through a 53u sieve (any powder too coarse to pass through the sieve was reduced by hand in an agate pestle and morter) this powder was dried at 110°c overnight and used in the production of pressed pellets and fusion discs. Pressed powder pellets were used for the analysis of MgO, MnO, $Na_2O$ and trace elements, and were prepared by mixing 7g of <53um fraction powder with 15 drops of Moviol binder solution (4g Moviol + 10ml ethanol + 50ml distilled water). The resultant mixture was pressed into a 4cm diameter disc under 5 tons pressure. Glass fusion discs were used in the analysis of major elements and were prepared by fusing a mixture of approx 0.6g < 53u rock powder and approx 3.3g of a flux at ≃ 990°c and casting the melt on to 4cm diameter aluminium platterns. The resultant glass disc was mounted on a backing disc for analysis.

Analytical proceedure: Major elements ($SiO_2$, $TiO_2$, $Al_2O_3$ , total iron as $Fe_2O_3$, MnO, MgO, CaO, $Na_2O$, $K_2O$, $K_2O$ and $P_2O_5$) and trace elements (Ba, Ce, Cr, La, Nd, Pb, Rb, Sc, Sr, Th V, Y, Zn and Zr) were determined by XRF at the Dept of Earth Sciences, Liverpool University. The equipment used consisted of a Siemens sequential X - ray spectrometer SRS - 1 powered by a Siemens Krystalloflex - 4 generator and controlled by an Apple II+ via a Hiltonbrooks controller and drive unit. Major elements were determined using Cr primary beam radiation at 50kV and 40mA,

trace elements using W primary beam radiation generated at 45kV and 60mA. Major elements were analysed after the procedure of Naggar & Atherton (1971) with a similar method used in determining trace elements (although a correction for major element concentration and interference between trace elements after Brown, Hughes & Esson (1973) was applied to the trace element data). Accuracy in major element analyses was checked by analysing a glass disc of a standard (USGS standard rock G2, Flanagan, 1973) at intervals during the analysis of the 49 unknown compositions. The precision for major element analyses is given below (data courtesy of J. Sharman).

| Element | x | $sigma_{n-1}$ | c% |
|---|---|---|---|
| $SiO_2$ | 72.60 | 0.24 | 0.33 |
| $TiO_2$ | 0.30 | 0.0041 | 1.36 |
| $Al_2O_3$ | 14.27 | 0.094 | 0.66 |
| $Fe_2O_3$ | 1.76 | 0.015 | 0.86 |
| MnO | 0.16 | 0.0040 | 2.46 |
| MgO | 1.46 | 0.046 | 3.15 |
| CaO | 1.86 | 0.0063 | 0.34 |
| $Na_2O$ | 5.81 | 0.101 | 1.74 |
| $K_2O$ | 4.10 | 0.011 | 0.27 |
| $P_2O_5$ | 0.08 | 0.012 | 15.1 |

The data produced by these analyses is presented in {Appendix C}.

Neutron activation analysis

In an attempt to quantify the results of field measurements of U, Th and radiogenic K selected samples of pelitic, semi - pelitic, amphibolitic and ultrabasic material were analysed for U, Th and certain other trace elements by instrumental neutron activation analysis. The procedure, similar to that of Brunfelt & Steinnes (1969), was carried out by Mr M.S. Brotherton at the Universities' Research Reaction at Risley near Warrington.

The raw data are tabulated in {Appendix C}.

Electron probe analysis

Sample preparation: Examination of ordinary thin sections enabled the selection of rocks suitable for electron microprobe analysis. New thin sections of these lithologies were produced, using where possible the offcuts remaining after the production of the ordinary sections. The new thin sections were prepared as normal thin sections, being cut and ground to ≃ 40 um , the final polishing being made using progressively finer diamond pastes (6um down to 1/4um). The resulting highly polished surface was made electrically conducting by coating it in a carbon film.

Analytical procedure: Two electron microprobe systems were used, a Cambridge Instruments Microscan 5 at University College, London and a modified Cambridge Instruments Geoscan at Manchester University. In both cases energy dispersive spectrometer (E.D.S) analyses were performed, using an accelerating voltage of 10 - 15kV, specimen current of 3nA (on cobalt) and take off angle of 75°. The beam diameter was adjusted to give 2 - 7 um on the specimen. Any drift in beam current was checked by making regular (1/2 to 1 hourly) analyses of a specific plagioclase feldspar and adjusting the controls to give 100% totals. X - ray spectra were converted into chemical analyses using Link Systems ZAF4/FLS software (Statham, 1977). It should be noted that the software did not include results where elements were present at <2 sigma levels (approx 0.2 wt% for most elements), any elements present at such low levels being recorded as a zero in the tabulated data. The data is presented in {Appendix C}.

## Table of contents

interbedded thin (20 - 50mm) grit-rich quartzitic and psammitic units. Thin psammitic beds are evident in the quartzite up to 20m below the contact zone.

2.1.2.1.2 Streamstown Formation

The Streamstown Formation shows a high degree of lateral variation (Figure 2.3) with three main lithological types being evident:

(i) Pale weathering, clean, gritty psammites (Derryinver psammite Member) and impure quartzites (Derryinver siliceous psammite Member);

(ii) Darker weathering 'striped' psammites and semipelites (Dawrosbeg striped psammite Member and Doongill garnet semipelite Member);

(iii) Mica rich schistose pelites (Roeillaun schist Member).

Derryinver psammite Member: This lithology is best developed in the Derryinver area to the south - east of Tully Mountain where it reaches its maximum thickness {Enclosure 1}. It consists of pale brown/buff coloured massive psammites with thin (up to 10mm) pink feldspar rich horizons and rare, scattered, semipelitic lenses (reaching 100mm by 1m). The dominant fabric is a spaced foliation, often defined by fine ( <1mm) partings of muscovite and chlorite. A variably developed grain shape lineation is evident in the quartz grains and grit clasts. Sedimentary structures are rare. Thin (5 - 10mm) grit bands locally show fining up. The contact of this unit with the underlying Bennabeola quartzite is marked by a grit-rich zone best seen around [GR 573 603].

Derryinver siliceous psammite Member: This unit overlies the Derryinver psammite and occurs only in the Ardagh - Derryinver area on the south coast of Renvyle peninsula. Its contact with the psammite is transitional, the psammite becoming increasingly siliceous over 5 - 10m. The siliceous psammite is a pink/brown weathering quartz rich psammite, often showing a saccharoidal texture, rarely containing feldspar clasts. These feldspars occur as fine ( <0.5mm) clasts which show extreme flattening in the tectonic foliation. A strong grain shape

## Appendix C

1, Whole rock XRF data: Lithology denoted by abbrevation
BQ = Bennabeola Quartzite Formation
ST = Streamstown Formation (Member not known)
ST2 = Streamstown Fm, Derryinver Siliceous psammite Mb
ST5 = Streamstown Fm, Roeilluan schist Mb
LM2 = Lakes Marble Formation, Doongill amphibolite Mb
KF = Kylemore Formation (R indicates regional, C indicates contact)
KFA = Kylemore Formation amphibolitic lithology
P = peridotitic lithologies

2, Mineral chemistry data
i, Garnet
ii, Biotite
iii, Muscovite (R indicates regional, C indicates contact)
iv, Chlorite (all lithologies)
v, Plagioclase feldspar (R indicates regional, C indicates contact)
vi, K - feldspar (contact only)
vii, Staurolite (regional only).

3, Radiogenic heat producing element concentrations
KF indicates Kylemore Formation (R indicates regional metamorphic assemblages, C inducates contact metamorphic assemblages)
ST indicates Streamstown Formation
LM indicates Lakes Marble Formation
BQ indicates Bennabeola Quartzite Formation
G indicates gabbroic lithologies
P indicates peridotitic lithologies

NB, The values of K% used in the calculation of heat production values are derived from analyses in this work unless stated otherwise.
Gabbro: Mean K% value of data from Boyle, McCarthy & Stewart (1987).
BQ: Mean K% value of quartzites from Senior & Leake (1978).

| Sample | 69631 | 69587 | D84-10 | 66795 | 66801 | 68760 | 68780 | 68790 | 68793 | 68804 | 68806 | 69215 | 69224 | 69230 | 69233 | 69236 | 68238 | 69242 | 69250 | 69259 |
|---|---|---|---|---|---|---|---|---|---|---|---|---|---|---|---|---|---|---|---|---|
| Code | LM2 | LM2 | BQ | KFC | KFC | BQ | KFC | P | KFC | KFC | KFR | KFC | P | ST5 | KFR | KFR | KFR | KFR | KFR | KFR |
| SIO2 | 48.96 | 50.14 | 91.54 | 67.83 | 66.97 | 80.80 | 66.24 | 48.32 | 57.92 | 61.00 | 58.06 | 65.63 | 51.46 | 48.66 | 48.20 | 70.54 | 56.90 | 57.16 | 68.32 | 54.41 |
| TIO2 | 0.92 | 1.34 | 0.14 | 1.55 | 1.05 | 0.32 | 1.36 | 1.24 | 1.54 | 1.79 | 1.75 | 1.07 | 0.19 | 2.09 | 2.83 | 0.79 | 1.89 | 2.25 | 1.14 | 1.80 |
| AL203 | 14.41 | 13.87 | 4.04 | 14.84 | 13.25 | 7.86 | 15.11 | 11.86 | 17.93 | 15.86 | 16.48 | 14.40 | 7.21 | 24.51 | 20.43 | 13.32 | 17.96 | 18.07 | 13.10 | 19.04 |
| FE203 | 13.02 | 13.58 | 0.13 | 6.28 | 8.87 | 0.84 | 7.74 | 15.31 | 12.25 | 9.62 | 11.23 | 7.77 | 8.16 | 10.26 | 13.51 | 5.35 | 10.95 | 9.80 | 7.29 | 10.28 |
| MNO | 0.18 | 0.25 | 0.01 | 0.07 | 0.08 | 0.02 | 0.09 | 0.22 | 0.20 | 0.05 | 0.33 | 0.11 | 0.13 | 0.11 | 0.12 | 0.09 | 0.12 | 0.06 | 0.08 | 0.07 |
| MGO | 7.57 | 6.86 | 0.13 | 2.28 | 2.07 | 0.38 | 2.59 | 7.52 | 3.16 | 2.54 | 1.98 | 3.31 | 16.35 | 2.32 | 3.38 | 1.40 | 2.60 | 2.73 | 2.36 | 2.61 |
| CAO | 9.69 | 7.40 | 0.26 | 1.73 | 1.49 | 0.26 | 1.15 | 8.75 | 2.07 | 2.11 | 1.43 | 0.98 | 11.43 | 0.93 | 0.95 | 1.46 | 1.94 | 1.66 | 0.77 | 1.51 |
| NA20 | 2.23 | 3.76 | 0.23 | 1.34 | 1.59 | 0.66 | 1.05 | 3.33 | 0.81 | 1.70 | 2.16 | 0.89 | 0.92 | 2.30 | 0.79 | 0.72 | 2.22 | 1.98 | 1.92 | 1.56 |
| K20 | 0.77 | 0.23 | 1.98 | 1.79 | 2.33 | 2.97 | 2.06 | 0.32 | 1.88 | 2.39 | 3.16 | 2.31 | 0.34 | 3.70 | 4.46 | 3.28 | 2.72 | 3.24 | 2.55 | 3.99 |
| TOTAL | 97.75 | 97.43 | 98.46 | 97.71 | 97.70 | 94.11 | 97.39 | 96.87 | 97.76 | 97.06 | 96.58 | 96.47 | 96.19 | 94.88 | 94.67 | 96.95 | 97.30 | 96.95 | 97.53 | 95.27 |
| BA | 164.00 | 0.00 | 667.00 | 1477.00 | 1026.00 | 381.00 | 1140.00 | 36.00 | 437.00 | 1535 | 551.00 | 993.00 | 1.00 | 1095.00 | 1325.00 | 773.00 | 634.00 | 714.00 | 772.00 | 791.00 |
| CE | 10.00 | 22.00 | 15.00 | 41.00 | 53.00 | 29.00 | 51.00 | 7.00 | 37.00 | 73.00 | 173.00 | 56.00 | 19.00 | 204.00 | 176.00 | 63.00 | 107.00 | 116.00 | 51.00 | 113.00 |
| CO | 64.00 | 57.00 | 145.00 | 105.00 | 72.00 | 117.00 | 87.00 | 50.00 | 97.00 | 80.00 | 66.00 | 78.00 | 64.00 | 50.00 | 49.00 | 72.00 | 57.00 | 54.00 | 58.00 | 44.00 |
| CR | 436.00 | 343.00 | 14.00 | 105.00 | 90.00 | 16.00 | 101.00 | 293.00 | 175.00 | 113.00 | 109.00 | 106.00 | 1857.00 | 145.00 | 112.00 | 99.00 | 115.00 | 108.00 | 105.00 | 121.00 |
| LA | 5.00 | 10.00 | 9.00 | 22.00 | 29.00 | 17.00 | 27.00 | 0.00 | 21.00 | 40.00 | 94.00 | 31.00 | 9.00 | 116.00 | 94.00 | 34.00 | 56.00 | 55.00 | 26.00 | 61.00 |
| ND | 11.00 | 20.00 | 14.00 | 23.00 | 27.00 | 22.00 | 29.00 | 9.00 | 17.00 | 37.00 | 91.00 | 31.00 | 12.00 | 106.00 | 92.00 | 35.00 | 61.00 | 61.00 | 30.00 | 63.00 |
| NI | 78.00 | 69.00 | 4.00 | 35.00 | 50.00 | 5.00 | 88.00 | 74.00 | 90.00 | 65.00 | 67.00 | 73.00 | 400.00 | 48.00 | 78.00 | 39.00 | 57.00 | 42.00 | 53.00 | 50.00 |
| PB | 5.00 | 14.00 | 5.00 | 20.00 | 16.00 | 12.00 | 17.00 | 9.00 | 11.00 | 19.00 | 30.00 | 12.00 | 4.00 | 26.00 | 23.00 | 17.00 | 26.00 | 21.00 | 19.00 | 22.00 |
| RB | 14.00 | 4.00 | 56.00 | 41.00 | 51.00 | 96.00 | 46.00 | 5.00 | 58.00 | 49.00 | 92.00 | 52.00 | 6.00 | 115.00 | 108.00 | 91.00 | 96.00 | 116.00 | 71.00 | 142.00 |
| SC | 52.00 | 38.00 | 1.00 | 10.00 | 10.00 | 0.00 | 9.00 | 40.00 | 38.00 | 10.00 | 13.00 | 8.00 | 32.00 | 29.00 | 18.00 | 7.00 | 16.00 | 11.00 | 10.00 | 19.00 |
| SR | 275.00 | 191.00 | 26.00 | 305.00 | 217.00 | 22.00 | 170.00 | 256.00 | 147.00 | 321.00 | 221.00 | 129.00 | 45.00 | 202.00 | 82.00 | 161.00 | 179.00 | 167.00 | 153.00 | 120.00 |
| TH | 0.00 | 1.00 | 0.00 | 7.00 | 12.00 | 6.00 | 14.00 | 0.00 | 1.00 | 13.00 | 30.00 | 13.00 | 0.00 | 38.00 | 34.00 | 10.00 | 21.00 | 21.00 | 11.00 | 23.00 |
| V | 266.00 | 309.00 | 8.00 | 129.00 | 104.00 | 16.00 | 157.00 | 365.00 | 227.00 | 178.00 | 145.00 | 147.00 | 138.00 | 193.00 | 174.00 | 73.00 | 150.00 | 157.00 | 110.00 | 144.00 |
| Y | 30.00 | 27.00 | 13.00 | 18.00 | 9.00 | 20.00 | 22.00 | 32.00 | 63.00 | 14.00 | 51.00 | 25.00 | 28.00 | 70.00 | 58.00 | 22.00 | 45.00 | 39.00 | 24.00 | 47.00 |
| ZN | 75.00 | 103.00 | 0.00 | 77.00 | 119.00 | 3.00 | 99.00 | 103.00 | 186.00 | 179.00 | 158.00 | 92.00 | 36.00 | 113.00 | 191.00 | 89.00 | 92.00 | 64.00 | 99.00 | 100.00 |
| ZR | 54.00 | 85.00 | 129.00 | 421.00 | 377.00 | 437.00 | 414.00 | 61.00 | 512.00 | 444.00 | 498.00 | 319.00 | 11.00 | 325.00 | 664.00 | 442.00 | 432.00 | 451.00 | 447.00 | 393.00 |

**Whole rock chemistry data**

| Sample | 69263 | 68268 | 69270 | 69273 | 69275 | 69277 | 69278 | 69590 | 69619 | 69623 | 69625 | 69627 | 69635 | 69636 | 71890 | 71898 | 71900 | 71901 | 71906 | 71912 |
|---|---|---|---|---|---|---|---|---|---|---|---|---|---|---|---|---|---|---|---|---|
| Code | KFR | ST | LM2 | LM2 | ST5 | ST | LM2 | KFA | KFC | ST5 | ST5 | ST5 | KFC | KFR | P | KFR | KFA | KFC | KFC | KFR |
| SI02 | 70.68 | 50.90 | 51.52 | 46.58 | 50.45 | 54.00 | 49.31 | 49.78 | 62.53 | 50.42 | 50.38 | 52.97 | 67.68 | 50.91 | 52.45 | 68.73 | 48.00 | 60.60 | 46.49 | 51.17 |
| TI02 | 1.30 | 1.73 | 1.17 | 0.51 | 2.58 | 1.32 | 0.77 | 1.92 | 1.26 | 1.96 | 2.24 | 1.60 | 1.56 | 1.63 | 0.14 | 0.92 | 1.94 | 1.15 | 2.14 | 2.09 |
| AL203 | 11.47 | 21.83 | 12.97 | 15.67 | 20.74 | 22.16 | 12.67 | 11.50 | 15.69 | 23.86 | 21.49 | 21.39 | 14.28 | 21.74 | 3.10 | 14.68 | 12.65 | 15.83 | 25.31 | 21.53 |
| FE203 | 6.96 | 11.03 | 12.54 | 11.74 | 10.49 | 8.33 | 15.57 | 14.50 | 8.84 | 10.13 | 11.88 | 8.55 | 7.13 | 13.43 | 5.88 | 6.80 | 16.69 | 8.98 | 13.58 | 10.82 |
| MN0 | 0.07 | 0.10 | 0.30 | 0.16 | 0.08 | 0.09 | 0.19 | 0.18 | 0.09 | 0.14 | 0.09 | 0.08 | 0.09 | 0.15 | 0.14 | 0.06 | 0.21 | 0.23 | 0.10 | 0.10 |
| MG0 | 1.44 | 2.60 | 8.05 | 10.29 | 3.33 | 2.39 | 6.21 | 7.98 | 2.17 | 2.51 | 3.10 | 2.07 | 1.59 | 2.25 | 22.06 | 1.58 | 6.15 | 2.22 | 3.48 | 2.70 |
| CA0 | 1.64 | 1.41 | 8.61 | 9.55 | 1.55 | 1.82 | 8.84 | 9.57 | 1.40 | 0.98 | 1.23 | 2.60 | 1.13 | 0.86 | 14.85 | 0.55 | 9.04 | 1.55 | 1.34 | 1.21 |
| NA20 | 2.09 | 1.70 | 2.74 | 2.00 | 1.78 | 1.66 | 3.39 | 1.02 | 1.13 | 2.38 | 1.20 | 3.02 | 1.27 | 1.52 | 0.54 | 1.46 | 1.24 | 2.32 | 1.04 | 1.36 |
| K20 | 2.32 | 3.57 | 0.05 | 0.44 | 4.13 | 3.79 | 0.27 | 1.38 | 3.39 | 3.17 | 4.06 | 3.33 | 3.11 | 4.52 | 0.09 | 2.80 | 1.64 | 3.78 | 3.43 | 4.06 |
| TOTAL | 97.97 | 94.87 | 97.95 | 96.94 | 95.13 | 95.56 | 97.22 | 97.83 | 96.50 | 95.55 | 95.67 | 95.61 | 97.84 | 97.01 | 99.25 | 97.58 | 97.56 | 96.66 | 96.91 | 95.04 |
| BA | 609.00 | 804.00 | 61.00 | 33.00 | 879.00 | 670.00 | 0.00 | 140.00 | 1001.00 | 1085. | 881.00 | 764.00 | 1017.00 | 873.00 | 0.00 | 659.00 | 247.00 | 650.00 | 15.83 | 814.00 |
| CE | 50.00 | 130.00 | 21.00 | 7.00 | 204.00 | 171.00 | 13.00 | 20.00 | 94.00 | 166.00 | 157.00 | 163.00 | 77.00 | 125.00 | 0.00 | 102.00 | 4.00 | 1.31 | 215.00 | 117.00 |
| CO | 73.00 | 46.00 | 62.00 | 64.00 | 45.00 | 54.00 | 51.00 | 73.00 | 76.00 | 59.00 | 74.00 | 42.00 | 79.00 | 55.00 | 60.00 | 60.00 | 73.00 | 56.00 | 73.00 | 51.00 |
| CR | 103.00 | 102.00 | 166.00 | 413.00 | 141.00 | 121.00 | 72.00 | 193.00 | 98.00 | 95.00 | 104.00 | 86.00 | 76.00 | 92.00 | 3254.00 | 73.00 | 99.00 | 103.00 | 195.00 | 75.00 |
| LA | 24.00 | 74.00 | 5.00 | 5.00 | 106.00 | 98.00 | 8.00 | 6.00 | 55.00 | 85.00 | 81.00 | 88.00 | 41.00 | 60.00 | 0.00 | 51.00 | 0.00 | 72.00 | 11.00 | 61.00 |
| ND | 30.00 | 70.00 | 17.00 | 8.00 | 104.00 | 89.00 | 11.00 | 17.00 | 50.00 | 93.00 | 84.00 | 87.00 | 39.00 | 67.00 | 0.00 | 54.00 | 13.00 | 68.00 | 110.00 | 62.00 |
| NI | 34.00 | 47.00 | 90.00 | 218.00 | 53.00 | 53.00 | 31.00 | 101.00 | 53.00 | 46.00 | 62.00 | 43.00 | 39.00 | 57.00 | 222.00 | 41.00 | 43.00 | 55.00 | 100.00 | 66.00 |
| PB | 18.00 | 20.00 | 10.00 | 2.00 | 27.00 | 25.00 | 14.00 | 10.00 | 24.00 | 26.00 | 23.00 | 34.00 | 17.00 | 28.00 | 5.00 | 14.00 | 10.00 | 22.00 | 20.00 | 29.00 |
| RB | 76.00 | 138.00 | 10.00 | 11.00 | 140.00 | 118.00 | 2.00 | 33.00 | 90.00 | 98.00 | 129.00 | 106.00 | 93.00 | 140.00 | 0.00 | 73.00 | 41.00 | 104.00 | 72.00 | 138.00 |
| SC | 10.00 | 24.00 | 39.00 | 41.00 | 25.00 | 21.00 | 52.00 | 43.00 | 14.00 | 29.00 | 27.00 | 23.00 | 12.00 | 18.00 | 73.00 | 8.00 | 54.00 | 11.00 | 14.00 | 22.00 |
| SR | 177.00 | 135.00 | 168.00 | 262.00 | 148.00 | 182.00 | 195.00 | 57.00 | 129.00 | 204.00 | 183.00 | 268.00 | 148.00 | 160.00 | 21.00 | 51.00 | 49.00 | 170.00 | 180.00 | 113.00 |
| TH | 10.00 | 17.00 | 0.00 | 0.00 | 40.00 | 27.00 | 0.00 | 0.00 | 21.00 | 26.00 | 23.00 | 25.00 | 18.00 | 23.00 | 0.00 | 29.00 | 0.00 | 27.00 | 45.00 | 26.00 |
| V | 120.00 | 185.00 | 275.00 | 204.00 | 195.00 | 164.00 | 307.00 | 330.00 | 120.00 | 197.00 | 217.00 | 173.00 | 116.00 | 134.00 | 197.00 | 82.00 | 435.00 | 129.00 | 195.00 | 154.00 |
| Y | 26.00 | 60.00 | 34.00 | 24.00 | 66.00 | 67.00 | 41.00 | 34.00 | 29.00 | 56.00 | 56.00 | 70.00 | 29.00 | 50.00 | 6.00 | 46.00 | 51.00 | 48.00 | 52.00 | 55.00 |
| ZN | 70.00 | 125.00 | 100.00 | 79.00 | 126.00 | 87.00 | 104.00 | 115.00 | 134.00 | 152.00 | 100.00 | 58.00 | 89.00 | 112.00 | 35.00 | 97.00 | 140.00 | 125.00 | 379.00 | 107.00 |
| ZR | 526.00 | 493.00 | 90.00 | 33.00 | 516.00 | 253.00 | 77.00 | 115.00 | 562.00 | 322.00 | 462.00 | 404.00 | 542.00 | 387.00 | 1.00 | 711.00 | 99.00 | 493.00 | 463.00 | 377.00 |

**Whole rock chemistry data**

| Sample Code | 71914 KFR | 71916 ST | 71918 ST5 | 71923 KFR | 71928 ST | 71932 KFR | 71934 KFR | 71937 KFR | 71939 P | 71941 KFR | 71934 P |
|---|---|---|---|---|---|---|---|---|---|---|---|
| SIO2 | 62.57 | 57.03 | 44.72 | 53.31 | 53.60 | 53.66 | 53.38 | 53.53 | 44.64 | 54.02 | 53.85 |
| TIO2 | 1.09 | 0.89 | 2.31 | 1.77 | 1.00 | 2.19 | 2.14 | 1.94 | 0.09 | 1.92 | 0.14 |
| AL203 | 15.64 | 19.27 | 24.61 | 21.03 | 20.76 | 19.64 | 18.37 | 19.98 | 1.52 | 20.65 | 3.65 |
| FE203 | 7.64 | 6.89 | 13.00 | 9.75 | 7.55 | 9.38 | 11.32 | 10.67 | 7.02 | 9.56 | 7.75 |
| MNO | 0.17 | 0.15 | 0.17 | 0.08 | 0.18 | 0.08 | 0.14 | 0.08 | 0.18 | 0.11 | 0.24 |
| MGO | 2.34 | 3.32 | 2.37 | 2.31 | 3.21 | 2.56 | 2.75 | 2.52 | 36.51 | 2.80 | 17.75 |
| CAO | 2.58 | 2.62 | 1.81 | 1.65 | 2.40 | 3.62 | 1.99 | 1.26 | 0.55 | 2.28 | 12.06 |
| NA20 | 2.20 | 1.81 | 1.34 | 2.22 | 1.89 | 3.10 | 1.53 | 1.95 | 0.16 | 2.16 | 0.54 |
| K20 | 2.67 | 4.24 | 4.58 | 3.03 | 5.02 | 1.36 | 3.97 | 3.11 | 0.03 | 3.20 | 0.16 |
| TOTAL | 96.90 | 96.22 | 94.91 | 95.15 | 95.61 | 95.59 | 95.59 | 95.04 | 90.70 | 96.70 | 96.14 |
| BA | 728.00 | 1555.00 | 1357.00 | 667.00 | 3451 | 322.00 | 1018.00 | 750.00 | 0.00 | 621.00 | 0.00 |
| CE | 80.00 | 183.00 | 154.00 | 43.00 | 202.00 | 111.00 | 163.00 | 100.00 | 7.00 | 152.00 | 0.00 |
| CO | 58.00 | 53.00 | 67.00 | 38.00 | 65.00 | 47.00 | 42.00 | 39.00 | 88.00 | 51.00 | 47.00 |
| CR | 142.00 | 38.00 | 117.00 | 83.00 | 45.00 | 90.00 | 80.00 | 87.00 | 2791.00 | 91.00 | 3243.00 |
| LA | 45.00 | 97.00 | 92.00 | 20.00 | 76.00 | 54.00 | 80.00 | 31.00 | 0.00 | 89.00 | 0.00 |
| ND | 45.00 | 89.00 | 79.00 | 28.00 | 79.00 | 64.00 | 85.00 | 42.00 | 1.00 | 88.00 | 4.00 |
| NI | 56.00 | 56.00 | 77.00 | 33.00 | 53.00 | 55.00 | 53.00 | 34.00 | 1990.00 | 74.00 | 229.00 |
| PB | 22.00 | 16.00 | 26.00 | 24.00 | 22.00 | 37.00 | 25.00 | 22.00 | 6.00 | 24.00 | 9.00 |
| RB | 73.00 | 137.00 | 151.00 | 86.00 | 180.00 | 52.00 | 120.00 | 105.00 | 0.00 | 96.00 | 1.00 |
| SC | 15.00 | 16.00 | 30.00 | 24.00 | 21.00 | 14.00 | 15.00 | 17.00 | 8.00 | 16.00 | 57.00 |
| SR | 247.00 | 194.00 | 208.00 | 217.00 | 312.00 | 231.00 | 152.00 | 157.00 | 10.00 | 210.00 | 9.00 |
| TH | 12.00 | 22.00 | 25.00 | 18.00 | 32.00 | 20.00 | 22.00 | 18.00 | 0.00 | 17.00 | 0.00 |
| V | 130.00 | 92.00 | 233.00 | 153.00 | 98.00 | 172.00 | 151.00 | 147.00 | 49.00 | 169.00 | 187.00 |
| Y | 38.00 | 63.00 | 69.00 | 38.00 | 59.00 | 44.00 | 54.00 | 38.00 | 5.00 | 60.00 | 4.00 |
| ZN | 108.00 | 149.00 | 134.00 | 102.00 | 154.00 | 110.00 | 165.00 | 157.00 | 39.00 | 141.00 | 96.00 |
| ZR | 351.00 | 325.00 | 318.00 | 400.00 | 311.00 | 473.00 | 776.00 | 336.00 | 4.00 | 340.00 | 6.00 |

**Whole rock chemistry data**

| Sample | 66795 | 68780 | 68780 | 68780 | 68780 | 68780 | 68780 | 68780 | 68780 | 68780 | 68780 | 68780 |
|---|---|---|---|---|---|---|---|---|---|---|---|---|
| SIO2 | 37.53 | 39.19 | 39.04 | 38.69 | 38.40 | 38.58 | 38.35 | 38.94 | 39.02 | 39.27 | 39.18 | 39.95 |
| TIO2 | 0.19 | 0.00 | 0.00 | 0.00 | 0.00 | 0.00 | 0.00 | 0.00 | 0.00 | 0.00 | 0.00 | 0.00 |
| AL203 | 22.66 | 21.96 | 22.27 | 22.05 | 21.48 | 22.17 | 21.40 | 21.87 | 22.05 | 22.27 | 21.96 | 22.54 |
| FEO | 31.87 | 32.58 | 33.28 | 33.72 | 33.25 | 33.57 | 33.50 | 34.13 | 33.55 | 33.77 | 34.55 | 33.72 |
| MNO | 1.55 | 1.16 | 1.16 | 0.92 | 1.01 | 1.14 | 0.80 | 0.77 | 1.21 | 1.18 | 0.90 | 1.13 |
| MGO | 4.08 | 5.89 | 6.24 | 5.67 | 5.53 | 5.29 | 5.39 | 5.06 | 5.61 | 5.52 | 5.55 | 5.57 |
| CAO | 1.58 | 1.65 | 1.35 | 1.27 | 1.91 | 2.70 | 2.43 | 2.09 | 1.52 | 1.44 | 1.41 | 1.49 |
| NA20 | 0.31 | 0.00 | 0.00 | 0.00 | 0.00 | 0.00 | 0.00 | 0.00 | 0.00 | 0.00 | 0.00 | 0.00 |
| K20 | 0.17 | 0.00 | 0.00 | 0.00 | 0.00 | 0.00 | 0.00 | 0.00 | 0.00 | 0.00 | 0.00 | 0.00 |
| TOTAL | 99.9 | 102.4 | 103.3 | 102.3 | 101.6 | 103.4 | 101.9 | 102.9 | 102.9 | 103.5 | 103.5 | 104.4 |
| | | | | | Cations for 24 oxygen | | | | | | | |
| SI | 5.96 | 6.03 | 5.97 | 5.98 | 6.00 | 5.93 | 5.98 | 6.01 | 6.00 | 6.01 | 6.00 | 6.04 |
| AL | 4.24 | 3.98 | 4.01 | 4.02 | 3.95 | 4.02 | 3.94 | 3.98 | 4.00 | 4.02 | 3.97 | 4.02 |
| FE2 | 4.23 | 4.19 | 4.25 | 4.36 | 4.34 | 4.31 | 4.37 | 4.41 | 4.31 | 4.32 | 4.43 | 4.26 |
| MN | 0.21 | 0.15 | 0.15 | 0.12 | 0.13 | 0.15 | 0.11 | 0.10 | 0.16 | 0.15 | 0.12 | 0.14 |
| MG | 0.96 | 1.35 | 1.42 | 1.31 | 1.29 | 1.21 | 1.25 | 1.16 | 1.29 | 1.26 | 1.27 | 1.26 |
| CA | 0.27 | 0.27 | 0.22 | 0.21 | 0.32 | 0.44 | 0.41 | 0.34 | 0.25 | 0.24 | 0.23 | 0.24 |
| | | | | | End member concentrations | | | | | | | |
| ALM | 74.59 | 70.26 | 70.36 | 72.69 | 71.38 | 70.51 | 71.25 | 73.25 | 71.82 | 72.40 | 73.28 | 72.20 |
| SPE | 3.67 | 2.54 | 2.48 | 2.01 | 2.19 | 2.42 | 1.72 | 1.67 | 2.62 | 2.56 | 1.92 | 2.45 |
| PYR | 17.00 | 22.65 | 23.50 | 21.78 | 21.18 | 19.81 | 20.42 | 19.35 | 21.40 | 21.09 | 20.96 | 21.27 |
| GRO | 4.74 | 4.55 | 3.66 | 3.52 | 5.26 | 7.26 | 6.62 | 5.74 | 4.16 | 3.95 | 3.84 | 4.08 |

**Garnet chemistry data**

| Sample | 68799 | 68799 | 68799 | 68799 | 68799 | 68799 | 68799 | 68799 | 68799 | 68799 | 68799 | 68799 | 68799 |
|---|---|---|---|---|---|---|---|---|---|---|---|---|---|
| SIO2 | 37.96 | 37.78 | 37.57 | 37.94 | 37.94 | 38.39 | 38.12 | 37.99 | 37.58 | 37.88 | 37.99 | 37.68 | 38.80 |
| TIO2 | 0.00 | 0.00 | 0.00 | 0.00 | 0.00 | 0.00 | 0.06 | 0.02 | 0.02 | 0.00 | 0.00 | 0.03 | 0.00 |
| AL2O3 | 20.95 | 21.25 | 20.71 | 21.08 | 21.23 | 21.43 | 21.47 | 20.94 | 21.16 | 21.06 | 21.18 | 20.81 | 21.12 |
| FEO | 23.42 | 23.33 | 23.15 | 23.39 | 22.90 | 23.17 | 23.63 | 22.93 | 23.02 | 23.42 | 23.50 | 22.63 | 23.68 |
| MNO | 9.74 | 11.12 | 11.01 | 10.24 | 11.03 | 11.35 | 10.84 | 10.87 | 11.26 | 10.75 | 10.57 | 11.17 | 9.70 |
| MGO | 3.35 | 3.05 | 2.66 | 3.20 | 2.77 | 2.92 | 3.18 | 2.88 | 2.84 | 2.79 | 3.37 | 3.02 | 3.32 |
| CAO | 4.46 | 4.59 | 4.49 | 4.71 | 4.53 | 4.41 | 4.59 | 4.62 | 4.08 | 4.99 | 4.45 | 4.58 | 4.53 |
| NA2O | 0.40 | 0.05 | 0.00 | 0.17 | 0.00 | 0.16 | 0.20 | 0.24 | 0.26 | 0.13 | 0.00 | 0.00 | 0.04 |
| K2O | 0.05 | 0.00 | 0.02 | 0.00 | 0.00 | 0.00 | 0.02 | 0.00 | 0.03 | 0.05 | 0.00 | 0.04 | 0.00 |
| TOTAL | 100.3 | 101.2 | 99.6 | 100.7 | 100.4 | 101.8 | 102.1 | 100.5 | 100.2 | 101.1 | 101.1 | 100.0 | 101.2 |

Cations for 24 oxygen

| | | | | | | | | | | | | | |
|---|---|---|---|---|---|---|---|---|---|---|---|---|---|
| SI | 6.05 | 5.98 | 6.04 | 6.02 | 6.03 | 6.03 | 5.98 | 6.05 | 6.01 | 6.01 | 6.01 | 6.03 | 6.09 |
| AL | 3.94 | 3.97 | 3.93 | 3.94 | 3.98 | 3.97 | 3.97 | 3.93 | 3.99 | 3.94 | 3.95 | 3.92 | 3.91 |
| FE2 | 3.12 | 3.09 | 3.11 | 3.10 | 3.05 | 3.04 | 3.10 | 3.05 | 3.08 | 3.11 | 3.11 | 3.03 | 3.11 |
| MN | 1.32 | 1.49 | 1.50 | 1.38 | 1.49 | 1.51 | 1.44 | 1.47 | 1.53 | 1.45 | 1.42 | 1.51 | 1.29 |
| MG | 0.80 | 0.72 | 0.64 | 0.76 | 0.66 | 0.68 | 0.74 | 0.68 | 0.68 | 0.66 | 0.79 | 0.72 | 0.78 |
| CA | 0.76 | 0.78 | 0.77 | 0.80 | 0.77 | 0.74 | 0.77 | 0.79 | 0.70 | 0.85 | 0.75 | 0.79 | 0.76 |

End member concentrations

| | | | | | | | | | | | | | |
|---|---|---|---|---|---|---|---|---|---|---|---|---|---|
| ALM | 52.07 | 50.83 | 51.69 | 51.40 | 51.09 | 50.89 | 51.20 | 50.95 | 51.48 | 51.28 | 51.20 | 50.08 | 52.36 |
| SPE | 21.94 | 24.55 | 24.91 | 22.79 | 24.93 | 25.25 | 23.78 | 24.46 | 25.51 | 23.84 | 23.32 | 25.04 | 21.73 |
| PYR | 13.28 | 11.83 | 10.57 | 12.54 | 11.02 | 11.44 | 12.28 | 11.42 | 11.32 | 10.87 | 13.07 | 11.90 | 13.07 |
| GRO | 12.71 | 12.80 | 12.84 | 13.27 | 12.95 | 12.42 | 12.74 | 13.16 | 11.69 | 14.01 | 12.41 | 12.98 | 12.84 |

**Garnet chemistry data**

| Sample | 68804 | 68804 | 68804 | 68804 | 68804 | 68804 | 68804 | 68806 | 68806 | 68806 | 68806 | 68806 |
|---|---|---|---|---|---|---|---|---|---|---|---|---|
| SIO2 | 38.64 | 39.38 | 38.94 | 39.47 | 38.93 | 39.06 | 38.76 | 38.24 | 38.35 | 38.15 | 35.56 | 38.13 |
| TIO2 | 0.00 | 0.00 | 0.00 | 0.00 | 0.00 | 0.00 | 0.00 | 0.00 | 0.00 | 0.26 | 0.00 | 0.00 |
| AL203 | 21.66 | 22.04 | 21.87 | 22.21 | 21.88 | 21.66 | 21.82 | 22.18 | 21.64 | 21.34 | 21.94 | 21.11 |
| FEO | 36.07 | 35.18 | 35.62 | 34.49 | 34.89 | 36.48 | 35.94 | 28.26 | 26.77 | 27.29 | 30.75 | 26.60 |
| MNO | 0.59 | 0.76 | 0.47 | 0.88 | 0.57 | 0.82 | 0.52 | 10.71 | 11.26 | 11.87 | 11.07 | 12.35 |
| MGO | 4.56 | 5.44 | 5.18 | 5.40 | 5.55 | 4.44 | 4.76 | 2.52 | 3.14 | 3.43 | 2.92 | 3.11 |
| CAO | 1.49 | 1.42 | 1.41 | 1.79 | 1.38 | 1.29 | 1.36 | 1.46 | 2.41 | 2.22 | 1.66 | 2.12 |
| NA20 | 0.00 | 0.00 | 0.00 | 0.00 | 0.00 | 0.00 | 0.00 | 0.00 | 0.00 | 0.00 | 0.00 | 0.00 |
| K20 | 0.00 | 0.00 | 0.00 | 0.00 | 0.00 | 0.00 | 0.00 | 0.00 | 0.00 | 0.00 | 0.00 | 0.00 |
| TOTAL | 103.0 | 104.2 | 103.5 | 104.2 | 103.2 | 103.7 | 103.1 | 103.4 | 103.6 | 104.6 | 103.9 | 103.4 |
| | | | | | Cations for 24 oxygen | | | | | | | |
| SI | 6.00 | 6.00 | 5.99 | 6.00 | 5.99 | 6.02 | 6.00 | 5.97 | 5.97 | 5.91 | 5.65 | 5.97 |
| AL | 3.96 | 3.96 | 3.97 | 3.98 | 3.97 | 3.94 | 3.98 | 4.08 | 3.97 | 3.90 | 4.11 | 3.90 |
| FE2 | 4.68 | 4.49 | 4.58 | 4.39 | 4.49 | 4.71 | 4.65 | 3.69 | 3.49 | 3.54 | 4.08 | 3.49 |
| MN | 0.08 | 0.10 | 0.06 | 0.11 | 0.07 | 0.11 | 0.07 | 1.42 | 1.49 | 1.56 | 1.49 | 1.64 |
| MG | 1.05 | 1.24 | 1.19 | 1.22 | 1.27 | 1.02 | 1.10 | 0.59 | 0.73 | 0.79 | 0.69 | 0.73 |
| CA | 0.25 | 0.23 | 0.23 | 0.29 | 0.23 | 0.21 | 0.22 | 0.24 | 0.40 | 0.37 | 0.28 | 0.36 |
| | | | | | End member concentrations | | | | | | | |
| ALM | 77.24 | 74.12 | 75.56 | 72.92 | 74.01 | 77.84 | 76.99 | 62.16 | 57.13 | 56.52 | 62.38 | 56.16 |
| SPE | 1.28 | 1.62 | 1.01 | 1.89 | 1.23 | 1.77 | 1.12 | 23.86 | 24.34 | 24.90 | 22.75 | 26.41 |
| PYR | 17.39 | 20.41 | 19.60 | 20.34 | 20.99 | 16.87 | 18.17 | 9.87 | 11.94 | 12.67 | 10.56 | 11.70 |
| GRO | 4.09 | 3.84 | 3.83 | 4.85 | 3.76 | 3.52 | 3.72 | 4.11 | 6.59 | 5.90 | 4.32 | 5.73 |

**Garnet chemistry data**

| Sample | 68806 | 68806 | 69215 | 69229 | 69229 | 69229 | 69229 | 69229 | 69229 | 69229 | 69229 | 69229 | 69229 | 69230 |
|---|---|---|---|---|---|---|---|---|---|---|---|---|---|---|
| SIO2 | 38.30 | 38.03 | 39.15 | 37.75 | 38.77 | 38.73 | 38.52 | 39.03 | 39.11 | 38.19 | 38.64 | 38.45 | 38.63 | 37.91 |
| TIO2 | 0.22 | 0.00 | 0.00 | 0.00 | 0.00 | 0.00 | 0.00 | 0.00 | 0.00 | 0.00 | 0.00 | 0.00 | 0.00 | 0.00 |
| AL203 | 21.26 | 22.00 | 21.74 | 21.43 | 22.36 | 21.90 | 22.08 | 22.16 | 21.82 | 21.88 | 21.55 | 21.82 | 21.92 | 21.32 |
| FEO | 26.69 | 28.53 | 35.75 | 33.77 | 30.71 | 32.42 | 32.26 | 33.06 | 32.03 | 31.90 | 32.42 | 34.14 | 33.68 | 34.05 |
| MNO | 12.15 | 10.38 | 0.98 | 1.52 | 2.58 | 3.54 | 3.48 | 3.08 | 2.88 | 3.18 | 2.41 | 1.62 | 1.07 | 3.46 |
| MGO | 3.24 | 3.02 | 4.74 | 1.33 | 1.19 | 1.04 | 1.03 | 1.09 | 1.01 | 1.13 | 1.00 | 1.44 | 1.34 | 2.26 |
| CAO | 2.03 | 0.05 | 1.38 | 6.28 | 8.03 | 7.08 | 6.97 | 7.05 | 7.19 | 7.32 | 7.28 | 6.31 | 6.82 | 2.50 |
| NA20 | 0.00 | 0.00 | 0.00 | 0.00 | 0.00 | 0.00 | 0.00 | 0.00 | 0.00 | 0.00 | 0.00 | 0.00 | 0.00 | 0.00 |
| K20 | 0.00 | 0.00 | 0.00 | 0.00 | 0.00 | 0.00 | 0.00 | 0.00 | 0.00 | 0.00 | 0.00 | 0.00 | 0.00 | 0.00 |
| TOTAL | 103.9 | 102.0 | 103.7 | 102.1 | 103.6 | 104.7 | 104.3 | 105.5 | 104.0 | 103.6 | 103.3 | 103.8 | 103.5 | 101.5 |

Cations for 24 oxygen

| | | | | | | | | | | | | | | |
|---|---|---|---|---|---|---|---|---|---|---|---|---|---|---|
| SI | 5.96 | 6.00 | 6.02 | 5.97 | 5.99 | 5.98 | 5.96 | 5.98 | 6.05 | 5.95 | 6.03 | 5.98 | 6.00 | 6.03 |
| AL | 3.90 | 4.09 | 3.94 | 4.00 | 4.07 | 3.99 | 4.03 | 4.00 | 3.98 | 4.02 | 3.96 | 4.00 | 4.02 | 3.99 |
| FE2 | 3.48 | 3.76 | 4.60 | 4.47 | 3.97 | 4.19 | 4.18 | 4.24 | 4.14 | 4.16 | 4.23 | 4.44 | 4.38 | 4.53 |
| MN | 1.60 | 1.39 | 0.13 | 0.20 | 0.34 | 0.46 | 0.46 | 0.40 | 0.38 | 0.42 | 0.32 | 0.21 | 0.14 | 0.47 |
| MG | 0.75 | 0.71 | 1.09 | 0.31 | 0.27 | 0.24 | 0.24 | 0.25 | 0.23 | 0.26 | 0.23 | 0.33 | 0.31 | 0.54 |
| CA | 0.34 | 0.01 | 0.23 | 1.07 | 1.33 | 1.17 | 1.16 | 1.16 | 1.19 | 1.22 | 1.22 | 1.05 | 1.14 | 0.43 |

End member concentrations

| | | | | | | | | | | | | | | |
|---|---|---|---|---|---|---|---|---|---|---|---|---|---|---|
| ALM | 56.34 | 64.14 | 76.13 | 73.84 | 67.14 | 69.06 | 69.30 | 70.10 | 69.70 | 68.59 | 70.51 | 73.54 | 73.38 | 76.02 |
| SPE | 25.98 | 23.63 | 2.10 | 3.37 | 5.72 | 7.65 | 7.58 | 6.62 | 6.35 | 6.92 | 5.31 | 3.53 | 2.36 | 7.82 |
| PYR | 12.18 | 12.11 | 17.99 | 5.18 | 4.64 | 3.96 | 3.93 | 4.13 | 3.91 | 4.31 | 3.88 | 5.52 | 5.21 | 9.00 |
| GRO | 5.50 | 0.13 | 3.77 | 17.61 | 22.50 | 19.33 | 19.19 | 19.16 | 20.03 | 20.18 | 20.30 | 17.41 | 19.04 | 7.15 |

**Garnet chemistry data**

| Sample | 69230 | 69230 | 69230 | 69230 | 69230 | 69230 | 69230 | 69230 | 69238 | 69238 | 69238 | 69238 | 69238 |
|---|---|---|---|---|---|---|---|---|---|---|---|---|---|
| SIO2 | 38.19 | 37.41 | 37.54 | 37.85 | 38.53 | 37.83 | 38.72 | 38.69 | 37.75 | 44.43 | 37.88 | 38.15 | 38.29 |
| TIO2 | 0.00 | 0.00 | 0.00 | 0.00 | 0.00 | 0.00 | 0.00 | 0.00 | 0.00 | 0.00 | 0.00 | 0.00 | 0.00 |
| AL2O3 | 21.63 | 21.77 | 21.50 | 21.64 | 21.73 | 21.50 | 21.57 | 21.47 | 21.74 | 19.30 | 21.30 | 21.15 | 21.48 |
| FEO | 32.73 | 28.76 | 29.42 | 30.94 | 29.29 | 33.61 | 34.99 | 34.94 | 34.86 | 29.66 | 33.53 | 33.41 | 34.03 |
| MNO | 6.57 | 7.19 | 7.71 | 7.71 | 7.26 | 4.83 | 2.11 | 2.55 | 3.79 | 2.72 | 3.08 | 3.42 | 3.30 |
| MGO | 1.93 | 0.96 | 0.87 | 1.29 | 1.22 | 2.04 | 2.49 | 2.39 | 2.18 | 0.95 | 1.23 | 1.39 | 1.62 |
| CAO | 2.00 | 4.44 | 4.55 | 3.26 | 4.98 | 2.56 | 3.26 | 1.81 | 2.45 | 6.53 | 6.39 | 5.67 | 5.12 |
| NA2O | 0.00 | 0.00 | 0.00 | 0.00 | 0.00 | 0.00 | 0.00 | 0.00 | 0.00 | 0.00 | 0.00 | 0.00 | 0.00 |
| K2O | 0.00 | 0.00 | 0.00 | 0.00 | 0.00 | 0.00 | 0.00 | 0.00 | 0.22 | 0.00 | 0.00 | 0.00 | 0.00 |
| TOTAL | 103.1 | 100.5 | 101.6 | 102.7 | 103.0 | 102.4 | 103.1 | 101.8 | 103.0 | 103.6 | 103.4 | 103.2 | 103.8 |
| | | | | | Cations for 24 oxygen | | | | | | | | |
| SI | 6.01 | 6.00 | 5.99 | 5.98 | 6.03 | 5.99 | 6.04 | 6.10 | 5.95 | 6.73 | 5.95 | 6.00 | 5.98 |
| AL | 4.01 | 4.12 | 4.04 | 4.03 | 4.01 | 4.01 | 3.97 | 3.99 | 4.04 | 3.45 | 3.95 | 3.92 | 3.95 |
| FE2 | 4.31 | 3.86 | 3.93 | 4.09 | 3.84 | 4.45 | 4.57 | 4.61 | 4.60 | 3.76 | 4.41 | 4.39 | 4.44 |
| MN | 0.88 | 0.98 | 1.04 | 1.03 | 0.96 | 0.65 | 0.28 | 0.34 | 0.51 | 0.35 | 0.41 | 0.45 | 0.44 |
| MG | 0.45 | 0.23 | 0.21 | 0.30 | 0.29 | 0.48 | 0.58 | 0.56 | 0.51 | 0.21 | 0.29 | 0.33 | 0.38 |
| CA | 0.34 | 0.76 | 0.78 | 0.55 | 0.84 | 0.43 | 0.54 | 0.31 | 0.41 | 1.06 | 1.08 | 0.95 | 0.86 |
| | | | | | End member concentrations | | | | | | | | |
| ALM | 72.11 | 66.19 | 65.96 | 68.44 | 64.80 | 74.00 | 76.53 | 79.25 | 76.24 | 69.83 | 71.28 | 71.67 | 72.70 |
| SPE | 14.67 | 16.76 | 17.52 | 17.27 | 16.27 | 10.77 | 4.66 | 5.85 | 8.39 | 6.48 | 6.63 | 7.42 | 7.14 |
| PYR | 7.57 | 3.95 | 3.47 | 5.07 | 4.82 | 8.00 | 9.69 | 9.64 | 8.49 | 3.99 | 4.67 | 5.33 | 6.16 |
| GRO | 5.66 | 13.10 | 13.06 | 9.22 | 14.11 | 7.23 | 9.12 | 5.25 | 6.87 | 19.71 | 17.42 | 15.58 | 14.01 |

**Garnet chemistry data**

| Sample | 69238 | 69238 | 69238 | 69238 | 69317 | 69317 | 69317 | 69317 | 69317 | 69317 | 69317 | 69317 | 69317 | 69317 | 69619 | 69619 | 69619 | 69619 | 69619 |
|---|---|---|---|---|---|---|---|---|---|---|---|---|---|---|---|---|---|---|---|
| SI02 | 38.44 | 38.60 | 38.52 | 38.69 | 38.52 | 38.88 | 39.13 | 38.78 | 38.72 | 38.92 | 39.10 | 39.03 | 38.44 | 38.68 | 37.74 | 37.82 | 37.41 | 38.20 | 36.97 |
| TI02 | 0.00 | 0.00 | 0.00 | 0.00 | 0.00 | 0.00 | 0.00 | 0.00 | 0.00 | 0.00 | 0.00 | 0.00 | 0.00 | 0.00 | 0.05 | 0.00 | 0.00 | 0.00 | 0.00 |
| AL203 | 21.87 | 21.78 | 21.78 | 21.80 | 21.74 | 21.78 | 21.87 | 21.77 | 21.38 | 21.17 | 21.72 | 21.54 | 21.99 | 21.68 | 21.10 | 21.19 | 21.39 | 21.74 | 20.69 |
| FE0 | 34.00 | 34.83 | 34.04 | 34.05 | 33.60 | 33.42 | 31.94 | 32.09 | 33.06 | 36.17 | 33.73 | 33.95 | 33.29 | 32.47 | 33.56 | 32.89 | 33.05 | 33.97 | 34.14 |
| MN0 | 3.38 | 3.64 | 2.76 | 2.98 | 3.72 | 4.18 | 4.18 | 4.23 | 4.17 | 2.27 | 3.25 | 3.34 | 3.96 | 4.06 | 4.96 | 5.37 | 4.88 | 4.72 | 6.64 |
| MG0 | 1.99 | 2.02 | 2.25 | 2.28 | 1.43 | 1.00 | 0.91 | 1.22 | 1.25 | 1.94 | 1.79 | 1.75 | 1.14 | 1.28 | 2.32 | 2.55 | 2.87 | 2.61 | 2.05 |
| CA0 | 4.68 | 3.49 | 4.30 | 4.36 | 4.43 | 4.78 | 5.88 | 5.61 | 5.60 | 2.73 | 3.92 | 4.28 | 5.51 | 5.53 | 1.58 | 1.58 | 1.64 | 1.67 | 1.81 |
| NA20 | 0.00 | 0.00 | 0.00 | 0.00 | 0.00 | 0.00 | 0.00 | 0.00 | 0.00 | 0.00 | 0.00 | 0.00 | 0.00 | 0.00 | 0.25 | 0.20 | 0.23 | 0.21 | 0.17 |
| K20 | 0.00 | 0.00 | 0.00 | 0.00 | 0.00 | 0.00 | 0.00 | 0.00 | 0.15 | 0.00 | 0.00 | 0.00 | 0.00 | 0.00 | 0.00 | 0.00 | 0.01 | 0.05 | 0.03 |
| TOTAL | 104.4 | 104.4 | 103.7 | 104.2 | 103.5 | 104.0 | 103.9 | 103.7 | 104.3 | 103.2 | 103.5 | 103.9 | 104.3 | 103.7 | 101.6 | 101.6 | 101.5 | 103.2 | 102.5 |

Cations for 24 oxygen

| | | | | | | | | | | | | | | | | | | | |
|---|---|---|---|---|---|---|---|---|---|---|---|---|---|---|---|---|---|---|---|
| SI | 5.96 | 5.99 | 5.99 | 5.99 | 6.02 | 6.04 | 6.06 | 6.03 | 6.02 | 6.09 | 6.08 | 6.06 | 5.97 | 6.02 | 6.03 | 6.02 | 5.97 | 6.00 | 5.93 |
| AL | 4.00 | 3.98 | 3.99 | 3.98 | 4.00 | 3.99 | 4.00 | 3.99 | 3.92 | 3.91 | 3.98 | 3.94 | 4.03 | 3.98 | 3.97 | 3.98 | 4.02 | 4.02 | 3.91 |
| FE2 | 4.41 | 4.52 | 4.43 | 4.41 | 4.39 | 4.35 | 4.14 | 4.17 | 4.30 | 4.74 | 4.38 | 4.41 | 4.32 | 4.23 | 4.48 | 4.38 | 4.41 | 4.46 | 4.58 |
| MN | 0.44 | 0.48 | 0.36 | 0.39 | 0.49 | 0.55 | 0.55 | 0.56 | 0.55 | 0.30 | 0.43 | 0.44 | 0.52 | 0.54 | 0.67 | 0.72 | 0.66 | 0.63 | 0.90 |
| MG | 0.46 | 0.47 | 0.52 | 0.53 | 0.33 | 0.23 | 0.21 | 0.28 | 0.29 | 0.45 | 0.41 | 0.40 | 0.26 | 0.30 | 0.55 | 0.60 | 0.68 | 0.61 | 0.49 |
| CA | 0.78 | 0.58 | 0.72 | 0.72 | 0.74 | 0.80 | 0.98 | 0.94 | 0.93 | 0.46 | 0.65 | 0.71 | 0.92 | 0.92 | 0.27 | 0.27 | 0.28 | 0.28 | 0.31 |

End member concentrations

| | | | | | | | | | | | | | | | | | | | |
|---|---|---|---|---|---|---|---|---|---|---|---|---|---|---|---|---|---|---|---|
| ALM | 72.38 | 74.78 | 73.44 | 72.89 | 73.70 | 73.36 | 70.48 | 70.17 | 70.80 | 79.63 | 74.59 | 73.90 | 71.76 | 70.67 | 75.00 | 73.27 | 73.11 | 74.61 | 72.88 |
| SPE | 7.29 | 7.91 | 6.03 | 6.47 | 8.26 | 9.30 | 9.33 | 9.37 | 9.05 | 5.06 | 7.27 | 7.36 | 8.65 | 8.94 | 11.24 | 12.12 | 10.93 | 10.49 | 14.37 |
| PYR | 7.56 | 7.71 | 8.66 | 8.70 | 5.59 | 3.91 | 3.59 | 4.73 | 4.77 | 7.61 | 7.05 | 6.79 | 4.38 | 4.97 | 9.24 | 10.11 | 11.32 | 10.20 | 7.81 |
| GR0 | 12.77 | 9.59 | 11.88 | 11.94 | 12.45 | 13.43 | 16.61 | 15.73 | 15.37 | 7.69 | 11.09 | 11.95 | 15.21 | 15.42 | 4.52 | 4.50 | 4.64 | 4.70 | 4.94 |

**Garnet chemistry data**

lineation is developed in the quartz and feldspar grains. No upper contact of this unit is seen.

Dawrosbeg striped psammite Member: This sequence forms the bulk of the Streamstown Formation on the Renvyle and Dawrosbeg peninsulas. The maximum thickness is reached to the south of Tully Mountain with a minimum thickness evident to the north of Tully Mountain where the Renvyle - Bofin slide cuts through the stratigraphy (Enclosures 1 and 2).

The sequence consists of interlayered units of dark weathering psammite and schistose semipelite. The scale of the layering shows a progressive change from west to east with layers up to 300mm on the SW of Renvyle peninsula to millimetre scale 'striping' in the Dawrosbeg area. The psammitic units show a gritty graded nature, especially in the western outcrops, and show thin (1 - 2mm) pelite partings and rare calcareous bands up to 5mm thick. The semipelitic lithologies are rich in foliation parallel quartz veins (1 - 2mm thick) which are best developed in the eastern parts of the area where the psammitic horizons are often reduced to fine partings or lenses. Graphitic pelite horizons (upto 100mm thick and laterally continuous) are present at [GR 646 633].

On the south side of Tully Mountain the striped psammites contain a laterally extensive 20m thick unit of massive garnetiferous semipelite.

Doongill garnet semipelite Member This unit is strongly foliated and contains rounded and subhedral garnets up to 10mm in diameter. A grading in garnet content is evident in some parts of this semipelite unit, the garnets being concentrated in the upper third of 200mm thick horizons. This distribution of garnets is considered to represent a primary variation in sedimentary composition, with the upper units of beds being more pelitic in composition, and inferring a greater percentage of clay grade material in the original sediment. These originally fining upward cycles show the lithology to be overturned in its present orientation.

Roeillaun schist Member: This lithology occurs on the

| Sample | 69619 | 69619 | 69619 | 69619 | 69619 | 69619 | 69623 | 69623 | 69623 | 69623 | 69623 | 69623 | 69623 | 69623 | 69623 | 69623 | 69625 | 69625 | 69625 | 69625 | 69625 |
|---|---|---|---|---|---|---|---|---|---|---|---|---|---|---|---|---|---|---|---|---|---|
| SIO2 | 37.82 | 37.83 | 37.68 | 37.58 | 37.10 | 37.45 | 37.67 | 37.61 | 37.76 | 38.04 | 37.89 | 38.18 | 37.63 | 37.61 | 37.20 | 38.14 | 37.89 | 38.03 | 37.89 | 37.86 | 37.61 |
| TIO2 | 0.00 | 0.00 | 0.02 | 0.00 | 0.00 | 0.06 | 0.23 | 0.11 | 0.22 | 0.17 | 0.00 | 0.22 | 0.09 | 0.09 | 0.06 | 0.21 | 0.06 | 0.04 | 0.16 | 0.07 | 0.07 |
| AL203 | 21.27 | 21.34 | 21.52 | 21.30 | 20.83 | 21.28 | 21.33 | 21.02 | 20.98 | 21.39 | 21.22 | 21.27 | 20.90 | 21.18 | 20.38 | 21.62 | 21.15 | 20.95 | 21.20 | 20.66 | 20.61 |
| FEO | 32.98 | 33.53 | 33.90 | 33.94 | 33.36 | 33.31 | 34.75 | 33.31 | 32.40 | 33.60 | 35.70 | 33.40 | 30.58 | 34.72 | 32.66 | 31.87 | 34.79 | 31.07 | 29.66 | 31.41 | 31.60 |
| MNO | 4.51 | 4.38 | 4.93 | 4.84 | 4.84 | 4.93 | 1.35 | 2.19 | 3.06 | 2.10 | 0.96 | 2.58 | 5.40 | 3.28 | 4.03 | 4.01 | 0.56 | 3.67 | 4.38 | 3.38 | 2.63 |
| MGO | 3.07 | 2.98 | 2.45 | 2.54 | 2.62 | 2.43 | 2.28 | 1.33 | 1.27 | 1.81 | 1.90 | 1.15 | 0.93 | 2.40 | 1.46 | 1.70 | 1.87 | 1.04 | 0.92 | 0.90 | 0.77 |
| CAO | 2.14 | 2.22 | 1.53 | 1.52 | 1.61 | 1.46 | 3.56 | 5.95 | 6.12 | 5.16 | 4.42 | 5.67 | 5.40 | 2.45 | 4.11 | 5.13 | 5.04 | 6.91 | 7.51 | 7.04 | 6.93 |
| NA20 | 0.09 | 0.33 | 0.34 | 0.12 | 0.28 | 0.06 | 0.12 | 0.21 | 0.08 | 0.12 | 0.06 | 0.07 | 0.00 | 0.11 | 0.00 | 0.19 | 0.37 | 0.20 | 0.00 | 0.00 | 0.00 |
| K20 | 0.04 | 0.05 | 0.00 | 0.00 | 0.00 | 0.07 | 0.01 | 0.01 | 0.04 | 0.01 | 0.01 | 0.03 | 0.00 | 0.06 | 0.03 | 0.06 | 0.05 | 0.00 | 0.03 | 0.03 | 0.04 |
| TOTAL | 101.9 | 102.7 | 102.4 | 101.9 | 100.6 | 101.1 | 101.3 | 101.7 | 101.9 | 102.4 | 102.2 | 102.6 | 100.9 | 101.9 | 99.9 | 102.9 | 101.8 | 101.9 | 101.7 | 101.3 | 100.3 |
| Cations for 24 Oxygens | | | | | | | | | | | | | | | | | | | | | |
| SI | 5.99 | 5.97 | 5.98 | 5.98 | 5.99 | 6.00 | 5.99 | 5.99 | 6.00 | 6.00 | 6.00 | 6.02 | 6.03 | 5.98 | 6.04 | 5.99 | 6.02 | 6.04 | 6.00 | 6.04 | 6.06 |
| AL | 3.97 | 3.97 | 4.03 | 4.00 | 3.96 | 4.02 | 4.00 | 3.95 | 3.93 | 3.97 | 3.96 | 3.95 | 3.95 | 3.97 | 3.90 | 4.00 | 3.96 | 3.92 | 3.96 | 3.89 | 3.91 |
| FE2 | 4.37 | 4.43 | 4.50 | 4.52 | 4.50 | 4.46 | 4.62 | 4.44 | 4.30 | 4.43 | 4.73 | 4.40 | 4.10 | 4.62 | 4.43 | 4.18 | 4.62 | 4.12 | 3.93 | 4.19 | 4.26 |
| MN | 0.61 | 0.59 | 0.66 | 0.65 | 0.66 | 0.67 | 0.18 | 0.30 | 0.41 | 0.28 | 0.13 | 0.34 | 0.73 | 0.44 | 0.55 | 0.53 | 0.08 | 0.49 | 0.59 | 0.46 | 0.36 |
| MG | 0.72 | 0.70 | 0.58 | 0.60 | 0.63 | 0.58 | 0.54 | 0.32 | 0.30 | 0.43 | 0.45 | 0.27 | 0.22 | 0.57 | 0.35 | 0.40 | 0.44 | 0.25 | 0.22 | 0.21 | 0.18 |
| CA | 0.36 | 0.38 | 0.26 | 0.26 | 0.28 | 0.25 | 0.61 | 1.02 | 1.04 | 0.87 | 0.75 | 0.96 | 0.93 | 0.42 | 0.71 | 0.86 | 0.86 | 1.18 | 1.28 | 1.20 | 1.20 |
| End member concentrations | | | | | | | | | | | | | | | | | | | | | |
| ALM | 72.07 | 72.69 | 74.97 | 74.88 | 74.16 | 74.86 | 77.67 | 73.17 | 71.05 | 73.74 | 78.08 | 73.69 | 68.53 | 76.38 | 73.21 | 69.99 | 77.05 | 68.28 | 65.39 | 69.12 | 70.98 |
| SPE | 9.99 | 9.61 | 11.03 | 10.82 | 10.89 | 11.21 | 3.06 | 4.87 | 6.80 | 4.67 | 2.13 | 5.77 | 12.26 | 7.31 | 9.15 | 8.92 | 1.26 | 8.16 | 9.78 | 7.53 | 5.98 |
| GRO | 5.99 | 6.17 | 4.34 | 4.30 | 4.58 | 4.21 | 10.19 | 16.75 | 17.19 | 14.51 | 12.39 | 16.03 | 15.50 | 6.91 | 11.80 | 14.43 | 14.30 | 19.47 | 21.21 | 19.84 | 19.95 |
| PYR | 11.95 | 11.53 | 9.65 | 10.00 | 10.36 | 9.71 | 9.08 | 5.21 | 4.96 | 7.08 | 7.41 | 4.52 | 3.71 | 9.41 | 5.83 | 6.65 | 7.39 | 4.09 | 3.61 | 3.51 | 3.08 |

**Garnet chemistry data**

| Sample | 69625 | 69625 | 69625 | 69625 | 69625 | 69625 | 69625 | 69625 | 69625 | 69627 | 69627 | 69627 | 69627 | 69627 | 69627 | 69627 | 69627 | 69627 | 69627 | 69627 | 69627 |
|---|---|---|---|---|---|---|---|---|---|---|---|---|---|---|---|---|---|---|---|---|---|
| SIO2 | 37.89 | 38.03 | 37.89 | 37.86 | 37.61 | 37.40 | 37.86 | 38.35 | 38.25 | 37.42 | 38.01 | 37.96 | 37.58 | 38.02 | 37.27 | 37.33 | 38.28 | 37.54 | 37.58 | 37.38 | 37.87 | 37.45 |
| TIO2 | 0.06 | 0.04 | 0.16 | 0.07 | 0.07 | 0.18 | 0.04 | 0.28 | 0.12 | 0.17 | 0.08 | 0.13 | 0.21 | 0.33 | 0.03 | 0.07 | 0.14 | 0.11 | 0.03 | 0.05 | 0.11 | 0.05 |
| AL2O3 | 21.15 | 20.95 | 21.20 | 20.66 | 20.61 | 21.12 | 21.58 | 21.14 | 20.97 | 20.80 | 21.12 | 21.04 | 20.78 | 20.20 | 20.74 | 20.99 | 21.64 | 21.17 | 21.05 | 20.66 | 21.06 | 20.71 |
| FEO | 34.79 | 31.07 | 29.66 | 31.41 | 31.60 | 34.36 | 35.95 | 29.79 | 28.71 | 36.19 | 35.49 | 35.37 | 33.90 | 32.14 | 34.94 | 36.55 | 36.25 | 36.44 | 36.33 | 31.90 | 35.81 | 35.84 |
| MNO | 0.56 | 3.67 | 4.38 | 3.38 | 2.63 | 1.04 | 0.28 | 4.12 | 5.31 | 0.40 | 0.45 | 0.18 | 1.67 | 3.16 | 1.35 | 1.20 | 0.17 | 0.23 | 1.24 | 4.53 | 0.40 | 0.22 |
| MGO | 1.87 | 1.04 | 0.92 | 0.90 | 0.77 | 1.39 | 2.05 | 1.13 | 0.72 | 1.67 | 1.79 | 2.09 | 1.63 | 1.41 | 1.98 | 2.30 | 2.35 | 1.90 | 1.86 | 1.02 | 1.85 | 2.39 |
| CAO | 5.04 | 6.91 | 7.51 | 7.04 | 6.93 | 5.74 | 4.22 | 7.14 | 7.78 | 3.96 | 4.01 | 4.25 | 4.81 | 4.66 | 3.61 | 2.30 | 4.04 | 3.85 | 3.33 | 5.45 | 4.52 | 3.29 |
| NA2O | 0.37 | 0.20 | 0.00 | 0.00 | 0.00 | 0.01 | 0.15 | 0.11 | 0.31 | 0.22 | 0.19 | 0.11 | 0.04 | 0.20 | 0.14 | 0.09 | 0.10 | 0.00 | 0.05 | 0.12 | 0.32 | 0.20 |
| K2O | 0.05 | 0.00 | 0.03 | 0.03 | 0.04 | 0.00 | 0.00 | 0.01 | 0.00 | 0.00 | 0.04 | 0.03 | 0.40 | 0.14 | 0.20 | 0.03 | 0.02 | 0.06 | 0.00 | 0.01 | 0.06 | 0.08 |
| TOTAL | 101.8 | 101.9 | 101.7 | 101.3 | 100.3 | 101.2 | 102.1 | 102.0 | 102.2 | 100.8 | 101.2 | 101.2 | 101.0 | 100.3 | 100.3 | 100.8 | 103.0 | 101.3 | 101.5 | 101.1 | 102.0 | 100.2 |

Cations for 24 oxygen

| | | | | | | | | | | | | | | | | | | | | | |
|---|---|---|---|---|---|---|---|---|---|---|---|---|---|---|---|---|---|---|---|---|---|
| SI | 6.02 | 6.04 | 6.00 | 6.04 | 6.06 | 5.97 | 5.99 | 6.05 | 6.05 | 6.02 | 6.06 | 6.04 | 6.03 | 6.13 | 6.03 | 6.00 | 5.99 | 5.99 | 6.01 | 6.01 | 6.02 | 6.04 |
| AL | 3.96 | 3.92 | 3.96 | 3.89 | 3.91 | 3.98 | 4.02 | 3.93 | 3.91 | 3.94 | 3.97 | 3.95 | 3.93 | 3.84 | 3.95 | 3.98 | 3.99 | 3.98 | 3.97 | 3.92 | 3.95 | 3.94 |
| FE2 | 4.62 | 4.12 | 3.93 | 4.19 | 4.26 | 4.59 | 4.75 | 3.93 | 3.80 | 4.87 | 4.73 | 4.71 | 4.55 | 4.33 | 4.72 | 4.91 | 4.74 | 4.87 | 4.86 | 4.29 | 4.76 | 4.83 |
| MN | 0.08 | 0.49 | 0.59 | 0.46 | 0.36 | 0.14 | 0.04 | 0.55 | 0.71 | 0.05 | 0.06 | 0.02 | 0.23 | 0.43 | 0.18 | 0.16 | 0.02 | 0.03 | 0.17 | 0.62 | 0.05 | 0.03 |
| MG | 0.44 | 0.25 | 0.22 | 0.21 | 0.18 | 0.33 | 0.48 | 0.27 | 0.17 | 0.40 | 0.43 | 0.50 | 0.39 | 0.34 | 0.48 | 0.55 | 0.55 | 0.45 | 0.44 | 0.24 | 0.44 | 0.57 |
| CA | 0.86 | 1.18 | 1.28 | 1.20 | 1.20 | 0.98 | 0.71 | 1.21 | 1.32 | 0.68 | 0.69 | 0.73 | 0.83 | 0.80 | 0.62 | 0.40 | 0.68 | 0.66 | 0.57 | 0.94 | 0.77 | 0.57 |

End member concentrations

| | | | | | | | | | | | | | | | | | | | | | |
|---|---|---|---|---|---|---|---|---|---|---|---|---|---|---|---|---|---|---|---|---|---|
| ALM | 77.05 | 68.28 | 65.39 | 69.12 | 70.98 | 75.95 | 79.38 | 66.03 | 63.32 | 81.09 | 80.13 | 79.08 | 75.90 | 73.35 | 78.60 | 81.57 | 79.17 | 80.98 | 80.45 | 70.43 | 79.05 | 80.46 |
| SPE | 1.26 | 8.16 | 9.78 | 7.53 | 5.98 | 2.33 | 0.64 | 9.24 | 11.85 | 0.90 | 1.03 | 0.41 | 3.79 | 7.31 | 3.07 | 2.70 | 0.38 | 0.53 | 2.78 | 10.12 | 0.89 | 0.50 |
| PYR | 7.39 | 4.09 | 3.61 | 3.51 | 3.08 | 5.46 | 8.05 | 4.46 | 2.84 | 6.65 | 7.22 | 8.32 | 6.50 | 5.73 | 7.94 | 9.16 | 9.14 | 7.54 | 7.34 | 4.02 | 7.27 | 9.56 |
| GRO | 14.30 | 19.47 | 21.21 | 19.84 | 19.95 | 16.26 | 11.93 | 20.27 | 21.99 | 11.36 | 11.62 | 12.18 | 13.81 | 13.62 | 10.39 | 6.57 | 11.31 | 10.95 | 9.44 | 15.43 | 12.80 | 9.47 |

**Garnet chemistry data**

| Sample | 69627 | 69627 | 69627 | 69627 | 69635 | 69635 | 69635 | 69635 | 69635 | 69635 | 69635 | 69635 | 69635 | 69635 | 69635 | 69635 | 69635 | 69635 | 69635 | 69635 |
|---|---|---|---|---|---|---|---|---|---|---|---|---|---|---|---|---|---|---|---|---|
| SIO2 | 37.22 | 38.13 | 37.78 | 37.70 | 37.17 | 37.51 | 37.49 | 37.06 | 37.59 | 37.86 | 37.61 | 37.59 | 37.66 | 37.45 | 37.64 | 37.14 | 36.85 | 36.96 | 37.72 | 37.41 |
| TIO2 | 0.44 | 0.05 | 0.02 | 0.15 | 0.00 | 0.00 | 0.00 | 0.03 | 0.04 | 0.04 | 0.00 | 0.00 | 0.00 | 0.00 | 0.06 | 0.05 | 0.00 | 0.19 | 0.00 | 0.00 |
| AL2O3 | 20.41 | 21.19 | 20.90 | 20.82 | 20.74 | 20.89 | 20.53 | 20.94 | 21.00 | 21.05 | 20.92 | 21.42 | 21.25 | 20.67 | 21.24 | 20.54 | 20.40 | 20.80 | 21.38 | 21.17 |
| FEO | 34.08 | 35.01 | 35.28 | 30.63 | 32.36 | 32.51 | 32.32 | 31.62 | 32.84 | 32.35 | 33.30 | 32.82 | 33.91 | 32.44 | 32.24 | 32.35 | 31.80 | 33.97 | 33.67 | 32.85 |
| MNO | 1.58 | 0.25 | 0.31 | 3.88 | 5.00 | 5.08 | 4.76 | 4.48 | 4.57 | 4.75 | 4.89 | 5.24 | 4.69 | 5.01 | 4.70 | 5.02 | 4.95 | 4.00 | 4.59 | 4.76 |
| MGO | 1.57 | 1.72 | 2.02 | 0.70 | 2.27 | 2.31 | 2.39 | 2.61 | 2.55 | 2.58 | 2.34 | 2.31 | 1.93 | 2.15 | 2.49 | 2.40 | 2.38 | 1.61 | 1.80 | 2.82 |
| CAO | 4.11 | 4.92 | 4.39 | 6.93 | 2.17 | 2.14 | 2.40 | 2.55 | 2.44 | 2.60 | 1.67 | 1.79 | 1.92 | 2.45 | 2.41 | 2.26 | 1.78 | 2.53 | 1.64 | 2.14 |
| NA2O | 0.20 | 0.37 | 0.28 | 0.01 | 0.14 | 0.01 | 0.02 | 0.25 | 0.13 | 0.00 | 0.38 | 0.00 | 0.04 | 0.00 | 0.00 | 0.20 | 0.20 | 0.00 | 0.00 | 0.29 |
| K2O | 0.07 | 0.11 | 0.04 | 0.05 | 0.00 | 0.02 | 0.01 | 0.07 | 0.00 | 0.00 | 0.02 | 0.00 | 0.04 | 0.01 | 0.02 | 0.00 | 0.00 | 0.02 | 0.00 | 0.02 |
| TOTAL | 99.7 | 101.8 | 101.0 | 100.9 | 99.8 | 100.5 | 99.9 | 99.6 | 101.1 | 101.2 | 101.1 | 101.2 | 101.4 | 100.2 | 100.8 | 99.9 | 98.4 | 100.1 | 100.8 | 101.5 |
| | | | | | | | | | | | Cations for 24 oxygen | | | | | | | | | |
| SI | 6.04 | 6.05 | 6.04 | 6.04 | 6.03 | 6.03 | 6.06 | 6.01 | 6.01 | 6.03 | 6.04 | 6.00 | 6.02 | 6.05 | 6.02 | 6.02 | 6.06 | 6.00 | 6.05 | 5.98 |
| AL | 3.91 | 3.97 | 3.94 | 3.93 | 3.97 | 3.96 | 3.91 | 4.00 | 3.96 | 3.95 | 3.96 | 4.03 | 4.00 | 3.94 | 4.00 | 3.93 | 3.95 | 3.98 | 4.04 | 3.99 |
| FE2 | 4.63 | 4.65 | 4.72 | 4.10 | 4.39 | 4.37 | 4.37 | 4.29 | 4.39 | 4.31 | 4.47 | 4.38 | 4.53 | 4.38 | 4.31 | 4.39 | 4.37 | 4.61 | 4.51 | 4.39 |
| MN | 0.22 | 0.03 | 0.04 | 0.53 | 0.69 | 0.69 | 0.65 | 0.61 | 0.62 | 0.64 | 0.66 | 0.71 | 0.63 | 0.69 | 0.64 | 0.69 | 0.69 | 0.55 | 0.62 | 0.64 |
| MG | 0.38 | 0.41 | 0.48 | 0.17 | 0.55 | 0.55 | 0.58 | 0.63 | 0.61 | 0.61 | 0.56 | 0.55 | 0.46 | 0.52 | 0.59 | 0.58 | 0.58 | 0.39 | 0.43 | 0.67 |
| CA | 0.72 | 0.84 | 0.75 | 1.19 | 0.38 | 0.37 | 0.42 | 0.44 | 0.42 | 0.44 | 0.29 | 0.31 | 0.33 | 0.42 | 0.41 | 0.39 | 0.31 | 0.44 | 0.28 | 0.37 |
| | | | | | | | | | | | End member concentrations | | | | | | | | | |
| ALM | 77.90 | 78.43 | 78.73 | 68.54 | 73.14 | 73.02 | 72.67 | 71.75 | 72.77 | 71.75 | 74.74 | 73.70 | 76.12 | 72.92 | 72.41 | 72.53 | 73.39 | 76.99 | 77.18 | 72.29 |
| SPE | 3.65 | 0.57 | 0.70 | 8.79 | 11.45 | 11.56 | 10.85 | 10.29 | 10.26 | 10.68 | 11.11 | 11.92 | 10.66 | 11.41 | 10.69 | 11.39 | 11.58 | 9.19 | 10.65 | 10.61 |
| PYR | 6.41 | 6.87 | 8.03 | 2.80 | 9.13 | 9.26 | 9.57 | 10.56 | 10.06 | 10.18 | 9.35 | 9.24 | 7.70 | 8.61 | 9.96 | 9.58 | 9.77 | 6.48 | 7.34 | 11.06 |
| GRO | 12.05 | 14.13 | 12.54 | 19.87 | 6.28 | 6.16 | 6.91 | 7.40 | 6.91 | 7.38 | 4.80 | 5.15 | 5.52 | 7.07 | 6.94 | 6.49 | 5.27 | 7.33 | 4.83 | 6.03 |

**Garnet chemistry data**

| Sample | 69635 | 71898 | 71898 | 71898 | 71901 | 71901 | 71901 | 71901 | 71901 | 71901 | 71901 | 71912 | 71912 | 71912 |
|---|---|---|---|---|---|---|---|---|---|---|---|---|---|---|
| SIO2 | 37.76 | 38.08 | 37.49 | 38.38 | 38.91 | 39.20 | 38.76 | 38.14 | 38.98 | 38.75 | 38.69 | 39.29 | 39.18 | 38.92 |
| TIO2 | 0.02 | 0.00 | 0.00 | 0.00 | 0.00 | 0.00 | 0.00 | 0.00 | 0.00 | 0.00 | 0.00 | 0.00 | 0.00 | 0.00 |
| AL2O3 | 21.57 | 21.14 | 21.01 | 21.54 | 21.41 | 21.38 | 20.99 | 20.50 | 21.15 | 20.51 | 21.55 | 21.90 | 21.84 | 21.30 |
| FEO | 33.86 | 29.25 | 29.56 | 30.03 | 29.95 | 27.47 | 22.56 | 21.39 | 23.33 | 24.96 | 29.60 | 33.27 | 32.60 | 30.37 |
| MNO | 4.83 | 8.14 | 9.29 | 7.35 | 10.03 | 10.79 | 13.67 | 14.56 | 13.32 | 10.34 | 9.27 | 2.19 | 4.34 | 5.88 |
| MGO | 2.03 | 3.62 | 1.74 | 3.36 | 1.78 | 2.23 | 1.71 | 1.56 | 1.66 | 1.92 | 2.26 | 1.12 | 0.84 | 0.58 |
| CAO | 1.70 | 2.07 | 2.82 | 1.74 | 2.35 | 4.14 | 5.16 | 5.58 | 5.11 | 5.44 | 3.48 | 6.52 | 5.89 | 6.60 |
| NA2O | 0.11 | 0.00 | 0.00 | 0.00 | 0.00 | 0.00 | 0.00 | 0.00 | 0.00 | 0.00 | 0.00 | 0.00 | 0.00 | 0.00 |
| K2O | 0.07 | 0.00 | 0.00 | 0.00 | 0.00 | 0.00 | 0.00 | 0.00 | 0.00 | 0.00 | 0.00 | 0.00 | 0.00 | 0.00 |
| TOTAL | 102.0 | 102.3 | 101.9 | 102.4 | 104.4 | 105.2 | 102.8 | 101.7 | 103.5 | 101.9 | 104.9 | 104.3 | 104.7 | 103.7 |
| | | | | | | Cations for 24 oxygen | | | | | | | | |
| SI | 6.00 | 6.10 | 5.99 | 6.06 | 6.05 | 6.03 | 6.07 | 6.06 | 6.07 | 6.11 | 5.98 | 6.06 | 6.05 | 6.07 |
| AL | 4.04 | 3.97 | 4.01 | 3.94 | 3.92 | 3.88 | 3.88 | 3.84 | 3.88 | 3.82 | 3.93 | 3.98 | 3.97 | 3.92 |
| FE2 | 4.50 | 4.04 | 4.18 | 4.29 | 3.89 | 3.53 | 2.96 | 2.84 | 3.04 | 3.29 | 3.83 | 4.29 | 4.21 | 3.96 |
| MN | 0.65 | 1.13 | 1.31 | 1.03 | 1.32 | 1.40 | 1.81 | 1.96 | 1.76 | 1.38 | 1.21 | 0.29 | 0.57 | 0.78 |
| MG | 0.48 | 0.47 | 0.40 | 0.47 | 0.41 | 0.51 | 0.40 | 0.37 | 0.39 | 0.45 | 0.52 | 0.26 | 0.19 | 0.14 |
| CA | 0.29 | 0.68 | 0.25 | 0.25 | 0.39 | 0.68 | 0.87 | 0.95 | 0.85 | 0.92 | 0.58 | 1.08 | 0.97 | 1.10 |
| | | | | | | End member concentrations | | | | | | | | |
| ALM | 76.00 | 67.90 | 68.12 | 67.07 | 64.70 | 57.62 | 48.98 | 46.42 | 50.37 | 54.47 | 62.35 | 72.58 | 70.83 | 66.29 |
| SPE | 10.99 | 18.90 | 21.40 | 17.30 | 21.96 | 22.91 | 30.05 | 32.01 | 29.12 | 22.85 | 19.77 | 4.85 | 9.55 | 13.00 |
| PYR | 8.12 | 8.40 | 6.50 | 7.94 | 6.85 | 8.35 | 6.61 | 6.04 | 6.39 | 7.48 | 8.48 | 4.35 | 3.24 | 2.27 |
| GRO | 4.90 | 4.80 | 4.01 | 4.13 | 6.49 | 11.12 | 14.35 | 15.52 | 14.12 | 15.20 | 9.40 | 18.22 | 16.39 | 18.44 |

**Garnet chemistry data**

| Sample | 71912 | 71912 | 71912 | 71912 | 71912 | 71914 | 71914 | 71914 | 71914 | 71914 | 71914 | 71916 | 71916 | 71916 | 71916 | 71916 | 71916 | 71918 | 71918 | 71923 |
|---|---|---|---|---|---|---|---|---|---|---|---|---|---|---|---|---|---|---|---|---|
| SIO2 | 38.49 | 38.67 | 38.70 | 38.77 | 38.09 | 37.88 | 38.37 | 38.25 | 38.09 | 38.61 | 37.92 | 39.00 | 38.72 | 38.99 | 39.08 | 39.22 | 39.14 | 40.18 | 40.30 | 37.49 |
| TIO2 | 0.00 | 0.00 | 0.00 | 0.00 | 0.00 | 0.00 | 0.00 | 0.00 | 0.00 | 0.00 | 0.00 | 0.00 | 0.00 | 0.00 | 0.00 | 0.00 | 0.00 | 0.00 | 0.00 | 0.00 |
| AL203 | 21.33 | 21.19 | 21.45 | 21.54 | 20.95 | 20.68 | 21.17 | 20.86 | 21.21 | 20.77 | 21.00 | 21.50 | 21.52 | 21.71 | 21.32 | 21.56 | 21.45 | 21.52 | 21.88 | 21.15 |
| FEO | 30.36 | 30.29 | 31.54 | 31.83 | 32.98 | 33.26 | 34.49 | 34.09 | 33.62 | 33.12 | 32.39 | 29.49 | 27.71 | 25.65 | 24.82 | 24.06 | 24.53 | 33.03 | 31.81 | 30.14 |
| MNO | 6.11 | 5.96 | 5.17 | 3.98 | 2.65 | 3.07 | 2.88 | 2.64 | 3.87 | 4.00 | 4.01 | 3.09 | 6.14 | 8.63 | 9.69 | 10.53 | 10.90 | 0.49 | 0.86 | 6.93 |
| MGO | 0.00 | 0.45 | 0.49 | 0.62 | 1.67 | 2.45 | 2.25 | 1.82 | 1.62 | 1.97 | 2.12 | 1.38 | 0.76 | 0.69 | 0.00 | 0.00 | 0.59 | 1.04 | 0.00 | 0.61 |
| CAO | 6.59 | 6.66 | 5.98 | 6.37 | 4.12 | 4.11 | 4.16 | 4.34 | 3.84 | 3.84 | 3.92 | 7.24 | 7.11 | 7.99 | 7.94 | 8.55 | 7.93 | 3.71 | 6.30 | 5.47 |
| NA20 | 0.00 | 0.00 | 0.00 | 0.00 | 0.00 | 0.00 | 0.00 | 0.00 | 0.00 | 0.00 | 0.00 | 0.00 | 0.00 | 0.00 | 0.00 | 0.00 | 0.00 | 0.00 | 0.00 | 0.00 |
| K20 | 0.16 | 0.00 | 0.00 | 0.00 | 0.00 | 0.00 | 0.00 | 0.00 | 0.00 | 0.00 | 0.00 | 0.00 | 0.00 | 0.14 | 0.00 | 0.00 | 0.00 | 0.00 | 0.23 | 0.00 |
| TOTAL | 103.0 | 103.2 | 103.3 | 103.1 | 100.5 | 101.4 | 103.3 | 102.0 | 102.3 | 102.3 | 101.4 | 101.7 | 102.0 | 103.8 | 102.8 | 103.9 | 104.5 | 100.0 | 101.4 | 101.8 |
| Cations for 24 oxygen | | | | | | | | | | | | | | | | | | | | |
| SI | 6.06 | 6.07 | 6.06 | 6.07 | 6.10 | 6.03 | 6.01 | 6.06 | 6.03 | 6.09 | 6.03 | 6.11 | 6.09 | 6.05 | 6.12 | 6.08 | 6.05 | 6.35 | 6.31 | 5.99 |
| AL | 3.96 | 3.92 | 3.96 | 3.97 | 3.95 | 3.88 | 3.91 | 3.90 | 3.96 | 3.86 | 3.94 | 3.97 | 3.99 | 3.97 | 3.93 | 3.94 | 3.91 | 4.01 | 4.04 | 3.98 |
| FE2 | 4.00 | 3.97 | 4.13 | 4.17 | 4.41 | 4.43 | 4.52 | 4.52 | 4.45 | 4.37 | 4.31 | 3.87 | 3.64 | 3.33 | 3.25 | 3.12 | 3.17 | 4.36 | 4.16 | 4.03 |
| MN | 0.81 | 0.79 | 0.69 | 0.53 | 0.36 | 0.41 | 0.38 | 0.35 | 0.52 | 0.54 | 0.54 | 0.41 | 0.82 | 1.13 | 1.28 | 1.38 | 1.43 | 0.07 | 0.11 | 0.94 |
| MG | 0.00 | 0.10 | 0.11 | 0.15 | 0.40 | 0.58 | 0.52 | 0.43 | 0.38 | 0.46 | 0.50 | 0.32 | 0.18 | 0.16 | 0.00 | 0.00 | 0.14 | 0.25 | 0.00 | 0.15 |
| CA | 1.11 | 1.12 | 1.00 | 1.07 | 0.71 | 0.70 | 0.70 | 0.74 | 0.65 | 0.65 | 0.67 | 1.22 | 1.20 | 1.33 | 1.33 | 1.42 | 1.31 | 0.63 | 1.06 | 0.94 |
| End member concentrations | | | | | | | | | | | | | | | | | | | | |
| ALM | 67.50 | 66.36 | 69.63 | 70.53 | 75.09 | 72.33 | 73.80 | 74.81 | 74.13 | 72.63 | 71.58 | 66.49 | 62.43 | 55.92 | 55.39 | 52.66 | 52.43 | 82.31 | 78.05 | 66.60 |
| SPE | 13.75 | 13.22 | 11.56 | 8.93 | 6.12 | 6.75 | 6.24 | 5.87 | 8.65 | 8.89 | 8.97 | 7.05 | 14.02 | 19.06 | 21.90 | 23.35 | 23.60 | 1.23 | 2.13 | 15.50 |
| PYR | 0.00 | 1.74 | 1.91 | 2.46 | 6.76 | 9.47 | 8.56 | 7.12 | 6.37 | 7.69 | 8.35 | 5.55 | 3.04 | 2.70 | 0.00 | 0.00 | 2.25 | 4.63 | 0.00 | 2.40 |
| GRO | 18.76 | 18.68 | 16.90 | 18.08 | 12.03 | 11.44 | 11.40 | 12.20 | 10.85 | 10.79 | 11.10 | 20.92 | 20.52 | 22.33 | 22.71 | 23.99 | 21.72 | 11.83 | 19.82 | 15.50 |

**Garnet chemistry data**

| Sample | 71923 | 71923 | 71923 | 71923 | 71923 | 71932 | 71932 | 71932 | 71932 | 71932 | 71932 | 71934 | 71934 | 71934 | 71934 | 71934 | 71934 | 71941 | 71941 | 71941 |
|---|---|---|---|---|---|---|---|---|---|---|---|---|---|---|---|---|---|---|---|---|
| SIO2 | 37.60 | 37.70 | 37.87 | 38.15 | 36.67 | 37.94 | 38.00 | 38.29 | 38.47 | 38.45 | 38.60 | 38.17 | 37.79 | 38.13 | 38.38 | 38.67 | 38.71 | 38.40 | 38.55 | 38.76 |
| TIO2 | 0.00 | 0.00 | 0.42 | 0.00 | 0.00 | 0.00 | 0.00 | 0.00 | 0.00 | 0.00 | 0.00 | 0.00 | 0.00 | 0.00 | 0.00 | 0.00 | 0.00 | 0.00 | 0.00 | 0.00 |
| AL2O3 | 21.00 | 21.43 | 21.13 | 21.42 | 20.36 | 20.56 | 21.23 | 21.46 | 21.21 | 22.13 | 21.47 | 21.26 | 20.82 | 21.12 | 21.19 | 21.40 | 21.74 | 21.47 | 21.57 | 21.38 |
| FEO | 29.84 | 29.66 | 29.97 | 29.87 | 30.03 | 33.60 | 29.51 | 29.88 | 29.64 | 32.71 | 33.13 | 34.71 | 32.74 | 31.94 | 30.57 | 31.41 | 34.57 | 33.29 | 32.14 | 34.31 |
| MNO | 7.50 | 7.17 | 7.74 | 7.39 | 6.45 | 3.98 | 5.63 | 5.34 | 5.34 | 3.98 | 4.21 | 2.67 | 4.47 | 5.35 | 7.17 | 6.19 | 2.99 | 4.14 | 4.29 | 1.74 |
| MGO | 0.77 | 0.79 | 0.78 | 0.65 | 0.91 | 1.69 | 1.07 | 1.05 | 1.07 | 1.91 | 1.61 | 2.22 | 1.69 | 1.39 | 0.98 | 1.41 | 2.10 | 0.49 | 0.82 | 1.20 |
| CAO | 5.56 | 5.50 | 5.12 | 5.55 | 5.21 | 1.89 | 6.16 | 6.44 | 6.63 | 4.29 | 3.66 | 3.59 | 4.39 | 4.15 | 4.95 | 4.63 | 3.56 | 6.28 | 6.21 | 5.36 |
| NA2O | 0.00 | 0.00 | 0.00 | 0.57 | 0.89 | 0.00 | 0.00 | 0.00 | 0.00 | 0.00 | 0.00 | 0.61 | 0.00 | 0.00 | 0.00 | 0.00 | 0.00 | 0.00 | 0.00 | 0.00 |
| K2O | 0.00 | 0.00 | 0.00 | 0.00 | 0.00 | 0.00 | 0.00 | 0.00 | 0.00 | 0.00 | 0.00 | 0.00 | 0.00 | 0.00 | 0.00 | 0.00 | 0.00 | 0.00 | 0.00 | 0.00 |
| TOTAL | 102.3 | 102.2 | 103.0 | 103.6 | 100.5 | 99.7 | 101.6 | 102.5 | 102.4 | 103.5 | 102.7 | 103.2 | 101.9 | 102.1 | 103.2 | 103.7 | 103.7 | 104.1 | 103.6 | 102.7 |
| | | | | | | | | | | | | | | Cations for 24 oxygen | | | | | | |
| SI | 5.99 | 5.98 | 5.98 | 6.01 | 5.99 | 6.14 | 6.03 | 6.03 | 6.06 | 5.98 | 6.06 | 6.01 | 6.02 | 6.04 | 6.04 | 6.04 | 6.02 | 6.00 | 6.02 | 6.08 |
| AL | 3.94 | 4.01 | 3.93 | 3.98 | 3.92 | 3.92 | 3.97 | 3.98 | 3.94 | 4.06 | 3.98 | 3.95 | 3.91 | 3.95 | 3.93 | 3.94 | 3.99 | 3.96 | 3.97 | 3.95 |
| FE2 | 3.97 | 3.94 | 3.96 | 3.94 | 4.10 | 4.55 | 3.92 | 3.93 | 3.90 | 4.26 | 4.35 | 4.57 | 4.36 | 4.24 | 4.02 | 4.10 | 4.50 | 4.35 | 4.20 | 4.50 |
| MN | 1.01 | 0.96 | 1.03 | 0.99 | 0.89 | 0.55 | 0.76 | 0.71 | 0.71 | 0.52 | 0.56 | 0.36 | 0.60 | 0.72 | 0.96 | 0.82 | 0.39 | 0.55 | 0.57 | 0.23 |
| MG | 0.18 | 0.19 | 0.18 | 0.15 | 0.22 | 0.41 | 0.25 | 0.25 | 0.25 | 0.44 | 0.38 | 0.52 | 0.40 | 0.33 | 0.23 | 0.33 | 0.49 | 0.11 | 0.19 | 0.28 |
| CA | 0.95 | 0.94 | 0.87 | 0.94 | 0.91 | 0.33 | 1.05 | 1.09 | 1.12 | 0.72 | 0.62 | 0.61 | 0.75 | 0.71 | 0.83 | 0.77 | 0.59 | 1.05 | 1.04 | 0.90 |
| | | | | | | | | | | | | | | End member concentrations | | | | | | |
| ALM | 64.97 | 65.35 | 65.50 | 65.47 | 66.96 | 78.02 | 65.56 | 65.81 | 65.20 | 71.66 | 73.70 | 75.53 | 71.34 | 70.73 | 66.57 | 68.11 | 75.31 | 71.74 | 70.03 | 76.12 |
| SPE | 16.54 | 16.01 | 17.13 | 16.42 | 14.56 | 9.36 | 12.66 | 11.91 | 11.90 | 8.83 | 9.48 | 5.88 | 9.86 | 11.99 | 15.82 | 13.58 | 6.60 | 9.04 | 9.46 | 3.90 |
| PYR | 2.99 | 3.12 | 3.04 | 2.52 | 3.60 | 6.99 | 4.24 | 4.12 | 4.21 | 7.46 | 6.39 | 8.59 | 6.55 | 5.49 | 3.82 | 5.43 | 8.15 | 1.87 | 3.18 | 4.73 |
| GRO | 15.50 | 15.53 | 14.33 | 15.59 | 14.87 | 5.63 | 17.53 | 18.17 | 18.69 | 12.05 | 10.42 | 10.00 | 12.25 | 11.78 | 13.80 | 12.87 | 9.94 | 17.35 | 17.33 | 15.25 |

**Garnet chemistry data**

| Sample | 66795 | 66801 | 68780 | 68780 | 68780 | 68793 | 68799 | 68799 | 68799 | 68799 | 68799 | 68799 | 68804 |
|---|---|---|---|---|---|---|---|---|---|---|---|---|---|
| SIO2 | 38.02 | 35.58 | 35.38 | 49.03 | 42.65 | 46.95 | 36.67 | 35.62 | 33.90 | 36.01 | 35.57 | 36.61 | 33.96 |
| TIO2 | 0.75 | 3.78 | 3.13 | 0.36 | 0.60 | 0.38 | 2.60 | 2.33 | 1.59 | 2.66 | 3.12 | 2.82 | 3.96 |
| AL203 | 27.16 | 18.18 | 19.15 | 32.65 | 26.39 | 33.18 | 16.82 | 16.84 | 16.66 | 16.97 | 16.48 | 16.68 | 17.85 |
| FEO | 13.66 | 18.95 | 18.04 | 4.41 | 10.40 | 5.19 | 19.95 | 19.95 | 20.09 | 18.13 | 19.45 | 19.00 | 24.52 |
| MNO | 0.13 | 0.21 | 0.00 | 0.00 | 0.00 | 0.00 | 0.30 | 0.47 | 0.46 | 0.46 | 0.42 | 0.36 | 0.00 |
| MGO | 7.23 | 8.66 | 11.16 | 1.56 | 6.97 | 2.53 | 10.23 | 10.51 | 11.88 | 9.74 | 9.07 | 10.30 | 10.01 |
| CAO | 0.02 | 0.00 | 0.00 | 0.00 | 0.32 | 0.00 | 0.04 | 0.10 | 0.27 | 0.03 | 0.02 | 0.03 | 0.00 |
| NA20 | 0.36 | 0.14 | 0.00 | 0.00 | 0.75 | 0.00 | 0.44 | 0.22 | 0.01 | 0.00 | 0.21 | 0.07 | 0.00 |
| K20 | 4.81 | 9.69 | 8.32 | 7.52 | 6.15 | 8.48 | 9.58 | 9.08 | 6.26 | 9.66 | 9.37 | 9.18 | 6.09 |
| TOTAL | 92.1 | 95.2 | 95.2 | 95.5 | 94.2 | 96.7 | 96.6 | 95.1 | 91.1 | 93.7 | 93.7 | 95.1 | 96.4 |
| | | | | | | Total cations | | | | | | | |
| SI | 5.54 | 5.43 | 5.32 | 6.45 | 5.98 | 6.20 | 5.53 | 5.47 | 5.37 | 5.57 | 5.54 | 5.57 | 5.16 |
| TI | 0.08 | 0.43 | 0.35 | 0.04 | 0.06 | 0.04 | 0.30 | 0.27 | 0.19 | 0.31 | 0.37 | 0.32 | 0.45 |
| ALIV | 2.46 | 2.57 | 2.68 | 1.55 | 2.02 | 1.80 | 2.47 | 2.53 | 2.63 | 2.43 | 2.46 | 2.43 | 2.84 |
| ALVI | 2.21 | 0.70 | 0.71 | 3.52 | 2.34 | 3.36 | 0.53 | 0.51 | 0.48 | 0.66 | 0.56 | 0.57 | 0.36 |
| FE2 | 1.67 | 2.42 | 2.27 | 0.49 | 1.22 | 0.57 | 2.52 | 2.56 | 2.66 | 2.34 | 2.53 | 2.42 | 3.12 |
| MN | 0.02 | 0.03 | 0.00 | 0.00 | 0.00 | 0.00 | 0.04 | 0.06 | 0.06 | 0.06 | 0.06 | 0.05 | 0.00 |
| MG | 1.57 | 1.97 | 2.50 | 0.31 | 1.46 | 0.50 | 2.30 | 2.40 | 2.81 | 2.24 | 2.10 | 2.34 | 2.27 |
| CA | 0.00 | 0.00 | 0.00 | 0.00 | 0.05 | 0.00 | 0.01 | 0.02 | 0.05 | 0.00 | 0.00 | 0.01 | 0.00 |
| NA | 0.10 | 0.04 | 0.00 | 0.00 | 0.20 | 0.00 | 0.13 | 0.07 | 0.00 | 0.00 | 0.06 | 0.02 | 0.00 |
| K | 0.89 | 1.89 | 1.60 | 1.26 | 1.10 | 1.43 | 1.85 | 1.78 | 1.27 | 1.91 | 1.86 | 1.78 | 1.18 |
| | | | | | | End member concentrations | | | | | | | |
| XFE | 0.51 | 0.55 | 0.48 | 0.61 | 0.46 | 0.53 | 0.52 | 0.51 | 0.48 | 0.50 | 0.54 | 0.50 | 0.58 |
| XMG | 0.48 | 0.45 | 0.52 | 0.39 | 0.54 | 0.47 | 0.47 | 0.48 | 0.51 | 0.48 | 0.45 | 0.49 | 0.42 |
| XMN | 0.00 | 0.01 | 0.00 | 0.00 | 0.00 | 0.00 | 0.01 | 0.01 | 0.01 | 0.01 | 0.01 | 0.01 | 0.00 |

**Biotite chemistry data**

| Sample | 68804 | 68806 | 69215 | 69215 | 69215 | 69215 | 69219 | 69229 | 69229 | 69229 | 69229 | 69230 | 69230 |
|---|---|---|---|---|---|---|---|---|---|---|---|---|---|
| SIO2 | 35.80 | 44.94 | 36.83 | 37.13 | 36.27 | 36.44 | 36.91 | 36.86 | 35.53 | 36.77 | 36.62 | 35.97 | 36.01 |
| TIO2 | 3.72 | 0.94 | 3.04 | 3.36 | 3.27 | 3.20 | 2.08 | 1.80 | 1.69 | 1.89 | 1.47 | 2.35 | 1.70 |
| AL203 | 17.79 | 32.89 | 19.05 | 19.60 | 19.66 | 20.23 | 21.31 | 20.30 | 19.83 | 20.62 | 21.20 | 24.27 | 20.17 |
| FEO | 19.80 | 3.80 | 18.67 | 18.86 | 19.66 | 19.86 | 16.38 | 20.07 | 21.47 | 20.53 | 21.03 | 19.11 | 21.23 |
| MNO | 0.00 | 0.00 | 0.00 | 0.00 | 0.00 | 0.00 | 0.00 | 0.00 | 0.00 | 0.00 | 0.00 | 0.00 | 0.00 |
| MGO | 9.63 | 0.62 | 10.77 | 10.80 | 9.86 | 9.62 | 11.57 | 9.89 | 9.32 | 9.14 | 9.08 | 5.30 | 9.43 |
| CAO | 0.00 | 0.00 | 0.00 | 0.00 | 0.00 | 0.00 | 0.00 | 0.00 | 0.00 | 0.00 | 0.00 | 0.20 | 0.00 |
| NA20 | 0.00 | 0.78 | 0.00 | 0.59 | 0.00 | 0.00 | 0.00 | 0.00 | 0.00 | 0.00 | 0.00 | 0.52 | 0.53 |
| K20 | 9.47 | 9.89 | 9.15 | 9.42 | 9.08 | 8.82 | 8.70 | 8.93 | 8.34 | 9.26 | 7.28 | 6.09 | 8.44 |
| TOTAL | 96.2 | 93.9 | 97.5 | 99.8 | 97.8 | 98.2 | 97.0 | 97.8 | 96.2 | 98.2 | 96.7 | 93.8 | 97.5 |
| SI | 5.41 | 6.16 | 5.42 | 5.36 | 5.35 | 5.34 | 5.37 | 5.42 | 5.36 | 5.41 | 5.42 | 5.39 | 5.35 |
| TI | 0.42 | 0.10 | 0.34 | 0.37 | 0.36 | 0.35 | 0.23 | 0.20 | 0.19 | 0.21 | 0.16 | 0.26 | 0.19 |
| ALIV | 2.59 | 1.84 | 2.58 | 2.64 | 2.65 | 2.66 | 2.63 | 2.58 | 2.64 | 2.59 | 2.58 | 2.61 | 2.65 |
| ALVI | 0.58 | 3.47 | 0.73 | 0.69 | 0.77 | 0.84 | 1.03 | 0.94 | 0.89 | 0.99 | 1.12 | 1.67 | 0.89 |
| FE2 | 2.50 | 0.44 | 2.30 | 2.28 | 2.43 | 2.44 | 1.99 | 2.47 | 2.71 | 2.53 | 2.60 | 2.39 | 2.64 |
| MN | 0.00 | 0.00 | 0.00 | 0.00 | 0.00 | 0.00 | 0.00 | 0.00 | 0.00 | 0.00 | 0.00 | 0.00 | 0.00 |
| MG | 2.17 | 0.13 | 2.36 | 2.32 | 2.17 | 2.10 | 2.51 | 2.17 | 2.09 | 2.00 | 2.00 | 1.18 | 2.09 |
| CA | 0.00 | 0.00 | 0.00 | 0.00 | 0.00 | 0.00 | 0.00 | 0.00 | 0.00 | 0.00 | 0.00 | 0.03 | 0.00 |
| NA | 0.00 | 0.21 | 0.00 | 0.17 | 0.00 | 0.00 | 0.00 | 0.00 | 0.00 | 0.00 | 0.00 | 0.15 | 0.15 |
| K | 1.82 | 1.73 | 1.72 | 1.73 | 1.71 | 1.65 | 1.62 | 1.68 | 1.60 | 1.74 | 1.37 | 1.16 | 1.60 |
| XFE | 0.54 | 0.78 | 0.49 | 0.49 | 0.53 | 0.54 | 0.44 | 0.53 | 0.56 | 0.56 | 0.57 | 0.67 | 0.56 |
| XMG | 0.46 | 0.22 | 0.51 | 0.51 | 0.47 | 0.46 | 0.56 | 0.47 | 0.44 | 0.44 | 0.43 | 0.33 | 0.44 |
| XMN | 0.00 | 0.00 | 0.00 | 0.00 | 0.00 | 0.00 | 0.00 | 0.00 | 0.00 | 0.00 | 0.00 | 0.00 | 0.00 |

**Biotite chemistry data**

| Sample | 69230 | 69236 | 69236 | 69238 | 69238 | 69238 | 69277 | 69277 | 69277 | 69619 | 69619 | 69623 | 69623 |
|---|---|---|---|---|---|---|---|---|---|---|---|---|---|
| SIO2 | 35.58 | 37.53 | 35.01 | 38.44 | 36.95 | 35.79 | 35.87 | 35.71 | 35.93 | 45.23 | 36.97 | 34.39 | 41.47 |
| TIO2 | 1.59 | 2.89 | 2.40 | 2.40 | 1.72 | 2.00 | 1.94 | 1.50 | 1.94 | 0.44 | 1.67 | 1.54 | 0.40 |
| AL203 | 19.90 | 18.97 | 19.65 | 18.35 | 20.30 | 20.11 | 21.40 | 20.41 | 20.07 | 29.45 | 19.90 | 19.74 | 32.16 |
| FEO | 20.75 | 23.57 | 26.84 | 22.25 | 21.19 | 22.93 | 21.27 | 21.74 | 21.53 | 7.02 | 24.03 | 21.58 | 10.72 |
| MNO | 0.00 | 0.00 | 0.00 | 0.00 | 0.00 | 0.18 | 0.00 | 0.00 | 0.00 | 0.14 | 2.06 | 0.11 | 0.03 |
| MGO | 9.35 | 7.65 | 8.61 | 7.20 | 7.38 | 8.15 | 7.60 | 9.24 | 8.34 | 2.19 | 7.37 | 9.11 | 3.36 |
| CAO | 0.00 | 0.21 | 0.00 | 0.00 | 0.18 | 0.00 | 0.00 | 0.00 | 0.00 | 0.10 | 0.86 | 0.02 | 0.02 |
| NA20 | 0.59 | 0.00 | 0.00 | 0.00 | 0.74 | 0.69 | 0.00 | 0.51 | 0.49 | 0.41 | 0.36 | 0.09 | 1.48 |
| K20 | 8.25 | 8.95 | 6.88 | 7.65 | 8.79 | 8.42 | 8.25 | 7.92 | 8.44 | 9.74 | 5.84 | 7.40 | 6.33 |
| TOTAL | 96.0 | 99.8 | 99.4 | 96.3 | 97.3 | 97.1 | 96.3 | 97.0 | 96.7 | 94.7 | 99.1 | 94.0 | 96.0 |

Total cations

| | | | | | | | | | | | | | |
|---|---|---|---|---|---|---|---|---|---|---|---|---|---|
| SI | 5.37 | 5.50 | 5.20 | 5.75 | 5.51 | 5.08 | 5.37 | 5.33 | 5.39 | 6.25 | 5.44 | 5.31 | 5.71 |
| TI | 0.18 | 0.32 | 0.27 | 0.27 | 0.19 | 0.21 | 0.22 | 0.17 | 0.22 | 0.05 | 0.19 | 0.18 | 0.04 |
| ALIV | 2.63 | 2.50 | 2.80 | 2.25 | 2.49 | 2.92 | 2.63 | 2.67 | 2.61 | 1.75 | 2.56 | 2.69 | 2.29 |
| ALVI | 0.90 | 0.78 | 0.64 | 0.98 | 1.07 | 0.44 | 1.15 | 0.93 | 0.94 | 3.05 | 0.89 | 0.90 | 2.92 |
| FE2 | 2.62 | 2.89 | 3.34 | 2.78 | 2.64 | 2.72 | 2.66 | 2.72 | 2.70 | 0.81 | 2.96 | 2.79 | 1.23 |
| MN | 0.00 | 0.00 | 0.00 | 0.00 | 0.00 | 0.02 | 0.00 | 0.00 | 0.00 | 0.02 | 0.26 | 0.01 | 0.00 |
| MG | 2.10 | 1.67 | 1.91 | 1.60 | 1.64 | 1.72 | 1.70 | 2.06 | 1.87 | 0.45 | 1.62 | 2.10 | 0.69 |
| CA | 0.00 | 0.03 | 0.00 | 0.00 | 0.03 | 0.00 | 0.00 | 0.00 | 0.00 | 0.02 | 0.14 | 0.00 | 0.00 |
| NA | 0.17 | 0.00 | 0.00 | 0.00 | 0.21 | 0.19 | 0.00 | 0.15 | 0.14 | 0.11 | 0.10 | 0.03 | 0.39 |
| K | 1.59 | 1.68 | 1.30 | 1.46 | 1.67 | 1.52 | 1.58 | 1.51 | 1.62 | 1.72 | 1.10 | 1.46 | 1.11 |

End member concentrations

| | | | | | | | | | | | | | |
|---|---|---|---|---|---|---|---|---|---|---|---|---|---|
| XFE | 0.55 | 0.63 | 0.64 | 0.63 | 0.62 | 0.49 | 0.61 | 0.57 | 0.59 | 0.64 | 0.61 | 0.57 | 0.64 |
| XMG | 0.45 | 0.37 | 0.36 | 0.37 | 0.38 | 0.31 | 0.39 | 0.43 | 0.41 | 0.35 | 0.33 | 0.43 | 0.36 |
| XMN | 0.00 | 0.00 | 0.00 | 0.00 | 0.00 | 0.20 | 0.00 | 0.00 | 0.00 | 0.01 | 0.05 | 0.00 | 0.00 |

**Biotite chemistry data**

| Sample | 69625 | 69627 | 69627 | 69635 | 71898 | 71901 | 71901 | 71901 | 71906 | 71906 | 71906 | 71906 |
|---|---|---|---|---|---|---|---|---|---|---|---|---|
| SI02 | 44.91 | 31.91 | 46.24 | 34.54 | 38.99 | 36.10 | 36.28 | 35.75 | 36.72 | 36.62 | 35.41 | 36.88 |
| TI02 | 0.53 | 1.66 | 0.72 | 2.85 | 0.51 | 3.60 | 3.53 | 3.04 | 4.56 | 6.42 | 4.26 | 4.76 |
| AL203 | 31.12 | 18.86 | 35.38 | 19.70 | 24.49 | 18.26 | 18.53 | 18.68 | 18.91 | 18.27 | 19.06 | 18.89 |
| FE0 | 5.19 | 24.63 | 0.88 | 22.10 | 19.26 | 21.81 | 22.09 | 21.67 | 19.58 | 19.58 | 22.26 | 20.27 |
| MN0 | 0.09 | 0.11 | 0.02 | 0.14 | 0.00 | 0.44 | 0.32 | 0.00 | 0.00 | 0.00 | 0.00 | 0.00 |
| MG0 | 2.21 | 8.19 | 0.62 | 6.54 | 4.81 | 8.01 | 7.76 | 8.50 | 8.76 | 9.34 | 9.05 | 9.17 |
| CA0 | 0.00 | 0.03 | 0.00 | 0.00 | 0.00 | 0.00 | 0.00 | 0.00 | 0.00 | 0.00 | 0.00 | 0.00 |
| NA20 | 0.34 | 0.28 | 1.24 | 0.15 | 0.00 | 0.00 | 0.00 | 0.00 | 0.00 | 0.00 | 0.00 | 0.00 |
| K20 | 8.82 | 7.17 | 9.70 | 9.63 | 6.12 | 9.81 | 9.89 | 9.59 | 9.88 | 9.90 | 8.37 | 10.06 |
| TOTAL | 93.2 | 92.8 | 94.8 | 95.6 | 94.2 | 98.0 | 98.4 | 97.2 | 98.4 | 100.1 | 98.4 | 100.0 |
| | | | | Total cations | | | | | | | | |
| SI | 6.20 | 5.11 | 6.16 | 5.32 | 5.75 | 5.41 | 5.42 | 5.39 | 5.41 | 5.31 | 5.25 | 5.36 |
| TI | 0.06 | 0.20 | 0.07 | 0.33 | 0.06 | 0.41 | 0.40 | 0.34 | 0.51 | 0.70 | 0.47 | 0.52 |
| ALIV | 1.80 | 2.89 | 1.84 | 2.68 | 2.25 | 2.59 | 2.58 | 2.61 | 2.59 | 2.69 | 2.75 | 2.64 |
| ALVI | 3.27 | 0.67 | 3.71 | 0.90 | 2.00 | 0.64 | 0.68 | 0.70 | 0.69 | 0.43 | 0.58 | 0.60 |
| FE2 | 0.60 | 3.30 | 0.10 | 2.85 | 2.37 | 2.74 | 2.76 | 2.73 | 2.41 | 2.37 | 2.76 | 2.46 |
| MN | 0.01 | 0.01 | 0.00 | 0.02 | 0.00 | 0.06 | 0.04 | 0.00 | 0.00 | 0.00 | 0.00 | 0.00 |
| MG | 0.45 | 1.95 | 0.12 | 1.50 | 1.06 | 1.79 | 1.73 | 1.91 | 1.92 | 2.02 | 2.00 | 1.99 |
| CA | 0.00 | 0.00 | 0.00 | 0.00 | 0.00 | 0.00 | 0.00 | 0.00 | 0.00 | 0.00 | 0.00 | 0.00 |
| NA | 0.09 | 0.09 | 0.32 | 0.04 | 0.00 | 0.00 | 0.00 | 0.00 | 0.00 | 0.00 | 0.00 | 0.00 |
| K | 1.55 | 1.46 | 1.65 | 1.89 | 1.15 | 1.88 | 1.88 | 1.84 | 1.85 | 1.83 | 1.58 | 1.86 |
| | | | | End member concentrations | | | | | | | | |
| XFE | 0.56 | 0.63 | 0.44 | 0.65 | 0.69 | 0.60 | 0.61 | 0.59 | 0.56 | 0.54 | 0.58 | 0.55 |
| XMG | 0.43 | 0.37 | 0.55 | 0.34 | 0.31 | 0.39 | 0.38 | 0.41 | 0.44 | 0.46 | 0.42 | 0.45 |
| XMN | 0.01 | 0.00 | 0.01 | 0.00 | 0.00 | 0.01 | 0.01 | 0.00 | 0.00 | 0.00 | 0.00 | 0.00 |

**Biotite chemistry data**

Figure 2.4: Field appearance of the Roeillaun Schist Member of the Streamstown Formation, showing the typical conspicuous garnet porphyroblasts. Lens cap is 49mm diameter.


Figure 2.5: Inverted graded grit horizon within the Tonabina Marble Member of the Lakes Marble Formation at [GR 684 586]. Note the typical saccharoidal weathering of the marble. Lens cap is 49mm diameter.

| Sample | 71906 | 71906 | 71912 | 71914 | 71914 | 71916 | 71916 | 71918 | 71918 | 71928 | 71932 | 71934 | 71934 | 71934 |
|---|---|---|---|---|---|---|---|---|---|---|---|---|---|---|
| SI02 | 35.64 | 36.87 | 39.70 | 28.68 | 34.70 | 36.56 | 36.65 | 37.25 | 37.08 | 38.24 | 34.49 | 36.21 | 35.85 | 43.43 |
| TI02 | 4.93 | 4.65 | 0.00 | 0.62 | 1.45 | 1.88 | 1.90 | 0.69 | 1.41 | 1.73 | 2.18 | 2.13 | 1.70 | 1.68 |
| AL203 | 19.09 | 19.75 | 28.90 | 18.64 | 19.56 | 19.61 | 18.89 | 22.17 | 21.30 | 18.24 | 19.10 | 19.33 | 19.44 | 20.39 |
| FE0 | 19.61 | 19.42 | 16.37 | 30.62 | 24.63 | 19.13 | 20.28 | 21.75 | 20.19 | 16.91 | 22.03 | 21.38 | 22.25 | 17.69 |
| MN0 | 0.00 | 0.00 | 0.00 | 0.00 | 0.00 | 0.00 | 0.00 | 0.00 | 0.00 | 0.00 | 0.00 | 0.00 | 0.00 | 0.00 |
| MG0 | 8.52 | 8.36 | 2.37 | 10.96 | 8.80 | 10.85 | 11.78 | 6.73 | 6.29 | 12.11 | 8.46 | 8.33 | 8.22 | 5.66 |
| CA0 | 0.00 | 0.00 | 0.00 | 0.00 | 1.10 | 0.00 | 0.00 | 0.00 | 0.00 | 0.00 | 0.00 | 0.00 | 0.00 | 0.68 |
| NA20 | 0.00 | 0.00 | 0.00 | 0.00 | 0.00 | 0.00 | 0.00 | 0.00 | 0.00 | 0.00 | 0.00 | 0.00 | 0.00 | 3.10 |
| K20 | 9.41 | 9.85 | 5.57 | 1.20 | 2.53 | 9.03 | 7.82 | 5.68 | 6.21 | 9.80 | 8.08 | 9.53 | 9.61 | 5.72 |
| TOTAL | 97.2 | 98.9 | 92.9 | 90.7 | 92.8 | 97.1 | 97.3 | 94.3 | 92.5 | 97.0 | 94.3 | 96.9 | 97.1 | 98.3 |

Total cations

| | | | | | | | | | | | | | | |
|---|---|---|---|---|---|---|---|---|---|---|---|---|---|---|
| SI | 5.31 | 5.38 | 5.77 | 4.71 | 5.35 | 5.41 | 5.41 | 5.59 | 5.66 | 5.62 | 5.33 | 5.45 | 5.42 | 6.12 |
| TI | 0.55 | 0.51 | 0.00 | 0.08 | 0.17 | 0.21 | 0.21 | 0.08 | 0.16 | 0.19 | 0.25 | 0.24 | 0.19 | 0.18 |
| ALIV | 2.69 | 2.62 | 2.23 | 3.29 | 2.65 | 2.59 | 2.59 | 2.41 | 2.34 | 2.38 | 2.67 | 2.55 | 2.58 | 1.88 |
| ALVI | 0.67 | 0.78 | 2.73 | 0.32 | 0.91 | 0.84 | 0.70 | 1.51 | 1.49 | 0.78 | 0.82 | 0.88 | 0.88 | 1.51 |
| FE2 | 2.45 | 2.37 | 1.99 | 4.21 | 3.18 | 2.37 | 2.50 | 2.73 | 2.58 | 2.08 | 2.85 | 2.69 | 2.81 | 2.09 |
| MN | 0.00 | 0.00 | 0.00 | 0.00 | 0.00 | 0.00 | 0.00 | 0.00 | 0.00 | 0.00 | 0.00 | 0.00 | 0.00 | 0.00 |
| MG | 1.89 | 1.82 | 0.51 | 2.68 | 2.02 | 2.40 | 2.59 | 1.50 | 1.43 | 2.65 | 1.95 | 1.87 | 1.85 | 1.19 |
| CA | 0.00 | 0.00 | 0.00 | 0.00 | 0.18 | 0.00 | 0.00 | 0.00 | 0.00 | 0.00 | 0.00 | 0.00 | 0.00 | 0.10 |
| NA | 0.00 | 0.00 | 0.00 | 0.00 | 0.00 | 0.00 | 0.00 | 0.00 | 0.00 | 0.00 | 0.00 | 0.00 | 0.00 | 0.85 |
| K | 1.79 | 1.84 | 1.03 | 0.25 | 0.50 | 1.71 | 1.47 | 1.09 | 1.21 | 1.84 | 1.59 | 1.83 | 1.85 | 1.03 |

End member concentrations

| | | | | | | | | | | | | | | |
|---|---|---|---|---|---|---|---|---|---|---|---|---|---|---|
| XFE | 0.56 | 0.57 | 0.79 | 0.61 | 0.61 | 0.50 | 0.49 | 0.64 | 0.64 | 0.44 | 0.59 | 0.59 | 0.60 | 0.64 |
| XMG | 0.44 | 0.43 | 0.21 | 0.39 | 0.39 | 0.50 | 0.51 | 0.36 | 0.36 | 0.56 | 0.41 | 0.41 | 0.40 | 0.36 |
| XMN | 0.00 | 0.00 | 0.00 | 0.00 | 0.00 | 0.00 | 0.00 | 0.00 | 0.00 | 0.00 | 0.00 | 0.00 | 0.00 | 0.00 |

**Biotite chemistry data**

| Sample | 66801 | 66801 | 68806 | 68806 | 68806 | 69229 | 69229 | 69229 | 69229 | 69230 | 69230 | 69230 | 69230 | 69236 | 69238 | 69238 | 69238 | 69277 | 69277 | 69277 | 69619 | 69619 |
|---|---|---|---|---|---|---|---|---|---|---|---|---|---|---|---|---|---|---|---|---|---|---|
| Code | C | C | R | R | R | R | R | R | R | R | R | R | R | R | R | R | R | R | R | R | C | C |
| SIO2 | 45.82 | 45.85 | 46.12 | 45.60 | 45.53 | 47.53 | 47.71 | 46.51 | 46.69 | 46.59 | 49.42 | 46.46 | 47.71 | 47.24 | 45.01 | 46.15 | 46.54 | 45.03 | 46.49 | 45.39 | 45.92 | 45.79 |
| TIO2 | 1.43 | 1.22 | 0.70 | 1.01 | 0.85 | 0.58 | 0.48 | 0.78 | 0.60 | 0.27 | 0.00 | 0.39 | 0.29 | 1.02 | 0.51 | 0.66 | 0.69 | 0.62 | 0.72 | 0.50 | 1.14 | 0.57 |
| AL203 | 33.04 | 33.25 | 33.59 | 32.88 | 32.13 | 35.31 | 34.14 | 36.68 | 35.35 | 34.03 | 34.26 | 35.01 | 35.22 | 34.86 | 34.10 | 34.89 | 35.12 | 33.86 | 36.72 | 35.43 | 34.70 | 35.49 |
| FEO | 2.98 | 2.90 | 3.62 | 3.38 | 3.60 | 1.02 | 1.22 | 0.96 | 1.63 | 2.28 | 1.63 | 1.84 | 1.41 | 1.71 | 3.32 | 2.54 | 2.82 | 5.25 | 1.04 | 2.92 | 1.63 | 1.36 |
| MNO | 0.00 | 0.00 | 0.00 | 0.00 | 0.00 | 0.00 | 0.00 | 0.00 | 0.00 | 0.00 | 0.00 | 0.00 | 0.00 | 0.00 | 0.00 | 0.00 | 0.00 | 0.00 | 0.00 | 0.00 | 0.00 | 0.07 |
| MGO | 0.46 | 0.59 | 1.11 | 0.83 | 0.73 | 0.40 | 0.43 | 0.00 | 0.39 | 0.77 | 0.99 | 0.45 | 0.74 | 0.41 | 0.57 | 0.00 | 0.43 | 0.84 | 0.40 | 0.41 | 0.53 | 0.47 |
| CAO | 0.00 | 0.00 | 0.21 | 0.00 | 0.00 | 0.00 | 0.00 | 0.00 | 0.00 | 0.00 | 0.00 | 0.00 | 0.00 | 0.00 | 0.00 | 0.00 | 0.00 | 0.00 | 0.00 | 0.00 | 0.00 | 0.00 |
| NA20 | 0.46 | 0.53 | 0.63 | 0.00 | 0.63 | 0.64 | 0.78 | 1.25 | 0.94 | 0.72 | 0.81 | 1.17 | 0.99 | 0.85 | 1.44 | 1.37 | 1.20 | 0.81 | 1.44 | 1.09 | 0.51 | 0.36 |
| K20 | 10.30 | 10.87 | 10.05 | 9.81 | 9.50 | 9.71 | 9.84 | 9.82 | 9.61 | 8.56 | 8.97 | 8.29 | 8.81 | 10.90 | 9.15 | 9.34 | 9.79 | 9.05 | 9.33 | 9.55 | 10.63 | 10.77 |
| TOTAL | 94.5 | 95.2 | 96.0 | 93.5 | 93.0 | 95.2 | 94.6 | 96.0 | 95.2 | 93.2 | 96.1 | 93.6 | 95.2 | 97.0 | 94.1 | 95.0 | 96.6 | 95.4 | 96.1 | 95.3 | 95.1 | 94.9 |

Total cations

| | | | | | | | | | | | | | | | | | | | | | | |
|---|---|---|---|---|---|---|---|---|---|---|---|---|---|---|---|---|---|---|---|---|---|---|
| SI | 6.21 | 6.18 | 6.16 | 6.22 | 6.26 | 6.28 | 6.35 | 6.11 | 6.20 | 6.29 | 6.44 | 6.23 | 6.29 | 6.20 | 6.11 | 6.18 | 6.14 | 6.08 | 6.09 | 6.07 | 6.15 | 6.13 |
| TI | 0.15 | 0.12 | 0.07 | 0.10 | 0.09 | 0.06 | 0.05 | 0.08 | 0.06 | 0.03 | 0.00 | 0.04 | 0.03 | 0.10 | 0.05 | 0.07 | 0.07 | 0.06 | 0.07 | 0.05 | 0.11 | 0.06 |
| ALIV | 1.79 | 1.82 | 1.84 | 1.78 | 1.74 | 1.72 | 1.65 | 1.89 | 1.80 | 1.71 | 1.56 | 1.77 | 1.71 | 1.80 | 1.89 | 1.82 | 1.86 | 1.92 | 1.91 | 1.93 | 1.85 | 1.87 |
| ALVI | 3.48 | 3.47 | 3.46 | 3.51 | 3.47 | 3.77 | 3.71 | 3.80 | 3.73 | 3.70 | 3.71 | 3.77 | 3.76 | 3.60 | 3.58 | 3.68 | 3.61 | 3.46 | 3.77 | 3.66 | 3.62 | 3.73 |
| FE2 | 0.34 | 0.33 | 0.40 | 0.39 | 0.41 | 0.11 | 0.14 | 0.11 | 0.18 | 0.26 | 0.18 | 0.21 | 0.16 | 0.19 | 0.38 | 0.28 | 0.31 | 0.59 | 0.11 | 0.33 | 0.18 | 0.15 |
| MN | 0.00 | 0.00 | 0.00 | 0.00 | 0.00 | 0.00 | 0.00 | 0.00 | 0.00 | 0.00 | 0.00 | 0.00 | 0.00 | 0.00 | 0.00 | 0.00 | 0.00 | 0.00 | 0.00 | 0.00 | 0.00 | 0.01 |
| MG | 0.09 | 0.12 | 0.22 | 0.17 | 0.15 | 0.08 | 0.09 | 0.00 | 0.08 | 0.16 | 0.19 | 0.09 | 0.15 | 0.08 | 0.12 | 0.00 | 0.08 | 0.17 | 0.08 | 0.08 | 0.11 | 0.09 |
| CA | 0.00 | 0.00 | 0.03 | 0.00 | 0.00 | 0.00 | 0.00 | 0.00 | 0.00 | 0.00 | 0.00 | 0.00 | 0.00 | 0.00 | 0.00 | 0.00 | 0.00 | 0.00 | 0.00 | 0.00 | 0.00 | 0.00 |
| NA | 0.12 | 0.14 | 0.16 | 0.00 | 0.17 | 0.16 | 0.20 | 0.32 | 0.24 | 0.19 | 0.21 | 0.30 | 0.25 | 0.22 | 0.38 | 0.36 | 0.31 | 0.21 | 0.37 | 0.28 | 0.13 | 0.09 |
| K | 1.78 | 1.87 | 1.71 | 1.71 | 1.67 | 1.64 | 1.67 | 1.65 | 1.63 | 1.47 | 1.49 | 1.42 | 1.48 | 1.83 | 1.59 | 1.59 | 1.65 | 1.56 | 1.56 | 1.63 | 1.81 | 1.84 |

**Muscovite chemistry data**

| Sample | 69619 | 69619 | 69623 | 69623 | 69625 | 69625 | 69625 | 69625 | 69627 | 69635 | 69635 | 71898 | 71898 | 71898 | 71901 | 71901 | 71901 | 71912 | 71914 | 71914 |
|---|---|---|---|---|---|---|---|---|---|---|---|---|---|---|---|---|---|---|---|---|
| Code | C | C | R | R | R | R | R | R | R | C | C | C | C | C | C | C | C | R | R | R |
| SI02 | 46.50 | 46.34 | 45.90 | 46.16 | 46.13 | 46.49 | 46.26 | 46.49 | 46.29 | 47.36 | 45.77 | 46.35 | 46.51 | 46.26 | 45.80 | 46.87 | 46.22 | 44.25 | 49.57 | 45.64 |
| TI02 | 1.03 | 1.00 | 0.61 | 0.53 | 0.76 | 0.72 | 0.73 | 0.50 | 0.54 | 1.18 | 1.24 | 1.19 | 0.77 | 1.21 | 1.13 | 1.09 | 1.05 | 0.00 | 0.00 | 0.96 |
| AL203 | 34.71 | 35.22 | 35.98 | 36.02 | 35.13 | 32.49 | 35.75 | 35.61 | 33.39 | 35.51 | 34.72 | 33.50 | 34.66 | 34.11 | 33.01 | 32.96 | 33.42 | 31.97 | 19.85 | 32.62 |
| FE0 | 1.50 | 1.77 | 1.28 | 1.65 | 0.93 | 1.42 | 1.02 | 1.33 | 2.20 | 1.19 | 1.23 | 2.36 | 2.38 | 2.79 | 4.11 | 3.41 | 3.74 | 1.74 | 10.79 | 3.63 |
| MN0 | 0.08 | 0.00 | 0.03 | 0.06 | 0.00 | 0.08 | 0.01 | 0.05 | 0.04 | 0.08 | 0.12 | 0.00 | 0.00 | 0.00 | 0.00 | 0.00 | 0.00 | 0.00 | 0.00 | 0.00 |
| MG0 | 0.33 | 0.35 | 0.26 | 0.52 | 0.32 | 1.00 | 0.28 | 0.64 | 0.60 | 0.57 | 0.34 | 0.00 | 0.00 | 0.00 | 0.00 | 0.00 | 0.00 | 0.00 | 3.56 | 0.00 |
| CA0 | 0.00 | 0.00 | 0.00 | 0.00 | 0.00 | 0.04 | 0.00 | 0.00 | 0.00 | 0.00 | 0.00 | 0.00 | 0.00 | 0.00 | 0.00 | 0.00 | 0.00 | 0.00 | 0.00 | 0.00 |
| NA20 | 0.46 | 0.70 | 1.83 | 1.68 | 0.98 | 0.72 | 0.88 | 1.12 | 0.82 | 0.93 | 0.52 | 0.00 | 0.00 | 0.00 | 0.00 | 0.00 | 0.00 | 0.00 | 1.47 | 0.00 |
| K20 | 10.87 | 10.65 | 8.85 | 8.87 | 9.90 | 9.57 | 9.58 | 9.60 | 9.53 | 10.56 | 10.27 | 10.04 | 10.21 | 10.19 | 10.50 | 10.68 | 10.51 | 9.19 | 9.43 | 10.33 |
| TOTAL | 95.5 | 96.0 | 94.7 | 95.5 | 94.1 | 92.5 | 94.5 | 95.3 | 93.4 | 97.4 | 94.2 | 93.4 | 94.5 | 94.6 | 94.5 | 95.0 | 94.9 | 87.2 | 94.7 | 93.2 |
| | | | | | | | | | | | | Total cations | | | | | | | | |
| SI | 6.20 | 6.14 | 6.11 | 6.11 | 6.19 | 6.35 | 6.16 | 6.16 | 6.28 | 6.17 | 6.16 | 6.29 | 6.24 | 6.22 | 6.23 | 6.31 | 6.24 | 6.39 | 6.99 | 6.27 |
| TI | 0.10 | 0.10 | 0.06 | 0.05 | 0.08 | 0.07 | 0.07 | 0.05 | 0.05 | 0.12 | 0.13 | 0.12 | 0.08 | 0.12 | 0.12 | 0.11 | 0.11 | 0.00 | 0.00 | 0.10 |
| ALIV | 1.80 | 1.86 | 1.89 | 1.89 | 1.81 | 1.65 | 1.84 | 1.84 | 1.72 | 1.83 | 1.84 | 1.71 | 1.76 | 1.78 | 1.77 | 1.69 | 1.76 | 1.61 | 1.01 | 1.73 |
| ALVI | 3.65 | 3.65 | 3.76 | 3.72 | 3.74 | 3.58 | 3.78 | 3.72 | 3.63 | 3.63 | 3.67 | 3.65 | 3.72 | 3.64 | 3.52 | 3.55 | 3.56 | 3.83 | 2.29 | 3.56 |
| FE2 | 0.17 | 0.20 | 0.14 | 0.18 | 0.10 | 0.16 | 0.11 | 0.15 | 0.25 | 0.13 | 0.14 | 0.27 | 0.27 | 0.31 | 0.47 | 0.38 | 0.42 | 0.21 | 1.27 | 0.42 |
| MN | 0.01 | 0.00 | 0.00 | 0.01 | 0.00 | 0.01 | 0.00 | 0.01 | 0.00 | 0.01 | 0.01 | 0.00 | 0.00 | 0.00 | 0.00 | 0.00 | 0.00 | 0.00 | 0.00 | 0.00 |
| MG | 0.06 | 0.07 | 0.05 | 0.10 | 0.06 | 0.20 | 0.06 | 0.13 | 0.12 | 0.11 | 0.07 | 0.00 | 0.00 | 0.00 | 0.00 | 0.00 | 0.00 | 0.00 | 0.75 | 0.00 |
| CA | 0.00 | 0.00 | 0.00 | 0.00 | 0.00 | 0.01 | 0.00 | 0.00 | 0.00 | 0.00 | 0.00 | 0.00 | 0.00 | 0.00 | 0.00 | 0.00 | 0.00 | 0.00 | 0.00 | 0.00 |
| NA | 0.12 | 0.18 | 0.47 | 0.43 | 0.26 | 0.19 | 0.23 | 0.29 | 0.22 | 0.24 | 0.14 | 0.00 | 0.00 | 0.00 | 0.00 | 0.00 | 0.00 | 0.00 | 0.40 | 0.00 |
| K | 1.85 | 1.80 | 1.50 | 1.50 | 1.69 | 1.67 | 1.63 | 1.62 | 1.65 | 1.76 | 1.76 | 1.74 | 1.75 | 1.75 | 1.82 | 1.83 | 1.81 | 1.69 | 1.70 | 1.81 |

**Muscovite chemistry data**

| Sample Code | 71916 R | 71916 R | 71918 R | 71918 R | 71923 R | 71928 R | 71928 R | 71934 R | 71934 R | 71934 R | 71934 R | 71941 R | 71941 R | 71941 R |
|---|---|---|---|---|---|---|---|---|---|---|---|---|---|---|
| SIO2 | 42.86 | 46.93 | 46.36 | 48.84 | 46.57 | 47.25 | 47.34 | 46.10 | 46.07 | 46.13 | 46.09 | 47.29 | 47.50 | 47.51 |
| TIO2 | 1.18 | 0.43 | 0.33 | 0.00 | 0.36 | 0.00 | 0.35 | 0.48 | 0.39 | 0.57 | 0.00 | 0.00 | 0.00 | 0.37 |
| AL203 | 31.58 | 34.67 | 36.26 | 36.17 | 35.99 | 32.20 | 34.26 | 34.37 | 33.93 | 34.77 | 35.24 | 35.87 | 35.75 | 35.63 |
| FEO | 5.25 | 1.82 | 1.91 | 1.76 | 1.36 | 3.78 | 3.24 | 2.27 | 4.05 | 2.22 | 2.20 | 1.65 | 0.98 | 1.38 |
| MNO | 0.00 | 0.00 | 0.00 | 0.00 | 0.00 | 0.00 | 0.00 | 0.00 | 0.00 | 0.00 | 0.00 | 0.00 | 0.00 | 0.00 |
| MGO | 2.37 | 0.00 | 0.00 | 0.00 | 0.00 | 0.00 | 0.00 | 0.00 | 0.52 | 0.00 | 0.00 | 0.00 | 0.00 | 0.00 |
| CAO | 0.48 | 0.00 | 0.00 | 0.00 | 0.00 | 0.00 | 0.00 | 0.00 | 0.00 | 0.00 | 0.00 | 0.00 | 0.00 | 0.00 |
| NA20 | 0.00 | 0.00 | 0.00 | 0.00 | 1.65 | 0.00 | 0.00 | 1.13 | 1.02 | 1.13 | 1.45 | 0.00 | 0.00 | 0.00 |
| K20 | 8.17 | 10.13 | 8.47 | 8.42 | 9.15 | 9.88 | 10.45 | 9.74 | 9.56 | 9.61 | 9.86 | 9.76 | 9.82 | 9.65 |
| TOTAL | 91.9 | 94.0 | 93.3 | 95.2 | 95.1 | 93.1 | 95.6 | 94.1 | 95.5 | 94.4 | 94.8 | 94.6 | 94.1 | 94.5 |

Total cations

| | | | | | | | | | | | | | | |
|---|---|---|---|---|---|---|---|---|---|---|---|---|---|---|
| SI | 6.01 | 6.30 | 6.21 | 6.38 | 6.18 | 6.46 | 6.31 | 6.23 | 6.18 | 6.20 | 6.18 | 6.28 | 6.32 | 6.30 |
| TI | 0.12 | 0.04 | 0.03 | 0.00 | 0.04 | 0.00 | 0.03 | 0.05 | 0.04 | 0.06 | 0.00 | 0.00 | 0.00 | 0.04 |
| ALIV | 1.99 | 1.70 | 1.79 | 1.62 | 1.82 | 1.54 | 1.69 | 1.77 | 1.82 | 1.80 | 1.82 | 1.72 | 1.68 | 1.70 |
| ALVI | 3.22 | 3.79 | 3.93 | 3.95 | 3.80 | 3.65 | 3.69 | 3.70 | 3.55 | 3.71 | 3.75 | 3.90 | 3.93 | 3.87 |
| FE2 | 0.62 | 0.20 | 0.21 | 0.19 | 0.15 | 0.43 | 0.36 | 0.26 | 0.45 | 0.25 | 0.25 | 0.18 | 0.11 | 0.15 |
| MG | 0.49 | 0.00 | 0.00 | 0.00 | 0.00 | 0.00 | 0.00 | 0.00 | 0.10 | 0.00 | 0.00 | 0.00 | 0.00 | 0.00 |
| CA | 0.07 | 0.00 | 0.00 | 0.00 | 0.00 | 0.00 | 0.00 | 0.00 | 0.00 | 0.00 | 0.00 | 0.00 | 0.00 | 0.00 |
| NA | 0.00 | 0.00 | 0.00 | 0.00 | 0.42 | 0.00 | 0.00 | 0.30 | 0.27 | 0.30 | 0.38 | 0.00 | 0.00 | 0.00 |
| K | 1.46 | 1.74 | 1.45 | 1.40 | 1.55 | 1.72 | 1.78 | 1.68 | 1.64 | 1.65 | 1.69 | 1.65 | 1.67 | 1.63 |

**Muscovite chemistry data**

| Sample | 66801 | 66801 | 68780 | 68804 | 68804 | 69236 | 69619 | 69627 | 69635 | 71912 | 71941 | 71941 |
|---|---|---|---|---|---|---|---|---|---|---|---|---|
| Code | C | C | C | C | C | C | C | C | C | C | C | C |
| SI02 | 26.49 | 25.62 | 28.04 | 32.27 | 27.45 | 29.10 | 25.69 | 25.43 | 24.78 | 27.21 | 26.61 | 26.33 |
| TI02 | 0.66 | 0.24 | 0.27 | 6.09 | 0.00 | 0.00 | 0.08 | 0.23 | 0.13 | 0.00 | 0.00 | 0.00 |
| AL203 | 20.36 | 21.38 | 22.36 | 18.19 | 22.20 | 18.97 | 19.33 | 21.83 | 21.38 | 21.83 | 24.19 | 23.96 |
| FEO | 26.69 | 26.24 | 28.15 | 27.50 | 29.00 | 36.86 | 32.88 | 28.53 | 31.86 | 32.51 | 29.00 | 28.12 |
| MNO | 0.46 | 0.35 | 0.00 | 0.00 | 0.00 | 0.00 | 0.40 | 0.13 | 0.44 | 0.00 | 0.00 | 0.00 |
| MGO | 12.59 | 12.87 | 13.55 | 10.39 | 14.01 | 10.80 | 9.23 | 12.19 | 9.35 | 11.25 | 13.17 | 13.26 |
| CAO | 0.17 | 0.11 | 0.00 | 0.16 | 0.00 | 0.17 | 0.06 | 0.00 | 0.00 | 0.00 | 0.00 | 0.00 |
| NA20 | 0.33 | 0.00 | 0.00 | 0.00 | 0.00 | 0.00 | 0.28 | 0.16 | 0.18 | 0.00 | 0.00 | 0.00 |
| K20 | 0.48 | 0.11 | 0.00 | 0.00 | 0.00 | 0.00 | 0.09 | 0.32 | 0.00 | 0.00 | 0.00 | 0.00 |
| TOTAL | 88.2 | 86.9 | 92.4 | 94.6 | 92.7 | 95.9 | 88.0 | 88.8 | 88.1 | 92.8 | 93.0 | 91.7 |

Total cations

| | | | | | | | | | | | | |
|---|---|---|---|---|---|---|---|---|---|---|---|---|
| SI | 5.61 | 5.47 | 5.62 | 6.25 | 5.52 | 5.87 | 5.63 | 5.38 | 5.39 | 5.56 | 5.33 | 5.33 |
| TI | 0.10 | 0.04 | 0.04 | 0.89 | 0.00 | 0.00 | 0.01 | 0.04 | 0.02 | 0.00 | 0.00 | 0.00 |
| ALIV | 2.39 | 2.53 | 2.38 | 1.75 | 2.48 | 2.13 | 2.37 | 2.62 | 2.61 | 2.44 | 2.67 | 2.67 |
| ALVI | 2.69 | 2.86 | 2.90 | 2.41 | 2.78 | 2.38 | 2.63 | 2.83 | 2.88 | 2.82 | 3.03 | 3.05 |
| FE2 | 4.73 | 4.69 | 4.72 | 4.46 | 4.88 | 6.22 | 6.03 | 5.05 | 5.80 | 5.56 | 4.86 | 4.76 |
| MN | 0.08 | 0.06 | 0.00 | 0.00 | 0.00 | 0.00 | 0.07 | 0.02 | 0.06 | 0.00 | 0.00 | 0.00 |
| MG | 3.97 | 4.10 | 4.05 | 3.00 | 4.20 | 3.25 | 3.01 | 3.85 | 3.03 | 3.43 | 3.93 | 4.00 |
| CA | 0.04 | 0.02 | 0.00 | 0.03 | 0.00 | 0.04 | 0.01 | 0.00 | 0.00 | 0.00 | 0.00 | 0.00 |
| NA | 0.13 | 0.00 | 0.00 | 0.00 | 0.00 | 0.00 | 0.12 | 0.07 | 0.07 | 0.00 | 0.00 | 0.00 |
| K | 0.13 | 0.03 | 0.00 | 0.00 | 0.00 | 0.00 | 0.03 | 0.09 | 0.00 | 0.00 | 0.00 | 0.00 |

End member concentrations

| | | | | | | | | | | | | |
|---|---|---|---|---|---|---|---|---|---|---|---|---|
| XFE | 0.54 | 0.53 | 0.54 | 0.60 | 0.54 | 0.66 | 0.66 | 0.57 | 0.65 | 0.62 | 0.55 | 0.54 |
| XMG | 0.45 | 0.46 | 0.46 | 0.40 | 0.46 | 0.34 | 0.33 | 0.43 | 0.34 | 0.38 | 0.45 | 0.46 |
| XMN | 0.01 | 0.01 | 0.00 | 0.00 | 0.00 | 0.00 | 0.01 | 0.00 | 0.01 | 0.00 | 0.00 | 0.00 |

**Chlorite chemistry data**

| Sample | 66795 | 66795 | 66795 | 66795 | 66801 | 66801 | 66801 | 66801 | 66801 | 68780 | 68790 | 68790 | 68790 | 68793 | 68793 | 68793 | 68799 | 68804 | 68804 | 68804 | 68804 | 68806 |
|---|---|---|---|---|---|---|---|---|---|---|---|---|---|---|---|---|---|---|---|---|---|---|
| Code | C | C | C | C | C | C | C | C | C | C | C | C | C | C | C | C | C | C | C | C | C | R |
| SI02 | 78.88 | 55.60 | 54.60 | 54.75 | 59.00 | 59.58 | 58.11 | 58.92 | 58.56 | 57.99 | 53.47 | 50.17 | 49.77 | 49.46 | 50.20 | 50.34 | 58.46 | 59.29 | 60.33 | 59.39 | 59.33 | 62.48 |
| TI02 | 0.00 | 0.06 | 0.02 | 0.00 | 0.00 | 0.05 | 0.01 | 0.02 | 0.00 | 0.00 | 0.00 | 0.00 | 0.00 | 0.00 | 0.00 | 0.00 | 0.01 | 0.00 | 0.00 | 0.00 | 0.00 | 0.00 |
| AL203 | 9.02 | 27.94 | 28.00 | 27.82 | 27.05 | 26.62 | 26.05 | 25.96 | 26.48 | 27.76 | 30.81 | 33.26 | 33.13 | 33.21 | 32.47 | 32.58 | 26.53 | 25.38 | 25.66 | 26.54 | 26.03 | 24.83 |
| FE0 | 0.37 | 0.16 | 0.03 | 0.06 | 0.03 | 0.00 | 0.02 | 0.00 | 0.05 | 0.00 | 0.00 | 0.37 | 0.31 | 0.00 | 0.00 | 0.00 | 0.22 | 0.00 | 0.00 | 0.00 | 0.00 | 0.00 |
| MN0 | 0.18 | 0.00 | 0.01 | 0.00 | 0.03 | 0.06 | 0.07 | 0.08 | 0.08 | 0.00 | 0.00 | 0.00 | 0.00 | 0.00 | 0.00 | 0.00 | 0.09 | 0.00 | 0.00 | 0.00 | 0.00 | 0.00 |
| MG0 | 0.06 | 0.00 | 0.10 | 0.00 | 0.00 | 0.04 | 0.00 | 0.00 | 0.00 | 0.00 | 0.00 | 0.00 | 0.00 | 0.00 | 0.00 | 0.00 | 0.00 | 0.00 | 0.00 | 0.00 | 0.00 | 0.00 |
| CA0 | 1.52 | 9.91 | 10.42 | 10.31 | 8.35 | 7.98 | 8.33 | 8.00 | 8.16 | 9.43 | 12.83 | 14.83 | 15.56 | 16.29 | 15.43 | 15.53 | 8.48 | 7.13 | 6.04 | 8.08 | 7.47 | 4.82 |
| NA20 | 0.21 | 5.40 | 5.50 | 5.38 | 6.90 | 7.09 | 6.73 | 6.85 | 6.65 | 6.03 | 4.02 | 2.72 | 2.51 | 2.13 | 2.09 | 1.92 | 6.87 | 7.36 | 7.00 | 7.24 | 6.95 | 8.28 |
| K20 | 0.93 | 0.34 | 0.04 | 0.11 | 0.21 | 0.23 | 0.18 | 0.24 | 0.23 | 0.24 | 0.21 | 0.60 | 0.18 | 0.00 | 0.00 | 0.14 | 0.10 | 0.24 | 0.74 | 0.17 | 0.13 | 0.39 |
| TOTAL | 91.2 | 99.4 | 98.7 | 98.4 | 101.6 | 101.6 | 99.5 | 100.1 | 100.2 | 101.5 | 101.3 | 102.0 | 101.5 | 101.1 | 100.2 | 100.5 | 100.8 | 99.4 | 99.8 | 101.4 | 99.9 | 100.8 |

Cations for 8 Oxygen

| | | | | | | | | | | | | | | | | | | | | | | |
|---|---|---|---|---|---|---|---|---|---|---|---|---|---|---|---|---|---|---|---|---|---|---|
| SI | 4.24 | 2.52 | 2.49 | 2.51 | 2.60 | 2.62 | 2.62 | 2.64 | 2.62 | 2.57 | 2.40 | 2.25 | 2.25 | 2.24 | 2.30 | 2.30 | 2.60 | 2.66 | 2.70 | 2.61 | 2.66 | 2.75 |
| AL | 0.57 | 1.49 | 1.51 | 1.50 | 1.40 | 1.38 | 1.38 | 1.37 | 1.40 | 1.45 | 1.63 | 1.76 | 1.76 | 1.78 | 1.75 | 1.76 | 1.39 | 1.34 | 1.36 | 1.38 | 1.37 | 1.29 |
| FE2 | 0.02 | 0.01 | 0.00 | 0.00 | 0.00 | 0.00 | 0.00 | 0.00 | 0.00 | 0.00 | 0.00 | 0.01 | 0.01 | 0.00 | 0.00 | 0.00 | 0.01 | 0.00 | 0.00 | 0.00 | 0.00 | 0.00 |
| CA | 0.09 | 0.48 | 0.51 | 0.51 | 0.39 | 0.38 | 0.40 | 0.38 | 0.39 | 0.45 | 0.62 | 0.71 | 0.75 | 0.79 | 0.76 | 0.76 | 0.40 | 0.34 | 0.29 | 0.38 | 0.36 | 0.23 |
| NA | 0.02 | 0.48 | 0.49 | 0.48 | 0.59 | 0.60 | 0.59 | 0.59 | 0.58 | 0.52 | 0.35 | 0.24 | 0.22 | 0.19 | 0.19 | 0.17 | 0.59 | 0.64 | 0.61 | 0.62 | 0.60 | 0.71 |
| K | 0.06 | 0.02 | 0.00 | 0.01 | 0.01 | 0.01 | 0.01 | 0.01 | 0.01 | 0.01 | 0.01 | 0.03 | 0.01 | 0.00 | 0.00 | 0.01 | 0.01 | 0.01 | 0.04 | 0.01 | 0.01 | 0.02 |

End member concentrations

| | | | | | | | | | | | | | | | | | | | | | | |
|---|---|---|---|---|---|---|---|---|---|---|---|---|---|---|---|---|---|---|---|---|---|---|
| AB | 12.79 | 48.66 | 48.73 | 48.27 | 59.20 | 60.84 | 58.76 | 59.95 | 58.78 | 52.91 | 35.71 | 24.04 | 22.33 | 19.11 | 19.71 | 18.15 | 59.14 | 64.23 | 64.67 | 61.25 | 62.24 | 73.92 |
| AN | 50.34 | 49.35 | 51.05 | 51.11 | 39.59 | 37.87 | 40.21 | 38.65 | 39.87 | 45.70 | 63.05 | 72.47 | 76.64 | 80.89 | 80.29 | 80.99 | 40.32 | 34.38 | 30.83 | 37.81 | 36.97 | 23.79 |
| OR | 36.86 | 1.99 | 0.22 | 0.62 | 1.21 | 1.29 | 1.03 | 1.39 | 1.34 | 1.40 | 1.25 | 3.49 | 1.03 | 0.00 | 0.00 | 0.86 | 0.54 | 1.39 | 4.50 | 0.94 | 0.79 | 2.29 |

**Plagioclase chemistry data**

| Sample Code | 68806 R | 68806 R | 68806 R | 68806 R | 69215 C | 69215 C | 69215 C | 69215 C | 69219 C | 69219 C | 69219 C | 69229 R | 69229 R | 69230 R | 69230 R | 69236 R | 69236 R | 69238 R | 69238 R | 69238 R |
|---|---|---|---|---|---|---|---|---|---|---|---|---|---|---|---|---|---|---|---|---|
| SIO2 | 63.36 | 62.77 | 62.66 | 62.95 | 59.90 | 59.74 | 61.25 | 61.02 | 56.27 | 57.39 | 57.82 | 59.60 | 63.31 | 66.96 | 66.70 | 53.66 | 53.54 | 61.53 | 59.41 | 61.57 |
| TIO2 | 0.00 | 0.00 | 0.00 | 0.00 | 0.00 | 0.00 | 0.00 | 0.00 | 0.00 | 0.00 | 0.00 | 0.00 | 0.00 | 0.00 | 0.00 | 0.00 | 0.64 | 0.00 | 0.00 | 0.00 |
| AL2O3 | 24.39 | 23.85 | 24.46 | 23.96 | 26.10 | 26.53 | 26.75 | 26.03 | 28.00 | 28.30 | 27.49 | 25.47 | 24.92 | 21.76 | 22.19 | 33.59 | 32.43 | 24.30 | 25.09 | 24.91 |
| FEO | 0.00 | 0.33 | 0.00 | 0.00 | 0.00 | 0.00 | 0.00 | 0.00 | 0.00 | 0.00 | 0.00 | 0.39 | 0.00 | 0.00 | 0.00 | 0.87 | 1.37 | 0.00 | 1.04 | 0.00 |
| MNO | 0.00 | 0.00 | 0.00 | 0.00 | 0.00 | 0.00 | 0.00 | 0.00 | 0.00 | 0.00 | 0.00 | 0.00 | 0.00 | 0.00 | 0.00 | 0.00 | 0.00 | 0.00 | 0.00 | 0.00 |
| MGO | 0.00 | 0.00 | 0.00 | 0.00 | 0.00 | 0.00 | 0.00 | 0.00 | 0.00 | 0.00 | 0.00 | 0.00 | 0.00 | 0.00 | 0.00 | 0.00 | 0.00 | 0.00 | 0.00 | 0.00 |
| CAO | 5.29 | 4.70 | 5.12 | 4.82 | 7.54 | 7.52 | 7.65 | 7.04 | 9.54 | 9.95 | 8.65 | 7.01 | 4.16 | 1.89 | 2.10 | 6.07 | 6.61 | 5.82 | 6.46 | 6.26 |
| NA2O | 8.01 | 8.43 | 8.33 | 8.61 | 7.49 | 7.18 | 7.39 | 7.35 | 5.86 | 6.30 | 5.92 | 8.27 | 8.42 | 10.56 | 10.37 | 5.23 | 5.69 | 8.45 | 5.99 | 8.01 |
| K2O | 0.17 | 0.18 | 0.19 | 0.20 | 0.00 | 0.44 | 0.19 | 0.19 | 0.14 | 0.00 | 0.43 | 0.00 | 0.87 | 0.00 | 0.00 | 0.61 | 0.66 | 0.00 | 0.92 | 0.00 |
| TOTAL | 101.2 | 100.3 | 100.8 | 100.6 | 101.0 | 101.4 | 103.2 | 101.6 | 99.8 | 101.9 | 100.3 | 100.7 | 101.7 | 101.2 | 101.4 | 100.0 | 101.0 | 100.1 | 98.9 | 100.7 |
| Cations for 8 Oxygen | | | | | | | | | | | | | | | | | | | | |
| SI | 2.79 | 2.78 | 2.76 | 2.78 | 2.64 | 2.63 | 2.65 | 2.68 | 2.53 | 2.53 | 2.59 | 2.63 | 2.76 | 2.91 | 2.89 | 2.42 | 2.42 | 2.73 | 2.71 | 2.72 |
| AL | 1.27 | 1.25 | 1.27 | 1.25 | 1.36 | 1.38 | 1.36 | 1.35 | 1.49 | 1.47 | 1.45 | 1.32 | 1.28 | 1.11 | 1.13 | 1.79 | 1.73 | 1.27 | 1.35 | 1.30 |
| FE2 | 0.00 | 0.01 | 0.00 | 0.00 | 0.00 | 0.00 | 0.00 | 0.00 | 0.00 | 0.00 | 0.00 | 0.01 | 0.00 | 0.00 | 0.00 | 0.03 | 0.05 | 0.00 | 0.04 | 0.00 |
| CA | 0.25 | 0.22 | 0.24 | 0.23 | 0.36 | 0.35 | 0.35 | 0.33 | 0.46 | 0.47 | 0.42 | 0.33 | 0.19 | 0.09 | 0.10 | 0.49 | 0.48 | 0.28 | 0.32 | 0.30 |
| NA | 0.68 | 0.73 | 0.71 | 0.74 | 0.64 | 0.61 | 0.62 | 0.63 | 0.51 | 0.54 | 0.51 | 0.71 | 0.71 | 0.89 | 0.87 | 0.42 | 0.41 | 0.73 | 0.53 | 0.69 |
| K | 0.01 | 0.01 | 0.01 | 0.01 | 0.00 | 0.02 | 0.01 | 0.01 | 0.01 | 0.00 | 0.02 | 0.00 | 0.05 | 0.00 | 0.00 | 0.05 | 0.05 | 0.00 | 0.05 | 0.00 |
| End member concentrations | | | | | | | | | | | | | | | | | | | | |
| AB | 72.50 | 75.67 | 73.79 | 75.48 | 64.25 | 61.76 | 62.90 | 64.69 | 52.23 | 53.38 | 53.87 | 68.12 | 74.56 | 90.99 | 89.92 | 43.90 | 42.94 | 72.43 | 58.90 | 69.82 |
| AN | 26.48 | 23.29 | 25.08 | 23.36 | 35.75 | 35.75 | 36.00 | 34.21 | 46.94 | 46.62 | 43.54 | 31.88 | 20.34 | 9.01 | 10.08 | 51.02 | 53.08 | 27.57 | 35.12 | 30.18 |
| OR | 1.02 | 1.04 | 1.13 | 1.16 | 0.00 | 2.49 | 1.09 | 1.09 | 0.83 | 0.00 | 2.58 | 0.00 | 5.10 | 0.00 | 0.00 | 0.51 | 0.66 | 0.00 | 5.98 | 0.00 |

**Plagioclase chemistry data**

| Sample | 69277 | 69277 | 69277 | 69277 | 69317 | 69317 | 69317 | 69317 | 69619 | 69619 | 69619 | 69619 | 69619 | 69619 | 69623 | 69623 | 69625 | 69627 | 69627 | 69627 | 69627 | 69635 |
|---|---|---|---|---|---|---|---|---|---|---|---|---|---|---|---|---|---|---|---|---|---|---|
| Code | R | R | R | R | R | R | R | R | C | C | C | C | C | C | R | R | R | R | R | R | R | C |
| SI02 | 50.38 | 62.40 | 57.08 | 61.45 | 69.28 | 66.18 | 67.26 | 66.76 | 61.07 | 60.98 | 61.37 | 61.25 | 62.67 | 60.85 | 69.40 | 65.38 | 61.96 | 63.45 | 65.60 | 64.52 | 61.85 | 59.77 |
| TI02 | 0.35 | 0.00 | 0.00 | 0.00 | 0.00 | 0.00 | 0.00 | 0.00 | 0.00 | 0.07 | 0.00 | 0.00 | 0.00 | 0.02 | 0.03 | 0.04 | 0.02 | 0.07 | 0.03 | 0.04 | 0.07 | 0.00 |
| AL203 | 35.39 | 23.92 | 24.67 | 24.97 | 20.98 | 22.39 | 22.11 | 22.22 | 24.35 | 25.08 | 24.23 | 24.41 | 23.58 | 24.21 | 19.50 | 22.37 | 24.64 | 23.12 | 22.85 | 21.72 | 22.86 | 24.45 |
| FE0 | 3.41 | 1.29 | 5.44 | 0.00 | 0.00 | 0.00 | 0.65 | 0.00 | 0.13 | 0.35 | 0.06 | 0.18 | 0.19 | 0.41 | 0.75 | 0.33 | 0.37 | 0.05 | 0.25 | 0.22 | 0.32 | 0.20 |
| MN0 | 0.00 | 0.00 | 0.00 | 0.00 | 0.00 | 0.00 | 0.00 | 0.00 | 0.11 | 0.00 | 0.06 | 0.06 | 0.00 | 0.01 | 0.00 | 0.00 | 0.04 | 0.01 | 0.02 | 0.00 | 0.02 | 0.00 |
| MG0 | 0.00 | 0.00 | 1.69 | 0.00 | 0.00 | 0.00 | 0.00 | 0.00 | 0.00 | 0.00 | 0.00 | 0.00 | 0.00 | 0.00 | 0.00 | 0.00 | 0.00 | 0.00 | 0.00 | 0.00 | 0.00 | 0.00 |
| CA0 | 2.35 | 3.33 | 2.04 | 6.16 | 0.75 | 1.13 | 0.75 | 0.60 | 5.89 | 6.55 | 5.36 | 4.87 | 2.32 | 3.02 | 0.06 | 3.19 | 5.77 | 4.60 | 3.60 | 2.15 | 4.51 | 4.57 |
| NA20 | 3.66 | 6.90 | 7.43 | 8.35 | 10.30 | 9.43 | 9.99 | 9.44 | 7.99 | 7.81 | 7.90 | 7.98 | 8.47 | 7.66 | 11.43 | 9.72 | 8.26 | 8.99 | 9.45 | 9.51 | 8.60 | 6.84 |
| K20 | 3.87 | 3.48 | 1.91 | 0.00 | 0.20 | 1.16 | 0.89 | 1.41 | 0.26 | 0.08 | 0.40 | 0.79 | 1.69 | 2.20 | 0.01 | 0.07 | 0.12 | 0.09 | 0.03 | 0.59 | 0.16 | 1.55 |
| TOTAL | 99.4 | 101.3 | 100.3 | 100.9 | 101.5 | 100.3 | 101.6 | 100.4 | 99.8 | 100.9 | 99.4 | 99.6 | 98.9 | 98.4 | 101.2 | 101.1 | 101.2 | 100.4 | 101.8 | 98.8 | 98.4 | 97.4 |
| | | | | | | | Cations for 8 Oxygen | | | | | | | | | | | | | | | |
| SI | 2.30 | 2.76 | 2.54 | 2.70 | 3.01 | 2.91 | 2.92 | 2.94 | 2.73 | 2.70 | 2.75 | 2.74 | 2.81 | 2.75 | 3.01 | 2.86 | 2.73 | 2.80 | 2.85 | 2.89 | 2.79 | 2.74 |
| AL | 1.90 | 1.25 | 1.29 | 1.29 | 1.07 | 1.16 | 1.13 | 1.15 | 1.28 | 1.31 | 1.28 | 1.29 | 1.24 | 1.29 | 1.00 | 1.15 | 1.28 | 1.20 | 1.17 | 1.14 | 1.22 | 1.32 |
| FE2 | 0.13 | 0.05 | 0.20 | 0.00 | 0.00 | 0.00 | 0.02 | 0.00 | 0.01 | 0.01 | 0.00 | 0.01 | 0.01 | 0.02 | 0.03 | 0.01 | 0.01 | 0.00 | 0.01 | 0.01 | 0.01 | 0.01 |
| CA | 0.11 | 0.16 | 0.10 | 0.29 | 0.04 | 0.05 | 0.03 | 0.03 | 0.28 | 0.31 | 0.26 | 0.23 | 0.11 | 0.15 | 0.00 | 0.15 | 0.27 | 0.22 | 0.17 | 0.10 | 0.22 | 0.22 |
| NA | 0.32 | 0.59 | 0.64 | 0.71 | 0.87 | 0.81 | 0.84 | 0.81 | 0.69 | 0.67 | 0.69 | 0.69 | 0.74 | 0.67 | 0.96 | 0.82 | 0.70 | 0.77 | 0.80 | 0.82 | 0.75 | 0.61 |
| K | 0.23 | 0.20 | 0.11 | 0.00 | 0.01 | 0.06 | 0.05 | 0.08 | 0.02 | 0.00 | 0.02 | 0.05 | 0.10 | 0.13 | 0.00 | 0.00 | 0.01 | 0.01 | 0.00 | 0.03 | 0.01 | 0.09 |
| | | | | | | | End member concentrations | | | | | | | | | | | | | | | |
| AB | 48.79 | 62.57 | 75.73 | 71.06 | 94.96 | 87.20 | 90.92 | 88.23 | 69.99 | 68.00 | 70.99 | 71.32 | 77.95 | 71.06 | 99.65 | 84.31 | 71.67 | 77.56 | 82.49 | 85.83 | 76.81 | 65.84 |
| AN | 17.27 | 16.68 | 11.46 | 28.94 | 3.84 | 5.77 | 3.75 | 3.11 | 28.48 | 31.52 | 26.64 | 24.03 | 11.80 | 15.49 | 0.29 | 15.29 | 27.66 | 21.93 | 17.35 | 10.70 | 22.24 | 24.31 |
| OR | 33.94 | 20.75 | 12.82 | 0.00 | 1.20 | 7.03 | 5.33 | 8.67 | 1.53 | 0.48 | 2.37 | 4.65 | 10.25 | 13.45 | 0.06 | 0.40 | 0.66 | 0.51 | 0.16 | 3.47 | 0.95 | 9.84 |

Plagioclase chemistry data

| Sample Code | 69635 C | 71898 C | 71898 C | 71898 C | 71901 C | 71901 C | 71912 R | 71912 R | 71912 R | 71914 R | 71914 R | 71916 R | 71916 R | 71916 R | 71916 R | 71918 R | 71918 R | 71918 R | 71923 R | 71928 R | 71928 R | 71928 R |
|---|---|---|---|---|---|---|---|---|---|---|---|---|---|---|---|---|---|---|---|---|---|---|
| SIO2 | 59.96 | 70.60 | 67.83 | 63.19 | 63.03 | 63.86 | 65.70 | 70.55 | 65.38 | 59.05 | 58.26 | 67.93 | 63.17 | 68.42 | 68.70 | 64.20 | 65.77 | 65.48 | 61.61 | 63.24 | 63.78 | 64.41 |
| TIO2 | 0.03 | 0.00 | 0.00 | 0.00 | 0.00 | 0.00 | 0.00 | 0.00 | 0.00 | 0.00 | 0.00 | 0.00 | 0.00 | 0.00 | 0.00 | 0.00 | 0.00 | 0.00 | 0.00 | 0.00 | 0.00 | 0.00 |
| AL203 | 25.07 | 20.00 | 21.95 | 24.53 | 23.34 | 24.16 | 22.98 | 19.98 | 21.80 | 25.91 | 25.72 | 21.02 | 24.13 | 20.56 | 21.33 | 23.64 | 22.46 | 22.68 | 23.70 | 24.28 | 25.32 | 24.79 |
| FEO | 0.23 | 0.00 | 0.00 | 0.49 | 0.00 | 0.00 | 0.27 | 0.00 | 0.35 | 0.00 | 0.00 | 0.32 | 0.00 | 0.35 | 0.00 | 0.36 | 0.00 | 0.00 | 0.00 | 0.00 | 0.00 | 0.00 |
| MNO | 0.04 | 0.00 | 0.00 | 0.00 | 0.00 | 0.00 | 0.00 | 0.00 | 0.00 | 0.00 | 0.00 | 0.00 | 0.00 | 0.00 | 0.00 | 0.00 | 0.00 | 0.00 | 0.00 | 0.00 | 0.00 | 0.00 |
| MGO | 0.00 | 0.00 | 0.00 | 0.00 | 0.00 | 0.00 | 0.00 | 0.00 | 0.00 | 0.00 | 0.00 | 0.00 | 0.00 | 0.00 | 0.00 | 0.00 | 0.00 | 0.00 | 0.00 | 0.00 | 0.00 | 0.00 |
| CAO | 7.07 | 0.00 | 0.38 | 0.75 | 5.04 | 5.13 | 2.36 | 0.25 | 1.47 | 7.78 | 7.87 | 1.51 | 5.46 | 1.36 | 5.31 | 1.39 | 3.92 | 4.07 | 5.61 | 6.05 | 5.65 | 5.98 |
| NA20 | 7.37 | 9.89 | 9.45 | 6.64 | 7.58 | 8.22 | 8.26 | 10.15 | 8.24 | 7.33 | 6.94 | 9.52 | 7.77 | 9.61 | 6.39 | 8.14 | 7.65 | 6.47 | 8.49 | 5.63 | 6.86 | 7.30 |
| K20 | 0.09 | 0.00 | 1.25 | 3.23 | 0.00 | 0.15 | 0.97 | 0.00 | 1.10 | 0.00 | 0.21 | 0.62 | 0.14 | 0.00 | 0.00 | 1.95 | 0.20 | 0.20 | 0.00 | 0.23 | 0.59 | 0.00 |
| TOTAL | 99.9 | 100.5 | 100.9 | 98.8 | 99.0 | 101.5 | 100.5 | 100.9 | 98.3 | 100.1 | 99.0 | 100.9 | 100.7 | 100.3 | 101.7 | 99.7 | 100.0 | 98.9 | 99.4 | 99.4 | 102.2 | 102.5 |

Cations for 8 Oxygens

| | | | | | | | | | | | | | | | | | | | | | | |
|---|---|---|---|---|---|---|---|---|---|---|---|---|---|---|---|---|---|---|---|---|---|---|
| SI | 2.68 | 3.11 | 2.97 | 2.86 | 2.85 | 2.80 | 2.91 | 3.09 | 2.96 | 2.63 | 2.63 | 2.98 | 2.80 | 3.03 | 3.07 | 2.86 | 2.95 | 2.99 | 2.75 | 2.89 | 2.80 | 2.82 |
| AL | 1.32 | 1.04 | 1.13 | 1.31 | 1.24 | 1.25 | 1.20 | 1.03 | 1.16 | 1.36 | 1.37 | 1.09 | 1.26 | 1.07 | 1.12 | 1.24 | 1.19 | 1.22 | 1.25 | 1.31 | 1.31 | 1.28 |
| FE2 | 0.01 | 0.00 | 0.00 | 0.02 | 0.00 | 0.00 | 0.01 | 0.00 | 0.01 | 0.00 | 0.00 | 0.01 | 0.00 | 0.01 | 0.00 | 0.01 | 0.00 | 0.00 | 0.00 | 0.00 | 0.00 | 0.00 |
| CA | 0.34 | 0.00 | 0.02 | 0.04 | 0.24 | 0.24 | 0.11 | 0.01 | 0.07 | 0.37 | 0.38 | 0.07 | 0.26 | 0.06 | 0.25 | 0.07 | 0.19 | 0.20 | 0.27 | 0.30 | 0.27 | 0.28 |
| NA | 0.64 | 0.85 | 0.80 | 0.58 | 0.66 | 0.70 | 0.71 | 0.86 | 0.72 | 0.63 | 0.61 | 0.81 | 0.67 | 0.82 | 0.55 | 0.70 | 0.67 | 0.57 | 0.73 | 0.50 | 0.59 | 0.62 |
| K | 0.00 | 0.00 | 0.07 | 0.19 | 0.00 | 0.01 | 0.05 | 0.00 | 0.06 | 0.00 | 0.01 | 0.03 | 0.01 | 0.00 | 0.00 | 0.11 | 0.01 | 0.01 | 0.00 | 0.01 | 0.03 | 0.00 |

End member concentrations

| | | | | | | | | | | | | | | | | | | | | | | |
|---|---|---|---|---|---|---|---|---|---|---|---|---|---|---|---|---|---|---|---|---|---|---|
| AB | 65.03 | 100.00 | 90.16 | 72.34 | 73.13 | 73.68 | 80.95 | 98.66 | 84.29 | 63.03 | 60.72 | 88.46 | 71.44 | 92.72 | 68.54 | 79.85 | 76.95 | 73.09 | 73.27 | 61.70 | 66.19 | 68.85 |
| AN | 34.47 | 0.00 | 1.99 | 4.52 | 26.87 | 25.42 | 12.79 | 1.34 | 8.28 | 36.97 | 38.07 | 7.76 | 27.73 | 7.28 | 31.46 | 7.54 | 21.76 | 25.41 | 26.73 | 36.66 | 30.09 | 31.15 |
| OR | 0.49 | 0.00 | 7.85 | 23.15 | 0.00 | 0.91 | 6.26 | 0.00 | 7.43 | 0.00 | 1.20 | 3.77 | 0.83 | 0.00 | 0.00 | 12.61 | 1.30 | 1.49 | 0.00 | 1.64 | 3.71 | 0.00 |

**Plagioclase chemistry data**

| Sample Code | 71932 R | 71932 R | 71932 R | 71934 R | 71934 R | 71934 R | 71941 R |
|---|---|---|---|---|---|---|---|
| SI02 | 60.60 | 61.32 | 61.22 | 60.44 | 61.78 | 64.55 | 64.15 |
| TI02 | 0.00 | 0.00 | 0.00 | 0.00 | 0.00 | 0.00 | 0.00 |
| AL203 | 24.82 | 25.49 | 25.14 | 24.91 | 24.94 | 21.60 | 24.00 |
| FE0 | 0.00 | 0.00 | 0.00 | 0.00 | 0.00 | 0.34 | 0.44 |
| MN0 | 0.00 | 0.00 | 0.00 | 0.00 | 0.00 | 0.00 | 0.00 |
| MG0 | 0.00 | 0.00 | 0.00 | 0.00 | 0.00 | 0.00 | 0.00 |
| CA0 | 6.57 | 6.96 | 6.45 | 6.46 | 6.57 | 3.24 | 1.65 |
| NA20 | 7.89 | 7.66 | 7.78 | 8.15 | 7.56 | 9.25 | 6.57 |
| K20 | 0.00 | 0.00 | 0.13 | 0.21 | 0.13 | 0.64 | 2.28 |
| TOTAL | 99.9 | 101.4 | 100.7 | 100.2 | 101.0 | 99.6 | 99.1 |

Cations for 8 Oxygen

| | | | | | | | |
|---|---|---|---|---|---|---|---|
| SI | 2.70 | 2.70 | 2.71 | 2.68 | 2.73 | 2.87 | 2.91 |
| AL | 1.30 | 1.32 | 1.31 | 1.30 | 1.30 | 1.13 | 1.28 |
| FE2 | 0.00 | 0.00 | 0.00 | 0.00 | 0.00 | 0.01 | 0.02 |
| CA | 0.31 | 0.33 | 0.31 | 0.31 | 0.31 | 0.15 | 0.08 |
| NA | 0.68 | 0.65 | 0.67 | 0.70 | 0.65 | 0.80 | 0.58 |
| K | 0.00 | 0.00 | 0.01 | 0.01 | 0.01 | 0.04 | 0.13 |

End member concentrations

| | | | | | | | |
|---|---|---|---|---|---|---|---|
| AB | 68.49 | 66.56 | 68.06 | 68.73 | 67.04 | 80.73 | 73.14 |
| AN | 31.51 | 33.44 | 31.19 | 30.10 | 32.21 | 15.62 | 10.16 |
| OR | 0.00 | 0.00 | 0.75 | 1.17 | 0.75 | 3.66 | 16.71 |

**Plagioclase chemistry data**

island of Roeillaun and in a strip in the central part of the south coast of the Renvyle peninsula. Characteristically the Roeillaun schists are pale grey (weathering to a rusty brown) muscovite rich schistose pelites (Figure 2.4). Red - brown garnets are common and reach up to 10mm diameter, generally being <5mm and showing subhedral to rounded forms, although euhedral crystals are present in the Renvyle coastal outcrops. Staurolite needles up to 10mm are present, lying within the foliation, but showing no preferred linear orientation. The schists show some fine ( <5mm) psammitic partings and scattered thicker psammite lenses [GR 680 593]. The stratigraphic position of the Roeillaun schist Mb is discused further in the addendum at the end of this chapter (after page 47).

2.1.2.1.3 Lakes Marble Formation

This formation is the stratigraphically highest encountered and is incompletely exposed, the top of the formation not occurring in the study area. The base of the Lakes Marble Formation is marked by a thin, but laterally continuous band of calc - silicate/marble (Figure 2.3).

Five main members can be defined in the formation and all show good lateral continuity, in spite of major variations in thickness.

Tonabina Marble Member: This unit is the base of the Lakes Marble Formation and consists of a thin (1 - 20m), laterally persistent siliceous marble. The variation in thickness across fold hinges is marked, with the marble being strongly attenuated in fold limbs and thickened in hinges. In outcrop this unit is variable in appearance, generally consisting of a poorly foliated blue/grey smooth weathering saccharoidal marble with strongly foliated thin ( <40mm) 'ribs' of more siliceous material. Saccharoidal dolomitic marble is the dominant lithology, although the siliceous ribs may form up to 50% of the total.

Pale weathering quartzose psammites and grits are evident in the marble, grit bands often reaching 300mm thickness and showing good grading features (Figure 2.5). Rare pelites and thin amphibolitic units are also present.

The marble can be traced from the end of Renvyle Point at Knocknasheeoge inland to the Kylemore valley and beyond.

| Sample | 66795 | 68790 | 68790 | 69236 | 69236 | 69236 | 69619 | 71906 |
|---|---|---|---|---|---|---|---|---|
| Code | C | C | C | C | C | C | C | C |
| SI02 | 46.37 | 60.09 | 48.98 | 49.54 | 48.50 | 56.01 | 63.31 | 65.25 |
| TI02 | 0.57 | 0.00 | 0.00 | 0.84 | 0.94 | 0.00 | 0.46 | 0.62 |
| AL203 | 31.40 | 27.01 | 32.89 | 35.76 | 36.17 | 30.26 | 18.38 | 18.80 |
| FE0 | 1.39 | 1.48 | 3.47 | 1.80 | 1.90 | 1.82 | 1.36 | 0.00 |
| MN0 | 0.10 | 0.00 | 0.00 | 0.00 | 0.00 | 0.00 | 0.02 | 0.00 |
| MG0 | 0.91 | 0.54 | 0.64 | 0.76 | 0.34 | 0.00 | 0.21 | 0.00 |
| CA0 | 0.38 | 0.00 | 0.00 | 0.00 | 0.00 | 0.83 | 0.00 | 0.00 |
| NA20 | 0.49 | 0.42 | 0.00 | 0.00 | 0.57 | 3.48 | 0.25 | 1.84 |
| K20 | 8.96 | 8.04 | 10.97 | 10.68 | 10.84 | 7.50 | 16.36 | 13.86 |
| TOTAL | 90.6 | 97.6 | 96.9 | 99.4 | 99.3 | 99.9 | 100.4 | 100.4 |

Cations for 8 Oxygen

| | | | | | | | | |
|---|---|---|---|---|---|---|---|---|
| SI | 2.35 | 2.86 | 2.32 | 2.29 | 2.24 | 2.54 | 2.94 | 3.00 |
| AL | 1.88 | 1.52 | 1.84 | 1.95 | 1.97 | 1.62 | 1.00 | 1.02 |
| FE2 | 0.06 | 0.06 | 0.14 | 0.07 | 0.07 | 0.07 | 0.05 | 0.00 |
| CA | 0.02 | 0.00 | 0.00 | 0.00 | 0.00 | 0.04 | 0.00 | 0.00 |
| NA | 0.05 | 0.04 | 0.00 | 0.00 | 0.05 | 0.31 | 0.02 | 0.16 |
| K | 0.58 | 0.49 | 0.66 | 0.63 | 0.64 | 0.43 | 0.97 | 0.81 |

End member concentrations

| | | | | | | | | |
|---|---|---|---|---|---|---|---|---|
| AB | 7.37 | 7.29 | 0.00 | 0.00 | 7.34 | 39.25 | 2.30 | 16.80 |
| AN | 3.21 | 0.00 | 0.00 | 0.00 | 0.00 | 5.14 | 0.00 | 0.00 |
| OR | 89.42 | 92.71 | 100.00 | 100.00 | 92.66 | 55.61 | 97.70 | 83.20 |

**K - feldspar chemistry data**

| Sample | 69229 | 69230 | 69230 | 69230 | 69238 | 69238 | 69277 | 69623 | 69623 | 69625 | 69625 | 69625 | 69627 | 71912 | 71912 | 71918 | 71918 |
|---|---|---|---|---|---|---|---|---|---|---|---|---|---|---|---|---|---|
| SIO2 | 29.69 | 29.23 | 28.64 | 30.28 | 29.15 | 29.32 | 29.31 | 30.14 | 28.45 | 27.97 | 28.57 | 28.30 | 27.98 | 29.24 | 29.98 | 30.15 | 30.09 |
| TIO2 | 0.44 | 0.61 | 0.73 | 0.42 | 0.71 | 0.62 | 0.47 | 0.56 | 0.68 | 0.53 | 0.57 | 0.63 | 0.54 | 0.45 | 0.67 | 0.00 | 0.48 |
| AL2O3 | 56.92 | 56.06 | 55.86 | 54.95 | 55.74 | 55.38 | 56.61 | 51.82 | 54.54 | 54.37 | 54.71 | 55.41 | 45.45 | 55.32 | 54.45 | 54.97 | 55.58 |
| FEO | 12.93 | 13.44 | 13.25 | 12.34 | 14.08 | 14.47 | 13.85 | 12.94 | 12.51 | 13.01 | 13.40 | 12.58 | 12.34 | 13.87 | 14.09 | 12.47 | 12.47 |
| MNO | 0.00 | 0.00 | 0.26 | 0.00 | 0.00 | 0.00 | 0.00 | 0.31 | 0.19 | 0.26 | 0.22 | 0.17 | 0.18 | 0.24 | 0.27 | 0.00 | 0.00 |
| MGO | 1.03 | 1.75 | 1.39 | 1.45 | 1.32 | 1.14 | 0.82 | 1.08 | 1.47 | 1.22 | 1.57 | 0.90 | 0.49 | 0.00 | 0.44 | 0.00 | 0.00 |
| CAO | 0.00 | 0.00 | 0.00 | 0.00 | 0.00 | 0.00 | 0.00 | 0.00 | 0.00 | 0.02 | 0.00 | 0.00 | 0.02 | 0.00 | 0.00 | 0.00 | 0.00 |
| NA2O | 0.00 | 0.00 | 0.00 | 0.00 | 0.00 | 0.00 | 0.00 | 0.18 | 0.04 | 0.27 | 0.27 | 0.15 | 0.39 | 0.00 | 0.00 | 0.00 | 0.00 |
| K2O | 0.00 | 0.00 | 0.00 | 0.00 | 0.00 | 0.00 | 0.00 | 0.95 | 0.00 | 0.00 | 0.03 | 0.02 | 0.02 | 0.00 | 0.00 | 0.00 | 0.00 |
| TOTAL | 101.0 | 101.1 | 100.1 | 99.4 | 101.0 | 100.9 | 101.1 | 98.0 | 97.9 | 97.7 | 99.4 | 98.2 | 87.4 | 99.1 | 99.9 | 97.6 | 98.6 |

Cations for 46 oxygen

| | | | | | | | | | | | | | | | | | |
|---|---|---|---|---|---|---|---|---|---|---|---|---|---|---|---|---|---|
| SI | 7.89 | 7.80 | 7.73 | 8.15 | 7.81 | 7.87 | 7.83 | 8.34 | 7.83 | 7.75 | 7.79 | 7.76 | 8.65 | 7.97 | 8.12 | 8.26 | 8.16 |
| TI | 0.09 | 0.12 | 0.15 | 0.08 | 0.14 | 0.13 | 0.10 | 0.12 | 0.14 | 0.11 | 0.12 | 0.13 | 0.13 | 0.09 | 0.14 | 0.00 | 0.10 |
| AL | 17.84 | 17.64 | 17.76 | 17.44 | 17.60 | 17.53 | 17.82 | 16.90 | 17.68 | 17.75 | 17.58 | 17.92 | 16.57 | 17.77 | 17.38 | 17.75 | 17.77 |
| FE2 | 2.87 | 3.00 | 2.99 | 2.78 | 3.16 | 3.25 | 3.09 | 3.00 | 2.88 | 3.01 | 3.05 | 2.89 | 3.19 | 3.16 | 3.19 | 2.86 | 2.83 |
| MN | 0.00 | 0.00 | 0.06 | 0.00 | 0.00 | 0.00 | 0.00 | 0.07 | 0.04 | 0.06 | 0.05 | 0.04 | 0.05 | 0.06 | 0.06 | 0.00 | 0.00 |
| MG | 0.41 | 0.70 | 0.56 | 0.58 | 0.53 | 0.46 | 0.33 | 0.45 | 0.60 | 0.51 | 0.64 | 0.37 | 0.23 | 0.00 | 0.18 | 0.00 | 0.00 |
| CA | 0.00 | 0.00 | 0.00 | 0.00 | 0.00 | 0.00 | 0.00 | 0.00 | 0.00 | 0.00 | 0.00 | 0.00 | 0.00 | 0.00 | 0.00 | 0.00 | 0.00 |
| NA | 0.00 | 0.00 | 0.00 | 0.00 | 0.00 | 0.00 | 0.00 | 0.10 | 0.02 | 0.15 | 0.14 | 0.08 | 0.24 | 0.00 | 0.00 | 0.00 | 0.00 |
| K | 0.00 | 0.00 | 0.00 | 0.00 | 0.00 | 0.00 | 0.00 | 0.34 | 0.00 | 0.00 | 0.01 | 0.01 | 0.01 | 0.00 | 0.00 | 0.00 | 0.00 |

**Staurolite chemistry data**

| Lithology | G.R. | Stripped field data (in counts per min) U | Th | p.p.m U | Th | Heat Production A |
|---|---|---|---|---|---|---|
| ST psammite | 681 600 | 87 | 4 | 0.07 | 1.0 | 0.41 |
| BQ quartzite | 680 601 | 74 | 10 | 0.58 | 1.4 | 0.32 |
| " " " | 679 601 | 93 | 16 | 0.73 | 6.9 | 0.84 |
| " " " | 678 603 | 129 | 23 | 1.02 | 9.9 | 1.13 |
| LM amphibolite | 675 603 | 24 | 12 | 0.19 | 5.1 | 0.49 |
| ST semipelite | 675 604 | 347 | 50 | 2.72 | 21.2 | 2.44 |
| BQ quartzite | 667 607 | 63 | 4 | 0.52 | 1.8 | 0.40 |
| ST pelite | 666 607 | 391 | 44 | 3.08 | 18.5 | 2.56 |
| LM amphibolite | 666 606 | 78 | 1 | 0.61 | 0.6 | 0.26 |
| LM marble | 666 605 | 79 | 35 | 0.62 | 1.4 | 0.33 |
| ST schist | 665 603 | 315 | 32 | 2.48 | 13.7 | 2.09 |
| LM psammite | 663 606 | 277 | 31 | 2.18 | 13.1 | 1.67 |
| ST schist | 663 607 | 266 | 28 | 2.09 | 11.8 | 1.85 |
| LM amphibolite | 663 606 | 44 | 4 | 0.35 | 1.6 | 0.26 |
| ST schist | 660 608 | 254 | 21 | 1.96 | 8.8 | 1.58 |
| LM semipelite | 659 608 | 207 | 31 | 1.60 | 13.1 | 1.53 |
| ST schist | 658 608 | 387 | 30 | 3.04 | 12.8 | 2.14 |
| LM marble | 657 608 | 315 | 13 | 2.48 | 5.5 | 1.06 |
| LM amphibolite | 658 609 | 35 | 3 | 0.27 | 1.5 | 0.23 |
| ST psammite | 660 600 | 270 | 30 | 2.11 | 12.8 | 1.64 |
| LM marble | 664 606 | 209 | 12 | 1.64 | 5.1 | 0.08 |
| ST semipelite | 664 608 | 250 | 42 | 1.97 | 17.9 | 1.98 |
| BQ quartzite | 665 608 | 67 | 10 | 0.53 | 4.4 | 0.60 |
| " " " | 665 609 | 72 | 15 | 0.57 | 6.3 | 0.75 |
| ST pelite | 663 608 | 231 | 28 | 1.82 | 11.8 | 1.74 |
| BQ quartzite | 655 614 | 27 | 19 | 0.21 | 8.2 | 0.80 |
| ST semipelite | 654 615 | 270 | 23 | 2.13 | 9.7 | 1.36 |
| BQ quartzite | 654 616 | 68 | 5 | 0.53 | 2.3 | 0.44 |
| ST semipelite | 652 617 | 356 | 51 | 2.00 | 21.7 | 2.30 |
| BQ quartzite | 652 618 | 63 | 11 | 0.49 | 4.8 | 0.62 |
| ST semipelite | 647 625 | 308 | 44 | 2.42 | 18.7 | 2.01 |
| BQ quartzite | 650 624 | 89 | 16 | 0.70 | 6.7 | 0.82 |
| ST psammite | 650 625 | 88 | 13 | 0.69 | 5.6 | 0.74 |
| BQ quartzite | 655 622 | 39 | 14 | 0.31 | 6.1 | 0.67 |
| " " " | 661 618 | 38 | 17 | 0.30 | 7.4 | 0.76 |
| " " " | 667 617 | 48 | 5 | 0.37 | 2.3 | 0.41 |
| " " " | 672 613 | 51 | 14 | 0.40 | 6.1 | 0.69 |
| " " " | 680 605 | 33 | 22 | 0.26 | 9.3 | 0.89 |
| " " " | 683 600 | 61 | 12 | 0.48 | 5.1 | 0.63 |
| ST psammite | 643 636 | 84 | 21 | 0.67 | 9.1 | 0.91 |
| " " " | 643 635 | 282 | 33 | 2.22 | 13.9 | 1.62 |
| LM marble | 644 634 | 149 | 1 | 1.17 | 0.4 | 0.39 |
| BQ quartzite | 650 630 | 262 | 20 | 2.06 | 8.4 | 1.30 |
| ST semipelite | 646 629 | 488 | 45 | 3.84 | 18.9 | 2.37 |
| KFC semipelite | 695 599 | 258 | 24 | 2.00 | 10.0 | 1.46 |
| Peridotite | 694 597 | 21 | 10 | 0.17 | 4.21 | 0.41 |
| KFC semipelite | 694 597 | 173 | 29 | 1.36 | 12.2 | 1.42 |
| " " " | 691 598 | 150 | 22 | 1.18 | 9.5 | 1.18 |
| " " " | 687 600 | 287 | 15 | 2.26 | 6.32 | 1.23 |
| " " " | 687 604 | 255 | 50 | 2.01 | 21.1 | 2.14 |

| Lithology | G.R. | Stripped field data (in counts per min) U | Th | p.p.m U | Th | Heat Production A |
|---|---|---|---|---|---|---|
| KFR semipelite | 643 643 | 330 | 28 | 2.10 | 11.1 | 1.73 |
| " " " | 644 643 | 358 | 54 | 2.11 | 22.0 | 2.46 |
| " " " | 646 644 | 282 | 52 | 2.00 | 22.0 | 2.27 |
| KFR psammite | 646 642 | 242 | 25 | 1.10 | 10.1 | 1.38 |
| " " " | 648 643 | 299 | 28 | 2.00 | 11.0 | 1.56 |
| KFR pelite | 654 643 | 388 | 35 | 2.68 | 14.2 | 2.13 |
| " " " | 656 641 | 334 | 50 | 2.01 | 21.3 | 2.48 |
| KFR semipelite | 655 640 | 248 | 31 | 1.02 | 13.0 | 1.57 |
| " " " | 656 636 | 268 | 12 | 2.07 | 5.2 | 1.04 |
| KFR pelite | 660 638 | 368 | 48 | 2.11 | 20.5 | 2.51 |
| " " " | 676 637 | 334 | 48 | 2.14 | 20.2 | 2.42 |
| Rushenduff peg | 670 641 | 236 | 22 | 1.13 | 8.7 | 1.36 |
| KFR semipelite | 673 643 | 253 | 30 | 1.02 | 12.3 | 1.53 |
| Rushenduff peg | 673 642 | 209 | 51 | 1.12 | 21.0 | 2.15 |
| KFR psammite | 673 639 | 229 | 41 | 0.93 | 16.8 | 1.80 |
| " " " | 668 637 | 258 | 35 | 1.82 | 14.1 | 1.75 |
| " " " | 669 635 | 251 | 33 | 1.06 | 14.0 | 1.63 |
| KFR semipelite | 677 634 | 193 | 32 | 1.05 | 13.1 | 1.49 |
| KFR pelite | 679 636 | 318 | 31 | 2.04 | 12.7 | 1.88 |
| KFR psammite | 683 640 | 232 | 35 | 1.03 | 14.0 | 1.65 |
| KFR pelite | 677 643 | 322 | 40 | 2.04 | 16.8 | 2.16 |
| KFR psammite | 680 635 | 188 | 14 | 1.00 | 5.1 | 0.94 |
| KFR semipelite | 686 637 | 226 | 43 | 1.13 | 17.6 | 1.87 |
| KFR psammite | 689 638 | 241 | 21 | 1.10 | 9.0 | 1.26 |
| KFR pelite | 695 632 | 371 | 35 | 2.05 | 14.3 | 2.11 |
| KFR psammite | 689 635 | 215 | 31 | 1.02 | 13.0 | 1.49 |
| KFR semipelite | 680 630 | 305 | 28 | 1.97 | 11.8 | 1.59 |
| " " " | 685 650 | 280 | 44 | 1.96 | 18.1 | 2.01 |
| " " " | 688 626 | 229 | 29 | 1.06 | 12.0 | 1.46 |
| KFR pelite | 689 627 | 237 | 34 | 1.04 | 14.0 | 1.81 |
| " " " | 691 620 | 366 | 39 | 2.32 | 16.3 | 2.22 |
| KFR psammite | 686 622 | 107 | 24 | 0.09 | 9.6 | 1.02 |
| KFR pelite | 684 624 | 283 | 41 | 1.97 | 17.1 | 1.87 |
| " " " | 676 617 | 393 | 46 | 3.00 | 19.0 | 2.52 |
| " " " | 675 618 | 296 | 45 | 1.92 | 18.1 | 2.28 |
| LM amphibolite | 674 619 | 23 | 16 | 0.01 | 6.1 | 0.62 |
| KFR semipelite | 674 620 | 289 | 40 | 1.98 | 16.1 | 1.89 |
| LM amphibolite | 671 621 | 76 | 13 | 0.48 | 5.1 | 0.65 |
| KFR semipelite | 688 623 | 195 | 29 | 1.02 | 12.0 | 1.40 |
| " " " | 665 624 | 304 | 25 | 1.96 | 10.0 | 1.50 |
| LM amphibolite | 665 623 | 140 | 6 | 1.00 | 2.0 | 0.54 |
| KFR psammite | 668 623 | 284 | 37 | 2.00 | 15.2 | 1.74 |
| KFR semipelite | 663 628 | 309 | 35 | 1.95 | 13.8 | 1.78 |
| KFR pelite | 666 625 | 332 | 36 | 1.97 | 14.0 | 2.08 |
| " " " | 667 624 | 295 | 29 | 1.86 | 13.2 | 1.79 |
| KFR psammite | 668 623 | 173 | 28 | 1.03 | 13.1 | 1.28 |
| ST semipelite | 673 617 | 337 | 26 | 2.01 | 11.2 | 1.73 |
| " " " | 676 614 | 196 | 14 | 1.02 | 5.3 | 1.11 |
| KFR semipelite | 677 614 | 264 | 43 | 2.02 | 17.6 | 1.93 |
| " " " | 680 610 | 321 | 35 | 2.31 | 13.8 | 1.81 |
| " " " | 679 618 | 170 | 38 | 0.93 | 15.7 | 1.60 |

| Lithology | G.R. | Stripped field data (in counts per min) U | Th | p.p.m U | Th | Heat Production A |
|---|---|---|---|---|---|---|
| KFC pelite | 687 606 | 217 | 42 | 1.71 | 17.9 | 2.02 |
| " " " | 690 604 | 311 | 41 | 2.45 | 17.5 | 2.18 |
| KFC semipelite | 695 605 | 226 | 31 | 1.78 | 13.3 | 1.53 |
| KFC psammite | 690 612 | 93 | 25 | 0.73 | 10.7 | 1.09 |
| KFC pelite | 701 610 | 293 | 38 | 2.30 | 16.2 | 2.05 |
| KFC semipelite | 701 609 | 271 | 23 | 2.13 | 9.7 | 1.36 |
| KFC pelite | 701 607 | 265 | 26 | 2.09 | 10.9 | 1.61 |
| KFC semipelite | 702 598 | 102 | 11 | 0.80 | 4.6 | 0.75 |
| " " " | 704 597 | 256 | 32 | 2.09 | 13.5 | 1.69 |
| Gabbro | 707 594 | 47 | 1 | 0.37 | 0.4 | 0.27 |
| KFC pelite | 712 600 | 276 | 23 | 2.10 | 9.9 | 1.57 |
| " " " | 714 605 | 176 | 30 | 1.38 | 12.9 | 1.60 |
| Peridotite | 716 604 | 18 | 9 | 0.14 | 3.7 | 0.35 |
| KFC pelite | 716 604 | 219 | 27 | 1.72 | 11.6 | 1.59 |
| KFC semipelite | 711 608 | 177 | 23 | 1.39 | 9.7 | 1.20 |
| KFC pelite | 711 607 | 201 | 24 | 1.58 | 10.3 | 1.47 |
| " " " | 709 604 | 152 | 26 | 1.20 | 10.9 | 1.44 |
| " " " | 700 598 | 162 | 23 | 1.27 | 9.7 | 1.37 |
| " " " | 701 590 | 151 | 24 | 1.19 | 10.1 | 1.18 |
| Gabbro | 702 591 | 43 | 1 | 0.34 | 0.2 | 0.32 |
| " " | 702 591 | 42 | 2 | 0.33 | 0.8 | 0.29 |
| " " | 702 592 | 18 | 9 | 0.14 | 3.8 | 0.47 |
| KFC pelite | 702 592 | 203 | 40 | 1.59 | 17.1 | 1.77 |
| Gabbro | 703 592 | 13 | 10 | 0.10 | 4.2 | 0.49 |
| KFC pelite | 703 591 | 84 | 1 | 0.66 | 0.6 | 0.38 |
| " " " | 704 591 | 82 | 25 | 0.64 | 10.5 | 1.07 |
| Gabbro | 704 594 | 34 | 1 | 0.26 | 0.2 | 0.22 |
| " " | 706 595 | 29 | 3 | 0.22 | 1.2 | 0.29 |
| KFC pelite | 710 592 | 66 | 3 | 0.52 | 1.7 | 0.41 |
| " " " | 704 593 | 22 | 23 | 0.18 | 9.7 | 0.89 |
| KFC semipelite | 703 588 | 70 | 10 | 0.55 | 4.2 | 0.57 |
| Gabbro | 702 588 | 27 | 7 | 0.21 | 3.2 | 0.44 |
| KFC semipelite | 701 588 | 29 | 16 | 0.22 | 6.9 | 0.68 |
| Peridotite | 701 588 | 24 | 8 | 0.18 | 3.3 | 0.33 |
| " " | 700 589 | 24 | 3 | 0.19 | 1.4 | 0.18 |
| KFC semipelite | 698 591 | 157 | 12 | 1.23 | 5.1 | 0.81 |
| KFC pelite | 697 592 | 201 | 15 | 1.58 | 6.5 | 1.06 |
| Peridotite | 698 593 | 32 | 1 | 0.25 | 0.6 | 0.13 |
| KFC semipelite | 697 593 | 51 | 16 | 0.40 | 6.7 | 0.65 |
| Gabbro | 696 592 | 40 | 0 | 0.31 | 0.0 | 0.22 |
| Peridotite | 695 591 | 23 | 4 | 0.18 | 1.9 | 0.21 |
| KFC semipelite | 694 592 | 141 | 7 | 1.11 | 3.2 | 0.64 |
| Peridotite | 692 592 | 36 | 3 | 0.28 | 1.5 | 0.21 |
| " " | 692 590 | 40 | 8 | 0.31 | 3.4 | 0.36 |
| KFC semipelite | 693 588 | 8 | 37 | 0.07 | 15.8 | 1.28 |
| " " " | 699 586 | 14 | 43 | 0.11 | 18.1 | 1.45 |
| " " " | 699 584 | 265 | 60 | 2.09 | 25.5 | 2.57 |
| Gabbro | 718 597 | 42 | 5 | 0.32 | 2.1 | 0.39 |
| " " | 720 597 | 38 | 3 | 0.30 | 1.2 | 0.32 |
| " " | 725 600 | 37 | 10 | 0.29 | 1.3 | 0.56 |

| Lithology | G.R. | Stripped field data (in counts per min) U | Th | p.p.m U | Th | Heat Production A |
|---|---|---|---|---|---|---|
| Gabbro | 730 607 | 104 | 5 | 0.82 | 2.3 | 0.54 |
| KFC semipelite | 730 608 | 387 | 50 | 3.05 | 21.3 | 2.56 |
| " " " | 731 608 | 222 | 26 | 1.75 | 10.9 | 1.49 |
| Gabbro | 731 607 | 30 | 10 | 0.24 | 4.2 | 0.49 |
| " " | 740 605 | 38 | 3 | 0.30 | 1.5 | 0.33 |
| " " | 740 604 | 57 | 5 | 0.44 | 2.1 | 0.42 |
| " " | 736 604 | 40 | 8 | 0.31 | 3.4 | 0.49 |
| KFC semipelite | 737 595 | 285 | 23 | 2.24 | 9.7 | 1.52 |
| " " " | 744 595 | 295 | 42 | 2.32 | 17.9 | 2.12 |
| Peridotite | 744 597 | 47 | 3 | 0.37 | 1.26 | 0.21 |
| Gabbro | 744 600 | 32 | 13 | 0.25 | 6.33 | 0.70 |
| " " | 741 602 | 64 | 4 | 0.51 | 1.89 | 0.42 |
| KFC semipelite | 741 603 | 233 | 18 | 1.83 | 7.6 | 1.26 |
| " " " | 738 608 | 296 | 43 | 2.30 | 18.1 | 2.14 |
| " " " | 746 608 | 223 | 26 | 1.76 | 10.9 | 1.59 |
| " " " | 750 610 | 307 | 38 | 2.41 | 16.0 | 2.12 |
| " " " | 751 609 | 240 | 31 | 1.89 | 13.0 | 1.77 |
| Gabbro | 733 601 | 30 | 8 | 0.23 | 3.6 | 0.48 |
| KFC semipelite | 761 599 | 403 | 50 | 3.17 | 21.1 | 2.67 |
| Gabbro | 761 598 | 14 | 15 | 0.11 | 6.3 | 0.66 |
| " " | 760 584 | 36 | 6 | 0.28 | 2.7 | 0.43 |
| KFC semipelite | 760 583 | 296 | 31 | 2.33 | 13.1 | 1.85 |
| " " " | 752 585 | 259 | 42 | 2.04 | 17.8 | 2.11 |
| " " " | 745 591 | 291 | 46 | 2.29 | 16.6 | 2.31 |
| " " " | 740 592 | 232 | 52 | 1.82 | 21.9 | 2.36 |
| " " " | 736 593 | 464 | 61 | 3.65 | 25.7 | 3.09 |
| " " " | 734 593 | 265 | 62 | 2.08 | 26.3 | 2.59 |
| Gabbro | 733 592 | 64 | 3 | 0.51 | 1.5 | 0.39 |
| " " | 732 592 | 67 | 9 | 0.53 | 4.0 | 0.59 |
| " " | 712 589 | 98 | 17 | 0.77 | 7.4 | 0.93 |
| KFC pelite | 712 590 | 193 | 28 | 1.52 | 12.0 | 1.42 |
| Gabbro | 713 589 | 142 | 16 | 1.11 | 6.9 | 0.99 |
| KFC pelite | 714 590 | 224 | 22 | 1.76 | 9.3 | 1.29 |

## Appendix D

Table of sample numbers used in this thesis, with rock type grid reference, Univ. of Liverpool catalogue No. and analytical details

Notes

1, Rock types

Igneous rocks - general lithological name.

Metaigneous - classified as above.

Metasediments - classified as above, with the addition of field characteristics (banded, graded, etc) and/or dominant porphyroblast type. Formation and member name denoted by abbrevation:

B.Q = Bennabeola Quartzite Formation
S.T = Streamstown Formation (Member not known)
S.T1 = Streamstown Fm, Derryinver psammite Mb
S.T2 = Streamstown Fm, Derryinver Siliceous psammite Mb
S.T3 = Streamstown Fm, Dawrosbeg striped psammite Mb
S.T4 = Streamstown Fm, Doongill garnet semipelite Mb
S.T5 = Streamstown Fm, Roeilluan schist Mb

L.M = Lakes Marble Formation (Member not known)
L.M1 = Lakes Marble Formation, Tonabina marble Mb
L.M2 = Lakes Marble Formation, Doongill amphibolite Mb
L.M3 = Lakes Marble Formation, Gubbatoor psammite Mb
L.M4 = Lakes Marble Formation, Gubbatoor marble Mb
L.M5 = Lakes Marble Formation, Trawmore psammite Mb
K.F = Kylemore Formation (undifferentiated)

2, Cat. No.

This is the catalogue number given to a rock specimen when a thin section is cut in the Dept. of Earth Sciences, Liverpool University. The thin section (or polished section) is also identified by this number.

3, Analytical details

XRF - indicates that this specimen was analysed for major and trace element concentrations by X - ray fluorescence spectrometry.

NAA - indicates analysis by neutron activation to determine U, Th and other trace element concentrations.

P - indicates mineral composition analysis by electron probe.

* indicates sample collection by Dr A.P.Boyle

| Loc No. | Locality | Grid Ref. | Rock type | Cat. No. | Anal. Detail |
|---|---|---|---|---|---|
| GA1* | Creggaun | 702 592 | Gabbro | 62405 | |
| GA2* | " " | 703 591 | Green Gabbro | 62406 | |
| GA3* | " " | 703 591 | Lichen Gabbro | 62407 | |
| P1* | approx 200m S of Creggaun | 703 588 | Serpentinised Peridotite | 62408 | |
| P2* | " " " " | 703 588 | Serpentinised Peridotite | 62409 | |
| P3* | Dawrosmore nr road | 699 588 | Layered Peridotite | 62410 | |
| P4* | Dawrosmore | 699 585 | Layered Peridotite | 62411 | |
| P5* | Small hill, SW Dawrosmore | 695 586 | Coarse orthopyroxenite | 62412 | |
| SS1* | S Dawrosmore | 695 584 | L.M Striped Amphibolite | 62738 | |
| SS1* | " " | 695 584 | " " | 62739 | |
| SS2* | " " | 695 585 | S.T mica schist | 62740 | |
| SS3* | " " | 696 585 | B.Q White quartzite | 62741 | |
| SS5* | Gubbatoor coast | 682 585 | S.T3 micaceous semipelite | 62744 | |
| SS6* | " " | 683 584 | L.M calc - silicate | 62745 | |
| SS7* | " " | 682 584 | L.M quartzose psammite | 62746 | |
| GN1* | Dawros Bridge | 701 597 | K.F augen gneiss | 62747 | |
| GN2* | " " | 700 595 | K.F Gneiss | 62748 | |
| GN3* | " " | 701 595 | K.F 'contorted' gneiss | 62749 | |
| GN4* | Creggaun | 702 592 | K.F Banded gneiss | 62750 | |
| GN5* | " " | 702 592 | K.F Basic boundin gneiss | 62751 | |
| GN6* | " " | 703 591 | K.F Granitic pegmatite | 62752 | |
| GN7* | Approx 200m S of Creggaun | 703 588 | K.F Contact gneiss | 62753 | |
| GN8* | " " 250m " " " " | 703 587 | K.F Schlieren gneiss | 62755 | |
| GN9* | Creggaun | 701 589 | K.F Quartzo - feldspathic gneiss | 62754 | |
| 83/68* | Creggaun nr boreen | 702 586 | K.F 5m above Creggaun thrust | 66760 | |
| 83/68* | " " | 702 586 | K.F 10m above Creggaun thrust | 66761a | |
| 83/68* | " " | 702 586 | K.F " " " " " " | 66761b | |
| 83/68* | " " | 702 586 | Serpentinite | 66762 | |
| 83/68* | " " | 702 586 | K.F quartzose psammite | 66763 | |
| 83/68* | " " | 702 586 | Serpentinite | 66764 | |
| 83/68* | " " | 702 586 | K.F in Creggaun thrust | 66765a | |
| 83/68* | " " | 702 586 | " " " " | 66765b | |
| 83/68* | " " | 702 586 | peridotite 5m below Creggaun thrust | 66766 | |
| 83/68* | " " | 702 586 | " " 4m " " " " " | 66767 | |
| 83/68* | " " | 702 586 | Talc schist | 66768 | |
| 83/5* | Dawrosmore | 702 596 | Gabbro 200mm above peridotite contact | 66781 | |
| 83/7* | " " | 703 596 | " " " " | 66782 | |
| 83/8* | " " | 703 596 | Gabbro / peridotite contact | 66783a | |
| 83/8* | " " | 703 596 | " " " | 66783b | |
| 83/9* | " " | 703 596 | Gabbro 50mm above contact | 66784 | |
| 83/10* | " " | 703 596 | Peridotite 300mm below contact | 66785 | |
| 83/30* | Creggaun | 702 592 | K.F contact lithology | 66795 | XRF, NAA, P |
| 83/14* | " " | 701 591 | " " " " " | 66800 | |
| 83/14* | " " | 701 591 | K.F feldspathic contact lithology | 66801 | XRF, P |
| 84/171* | " " | 702 586 | L.M2 amphibolite | 69587 | |
| 84/190* | Dawrosmore | 703 599 | S.T5 garnet staurolite schist | 69588 | |
| 84/248* | " " | 708 597 | K.F psammite | 69589 | |
| 84/248* | " " | 708 597 | K.F amphibolite | 69590 | XRF |
| 84/275* | Dawros River | 712 589 | K.F schistose garnet pelite | 69591 | |
| 84/283* | " " " " | 711 592 | Lineated green gabbro | 69592 | |
| 84/285* | E of Tully Cross Road | 712 594 | K.F lineated psammite | 69593 | |
| 84/189* | Dawrosmore | 702 586 | L.M2 amphibolite | 69594 | XRF |
| 84/190* | " " | 702 586 | S.T5 garnet staurolite schist | 69595 | |
| 84/173* | " " | 702 586 | " " " " " " " | 69596 | |

| Loc No. | Locality | Grid Ref. | Rock type | Cat. No. | Anal. Detail |
|---|---|---|---|---|---|
| 84/213* | Dawrosmore | 703 587 | L.M psammite | 69597 | |
| 84/126* | Creggaun | 702 586 | K.F semipelite | 69598 | |
| 84/93* | " " | 704 587 | K.F semipelite | 69599 | |
| 84/101* | " " | 705 587 | " " " | 69601 | |
| 84/102* | " " | 705 587 | " " " | 69602 | |
| 84/113* | " " | 705 587 | " " " | 69603 | |
| 84/115* | " " | 705 586 | " " " | 69604 | |
| 84/116* | " " | 705 586 | " " " | 69605 | |
| 84/117* | " " | 704 586 | K.F banded psammite | 69606 | |
| 84/118* | " " | 705 586 | K.F quartzite | 69607 | |
| 84/100* | " " | 705 586 | K.F semipelite | 69608 | |
| 84/92* | " " | 705 587 | " " " | 69609 | |
| 84/86* | " " | 705 587 | " " " | 69610 | |
| 84/142* | " " | 704 587 | " " " | 69611 | |
| 84/288* | E of Tully Cross Road | 702 602 | K.F garnet semipelite | 69612 | |
| 84/289* | " " " " " " " | 702 602 | " " " " " | 69613 | |
| 84/291* | " " " " " " " | 702 601 | K.F amphibolite | 69614 | |
| 84/291* | " " " " " " " | 702 601 | K.F semipelite | 69615 | |
| 84/293* | " " " " " " " | 702 601 | " " " | 69616 | |
| 84/296* | " " " " " " " | 704 602 | K.F amphibolite | 69617 | |
| 84/239* | " " " " " " " | 704 600 | K.F pelite | 69618 | |
| 84/250* | " " " " " " " | 706 600 | " " " | 69619 | XRF, P |
| 84/257* | " " " " " " " | 710 597 | " " " | 69620 | |
| 84/257* | " " " " " " " | 710 597 | Gabbro | 69621 | |
| 84/228* | Creggaun | 701 599 | K.F amphibolite | 69622 | |
| 84/35* | Dawrosbeg peninsula | 688 588 | S.T5 garnet staurolite schist | 69623 | XRF, P |
| 84/50* | " " " " | 688 585 | S.T3 crenulated pelite | 69624 | |
| 84/63* | " " " " | 682 583 | S.T5 garnet staurolite schist | 69625 | XRF, P |
| 84/68* | " " " " | 684 582 | S.T3 psammite | 69626 | |
| 84/68* | " " " " | 684 582 | S.T5 garnet staurolite schist | 69627 | XRF, NAA, P |
| 84/22* | " " " " | 682 587 | L.M psammite | 69628 | |
| 84/19* | " " " " | 682 587 | L.M pelite | 69629 | |
| 84/29* | " " " " | 685 590 | L.M psammite | 69630 | |
| 84/177* | Dawrosmore | 700 585 | L.M2 amphibolite | 69631 | |
| 84/298* | Creggaun | 707 604 | K.F granitic migmatite | 69632 | |
| 84/298* | " " | 707 604 | " " " " " | 69633 | |
| 84/303* | " " | 701 602 | K.F banded psammite | 69634 | |
| 84/243* | " " | 712 600 | K.F garnet semipelite | 69635 | XRF, P |
| 84/RENA* | Rinvyle Quay | 657 638 | K.F andalusite pelite | 69636 | XRF, NAA |
| 84/RENB* | " " " " | 657 638 | " " " " " | 69637 | |
| 84/A1.1 | Dawrosbeg coast, Gubbatoor | 682 584 | L.M3 Calcareous Psammite | 68752 | |
| 84/A1.3 | " " " " " " | 682 584 | L.M3 Calcareous semipelite | 68753 | |
| 84/A2 | " " " " " " | 682 584 | L.M3 Quartzose psammite | 68754 | |
| 84/A3 | " " " " " " | 682 585 | L.M3 Massive psammite | 68755 | |
| 84/A4 | " " " " " " | 682 585 | L.M3 Micaceous semipelite | 68756 | |
| 84/A6.1 | " " " " " " | 683 585 | S.T3 Schistose semipelite | 68757 | |
| 84/A7.3 | " " " " Doleengarve | 683 586 | S.T3 Semipelite | 68758 | |
| 84/A8.2 | " " " " " " | 684 586 | S.T3 Psammite | 68759 | |
| 84/A9.1 | " " " " " " | 684 586 | B.Q White quartzite | 68760 | |
| 84/A12.1 | " " " " " " | 683 587 | S.T5 Garnet mica schist | 68761 | |
| 84/A12.3 | " " " " " " | 683 587 | S.T5 Mica schist | 68762 | |
| 84/B1 | Dawrosmore | 693 587 | Coarse grain orthopyroxenite | 68763 | |
| 84/B4 | " " | 692 588 | K.F schistose psammite | 68764 | |
| 84/B5 | " " | 692 587 | Medium grain size pyroxenite | 68765 | |

| Loc No. | Locality | Grid Ref. | Rock type | Cat. No. | Anal. Detail |
|---|---|---|---|---|---|
| 84/B8 | Dawrosmore | 691 588 | K.F gneissose psammite | 68766 | |
| 84/B11 | " " | 691 589 | K.F feldspar porphyroblast schist | 68767 | |
| 84/B18 | " " | 692 592 | K.F schistose garnetiferous psammite | 68768 | NAA |
| 84/B19 | " " | 692 592 | " " " " " " " | 68769 | |
| 84/B23 | " " | 693 592 | " " " " " " " | 68770 | |
| 84/B28 | " " | 692 588 | K.F feldspar porphyroblast psammite | 68771 | |
| 84/B30 | " " | 693 587 | K.F foliated gneissose psammite | 68772 | |
| 84/B32 | " " | 694 588 | Layered Lherzolite | 68773 | |
| 84/B37 | " " | 696 583 | " " " " | 68774 | |
| 84/B38 | " " | 695 596 | K.F hornfelsic mylonitised semipelite | 68775 | |
| 84/B40 | " " | 697 591 | K.F feldspar porphyroblast psammite | 68776 | |
| 84/B42 | " " | 697 589 | Layered Lherzolite | 68777 | |
| 84/B43.1 | " " | 697 590 | K.F quartzose vein in psammites | 68778 | |
| 84/B43.2 | " " | 697 590 | K.F coarse grained schist | 68789 | |
| 84/B44 | " " | 698 591 | K.F garnet psammite | 68780 | XRF, P |
| 84/B45 | " " | 699 594 | K.F feldspar porphyroblast psammite | 68781 | |
| 84/B46 | " " | 699 594 | K.F basic sheet in psammites | 68782 | |
| 84/C1.1 | Gortnaling, nr Gawlaun | 728 628 | K.F garnet semipelite | 68783 | |
| 84/C1.2 | " " " " " | 728 628 | Serpentinised ultrabasic | 68784 | |
| 84/C2 | " " " " " | 727 628 | K.F mica schist | 68785 | |
| 84/C3 | " " " " " | 727 628 | K.F semipelite | 68786 | |
| 84/C4 | " " " " " | 726 627 | K.F coarse psammite | 68787 | |
| 84/C5 | " " " " " | 726 627 | K.F flaggy semipelite | 68788 | |
| 84/C6 | " " " " " | 726 627 | K.F garnet pelite | 68789 | |
| 84/C7 | " " " " " | 728 628 | Lineated amphibolite | 68790 | NAA |
| 84/C8 | " " " " " | 728 629 | K.F garnet mica schist | 68791 | |
| 84/C9 | " " " " " | 728 627 | Pyroxenite | 68792 | |
| 84/D16 | Dawros River | 712 593 | K.F garnet semipelite | 68793 | XRF, P |
| 84/E3 | W side of Currywongaun | 721 593 | K.F garnet hornfels | 68794 | |
| 84/E7 | " " " " " | 716 594 | K.F schist | 68795 | |
| 84/F1 | Bog NE of Dawros Bridge | 701 607 | K.F micaceous semipelite | 68796 | |
| 84/F3 | " " " " " " | 701 605 | K.F foliated semipelite | 68797 | |
| 84/F5 | " " " " " " | 701 604 | K.F mylonitic garnet semipelite | 68798 | |
| 84/F6.1 | " " " " " " | 701 603 | K.F garnet pelite | 68799 | P |
| 84/F8 | Dawros Bridge | 700 598 | K.F feldspathic semipelite | 68800 | |
| 84/H1 | North of Shanaveag Bridge | 708 610 | K.F micaceous semipelite | 68801 | |
| 84/H3 | " " " " " " | 712 604 | K.F feldspathic psammite | 68802 | |
| 84/H5 | " " " " " " | 717 601 | K.F Gneissic feldspathic psammite | 68803 | |
| 84/H7 | NW slope of Currywongaun | 720 598 | K.F garnet pelite | 68804 | XRF, NAA, P |
| 84/H8 | " " " " " | 721 597 | Feldspar porphyroblast gabbro | 68805 | |
| 84/I1 | Bog N of Dawros River | 705 604 | K.F micaceous semipelite | 68806 | XRF, P |
| 84/I2 | " " " " " " | 706 603 | K.F feldspathic semipelite | 68807 | |
| 84/I4 | " " " " " " | 705 600 | K.F feldspar porphyroblast pelite | 68808 | |
| 84/I5 | " " " " " " | 704 598 | K.F feldspar porphyroblast semipelite | 68809 | |
| 84/J1 | " " " " " " | 712 600 | K.F micaceous psammite | 68810 | |
| 84/J2 | " " " " " " | 711 599 | K.F garnet semipelite | 68811 | |
| 85/31 | Dawrosbeg | 690 594 | K.F pelite | 69213 | |
| 85/40 | " " | 697 594 | K.F feldspar porphyroblast psammite | 69214 | |
| 85/44 | " " | 697 594 | K.F garnet pelite | 69215 | XRF,P |
| 85/60 | " " | 696 595 | Massive harzburgite | 69216 | |
| 85/72 | " " | 695 592 | Serpentinised harzburgite | 69217 | |
| 85/110 | " " | 700 593 | K.F garnet semipelite | 69218 | |
| 85/119 | " " | 700 590 | K.F mylonitic garnet pelite | 69219 | P |
| 85/126 | " " | 695 590 | Layered harzburgite | 69220 | |

Doongill Amphibolite Member: This lithology is best developed to the south of Tully Mountain, in the coastal strip between Doongill and Tonabina. In this area the base of the amphibolite is not exposed and a minimum thickness of >70m is present. Inland the amphibolite is considerably thinner, being reduced to a thickness of 20m on the north side of Tully Mountain, where the RBS cuts the stratigraphy. On the Dawrosbeg peninsula the amphibolite reaches thicknesses of only 1 - 2m and is laterally impersistent.

The amphibolite is typically dark green/grey weathering with a strong foliation. A lineation defined by amphibole needles up to 2mm long is variably developed on the foliation planes. A compositional striping (Evans & Leake 1960), parallel to the dominant foliation, is defined by 1 - 10mm thick, green hornblende rich horizons which are interlaminated with plagioclase rich pale horizons of a similar thickness. The compositional fabric is interrupted by scattered 100-200mm long lenticular pods of feldspathic material (Figure 2.6).

In some areas, e.g. [GR 660 508, 728 592] large (10 - 20mm) sub to euhedral amphibole crystals are developed which randomly overgrow the main tectonic fabric.

Gubbatoor Psammite Member: This lithology has contacts with the amphibolite and marble members described above. Direct contacts between this psammite and the Tonabina marble are exposed on the Dawrosbeg peninsula where the amphibolite is locally absent. The psammite consists of pale weathering, bedded (100 - 200mm) siliceous units with a strongly developed spaced foliation and thin (20 - 30mm) penetratively foliated micaceous horizons. Grit bands are developed, with lineated quartz clasts occurring in graded sets (Figure 2.7). The contact of this unit with the marble is sharp, with no evidence of transition between the two units. The contact with the amphibolite is less well exposed, and it is possible that the psammite cuts down into the amphibolite, the local absence of amphibolite representing an original sedimentary feature rather than a tectonic effect.

Gubbatoor Marble Member: This lithology is best exposed on

| Loc No. | Locality | Grid Ref. | Rock type | Cat. No. | Anal. Details |
|---|---|---|---|---|---|
| 85/149 | Dawrosbeg | 695 590 | Massive metagabbro | 69221 | |
| 85/160 | " " | 698 590 | Foliated metagabbro | 69222 | |
| 85/172 | " " | 695 592 | K.F mylonitic semipelite | 69223 | |
| 85/174 | " " | 695 592 | Feldspathic xenolith in peridotite | 69224 | XRF |
| 85/101 | " " | 698 592 | Spinel lherzolite | 69225 | |
| 85/87 | " " | 695 590 | Ultrabasic pod within metagabbro | 69226 | |
| 85/150 | " " | 695 589 | Pyroxene rich ultrabasic | 69227 | |
| 85/500 | Roeillaun | 683 591 | S.T5 banded psammite | 69228 | |
| 85/504 | " " | 683 593 | S.T5 garnet - staurolite schist | 69229 | P |
| 85/506 | " " | 682 593 | S.T5 " " " " " " | 69230 | XRF, P |
| 85/522 | " " | 677 592 | S.T5 " " " " " " | 69231 | |
| 85/525 | " " | 680 590 | S.T5 " " " " " " | 69232 | |
| 85/529 | N Renvyle peninsula | 681 543 | K.F pelite | 69233 | XRF, NAA |
| 85/537 | " " " " " | 680 639 | K.F semipelite | 69234 | |
| 85/543 | " " " " " | 680 636 | K.F micaceous semipelite | 69235 | |
| 85/546 | " " " " " | 677 636 | K.F garnet pelite | 69236 | XRF, P |
| 85/556 | " " " " " | 680 631 | K.F semipelite | 69237 | NAA |
| 85/561 | " " " " " | 679 630 | K.F garnet pelite | 69238 | XRF, P |
| 85/571 | " " " " " | 681 630 | K.F semipelite | 69239 | |
| 85/576 | " " " " " | 682 620 | K.F semipelite | 69240 | |
| 85/577 | " " " " " | 681 620 | Porphyritic dyke | 69241 | |
| 85/578 | " " " " " | 681 620 | K.F crenulated garnet pelite | 69242 | XRF, NAA |
| 85/584 | " " " " " | 681 620 | K.F " " " " " " | 69243 | |
| 85/588 | " " " " " | 681 610 | K.F " " " " " " | 69244 | |
| 85/590 | " " " " " | 676 621 | K.F schistose semipelite | 69245 | |
| 85/598 | " " " " " | 676 617 | K.F chloritic schist | 69246 | |
| 85/599 | " " " " " | 675 617 | K.F crenulated semipelite | 69247 | |
| 85/600 | " " " " " | 675 617 | K.F psammite | 69248 | |
| 85/601 | " " " " " | 675 617 | K.F garnet semipelite | 69249 | |
| 85/615 | Derryinver | 686 598 | K.F feldspathic psammite | 69250 | XRF |
| 85/618 | " " | 686 600 | K.F semipelite | 69251 | |
| 85/621 | S Tully Mountain coast | 674 601 | S.T4 garnet mica schist | 69252 | |
| 85/622 | Dawrosbeg peninsula | 676 586 | S.T3 staurolite pelite | 69253 | |
| 85/628 | " " " " | 678 584 | S.T3 semipelite | 69254 | |
| 85/627 | " " " " | 675 585 | L.M1 marble | 69255 | |
| 85/631 | Coast N of Rinvyle | 692 636 | K.F semipelite | 69256 | |
| 85/633 | " " " " " " | 693 635 | " " " | 69257 | |
| 85/638 | W of Tully Cross | 690 628 | K.F crenulated garnet semipelite | 69258 | |
| 85/642 | " " " " " " | 690 628 | K.F crenulated semipelite | 69259 | XRF |
| 85/652 | " " " " " " | 688 625 | K.F garnet semipelite | 69260 | |
| 85/657 | Tully Lough | 693 605 | K.F mica schist | 69261 | |
| 85/667 | S of Tully Lough | 691 603 | K.F garnet semipelite | 69262 | |
| 85/677 | Roeillaun, Derryinver | 691 597 | K.F feldspathic psammite | 69263 | XRF |
| 85/679 | " " " " | 690 596 | K.F feldspathic psammite | 69264 | |
| 85/688 | N coast of Bunlahy Bay | 694 598 | K.F lineated psammite | 69265 | |
| 85/700 | Derryinver | 689 600 | K.F feldspathic psammite | 69266 | |
| 85/707 | N coast of Bunlahy Bay | 692 592 | K.F semipelite | 69267 | |
| 85/725 | Dawrosbeg peninsula | 693 585 | S.T3 semipelite | 69268 | XRF |
| 85/728 | " " " " | 692 589 | S.T3 schist | 69269 | |
| 85/732 | Dawrosmore | 700 585 | L.M2 amphibolite | 69270 | XRF |
| 85/733 | " " | 710 585 | S.T garnet semipelite | 69271 | |
| 85/734 | Lough Touther | 735 594 | K.F garnet semipelite | 69272 | |
| 85/740 | Currywongaun Village | 731 590 | L.M2 amphibolite | 69273 | XRF, NAA |

| Loc No. | Locality | Grid Ref. | Rock type | Cat. No. | Anal. Details |
|---|---|---|---|---|---|
| 85/746 | " " " " | 732 591 | K.F semipelite | 69274 | XRF |
| 85/747 | " " " " | 733 591 | " " " | 69275 | XRF |
| 85/748 | " " " " | 732 592 | K.F garnet semipelite | 69276 | |
| 85/750 | Tullywee Bridge | 728 591 | S.T garnet staurolite schist | 69277 | XRF, P |
| 85/752 | " " " " | 728 591 | L.M2 amphibolite | 69278 | XRF, NAA |
| 85/354 | Dawrosmore | 699 597 | K.F lineated garnet semipelite | 69279 | |
| 85/365 | " " | 699 598 | " " " " " " " | 69280 | |
| 86/1 | Shanaveag Bridge | 716 604 | Amphibolitic ultrabasic pod | 71890 | XRF |
| 86/7 | " " " " | 716 604 | K.F pelitic gneiss | 71891 | |
| 86/10 | " " " " | 714 605 | K.F pelitic schist | 71892 | |
| 86/12 | " " " " | 716 604 | Amphibolitic ultrabasic pod | 71893 | |
| 86/14 | Plateau N of Currywongaun | 725 607 | K.F foliated gneiss | 71894 | |
| 86/15 | " " " " " " | 730 608 | K.F gneiss | 71895 | |
| 86/27 | N of Doughruagh | 742 609 | K.F feldspar porphyroblastic psammite | 71896 | |
| 86/30 | W slope of Altnagaighera | 749 605 | K.F siliceous psammite | 71897 | |
| 86/47 | " " " " " " | 752 602 | K.F feldspathic semipelite | 71898 | XRF, P |
| 86/55 | " " " " " " | 755 605 | K.F semipelite | 71899 | |
| 86/61 | " " " " " " | 754 606 | K.F amphibolite | 71900 | XRF |
| 86/64 | " " " " " " | 753 608 | K.F garnet semipelite | 71901 | XRF, P |
| 86/69 | " " " " " " | 748 612 | K.F psammite | 71902 | |
| 86/76 | " " " " " " | 760 601 | K.F foliated migmatite | 71903 | |
| 86/87 | Corrie E of Doughruagh | 762 598 | K.F semipelitic gneiss | 71904 | |
| 86/106 | " " " " " " | 762 598 | K.F garnet feldspar gneiss | 71905 | |
| 86/108 | " " " " " " | 761 597 | K.F sillimanite pelite | 71906 | XRF, P |
| 86/113 | SE of Doughruagh | 762 597 | K.F silimanitic gneiss | 71907 | |
| 86/114 | " " " " | 762 597 | " " " " " | 71908 | |
| 86/142 | N side of Kylemore valley | 760 587 | K.F psammite | 71909 | |
| 86/147 | " " " " " " " | 759 588 | K.F gneiss | 71910 | |
| 86/155 | " " " " " " " | 754 588 | K.F semipelite | 71911 | |
| 86/162 | " " " " " " " | 747 589 | K.F garnet semipelite | 71912 | XRF, P |
| 86/166 | Lough Touther | 743 589 | " " " " " | 71913 | |
| 86/172 | " " " " | 737 594 | " " " " " | 71914 | XRF, P |
| 86/186 | " " " " | 737 592 | K.F semipelite | 71915 | |
| 86/263 | S side of Tully Mountain | 674 603 | S.T4 garnet pelite | 71916 | XRF, P |
| 86/266 | " " " " " " " " | 674 602 | L.M2 amphibolite | 71917 | |
| 86/356 | Doongill | 660 607 | S.T5 garnet staurolite schist | 71918 | XRF, P |
| 86/409 | " " | 662 609 | L.M1 marble | 71919 | |
| 86/446 | Lettermore | 667 605 | S.T4 garnet pelite | 71920 | |
| 86/447 | N side of Tully Mountain | 680 611 | S.T3 siliceous psammite | 71921 | |
| 86/500 | " " " " " " " | 675 617 | S.T3 semipelite | 71922 | |
| 86/501 | " " " " " " " | 676 617 | K.F garnet pelite | 71923 | XRF, P |
| 86/503 | " " " " " " " | 674 619 | " " " " " | 71924 | |
| 86/522 | " " " " " " " | 665 624 | L.M2 amphibolite | 71925 | |
| 86/525 | " " " " " " " | 664 624 | " " " | 71926 | |
| 86/604 | Braadillaun | 654 615 | S.T3 garnet semipelite | 71927 | |
| 86/646 | " " | 652 618 | " " " " " | 71928 | XRF, P |
| 86/719 | Rinvyle Point | 643 636 | L.M amphibolite | 71929 | |
| 86/727 | " " " " | 645 634 | S.T3 chloritic semipelite | 71930 | |
| 86/728 | " " " " | 645 638 | K.F chloritic semipelite | 71931 | |
| 86/750 | Ardnagreevagh | 656 643 | K.F garnet pelite | 71932 | XRF, P |
| 86/781 | " " | 664 630 | K.F crenulated semipelite | 71933 | |
| 86/796 | Rushenduff coast | 674 643 | K.F crenulated semipelite | 71934 | XRF, P |
| 86/804 | Rushenduff | 673 637 | K.F semipelite | 71935 | |
| 86/828 | N side of Tully Mountain | 674 611 | K.F crenulated semipelite | 71936 | |
| 86/842 | Eagles' Nest School | 665 627 | K.F garnet semipelite | 71937 | XRF, P |

| Loc No. | Locality | Grid Ref. | Rock type | Cat. No. | Anal. Detai |
|---|---|---|---|---|---|
| 86/863 | Cloonooaun | 675 620 | " " " " " | 71938 | |
| 86/876 | Tully Pier | 696 631 | Serpentinised ultrabasic | 71939 | XRF |
| 86/876 | " " " " | 696 631 | " " " " | 71940 | |
| 86/876 | " " " " | 696 631 | K.F pelitic schist | 71941 | XRF, P |
| 86/918 | Mullaghglass | 717 628 | K.F pelitic schist | 71942 | |
| 86/920 | " " | 718 628 | K.F amphibolite | 71943 | XRF |
| 86/921 | " " | 718 628 | " " " | 71944 | |
| 86/936 | Rushenduff | 674 635 | K.F garnet semipelite | 71945 | |
| 86/941 | " " | 674 636 | Rushenduff pegmatite | 71946 | |
| 86/940 | " " | 674 636 | " " " " | 71947 | |

AGUIRRE, L. & ATHERTON, M.P. 1987. Low grade metamorphism and geotectonic setting of the Macuchi Formation, Western Cordillera of Ecuador. *Journal of Metamorphic Geology*, 5, 473-494.

ANDERSON, D.E. & OLIMPIO, J.C. 1977. Progressive homogenisation of metamorphic garnets, South Morar, Scotland: Evidence for volume diffusion. *Canadian Mineralogist*, 15, 205-216.

ANDERTON, R. 1985. Sedimentation and tectonics in the Scottish Dalradian. *Scottish Journal of Geology*, 21, 407-436.

----- . 1988. Dalradian slides and basin development: a radical interpretation of stratigraphy in the SW and Central Highlands of Scotland. *Journal of the Geological Society, London*, 145, 669-678.

ANGUS, N.S. & MIDDLETON, R. 1985. Compositional variation in Hogbomites from North Connemara, Ireland. *Mineralogical Magazine*, 49, 649-654.

-----, ----- & KANARIS-SOTIRIOU, R. 1980. The petrogenetic significance of a peridotite xenolith from the Currywongaun-Doughraugh intrusion, Connemara. *Journal of Earth Sciences of the Royal Dublin Society*, 2, 153-160.

ANOVITZ, L.M & ESSENE, E.J. 1987. Compatibility of geobarometers in the system CaO - FeO - $Al_2O_3$ - $SiO_2$ - $TiO_2$ (CFAST): Implications for garnet mixing models. *Journal of Gelogy*, 95, 633-645.

ASHWORTH, J.R. & EVIRGEN, M.M. 1985. Plagioclase relations in pelites, central Menderes Massif, Turkey I. The peristite gap with coexisting kyanite. *Journal of Metamorphic Geology*, 3, 207-218.

ATHERTON, M.P. 1968. The variation in garnet, biotite, and chlorite composition in medium grade pelitic rocks from the Dalradian, Scotland, with particular reference to the zonation in garnet. *Contributions to Mineralogy and Petrology*, 18, 347-371.

----- 1977. Carnegie Review Article - The metamorphism of the Dalradian rocks of Scotland. *Scottish Journal of Geology*, 13, 331-370.

----- & BROTHERTON, M.S. 1972. The composition of some kyanite-bearing regionally metamorphosed rocks from the Dalradian. *Scottish Journal of Geology*, 8, 203-213.

----- & ----- 1979. Thorium and uranium in some pelitic rocks from the Dalradian, Scotland. *Chemical Geology*, 27, 329-342.

----- & ----- 1982. Major element composition of the pelites of the Scottish Dalradian. *Geological Journal*, 17, 185-222.

BADLEY, M.E. 1976. Stratigraphy, structure and metamorphism of Dalradian rocks of the Maumturk mountains, Connemara, Eire. *Journal of the Geological Society, London*, 132, 509-520.

BARBER, J.P. & YARDLEY, B.W.D. 1985. Conditions of high grade metamorphism in the Dalradian of Connemara, Eire. *Journal of the Geological Society, London*, 142, 87-96.

BARKER, A.J. & GAYER, R.A. 1985. Caledonide - Appalachian tectonic analysis and evolution of related oceans. *In:* GAYER R.A. (ed) *The tectonic evolution of the Caledonian - Appalachian orogen.* pp126-165. Bransheig/Wiesbaden: Friedr Viewg & Sohn.

BELL, T.H. 1985. Deformation partitioning and porphyroblast rotation in metamorphic rocks: a radical reinterpretation. *Journal of Metamorphic Geology*, 3, 109-118.

-----. 1986. Foliation development and refraction in metamorphic rocks: reactivation of earlier foliations and decrenulation due to shifting patterns of deformation partitioning. *Journal of Metamorphic Geology*, 4, 421-444.

----- & RUBENACH, M.J. 1983. Sequential porphyroblast growth and crenulation cleavage development during progressive deformation. *Tectonophysics*, 92, 171-194.

----- , ----- . & FLEMING, P.D. 1986. Porphyroblast nucleation, growth and dissolution in regional metamorphic rocks as a function of deformation partitioning during foliation development. *Journal of Metamorphic Geology*, 4, 37-67.

BENNETT, M.C. & GIBB, F.G.F. 1983. Younging directions in the Dawros Peridotite, Connemara. *Journal of the Geological Society, London*, 140, 63-73.

BLUCK, B.J. & LEAKE, B.E. 1986. Late Ordovician to early Silurian amalgamation of the Dalradian and adjacent Ordovian rocks in the British Isles. *Geology*, 14, 917-919.

BOYLE, A.B., McCARTHY, P.M & STEWART, D. 1987. Geochemical control of saxicolous lichen communities on the Creggaun Gabbro, Letterfrack, Co. Galway, Western Ireland. *Lichenoligist*, 19, 307-317.

BREMNER, D.L & LEAKE, B.E. 1980. The geology of the Roundstone Ultrabasic Complex, Connemara. *Proceedings of the Royal Irish Academy*, 80, 395-433.

BROWN,G.C., HUGHES, D.J. & ESSON, J. 1973. New XRF data retrieval techniques and their application to USGS standard data. *Chemical Geology*, 11, 223-229.

BRUNFELT, A.O. & STEINNES, E. 1969. Instrumental activation

analysis of silicate rocks with epithermal neutrons. *Analytica Chimica Acta*, 48, 13-24.

BURTON, K.W. 1986. *Fluid controls on crystal growth during metamorphism.* Ph.D thesis, University College, London.

CASSIDY, J. 1981. Techniques of field gamma - ray spectrometry. *Mineralogical Magazine*, 44, 391-398.

CARMICHAEL, D.M. 1969. On the mechanism of prograde metamorphic reactions in quartz - bearing pelitic rocks. *Contributions to Mineralogy and Petrology*, 20, 244-267.

----- . 1970. Intersecting isograds in the Whetstone Lake area, Ontario. *Journal of Petrology*, 11, 147-181.

CARSLAW, H.S & JAEGER, J.C. 1959. Conduction of heat in solids. *Oxford University Press*, 2nd ed, pp510.

CHAMBERLAIN, C.P. 1986. Evidence for the repeated folding of Isotherms during regional metamorphism. *Journal of Petrology*, 27, 63-89.

----- & KARABINOS, P. 1987. Influence of deformation on pressure-temperature paths of metamorphism. *Geology*, 15, 42-44.

CHATTERJEE, N.D. & JOHANNES, W. 1974. Thermal stability and standard thermodynamic properties of synthetic $2M_1$ muscovite, $KAl_2[AlSi_3O_{10}(OH)_2]$. *Contributions to Mineralogy and Petrology*, 48, 89-114.

CHINNER, G.A. 1961. The origin of sillimanite at Glen Clova, Angus. *Journal of Petrology*, 2, 312-323.

CLARK (Jr), S.P. 1966. Thermal conductivity. In: CLARK (Jr), S.P. (ed) *Handbook of physical constants*, The Geological Society of America Memoir 97.

COBBING, E.J. 1969. The geology of the district NW of Clifden, Co. Galway. *Proceedings of the Royal Irish Academy*, 67, 303-305.

CRESSEY, G., SCHMID, R. & WOOD, B.J. 1978. Thermodynamic properties of almandine-grossular garnet solid solutions. *Contributions to Mineralogy and Petrology*, 67, 397-404.

CRUSE, M.A.J.B. 1963. *The geology of Renvyle, Inishbofin and Inishshark, Northwest Connemara, Co. Galway.* PhD thesis, Bristol.

----- & LEAKE, B.E. 1969. The geology of Renvyle, Inishbofin and Inishshark, NW Connemara, Co. Galway. *Proceedings of the Royal Irish Academy, 67B*, 1-36.

DALLMEYER, R.D. 1974. The role of cystal structure in

controlling the partitioning of Mg and $Fe^{2+}$ between coexisting garnet and biotite. *American Mineralogist*, **59**, 201-203.

DALY, R.A., MANGER, G.E. & CLARK (Jr), S.P. 1966. Density of rocks. In: CLARK (Jr), S.P. (ed) *Handbook of physical constants*, The Geological Society of America Memoir **97**.

DAVY, P. & GILLET, P. 1986. The stacking of thrust slices in collision zones and its thermal consequences. *Tectonics*, **5**, 913-929.

DEER, W.A., HOWIE, R.A. & ZUSSMAN, J. 1966. *An introduction to the rock - forming minerals*. Longman.

DEMPSTER, T.J. 1985. Garnet zoning and metamorphism in the Barrovian type area, Scotland. *Contributions to Mineralogy and Petrology*, **89**, 30-38.

DE BETHUNE, P., LADURON, D. & BOCQUET, J. 1975. Diffusion processes in resorbed garnets. *Contributions to Mineralogy and Petrology*, **50**, 197-204.

DEWEY, J.F. & HUTTON D.H.W. 1986. Paleozoic terrane accretion in the Western Irish Caledonides. *Tectonics*, **7**, 1115-1124.

----- & SHACKLETON, R.M. 1984. A model for the evolution of the Grampian tract in the early Caledonides and Appalachians. *Nature*, **312**, 115-121.

DRURY, M.J. & LEWIS, T.J. 1983. Water movement within Lac du Bonnet Batholith as revealed by detailed thermal studies of three closely - spaced boreholes. *Tectonophysics*, 337-351.

DYMEK, R.F. 1983. Titanium, aluminium and interlayer cation substitutions in biotite from high -grade gneisses, West Greenland. *American Mineralogist*, **68**, 880-899.

ELIAS, E.M., MacINTYRE, R.M. & LEAKE, B.E. 1988. The cooling history of Connemara, western Ireland, from K - Ar and Rb - Sr age studies. *Journal of the Geological Society, London*, **145**, 649-660.

ELLIS, M.A. 1986. Structural morphology and associated strain in the central Cordillera (British Columbia and Washington): Evidence of oblique tectonics. *Geology*, **14**, 647-650.

----- & WATKINSON, A.J. 1987. Orogen - parallel extension and oblique tectonics: The relation between stretching directions and relative plate motions. *Geology*, **15**, 1022-1026.

ENGLAND, P.C. & RICHARDSON, S.W. 1977. The influence of erosion upon the mineral facies of rocks from different metamorphic environments. *Journal of the Geological Society, London* , **134**, 201-213.

----- & ----- . 1980. Erosion and the age dependence of continental heat flow. *Geophysical Journal of the Royal Astronomical Society*, **62**, 421-437.

----- & THOMPSON, A.B. 1984. Pressure-Temperature-Time paths of regional metamorphism I. Heat transfer during the evolution of regions of thickened continental crust. *Journal of Petrology*, **25**, 894-928.

ESSENE, E.J. 1982. Geologic thermometry and barometry. *In:* FERRY, J.M. (ed) *Characterisation of metamorphism through mineral equilibria, Mineralogical Society of America, Reviews in Mineralogy Volume* **10.**

EVANS, B.W. & LEAKE, B.E. 1960. The composition and origin of the striped amphibolites of Connemara, Ireland. *Journal of Petrology*, **1**, 337-363.

FEELY, M. & MADDEN, J.S. 1987. The spatial distribution of K, U, Th and surface heat rpoduction in the Galway Granite, Connemara, western Ireland. *Irish Journal of Earth Sciences*, **8**, 155-164.

----- . & ----- . 1970. The geology of the Toombeola district, Connemara, Co. Galway. *Proceedings of the Royal Irish Academy*, **70B**, 105-139.

FERGUSON, C.C. 1984. A probabilistic model for the persistence of early planar fabrics in polydeformed pelitic schists. *Journal of Structural Geology*, **6**, 135-146.

----- & AL-AMEEN, S.I. 1986. Geochemistry of Dalradian Pelites from Connemara, Ireland: new constraints on kyanite genesis and conditions of metamorphism. *Journal of the Geological Society, London* , **143**, 236-253.

----- & HARVEY, P.K. 1978. Thermally overprinted Dalradian rocks near Cleggan, Connemara, Western Ireland. *Proceedings of the Geologists Association*, **90**, 43-50.

FERRY, J.M. 1976. P, T, $f_{CO_2}$, and $f_{H_2O}$ during metamorphism of calcareous sediments in the Waterville - Vassalboro area, south - central Maine. *Contributions to Mineralogy and Petrology*, **57**, 119-143.

----- . 1979. A map of chemical potential differences within an outcrop. *American Mineralogist*, **64**, 966-985.

----- . 1980. A case study of the amount and distribution of heat and fluid during metamorphism. *Contributions to Mineralogy and Petrology*, **71**, 373-385.

----- . 1988. Contrasting mechanisms of fluid flow through adjacent stratigraphic units during regional metamorphism, south-central Maine, USA. *Contributions to Mineralogy and*

*Petrology*, **98**, 1-12.

----- & SPEAR, F.S. 1978. Experimental calibrations of the partitioning of Fe and Mg between biotite and garnet. *Contributions to Mineralogy and Petrology*, **66**, 113-117.

FLANAGAN, F.J. 1973. 1972 values for international geochemical reference samples. *Geochimica et Cosmochimica Acta*, **37**, 1189-1200.

FOWLER, C.M.R. & NISBET, E.G. 1982. The thermal background to metamorphism - II. Simple two-dimensional conductive models. *Geoscience Canada*, **9**, 208-214.

FRONDEL, C. & COLLETTE, R.L. 1957. Synthesis of tourmaline by reaction of mineral grains with NaCl - $H_3BO_3$ solution, and its implications in rock metamorphism. *American Mineralogist* , **42**, 754-758.

GANGULY, J. 1979. Garnet and clinopyroxene solid solutions, and geothermometry based on Fe - Mg distribution coefficient. *Geochimica et Cosmochimica Acta*, **43**, 1021-1029.

----- & SAXENA, S.K. 1984. Mixing properties of aluminosilicate garnets: constraints from natural and experimental data, and applications to geothermo-barometry. *American Mineralogist*, **69**, 88-97.

GEIGER, C.A, NEWTON, R.C. & KLEPPA, O. 1987. Enthalpy of mixing of synthetic almandine - grossular and almandine - pyrope garnets fgrom high - temperature solution calorimetry. *Geochimica et Cosmachimica Acta* **51**, 1755-1763.

GHENT, E.D. 1976. Plagioclase-garnet-$Al_2SiO_5$-Qtz; A potential geobarometer-geothermometer. *American Mineralogist*, **61**, 710-714.

----- , ROBBINS, D.B. & STOUT, M.Z. 1979. Geothermometry, geobarometry and fluid compostions of metamorphosed calc-silicates and pelites, Mica creek, British Columbia. *American Mineralogist*, **64**, 874-885.

----- & STOUT, M.Z. 1981. Geothermometry and geobarometry of plagioclase - biotite - garnet - muscovite assembelages. *Contributions to Mineralogy and Petrology*, **76**, 92-97.

GOLDMAN, D.S & ALBEE, A.L. 1977. correlation of Mg/Fe partitioning between garnet and biotite with $^{18}O/^{16}O$ partitioning between quartz and magnetite. *American Journal of Science*, 277, 750-767.

GUIDOTTI, C.V. 1984. Micas in metamorphic rocks. *In* Bailey, S.W. (ed) *Reviews in Mineralogy, Volume 13 Micas*, Mineralogical Society of America, 357-468.

HARLAND, W.B., COX, A.V., LLEWELLYN, P.G, PICKTON, C.A.G., SMITH,

A.G. & WALTERS. R. 1982. *A geologic time scale*, Cambridge University Press.

HARRIS, A.L. & PITCHER, W.S. 1975. The Dalradian supergroup. *In*: HARRIS, A.L., SHACKLETON, R.M., WATSON, J., DOWNIE, C. HARLAND, W.B. & MOORBATH, S. (eds) *Geological Society of London Special Report 6: A correlation of precambrian rocks in the British Isles.*

HARTE, B. & DEMPSTER, T.J. 1987. Regional metamorphic zones: tectonic controls. *Philosphical Transactions of the Royal Society of London, Series A*, **321**, 105-127.

----- . & HENLEY, K.J. 1966. Occurence of compositionally zoned almanditic garnets in regional metamorphosed rocks. *Nature*, **210**, 689-692.

HARVEY, P.K. & FERGUSON, C.C. 1973. Spherically arranged inclusions in post-tectonic garnet porphyroblasts. *Mineralogical Magazine*, **39**, 85-88.

HASLAM, H.W. 1983. An isotropic alteration product of Cordierite. *Mineralogical Magazine*, **47**, 238-240.

HEY, M.H. 1954. A new review of the chlorites. *Mineralogical Magazine*, **30**, 277-292.

HODGES, K.V. & CROWLEY, P.D. 1985. Error estimation and empirical geothermobarometry for pelitic systems. *American Mineralogist*, **70**, 702-709.

----- . & McKENNA, L.W. 1987. Realistic propagation of uncertainties in geologic thermobarometry. *American Mineralogist*, **72**, 671-680.

----- & SPEAR, F.S. 1982. Geothermometry, geobarometry and the $Al_2SiO_5$ triple point at Moosilauke, New Hampshire. *American Mineralogist*, **67**, 1118-1134.

HOLDAWAY, M.J. 1980. Chemical formulae and activity models for biotite, muscovite and chlorite applicable to pelitic metamorphic rocks. *American Mineralogist*, **65**, 711-719.

HOLLISTER, L.S. 1966. Garnet zoning: an interpretation based on the Rayleigh fractionation model. *Science*, **154**, 1647-1651.

HUTTON, D.H.W. 1987. Strike - slip terranes and a model for the evolution of the British and Irish Caledonides. *Geological Magazine*, **124**, 405-425.

----- . & DEWEY, J.F. 1986. Palaeozoic terrane accretion in the western Irish Caledonides. *Tectonics*, **5**, 1115-1124.

INDARES, A. & MARTIGNOLE, J. 1985. Biotite - garnet geothermometry in the granulite facies: the influence of Ti and

Figure 2.6: Feldspathic pods wrapped by foliation and compositional striping in the Doongill Amphibolite Member of the Lakes Marble Formation at [GR 664 603]. Compass is 175mm long.


Figure 2.7: Graded bedding in the Gubbatoor Psammite Member of the Lakes Marble Formation at [GR 683 585]. Lens cap is 49mm diameter.

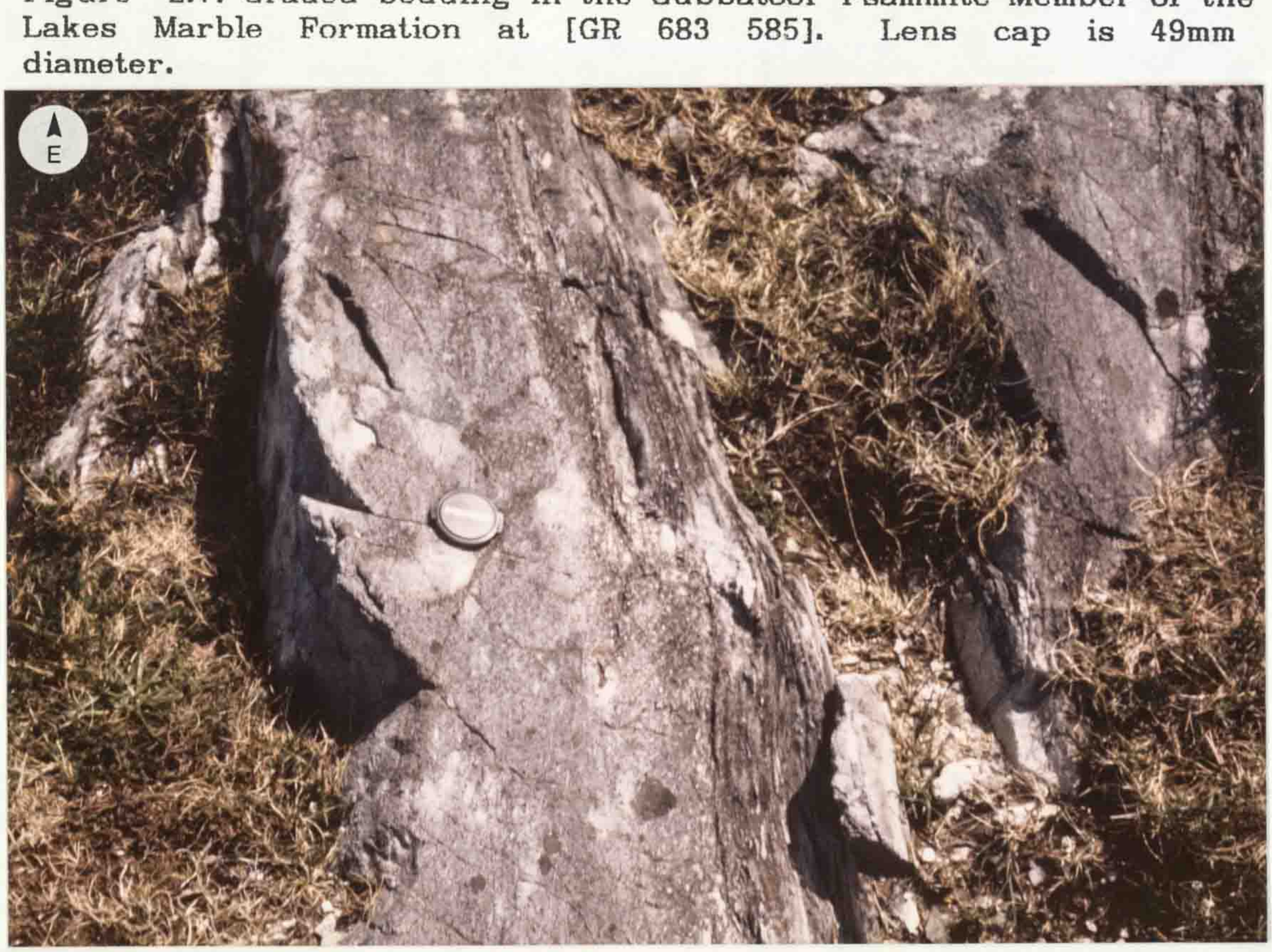

Al in biotite. *American Mineralogist*, **70**, 272-278.

INGOLD, L.M. 1937. The geology of the Currywongaun - Doughruagh area, Co. Galway. *Proceedings of the Royal Irish Academy*, **43B**, 135-159.

IRVINE, T.N. 1974. Petrology of the Duke Island ultramafic complex. *Memoir of the Geological Society of America*, **138.**

----- . 1982. Terminology for layered intrusions. *Journal of Petrology*, **23**, 127-162.

JAEGER, J.C. 1961. The cooling of irregularly shaped igneous bodies. *American Journal of Science*, **259**, 721-734.

JAGGER, M.D., MAX, M.D, AFTALION, M. & LEAKE, B.E. 1988. U - Pb zircon ages of basic rocks and gneisses intruded into the Dalradian rocks of Cashel, Connemara, western Ireland. *Journal of the Geological Society, London*, **145**, 645-648.

JAMIESON, R.A. & BEAUMONT, C. Orogeny and metamorphism: A model for deformation and P - T - t paths with applications to the central and southern Appalachians. *Tectonics*, in press.

JONES, D.J, HOWELL, D.G., CONEY, P.J. & MONGER, W.H. 1983. Recognition, character, analysis of tectonostratigraphic terranes in western North America. *In:* HASHIMOTO, M. & UYEDA, S. (eds) *Accretionary tectonics in the Circum - Pacific regions*, Advances in Earth and Planetary Science, Terra Science Publishing Co. Tokyo.

KANARIS-SOTIRIOU, K. & ANGUS, N.S. 1976. The Currywongaun - Doughruagh syntectonic intrusion, Connemara, Ireland. *Journal of the Geological Society, London*, **132**, 485-508.

KELLY, T.J & MAX, M.D. 1979. A strain section across part of the Caledonian orogen in W. Ireland. *In:* HARRIS, A.L., HOLLAND, C.H. & LEAKE, B.E. (eds) *Caledonides of the British Isles - reviewed, Geological Society, London, Special Publication*, 8, 275-280.

KENNAN, P.S., FELLY, M. & MOHR, P. 1987. The age of the Oughterard granite, Connemara, Ireland. *Geological Journal*, **22**, 273-280.

----- & MURPHY, F.C. 1987. Tectonically reset Rb - Sr system during Late Ordovician terrane assembly in Iapetus, western Ireland. *Geology*, **15**, 115-1158.

KENNEDY, M.J. 1984. Ophiolitic melanges in the Irish Dalradian and the Canadian Appalachians. In *Programme and Abstracts: Tectonic Studies Group Annual General Meeting 1984*, University College, Swansea.

KILBURN, C., PITCHER, W.S. & SHACKLETON, R.M. 1965. The

stratigraphy and origin of the Portaskaig boulder bed series (Dalradian). *Geological Journal*, 4, 343-360.

KILROE, J.R. 1907. The Silurian and metamorphic rocks of Mayo and North Galway. *Proceedings of the Royal Irish Academy*, 26, 129-160.

KINAHAN, G.H., NOLAN, J., LEONARD, H. & CRUISE, R.J. 1878. Geological structure of the district around Clifden, Connemara. *Geological Survey of Ireland, Explanatory Memoir*, Sheets 93 and 94.

KRETZ, R. 1973. Kinetics of the crystallisation of garnet at two localities near Yellowknife. *Canadian Mineralogist*, 12, 1-20.

----- . 1983. Symbols for rock forming minerals. *American Mineralogist* , 68, 277-279.

KWAK, T.A.P. 1968. Ti in biotite and muscovite as an indicator of metamorphic grade in almandine amphibolite facies rocks from Sudbury, Ontario. *Geochemica et Cosmochimica Acta*, 32, 1222-1229.

LABOTKA, T.C. 1980. Petrology of a medium - pressure regional metamorphic terrane, Funeral Mountains, California. *American Mineralogist*, 65, 670-689.

LASAGA, A.C. 1983. Geospeedometry: an extension of geothermometry. *In*: SAXENA, S.K. (ed) *Kinetics and equilibrrium in mineral reactions*, Springer Verlag NY. 81-115.

LEAKE, B.E. 1958a. Composition of pelites from Connemara, Co. Galway, Ireland. *Geological Magazine*, 95, 281-296.

----- . 1958b. The Cashel - Lough Wheelan intrusion. *Proceedings of the Royal Irish Academy*, 59B, 155-203.

----- . 1964b. New light on the Dawros peridotite, Connemara, Eire. *Geological Magazine*, 101, 63-75.

----- . 1965. A cordierite-rich magnetite - hogbomite - opx hornfels from Currywongaun, Connemara, Ireland. *American Mineralogist*, 50, 1092-1095.

----- . 1970b. The fragmentation of the Connemara basic and ultrabasic intrusions. *In*: NEWALL, G. & RAST, N. (eds) *Mechanisms of igneous intrusion, Geological Journal Special Issue*, 2, 103-122.

----- . 1986. The geology of SW Connemara, Ireland: a fold and thrust Dalradian and metagabbroic - gneiss complex. *Journal of the Geological Society, London*, 143, 221-236.

----- . & SINGH, D. 1986. The Delaney Dome Formation, Connemara, W. Ireland and the geochemical distinction of ortho-

and para- quartzitic rocks. *Mineralogical Magazine*, 50, 205-215.

----- , TANNER, P.W.G., MACINTYRE, R.M. & ELIAS, E. 1984. Tectonic postion of the Dalradian rocks of Connemara and its bearing on the evolution of the Midland Valley of Scotland. *Transactions of the Royal Society of Edinburgh: Earth Sciences*, **75**, 165-171.

----- , ----- , & SENIOR, A. 1981. The geology of Connemara: geological map (1:63,360) with cross sections, fold traces and metamorphic isograd map. University of Glasgow.

----- , ----- , SINGH, D. & HALLIDAY, A.N. 1983. Major southward thrusting of the Dalradian rocks of Connemara, W Ireland. *Nature*, **305**, 210-213.

LEGGO, P.J., COMPSTON, W. & LEAKE, B.E. 1966. The geochronology of the Connemara granites and its bearing on the antiquity of the Dalradian series. *Journal of the Geological Society, London*, **122**, 91-118.

----- & PIDGEON, R.T. 1970. Geochronological investigations of Caledonian history in Western Ireland. *Eclogae Geologicae Helvetiae*, **23**, 207-212.

LEWIS, S.D., LADD, J.W. & BRUNS, T.R. 1988. Structural development of an accretionary prism by thrust and strike - slip faulting: Shumagin region, Aleutian Trench. *Geological Society of America, Bulletin*, **100**, 767-782.

LOOMIS, T.P. 1975. Reaction zoning of garnet. *Contributions to Mineralogy and Petrology*, **52**, 285-303.

MALTMAN, A.J. 1978. Serpentinite textures in Anglesey, North Wales, United Kingdom. *Geological Society of America Bulletin*, **89**, 972-980.

McCURRY, P. 1971. The relationship between optical properties and occurrence of some black tourmalines from Northern Nigeria. *Mineralogical Magazine*, **38**, 368-373.

McKENZIE, D. 1978. Some remarks on the development of sedimentary basins. *Earth and Planetary Science Letters*, **4 0**, 25-32.

McLELLEN, E.L. 1983. Problems of structural analysis in migmatite terrains. *In:* ATHERTON, A.P. & GRIBBLE C.D. (eds) *Migmatites, melting and metamorphism.* Shiva Publishing Ltd.

----- . 1988. Migmatite structures in the Central Gneiss Complex, Boca de Quadra, Alaska. *Journal of Metamorphic Geology*, **6**, 517-542.

MIYASHIRO, A. 1973. *Metamorphism and metamorphic belts.* London: George Allen & Unwin.

MOORBATH, S., BELL, K., LEAKE, B.E. & McKERROW, W.S. 1968. Geochronlogical studies in Connemara and Murrisk, Western Ireland. *In*: HAMILTON, E.I. & FARQUHAR, R.M. (eds.) *Radiometric Dating for Geologists*, Wiley-Interscience, 259-298.

MORRIS, W.A. & TANNER, P.W.G. 1977. The use of paleomagnetic data to delineate the history of the development of the Connemara antiform. *Canadian Journal of Earth Sciences*, 14, 2601-2613.

NAGGER, M.H. & ATHERTON, M.P. 1970. The composition and metamorphic history of some aluminium silicate - bearing rocks from the aureoles of the Donnegal granite. *Journal of Petrology*, 11, 549-589.

----- & ----- . 1971. The X - ray spectrochemical analysis of pelitic rocks by a limited compositional range technique. *United Arab Republic Journal of Geology*, 15, 1-27.

NEWTON, R.C. 1983. Geobarometry of high - grade metamorphic rocks. *American Journal of Science*, 283A, 1-28.

----- . & HASELTON, H.T. 1981. Thermodynamics of the garnet - plagioclase - $Al_2SiO_5$ - quartz geobarometer. *In:* NEWTON, R.C., NAVROTSKY, A. & WOOD, B.J. (eds) *Thermodynamics of minerals and melts*, Springer-Verlag, New York.

NISBET, E.G. & FOWLER, C.M.R. 1982. The thermal background to metamorphism - 1. Simple one-dimensional models. *Geoscience Canada*, 9, 16-26.

NORRIS, R.J. & HENLEY, R.W. 1976. Dewatering of a metamorphic pile. *Geology*, 4, 333-336.

OXBURGH, E.R. & TURCOTTE, D.L. 1974. Thermal gradients and regional metamorphism in overthrust terrains with special reference to the Eastern Alps. *Schweiz Mineralogie Petrologie Mittielung*, 54, 641-662.

PERCHUK, L.L. 1967. The biotite garnet thermometer. *Doklady Akademii Nauk SSSR*, 177, 411-414.

PIDGEON, R.T. 1969. Zircon U-Pb ages from the Galway granite and the Dalradian, Connemara, Ireland. *Scottish Journal of Geology*, 5, 375-392.

PIGAGE, L.C. & GREENWOOD, H.J. 1982. Internally consistant estimates of pressure and temperature: the staurolite problem. *American Journal of Science*, 282, 943-969.

POWELL, D. & TREAGUS, J.E. 1967. On the geometry of S-shaped inclusion trails in some garnet porphyroblasts. *Mineralogical Magazine*, 36, 453-456.

----- & ----- . 1970. Rotational fabrics in metamorphic minerals. *Mineralogical Magazine*, 37, 801-814.

RAMSEY, J.G. 1967. *Folding and fracturing of rocks.* McGraw - Hill, New York.

----- & HUBER, M.I. 1987. *The techniques of modern structural geology. Volume 2: Folds and Fractures.* Academic Press Inc. (London) Ltd.

RIBBE, P.H. 1983. Exsolution textures in ternary and plagioclase feldspars: Interference colours. *In* RIBBE, P.H. (ed) *Feldspar mineralogy, Mineralogical Society of America, Reviews in Mineralogy, Volume* 2, second edition.

RICHARDSON, S.W. 1970. The relation between a petrogenetic grid, facies series and the geothermal gradient in metamorphism. *Fortschrift Mineralogie*, 47, 65-76.

----- & ENGLAND, P.C. 1979. Metamorphic consequences of crustal eclogite production in overthrust orogenic zones. *Earth and Planetary Science Letters*, 42, 183-190.

ROTHSTEIN, A.T.V. 1954. *Studies in the serpentine rocks.* Ph.D thesis, Oxford.

----- . 1956. The Dawros peridotite, Connemara, Eire. *Journal of the Geological Society, London*, 63, 2-25.

----- . 1958. Pyroxenes from the Dawros peridotite. *Geological Magazine*, 95, 456-462.

----- . 1961. A synorogenic peridotite at Dawros, Connemara. *Acta Geologica Hungaricae*, 7, 221-232.

----- . 1964. New light on the Dawros Peridotite - reply to Leake 1964. *Geological Magazine*, 101, 283-285.

----- . 1972. Spinels from the Dawros peridotite, Connemara, Ireland. *Mineralogical Magazine*, 38, 957-960.

----- . 1983. Discussion on younging directions in the Dawros Peridotite, Connemara, *Journal*, 140, 63-73. *Journal of the Geological Society, London*, 140, 843-844.

ROY, R.F., BLACKWELL, D.D. & BIRCH, F. 1968. Heat generation of plutonic rocks and continental heat flow provinces. *Earth and Planetary Science Letters*, 5, 1-12.

RUMBLE (III), D., FERRY, J.M., HOERING, T.C. & BOUCOT, A.T. 1982. Fluid flow during metamorphism at the Beaver Brook fossil locality, New Hampshire. *American Journal of Science*, 282, 886-919.

RYAN, P.D. 1983. The Silurian succession. *In:* ARCHER, J.B & RYAN, P.D. (eds) *Geological guide to the Caledonides of*

*western Ireland*, The Geological Survey of Ireland.

RYE, R.O., SCHULING, R.D., RYE, D.M. & JANSEN, J.B.H. 1976. Carbon, hydrogen, and oxygen isotpe studies of the regional metamorphic complex at Naxos, Greece. *Geochimica et Cosmochimica Acta*, **40**, 1031-1049.

SALJE, E. 1986. Heat capacities and entropies of andalusite and sillimanite: the influence of fibrolitization on the phase diagram of the $Al_2SiO_5$ polymorphs. *American Mineralogist*, **71**, 1366-1371.

SAXENA, S.K. 1969. Silicate solid solution and geothermometry. 3. distribution of Fe and Mg between coexisting garnet and biotite. *Contributions to Mineralogy and Petrology*, **22**, 259-267.

SELVERSTONE, J. & SPEAR, F.S. 1985. Metamorphic P-T paths from pelitic schists and greenstones from the South-west Tauern window, Eastern Alps. *Journal of Metamorphic Geology*, **3**, 439-465.

SENIOR, A. & LEAKE, B.E. 1978. Regional metasomatism and the geochemistry of the Dalradian metasediments of Connemara, Western Ireland. *Journal of Petrology*, **19**, 585-625.

SHAOCHENG, J. & MAINPRICE, D. 1988. Natural deformation fabrics of plagioclase: implications for slip - systems and seismic anisotropy. *Tectonophysics*, **147**, 145-163.

SHAW, D.M. 1956. Geochemistry of pelitic rocks. Part III: major elements and general geochemistry. *Bulletin of the Geological Society of America*, *67*, 913-934.

SHI, Y. & WANG, C - Y. 1987. Two - dimensional modelling of the P - T - t paths of regional metamorphism in simple overthrust terrains. *Geology*, **15**, 1048-1051.

SIMPSON, C. 1986. Determination of movement semse in mylonites. *Journal of Geological Education*, **34**, 246-261.

SLEEP, N.H. 1979. A thermal constraint on the duration of folding with reference to Acadian geology, New England. *Journal of Geology*, **87**, 583-589.

SMITH, J.V. 1974. *Feldspar Minerals*, Springer - Verlag.

SOPER, N.J. & HUTTON, D.H.W. 1984. Late Caledonian sinstral displacements in Britain: implications for a three plate collision model. *Tectonics*, **3**, 781-794.

SPEAR, F.S. 1986. PT path: a FORTRAN progrom to calculate pressure - temperature paths from zoned metamorphic garnets. *Computers and Geosciences*, **12**, 247-266.

----- , FERRY, J.M. & RUMBLE, D. III. 1982. Analytical formulation of phase equilibria: The Gibbs method. *In* FERRY, J.M. (ed) *Characterisation of metamorphism through mineral equilibria. Mineralogical Society of America, Reviews in Mineralogy, Volume* 10.

----- . & RUMBLE, D. (III). 1986. Pressure, temperature and structrual evolution of the Orfordville belt, West-Central New Hampshire. *Journal of Petrology*, 27, 1071-1093.

----- .& SELVERSTONE, J. 1983. Quantitative P-T paths from zoned minerals: theory and tectonic applications. *Contributions to Mineralogy and Petrology*, 83, 384-357.

----- , ----- , HICKMOTT, D., CROWLEY, P. & HODGES, K.V. 1984. P-T paths from garnet zoning: a new technique for deciphering tectonic processes in crystalline terranes. *Geology*, 12, 87-90.

SPRY, A. 1963a. The origin and significance of snowball structure in garnet. *Journal of Petrology*, 4, 211-222.

STATHAM, P.J. 1977. Deconvolution and background subtraction by least - squares fitting with prefilter of spectra. *Analytical Chemistry*, 49, 2149-2145.

STURT, B.A. & HARRIS, A.L. 1961. The metamorphic history of the Loch Tummel area, Central Perthshire, Scotland. *Liverpool and Manchester Geological Journal*, 2, 689-711.

TANNER, P.W.G. 1967. The Dalradian of Connemara, Eire. *11th Annual Report of the Research Institute for African Geology of the University of Leeds*, 26-28.

----- . & SHACKLETON, R.M. 1979. Structure and stratigrahy of the Dalradian rocks of the Bennabeola area, Connemara, Eire. *In:* HARRIS, A.L., HOLLAND, C.H. & LEAKE, B.E. (eds) *The Caledonides of the Britsh isles - Reviewed.* Special Publication of the Geological Society of London, 8, 243-249.

THOMPSON, J.B. 1957. The graphical analysis of mineral assemblages in pelitic schists. *American Mineralogist*, 42, 842-858.

THOMPSON, A.B. 1976a. Mineral reactions in pelitic rocks: I prediction of P-T-X (Fe-Mg) phase relations. *American Journal of Science*, 276, 401-424.

----- . 1976b. Mineral reactions in pelitic rocks: II recalculation of some P-T-X (Fe-Mg) phase relations. *American Journal of Science*, 276, 425-454.

----- . 1981. The pressure - temperature (P, T) plane viewed by geophysists and petrologists. *Terra Cognita, Journal of the European Union of Geosciences*, 1, 11-20.

----- . 1987. Some aspects of fluid motion during metamorphism. *Journal of the Geological Society, London*, 144, 309-312.

----- . & ENGLAND, P.C. 1984. Pressure - temperature - time paths of regional metamorphism II. Their influence and interpretation using mineral assembelages in metamorphic rocks. *Journal of Petrology*, 25, 929-955.

----- . & RIDLEY, J.R. 1987. Pressure - temperature - time (P-T-t) histories of orogenic belts. *Philosphical Transactions of the Royal Society of London, Series A*, 321, 27-45.

THOMPSON, P.H. 1976. Isograd patterns and pressure - temperature distributions during regional metamorphism. *Contributions to Mineralogy and Petrology*, 57, 277-295.

TILLEY, C.E. 1924b. The facies classification of metamorphic rocks. *Geological Magazine*, 61, 167-171.

TRACY, R.J. 1982. Compositional zoning and inclusions in metamorphic minerals. *In:* FERRY, J.M. (ed) *Characterisation of metamorphism through mineral equilibria. Mineralogical Society of America, Reviews in Mineralogy, Volume* 10.

----- . , ROBINSON, P. & THOMPSON, A.B. 1976. Garnet composition and zoning in the determination of temperature and pressure of metamorphism, Central Massachusetts. *American Mineralogist*, 61, 762-775.

TRELOAR, P.J. 1981. Gnt - bio - cord thermometry and barometry in the Cashel aureole, Connemara, Ireland. *Mineralogical Magazine*, 44, 183-189.

----- . 1982. The stratigraphy and structure of the rocks of the Lissoughter area, Connemara. *Proceedings of the Royal Irish Academy*, 82B, 83-107.

----- . 1985. Metamorphic conditions in central Connemara, Eire. *Journal of the Geological Society, London*, 142, 77-86.

----- . & McINNES, J.L. 1981. Complex deformation of ore bands in Dalradian quartzites at Cleggan, Connemara, Ireland. *Journal of Earth Sciences of the Royal Dublin Society*, 4, 75-82.

TRZCIENSKI, W.E. ((Jr)). 1977. Garnet zoning - production of a continous reaction. *Canadian Mineralogist*, 15, 250-256.

TOWNEND, R. 1966. The geology of some granite plutons from western Connemara, Co. Galway. *Proceedings of the Royal Irish Academy*, 65B, 157-202.

VERNON, R.H. 1987. Growth and concentrations of fibrous sillimanite related to heterogeneous deformation in K - feldspar - sillimanite metapelites. *Journal of Metamorphic Geology*, 5, 51-58.

WAGER, L.R. 1932. The geology of the Roundstone district, County Galway. *Proceedings of the Royal Irish Academy*, 41B, 46-72.

----- . 1939. Outline of the geology of Connemara. *Proceedings of the Geologists Association*, 50, 346-351.

----- . & ANDREW, G. 1930. The age of the Connemara schists and of their metamorphism. *Geological Magazine*, 67, 271-275.

WALTHER, J.H. & ORVILLE, P.M. 1982. Volatile production and transport in regional metamorphism. *Contributions to Mineralogy and Petrology*, 79, 252-257.

WICKHAM, S.M. & TAYLOR, H.P. ((Jr)). 1987. Stable isotope constraints on the orign and depth of penetration of hydrothermal fluids associated with Hercynian regional metamorphism and crustal anatexis in the Pyrenees. *Contributions to Mineralogy and Petrology*, 95, 255-268.

WINKLER, H.G.F. 1965. *Petrogenesis of metamorphic rocks*, Springer - Verlag, New York.

WOOD, B.J. & FRASER, D.G. 1977. *Elementary thermodynamics for geologists*, Oxford University Press.

WOODSWORTH, G.J. 1977. Homogenisation of zoned garnets from pelitic schists. *Canadian Mineralogist*, 15, 230-242.

YARDLEY, B.W.D. 1976. Deformation and metamorphism of Dalradian rocks and the evolution of the Connemara cordillera. *Journal of the Geological Society, London*, 132, 521-542.

----- . 1977a. An empirical study of diffusion in garnet. *American Mineralogist*, 62, 793-800.

----- . 1977b. Relationships betwwen the chemical and modal compositions of metapelites from Connemara, Ireland. *Lithos*, 10, 235-242.

----- , BARBER, J.P. & GREY, J.R. 1987. The metamorphism of the Dalradian rocks of western Ireland and its relation to tectonic setting. *Philosphical Transactions of the Royal Society of London, Series A*, 321, 243-270.

----- , LEAKE, B.E. & FARROW, C.M. 1980. Metamorphism of Fe-rich pelites from Connemara, Ireland. *Journal of Petrology*, 21, 365-399.

----- . & SENIOR, A. 1982. Basic magmatism in Connemara, Ireland: evidence for a volcanic arc? *Journal of the Geological Society, London*, 139, 67-70.

----- , SHEPHERD, T.J. & BARBER, J.P. 1983. Fluid inclusion studies in high grade rocks from Connemara, Ireland. *In:* ATHERTON, M.P. & GRIBBLE, C.D. (eds), *Migmatites, melting and*

*metamorphism*, Shiva Publishing Ltd.

----- , VINE, F.J. & BALDWIN, C.T. 1982. The plate tectonic setting of NW Britain and Ireland in late Cambrian and early Ordovician times. *Journal of the Geological Society, London*, 139, 457-466.

Figure 2.8: Contact between the Gubbatoor Psammite and Marble Members of the Lakes Marble Formation at [GR 643 635].


Figure 2.9: Typical field appearance of hornfelsic Kylemore Formation at [GR 695 594]. Lens cap is 49mm diameter.

the Dawrosbeg peninsula. The contact of this unit with the Gubbatoor psammite is locally well exposed in fold closures [GR 682 585] (Figure 2.8) and is sharp, with the marble showing features similar to those described previously for the Tonabina marble Member. The marble is laterally variable, being rich in thick (up to 300mm) grit and psammite bands in the Gubbatoor area, poor in siliceous ribs on the west coast of Dawrosbeg and showing regularly spaced 5 - 10mm siliceous ribs at Knocknasheeoge.

Trawmore Psammite Member: This is the highest stratigraphic horizon seen in the study area. The lower contact is not exposed, the maximum thickness exposed being 20 - 30m. The unit is very similar to the Gubbatoor psammite in appearance, sometimes being darker weathering and more micaceous in nature, but generally showing identical features. On the south side of Trawmore Bay [GR 645 636] the psammite contains graded pebble beds with quartz clasts which can reach maximum dimensions of 50x20x10mm.

### 2.1.2.2 Lithologies to the north of the Renvyle - Bofin slide

The sequence of lithologies to the north of the RBS, the Kylemore Formation (Morris & Tanner 1977), is much more homogeneous than that which lies to the south. The Kylemore Formation lacks good marker horizons and is often poorly exposed. The evaluation of the large scale structures developed in these lithologies could not be performed with the same degree of detail as could be achieved in the southern area.

The Kylemore Formation consists of a sequence of interbedded psammites, semipelites and pelites. The thickness of the bedding varies from 1 - 2m thick psammites with wispy, 10 - 20mm semipelite partings seen on the north coast of the Renvyle peninsula, to massive pelites and semipelites with 10 - 20cm psammite bands at Mweelbeg (the western tip of Renvyle). To the east of Eagle's Nest school [GR 666 626] grit bands up to 100mm thick are present in a sequence of banded semipelites and psammites. These grit bands, now strongly lineated, consist of rounded quartz clasts up to 50x20x10mm which rarely develop as

Figure 2.10: Typical field appearance of schistose Kylemore Formation at [GR 703 628]. Notebook is 210 X 150mm.

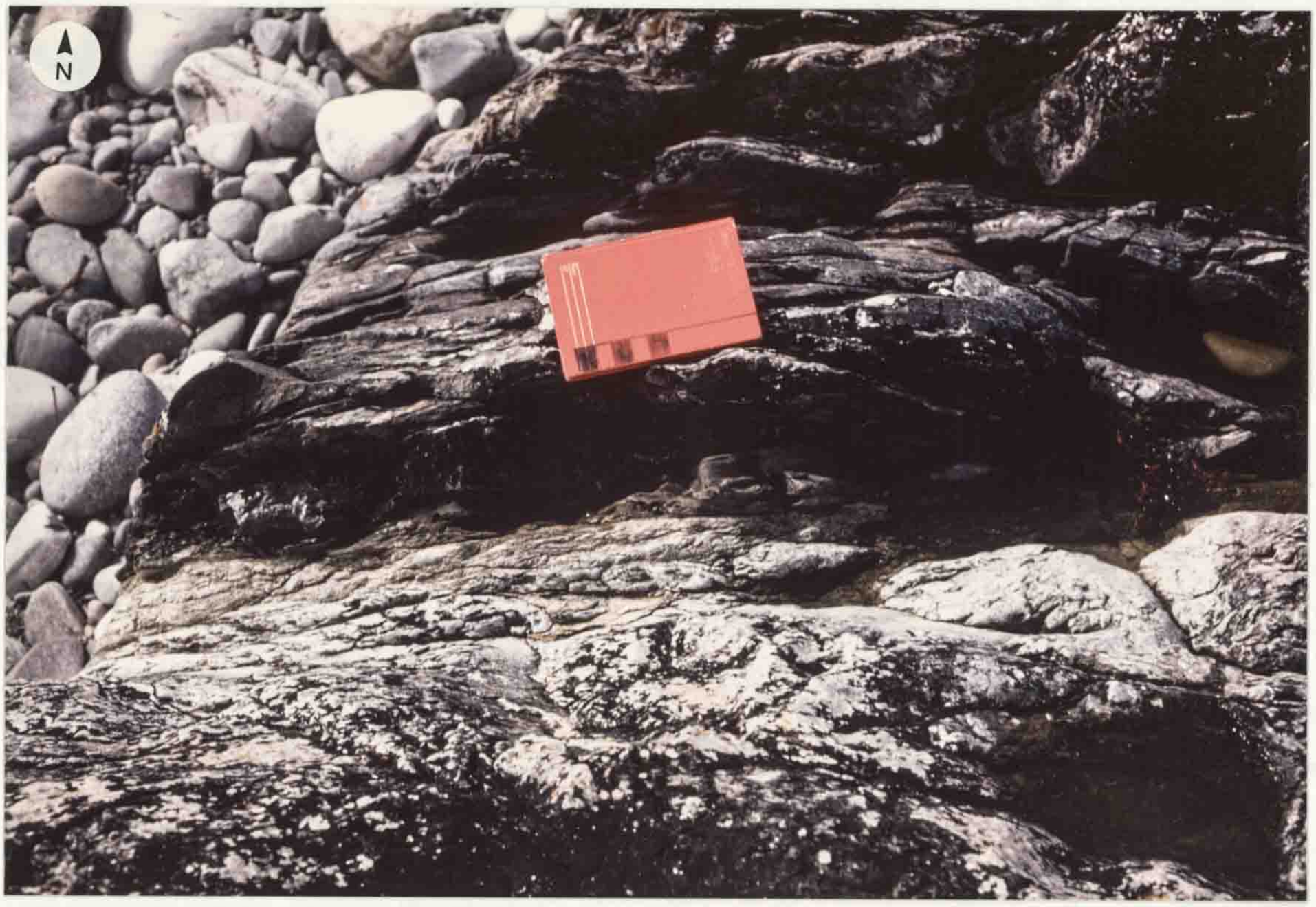


Figure 2.11: Amphibolite sheet in Kylemore Formation psammites and semipelites at [GR 756 604]. Compass is 175mm long.

fining upwards sequences. These show the Kylemore Formation to upward facing, although locally inverted.

The field appearance of the Kylemore Formation is variable, and largely dependent on metamorphic grade, as, unlike the lithologies south of the RBS, the Kylemore Formation shows a range of metamorphic grades. Adjacent to the Dawros - Currywongaun - Doughruagh igneous complex the Kylemore Formation lithologies show sillimanite - bearing migmatitic assemblages and are typically massive, dark weathering, gneisses and hornfelses, often with only a 'ghost' foliation (Figure 2.9). Feldspar porphyroblasts are common in these gneissic and hornfelsic lithologies, and can be used to delineate the aureole effects of the Dawros - Currywongaun - Doughruagh igneous complex (Tanner & Shackleton 1979, Leake, Tanner & Senior 1981). Away from the igneous bodies the metamorphic grade falls, with the bulk of the sequence showing garnet/staurolite grades and being schistose in appearance. These schistose lithologies are commonly grey/brown weathering (Figure 2.10) although they show increasingly green weathering colour in the NW Renvyle area as chloritic micas replace earlier biotites. The variation in metamorphic assemblages across the area is discussed in {Chapter 4}.

Thin (100 - 200mm) transgressive sheets of amphibolite crosscut the Kylemore Formation (Figure 2.11) in the area around the igneous bodies. These sheets often show poorly developed fabrics of similar orientation to those in the metasediments. The contact relations of the sheets are generally sharp, although deformed (Figure 2.11), with apparent syn - migmatitic sheets being locally developed.

## 2.2 Igneous bodies and their contact relations

### 2.2.1 The Dawros Peridotite

2.2.1.1 Introduction: The Dawros peridotite outcrops over an area of <1km² on the Dawrosmore peninsula (Figure 2.12) and lies at the western end of the chain of basic and ultrabasic bodies, which form the Dawros - Currywongaun - Doughruagh complex.

In the Irish Geological Survey memoir (Kinahan *et al.*

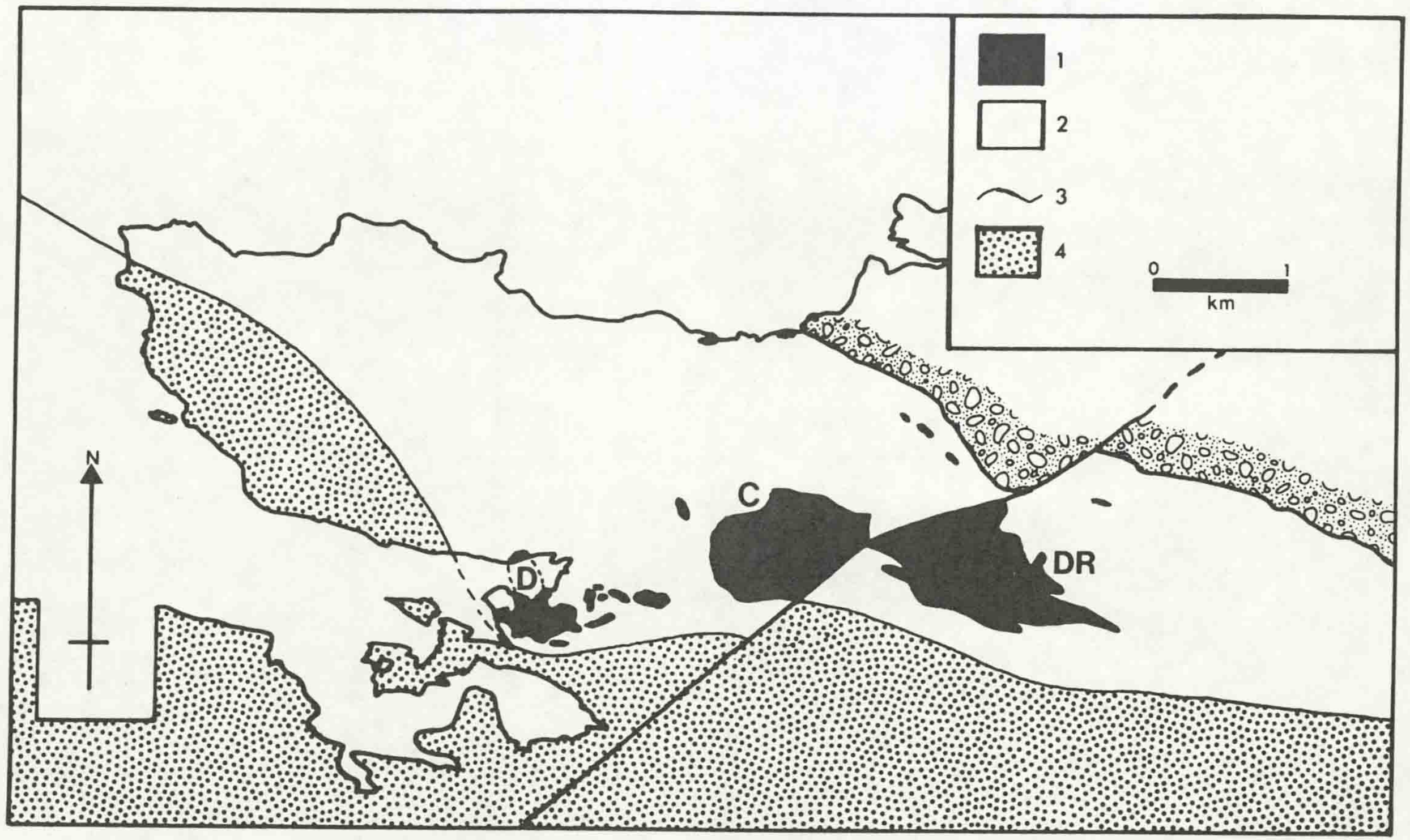


Figure 2.12: The distribution of basic and ultrabasic bodies within the study area. D: Dawros peridotite, C: Currywongaun, DR: Doughruagh. 1: Basic and ultrabasic igneous lithologies; 2: Kylemore Formation; 3: Renvyle - Bofin slide; 4: Lithologies to the south of the RBS.

1878) the peridotite is described as 'a large irregular tract of ophite' (serpentinite) with associated talcose and hornblendic lithologies. The body is described as having a sill - like form and lying on the '*bedding*' of the schists and is interpreted as a doleritic / tuffose intrusion now altered to serpentinite.

Wager (1932, 1939) considered the relation of the Dawros - Currywongaun - Doughruagh igneous complex to the ultramafic intrusions in south Connemara concluding that the two groups of ultrabasic intrusions, although superficially similar were intruded at different times and not related. Wager (1939) suggests that the intrusions in the north of Connemara are pre - Silurian in age as no similar bodies are evident in the (non - metamorphic) Silurian sequence.

Ingold (1937) studied the Dawros - Currywongaun - Doughruagh area and discussed the peridotite and its relations to the gabbroic intrusions. She suggests that the peridotite has a sill - like form, dipping under the metasediments to the N/NNE at 60-80° with local '*detached*' masses of serpentinised peridotite occurring around the main outcrop. Some gabbroic lithologies were noted within the peridotite, although no localities are given and these zones are not recorded on the map of the area. Ingold interprets the Dawros peridotite as the early differentiate of the magma which produced the Currywongaun - Doughruagh intrusions.

Rothstein (1954, 1956, 1958, 1961, 1964, 1972, 1983) made a detailed study of the peridotite and its environs, covering the petrology and petrogenetic evolution of the body. Rothstein states that the present form of the peridotite is lensoid, being approx 160m (500ft) thick and a maximum of 1280m (4000ft) across, with a rim of massive harzburgite and dunite and a central zone of layered dunite and pyroxenite. The contacts between the peridotite and the metasediments are described as sharp with local preservation of hornfelses. The unaltered peridotite has feldspar free, Ol - Opx - Cpx - Cr Spl, ultrabasic, assemblages which show primary igneous cumulate layering, with evidence of density stratification and 'wedge bedding'. A fractionation sequence is evident in the peridotite enabling the establishment of an internal stratigraphy for the body. This fractionation sequence (Rothstein 1954, 1957, 1961) shows a variation from

basal assemblages of Ol + Opx, through Ol + Opx + Cpx and Ol + Opx + Cpx + Spl zones, to Ol + Cpx lithologies in the highest exposed levels of intrusion. The sequence is compared (Rothstein 1958, 1961) with experimental work on Fo - Fa - Di - Qtz systems and Rothstein concludes that the assemblages developed in the peridotite would result from the fractional crystallization of a silica - saturated basaltic melt under conditions of high water pressure.

The gabbroic material noted by Ingold is recorded by Rothstein (1954, 1957) (Figure 2.13) who recognized the existence of fragments of ultrabasic material within the gabbroic areas suggesting that the gabbro is intrusive into the peridotite and represents a later magmatic event.

The peridotite shows evidence of post crystallization deformation (Rothstein 1957). The growth of hypersthene in the deformation fabrics suggests that this deformation occurred whilst the body was still at an elevated temperature, possibly during sub-solidus cooling. This deformation may also have resulted in the removal of the higher, more fractionated, parts of the body.

Rothstein concludes that the peridotite represents a syn-orogenic magmatic cumulate which has been deformed, possibly during *'emplacement in to higher crustal levels'* and subsequently underwent serpentinitic and talcose alteration.

Leake (1964b) notes the occurrence of feldspar, now saussuritised and sericitised, within the peridotite and suggests that the gabbroic material represents a continuation of the fractionation sequence, forming the upper part of the intrusion. The fragments of peridotite noted by Rothstein are interpreted by Leake (1964b) as igneous layers in the gabbro. Leake (1964b, 1970b) suggests that the Dawros and Currywongaun - Doughruagh bodies represent a single magma body which has been tectonically disrupted during its crystallization. Leake notes that all the intrusions *'possess hornfelsed, desilicated pelitic envelopes proving that they (the ultrabasic bodies) were intruded in a hot state'*. Leake (1958, 1970b) correlates, on petrological and geochemical grounds, the Dawros - Currywongaun - Doughruagh complex with the south Connemara ultrabasics, considering the two groups of intrusions to belong to one magma series.

**Figure 2.13: Lithological maps of the Dawros peridotite area;**
**a, Ingold (1937),**
**b, Rothstein (1957),**
**c, Leake (1970) (schematic profile section)**
**d, Bennett & Gibb (1983)**

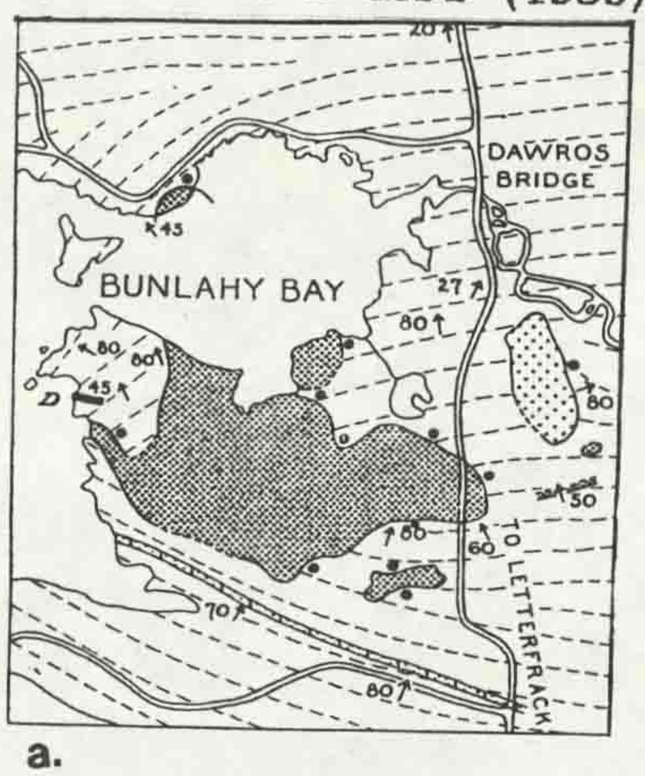


a.

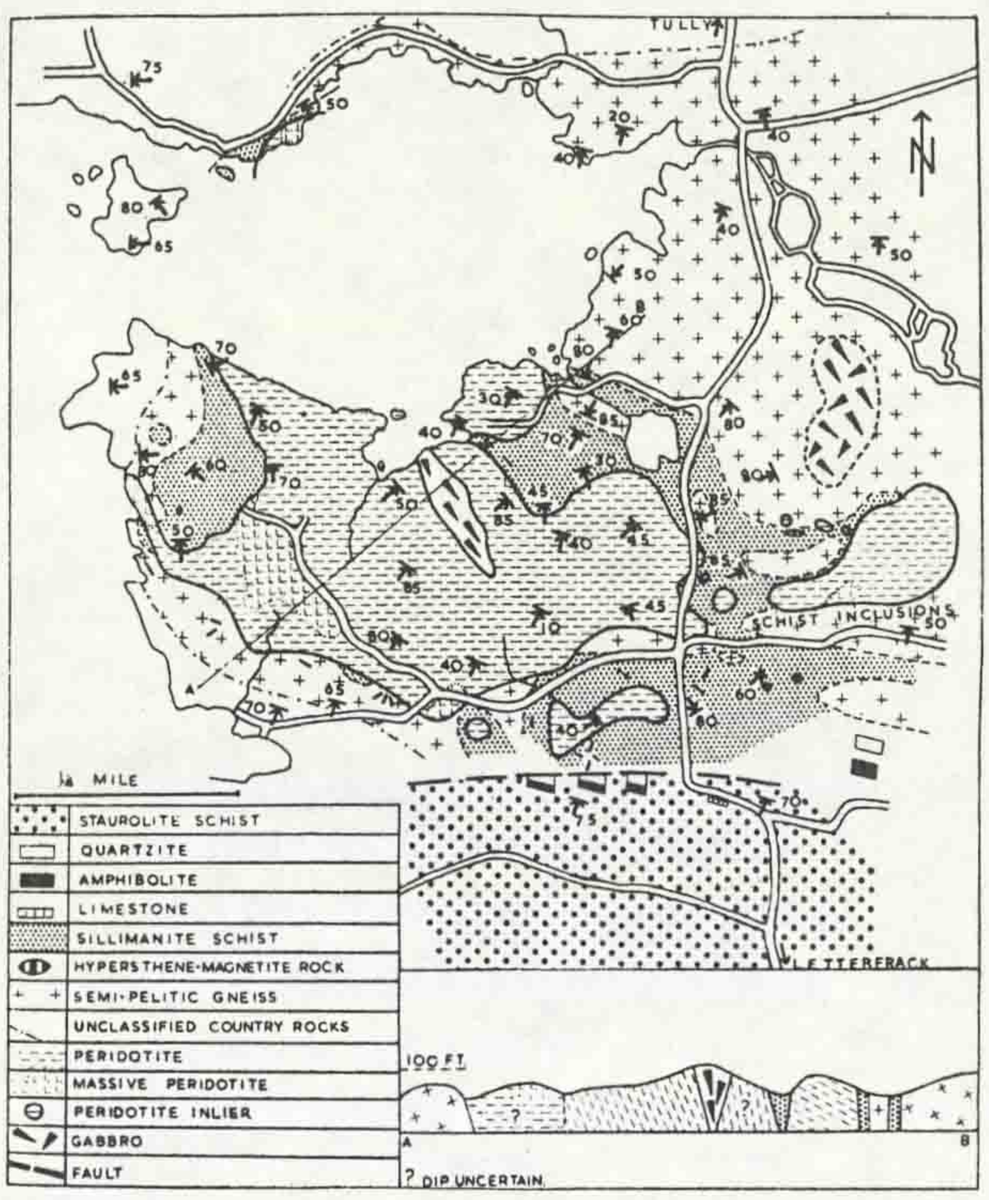


b.

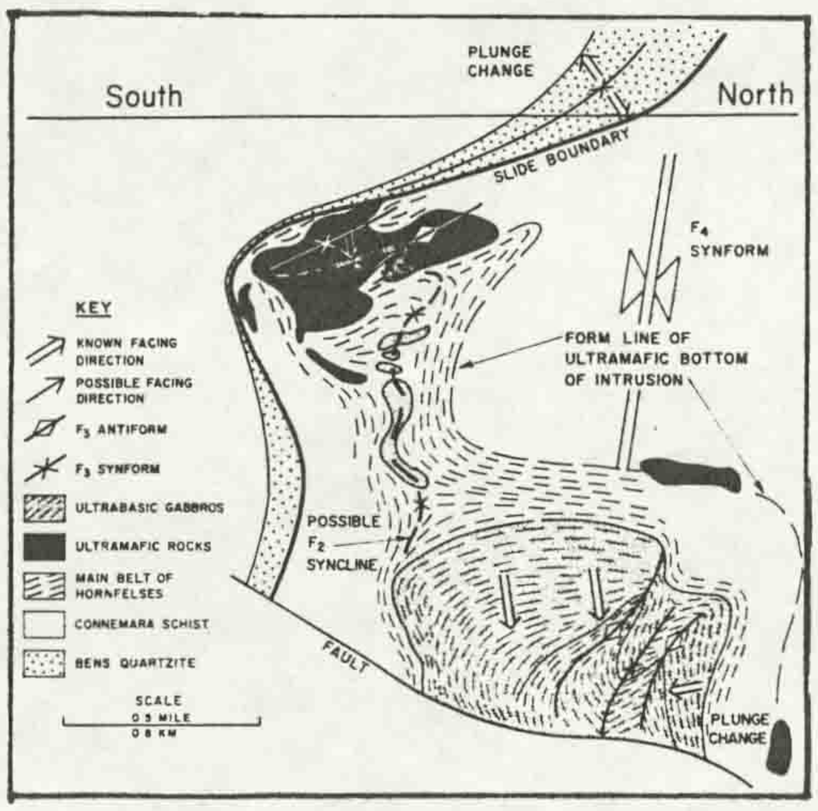


c.

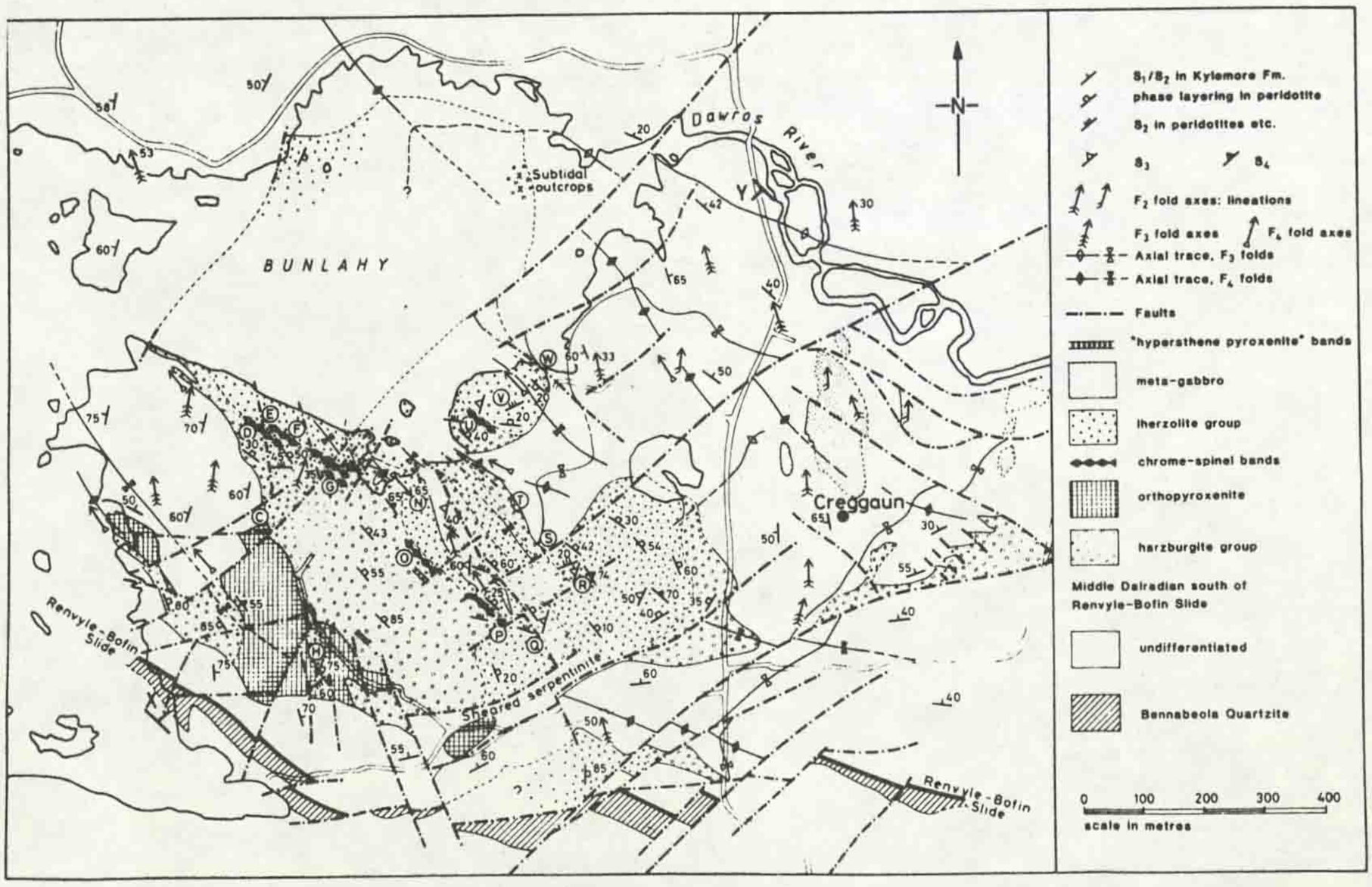


d.

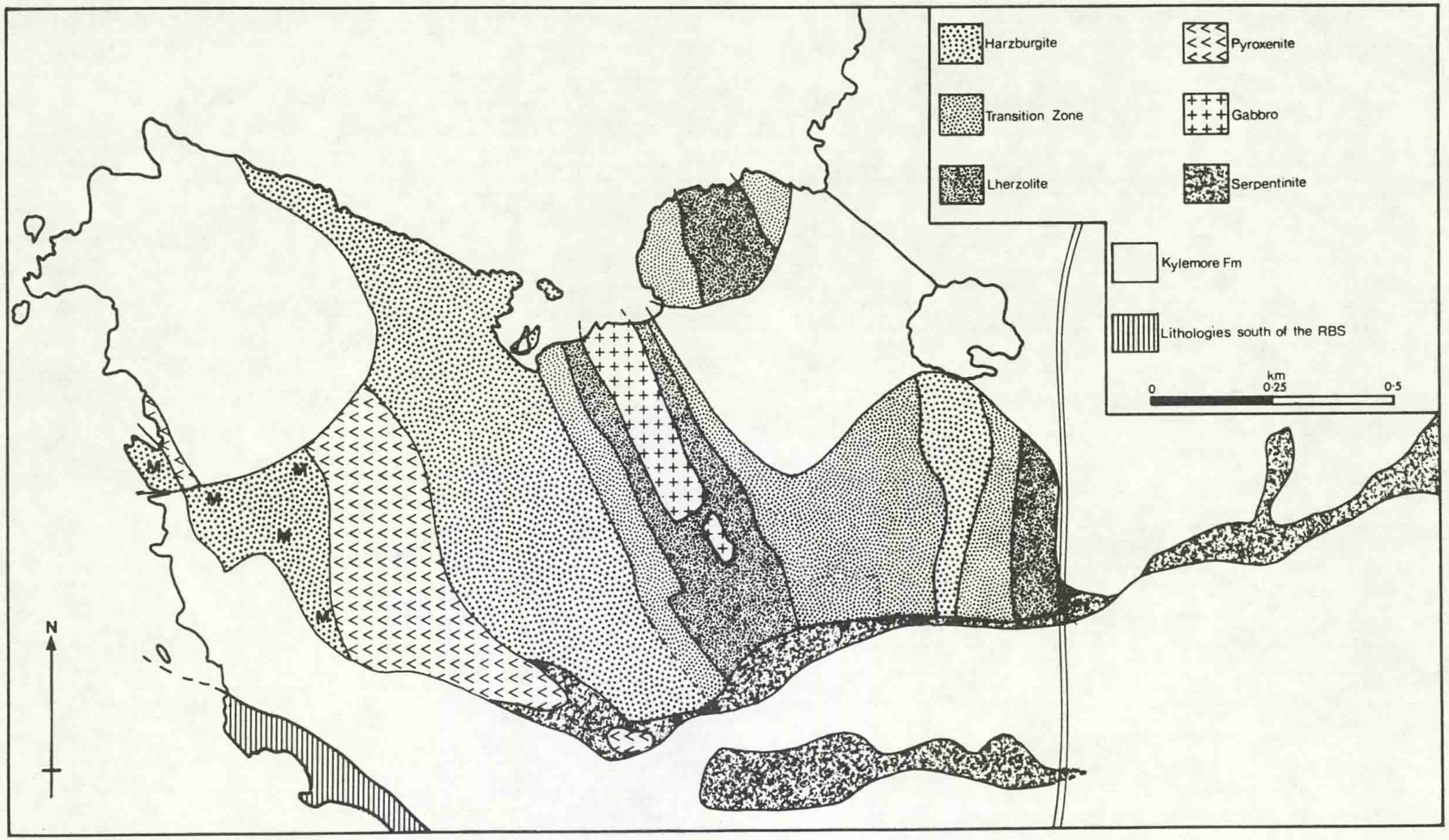


**(Figure 2.13 cont) e, Lithological map of the Dawros peridotite produced in this study.**

In a study of the Currywongaun - Doughruagh intrusion Kanaris - Sotiriou & Angus (1976) noted the existence of peridotite bodies, similar in appearance and composition to the Dawros peridotite, which occur either as xenoliths in the gabbros or are cross-cut by gabbroic material. These relations suggest that the gabbroic bodies postdate the peridotites, although compositional data (Kanaris - Sotiriou & Angus 1976, Angus, Middleton & Kanaris - Sotiriou 1980), show the peridotites and gabbros lie on a common differentiation trend {4.2}. Kanaris - Sotiriou & Angus (1976) suggest that the peridotite represents the early, basal cumulate products of a large, syn-tectonic, magma chamber which was tectonically disrupted during crystallization with the peridotite being emplaced to its current location.

Bennett & Gibb (1983) remapped the peridotite area to determine the lithological sequence and structure of the body and its metasedimentary envelope. Coupled with this work was a geochemical investigation which aimed to determine variation in Mg / Fe partitioning between coexisting Ol and Opx across the outcrop and so clarify the younging directions within the sequence. The gabbro is interpreted by Bennett & Gibb as being transgressive through the peridotite layering although the layering within the gabbro is concordant with that in the peridotite. The gabbro is considered to be syntectonic, and was probably injected during $D_2$ into the largely crystallized peridotite. The contacts of the body with the metasediments are described as mylonitic due to '*extensive shear along the peridotite margins*' during $D_2$ and $D_3$.

2.2.1.2 Lithological sequence

2.2.1.2.1 Previous work: Previous investigations of the peridotite (eg, Rothstein 1954, 1957, Leake 1964, 1970b, Bennett & Gibb 1983) agree that the body represents a fractionated sequence of igneous cumulate lithologies which show greater or lesser amounts of alteration. Rothstein interprets the mineralogical layering within the peridotite as being primary igneous in nature with features typical of a cumulate origin. Leake (1964b) and Bennett & Gibb (1983) suggest that the layering may not be entirely a primary igneous feature and may be due to deformation (and metamorphism) during the crystallization of the

**Figure 2.14: Generalized lithological sequences in the Dawros peridotite.**

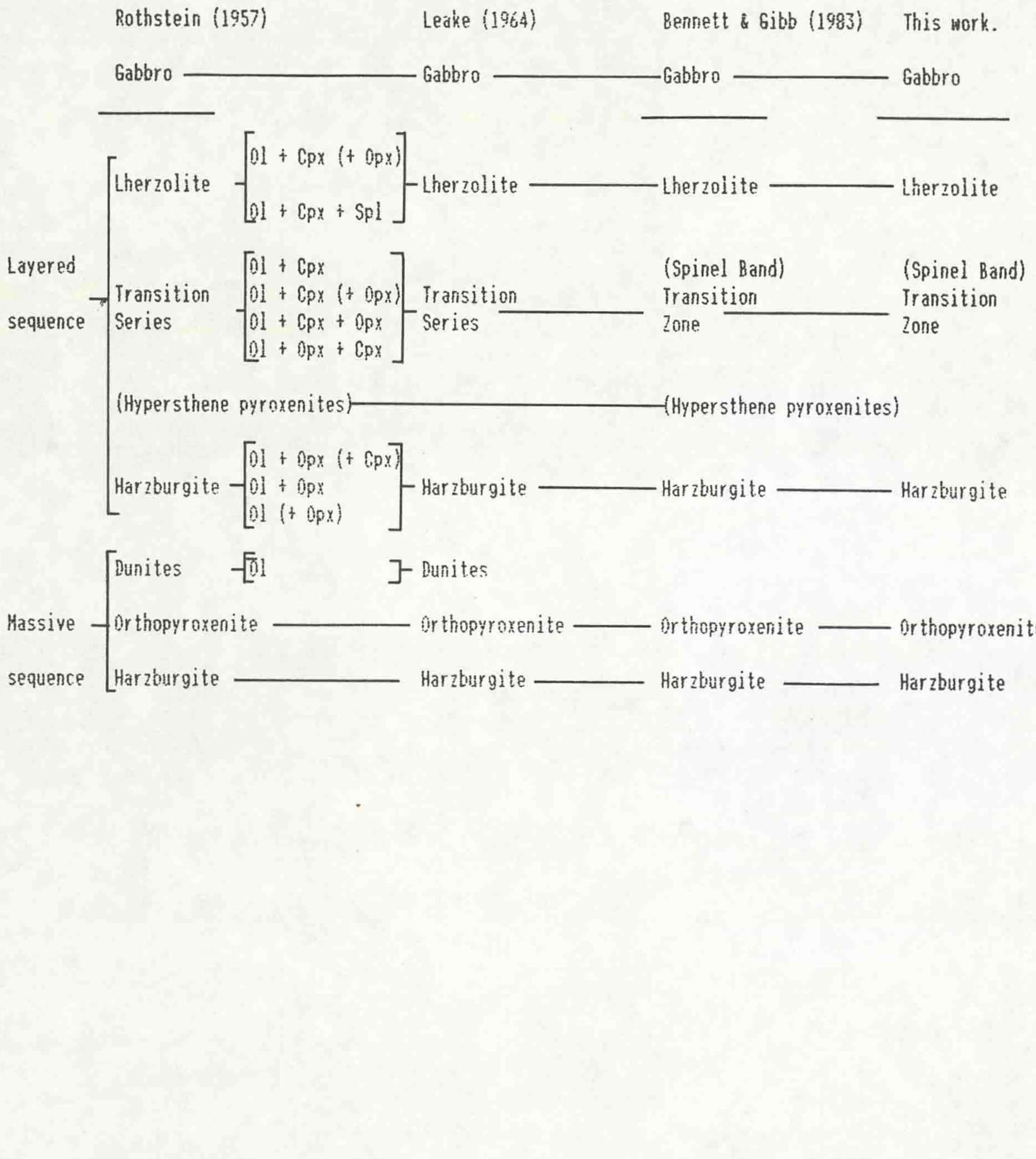

body. Bennett & Gibb provide no evidence to support this suggestion and use the chemical variation between layers, which they interpret as primary, as a means of determining the way - up of the body.

Rothstein (1954, 1957) subdivided the peridotite body into a series of units representing an igneous fractionation sequence (Figure 2.14) from a dunitic base through a sequence of harzburgites, showing a trend of increasing Fe in pyroxene, a transition zone of chrome - spinel bearing wherlitic lithologies to the higher parts of the sequence which are lherzolitic in nature.

Leake (1964, 1970b), provides no section through the body, using Rothstein's stratigraphy as a basis for his work, although he does add the gabbro to the top of the sequence above the lherzolites, thus extending the fractionation sequence (Figure 2.14).

Bennett & Gibb (1983) use the Rothstein sequence as a basis for remapping and cryptic layering determination through geochemical analysis. The results of this work (Figure 2.14) confirm Rothstein's sequence to be essentially correct, although the relation of the gabbro to this sequence remains a contentious issue.

2.2.1.2.2 Lithologies

2.2.1.2.2.1 Massive lithologies: These are best developed in the SW corner of the peridotite (Figure 2.13), although patches of massive lithologies are evident along the margins, and represent the 'marginal facies' of Rothstein and Leake, and the basal parts of Bennett & Gibb's sequence. Two main lithological types are evident in this part of the body, harzburgites and orthopyroxenites.

Massive Harzburgites: These lithologies are generally found in low - lying flat areas as scattered smooth weathering pale green/grey outcrops. The lithology is fine grained (1 - 2mm) and serpentine rich, with scattered yellow/brown irregular pyroxene grains up to 10mm (Figure 2.15). A steeply dipping, NNE/SSW striking, spaced (5 - 10mm) foliation is developed, locally

Figure 2.15: Massive Harzburgite cross cut by upright foliation associated with calcite veins [GR 693 588]. Lens cap is 49mm diameter.


Figure 2.16: Field appearance of the massive pyroxenite [GR 693 590] showing large sub to euhedral laths of bronzitic orthopyroxene, most evident below and right of the lens cap. Lens cap is 49mm diameter.

associated with veins of fibrous pale grey serpentinite which occasionally contain calcite as a core to the vein. This foliation is observed to crosscut a flatter lying, more patchily developed, planar fabric which is again associated with serpentinisation effects.

Massive Pyroxenites: This lithology is best exposed in a low irregular hill [GR 693 590] as blocky, brown weathering outcrops, consisting of a mesh of coarse grained tabular laths of bronzitic pyroxene (Figure 2.16). The grain size is variable from 5 - 50mm with 10 - 20 mm being most common. A foliation is variably developed, with talc - carbonate veins and rare fibrous serpentinite veins occurring parallel to the foliation. The contact of the massive pyroxenite material with the massive harzburgite is exposed in a low crag at [GR 692 589] and shows the pyroxenite overlying the harzburgite above a sharp contact. Lensoid pods of the pyroxenite up to 1m are developed in the underlying harzburgite. This boundary represents an original igneous contact. The boundary of the massive pyroxenite with the layered series is not exposed.

The euhedral laths seen in outcrop are enstatitic orthopyroxenite and form up to 80% of the total rock.

2.2.1.2.2.2 Layered sequence

The layered peridotite lithologies make up the bulk of the body. Despite the thinly layered nature of these lithologies it is possible to subdivide them into a series of units, because the sequence shows a progressive change in composition and mineralogy from base to top. The units chosen are based on the subdivisions mapped in the field backed up by thin section work to confirm mineralogies in areas where serpentinisation or poor exposure made it difficult to define the boundaries between units.

Three units are defined:

(i) harzburgite, a sequence of Ol - Opx bearing lithologies;

(ii) transition zone, a sequence of mixed Ol - Opx - Cpx bearing lithologies, with variable concentrations of chrome spinel;

(iii) lherzolite, a sequence of Ol - Cpx lithologies often spinel bearing.

The relations of these lithological groups to the previous

subdivisions are shown in Figure 2.14.

The following descriptions of the layered lithologies use the terminology of Irvine (1982).

Harzburgite: This sequence of lithologies crops out over much of the area and shows a high degree of variability. The best preserved igneous mineralogies and textures are seen in the western part of the body although the layering in this area is often irregular and laterally discontinuous. Well developed layering is evident in the area around [GR 698 591] where patchy but good outcrop exists.

The lithology consists of irregular, planar, modally interbanded, pale green/grey, olivine rich units and brown/rust coloured pyroxene rich units. The banding commonly occurs on a 100 - 150mm scale, although both thicker and thinner bands are evident. The contacts between the units can be sharp or transitional in nature the former being more common. Where transitional boundaries are seen [GR 697 591] the dunite unit becomes increasingly pyroxene rich, grading into the adjacent pyroxene band. Both normal and reverse grading is developed. The layering is often irregular in form, with laterally persistent units showing wedging and variable thicknesses, a feature noted by Rothstein (1957) as an original feature, and by Leake (1964) as a tectonic effect.

Mineralogically this unit is typified by forsteritic olivine and enstatite assemblages, developed as anhedral, equigranular crystals up to 2mm in size. Rare, scattered, irregular spinel grains are evident in the higher parts of the harzburgite zone, but not in the lower zone. Serpentinisation variably replaces the original igneous mineralogy.

Transition zone: This unit is developed between the harzburgites and lherzolites. In outcrop the layering features are similar to those described in the previous section, consisting of planar, locally irregular, bands of olivine rich and pyroxene rich assemblages. The main feature which distinguishes this band from the harzburgitic lithologies is the development of pale brown spinel grains (rounded, 3 - 15mm size). The spinel occurs either in discrete, often multiple, 2 - 25mm

thick bands or distributed within the main layering with local concentrations in the olivine rich units. The association of spinel within the layering is best seen in the North West of the body where spinels up to 30mm are developed within discontinuously layered harzburgitic lithologies. The spinel bands can be used as marker horizons, with one particular unit being traceable across much of the eastern area of the peridotite.

Lherzolite: The lherzolitic lithologies overlie the transition zone, the contact between the two zones being transitional over 5 - 10m as the pyroxene content changes from orthopyroxene to clinopyroxene dominated. The weathering colour of the lherzolite reflects this change, becoming increasingly blue - grey in hue, against the greener weathering Opx lithologies. The layering is similar in appearance to that seen in the other layered zones, with irregular thickness (Figure 2.17) and parallel layers being evident. Cross stratification of the layers is seen at [GR 692 588] (Figure 2.18 and 2.19), dunitic and pyroxene rich units being truncated to form troughs into which the overlying layers are draped. These features are typical of those produced by the action of magmatic currents on cumulate material (eg, Irvine 1974, 1982), and indicate that the peridotite is right way up at this locally. The significance of such features is discussed later. Graded layers, like those in the transition zone are also developed.

2.2.1.2.2.3 Gabbro: The gabbroic lithologies crop out as a NNW/SSE trending ridge in the centre of the body. Lithologically the gabbro consists of a variably foliated, locally layered, pale - green weathering rock (Figure 2.20) with local inclusions of more basic material (Figure 2.21). The layered portions of the gabbro consist of thin (10 - 20mm) layers of pale cream weathering feldspathic material interlaminated with similar thicknesses of green weathering mafic layers. This layering probably represents a primary igneous texture, similar to those seen in the nearby Creggaun gabbro (Boyle, McCarthy & Stewart 1987), as the tectonic foliation can locally be seen to crosscut this lamination.

Figure 2.17: Irregular phase layering in layered Lherzolite cut by spaced $S_3$ foliation [GR 697 591]. Lens cap is 49mm diameter.

**Figure 2.18: Cross bedding within layered Lherzolite at [GR 695 587]. Lens cap is 49mm diameter.**


**Figure 2.19: Line drawing of Figure 2.18 showing the nature of the cross bedding.**

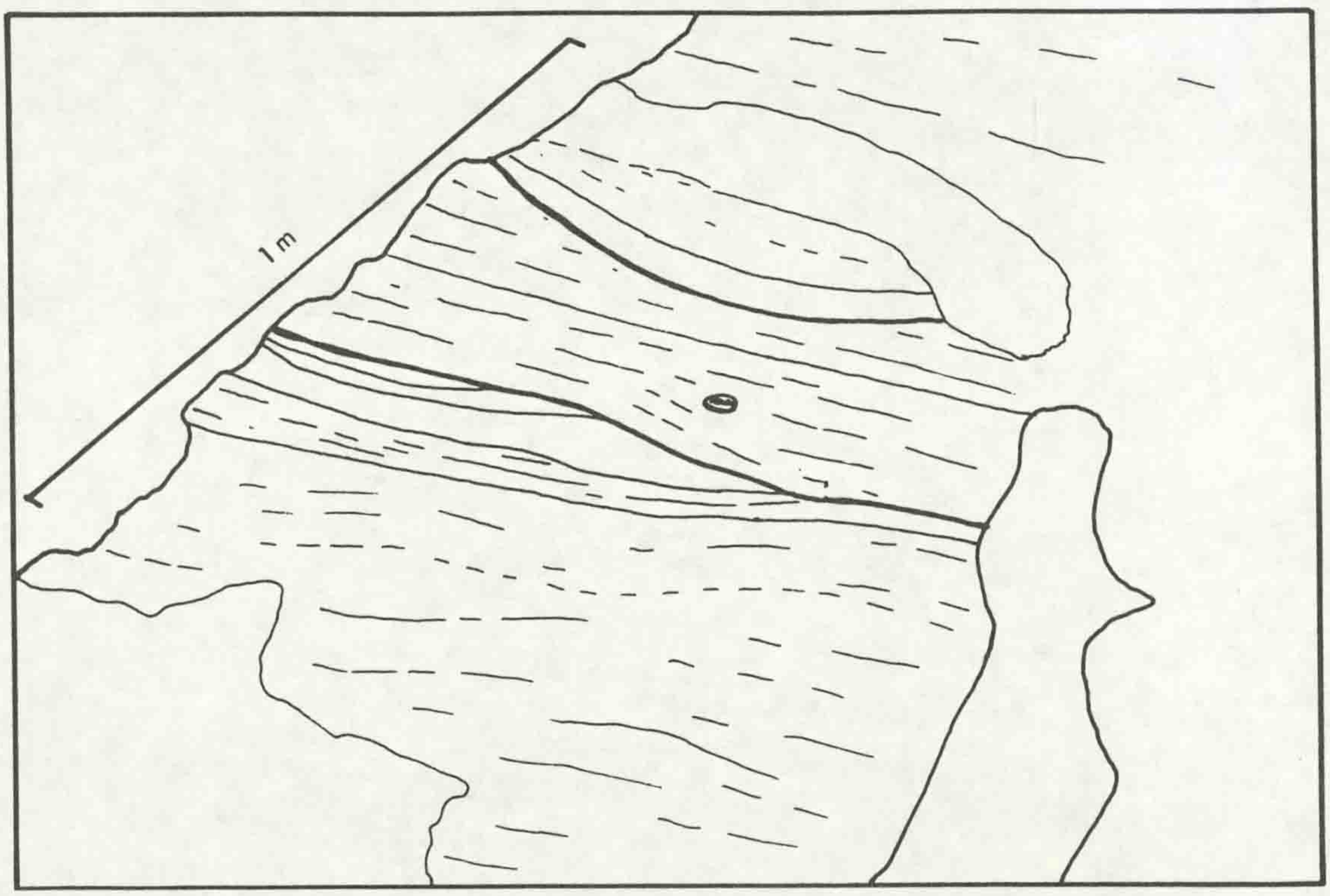

Figure 2.20: Foliated metagabbro at [GR 696 592]. Clothes peg is 74mm long.


Figure 2.21: Metagabbro with containing angular fragments of feldspar free material [GR 697 591]. Lens cap is 49mm diameter.

Figure 2.22: Contact between foliated metagabbro and rusty weathering peridotite at [GR 696 590] showing thin, glassy irregular serpentinised zone between the two lithologies. Lens cap is 49mm diameter.

The contact of the gabbro and the surrounding peridotite is poorly exposed, relations being evident in only two places, [GR 696 589] and [GR 696 590]. At the first locality the actual contact is not exposed although it can be traced into a 1-2m exposure gap. The gabbroic lithologies occur in a steep slope with the crest of the slope consisting of lherzolitic peridotite, the gabbro underlying the peridotite in this area. At [GR 696 590] the contact itself is exposed, with the gabbro overlying the peridotite, the contact being a thin (10 - 50mm), N - S striking, E dipping, irregular layer of glassy serpentinite (Figure 2.22). The layering within the peridotite is absent within 1 - 2m of the contact although a strong foliation fabric, showing lineated fibrous serpentinite growth, lies subparallel to the contact zone. The gabbro is strongly foliated parallel to the contact zone. The layering within the gabbro also runs parallel or subparallel to the contact.

The original nature of this contact is not clear although the irregularity of the zone even in its present deformed state, suggests an original irregular igneous contact. This evidence, along with the existence of fragments of peridotitic material as angular blocks within the gabbro, suggest that the gabbro is intrusive into the peridotite, with subsequent deformation partially obscuring the original contact relations.

2.2.2 Gabbroic lithologies

The petrology, petrogenetic evolution and structure of the Currywongaun - Doughruagh gabbros are well documented (Ingold 1937, Leake 1964b, 1970b, Kanaris - Sotiriou & Angus 1976, Boyle *et al.* 1987). The complex consists of anorthosite - norite - pyroxenite lithologies, typically containing highly calcic feldspar ( $>An_{80}$), with subordinate acid gneiss and pegmatitic lithologies. Primary igneous layering is present in the gabbros, most evidently in Currywongaun, and along with cryptic variation data provides evidence for the way up and structure of the body.

2.2.3 Ultrabasic Pods and Sheets: Small ( <30m), lenticular pods of ultrabasic material are developed within the Kylemore Formation (Figure 2.12). These pods appear to define an horizon

within the Kylemore Formation and have been previously interpreted (Kennedy 1984) as olistolithic material, the present pod - like form of the ultrabasic bodies being a tectonic modification of original sedimentary clasts.

On the north coast of the Renvyle peninsula a series of variably serpentinised ultrabasic pods are developed within the schistose Kylemore Formation. At Garraun [GR 729 628] a pod of ultrabasic material with Ol - Opx assemblages is developed in semi-pelitic schistose Kylemore Formation. Along strike to the west a series of serpentinised pods of similar material are evident. The serpentinised material typically shows talc - carbonate assemblages with tremolitic amphiboles and rare relict pyroxenes. Similar assemblages are noted by Cruse (1963) in the zone of the Renvyle - Bofin slide on Inishbofin.

Inland, similar pods are evident [GR 713 605 & 749 610], but they are generally poorly exposed with their contacts with the Kylemore Formation being unclear. In the wall of the corrie NNE of Doughruagh [GR 761 601] a pod approx 30m long is developed within a series of platey psammitic schists, the margins of this pod consisting of a 1 - 2m zone of strongly foliated talc schist. This schistosity becomes less well developed away from the pod margins, being absent 5m from the contact. Within the pod a fine grained serpentinitic assemblage is developed, with local preservation of phase layering like that seen in the Dawros peridotite. The talc schist zone 'wraps' the pod as does the foliation within the metasediments.

The metasediments around these ultrabasic pods commonly show the development of sillimanite bearing assemblages, away from the pods the metasediments show garnet - staurolite grades of metamorphism. This evidence, coupled with evidence of an original sheet-like form to the now pod - like ultrabasic material (Figure 2.23), suggests that these pods represent an intrusive sheet, now tectonically dismembered.

**Figure 2.23:** Structure of the serpentinised peridotitic material (stippled) in coastal exposures of Kylemore Formation at [GR 705 630]. Note that the apparently irregular pods form a folded and locally disrupted sheet which lies within the shallowly dipping, gently folded ($F_3$ folds) $S_2$ foliation of the metasediments.

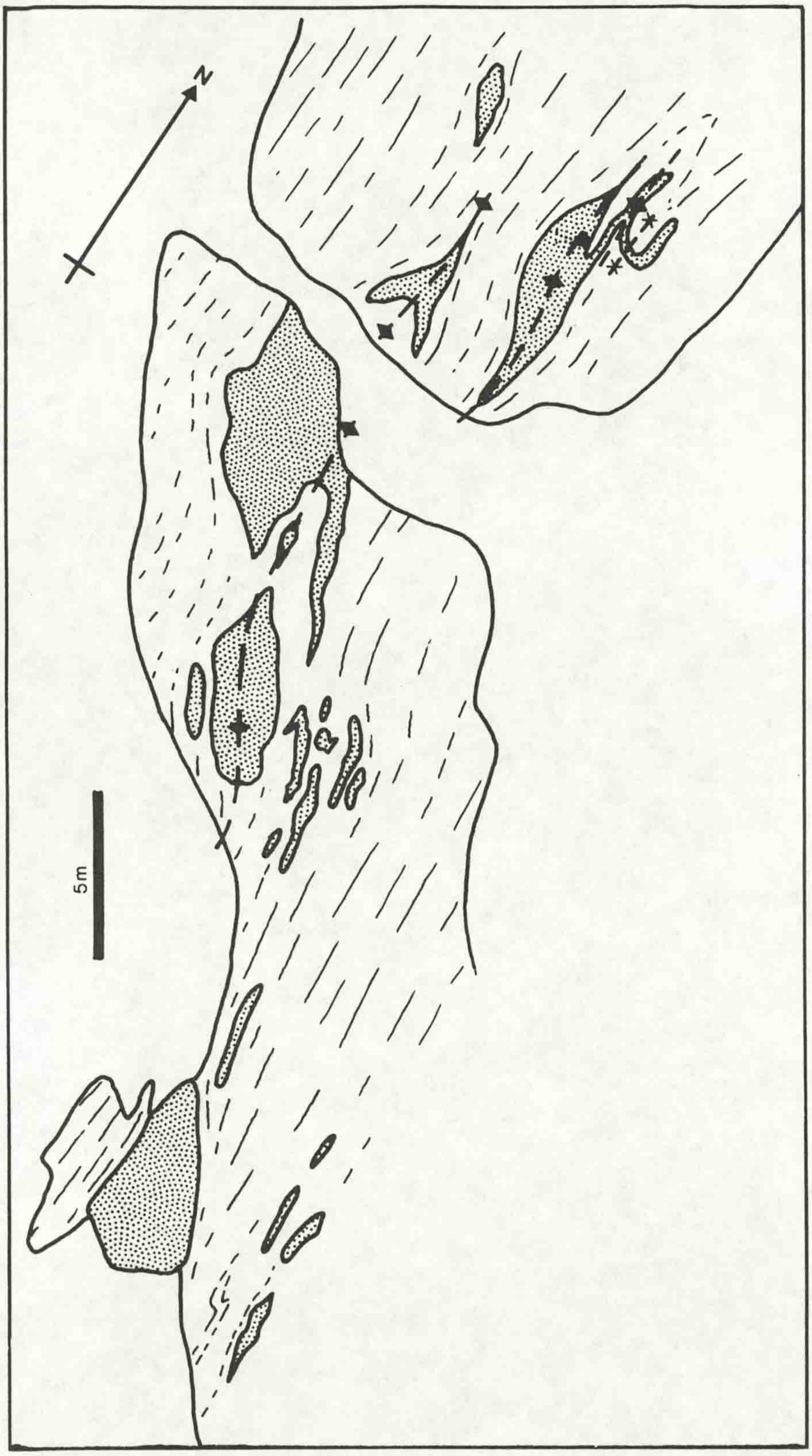

Addendum to {2.1.2.1.2}

As noted in {2.1.2.1} the garnet - staurolite pelite lithologies here described as the Roeillaun schist Member of the Streamstown Formation have previously been interpreted (Tanner & Shackleton 1979) as belonging to the Ballynakill Formation. This proposed change has been made for the following reasons.

The garnet - staurolite pelites found on the south side of the $F_3$ Doongill antiform on the south side of Tully Mountain {Enclosure 1, 2} are at a structural level equivalent to the psammites and semipelites of the Dawrosbeg striped psammite and the Derryinver psammite Members of the Streamstown Formation. The pelitic lithologies on Roeillaun are developed in an $F_3$ antiformal structure {Enclosure 1, 2} at a structural level equivalent to Streamstown Formation lithologies (i.e. structurally beneath the Bennabeola Quartzite Formation and above the Lakes Marble Formation).

The contact between the garnet - staurolite pelite lithologies and the Dawrosbeg striped psammite on the northern side of the Dawrosbeg peninsula (adjacent to Roeillaun) is transitional in nature. Lenses of psammitic material up to 300mm in thickness and 2 - 3m in lateral extent are present in the garnet - staurolite pelites, and increase in frequency towards the boundary with the Dawrosbeg striped psammite which locally contains thin ( <100mm) partings of garnetiferous pelitic material. The across strike transition from garnet - staurolite pelites to the Dawrosbeg striped psammite occurs over 10 - 20m in the Dawrosbeg area, although on the south side of Tully Mountain the (unexposed) contact between pelite and psammitic lithologies is much sharper ( <2 - 3m).

The occurrence of garnet - staurolite schists apparently within the Streamstown Formation in the study area can be explained in a number of ways.

a, The garnet - staurolite schists are part of the Ballynakill Formation, but in the study area the Lakes Marble Formation, which should be found between the Streamstown and Ballynakill Formations, is locally absent. This absence may be due to faulting or sliding. However, no evidence of fabrics typical of such processes are evident. The absence of the Lakes Marble Fm could also be due to facies variation such that the Lakes Marble Fm is totally absent or is missing characteristic lithologies in

the part of the study area where the garnet - staurolite schists are in contact with Streamstown Fm units. However, the lateral persistence of the Lakes Marble Fm within the rest of Connemara and the occurrence of the Tonabina Marble Member stratigraphically above, but structurally beneath, [GR 661 608] the garnet - staurolite schists suggests that the Lakes Marble is present in the study area.

b, The garnet - staurolite schist lithologies do belong to the Streamstown Fm and represent a local facies variation. The transitional contacts between schists and other Streamstown Fm members, together with the structural relations, are consistant with this.

Within the poorly exposed ground around Bunnaboghee Lough scattered outcrops of garnet - staurolite pelite are associated with lithologies of the Lakes Marble Fm. The paucity of exposure makes detailed structural interpretation difficult. The pelites may represent either infolded portions of the Streamstown Formation within $F_3$ synforms, or portions of the underlying Ballynakill Fm lying within the cores of $F_3$ antiforms. No clear relations can be determined in this area.

The evidence of consistent structural position and transitional boundaries with the Streamstown Formation have led to the inclusion of the garnet - staurolite pelites in the Streamstown Formation as the Roeillaun Schist Member.

# Chapter 3: Structural and igneous contact relationships

## 3.1 Introduction

The structure of the Connemara massif has been extensively studied (eg, Tanner 1967, Treloar 1982) and a sequence of four main deformational stages has been established (Figure 3.1). The intensities of the various deformation stages varies greatly across the massif, as does the relative timing of deformational and metamorphic events. The relations between structural and metamorphic events are discussed in chapters 4, 6 and 7.

The Renvyle - Bofin slide {2.1.1} divides the study area into two 'units', a southern sequence of Argyll Group (Dalradian) lithologies which are in structural continuity with the rest of the Connemara massif, and a more enigmatic northern sequence, the Kylemore Formation which is associated with the basic and ultrabasic bodies of the DCD. The fabrics and structures developed within the southern and northern units are discussed separately in {3.2.1 and 3.2.2} respectively, with the structural effects of the igneous bodies considered in {3.2.2.4}. The internal structure and contact relations of the igneous bodies are considered in {3.4}. The Renvyle - Bofin slide is discussed in {3.3}.

## 3.2 Structural features and fabrics of the Metasedimentary lithologies

### 3.2.1 Structures developed in the lithologies south of the Renvyle-Bofin slide

3.2.1.1 Planar fabrics: At outcrop, two main schistose fabrics are commonly evident, a bedding parallel to subparallel penetrative foliation and a spaced steeply dipping fabric.
The penetrative fabric is defined by strong alignment of platy and tabular minerals, flattened grain aggregates and original sedimentary clasts which display boudinage in the fabric. Within amphibolitic lithologies incipient feldspar / qtz segregations are developed parallel to the penetrative foliation, producing the 'striping' described in {2.1.2}. Siliceous ribs are developed in the fabric within the marble and calcsilicate lithologies. The segregation fabrics and foliation are deformed around $F_3$ {3.2} folds.

Figure 3.1: Simplified deformation history for Connemara (after Tanner & Shackleton 1979).

$D_1$: Evident only as fine, often crenulated, $MP_1$ fabrics within garnet and plagioclase porphyroblasts and rare folds (possibly representing sedimentary slump folds) with clear relations to later fabrics and folds.

$D_2$: *'Derryclare stage'*, major nappe - like folds with probable WNW - ESE axial traces, evident only by stratigraphic repetition (and facing changes). Minor folds more clearly evident, typically tight, with axial planar schistosity, and cut by later crenulation fabrics. The dominant 'regional' penetrative schistosity is axial planar to these folds.
Strongly developed lineation of boulders, pebbles, clasts and mineral segregations (feldspathic spots and fibrolitic clots) generally eastward plunging, although NNE plunges are developed in NW Connemara.

$D_3$: *'Glen Coaghan stage'*, the dominant fold closures developed in the Connemara massif are of $D_3$ age, and are most clearly evident where a well defined stratigraphy is deformed. No major $F_3$ folds are evident in the Kylemore Formation. E - W trending axial planes with variable plunges. A crenulation fabric (often resembling a penetrative schistosity in the field) is axial planar to these folds. This crenulation forms an intersection lineation and folds the $L_2$ lineation.
The intensity of deformation appears to increase from N to S.

$D_4$: *'Connemara antiform stage'*, large scale, rounded, open structure, with overall eastward plunge ( $<25^o$) with local variation. Axial plane dips north at $>70^o$.

Tectonic slides: Timing generally poorly constrained, can locally be traced around $F_3$ structures, although reactivation of the structures during $D_3$ is likely.

**Figure 3.2: Segregated $S_2$ fabric in Lakes Marble amphibolite (X 29) PPL.**

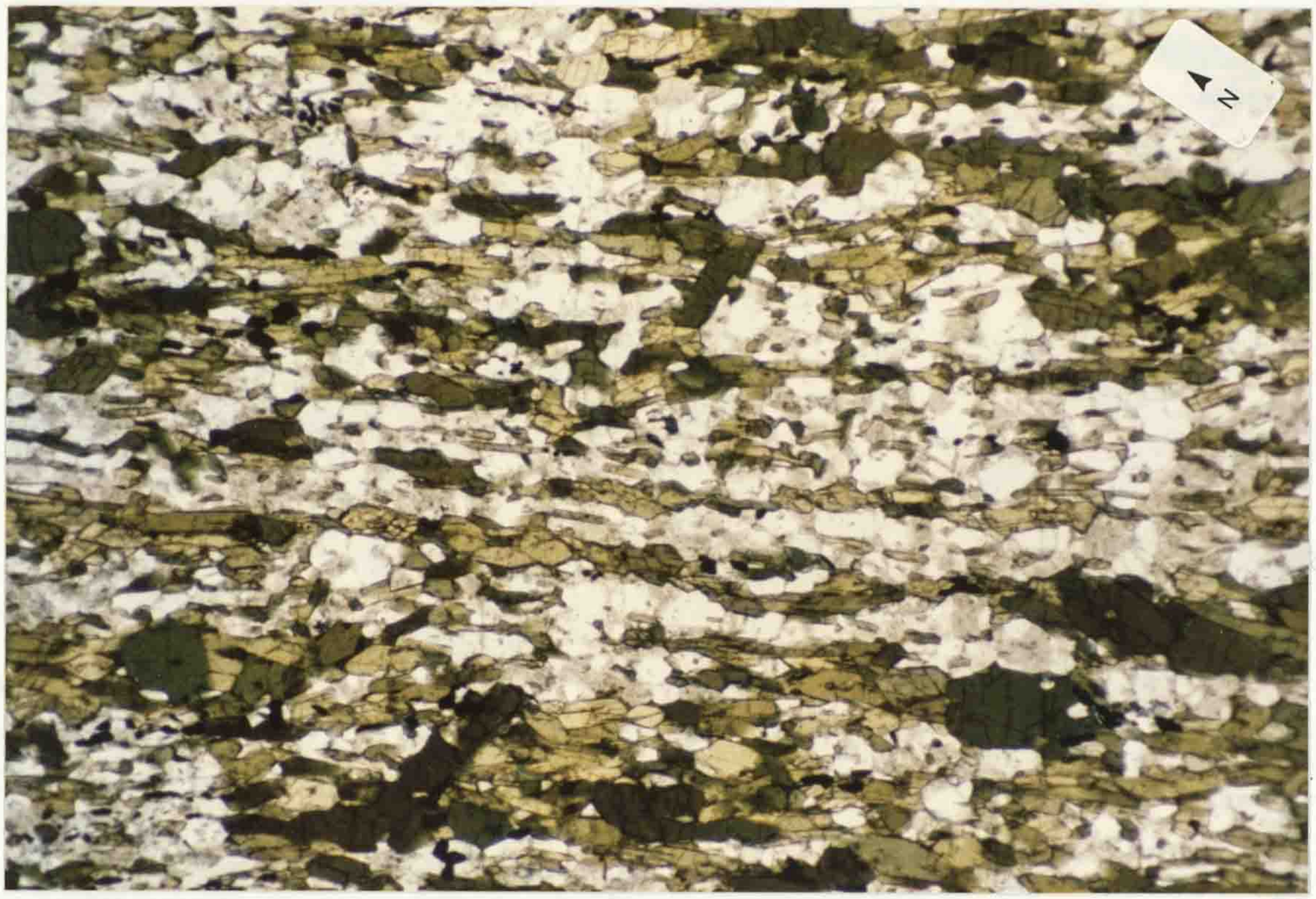


**Figure 3.3: Segregated $S_2$ fabric in Streamstown Formation pelite (X 29) XPL.**

The penetrative fabrics are variably overprinted by a spaced foliation which is axial planar to $F_3$ folding. $F_3$ folding is tight and locally isoclinal in form {3.2.1.3} which often means that $S_3$ and $S_2$ are parallel or subparallel to one another in fold limbs but show good crenulation relations in fold hinges. The degree of replacement of the earlier $S_2$ fabric by the $S_3$ axial planar foliation is highly dependent on the lithologies involved, with pelitic $S_2$ foliation often appearing to be totally transposed into the later $S_3$ fabric, whereas psammitic and quartzitic lithologies show widely spaced $S_3$ partings cross - cutting the penetrative $S_2$ fabrics.
In fold limbs a composite fabric is produced with a variably spaced fabric running parallel to the penetrative fabric. Within many of the quartzitic and psammitic lithologies uneqivocal identification of the phase of fabric developed is difficult unless folding is present.

The segregated nature of the earlier penetrative fabric is best seen in thin sections of pelitic and amphibolitic lithologies where biotite or amphibole foliae separate quartz / feldspar rich zones (Figures 3.2 and 3.3). In pelites the penetrative fabric wraps porphyroblasts of garnet and feldspar which contain inclusion fabrics. These inclusion trails are best developed in garnet porphyroblasts and the variation in the nature of the inclusion fabrics and their relation to external fabrics are discussed in {3.2.3}. The fabric seen in inclusion trails is occasionally preserved within the elongate quartzofeldspathic lenses of the penetrative fabric. As the penetrative fabric overprints an earlier, now largely obscured, fabric it must be considered as an $S_2$ fabric with the included fabric being $S_1$. The dominance of $S_2$ in the Connemara massif is noted by many workers (e.g. Badley 1976, Yardley 1976) although Treloar & McInnes (1981) suggest that the dominant fabric is a composite $S_2$ / $S_3$ foliation.

The crenulation fabric, $S_3$, is most apparent in $F_3$ fold hinges, especially in schistose pelitic lithologies where it develops as buckle folds of $S_2$. In the pelitic lithologies the crenulation shows a range in morphologies from gentle rounded folds to tight chevron-like forms (Figures 3.4 and 3.5). Within these crenulations the biotite defining $S_2$ is often deformed

**Figure 3.4: Gentle $D_3$ crenulation deforming $S_2$ foliation in Streamstown Formation pelite (X 29) PPL.**


**Figure 3.5: Tight angular $D_3$ crenulations deforming $S_2$ in Streamstown Formation pelite (X 29) XPL.**

**Figure 3.6: Equal area stereonet projections of orientation data from lithologies south of the Renvyle Bofin Slide;**
**a, Foliations (poles, 387 pts).**
**b, Mineral lineation (260 pts).**
**c, $F_3$ fold axial planes (poles, 96 pts).**
**d, $F_3$ fold hinges (96 pts).**

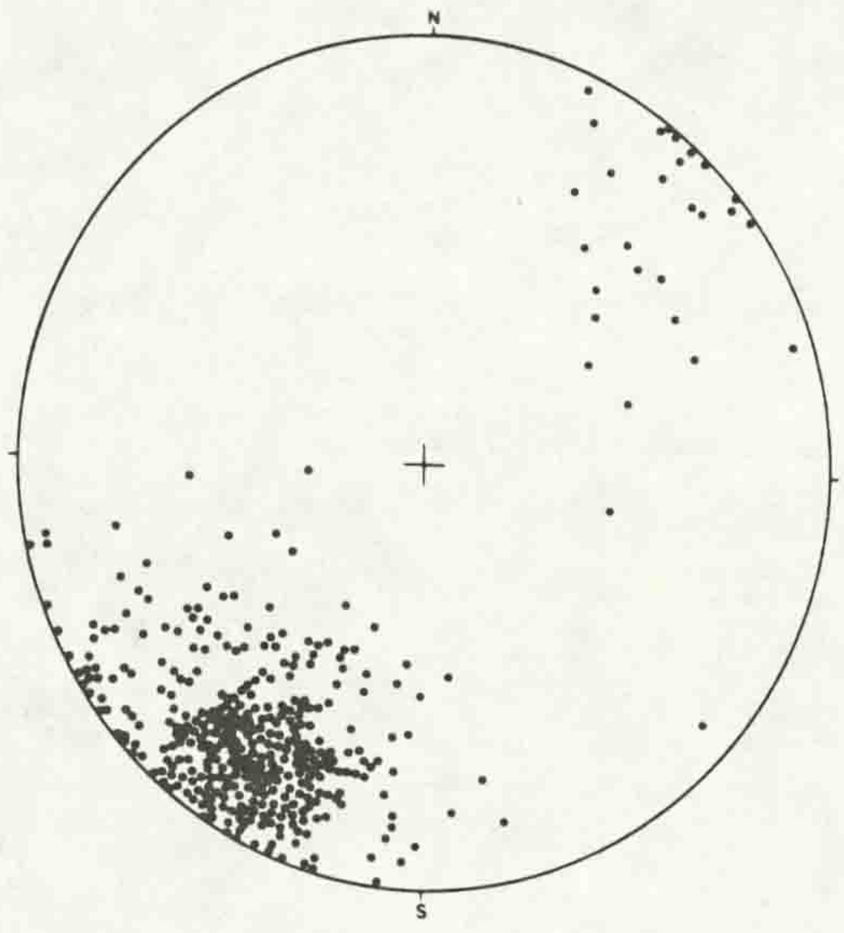


a.

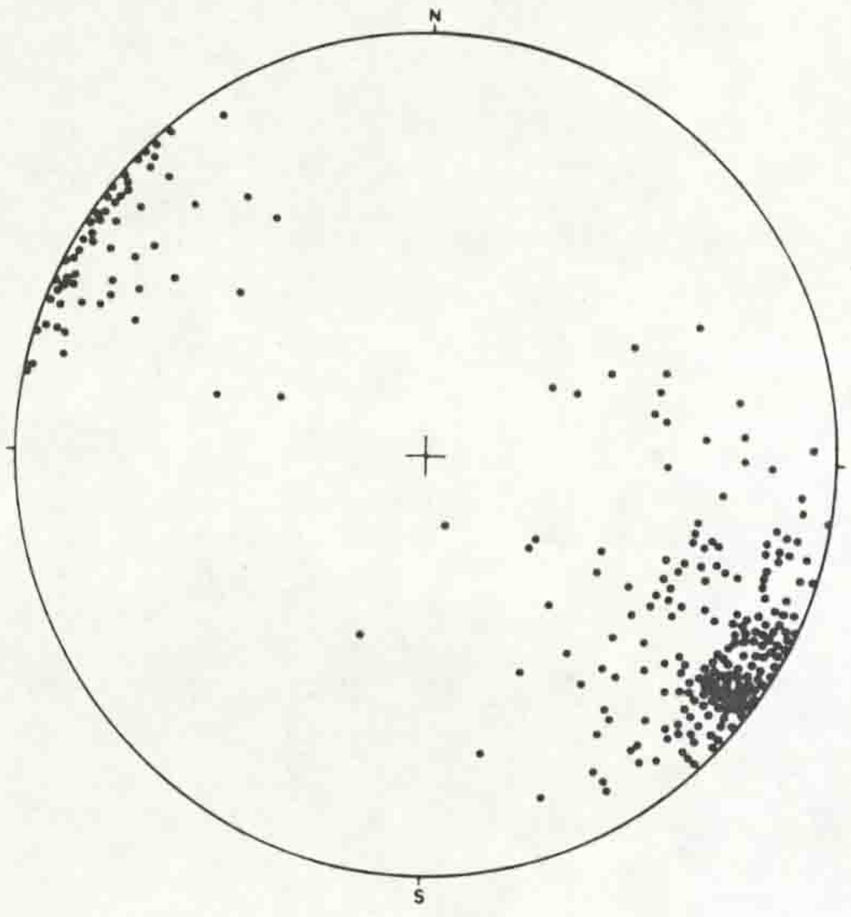


b.

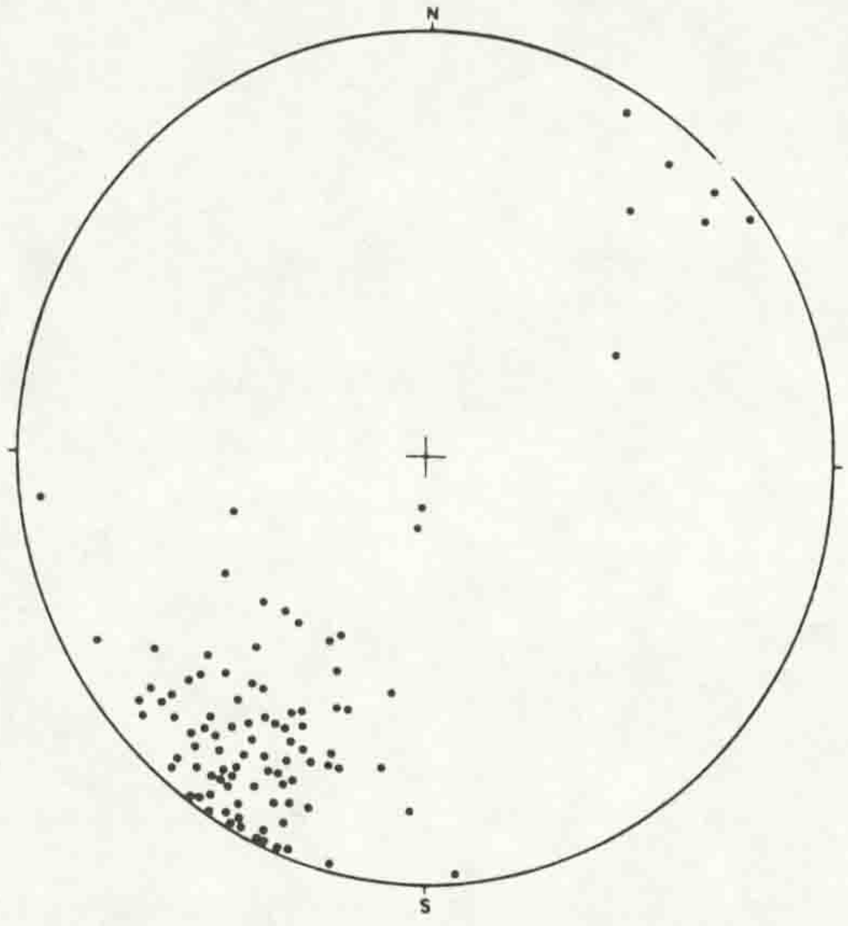


c.

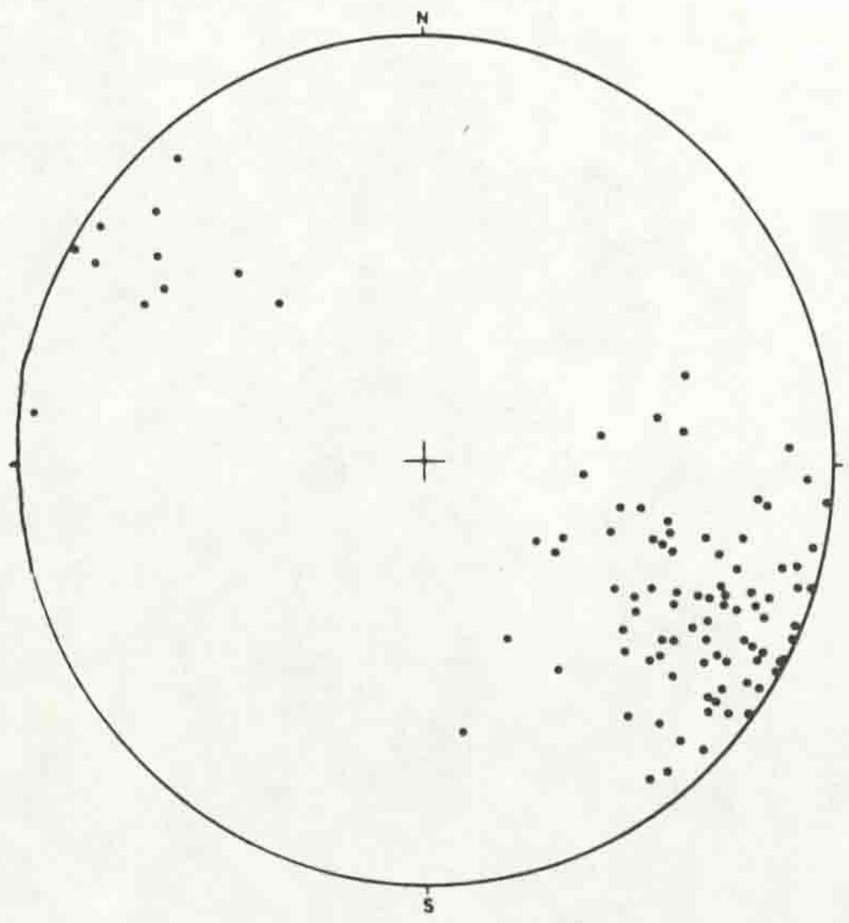


d.

(lower hemisphere projections)

in a brittle manner and variably replaced by chlorite. In psammitic and quartzitic lithologies the $S_3$ fabrics are poorly defined, the foliation being penetrative in nature and resembling $S_2$. Treloar (1982) describes a similar lack of clear $S_2$ / $S_3$ relations as being the result of the transposition of $S_2$ into $S_3$ during $D_3$.

3.2.1.2 Linear fabrics: Linear fabrics are commonly developed in siliceous lithologies with extensional grain shape (qtz rodding) and clast fabrics, and foliation intersection lineations showing general E - W azimuths and relatively shallow plunges (Figure 3.6). Within other lithologies lineations are variably developed, occurring as quartz rodding within siliceous ribs and pods in marbles and pelites, and as rare dimensionally orientated amphibole needles within amphibolitic units. $F_3$ fold hinges within the Bennabeola quartzite often display mullion forms parallel to the lineation direction. The linear fabrics are parallel to the axes of $F_3$ folds, a feature typical of lineations over much of Connemara (Tanner & Shackleton 1979). In many of the lithologies the relation between linear fabrics and foliations is unclear, but in psammitic units extended and flattened clasts can be seen to be deformed around $F_3$ folds, showing the extension lineation to be at least partly pre - $F_3$. Interpreting the timing of foliation / bedding intersection lineations is dependent on clear identification of the foliation fabric involved {3.2.1.1}.

3.2.1.3 Folds: No $F_1$ folds were identified in the study area, although it is likely that the intense $S_2$ fabrics overprint and obscure any earlier folding {3.2.1.1}. Previous workers (e.g. Yardley 1976, Tanner & Shackleton 1979) have suggested that the relic $S_1$ fabrics are not the product of deformation but are mimetic after bedding, with $D_2$ fabrics representing the earliest deformation.

Inspite of the intensity of $S_2$ fabrics, obvious $F_2$ folds are relatively rare. Where evident, e.g. [GR 664 603], $F_2$ folds are small scale structures, typically with amplitudes of <100mm, with axial planar $S_2$ foliation. Where the hinges of $F_2$ folds can be seen they are highly

**Figure 3.7: $F_2$ eye closures deformed by upright $F_3$ folds in the Gubbatoor Psammite Member of the Lakes Marble Formation [GR 664 603]. Lens cap is 49mm diameter.**


**Figure 3.8: Typical $F_3$ folding in the Tonabina Marble Member of the Lakes Marble Formation [GR 643 635]. Lens cap is 49mm diameter.**

## List of Figures

**Figure 3.9: Typical $F_3$ folding in the Gubbatoor Psammite Member of the Lakes Marble Formation [GR 644 633]. Notebook is 210 x 150mm.**


**Figure 3.10: $F_3$ folds of boudinaged $F_2$ closures of amphibolite within the Tonabina Marble Member of the Lakes Marble Formation [GR 643 635]. Lens cap is 49mm diameter.**

curvilinear, with the fold axis changing direction by up to 120°. More often $F_2$ folds are evident as 'eye' and doubly verging structures (Figure 3.7). The $L_2$ extension lineation {3.2.1.2} bisects the hinge angle of the curvilinear folds.

$F_3$ folds, clearly identifiable by their deformation of $S_2$ fabrics, are the most commonly developed folds in the study area. These folds show steeply dipping axial planes (Figure 3.6) and variable, though generally shallow, plunges (Figure 3.6). Folds on all scales show hinge line culmination and depression features. The vergence of minor $F_3$ folds defines large scale structures, such as the Tully Mountain Synform. Way up evidence within the metasediments show the $F_3$ folds to be downward and north facing. Typical fold forms are tight to isoclinal in nature, resembling similar folds (class 2 folds Ramsay & Huber 1987) although hybrid type 3/1c folds are reported as the common fold style in other areas of Connemara (e.g. Badley 1976, Yardley 1976). The detailed fold morphology is variable and controlled by lithology, the best developed folding being evident in marble and psammitic units (Figures 3.8 and 3.9). More pelitic units show only rare folds preserved in quartz veins. Where $F_2$ folds are deformed by $F_3$, a range of interference patterns are produced (Figure 3.10).

Kink bands, locally producing box folds, cut across the $F_3$ structures. These kinks may be related to the $D_4$ deformation although no direct evidence for large scale $F_4$ structures was detected in the study area. The dominant structural effects of $F_4$ folding are related to the development of the Connemara Antiform (Tanner & Shackleton 1979), the hinge of which lies to the south of the study area. The formation of the Connemara Antiform led to a tilting of the study area to the north by up to 70° (Figure 3.11). The removal of this tilting rotates the $F_3$ structures to a shallow orientation similar to that shown by Morris & Tanner (1977), with the folds in the study area having subhorizontal axial planes and facing north. The structural evolution of the study area, and its relation to the rest of Connemara are discussed in section {3.5}.

**Figure 3.11: Cross section of the Bennabeola area (From Tanner & Shackleton 1979) showing the northward tilting of the study area due to the $F_4$ Connemara Antiform (CA).**

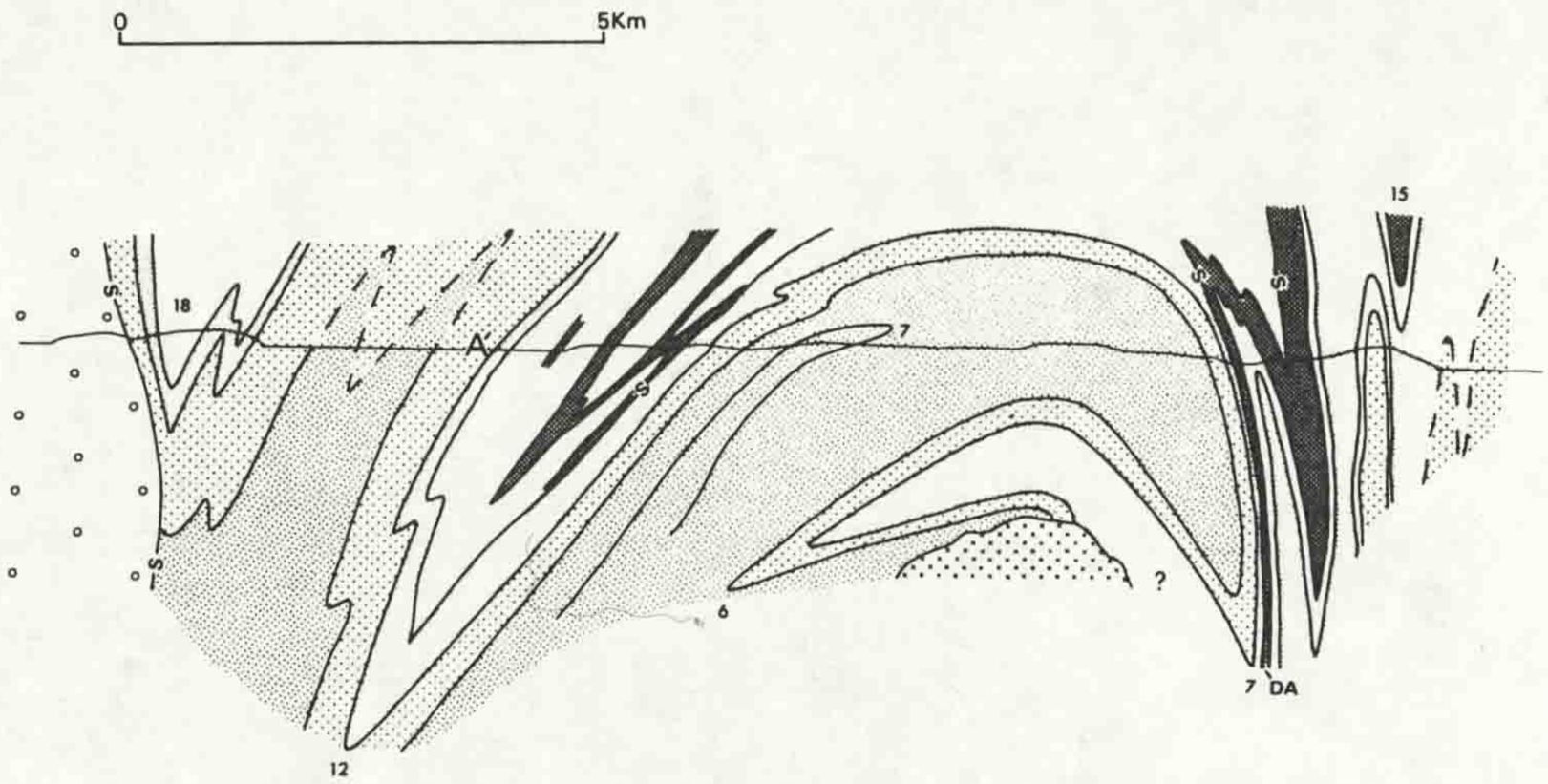

### 3.2.2 Structures developed in the lithologies north of the Renvyle - Bofin slide (the Kylemore Formation)

**3.2.2.1 Planar Fabrics:** The foliation fabrics developed within the Kylemore Fm are very similar to those seen in lithologies to the south of the RBS {3.2.1.1}, with two foliations being evident in the field. The earlier of these fabrics is penetrative, parallel to bedding and often associated with an incipient compositional layering in pelitic lithologies. This fabric shows an orientation similar to the fabrics in the lithologies to the south of the RBS (Figure 3.12). Along with the compositional layering, an alignment of platey and tabular minerals and flattened grain aggregates define the foliation. Where original sedimentary clasts are present they show flattening in the penetrative foliation. Penetrative fabrics are deformed around the hinges of $F_3$ folds.

A spaced second foliation, axial planar to the $F_3$ folds (Figure 3.12), crenulates and locally obscures the penetrative fabric. The nature of the crenulation fabric is somewhat variable, ranging from gentle warps of the penetrative fabric (Figure 3.13) to tight chevron-like folding (Figure 3.14). Axial planar foliations can locally obscure the penetrative fabric, a feature best seen within pelitic lithologies.

In thin section the penetrative fabric can be seen to be a replacement of an earlier fabric, which is preserved as inclusion trails within porphyroblasts {3.2.3} and in scattered relicts throughout the bulk of the rock (Figure 3.15). The penetrative foliation is, like the penetrative fabrics developed to the south of the RBS, an $S_2$ fabric, with the crenulation being $S_3$ in age. Despite the high strains inferred for the $D_2$ deformation (Kelly & Max 1979) pre - $D_2$ fabrics are often preserved; a feature also noted by Ferguson (1984).

**3.2.2.2 Linear fabrics:** As in the lithologies to the south of the RBS, strong linear fabrics are present in the Kylemore Fm. These linear fabrics are typically defined by 'rodded' quartz grain aggregates and vein bodies (Figure 3.16), and by scattered dimensionally orientated amphiboles in amphibolitic units.

Figure 3.12: Equal area stereonet projections of orientation data from the Kylemore Formation;
a, $S_2$ foliation, regional metamorphic lithologies (Poles, 386 pts).
b, $S_3$ crenulation, regional metamorphic lithologies (poles, 247 pts).
c, Foliation, aureole lithologies (poles, 401 pts).
d, Mineral lineation, aureole lithologies (215 pts).
e, Mineral lineation, regional metamorphic lithologies (143 pts).

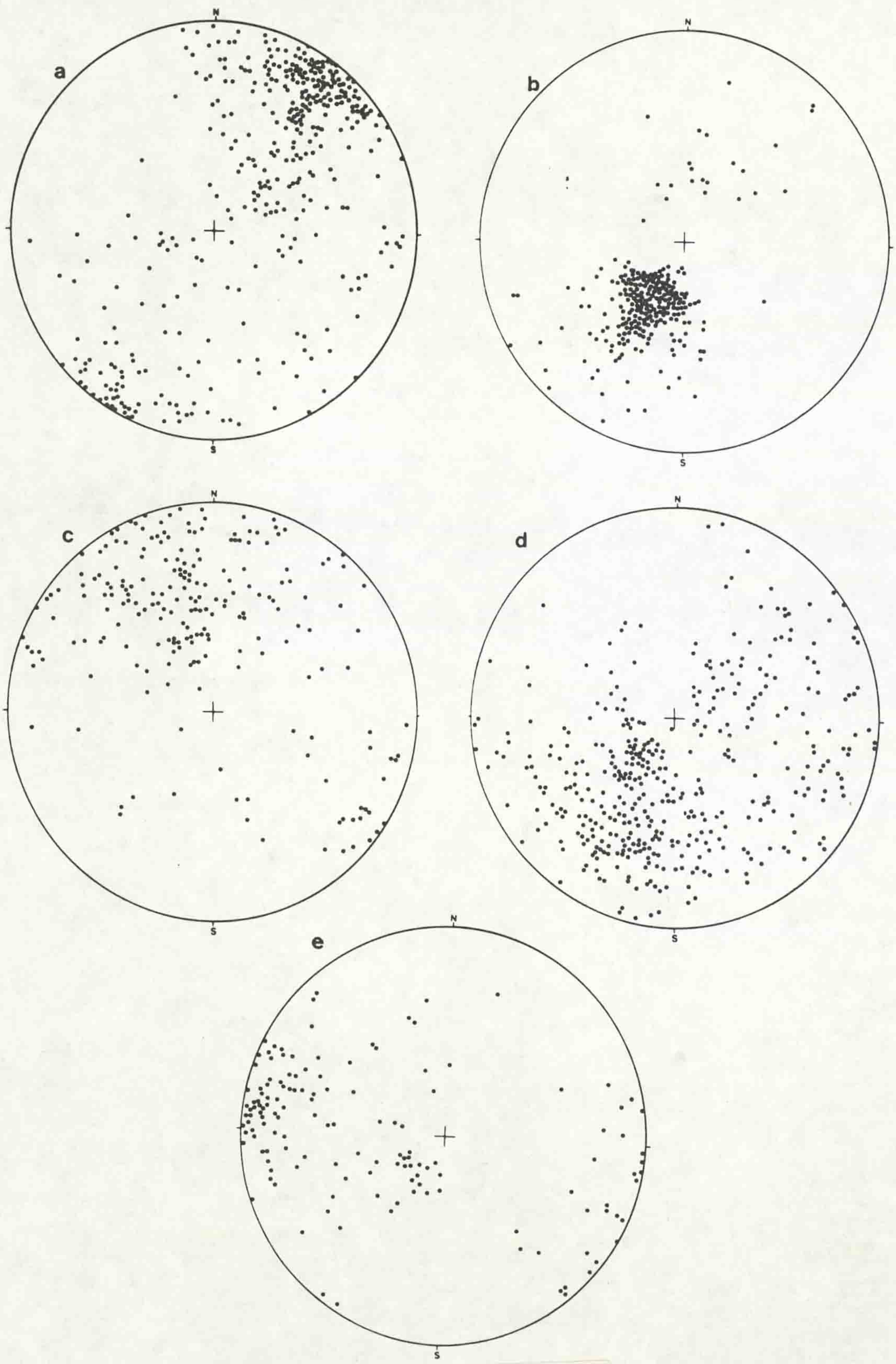


(lower hemisphere projections)

(Figure 3.12 cont)
f, Fold ($F_3$) axial planes, all area (poles, 160 pts).
g, Fold ($F_3$) hinges, all area (160 pts).

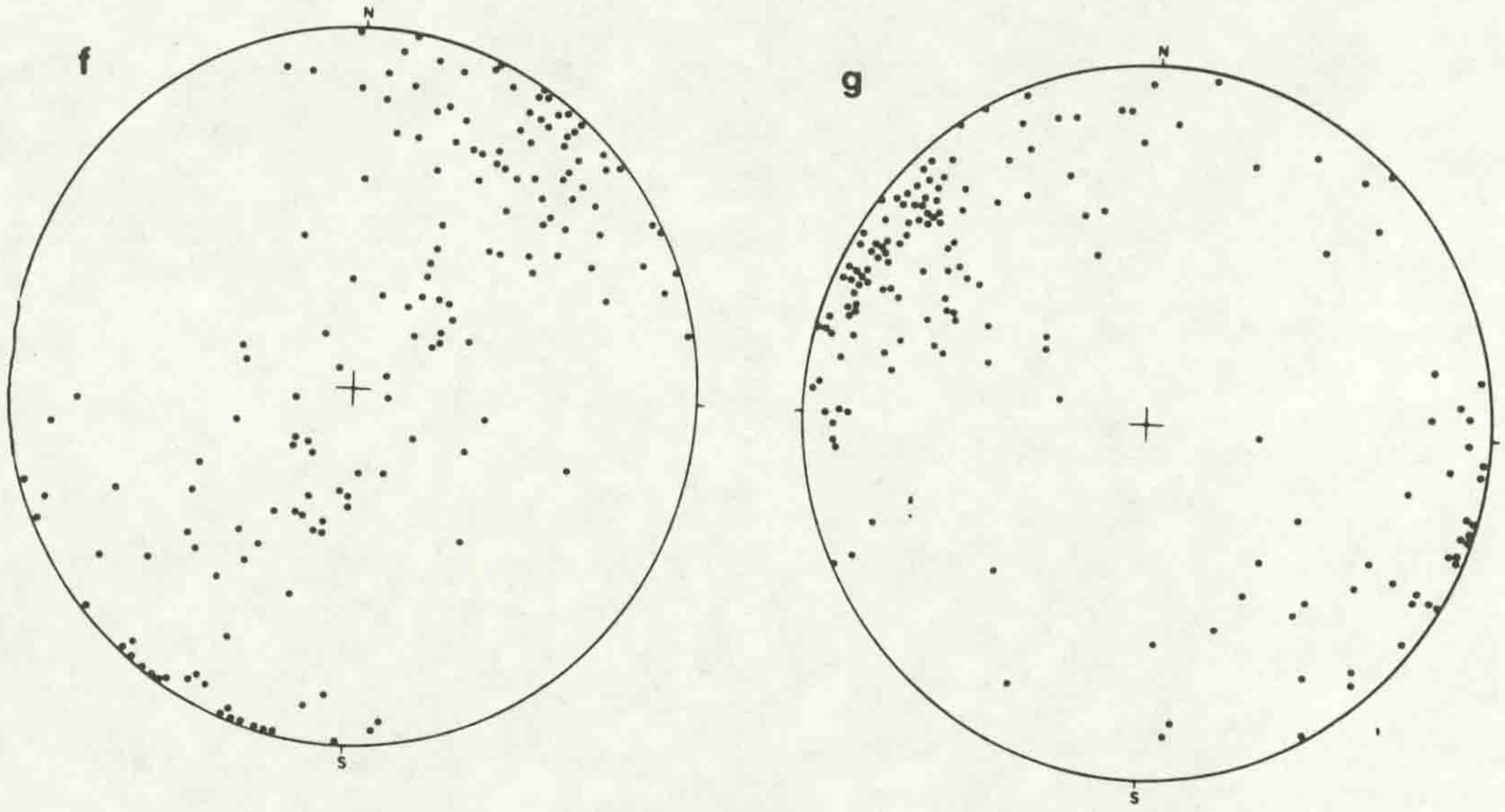


Figure 3.13: Penetrative $S_2$ foliation deformed by upright $D_3$ crenulation (X 29) PPL.

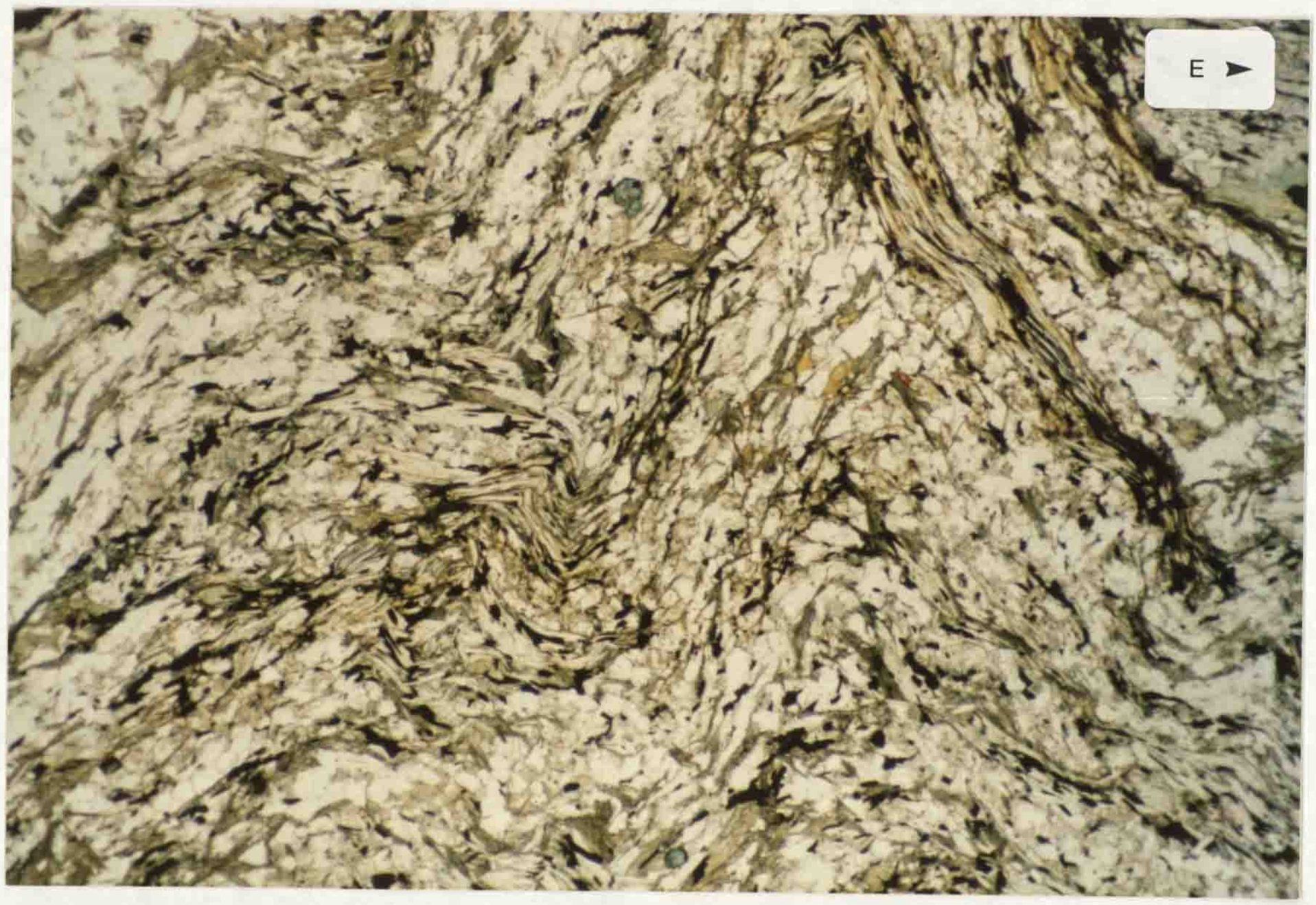

**Figure 3.14: Angular $D_3$ crenulation deforming $S_2$ foliation in Kylemore Formation pelite (X 29) PPL.**

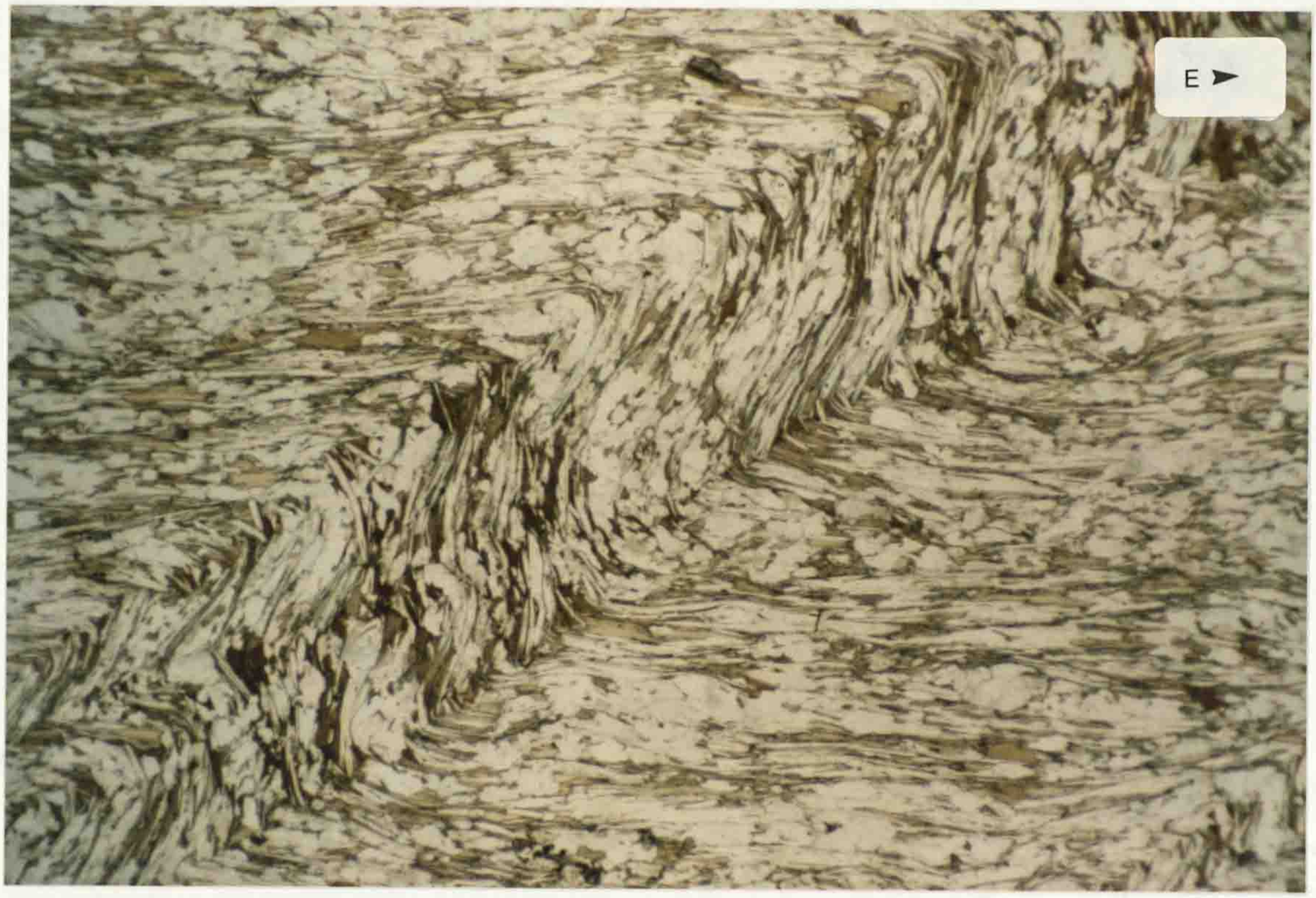


**Figure 3.15: Relic $S_1$ fabrics preserved within segregated $S_2$ foliation which is crenulated by upright $F_3$ microfolds (X 56) PPL.**

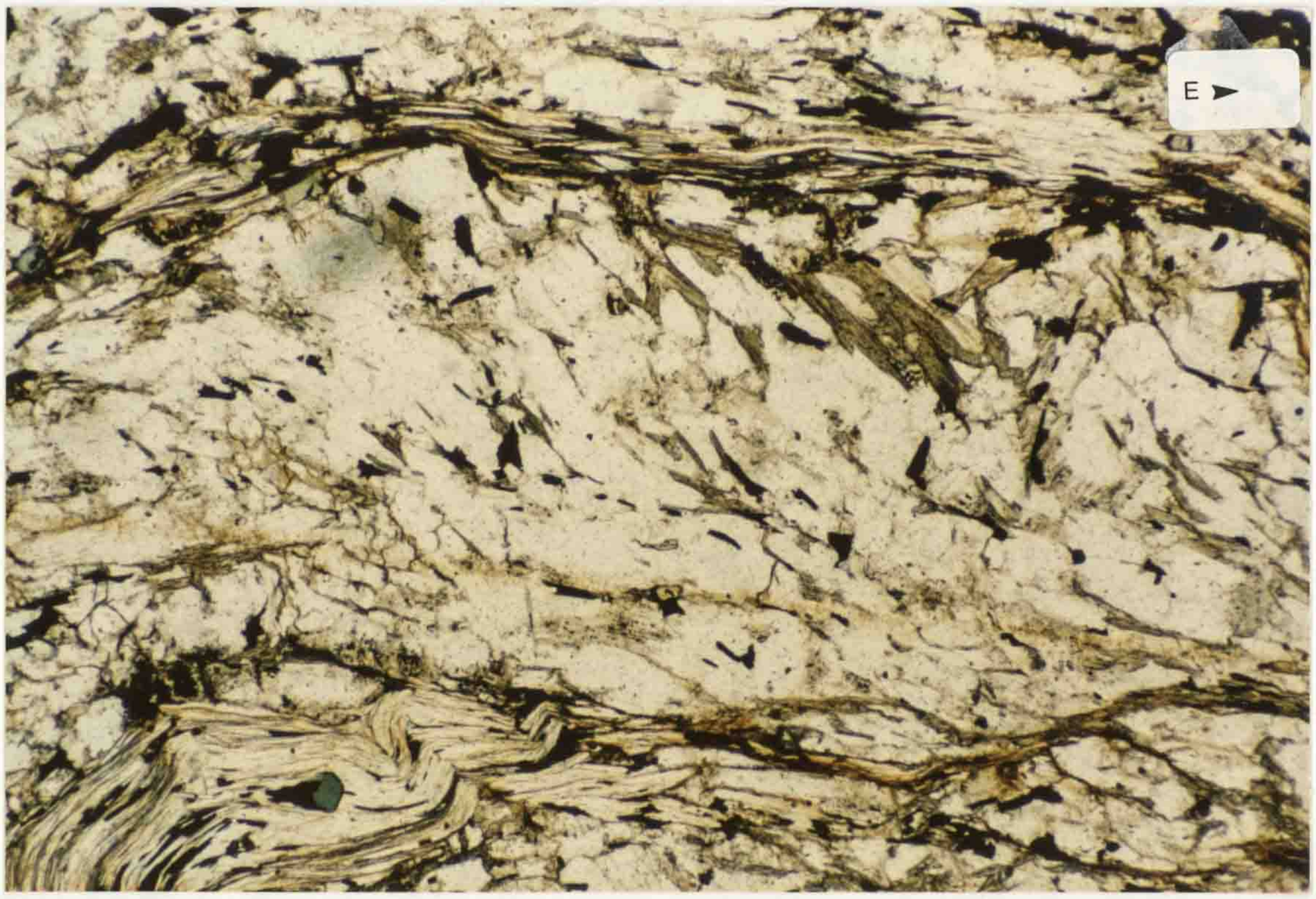

**Figure 3.16: Lineated Kylemore Formation at [GR 688 606]. Lens cap is 49mm diameter.**


**Figure 3.17: $F_3$ fold deforming $S_2$ foliation and $L_2$ lineation [GR 692 604]. Lens cap is 49mm diameter.**

**Figure 3.18: Crenulated $S_2$ fabrics in pelitic Kylemore Formation [GR 687 611]. Lens cap is 49mm diameter.**


**Figure 3.19: $D_4$ kink band cutting across $F_3$ fold [GR 681 632]. Lens cap is 49mm diameter.**

These fabrics fall into two groups which have different orientations (Figure 3.12), an E - W trending, relatively shallow plunging set which is possibly associated with the RBS {3.3}, and a more steeply plunging N - S trending group which is developed through out the study area, although more evident in the lithologies adjacent to the DCD igneous bodies. The time relations of the two groups of linear fabrics are often unclear, with no clear overprinting relations between the two orientations having been observed. The scatter in orientations of the N-S set (Figure 3.12) suggests that their orientation has been affected by the $F_3$ fold events. The E-W trending set of lineations trend parallel to the $F_3$ fold hinges.

3.2.2.3 Folds: As in the metasedimentary sequence lying to the south of the RBS the dominant folding in the Kylemore Fm can be ascribed to $D_3$. East - West striking and variably plunging $F_3$ folds with axial planar $S_3$ deform the $S_2$ and linear fabrics (Figures 3.12 and 3.17). Within pelitic units of the Kylemore Fm, $F_3$ folding is evident as a strong crenulation of the earlier fabrics and compositional banding (Figure 3.18). Where psammitic bands are developed they are tightly folded, the folds locally being almost isoclinal in form. Way up and younging evidence is sparse within the Kylemore Fm {2.1.2.2} although where present it shows the $F_3$ folds to be upward and southward facing. Lithologies are locally inverted on the overturned limbs of $F_3$ folds.

Some evidence of pre $F_3$ folding is developed at [GR 729 628] where eye structures and doubly verging folds are deformed in the $F_3$ structures.

Post - $F_3$ structures consist of kink bands, often showing brittle deformation, which cut across earlier fabrics and folds (Figure 3.19). No large scale $F_4$ structures were detected, although the overall north tilting of the study area due to the development of the Connemara Antiform {3.2.1.3} is clearly evident.

3.2.2.4 Fabric changes adjacent to igneous bodies: The foliation and linear fabrics developed in the Kylemore Fm show substantial modification within the contact aureole around the

**Figure 3.20: Irregular granitic veins and structureless migmatitic patches in Kylemore Formation migmatites [GR 703 594]. Hammer is 360mm long.**


**Figure 3.21: Irregular disharmonic folding in Kylemore Formation migmatites [GR 701 593]. Lens cap is 49mm diameter.**

DCD. The main changes in fabrics can be ascribed to the thermal effects of the DCD, although the presense of the igneous material has a significant effect on the local structural style.

The dominant planar fabric within the Kylemore Fm, $S_2$, is associated with a compositional banding {3.2.2.1} which is overprinted by hornfelsic textures at the margins of the DCD. Within the hornfelsic lithologies the phyllosilicate minerals which typically define planar fabrics, biotite and muscovite, are developed in random orientations in the foliae and locally replaced by sillimanite {Chapter 4}. This random regrowth of minerals within an initially planar fabric becomes increasingly strong closer to the igneous bodies, with the development of large (upto 20mm) porphyroblastic feldspar (typically $An_{45-60}$) grains (producing the andesine porphyroblast schist of Tanner & Shackleton 1979). Granoblastic textures are often developed within 20 - 30m of the contacts with the larger gabbroic bodies, although the development of hornfelsic lithogies at the peridotite contacts is less common {3.4.1.4}. Migmatitic lithologies are common at the contacts with gabbroic bodies; Kylemore Fm lithologies being cut by irregular granitic veins and structureless nebulitic patches (Figure 3.20). In the migmatitic areas, $S_2$ fabrics are often irregularly folded, with the folding typically being disharmonic, with a wide range in amplitude, wavelength and axial planar orientation (Figure 3.21). Bennett & Gibb (1983) described the complex nature of folding within the contact aureole of the Creggaun gabbro as being due to interference between several fold phases, tracing large scale 'regional' $F_4$ folds through the migmatitic lithologies. However, such large scale interference structures cannot be identified elsewhere in the study area.

The small scale structures developed in the migmatitic lithologies are often highly complex, showing evidence of multiple fold phases and disrupted folds. At [GR 701 593] a disrupted amphibolitic sheet occurs within convolutely folded migmatitic semipelites (Figure 3.22). In the semipelitic lithologies isolated fold hinges, typically showing multiple fold relations, are 'floating' within a variably foliated feldspar porphyroblastic psammitic migmatite. The amphibolitic unit shows evidence of less ductile behaviour, being a series of angular

**Figure 3.22: Disrupted amphibolite sheet (brown weathering) within convolutely folded migmatites (pale weathering) [GR 701 593]. Hammer is 360mm long.**


**Figure 3.23: Poorly foliated migmatitic fabrics swinging into strongly foliated ductile shear zone [GR 598 586]. Lens cap is 49mm diameter.**

**Figure 3.24: Typical mylonitic fabric developed in aureole lithologies [GR 696 593]. Foliae of biotite, prismatic sillimanite and fibrolite wrapping garnet and feldspar porphyroclasts (X 29) PPL.**


**Figure 3.25: Mylonitic fabric developed in reactivated ductile shear zone [GR 704 588]. Note the dominant phyllosilicate is chlorite, the absence of sillimanite, and the dusty appearance of altered feldspar porphyroclasts (X 29) PPL.**

blocks which sit within the migmatitic lithologies. The relations between deformation and migmatite development are often unclear, with both pre and post deformational migmatite veining being developed along with localised structureless migmatitic lithologies which cross cut folding. This work interprets the complexity of structure in the contact zone migmatitic lithologies as being due to deformation synchronous with the development of the migmatites. Under such circumstances a variety of deformation / migmatisation relationships can develop (McLellen 1983) and the mechanical behaviour of the deforming lithologies is controlled by the percentage of melt present resulting in complex relations in the structures produced.

A strong N-S lineation is developed in the bulk of hornfelsic and migmatitic lithologies, often obscuring the foliation. This lineation is developed within the convolutely folded migmatites. Detailed mapping by Dr A.P. Boyle (pers. comm) in the well exposed aureole of the Creggaun gabbro has revealed that the convolute foliation is locally reoriented into 1-2m zones of flat-lying regular mylonitic fabrics (Figure 3.23) which are commonly cross cut by granitic migmatite veins. These zones run E-W across the area and swing into steep N-S zones of similar regular mylonitic fabric. One such flat lying zone separates migmatitic and gabbroic lithologies from serpentinised peridotite lithologies [GR 705 590] {3.4.1.4}. The lineation fabric is strongly developed within these regular zones as are eye closures and doubly verging folds. These were interpreted by Bennett & Gibb as being due to interference between $F_2$ and $F_3$ folds, but are here interpreted as sheath folds formed during progressive simple shear. The small scale fabrics within the regularly foliated units are typically mylonitic, with ribbon aggregates of quartz and porphyroclastic feldspar, and with garnet grains wrapped by an anastomosing fabric of phyllosilicates and sillimanite (Figure 3.24). In some of the zones the mylonitisation shows evidence of development during retrogression, having strongly altered feldspars and chloritised micas within the fabric (Figure 3.25). In the intervening convolutely folded lithologies hornfelsic fabrics dominate.

The contact zone fabrics are discussed further in {3.4.1.4 and 3.4.2} and in the addendum at the end of the chapter (after page 104).

### 3.2.3 Fabrics within porphyroblastic minerals

As noted in {3.2.1.1 and 3.2.2.1} an early fabric ($S_1$) is preserved within garnet and feldspar porphyroblasts which are wrapped by the dominant $S_{2/3}$ foliation. Within feldspar porphyroblasts the included fabric, $S_1$, is typically straight and at a high angle to the $S_2$ fabric (Figure 3.26). The feldspar grains lie within the quartzofeldspathic domains of the segregated $S_2$ and are wrapped by anastomosing phyllosilicate foliae. Feldspar and quartz grains appear truncated where they abut against phyllosilicate rich zones.

The inclusion fabrics seen in garnet porphyroblasts are more complex than those seen in feldspars, ranging from straight to spiral and crenulated trails. Inclusions within garnet porphyroblasts developed adjacent to the DCD are typically rounded and xenoblastic. These fabrics are not attributable to syntectonic development of porphyroblasts and are discussed in {Chapter 4}. The inclusion fabrics which show syntectonic origins can be interpreted as a developmental sequence (Figure 3.27).

The crenulated inclusion fabrics are not readily explicable by standard models for the development of syntectonic porphyroblasts which involve rotation of porphyroblast relative to matrix (e.g. Spry 1963 , Powell & Treagus 1967, 1970), although rare spiral trails are developed (Figure 3.28) which can be considered in terms of rotational models. The models of syndeformational porphyroblast formation proposed by Bell & Rubenach (1983) (with modifications by Bell 1985, 1986 and Bell, Rubenach & Fleming 1986) in which a developing porphyroblast overgrows an actively deforming foliated matrix, better explain the fabrics seen.

Bell & Rubenach define six stages in the development of a segregated foliation from an original fabric via a crenulation cleavage (Figure 3.29). In this model the porphyroblasts do not rotate relative to the matrix, inclusion trails are produced by extremely rapid porphyroblast growth (relative to the strain rate) preserving 'snapshots' of individual stages in the foliation development.

Bell & Rubenach's model is based on the strain field produced

**Figure 3.26: Relict $S_1$ fabrics within feldspar grains within a segregated $S_2$ foliation (X 56) PPL.**

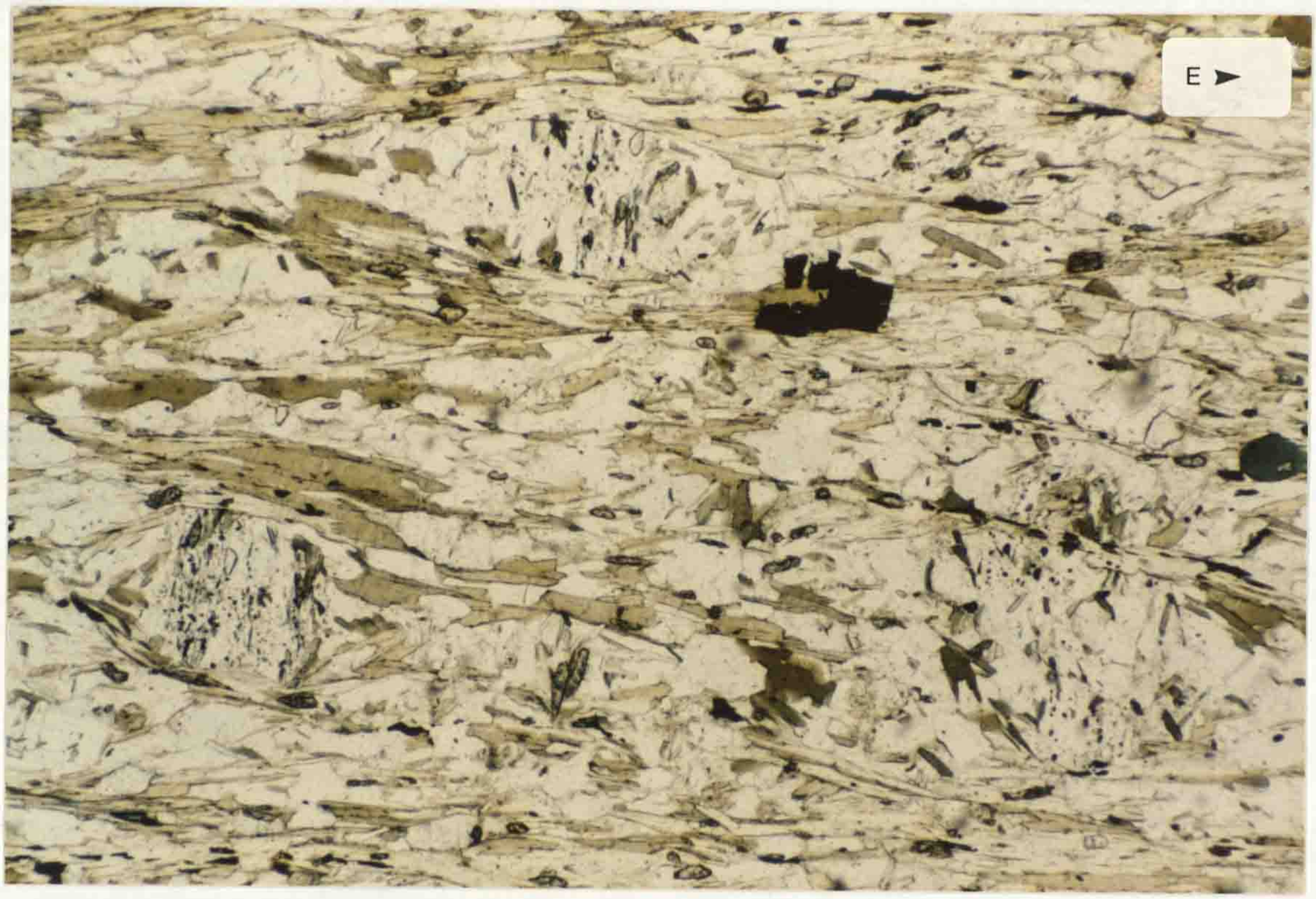


**Figure 3.27: Inclusion fabrics within garnet porphyroblasts from the Roeillaun Schist Member of the Streamstown Formation (NB. all sections cut perpendicular to the external $S_2$ fabric).**
**a, Straight inclusion trails of opaque minerals (largely ilmenite), quartz and feldspar within rounded, anhedral garnet porphyroblast (X 56) PPL.**

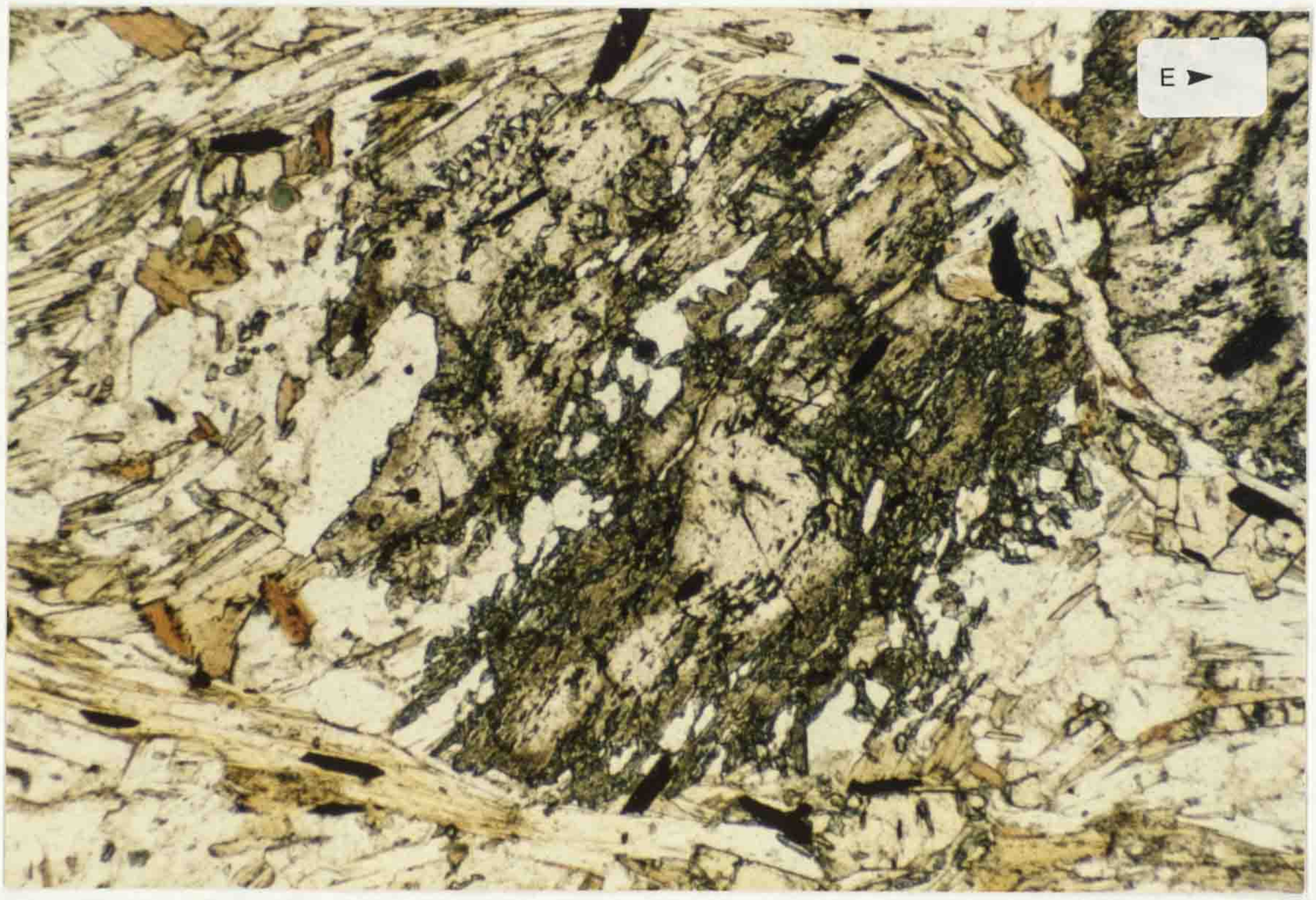

**(Figure 3.27 cont)**
**b, Continuous crenulated trails of quartz, feldspar and opaque minerals (X 56) PPL.**


**c, Crenulated trail showing loss of quartz and feldspar within crenulation hinges, although tabular opaque minerals are preserved in these zones (X 29) PPL.**

**(Figure 3.27 cont)**
**d, Crenulated hinges only locally preserved, with inclusion free garnet domains developed between the remaining hinges (X 56) PPL.**

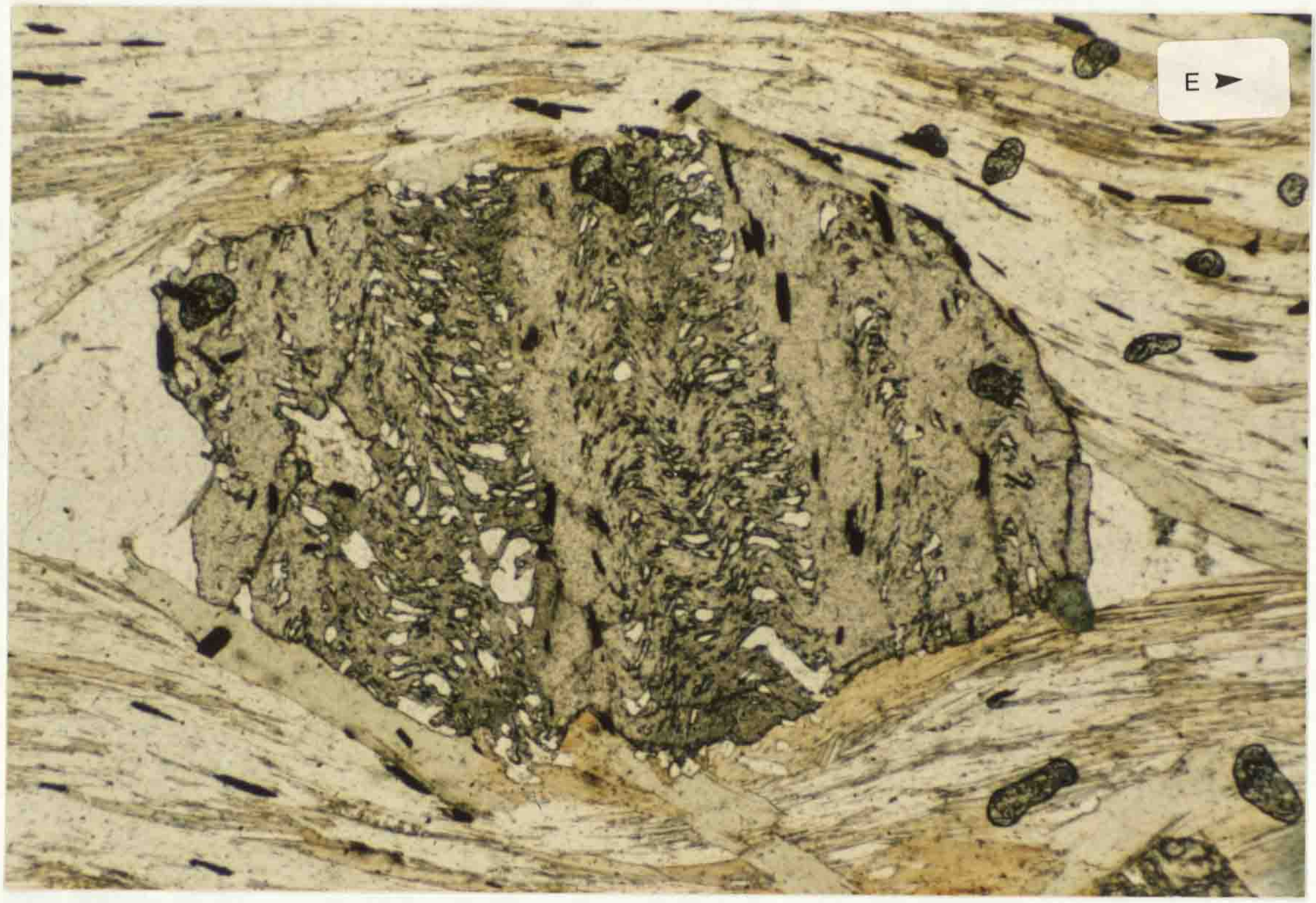


**e, Inclusion zones of quartz and feldspar, with no apparent preservation of crenulation hinges, separated by inclusion free garnet domains (X 56) PPL.**

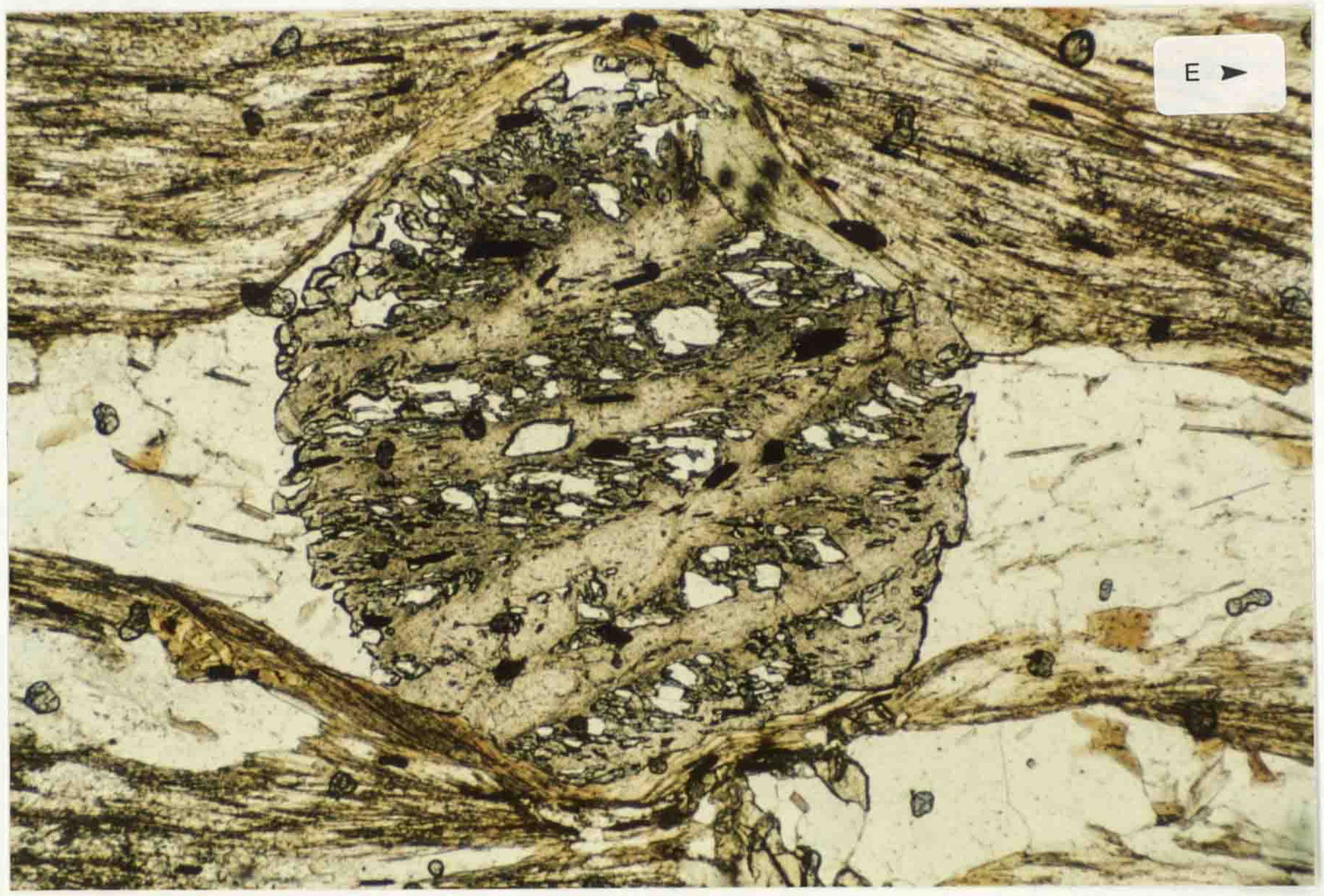

**Figure 3.28: Apparent rotational trail in a garnet porphyroblast from the Kylemore Formation (X 56) PPL.**

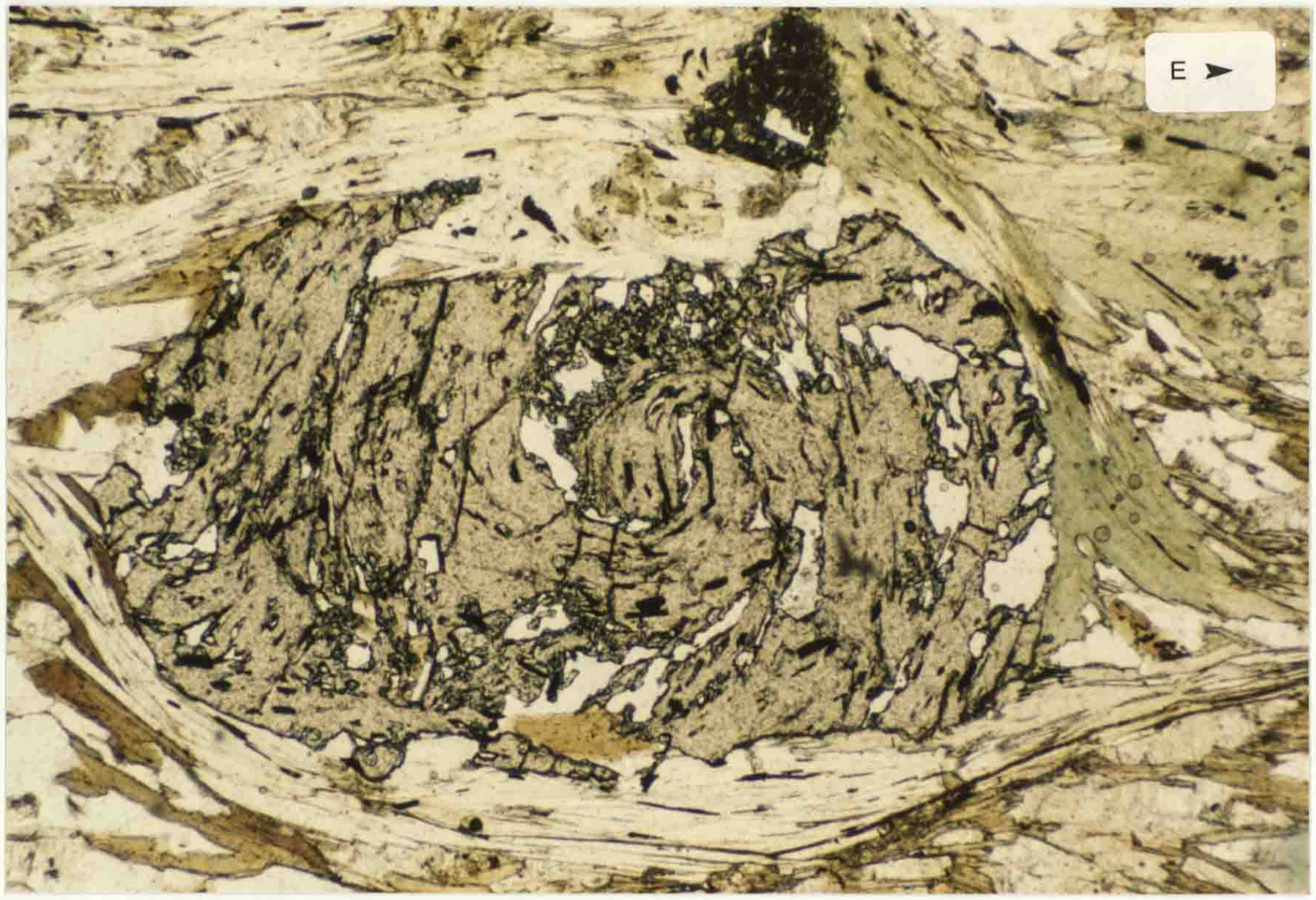


**Figure 3.29: The progressive modification of an original foliation through a crenulation cleavage to a new penetrative foliation (from Bell 1985). 1, Uncrenulated original foliation; 2, Crenulated foliation; 3, Differentiated crenulation cleavage with continuity across the crenulation; 4, Differentiated crenulation cleavage with new phyllosilicates along the crenulation; 5, Differentiated layering due to the destruction of crenulation hinges by further deformation; 6, Homogenised cleavage.**
**Note the similarity in form of stages 1 to 5 to the inclusion trails shown in Figure 3.27 a to e.**

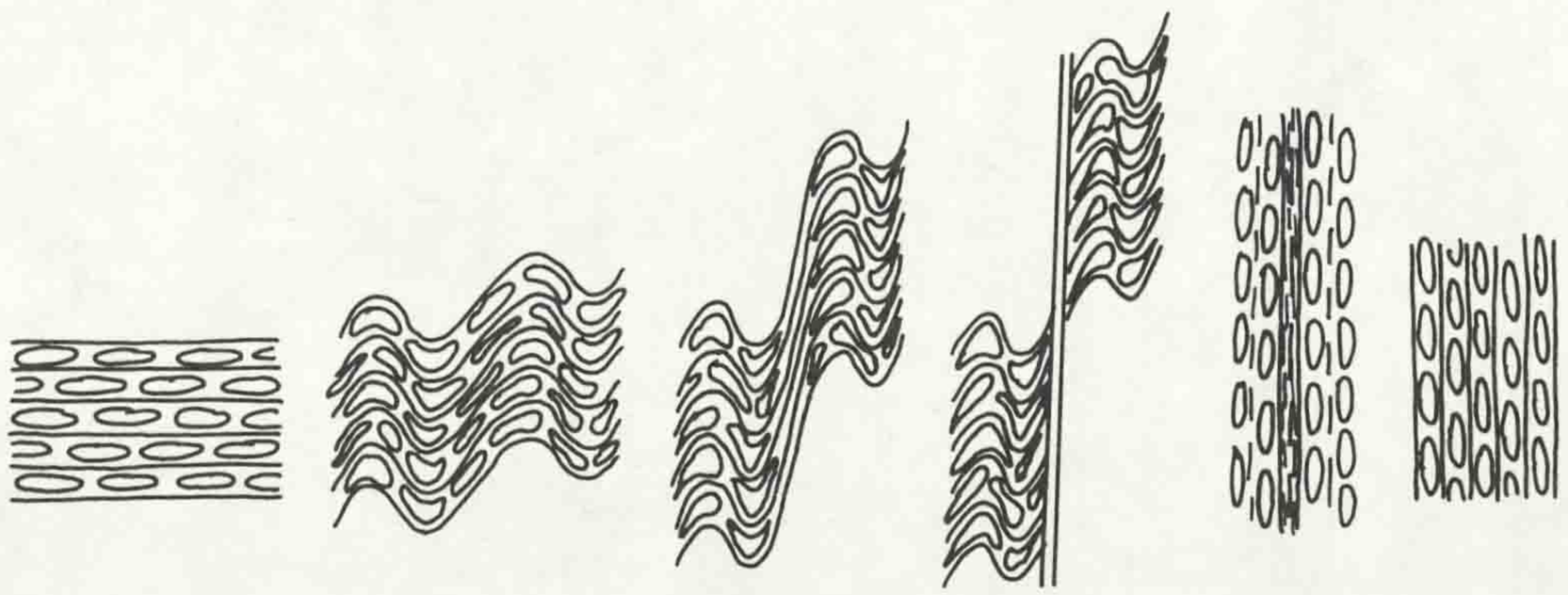

**Figure 3.30: Tabular garnet porphyroblast from Kylemore Fm pelite (X 56) PPL.**

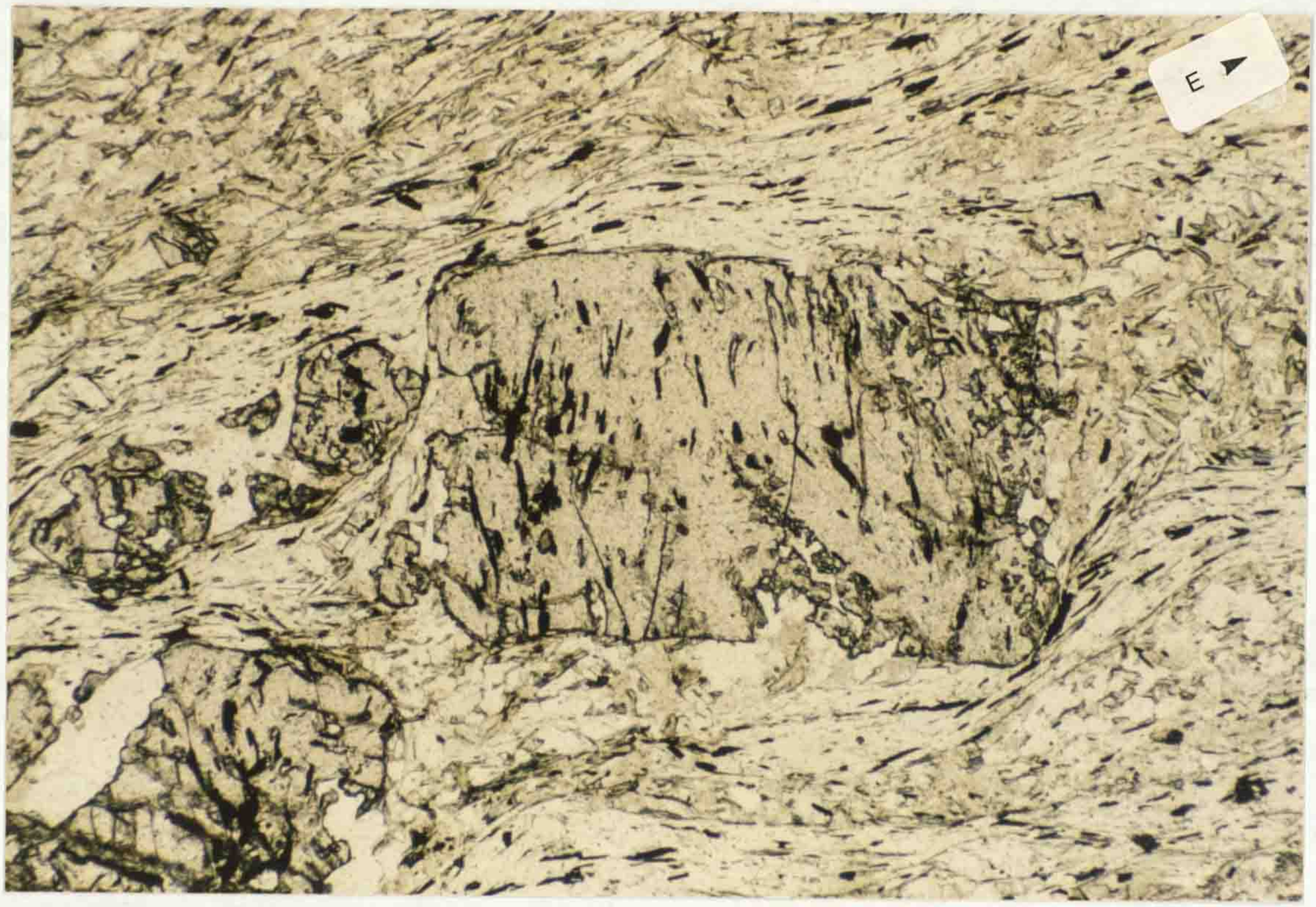


**Figure 3.31a: Morris & Tanners' (1977) correlation of the Renvyle - Bofin Slide across the $F_4$ Connemara Antiform.**

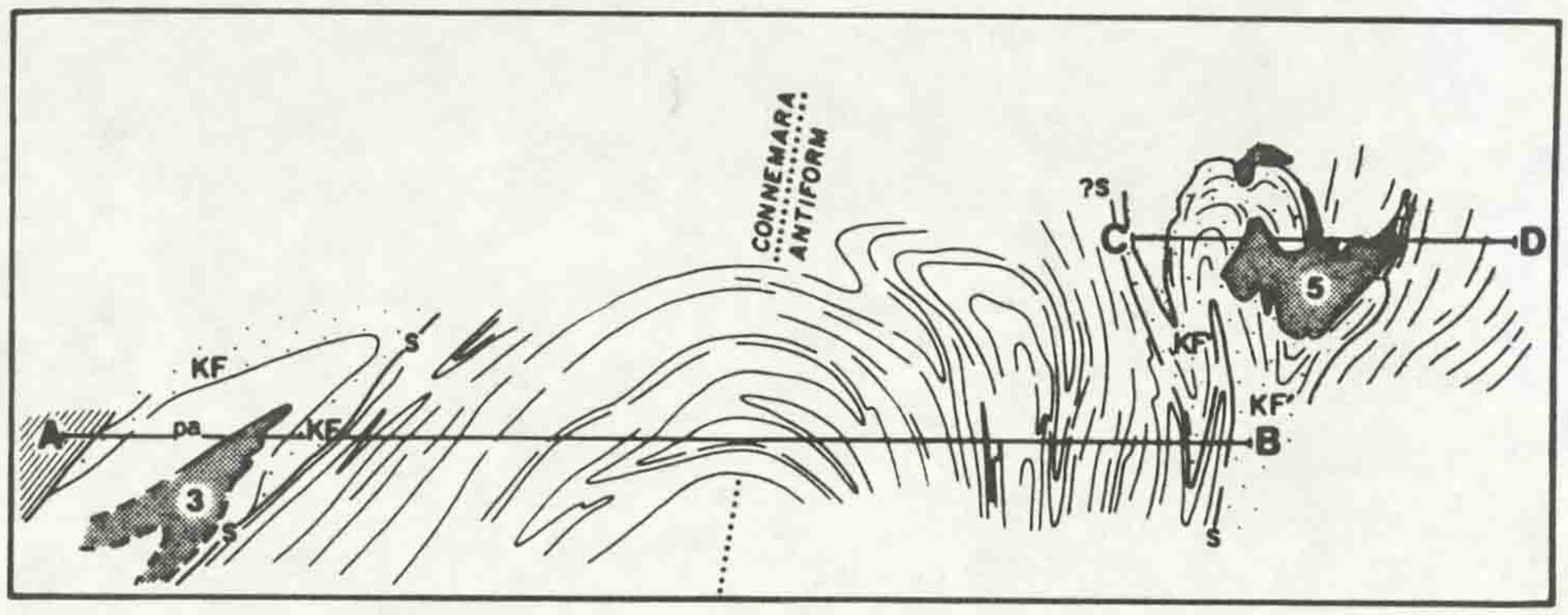

**Figure 3.31 (continued)**
**b, Tanner & Shackleton's (1979) correlation of the Renvyle - Bofin Slide across the $F_4$ Connemara Antiform.**

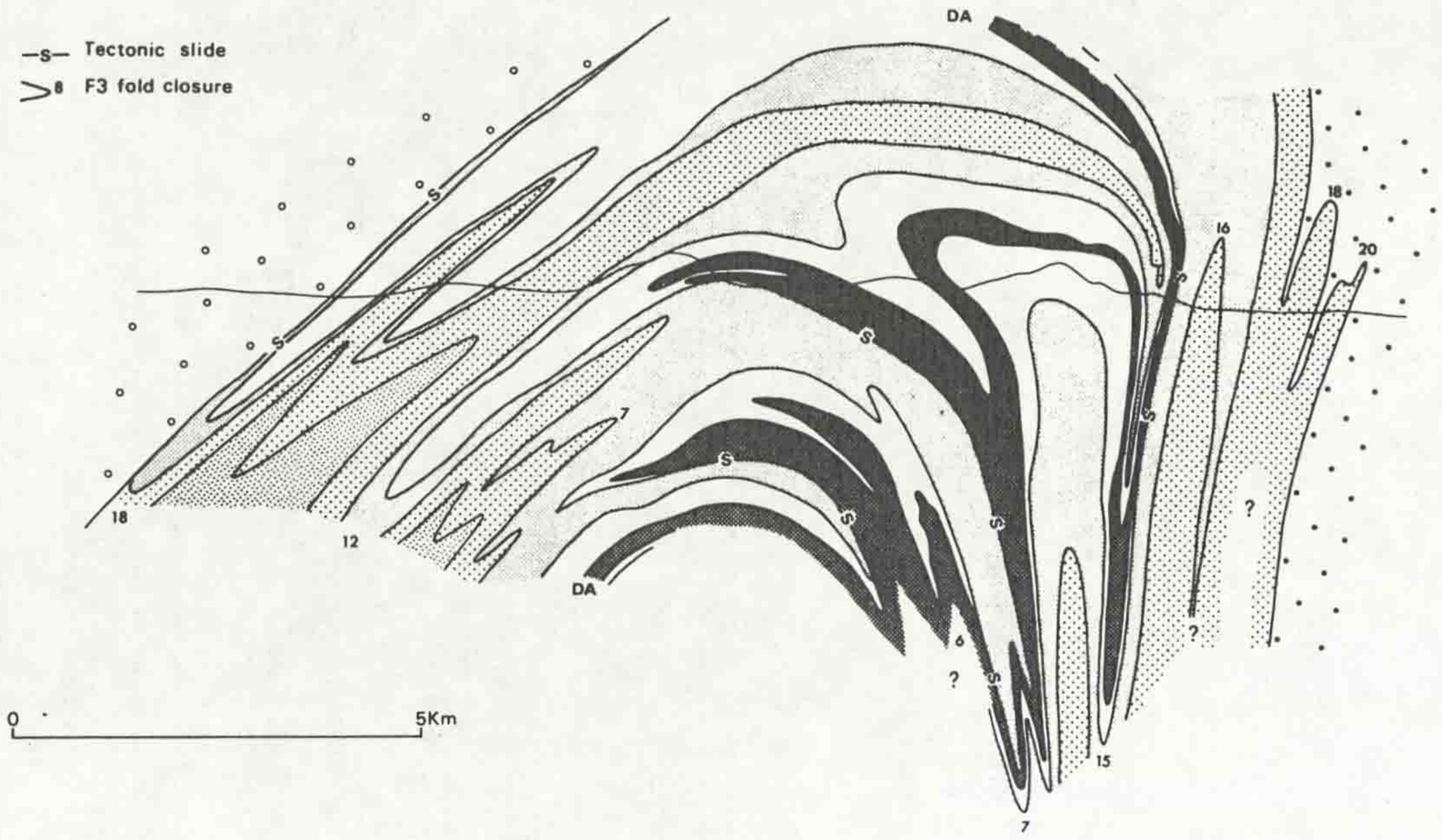


**c, Pre $F_4$ orientation of the Renvyle - Bofin Slide (from Morris & Tanner 1977).**

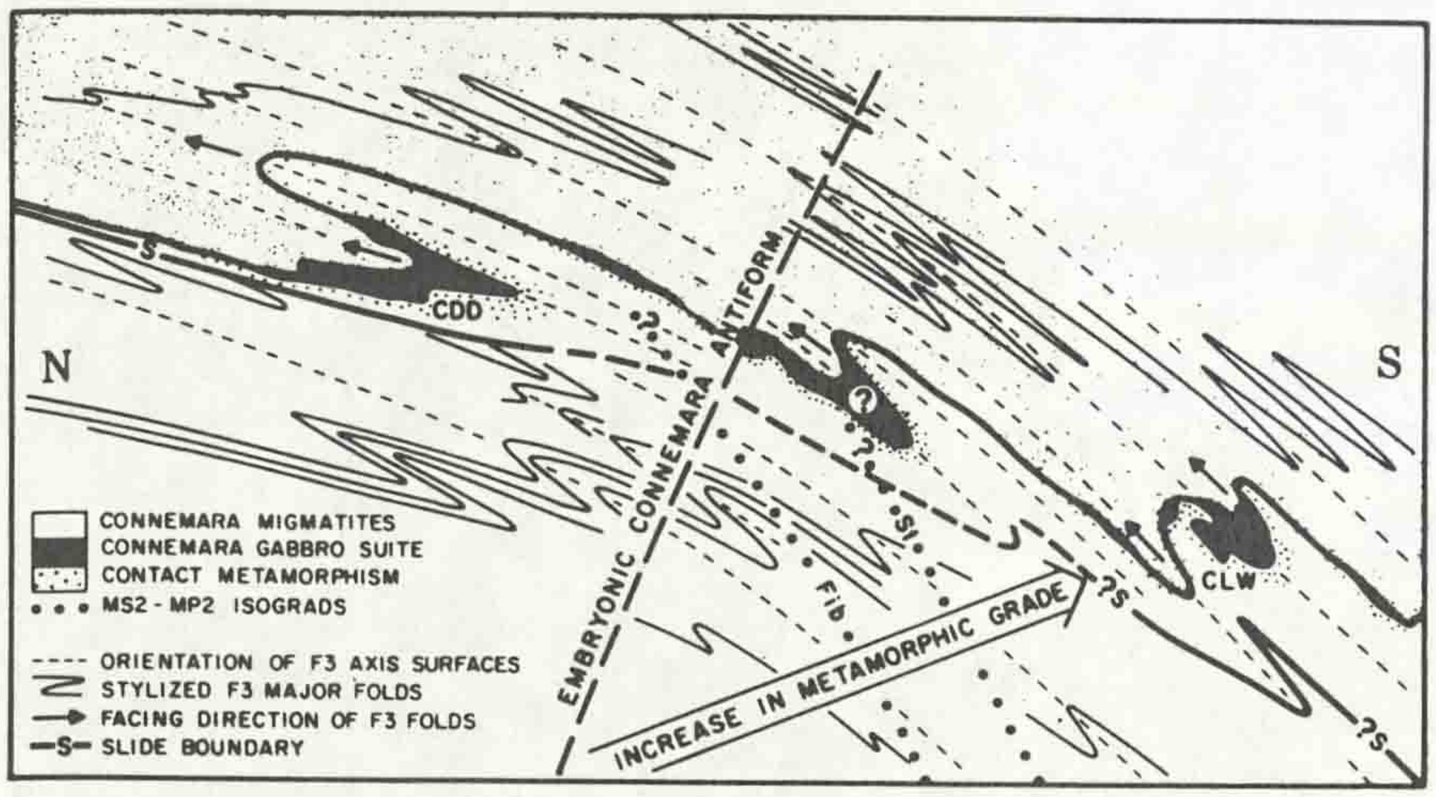

during the deformation being hetrogeneous; deformation being partitioned into domains of low strain (primarily shortening strains) wrapped by anastomosing high strain zones (with a large shear component to the strain). As deformation proceeds the strain field does not remain constant, but shifts such that intial low strain zones can receive high strains. In high strain zones phyllosilicate minerals are more readily able to absorb the high shear strains, whereas other minerals (Qtz, Pl, Grt) will develop large dislocation densities and undergo dissolution. As a result of this dissolution of rigid lattice minerals the high strain zones become enriched in phyllosilicate minerals. The low strain zones provide suitable sites for precipitation of the dissolved minerals and Bell & Rubenach suggest that porphyroblastic minerals preferentially nucleate in low strain zones.

However, as the strain field shifts during the deformation, the initial low strain nucleation sites of porphyroblasts can become subject to high shear strains. As a result, porphyroblasts can undergo dissolution as the high strain migrates through the porphyroblast. Within pelitic lithologies tabular garnet porphyroblasts are common (Figure 3.30), with their longest sides lying parallel to the foliation fabrics suggesting dissolution.

The fabrics developed in porphyroblastic minerals, particularly in garnets, preserve information on the early strain history of the study area, the details of which are considered in {3.5}.

## 3.3 The Renvyle - Bofin slide

3.3.1 Previous work: The Irish geological survey (Kinahan *et al.* 1878) noted the existence of a zone of disruption, the Kylemore valley fault, running E-W along the Kylemore valley and along the axis of the Dawros peninsula. This fault separates well stratified lithologies to the south from a more homogeneous northern series, within which the Dawros - Currywongaun - Doughruagh igneous complex is developed. The survey considered the Kylemore valley fault to be a brittle structure and did not correlate it with features seen elsewhere in the Ballynakill

district.

Cruse (1963) noted the existence of a tectonised zone on the island of Inishbofin, where a fault associated with serpentinitic and talc - schist pods is exposed on the coast near Inishbofin harbour. Cruse correlated this zone with features on the Renvyle peninsula, where a zone of *'shattering and recrystallisation'*, best seen around Eagles Nest school [GR 665 626], runs to the south of Lakes Marble Fm lithologies which Cruse interpreted as being in stratigraphic continuity with adjacent Kylemore Fm semipelites. This tectonic break was christened the Renvyle - Bofin slide (RBS) by Cruse (1963). Cruse & Leake (1968) postulated that this largely unexposed feature dipped steeply to the north and had downthrown the northern area late in, or after, the $D_3$ deformation.

Morris & Tanner (1977) consider the RBS to be a large scale feature, reappearing in South Connemara, and schematically depicted (Figure 3.31) the RBS running across the top of the Connemara antiform to outcrop north of the Cashel - Lough Wheelaun igneous bodies. This correlation suggests that the Kylemore Fm and the lithologies surrounding the igneous bodies in the south represent the same stratigraphic unit. Morris & Tanner show the slide to be deformed by $F_3$ folds (Figure 3.31) implying that the slide developed pre/syn $F_3$ and was deformed by that folding.

Tanner & Shackleton (1979) suggest the RBS runs across the Connemara Antiform (CA) to reappear north of the south Connemara ultrabasic bodies, correlating the Kylemore Fm with the Cashel Fm in the south. Tanner & Shackleton trace the RBS east from the limit of Cruse's area across the Dawros peninsula and through the Kylemore valley. The slide cuts out two formations, the Streamstown and Lakes Marble Fms on the north limb of the Tully Mountain synform. The displacement is considered by Tanner & Shackleton to be laterally variable, reaching a maximum adjacent to Kylemore Lough and falling away to the east and west, although no displacement direction is given. The slide is suggested by Tanner & Shackleton to postdate the peak of regional metamorphism (late $F_3$) and to be associated with the development of mylonites and blastomylonites in the Kylemore Fm.

Leake, Tanner, Macintyre & Elias (1984) suggest that the RBS,

along with other late - post $D_3$ slides, are precursors of the Mannin thrust {1.2}. More recently Leake (1986) has suggested that the RBS is related, at least in part, to a feature in southern Connemara, the Clifden Bay dislocation (a late / post $F_4$ feature). Leake considers that these two features represent normal faults, downthrowing the north and south Connemara areas with central Connemara being uplifted. The implied mechanism for this movement is the isostatic uplift of the *'low density quartzite - dominated region of the Connemara antiform'* and the relative sinking of the denser basic and ultrabasic intrusive rich north and south areas.

In the majority of interpretations the development of the RBS is considered to be prior to the formation of the $F_4$ Connemara antiform {3.2.1.3 and 3.2.2.3}. Palaeomagnetic studies of the development of the Connemara Antiform by Morris & Tanner (1977) show the RBS to have had a shallow, possibly south dipping orientation prior to later $D_4$ folding (Figure 3.31). This shallow early orientation is implied by Tanner & Shackleton (1979), who show the RBS to be deformed around the CA. In interpreting the nature of the RBS and its regional significance, it is important to determine its timing relative to the CA and to discern the original orientation of the slide.

In spite of its local and regional significance the RBS remains a contentious feature; its timing, movement sense and relation to the regional structure being unclear. The following section {3.3.2} describes the lithological, structural and textural features developed around the slide; the significance of these features is discussed in {3.5}.

3.3.2 Field observations: The path of the RBS through the study area is shown on Figure 3.32. The slide zone itself is largely unexposed lying in a shallow gully for much of its length. Adjacent to the slide the stratigraphic sequence is often highly attenuated, with the Bennabeola Quartzite Fm, which reaches a maximum thickness of >250m in the core of the Tully Mountain synform, typically being reduced to <20m. The slide runs parallel / subparallel to the foliation and lithological boundaries for much of its course, generally juxtaposing the Bennabeola Quartzite Fm with Kylemore Fm schistose pelites and

**Figure 3.32: The path of the Renvyle - Bofin Slide through the study area.**
**1: Kylemore Formation**
**2: Bennabeola Quartzite, Streamstown and Lakes Marble Formations**
**3: Silurian**

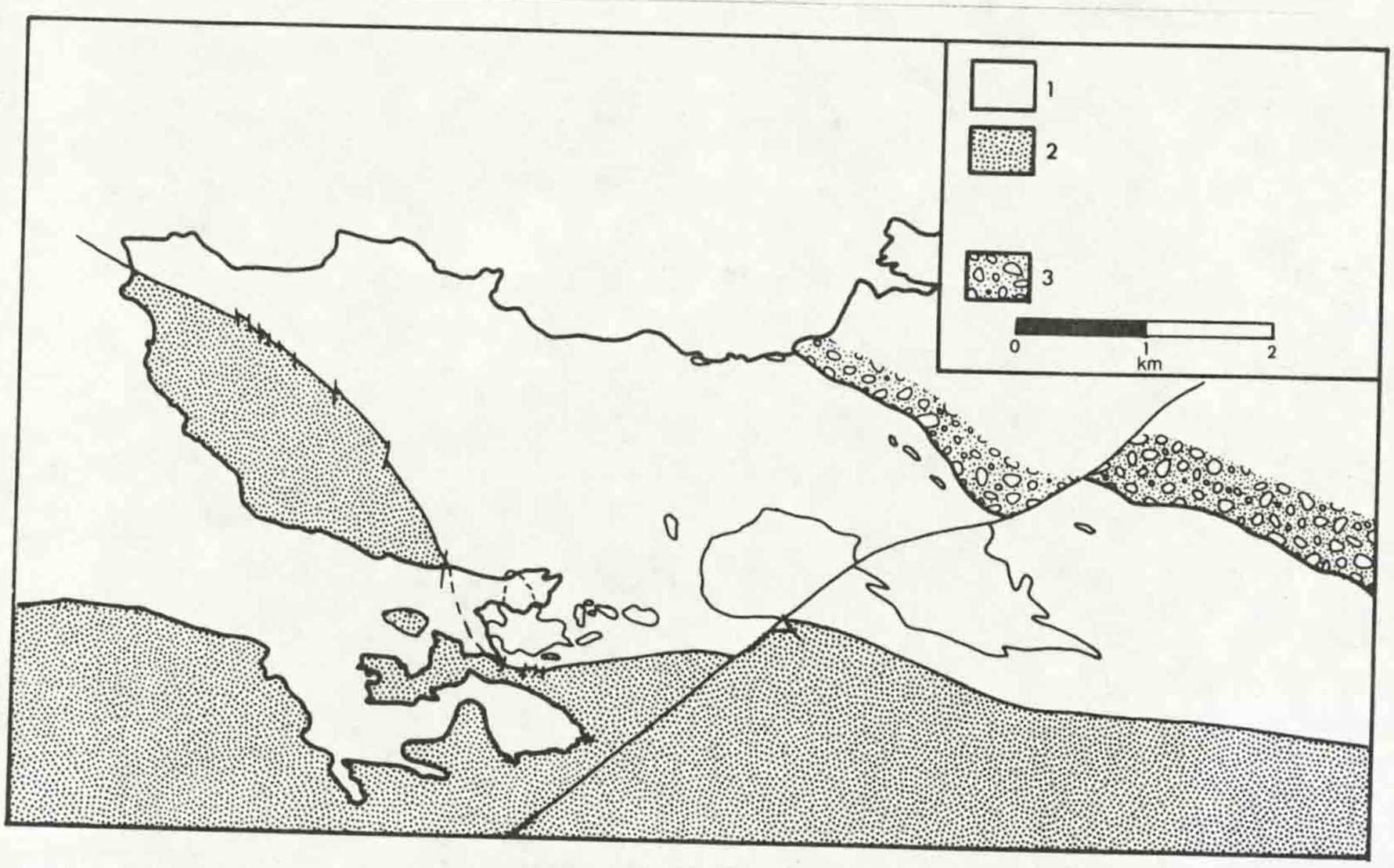


**Figure 3.33: The Renvyle - Bofin Slide exposed at Derryinver [GR 683 599] (photograph looking NW). The pale weathering Bennabeola Quartzite Formation to the south (left of photograph) is separated from flaggy feldspar porphyroblast semipelites of the Kylemore Formation (right of picture) by a zone of phyllonitic material which shows brittle disruption. Hammer is 360mm long.**

semipelites. However, in the Derryinver area and to the north of Tully Mountain the slide cuts down through the Streamstown and Lakes Marble Fms to place the Kylemore Fm against the Lakes Marble Fm for the remainder of its (largely unexposed) course (Figure 3.32). This placing of the RBS between the Lakes Marble Fm and Kylemore Fm contradicts the interpretation by Cruse (1963) of this boundary as a stratigraphic passage. The actual contact is poorly exposed, but fabrics typical of the slide zone (chloritised phyllitic lithologies, brittle disruption of ductile fabrics) are best developed to the north of the Lakes Marble Fm lithologies, suggesting the RBS to lie between them and the Kylemore Fm. The metamorphic grades of the lithologies adjacent to the RBS are similar across much of the northwestern part of the study area, although where the Kylemore Fm is associated with the DCD the slide juxtaposes contact aureole sillimanite - bearing migmatitic Kylemore Fm with regional garnet - staurolite grade lithologies to the south {Chapters 4, 5}. The aureole effects of the syn - $D_2$ DCD are not evident in the lithologies to the south of the RBS suggesting that the slide developed after the intrusion and cooling of the igneous bodies. The timing of the RBS can be constrained more tightly by consideration of the relations of structures and fabrics in the lithologies on either side of the slide.

The slide itself is exposed in only two places in the study area, [GR 683 599 & 692 589]. At [GR 683 599] it is marked by a 1 - 2m thick zone of chloritic phyllite which separates platey Bennabeola Quartzite Fm from feldspar porphyroblast rich Kylemore Fm semipelite (Figure 3.33). This zone shows evidence of strong brittle disruption of an originally ductile feature. Adjacent to the phyllitic material the quartzite has a platey appearance with a closely spaced foliation and a grain shape lineation being the dominant fabrics. Away from the slide zone the fabrics are less intense, the dominant ($S_{2/3}$) foliation being widely spaced (20 -30 mm) with only localised 1-2m thick zones of platey quartzite, a variably developed grain shape lineation, and tight to isoclinal $F_3$ fold closures. In the Kylemore Fm the lithologies adjacent to the slide consist of flaggy feldspar porphyroblastic psammites. The feldspars occur as augen within the foliation and are locally associated with a strong E - W

trending grain shape lineation. This lineation is developed within 100m of the slide zone and its orientation contrasts strongly with the N - S lineations recorded elsewhere in the Kylemore Fm {3.2.2.2}. It is notable that the mylonitic zones adjacent to the slide show no clear evidence of shear criteria (e.g. Simpson 1986) through which the movement sense can be determined.

The other exposure of the slide, [GR 692 589], again juxtaposes Bennabeola Quartzite Fm against Kylemore Fm, the quartzite being highly attenuated with a thickness of 15 - 20m. The Streamstown and Lakes Marble Fms in this area also show considerable thinning in the zone adjacent to the slide, typically reaching thicknesses of only 20 - 30m, compared with the typical thicknesses of several hundred metres away from the slide.

In those areas where the slide is unexposed the contact can often be located to within 5m, although where the quartzite is not adjacent to the slide such precise location is often difficult.

Brittle deformation within lithologies adjacent to the slide (Cruse 1963), is not widespread, generally only being developed within 5 - 10m of the actual slide zone. The zone around Eagles Nest School [GR 665 626], noted by Cruse as being typical of the *'shattering'* associated with the RBS, contains a series of minor ( <5m displacement) brittle faults (Figure 3.32) which locally produce the appearance of large scale brittle disruption. A gently dipping lineation trending parallel to the trace of the slide is variably developed in lithologies adjacent to the RBS.

The mineral assemblages in lithologies adjacent to the slide {4.1} show little evidence of retrogression related to ductile deformation, although a chlorite grade overprint is common in phyllitic zones and where brittle deformation is developed.

## 3.4 Structure and contact relations of the igneous bodies

### 3.4.1 The structure of the Dawros Peridotite: Introduction

Despite the body of work covering the structure of the Dawros

**Figure 3.34: Previous interpretations of the structure of the Dawros peridotite;**

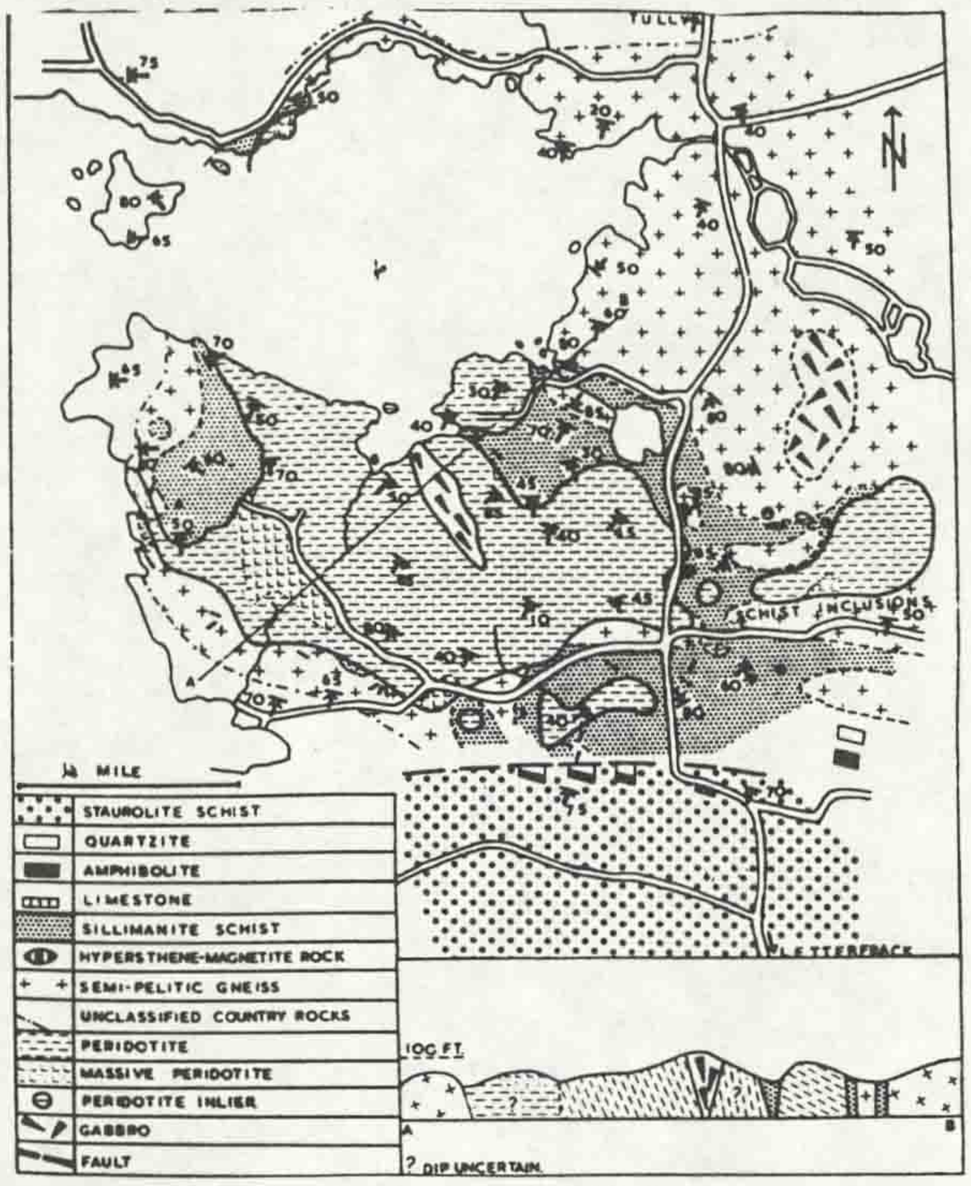


**a, Rothstein (1957),**

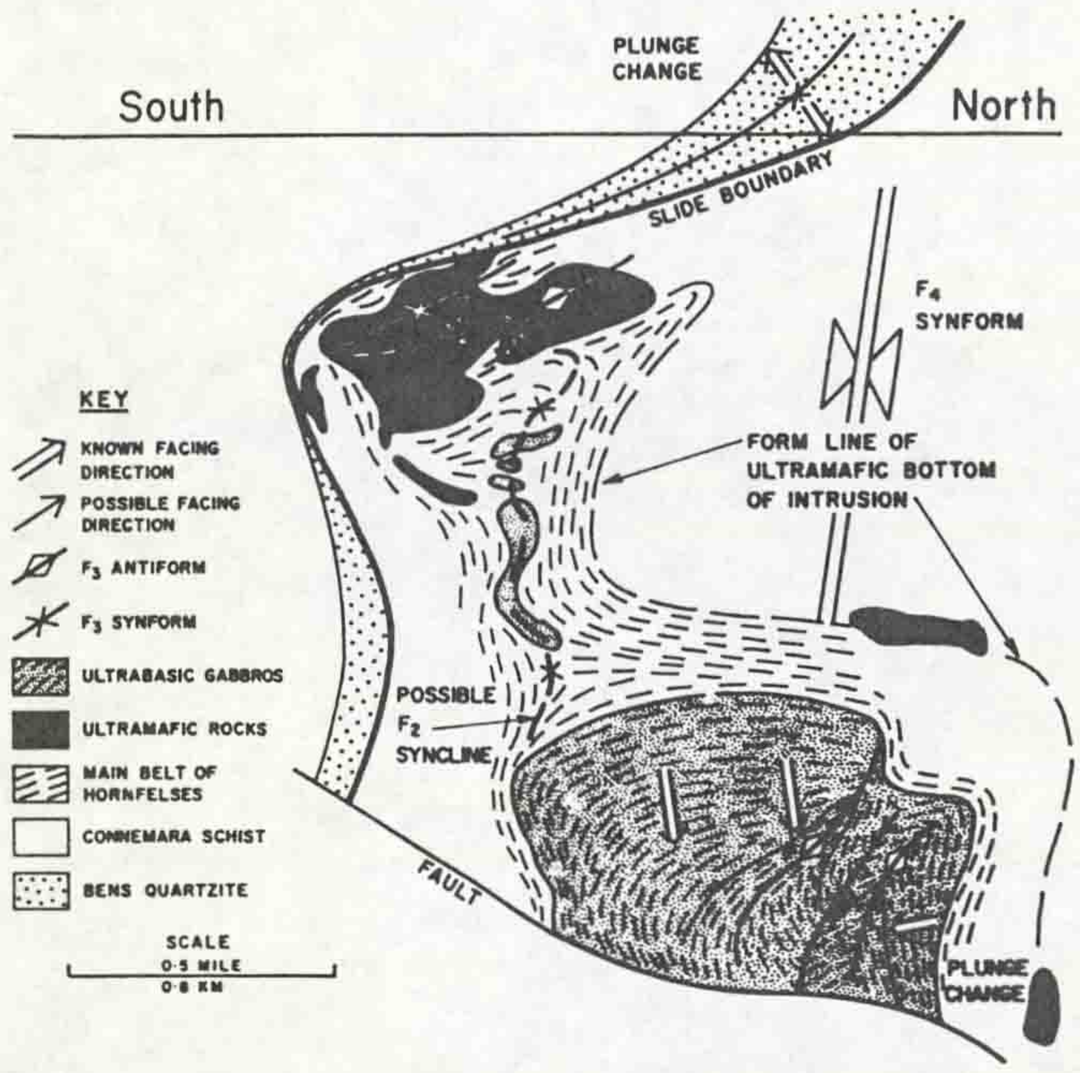


**b, Leake (1970b),**

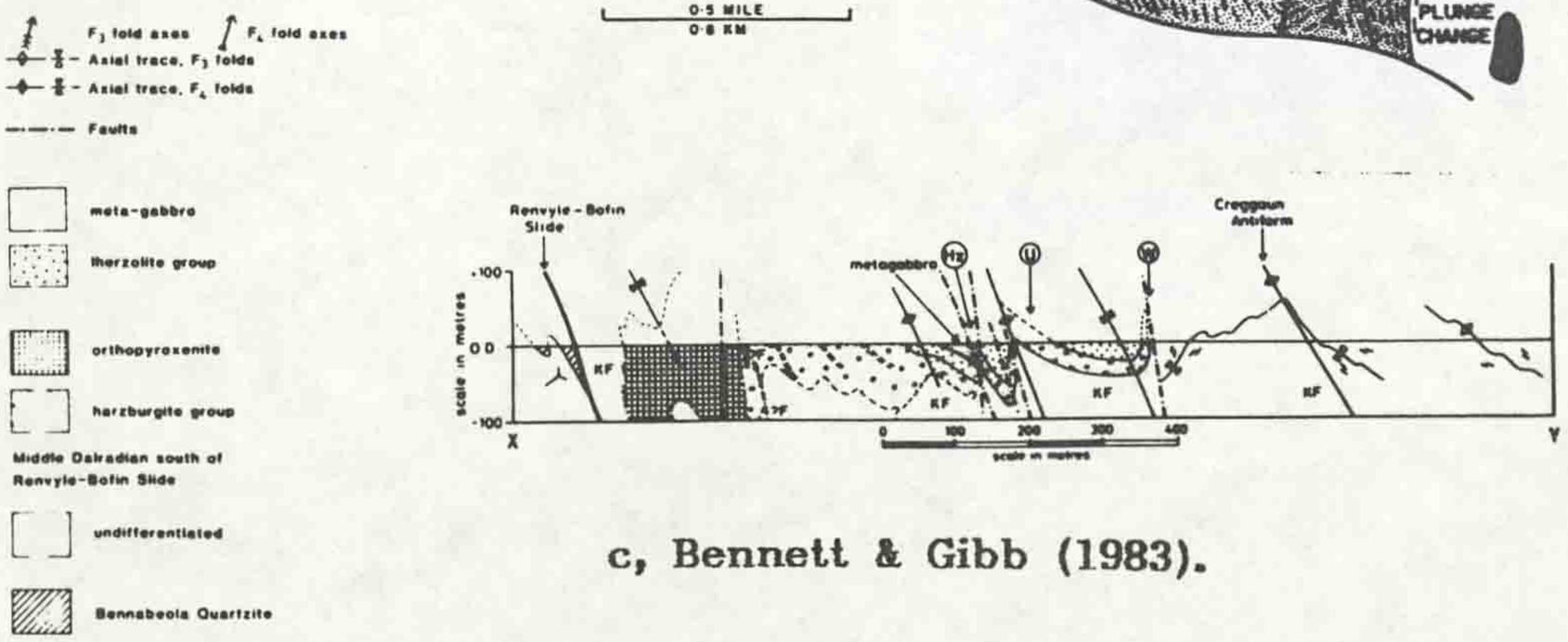


**c, Bennett & Gibb (1983).**

**Figure 3.35: Equal area stereonet projections of the peridotite orientation data (all planes plotted as poles);**
**a, Phase layering (131 pts)**
**b, $S_1$ foliation (153 pts)**
**c, $S_2$ foliation (122 pts)**
**d, Phase layering (dots, 36 pts) and foliation (triangles, 14 pts) in gabbroic lithologies.**